UNIVERSITÉ DU QUÉBEC À MONTRÉAL

IMPACT DE L'EPIGALLOCATECHINE-3-GALLATE SUR LA RÉGULATION PARACRINE DES MÉCANISMES DE DIFFÉRENCIATION ET DE TRANSFORMATION ONCOGÈNIQUE DES CELLULES SOUCHES PRÉADIPOCYTAIRES

THÈSE
PRÉSENTÉE
COMME EXIGENCE PARTIELLE
DU DOCTORAT EN BIOCHIMIE

PAR
NARJARA GONZALEZ SUAREZ

OCTOBRE 2023

UNIVERSITÉ DU QUÉBEC À MONTRÉAL

IMPACT OF EPIGALLOCATECHIN-3-GALLATE ON THE PARACRINE REGULATION AND PREADIPOCYTES STEM CELLS MECHANISMS OF DIFFERENTIATION AND ONCOGENIC TRANSFORMATION

THESIS
SUBMITTED
AS PARTIAL REQUIREMENT
OF THE DOCTORATE IN BIOCHEMISTRY

BY
NARJARA GONZALEZ SUAREZ

OCTOBER 2023

DEDICATION

To my dear family.

The one who raised me with love and support: my mom, grandparents, and aunt Pucha.
They taught me to be resilient and to trust myself above all else.

To my dear husband and son. You give me all the motivation to continue and sort out each obstacle.

This work is for you and thanks to you.

ACKNOWLEDGMENTS

This work is the closure of a journey that I stared in January 2019, and that involved the contribution of several people that I would like to acknowledge and thank.

First, I would like to start by thanking my supervisor Dr. Borhane Annabi for accepting me in his lab. I really appreciated your support and guidance all these years, but above all, thank you very much for believing in me and help in overcoming each obstacle.

I would like to continue to thank Dr. Denis Flipo and Dr. Grégoire Bonnamour for their contribution with the microscopy experiments. You were always kind and willing to help me and I will never forget that.

I recognize the support of our collaborator Prof. Luc Boudreau, which helped us to boost the part of the project associated with the EV and who was always very optimistic and motivated. Also, to my colleague and collaborator Dr. Yuniel Fernández-Marero for giving me his time and making big data analysis possible in our project.

I would also like to extent my acknowledgements to all UQAM professors that despite my lack of French, were very supportive in and outside the classroom. Especially to Prof. Dr. Claire Bénard, my most sincere thanks for your trust in me, encouragement and advice.

I would like to recognize the scholarships I received from CERMO-FC and from the FRQNT, which validated the pertinence of my research project and definitively made this journey easier.

Thank you so much to the members of the Committee of my Doctoral Exam: Prof. Isabelle Plante, Prof. Diana Alison Averill, and twice for Prof. Mircea A. Mateescu, that was also part of my evaluation committed in the Projet de Thèse. I am extremely grateful for accepting to revise my PhD thesis, the contribution of your suggestions improved the quality of my work.

My most sincere thanks to all the past and present members of Dr. Annabi's lab at UQAM: Marbelis Francisco Fernandez and Tiziana Dao, you welcomed me into the lab and taught me not only the techniques but also helped me with the cells or the experiments on those days when I couldn't come or had to rush out because my son was adapting his immune system to the cold temperatures. To, the girls that arrived almost at the end but again were more than colleagues: Layal El Cheikh-Hussein, Marie-Eve Roy, Celia Kassouri, Sahily Rodriguez Torres and Sima Torabidastgerdooei, Carolane Veilleux; and especially Souad Djediai for your

friendship and support beyond the lab. Also, to my colleagues at the lab: Cyndia, Jean Christophe, Naoufal, Isabelle, Mary-Cruz, Damiil and Bogdan, it has been a pleasure to share this time with you guys.

Many thanks to all my friends for making me feel like home in those short but great lunches to recharge batteries: Alexis, Anna Caridis, Yarelys, Mariela y Ana.

Finally, I would like to thank my family. My grandparents, my aunt Puchita, my dad Paul, my brother and my mom because they have believed in my abilities and decisions throughout my life, which have strengthened my confidence enough to allow me to accept this and rest of the challenges that lie ahead. To my dear mother-in-law, Mama, you had my back just when I needed it most, thank you very much.

My infinitive love to my husband and son.

Ale, this work is as much mine as yours, without your support I would never have gotten to this point and certainly not so fast. I believe that together we can accomplish everything we want to.

To my son Arian because your laugh and the way you look at me are my greatest drivers.

TABLE OF CONTENTS

LIST OF FIGURES

LIST OF TABLES

LIST OF ABBREVIATIONS AND ACRONYMS

ADM: Adrenomedullin

AKT: Protein kinase B

ALDH1: Aldehyde dehydrogenase 1

ALIX: Programmed cell death 6-interacting protein

AML: Acute myeloid leukemia

AMP: Adenosine monophosphate

AMPK: 5' adenosine monophosphate-activated protein kinase

AP-1: Activator protein 1

aP2: Adipocyte protein 2

ATP: Adenosine trisphosphate

Bad: BCL2 associated agonist of cell death

BAI: Body adiposity index

BAT: Brown adipose tissue

Bax: Bcl-2 associated X-protein

BC: Breast cancer

Bcl-2: B-cell lymphoma-2 protein

Bcl-XL: B-cell lymphoma-extra large protein

BCSCs: Breast cancer stem cells

BIP: Binding immunoglobulin protein

BMI: Body mass index

BRAF: B-Raf proto-oncogene, serine/threonine kinase

BRCA1/2: Breast and ovarian cancer susceptibility protein 1 and 2

C/EBPA: CCAAT/enhancer binding proteins alpha

C/EBPB: CCAAT/enhancer binding proteins beta

C/EBPD: CCAAT/enhancer binding proteins delta

CAA: Cancer-associated adipocytes

CAF: Cancer-associated fibroblasts

cAMP: Cyclic adenosine monophosphate

CCL2: C-C motif chemokine ligand 2

CCL5/RANTES: C-C motif chemokine ligand 5

CDK2: Cyclin-dependent kinase 2

CDK4: Cyclin-dependent kinase 4

CDK6: Cyclin-dependent kinase 6

CDKN1A: Cyclin dependent kinase inhibitor 1A

CDKN2A/B: Cyclin dependent kinase inhibitor 2A/2B

cGMP: Cyclic guanosine monophosphate

CM: Conditioned media

COX2/PTGS: Cyclooxygenase 2 / prostaglandin-endoperoxide synthase 2

CREB: Cyclic AMP response binding element

CSC: Cancer stem cells

CTLA-4: Lymphocyte-associated protein 4

CXCL-11: C-X-C motif chemokine ligand 11

CXCL-12: C-X-C motif chemokine ligand 12

CXCL-12: C-X-C motif chemokine ligand 12

CXCL-8/IL-8: C-X-C motif chemokine ligand 8/ Interleukin 8

CXCR4: C-X-C chemokine receptor 4

DAPI: 4′,6-diamidino-2-phenylindole

DCIS: Ductal carcinoma in situ

DEX: Dexamethasone

DNA: Deoxyribonucleic acid

DNMT1: DNA methyltransferase 1

ECM: Extracellular matrix

EGCG: Epigallocatechin-3-gallate

EGF: Epidermal growth factor

EGFR: Epidermal growth factor receptor

EMT: Epithelial-to-mesenchymal transition

ER: Estrogen receptor

ERBB2/HER2: Epidermal growth factor receptor 2

ERK1/2 or MAPK: Mitogen-activated protein kinase 1/2

ESCRT: Endosomal sorting complex required for transport

EV: Extracellular vesicles

FABP4: Fatty acid binding protein

FAS: Fatty acid synthase

FasL: Fas ligand

FFA: Free fatty acids

FLOT1: Flotillin

FN: Fibronectin

GAPDH: Glyceraldehyde-3-phosphate dehydrogenase

GATA2/ 3: GATA binding proteins 2 and 3

GIP: Gastric inhibitory polypeptide

GLP-1: Glucagon-like peptide-1

GLUT1: Glucose transporter 1

GLUT4: Glucose transporter 4

GSH: Glutathione

GSK-3β: Glycogen synthase kinase-3 beta

GSTP1: Glutathione s-transferase P1

hADMSC: Human adipose-derived mesenchymal stem cells

HDAC: Histone deacetylase

HGF: Hepatocyte growth factor

Hh: Hedgehog

HIF-1A: Hypoxia-inducible factor-1 alpha

HSP70: Heat shock proteins 70

HSP90: Heat shock proteins 90

IDO: Indoleamine 2,3-dioxygenase

IGF-1: Insulin-like growth factor 1

IGF-1R: Insulin-like growth factor1 receptor

IGFPB1: IGF binding protein 1

IGFPB3: IGF binding protein 3

IKBA/B/E: Nuclear factor of the kappa light polypeptide gene enhancer in B-cells inhibitor-alpha/beta/epsilon

IL-6/10/12/17: Interleukin 6, 10, 12 and 17

IL-1B: Interleukin beta

ILV: Intraluminal vesicles

iNOS: Inducible nitric oxide synthase

ISEV: International Society for Extracellular Vesicles

JAK: Janus kinases

JNK: c-Jun N-terminal kinase

KLF3: Kruppel-like transcription factors 3

KLF4: Kruppel-like transcription factors 4

KLF5: Kruppel-like transcription factors 5

KRAS: Kirsten rat sarcoma viral oncogene homolog

67LR: 67kDa Laminin receptor

LDH-A: Lactate dehydrogenase

lncRNAs: Long non-coding RNAs

LOX: Lipoxygenase

LPL: Lipoprotein lipase

MCP-1: Monocyte chemoattractant protein-1

MDSC: Myeloided-derived suppressor cells

MET: Proto-oncogene receptor tyrosine kinase

miRNA: Micro RNAs

MMP 2/9/11: Metalloproteinase 2, 9, and 11

MS: Metabolic syndrome

MSC: Mesenchymal stem cells

mTOR: Mammalian Target of Rapamycin

MVB: Multivesicular bodies

MYC: Proto-oncogene, BHLH transcription factor

NDRG1: *N*-myelocytomatosis viral related oncogene (myc) downstream regulated

NF-KB: Nuclear factor kappa B

NK: Natural killer

NKG2D: Killer cell lectin like receptor K 1

p38MAPK: p38 mitogen-activated protein kinases

PAI1: Plasminogen activator inhibitor 1

PD-1: Programmed cell death protein-1

PD-L1: Programmed cells death ligand 1

PECAM: Platelet and endothelial cell adhesion molecule

PI3K: Phosphatidylinositol-3-kinase

PIK3CA: Phosphatidylinositol-4,5-bisphosphate 3-kinase catalytic subunit alpha

PIK3CD: Phosphatidylinositol-4,5-bisphosphate 3-kinase catalytic subunit delta

PIPs: Phosphatidylinositol phospholipids

PKA: Protein kinase A

PKC: Protein kinase C

PP2A: Protein phosphatase 2A

PPARG: Peroxisome proliferator-activated receptor ganma

PR: Progesterone receptor

PTEN: Phosphatase and TENsin homolog deleted on chromosome 10

RB1: Retinoblastoma 1

RNA: Ribonucleic acid

ROS: Reactive oxygen species

SASP: Senescence-associated secretory phenotype

SGLT-2: Sodium-glucose co-transporter-2

SNARE: Soluble N-ethylmaleimide-sensitive factor-attachment protein (SNAP) receptor

SOD: Superoxide dismutase

SREBP1: Sterol regulatory element-binding protein 1

STAT3/5: Signal transducers and activators of transcription 3 and 5

TAM: Tumor-associated macrophages

TGFBR1: TGFB receptor 1

TGFB: Transforming growth factors beta

TILs: Tumor-infiltrating lymphocytes

TLR4: Toll-like receptor 4

TME: Tumor microenvironment

TNBC: Triple-negative breast cancer

TNFA: Tumor necrosis factor alpha

TP53: Tumor protein p53

Tregs: Regulatory T cells

UCP1/2: Uncoupling protein 1 and 2

VEGF: Vascular endothelial growth factor

VM: Vasculogenic mimicry

VPS4: Vacuolar protein sorting homolog A

WAT: White adipose tissue

WHO: World Health Organization

Wnt: Wingless-type MMTV integration site family members

WNT3A: Wnt family member 3A

WNT5: Wnt ligand 5

α-SMA: Alpha-smooth muscle actin

β-gal: Senescence-associated β-galactosidase

RÉSUMÉ

L'émergence et le développement du cancer est un phénomène multifactoriel. Des données récemment recueillies ont mis en évidence le rôle pro-tumoral de l'obésité en entretenant un état d'inflammation chronique de bas grade. Dans ce contexte, le sécrétome du tissu adipeux pourrait donc jouer un rôle régulateur paracrine crucial dans la promotion et la progression du cancer du sein. Cependant, les mécanismes moléculaires impliqués demeurent peu documentés. D'autre part, des études épidémiologiques suggèrent que la consommation d'aliments riches en polyphénols réduit l'incidence de certains cancers liés à l'obésité. L'épigallocatéchine-3-gallate (EGCG) est le composé principal du thé vert et, dans un modèle murin, il a été démontré qu'il réduit l'expression des marqueurs adipocytaires, leur prolifération et l'accumulation de lipides. Il reste à déterminer si les polyphénols dérivés de l'alimentation peuvent modifier le profil du sécrétome des adipocytes. Compte tenu de ces faits, ce project doctoral visait à identifier les mécanismes moléculaires impliqués dans la régulation paracrine adipocytaire du phénotype invasif des cellules cancéreuses du sein et l'efficacité d'une intervention dérivée de l'alimentation pouvant modifier ce phénomène. Pour modéliser l'interaction entre le tissu adipeux et les cellules cancéreuses du sein, nous avons utilisé des cellules souches mésenchymateuses dérivées d'adipocytes humains (h-ADMSC), qui peuvent se différencier en adipocytes matures et soutenir l'expansion du tissu adipeux. Quant à la lignée cellulaire tumorale, nous avons utilisé les cellules MDA-MB-231, un modèle de cancer du sein triple négatif, un sous-type très agressif. Premièrement, nous avons constaté que le sécrétome des adipocytes matures augmentait la capacité de migration des cellules MDA-MB-231 ainsi que leur potentiel à former de nouveaux vaisseaux sanguins (mimétisme vasculogénique). Fait intéressant, cet effet est en corrélation avec l'induction de la voie de signalisation STAT3, et l'EGCG l'a effectivement réduit. De plus, le polyphénol a inhibé la différenciation des h-ADMSC en adipocytes en réduisant l'expression de biomarqueurs adipogéniques clés. Deuxièmement, nous avons démontré que le sécrétome du TNBC pouvait attirer les h-ADMSC vers le microenvironnement tumoral et remodeler les pré-adipocytes pour acquérir un phénotype de type adipocyte associé au cancer (CAA), via la régulation positive de l'expression de cytokines telles que CCL2, CCL5, IL-1B et IL-6 et des immunomodulateurs COX2, HIF-1, VEGF et PD-L1. Nous avons également découvert que l'EGCG inhibait l'induction de ces gènes et la réponse chimiotactique induite. Enfin, nous nous sommes concentrés sur les vésicules extracellulaires (VE) au sein du sécrétome du TNBC et leur capacité à induire un phénotype pro-inflammatoire dans les h-ADMSC. Les VE ont induit l'expression des marqueurs CAA au sein du h-ADMSC. En revanche, les VE obtenus à partir de MDA-MB-231 traitées à l'EGCG (EGCG-EV) ont réduit l'expression de CCL2, CCL20 et IL-1Btout en augmentant les niveaux de CXCL8 et IL-6. De plus, les EGCG-EV ont spécifiquement réduit l'activation des voies de signalisation AKT et GSK-3β dans h-ADMSC, les sauvant de la sénescence induite par la déprivation de sérum. Dans

l'ensemble, nous avons démontré que l'EGCG prévient l'apparition d'un environnement obésogène qui favorise le développement de TNBC, en réduisant la modulation pro-inflammatoire du profil des sécrétomes des adipocytes et des cellules tumorales et en modulant le profil tumoral en contenu génétique des VE.

MOTS-CLÉS: Adipogenèse, adipocytes associés au cancer, obésité, épigallocatéchine-3-gallate, cellules cancéreuses du sein triple négatif, vésicules extracellulaires, inflammation.

ABSTRACT

The emergence and development of cancer is a multifactorial phenomenon. Recently collected data has pointed out the pro-tumoral role of obesity by sustaining a low-grade chronic inflammation state. In this context, the adipose tissue secretome could play a crucial paracrine regulatory role in the promotion and progression of breast cancer. However, little is known about the molecular mechanisms involved. On the other hand, epidemiological studies suggest that consuming a polyphenol-rich food reduces the incidence of some obesity-related cancers. Epigallocatechin-3-gallate (EGCG), the main compound in green tea, has reduced adipocytes markers' expression, proliferation, and lipid accumulation in a murine model. Whether diet-derived polyphenols can consequently alter the adipocyte secretome profile remains to be addressed. Considering these facts, this doctoral project aimed to identify the molecular mechanisms involved in the adipocyte paracrine regulation of cancer cells' invasive phenotype and how efficient diet-derived intervention may alter such a phenomenon. To model the interaction between adipose tissue and breast cancer cells, we used human adipocyte-derived mesenchymal stem cells (h-ADMSC), which can differentiate into mature adipocytes and sustain the expansion of the adipose tissue. As tumor cell line model, we used MDA-MB-231, a highly aggressive subtype model of triple-negative breast cancer (TNBC). *Firstly*, we found that the secretome of mature adipocytes increased the migratory capacity of the MDA-MB-231 cells as well as their potential to form new blood vessels (vasculogenic mimicry). Interestingly, this effect correlates with the induction of the STAT3 oncogenic signaling pathway and was effectively reduced by EGCG. In addition, the polyphenol inhibited the differentiation of h-ADMSCs into adipocytes by reducing the expression of key adipogenic biomarkers. *Secondly*, we demonstrated that the secretome of the TNBC could attract the h-ADMSC to the tumor microenvironment and reshape the pre-adipocytes to acquire a cancer-associated adipocyte (CAA)-like phenotype by upregulating the expression of cytokines like CCL2, CCL5, IL-1, and IL-6 and immunomodulators COX2, HIF-1, VEGF and PD-L1. Additionally, we found that EGCG inhibited the induction of these genes and the induced chemotactic response. *Finally*, we focused on the extracellular vesicles (EV) within the secretome of the TNBC and their capacity to modulate the h-ADMSC phenotype. Interestingly, while EV induced the expression of the CAA markers within the h-ADMSC, the vesicles obtained from the EGCG-treated MDA-MB231 cells (EGCG-EV) reduced the expression of *CCL2*, *CCL20* and *IL-1B*while increasing *CXCL8* and *IL-6* levels. In addition, EGCG-EV specifically reduced the activation of AKT and GSK-3β signaling pathways in h-ADMSC, rescuing them from serum starvation-induced senescence. Overall, we demonstrated that EGCG prevents the onset of an obesogenic environment that favours TNBC development by acting at different nodes: preventing the expansion of the adipose tissue, reducing the pro-inflammatory modulation of both adipocyte and tumor cells secretome profile and modulating the tumor-derived EV' genetic content.

KEYWORDS: Adipogenesis, cancer-associated adipocytes, obesity, epigallocatechin-3-gallate, triple-negative breast cancer cells, extracellular vesicles, inflammation.

CHAPTER I

INTRODUCTION

1.1 Cancer in the context of obesity

1.1.1 Obesity: a modern pandemic

Obesity is a condition that has increased worldwide, both for adults and children regardless of the country's income level (Avgerinos *et al.*, 2019). It is defined as an individual with a body mass index (BMI) equal to or greater than 30, calculated according to the weight and height (weight [kg]/ height [m^2]) of the person (Pischon et Nimptsch, 2016). Fat deposition can lead to a chronic condition that increases the risk of other comorbidities. For instance, abdominal obesity is associated with diabetes, cardiovascular disease, and cancer (Hu *et al.*, 2017). Hence, an alternative method has been established to include measuring the body fat percentage called the body adiposity index (BAI) (Bergman, 2012), although difficult to standardize.

Several factors can trigger this condition in adulthood, from social factors, lifestyles, and nutritional habits to genetics (Safaei *et al.*, 2021). As for the latter, factors include the brain-gut axis, gut microbiome, neuroendocrine conditions, and viruses (Kadouh et Acosta, 2017). With the increase in obesity, the incidence of other comorbidities like diabetes, heart disease, stroke, and several cancer types, has also increased (Andolfi et Fisichella, 2018; Avgerinos *et al.*, 2019). As a result, a high percentage of global deaths has been attributed to obesity as a risk factor. The figure below shows the increases in the percentage of obesity-related deaths worldwide within a ten-years laps (Figure 1. 1).

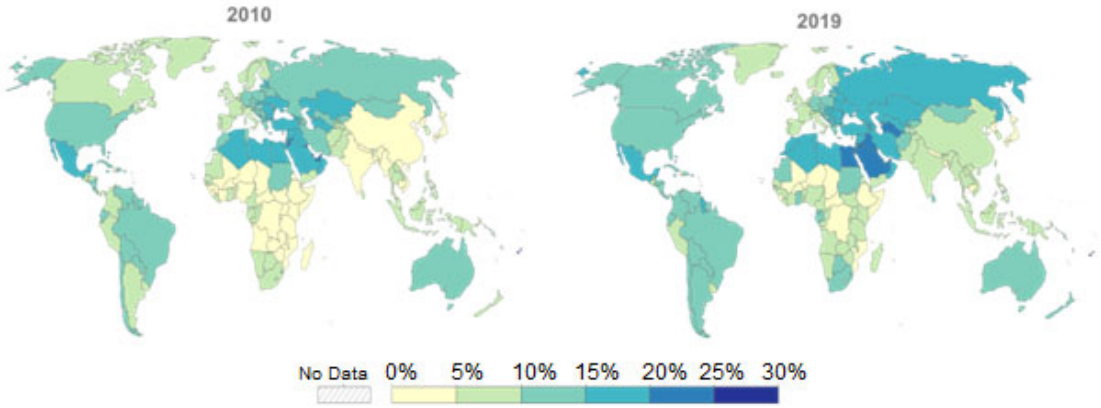

Figure 1. 1. Comparative world map showing the percentage of obesity-related deaths in 2010 and 2019.
Adapted from OurWorldInData.org/obesity (Obesity - Our World in Data).

It has been recognized that obesity is a multifactorial disease that links low-grade inflammation with metabolic, mitochondrial, and adipose tissue dysfunction (Kawai et al., 2021; Perez et al., 2016). Obesity manifests as the expansion of the white adipose tissue (WAT) localized near the visceral organs and under the skin. This expansion is often characterized by an increase in the size (hypertrophy) and number (hyperplasia) of adipocytes, followed by disruption of the hormonal and secretory profile (Zatterale *et al.*, 2019). Losing weight through changes in diet and lifestyle are the primary interventions against obesity, but diet adherence in the long term is a challenge. Sometimes surgical intervention and pharmacotherapy are required (Williams *et al.*, 2020).

1.1.2 The adipose tissue as a secretory gland

Besides WAT, the adipose tissue can be mainly classified as brown (BAT) or beige (Correa et al., 2019). BAT is associated with thermogenesis (Shin *et al.*, 2006), and is characterized by the expression of the uncoupling protein 1 (UCP1) gene and mitochondria enrichment (Wankhade *et al.*, 2016). It is predominant in newborns but

decreases in adulthood, where it localizes in the neck and interscapular region (Wankhade *et al.*, 2016). Also, a pro-tumoral role ascribed to BAT has been associated with cancer-induced cachexia (Vaitkus et Celi, 2017).

The expansion of the WAT is a characteristic of obesity (Correa *et al.*, 2019). This tissue is involved in energy storage and regulates the metabolisms throughout the secretion of cytokines and chemokines, referred to as adipokines (Perez *et al.*, 2016). It is divided into subcutaneous and visceral fat, where the subcutaneous is associated with hormonal secretion and a beneficial role (Ma *et al.*, 2015), while the visceral fat is associated with metabolic syndrome (MS) and complications (Mathieu *et al.*, 2010). MS is a group of conditions including high blood pressure, sugar levels, triglycerides, and cholesterol; that foster the risk of severe health problems like diabetes, stroke and heart disease (Mathieu *et al.*, 2010). Interestingly, the adipose tissue has a high plasticity for responding to metabolic demands. During exercise-mediated weight loss, the subcutaneous WAT undergoes a browning or beige process, adopting a brown-like phenotype (Stanford *et al.*, 2015). Hence, beige adipocytes are characterized as an intermediary between BAT and WAT, with mitochondria and brown fat-associated genes (UCP-1) but with more multilocular lipid droplets than BAT (Correa *et al.*, 2019). On the other hand, a group of researchers have reported the existence of pink adipocytes in mice, restricted to the breast and originating from subcutaneous WAT during pregnancy and lactation (Cinti, 2018; Giordano *et al.*, 2014). However, its existence in humans remains unclear.

The adipocytes are the main cellular component of the breast, followed by preadipocytes, adipose-derived stem cells, endothelial and immune cells (Esteve Rafols, 2014). Significantly, the adipokine pattern depends on whether the fat depot's origin is subcutaneous or visceral (Dommel et Bluher, 2021). Several adipokines like adiponectin, tumor necrosis factor alpha (TNFA) and leptin are secreted in the adipose tissue and intervene in their paracrine regulation mechanisms (Correa *et al.*, 2019). Leptin is one of the critical adipokines involved in regulating nutritional status, inducing anorexic effects, and regulating lipogenesis in the liver (Cohen *et al.*, 2002).

In tumor cells, leptin activates the phosphatidylinositol-3-kinase (PI3K) signaling pathway promoting cell proliferation and migration (Correa *et al.*, 2019). Adiponectin, in contrast, protects against insulin resistance, fatty acid oxidation in the liver and obesity-associated metabolic stress (Yamauchi *et al.*, 2002; Yamauchi *et al.*, 2001). The ratio of circulating levels of adiponectin (low) versus leptin (high) has been used as an indicator of adipose tissue dysfunction, cardiometabolic alterations and insulin resistance (Fruhbeck *et al.*, 2018). Hence, it has been proposed as a predictor for MS (Fruhbeck *et al.*, 2019).

The adipose secretion of the pro-inflammatory cytokines TNFA, and interleukin 6 (IL-6), as well as the monocyte chemoattractant protein-1 (MCP-1), also known as C-C motif chemokine ligand 2 (CCL2), links obesity to inflammation (Hotamisligil, 2006; Hotamisligil *et al.*, 1993). Among the cytokines, TNF-A directly inhibits the insulin signaling pathway (Hotamisligil *et al.*, 1994). It is mainly secreted by the resident macrophages within the adipose tissue and is responsible for sustained metabolic inflammation (Park *et al.*, 2010a). IL-6, in addition to its well-known pro-inflammatory role (Tanaka *et al.*, 2014), is involved in the regulation of glucose metabolism and adipose tissue dysfunction (Lehrskov et Christensen, 2019). This cytokine can be secreted by a broad range of cell subtypes, triggering in the target cells several pathways such as PI3K, mitogen-activated protein kinase (MAPK), adenosine monophosphate (AMP)-activated protein kinase (AMPK) and Janus kinases (JAK)-signal transducers and activators of transcription (STAT3) (Kamimura *et al.*, 2003; Yang *et al.*, 2003). Induced IL-6 levels cause translocation of the glucose transporter 4 (GLUT4) to the membrane, augmenting glucose uptake and fatty acid oxidation (Lehrskov et Christensen, 2019). A high level of this cytokine in serum has been linked to insulin resistance in obese patients, which is a characteristic of MS (Vozarova *et al.*, 2001). Blocking the IL-6 receptors showed a beneficial effect on MS (Castaneda *et al.*, 2019).

Other identified adipokines are resistin, the retinol transport protein (Rbp4), secreted frizzled-related protein 5 (Sfrp5) and FABP4, also known as a lipid-activated

adipocytokine (aP2) (Cao, 2014). The latter controls glucose metabolism and lipid regulation in the liver (Cao et al., 2013), and it is implicated in metabolic inflammation (Cao, 2014).

1.1.3 A molecular insight into adipogenesis

Adipogenesis is a process that involves several rounds of cell differentiation. First, adipose-derived mesenchymal stem cells (ADMSC) are committed and become preadipocytes, followed by mitotic clonal expansion to finally acquire a fully mature adipocyte phenotype. (Tang et Lane, 2012). This process involves a network of transcriptional factors regulating adipocytes' morphological, metabolic, and secretory changes (Lefterova et Lazar, 2009). At early stages of differentiation, there is an increase in the expression of markers such as the CCAAT/enhancer binding proteins beta and delta (C/EBPB and C/EBPD) (Farmer, 2006), the Kruppel-like transcription factors 4, 5 (KLF4 and KLF5) (Birsoy *et al.*, 2008; Oishi *et al.*, 2005), the early beta-cell factor 1 (EBF1) (Rosen *et al.*, 2009) and the cyclic AMP response binding element (CREB) (Reusch *et al.*, 2000). Apart from KLF4, the rest of the markers have demonstrated *in vitro* to directly induce the expression of the main transcriptional factors of adipogenesis, the peroxisome proliferator-activated receptor gamma (PPARG) and the CCAAT/enhancer binding proteins alpha (C/EBPA) (Rosen *et al.*, 2009). These are the master regulators of the adipocyte's terminal differentiation markers. C/EBPA controls the induction of phosphoenol pyruvate carboxykinase (PEPCK), fatty acid binding protein (aP2/FABP4), glucose transporter 4 (GLUT4) and stearoyl CoA desaturase-1 (SCD1) (Moseti *et al.*, 2016); while PPARG regulates lipoprotein lipase (LPL), acyl-CoA synthase (ACS), as well as aP2/FABP4 (Rosen *et al.*, 1999; Wahli, 2002). Hence, cooperation between both transcriptional factors is required to maintain the terminal differentiation state (Sarjeant et Stephens, 2012). The sterol regulatory element-binding protein 1 (SREBP1) is another transcriptional factor of adipogenesis involved in cholesterol homeostasis and the expression of fatty acid

synthase (FAS) and LPL (Kim et Spiegelman, 1996). On the other hand, KLF3 (Sue *et al.*, 2008), KLF7 (Cho *et al.*, 2007), GATA binding proteins 2 and 3 (GATA2 and 3) (Sarjeant et Stephens, 2012; Tong *et al.*, 2005), and the interferon regulatory factors 3 and 4 (IRF-3/4) (Eguchi *et al.*, 2008), are transcriptional suppressors of adipocyte differentiation. The different stages and transcriptional regulators of adipogenesis are summarized in the following figure (

Figure 1. *2*).

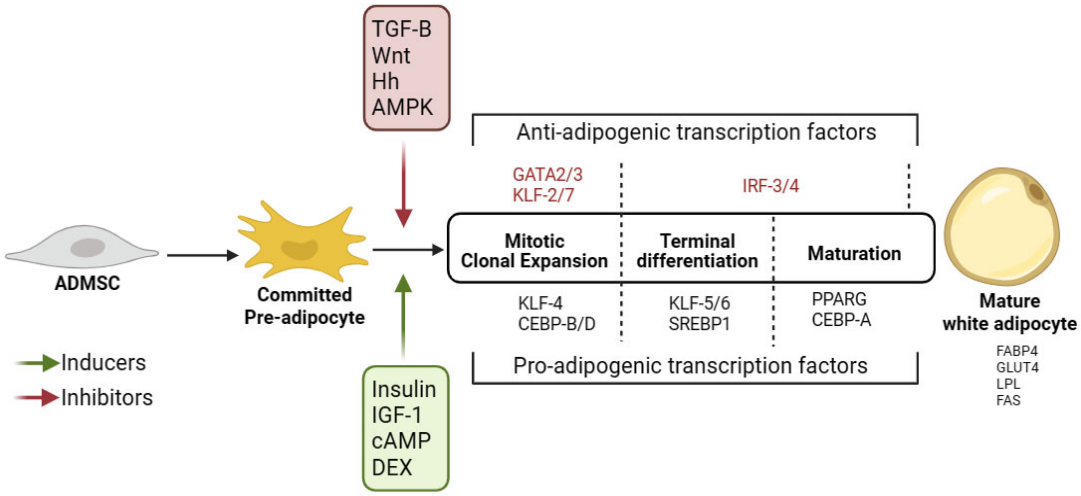

Figure 1. 2. Transcriptional regulators of adipogenesis
Created in BioRender with information from (Eguchi *et al.*, 2008; Lefterova et Lazar, 2009). AMPK (adenosine monophosphate-activated protein kinase); cAMP (cyclic adenosine monophosphate); CEBP-A/B/D (CCAAT/enhancer binding proteins alpha, beta and delta); DEX (dexamethasone); FABP4 (fatty acid binding protein); FAS (fatty acid synthase); GATA (GATA-binding factor) GLUT4 (glucose transporter 4); Hh (Hedgehog); IGF-1 (insulin-like growth factor 1); IRF (interferon regulatory factors); KLF (Kruppel-like transcription factors); LPL (lipoprotein lipase); PPARG (peroxisome proliferator-activated receptor gamma); SREBP1 (sterol regulatory element-binding protein 1); TGF-B (transforming growth factor); Wnt (Wingless-type MMTV integration site family members).

In addition, the signaling pathways of transforming growth factor beta (TGFB), the Wingless-type MMTV integration site family members (Wnt), Hedgehog (Hh) and

AMPK negatively regulate adipogenesis (Habinowski and Witters, 2001). AMPK is a kinase involved in regulating lipid and glucose homeostasis, mitochondrial biogenesis, and redox equilibrium (Ceddia, 2013; Xu *et al.*, 2012). Hence, AMPK can be activated in response to various stimuli from exercise, cold, nutrient deprivation and adipokines (IL-6, adiponectin, and leptin) (Daval et al., 2006; Katwan et al., 2019).

During *in vitro* studies, TGF-B1 inhibited pre-adipocyte differentiation, repressing the expression of C/EBPA, C/EBPB and PPARG (Margoni *et al.*, 2012; Moseti *et al.*, 2016). Besides, activating the canonical Wnt/β-catenin pathway leads to the differentiation of ADMSC into myocytes or osteocytes rather than adipocytes (Li *et al.*, 2007). The Wnt ligand 5 (WNT5)-mediated activation of the non-canonical pathways has been reported to promote adipogenesis by inhibiting the Wnt/β-catenin and blocking the PPARG downregulation (van Tienen *et al.*, 2009).

The natural inducers of this biological process include hormones (insulin) (Klemm *et al.*, 2001), growth factors like the insulin-like growth factor 1 (IGF-1) (Lefterova et Lazar, 2009), and adrenergic factors such as cyclic adenosine monophosphate (cAMP) and epinephrine (Tang and Lane, 2012). *In vitro*, adipogenesis can be induced with a corticosteroid such as dexamethasone (DEX) and isobutyl methylxanthine, a non-specific inhibitor of the cAMP and cyclic guanosine monophosphate (cGMP) phosphodiesterase (Farmer, 2006). Also, during adipogenesis cells undergo a morphological change and become spherical, which causes the remodeling of the extracellular matrix (ECM) and the loss of actin expression (Lazar, 2018).

1.1.4 Mechanisms linking obesity with cancer etiopathogenesis

The increased ectopic fat accumulation within tissues happens during obesity and it is associated with the incidence of adipocyte hypertrophy, insulin resistance and cancer (Pischon and Nimptsch, 2016). Several mechanisms have been proposed to explain how this environment contributes to cancer progression (Avgerinos *et al.*,

2019). Among these are i) chronic low-grade inflammation levels, ii) aberrations in the IGF-1 signaling axis linked to hyperinsulinemia and insulin resistance, iii) oxidative stress, iv) alteration of sex hormone production and pathways, v) adipose tissue dysfunction, and vi) stresses within the microenvironment (Avgerinos et al., 2019). Due to their relevance in breast cancer (BC), low-grade inflammation and adipose pathophysiology will be addressed more extensively in the following sections.

IGF-1 and IGF-II are growth factors ubiquitously secreted within the organism where they mediate cell growth and survival (Moschos et Mantzoros, 2002). Insulin binds to its cell surface receptors (IGF-IR and IGF-IIR) and activates the PI3K/ protein kinase B (AKT) pathways releasing anti-apoptotic molecules like the B-cell lymphoma-2 protein (Bcl-2) (Zha and Lackner, 2010). It also promotes glucose metabolism through the inhibition of glycogen synthase kinase-3 beta (GSK-3β) (Zha and Lackner, 2010). These growth factors and their receptors are overexpressed in many tumors including colon, breast, and prostate (Nguyen et al., 2022; Vigneri et al., 2016), and have been associated with drug resistance (Denduluri et al., 2015). Since insulin regulates glucose, protein and lipid metabolism (Magkos et al., 2010), it is also linked to oxidative stress (Hurrle et Hsu, 2017).

A disturbance in the redox equilibrium might cause the accumulation of reactive oxygen species (ROS) and the emergence of an oxidative stress state, which in turn causes DNA and mitochondrial damage (Sabharwal and Schumacker, 2014). Nevertheless, high levels of ROS have dual tumor-promoting and suppressing functions (Azmanova and Pitto-Barry, 2022). ROS, like superoxide and hydroxyl ions, fuel genomic instability and enhance mutational rates, in favour of cancer development, (Liou and Storz, 2010; Sabharwal and Schumacker, 2014). Also, ROS activate transcription factors involved in carcinogenesis, such as hypoxia-inducible factor-1 alpha (HIF-1A), nuclear factor kappa B (NF-KB), activator protein 1 (AP-1) and tumor protein p53 (TP53), promoting angiogenesis and metastasis (Marinho *et al*., 2014). However, above a certain threshold, very high ROS levels induce apoptosis via extrinsic or intrinsic pathways (Azmanova et Pitto-Barry, 2022).

The adipose tissue conversion of androgens (like testosterone) to estrogen is mediated by the aromatase enzyme, which has a high activity in obese individuals and is responsible for their high estrogen levels (Crosbie et al., 2010). As a consequence, obese postmenopausal women with high circulating estrogen levels (mainly estradiol) have an increased risk of developing BC (Key *et al.*, 2003) and endometrial cancer (Shaw et al., 2016). In premenopausal women, estrogen levels vary according to the menstrual cycle, which limits determining its association with BC risk. In this population, testosterone concentrations were found to be positively associated with BC risk (Zeleniuch-Jacquotte *et al.*, 2012), and to have a positive correlation with BMI (Harvie *et al.*, 2011). Nevertheless, it is unclear whether obesity causes increased androgen levels or whether women with hyperandrogenemia syndrome (polycystic ovary syndrome) are more likely to be obese (Moulana *et al.*, 2011).

Lastly, obesity alters cell signaling and the tumor microenvironment (TME) (Avgerinos *et al.*, 2019). It activates endothelial cells, forming the tumor-associated vasculature (Kwaifa et al., 2020) and triggers the epithelial-to-mesenchymal transition (EMT) program (Gilbert and Slingerland, 2013). This is a program in which epithelial cells acquire a more mesenchymal phenotype and lose their tissue attachment, allowing cells to invade and metastasize (Hursting and Dunlap, 2012). EMT can be triggered in the tumor cells by cytokines often present within the inflammatory adipose tissue like IL-6, IL-8, CCL5 (RANTES) and CCL2 (Gilbert and Slingerland, 2013; Kwaifa *et al*., 2020). Also, high circulating levels of free fatty acids (FFA) are often detected in obese people and linked with ROS-mediated oxidation of proteins (Iyengar *et al*., 2016). This causes endoplasmic reticulum stress and contributes to an inflammatory state (Iyengar et al., 2016). Besides, mesenchymal stem adipose-derived progenitors from the WAT can migrate to the TME (Zhang *et al.*, 2010), and differentiate into cancer-associated fibroblasts (CAF) (Bertolini *et al*., 2015). CAF are abundant in the TME and contribute to the malignancy development by suppressing the functions of immune cells, and by secreting factors responsible for the ECM remodelling (Hu *et al.*, 2022b).

1.1.5 Low-grade inflammation increases the risk of cancer

The WAT expansion during obesity causes a remodelling of the tissue characterized by high infiltration of immune cells, and an inflammatory state with some level of fibrosis. In this context, several factors can trigger the state of chronic inflammation like hypoxia, dysregulation of FFA homeostasis, mechanical stress associated with tissue expansion, cell death (Zatterale *et al.*, 2019), and infiltration of immune cells, mainly macrophages (Weisberg *et al*., 2003). In fact, pro-inflammatory macrophages are found near dead adipocytes forming crown-like structures, associated with local inflammation (Haase *et al.*, 2014).

Adipokines are implicated in the inflammatory response and the regulation of tumor cell metabolism, establishing a link between this process and increased cancer risk (Avgerinos *et al.*, 2019). For instance, the secretion of TNFA from the tissue-resident macrophages occurs in response to the release of FFA from the adipocytes, and a positive loop between both molecules is established (Nguyen *et al.*, 2005). Then, TNFA induces the production of pro-inflammatory cytokines by the adipocytes such as IL-6 and CCL2, stimulating the NF-KB pathway (Dommel and Bluher, 2021; Tanaka *et al.*, 2014). The relevance of TNFA and IL-6 in raising the risk of tumor development was confirmed in a study in mice, where chronic liver inflammation sustained the activation of the STAT3 pathway, enhancing hepatocellular carcinoma incidence and proliferation rate (Park *et al.*, 2010a).

Due to its role during chronic inflammation by acting as an attractant for macrophages and monocytes, MCP-1/CCL2 has been associated with malignancy of different cancer types like breast (Chen *et al.*, 2022), prostate (Hao *et al.*, 2020) and glioma (Qian *et al.*, 2022). Among the mechanisms proposed was its capacity to trigger macrophage polarization to the regulatory M2 phenotype (McClellan *et al.*, 2012), induce cell proliferation, promote migration, stemness and chemoresistance (Chen *et al.*, 2022; Hao *et al.*, 2020; Qian *et al.*, 2022).

The researchers found that obese mice fed with a high-fat diet had high levels of FABP4, which caused an upregulation of the STAT3/IL-6 axis leading to the overexpression of the DNA methyltransferase 1 (DNMT1) and the abrogation of the tumor suppressor gene p15INK4B, which encodes for the cyclin dependent kinase inhibitor 2B (CDKN2B) (Yan *et al*., 2017). In another report, obesity was linked to acute myeloid leukemia (AML) aggressiveness, because adipokines induced and sustained tumoral cell proliferation (Cao, 2014). In general, a dysfunction in the adipose tissue provides the energy and the inflammatory state required to increase the risk of developing a malignancy like cancer.

1.1.6 Evidence of the obesity pro-tumoral role in breast cancer

According to the World Health Organization (WHO), in 2020, BC was the most prevalent cancer in women, with 7.8 million diagnosed in the last five years (WHO, 2021). Many factors influence the development of this disease, from the genetic background, like mutations in the breast and ovarian cancer susceptibility protein (BRCA1/2), to the hormonal state (Avgerinos *et al.*, 2019). Estrogen and progesterone levels regulate the growth and development of the mammary gland (milk ducts and lobules) (Alferez *et al.*, 2018). Therefore, an imbalance in their levels is also involved in the development of BC (Satpathi *et al.*, 2023).

Epidemiological studies relating obesity to BC risk have yielded contrasting results regarding the women's hormonal status (Avgerinos *et al.*, 2019; Lauby-Secretan *et al.*, 2016). For instance, in postmenopausal women, BC risk has a positive association with increasing BMI, waist circumference and body weight gain (Renehan *et al.*, 2008). In premenopausal women, a high BMI reduces the incidence of BC, but no clear association has been found regarding waist circumference and weight gain (Renehan *et al.*, 2008). This double effect of obesity has been partially explained through its impact on endogenous sources of estrogen. Premenopausal obese women might have greater anovulation periods, lowering the circulating levels of estrogen and

progesterone increasing the clearance rate of both hormones by the liver (Key and Pike, 1988). Opposite, in postmenopausal women, obesity increases the level of estrogen in circulation by increasing androgen precursor availability which can be converted into estrogen in peripheral tissue, especially by the aromatase enzyme present in the peripheral adipose tissue. Also, a reduction in the sex-hormone-binding globulin (SHBG) levels has been observed during obesity, and this protein binds to estradiol reducing its availability (Siiteri, 1987). In fact, in postmenopausal women, obesity has been suggested to increase the risk of hormone-receptor-positive BC, associated with high levels of estrogen (Key *et al.*, 2003; Li *et al.*, 2019a; Zeng *et al.*, 2020). In addition, the BMI has a different impact on the BC risk depending on the molecular subtype (Yang *et al.*, 2007).

There are approximately 18 histological types of BC, and the most common have epithelial origin like the infiltrating duct carcinoma no special type (IDC-NST, 70-80%) and the invasive lobular carcinomas (ILC, 10%), (Lokuhetty *et al.*, 2019; Van Baelen *et al.*, 2023). To complement the histology, BC are also classified molecularly and according to their immunophenotype (Weigelt *et al.*, 2010). The immunophenotyping considers the expression levels of the hormonal receptors for estrogen (ER+) and progesterone (PR+), and the human epidermal growth factor receptor 2 (ERBB2/HER2+) (Weigelt *et al.*, 2008; Weigelt et Reis-Filho, 2009). Based on a microarray dataset analysis, five molecular subtypes have been described: luminal A, luminal B, HER2, basal-like and triple negative (TNBC) (Anders and Carey, 2008; Hu *et al.*, 2006; Perou *et al.*, 2000). This adds complexity to our understanding of obesity as a risk factor for different BC subtypes. For instance, during a population-based study (Poland), in premenopausal women increasing BMI had a protective effect for luminal A, but not for basal-like tumors (Yang *et al.*, 2007). Interestingly, obesity increased the risk of TNBC development and recurrence in premenopausal women, but in postmenopausal was not clearly established (Picon-Ruiz *et al.*, 2017; Sun *et al.*, 2017). Table 1. 1 summarizes the different classifications of BC, their prevalence, and stage definitions according to the TNM systems (Barzaman *et al.*, 2020; Lachapelle

and Foulkes, 2011; Orrantia-Borunda *et al.*, 2022). This staging system describes anatomically the primary tumor site and size (T), the involvement of lymph node (N) and the presence of metastasis (M) (Stages of breast cancer | Canadian Cancer Society).

Table 1. 1. Breast cancer classification and stages.

Classification (% of prevalence)	**Immunophenotype**	**Aggressiveness**	**Proposed therapies**
Luminal A (40-50%)	ER+, PR+ (≥50%), HER2-	Low proliferation rate and mutational burden.	Hormone therapy (tamoxifen and aromatase inhibitors).
Luminal B (10-20%)	ER+, PR+ (<20%), HER2+/-	Medium. BRCA2 mutation	Hormone therapy, and chemotherapy.
HER2 + (15%)	ER-, PR-, HER2+	Medium/High High proliferation rate and mutations in p53.	Chemotherapy and targeting HER2 treatments (trastuzumab, pertuzumab and TKI).
Basal-like (10-20%)	ER+(≤20), PR-, HER2+(≤20). CK-5/6 and EGFR+	High proliferation rate and mutations in BRCA1	Chemotherapy/ immunoth
TNBC (15%)	ER-, PR-, HER2-	High proliferation rate and mutations in p53 and BRCA1/2.	Chemotherapy (docetaxel or paclitaxel) /Experimental (Anthracycline-based regimens, immune checkpoint therapy)
STAGES			
0/ DCIS	Cancer cells only in the lining of a breast duct		
IA	Tumor ≤ 2 cm		
IB	Tumor ≤ 2 cm, but the presence of micrometastases in the lymph nodes (< 2 mm).		
IIA	Tumor ≤ 2 cm + presence of cancer cells in 1-3 lymph nodes of axillar and/or internal mammary gland. Or tumor mass between 2-5 cm		

IIB	2 cm > Tumor < 5 cm + presence of cancer cells in 1-3 lymph nodes of axillar and/or internal mammary gland. Or tumor > 5 cm
IIIA	Tumor ≤ 5 cm + presence of cancer cells in 4-9 internal mammary gland lymph nodes. Or tumor > 5 cm + presence of cancer cells in 1-9 lymph nodes of axillar and/or internal mammary gland.
IIIB	Tumor has grown into the muscles of the chest wall and/or skin + presence of cancer cells in 1-9 lymph nodes of axillar and/or internal mammary gland. Or inflammatory BC
IIIC	presence of cancer cells on > 10 lymph nodes of the axillar and/or internal mammary gland. Or tumor cells in supraclavicular lymph nodes
IV/Metastatic cancer	Spread to other organs (bone, liver, lungs, or brain)

CK (cytokeratins), EGFR (epidermal growth factor receptor 1), ER (estrogen receptor), PR (progesterone receptor), HER2 (epidermal growth factor receptor 2/ ERBB2), DCIS (ductal carcinoma in situ) and TNBC (triple-negative breast cancer). Source: Stages of breast cancer | Canadian Cancer Society.

Finding an effective therapy against TNBC is an open field in cancer research, where a subgroup of patients showed benefits with a combination of chemotherapy and anti-immune checkpoint blockage (Schmid *et al*., 2018; Wang *et al.*, 2019b). In this regard, obesity has been related to immune response dysregulation (Naik *et al*., 2019), affecting the efficacy of immunotherapies through a direct effect on several immune elements (Wang *et al.*, 2019d). For instance, obese individuals showed an exhausted T-cell phenotype related to the low-chronic inflammation state (Wang *et al.*, 2019c) and a reduction of the T-cell progenitor pool (Dooley and Liston, 2012) in the thymus by promoting the differentiation of thymic fibroblast into adipocytes (Dixit, 2010). Nevertheless, studies have reported that the blockage of the immune checkpoint interaction of programmed death 1 receptor with its ligand (PD-1/PD-L1) in TNBC obese patients, reverses the T cell exhaustion (Vonderheide *et al*., 2017; Yeong *et al.*, 2017). There are biases in determining obesity based on anthropomorphic measures of BMI and waist-to-hip ratio, such as not taking into account factors of race and ethnicity, which also impact what researchers have defined as "metabolically healthy" individuals (Dietze *et al*., 2018). Therefore, the direct impact of obesity on TNBC risk is not conclusive and varies among studies.

The presence of the adipose tissue within the mammary gland is extensive. Hence, it is an important component of the TME, and the contribution of adipokines in the oncogenesis and development of BC has been reported. FABP4, for example, regulates the traffic of FFA, and during obesity, its circulating levels are increased (Hao *et al.*, 2018b). It has been described that circulating FABP4 can trigger a stem-like phenotype within the tumor cells by interacting with cell membrane phosphatidylinositol phospholipids (PIPs), causing the activation of NF-KB which in turn promotes the autocrine production of IL-6 and the stimulation of the axis IL-6/STAT3/aldehyde dehydrogenase 1 (ALDH1) (Ginestier *et al.*, 2007; Zeng *et al.*, 2020). In addition, IL-6 secretion is sustained by the tumor-associated macrophages (TAM), where FABP4 induces its secretion via NF-KB activation (Hao *et al.*, 2018a).

In BC, CCL2 has also been reported to induce proliferation (Soria *et al.*, 2008) and bone metastasis, and it is a predictor of the advanced state of the disease (Hao *et al.*, 2020). Interestingly TAM-derived CCL2 was shown to increase the resistance to Tamoxifen, an ER modulator, by activating the PI3K/AKT/mechanistic target of Rapamycin (mTOR) pathway (Li *et al.*, 2020a). The relevance of CCL2 circulating level was later correlated with disease outcome because patients with endocrine-resistance cancer and high levels of CCL2 had shorter progression-free survival (Li *et al.*, 2020a).

Another vital aspect of BC pathology is the crown-like structures the macrophages form surrounding dead/dying adipocytes. This has been considered a histological marker of local inflammation and is under consideration for its value as a marker for unfavourable prognosis (Maliniak et al., 2021). Mechanistically, the dying adipocytes, release FFA that can be used as an energy source for the highly metabolically active tumoral cells (Nieman *et al*., 2013).

1.2 Cancer as a multi-factorial disease

1.2.1 The hallmarks of cancer

Cancer is a highly complex disease that requires the whole organism's participation in its development. The tumor does not only consist of malignant cells, but bears other cell types present within the TME (Hanahan and Weinberg, 2011). Hanahan and Weinberg described the regulatory mechanisms that cancer must bypass to develop as a disease, becoming a reference for all researchers in the field (Hanahan and Weinberg, 2011). In general, all cancers have a high rate of proliferation with resistance to cell death and adjusted energy metabolism due to genomic instability, which allows a high mutation rate and enables replicative immortality. Sustained inflammation conditions genomic instability and protects the tumors from immune elimination. Angiogenesis is another hallmark of cancer, although aberrant vessel

forms are often found within the malignancy, they are effective in providing nutrient supply (Hanahan and Weinberg, 2011). Finally, tumors can invade distant tissues and create metastasis (Hanahan and Weinberg, 2011), adding complexity to the disease.

Besides these well-established hallmarks, four emerging characteristics have been recently added, which help to better understand cancer as a disease that evolves. These new traits are unlocking phenotypic plasticity, non-mutational reprogramming, polymorphic microbiomes and senescent cells (Hanahan, 2022). Unlocking phenotypic plasticity refers to the disruption of the normal process of cellular differentiation, which allows cells to escape from terminal differentiated states and become more parenteral-like (dedifferentiation), or when progenitor cells keep a partially differentiated state (blocked differentiation or trans-differentiation) (Hanahan, 2022; Yuan *et al.*, 2019). As an advantage, cells are more flexible in responding and adapting to the tissue's environment.

In the beginning, all aberrant phenotypes were described as mutation associated. However, evidence from the tumor's genetic screen have highlighted the contribution of epigenetic regulation to the malignant phenotype (Baylin and Jones, 2016), named non-mutational reprogramming. For example, tumor microenvironment conditions like hypoxia and nutrient deprivation, can trigger epigenetic modifications, and act as a selective force for clonal expansion (Hanahan, 2022). This is one of the mechanisms that contribute to explaining the origin of intratumor heterogeneity (Lu *et al.*, 2020).

Senescent cells are non-proliferative, with metabolic and morphological changes that include a secretory profile called senescence-associated secretory phenotype (SASP) (Gorgoulis *et al.*, 2019). A protective role has been described for this mechanism against malignant progression (He and Sharpless, 2017), although other studies support the contrary (Faget *et al.*, 2019; Lee and Schmitt, 2019; Ruhland *et al.*, 2016b). Molecules within the SASP of senescent tumor cells have a paracrine regulatory function in the TME, triggering apoptosis, immune evasion and inducing other pro-tumoral effects (Hanahan, 2022; Hwang *et al.*, 2020; Ruhland *et al.*, 2016b). Besides, senescence is not irreversible, and cells can reassume proliferation once

favourable conditions are set, allowing malignant cells to enter and exit dormancy (De Blander *et al.*, 2021). Indeed, a senescence phenotype has been reported for cells from the TME such as cancer-associated fibroblasts (CAF) (Wang *et al.*, 2020a) and tumor endothelial cells (Hwang *et al.*, 2020; Wang *et al.*, 2020b), with great implication in tumor development.

1.2.2 Breast cancer and its tumor microenvironment

Breast cancers are highly heterogeneous in terms of clinical manifestations, and therapy response. Biologically, they are grouped according to their histological origin (Ellis *et al.*, 1992) and degree of differentiation (Elston and Ellis, 1991) as mentioned before (Table 1. 1). Tumors develop from the normal tissue and conserve some of their original characteristics, which are used for their classification. Normal breast tissue is mainly composed of epithelial and non-epithelial cells with a heterogeneous profile. Two luminal and two basal phenotypes have been described for the epithelial (Keller *et al.*, 2010). The luminal progenitor epithelial cells are characterized by the surface expression of the epithelial cell adhesion molecule (EpCAM), and the lack of $CD49f^{+}$ (alpha-6 integrin) (Shipitsin *et al.*, 2007), while mature luminal epithelial express an $EpCAM^{+}/CD49f^{+}$ phenotype (Keller *et al.*, 2010; Shipitsin *et al.*, 2007). They are both positive for cytokeratin 8 and 18 (CK-8 and CK-18) (Dairkee *et al.*, 1988) and the expression of CD24, a surface marker for genes involved in hormone responses. On the other hand, the basal cells express CK-5/5/14 (Raouf *et al.*, 2008; Shipitsin *et al.*, 2007), and have two phenotypes, one has $EpCAM^{+/lo}/CD24^{-}/CD49f^{+}$ cells and the other is $EpCAM^{-}/CD24^{-}/CD49f^{+}$ cells (mesenchymal) (Keller *et al.*, 2010). Then, luminal-derived tumors are associated with the expression of hormonal receptors (like the estrogen receptor, ER) and HER2 (Sorlie *et al.*, 2001), however immunohistochemical studies in BC biopsies reported the expression of luminal markers in all the different molecular subtypes (Park *et al.*, 2010b).

In addition to the intrinsic characteristics of tumors, the different components of the TME (Figure 1. 3) are essential in the development and clinical response of malignancies. In this section, we will focus on studies describing their contribution to BC progression, metastatic capacity, and drug resistance.

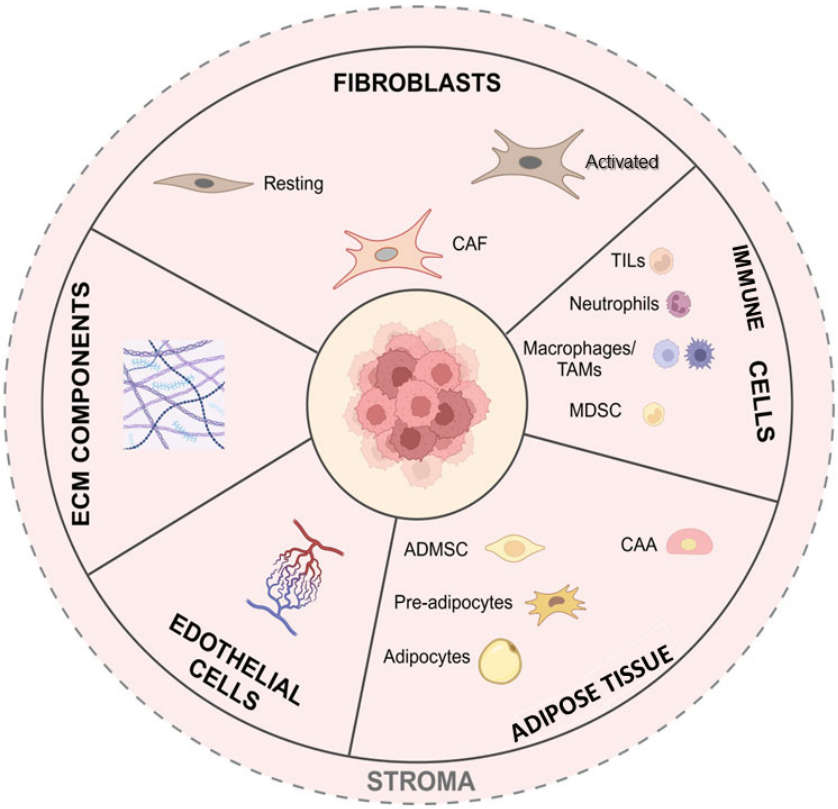

Figure 1. 3. Main components of the TME in BC.
Created in BioRender. ADMSC (adipo-derived mesenchymal stem cell); CAA (cancer-associated adipocytes); CAF (cancer-associated fibroblasts); ECM (extracellular matrix); MDSC (myeloid-derived suppressor cells); TAMs (tumor-associated macrophages); TILs (tumor-infiltrating lymphocytes).

One of the components altered within the TME is the ECM, which in the obese adipose tissue is rich in fibrillar collagen and myofibroblast-secreted fibronectin (Quail and Dannenberg, 2019). These myofibroblasts have been described as preadipocytes recruited by the tumor into the TME through chemokines like C-X-C motif chemokine ligand 11 (CXCL11) (Zhang et al., 2016), and differentiated to this phenotype,

contributing to tumoral angiogenesis (Correa *et al.*, 2019). Besides, during obesity, the accumulation of collagen fibres causes the ECM to be tighter, inducing the formation of integrin clusters, and promoting tumor proliferation and invasiveness (Gehler *et al.*, 2013; Mittal *et al.*, 2018).

Different immune cells infiltrate the TME with pro-tumoral roles. One of the best described cells are macrophages, which become tumor-associated macrophages (TAM) responsible for the crown-like structures previously mentioned. There are two populations of macrophages with opposite functions: the M1 (inhibitors) and the M2 (tumor-promoter). The latter has been demonstrated to support BC metastasis by inducing the EMT in malignant cells (Yang *et al.*, 2016) and degrading the ECM (Mittal *et al.*, 2018), favouring invasion and metastasis. On the other hand, tumor-infiltrating regulatory T cells (Tregs) are often associated with tumor malignancy. They have high expression of programmed cell death protein-1 (PD-1) (Taylor *et al.*, 2017), an inhibitory immuno-checkpoint protein that abrogates T effector cell-mediated cytotoxicity, helping tumors evade the anti-tumor immune response (Taylor *et al.*, 2017). The role of neutrophils in tumor promotion has been recently described; not only they suppress the T-cells and natural killer (NK) function (Spiegel *et al.*, 2016), but also produce DNA extracellular traps that contribute to cancer progression by preventing effector cells from reaching the cancer cells (Park *et al.*, 2016). Another critical component of the tumor-infiltrating immune cells are the myeloid-derived suppressor cells (MDSC), primarily associated with immune evasion and pro-tumoral role (Bergenfelz *et al.*, 2015). Their blood circulation levels are associated with recurrence and metastasis, reducing patients' overall survival (Diaz-Montero *et al.*, 2009). Within the TME, they are called tumor infiltrating MDSC (tiMDSC) and secrete indoleamine 2,3-dioxygenase (IDO), an inhibitory molecule of T cell activation (Yu *et al.*, 2014). The localization and predominance of the tumor infiltrating immune cells have been studied and characterized, creating an immune score that can predict the patient's clinical evolution and recurrence rate (Curigliano et Perez, 2014).

Encompassing the BC TME are non-inflammatory cells with an equally important role in cancer development, such as breast cancer stem cells (BCSCs), endothelial cells, CAFs and adipocytes. The BCSCs are a small subset of the tumor cells, although they are responsible for tumor heterogenicity (Cabrera *et al.*, 2015), recurrence (Li *et al.*, 2008), and chemoresistance. Their plasticity allows them to resist different stressful stimuli and proliferate. Critical pathways have been associated with the biological properties of BCSC, like JAK/STAT (Wang *et al.*, 2018b) in the self-renewal potential; while Wnt/β-catenin, hedgehog and Notch are related to resistance and metastasis (Cochrane *et al.*, 2015; Pires *et al.*, 2016). Recently, a new phenotype of BCSC has been described as energetic-CSC, characterized by a high mitochondrial mass, oxidative metabolism, and increased proliferation rate (Fiorillo *et al.*, 2018). These cells have a hybrid phenotype with the expression of markers for senescence (cyclin-dependent kinase inhibitor 1A, CDKN1A expression), and stemness such as the brain-enriched myelin-associated protein 1 (BCAS1), and ALDH (Fard *et al.*, 2017; Sotgia *et al.*, 2019).

Endothelial cells are essential in tumoral angiogenesis because they form the neovasculature, providing nutrients to solid tumors. Besides this notable contribution to tumor progression, a new study showed that senescent endothelial cells promoted BC aggressiveness, mediated by the secretion of specific cytokines (Hwang *et al.*, 2020; Wang *et al.*, 2020a). For instance, the chemokine CXCL11 present within the SASP of endothelial cells, increased the migration and spheroid formation capacity of the TNBC cell line MDA-MB-231, both *in vitro* and *in vivo* (Hwang et al., 2020). This pro-tumorigenic effect of CXCL11 was associated with the activation of AKT-ERK pathways, through its binding with the CXCR3 receptor expressed in the MDA-MB-231 (Hwang *et al.*, 2020). In another study, a tyrosine kinase inhibitor (sunitinib) induced senescence in endothelial cells (Wang *et al.*, 2020b). The SASP was enriched in pro-inflammatory cytokines, serving as a chemoattractant for tumor cells, macrophages, and neutrophils (Wang *et al.*, 2020b). These findings emphasize the

importance of the mechanisms by which senescence is induced because it affects the composition of the SASPs and their pro-tumoral role.

The pro-tumoral role of the CAF has been well characterized due to their abundance within the stroma of the TME. This population derives from bone marrow-derived mesenchymal stem cells and resident fibroblasts (Mittal *et al.*, 2018). Also, it has been described that epithelial carcinoma undergoing EMT can differentiate into CAF (Hanahan et Weinberg, 2011; Soda *et al.*, 2011; Zhou *et al.*, 2014) which in turn secrete growth factors and cytokines that promote proliferation (Mittal *et al.*, 2018), angiogenesis, and metastasis (Orimo *et al.*, 2005). Also, it has been reported that CAF promote therapy resistance (Amornsupak *et al.*, 2014; Shekhar *et al.*, 2007), protecting cells from drug-mediated apoptosis (Martinez-Outschoorn *et al.*, 2011). Besides, human fibroblasts that became senescent *in vitro* by replicative exhaustion could induce proliferation in epithelial cells with different grades of malignancy (Krtolica *et al.*, 2001), establishing senescence as a mechanism linking aging with the increased cancer risk.

As previously mentioned, TNBC is the most aggressive form of BC with a high metastatic potential in the lung, bones and brain (Anders and Carey, 2008; Deepak *et al.*, 2020); and high mortality associated with the lack of effective therapy. To explain its aggressiveness, it is important to highlight that in comparison with the other subtypes, TNBC has twelve times more BRCA1 mutational rate (Haffty *et al.*, 2006), and overexpression of the epidermal growth factor receptor 1 (EGFR) and TP53 among others (Rakha *et al.*, 2007; Wu *et al.*, 2021). In fact, according to its molecular profiling, six subtypes of TNBC have been well described: basal like-1 and 2 (BL1 and BL2), immunomodulatory (IM), mesenchymal (M), mesenchymal stem-like (MSL), luminal androgen receptor (LAR) (Lehmann *et al.*, 2011).

The BL1 subtype is characterized by the BRCA1 and BRCA2 mutations, which abrogate their role as tumor suppressor genes by inhibiting their capacity to regulate DNA repair, genome stability and cell cycle control (Yoshida and Miki, 2004). In the BL1 subtype, the most frequent deletions are found in the genes related to DNA repair:

phosphatase and TENsin homolog (PTEN) deleted on chromosome 10, retinoblastoma 1 (RB1) and TP53 among others (Yin *et al.*, 2020). This subtype is also characterized by a high amplification of several molecules associated with intracellular signal transducing pathways like the proto-oncogene BHLH transcription factor (MYC), phosphatidylinositol-4,5-bisphosphate 3-kinase catalytic subunit alpha (PIK3CA), AKT2, Kirsten rat sarcoma viral oncogene homolog (KRAS) and CDKN2A/B (Yin *et al.*, 2020). On the other hand, BL2 is associated with genetic abnormalities in glycolysis, glucogenesis and growth factors signaling pathways like Wnt/β-catenin, proto-oncogene receptor tyrosine kinase (MET), epidermal growth factor receptor (EGFR) and IGF-1R (Yin *et al.*, 2020).

The IM is the TNBC-subtype with the better prognosis since it has been associated with increased chemotherapy sensitivity (Yin *et al.*, 2020), especially targeting the immune checkpoints PD1, programmed cells death ligand 1 (PD-L1) and cytotoxic T-lymphocyte associated protein 4 (CTLA-4) (O'Meara *et al.*, 2020). This subtype has enriched expression of genes associated with cytokine-cytokine receptor interaction responses like interleukins 12 and 17 (IL-12 and IL-17) and the NF-KB pathway (Yin *et al.*, 2020). In the M subtype, there is an increased expression of genes associated with cell migration (PTEN, TP53 and PIK3CA), epithelial cells-like physical characteristics, and interaction with the ECM (Gibson *et al.*, 2005; Lehmann et Pietenpol, 2014). Compared with M, MSL has higher levels of stemness and angiogenesis-associated genes (Yin *et al.*, 2020).

Pathways related to cell differentiation, like Wnt and TGFB (Deepak *et al.*, 2020; Yin *et al.*, 2020), are involved in the metabolism of androgen, estrogen, and steroid synthesis (Yin *et al.*, 2020). Unlike the other subtypes, LAR has high activation in hormone-related signaling, associated with the increase in the expression of the androgen receptor (AR) and its downstream mediators (Liu *et al.*, 2016). Besides high AR expression, it has mutations in genes such as PIK3CA (55%), AKT (13%) and cadherin 1 (CDH1, 13%) (Bareche *et al.*, 2018; Lehmann and Pietenpol, 2014). In a recent study, after standard chemotherapy, patients with the LAR subtype had the

poorest probability of 5-years overall survival compared with the other subtypes (Hartung *et al.*, 2021). All these differences have a direct influence on tumor sensitivities and are taken into consideration for therapy selection. For instance, BL1 is sensitive to the unspecific cell cycle inhibitory drug cisplatin (Lehmann et Pietenpol, 2014), BL2 to mTOR and growth factor inhibitors (Lehmann et Pietenpol, 2014), while M and MSL to PI3K, mTOR and the non-receptor protein-tyrosine kinase Src pathways inhibitors (Abramson *et al.*, 2015; Yin *et al.*, 2020). LAR is also sensitive to PI3K pathway inhibitors and androgen receptor antagonists (Burstein *et al.*, 2015).

The presence of hypoxia is a general characteristic in many solid tumors and within the TME of TNBC. Most importantly, hypoxia promotes fibrosis of the tissues and regulates the interaction between cells and the ECM (Petrova *et al*., 2018). It augments the expression of metalloproteinases (MMP9), increasing invasiveness (Choi et al., 2011). Low oxygen levels induced the expression of HIF-1A in the CAF (Chiavarina et al., 2010), secreting not only enzymes that remodel the ECM (Cirri et Chiarugi, 2011) but also TGFB, vascular endothelial growth factor (VEGF), hepatocyte growth factor (HGF) and C-X-C motif chemokine ligand 12 (CXCL12), increasing their availability for the tumor cells in the ECM (Petrova *et al*., 2018).

1.2.3 The role of cancer-associated adipocytes in tumor progression

The contribution of adipocytes to tumoral development has remained unknown for many years despite being among the main components of TME in the breast. Human histological sections of breast biopsies have shown the presence of adipocytes and dedifferentiated adipocytes in the periphery of the tumor invasive front, referred to as cancer-associated adipocytes (CAA) (Dirat *et al.*, 2011). CAA have different morphology, with a fibroblast shape and expressed markers like the fibroblast activation protein (FAP), alpha-smooth muscle actin (α-SMA) and chondroitin sulphate proteoglycan (Bochet *et al.*, 2013). They are smaller, with dispersed droplet accumulation and loss of terminal differentiation markers like FABP4, resistin and

C/EBPA (Dirat *et al.*, 2011; Fujisaki *et al.*, 2015; Gonzalez Suarez *et al.*, 2022). Furthermore, CAA express the BAT-associated protein UCP1 (Wang *et al.*, 2014), which makes them resemble an intermediary phenotype. Also, they have a high proliferation rate (Fujisaki *et al.*, 2015) and an increased expression of pro-inflammatory cytokines such as IL-6, IL-1β, TNFA and CCL2, as well as metalloproteinase-2, -9 and -11 (MMP-2, -9, -11) (Dirat *et al.*, 2011; Fujisaki *et al.*, 2015; Rybinska *et al.*, 2021). A higher level of IL-6 expression was correlated with larger tumors and lymph node participation (Dirat *et al.*, 2011). This cytokine is critical in linking obesity with cancer progression because resistance to anti-VEGF therapies in obese BC patients correlates with its high levels in circulation (Incio *et al.*, 2018). CAA demonstrated a capacity to improve human BC cells' migration and metastatic ability *in vitro* and *in vivo* (Dirat *et al.*, 2011; Fujisaki *et al.*, 2015).

The emergence of CAA has been proposed as a process of dedifferentiation of mature adipocytes in response to tumor-secreted factors (Dirat *et al.*, 2011; Fujisaki *et al.*, 2015). More interestingly, the dedifferentiation of adipocytes to fibroblasts has been described in BC and related to the fibrotic environment near the tumor (Bochet *et al.*, 2013). The expression of CCL5 and IGF-1 within the adipocytes increases the invasiveness of the MDA-MB-231 TNBC cell line *in vitro* (D'Esposito *et al.*, 2016). A result later confirmed in a clinical setting where the CCL5 detection in the peritumoral adipose tissues of patients with TNBC showed a negative correlation with overall survival (D'Esposito *et al.*, 2016). The co-culture of TNBC with adipocytes triggered the activation of the Src signaling pathway, resulting in the autocrine production of pro-inflammatory cytokine, and raising the metastatic potential (Picon-Ruiz *et al.*, 2016). Src activation also triggered the upregulation of the tumorigenic driving pathways SRY-Box Transcription Factor 2 (SOX2), c-MYC, and Nanog (Picon-Ruiz *et al.*, 2016).

Several stimuli can lead to the development of CAA. The activation of the Wnt/β-catenin pathway is required for the differentiation of CAA in response to the tumor-secreted TNFA (Gustafson et Smith, 2010). Mechanistically, β-catenin inhibits the

activity of the adipogenic master regulator PPARG (Liu *et al.*, 2006), favoring the loss of terminal differentiation markers and the transition to a dedifferentiated state. Additionally, the WNT3A-mediated activation of Wnt is also required to initiate an immature phenotype (Rybinska *et al.*, 2021). Hepatocellular carcinoma-derived exosomes induced a CAA-like phenotype in human adipose-derived mesenchymal stem cells by activating mitogen-activated protein kinase 1/2 (ERK1/2 or MAPK), AKT, NF-KB, GSK-3β, and the signal transducers and activators of transcription-5 alpha (STAT5α) pathways (Wang *et al.*, 2018a). Soluble factors like the mammosphere-secreted adrenomedullin caused the conversion of white adipocytes into a brown-like phenotype, by inducing UCP1 and activating MAPK pathways (Pare *et al.*, 2020). Numerous molecular mechanisms unveil how cancer cells and adipocyte crosstalk regulates such a phenotype. Figure 1. *4* is a representation of the pathways and markers reported to describe the CAA induction and phenotype.

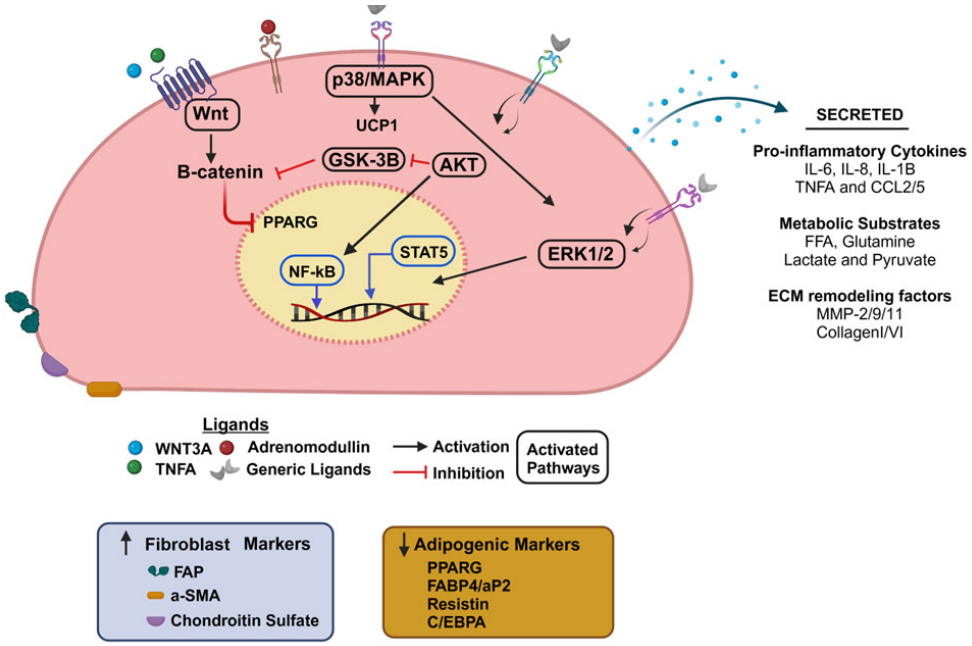

Figure 1. 4.**Error! Not a valid bookmark self-reference.**
Created in Biorender with information from (Dirat *et al.*, 2011; Fujisaki *et al.*, 2015; Pare *et al.*, 2020; Rybinska *et al.*, 2021; Wang *et al.*, 2018a). p38MAPK (p38 mitogen-

activated protein kinases); UCP1 (uncoupling protein 1); AKT (or protein kinase B, PKB); ERK1/2 (extracellular signal-regulated kinase 1/2); GSK-3β (glycogen synthase kinase-3 beta); PPARG (peroxisome proliferator-activated receptor gamma); NF-κβ (AP-1factor kappa light chain enhancer of activated B cells); STAT5a (signal transducer and activator of transcription 5A); TNFα (tumor necrosis factor alpha); CCL2/5 (C-C Motif chemokine ligand 2/5); FFA (free fatty acid); MMP-2/9/11 (metalloproteinase 2/9/11); WNT3A (Wnt family member 3A); FAP (fibroblast activation protein alpha); α-SMA (smooth muscle alpha-actin); FABP4/aP2 (fatty acid-binding protein 4/adipocyte binding protein 2); C/EBPA (CCAAT/enhancer-binding protein alpha).

CAA are delipidated and consequently released FFA, which in turn is transferred to the BC tumor cells, directly or by extracellular vesicles (Clement *et al.*, 2020), There, FFA induces cell growth and epigenetic changes that drive metabolic adaptation, and contribute to the acquisition of an aggressive phenotype (Attane and Muller, 2020; Rybinska *et al.*, 2021). Besides, CAA can regulate ECM remodelling through the over-expression of collagen VI and MMP11, contributing to fibrosis, angiogenesis, and tumor growth (Iyengar *et al.*, 2005; Wei *et al.*, 2019). The broad pro-inflammatory secretory profile of CAA contributes to the recruitment of immunomodulatory cells like MDSC, neutrophils and TAMs to the TME (Rybinska *et al.*, 2021), which in turn reinforces the pro-tumoral conditions.

1.3 Targeting pro-tumoral processes with diet-derived polyphenols

Diet-derived polyphenols are gaining more attention in the clinical scenario because of evidence highlighting their protective role through strong antioxidant properties (Khan *et al.*, 2021), making them suitable not only in prevention but also in combination with therapies (Lee *et al.*, 2021). These compounds can be found in fruits, vegetables, cereals and beverages like tea and wine (Arts and Hollman, 2005). Commonly, these include catechins, anthocyanidins, flavonoids, stilbenes, phenolic acids, lignans, tannins and flavonoids (Rudrapal *et al.*, 2022). Figure 1. *5* shows the

classification of polyphenols and the chemical structures of some of the most studied compounds in each sub-group.

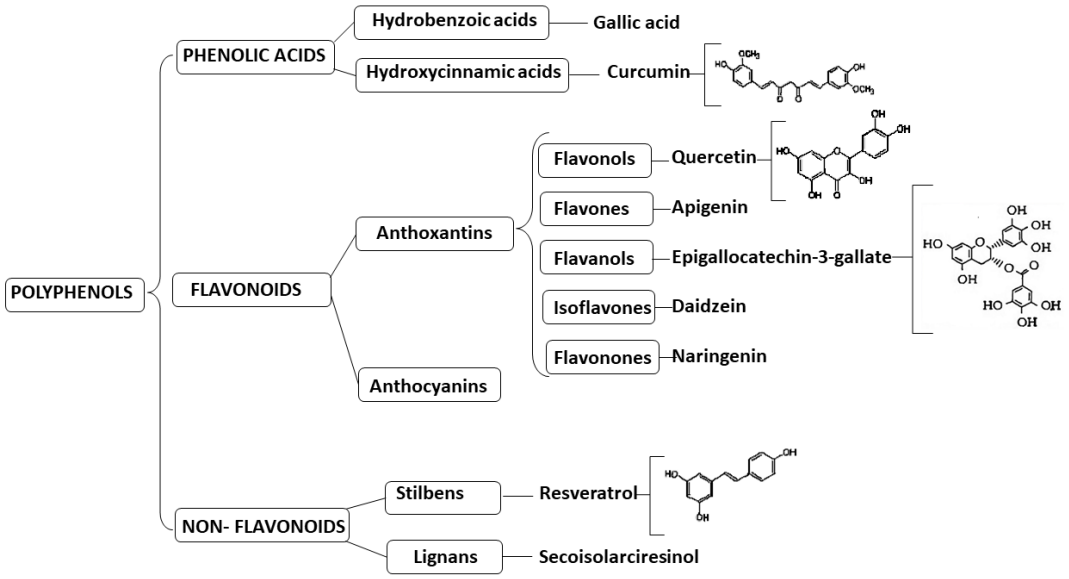

Figure 1. 5. Classification and chemical structure of natural polyphenols
Adapted from (Mao *et al*., 2018; Zhou *et al*., 2016).

Polyphenols are a class of organic compounds that have at least one aromatic ring with several hydroxyl groups within their chemical structure (Tsao, 2010). This allows them to act as scavengers for ROS and prevent cellular damage (Zhang, 2016). ROS induce several pathways with a pro-survival role, such as ERK, PI3K and NF-κB, or that are linked to apoptosis like c-Jun N-terminal kinase (JNK), TP53 and MAPK (p38) (Finkel et Holbrook, 2000). ROS can be generated by external (irradiation, drugs and toxins) or internal (hypoxia, mitochondrial activity and inflammatory cell responses) signals, and trigger oxidative stress causing modifications in all macromolecules (Rudrapal *et al.*, 2022) leading to cell death (Aguiar *et al.*, 2013). Therefore, ROS dysregulation has been linked to several pathologies (Law *et al.*, 2017). Antioxidant enzymes like catalase (CAT), superoxide dismutase (SOD) and reduced glutathione (GSH) are essential for maintaining homeostasis (Mao *et al.*, 2018). Besides, sustaining ROS production at a low level can lead to genetic instability and pro-inflammatory

cytokine release, increasing the risk for cancer development (Khansari *et al.*, 2009), and linking oxidative stress to cancer progression.

1.3.1 Diet-derived polyphenols with anti-tumoral roles

The anti-cancer properties of dietary polyphenols are correlated with the regulation of ROS and linked to their antioxidant impact. Nutraceuticals have been demonstrated to impact cell proliferation and inflammation (Maiuolo *et al.*, 2021). However, their rapid metabolic transformation, short half-life, low water solubility, absorption and biodistribution, limit their biological effects. In this sense, strategies to bypass these limitations have included chemical modifications (Bulotta *et al.*, 2013) and nanoencapsulation (Vinayak and Maurya, 2019). Still, no robust clinical validations have been performed so far. In the following section, we will describe the molecular mechanisms of some of these natural compounds.

Quercetin belongs to the flavonoids group, a subclass of flavonols. It is present in a wide variety of fruits and vegetables, with a high concentration in onions (Neveu *et al.*, 2010). It has antioxidant and anti-inflammatory effects. Besides, quercetin negatively impacts the cell cycle, and proliferation, inducing apoptosis in models of the prostate (Ward *et al.*, 2018), ovarian (Catanzaro *et al.*, 2015), TNBC (Choi *et al.*, 2008) and melanoma (Kim *et al.*, 2019) cancers. The general mechanism of action triggers the inhibition of cyclins (D1, A and B) and cyclin-dependent kinase 2 (CDK2), causing DNA damage at physiological concentrations. Additionally, it triggers apoptosis-mediated cell death by the mitochondrial associated pathway, causing an increase in pro-apoptotic (caspases 3, 8 and 9, Bax and Bad) mediators and a decrease in some anti-apoptotic ones (Bcl-XL and Bcl-2). Necroptosis is another cell death pathway induced by this compound, which increased the expression of receptor-interacting serine/threonine-protein kinase 1 and 3 (RIPK1 and RIPK3) in a model of BC (Khorsandi *et al.*, 2017). Quercetin also hampers the activation of the pro-survival pathways AKT and NF-KB (Ward *et al.*, 2018) while increasing the activation of the

stress-activated pathways JNK-p38, leading to cell apoptosis (Kim *et al.*, 2019). Moreover, quercetin regulates mitochondrial function and glucose metabolism (Lang et Racker, 1974). In several studies performed in colon and BC, the compound inhibited the activity of lactate dehydrogenase (LDH-A), monocarboxylate transporter (MCT), pyruvate kinase isoenzyme M2 (PKM2) and GLUT1, contributing to the inhibition of glycolysis, a critical metabolic pathway for tumor promotion (Aslan *et al.*, 2016; Jia *et al.*, 2018; Reyes-Farias et Carrasco-Pozo, 2019).

Curcumin is the principal polyphenol of the ginger family plant Curcuma Longa. It has an anti-proliferative and anti-inflammatory effect. The latter is supported by inhibiting NF-kB in BC and leukemia (Farghadani and Naidu, 2021). Similar to quercetin, curcumin causes cell cycle arrest and apoptosis in different cancer cell models. It regulates genes like *TP53*, *P21*, *P27* and caspases (3, 8, 9), and downregulates the AKT and STAT3 pathways (Farghadani et Naidu, 2021; He *et al.*, 2019). It has a protective effect. Curcumin's anti-inflammatory effect is mediated by its ability to decrease the expression of the enzymes cyclooxygenase 2 (COX2), lipoxygenase (LOX) and inducible nitric oxide synthase (iNOS), while blocking the TNFA signaling pathway (Maiuolo *et al.*, 2021). Additionally, curcumin exerted epigenetic regulation by modulating the expression of **s**mall (21-23 nucleotides), single-stranded, non-coding RNA (microRNAs) that regulate gene expression. It was demonstrated that in MCF-7, a cellular model of a human hormone-sensitive mammary tumor, the polyphenol induced the expression of the tumor suppressor cluster of microRNAs (miRNA)-15a/16 (Qin *et al.*, 2014).

Resveratrol is a polyphenol present in the peel of grapes (berries and peanuts), with a potential regulatory role in the expression of miRNAs. In BC cells, it has demonstrated a capacity to decrease the expression of DNA methyltransferase (DNMT) 3b in tumors but not in normal tissue, increasing the expression of tumor suppressors miRNAs- 129, 204, and 489 (Qin *et al.*, 2014). In rectal cancer, resveratrol shows a pro-apoptotic and anti-survival effect, inducing the expression of caspase 3,

TP53 and stabilizing PTEN, especially in models expressing wild type TP53 (Almatroodi *et al.*, 2022; Chen *et al.*, 2018). As an inducer of apoptosis, resveratrol reduces Bcl2 expression and activation levels of AKT (She *et al.*, 2001), which is responsible for the mitochondrial translocation of Bax, and interrupting mitochondrial transmembrane potential (Mahyar-Roemer *et al.*, 2002). In several cancer models, resveratrol demonstrated diminished angiogenesis by reducing the production of HIF-1A and VEGF (Kimura et Okuda, 2001). Also, it induces STAT3 and PI3K/AKT-mediated cell proliferation and invasion (Almatroodi *et al.*, 2022).

Green tea is rich in catechins among which epigallocatechin-3-gallate (EGCG) is the most abundant, with anti-proliferative, anti-angiogenic, and anti-metastatic capacity (Shankar *et al.*, 2008). These antitumoral effects have been demonstrated in different cancer cell models and through several mechanisms of action (Rady, 2018). In a study with pancreatic tumor cells and a xenograft tumor model, EGCG induced cancer cell apoptosis, inhibited tumoral cell proliferation, angiogenesis, and metastasis (Shankar *et al.*, 2008). The polyphenol diminished the ERK pathway signaling in the tumor while increasing P38 and JNK activation (Shankar *et al.*, 2008). Also, EGCG induced epigenetic modifications by inhibiting histone deacetylase (HDAC) activity, which increases the kinase inhibitor protein's expression (RKIP). As a result, genes associated with the EMT program were reduced, such as *SNAIL1*, and the activity of MMP2 and MMP9 (Kim et Kim, 2013). In a gastric cancer model, besides reducing the tumor burden, the catechin suppressed the expression of VEGF and inhibited the STAT3 activation (Zhu *et al.*, 2007). Its inhibitory effect on VEGF secretion and pro-angiogenic capacity was confirmed in both *in vitro* and *in vivo* in a human non-small cell lung cancer cell model, where it also downregulated the induction of HIF-1A (Li *et al.*, 2013). Also, in a human adrenal cancer cell model, the catechins affected mitochondrial membrane potential, increasing the influx of Ca^{2+} and causing cell growth arrest and apoptosis. Among the proteins involved in these effects, EGCG triggered the expression of regulatory proteins involved in the mitochondrial apoptotic pathway, such as Bad, Bax, cytochrome c, apoptosis protease-activating factor-1

(Apaf-1), and FAS/CD95, as well as the effectors caspases 3, 7, 8, and 9 (Rady, 2018). EGCG also downregulated anti-apoptotic mediators like Bcl-2, Bcl-XL, and heat shock proteins 70 and 90 (HSP70 and HSP90) (Wu *et al.*, 2009). EGCG arrests the cell cycle in cellular models of pancreatic (Shankar *et al.*, 2007), lung (Ma *et al.*, 2014), prostate (Gupta *et al.*, 2000), cervical (Sharma *et al.*, 2012) and colorectal cancers (Zhang *et al.*, 2012). It inhibits the signaling axis EGFR/cyclin D1 (Ma *et al.*, 2014) and regulates the expression of proliferation master regulators CDK4/6, P21 and P27 (Rady, 2018). In general, EGCG inhibits a plethora of signaling pathways like AKT, ERK, Src, c-Met, STAT3 and NF-KB, associated with several biological processes involved in cancer development (Chen *et al.*, 2011; Gonzalez Suarez *et al.*, 2022; Koh *et al.*, 2011; Sen et Chatterjee, 2011; Shi *et al.*, 2015; Zhou *et al.*, 2012; Zhu *et al.*, 2011).

Importantly, EGCG discriminates normal cells from cancer epithelial cells and only triggers apoptosis in malignant epithelial cells. This effect was described for prostate (Tang *et al.*, 2010), BC (Mineva *et al.*, 2013), colon (Toden *et al.*, 2016) and neuroblastoma (Nishimura *et al.*, 2012) cancer cell models, sharing some common mechanisms with other polyphenols like the downregulation of anti-apoptotic proteins Bcl-2, and the activation of the pro-apoptotic caspases -3 and -7, and the pro-invasive Vimentin, SLUG and SNAIL1 (Tang *et al.*, 2010). The catechin also increased the chemo-sensitivity of cancer stem cells (CSC) and downregulated stem cell markers (OCT4 and Nanog), key pathways (Notch1) and negative regulatory microRNAs linked to stem cell self-renewal (miRNAs, miR-34a, miR-145, and miR-200c), as well as molecules associated with chemoresistance (BMI-1, SUZ12 and EZ2) (Toden *et al.*, 2016).

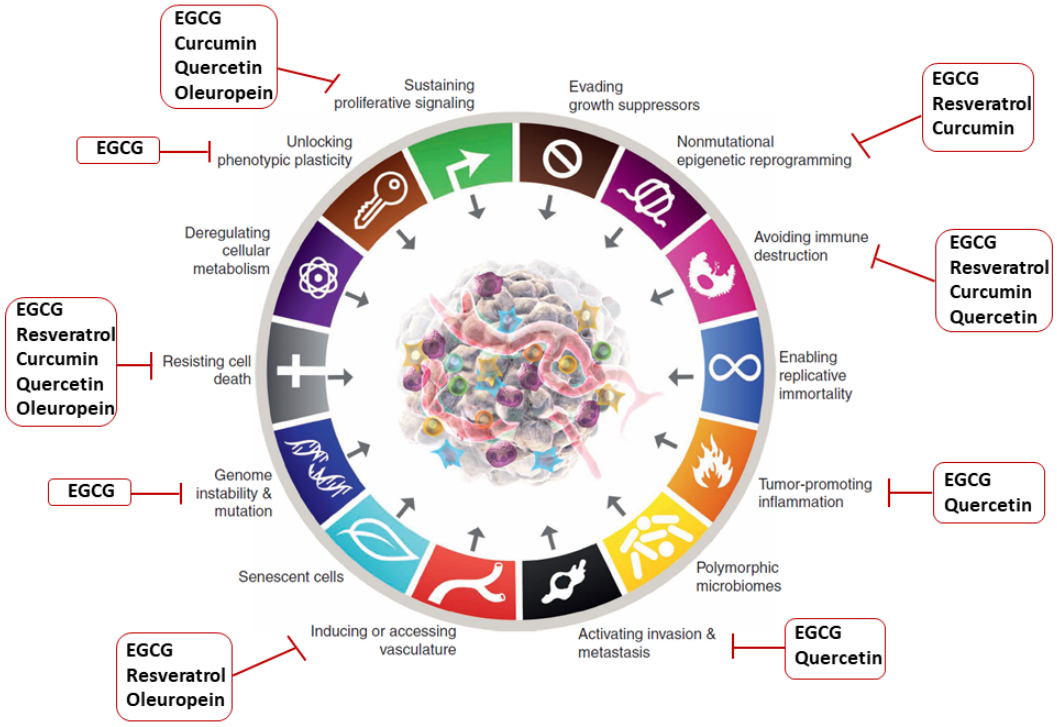

Figure 1. 6. Polyphenols target several hallmarks of cancer.
Adapted from (Hanahan, 2022). EGCG (epigallocatechin-3-gallate).

Overall, polyphenols target several pathways involved in carcinogenesis establishment and development (Figure 1. *6*). Hence, recent approaches have been designed to combine their potential to influence the entire TME to improve the effectiveness of other therapeutic agents like immune checkpoint inhibitors (Lee *et al.*, 2021). In this regard, most of the studies for EGCG and quercetin have been inhibiting the PD-1/PD-L1 axis, while resveratrol and curcumin affected the expression of CTLA-4 (Lee *et al.*, 2021). However, more studies are required to unveil these compounds' best combinatory strategy and delivery format. Nevertheless, EGCG affects protein expression by several mechanisms, including disrupting lipid rafts, receptor signalization and epigenetic modulation, and regulating miRNA expression. In a study with highly aggressive melanoma, the polyphenol inhibited tumor proliferation by activating its 67kDa laminin receptor (67LR). Consequently, the 67LR-mediated activation of cAMP/protein kinase A (PKA)/protein phosphatase 2A

(PP2A) led to the upregulation of let-7b (Yamada *et al.*, 2016). This miRNA inhibits the expression of tumor progression-associated genes like the high mobility group (HMGA2), involved in other cancer types (Liu *et al.*, 2014).

1.3.2 Anti-inflammatory effect of EGCG

NF-κB acts as a master regulator of genes involved in cellular processes such as differentiation, response to oxidative stress, survival, inflammation, angiogenesis and metastasis, establishing a link between inflammation and cancer (Gupta et al., 2010; (Gupta *et al.*, 2018). The modulation of the NF-κB transcription factor expression represents the primary mechanism described by nutraceuticals with anti-inflammatory effects (Gupta *et al.*, 2018). When cells are not activated, NF-κB proteins remain associated with inhibitory molecules called nuclear factor of kappa light polypeptide gene enhancer in B-cells inhibitor-alpha/beta/epsilon (IKBA/B/E) in the cytoplasm (Hayden et Ghosh, 2004). Once cells are activated, the IKK complex phosphorylates the IκB, inducing their degradation, and releasing NF-κB. Then, NF-κB is translocated to the nucleus to exert its transcriptional role (Hayden et Ghosh, 2004). Besides IKK intervention, protein kinases such as GSK-3β, PI3K, AKT and p38 MAPK, can directly phosphorylate and activate NF-κB (Gupta *et al.*, 2010).

EGCG affects downstream signaling cascades upon cell surface receptors' activation and it is the only catechin with a known receptor, the 67LR. Upon activation, 67LR leads to apoptosis and inhibition of the TLR4/MAPK-mediated inflammation (Xu *et al.*, 2017). Moreover, EGCG inhibited the activation of NF-kB in several malignancy models by blocking the IKK-mediated phosphorylation of IKBA (Nomura *et al.*, 2000) and the activity of MAPK (Afaq *et al.*, 2003). The latter pathways mainly encompass the inhibition of the growth factor and mitogen stimulator ERK1/2, and the pro-inflammatory, cell differentiation, and pro-apoptotic inducers JNK/p38. The effect of EGCG on the MAPK family-mediated process has been documented (Mokra *et al.*,

2022). For example, in mice, EGCG downregulated ROS and MAPK mediated activation of the inflammasome NLR family pyrin domain-containing protein 3 (NLRP3) (Liu *et al.*, 2021), a multimeric intracellular protein complex that mediates the inflammatory response. In human cancer cells, EGCG has been demonstrated to inhibit pro-inflammatory mediators such as COX-2, IL-8, IL-1β, and iNOS, as well as the STAT1/3 inflammatory responders TNFA and IL-6 (Mokra *et al.*, 2022), highlighting its potent anti-inflammatory properties.

1.3.3 Anti-obesogenic effect of EGCG

EGCG downregulates significant genes involved in adipogenesis, such as the C/EBPA, PPARG, FAS, and FABP4 (Gonzalez Suarez *et al*., 2021; Lee *et al*., 2013). EGCG negatively impacts adipocyte differentiation and lipid accumulation (Gonzalez Suarez *et al*., 2021), as well as their proliferation by inducing cell cycle arrest and apoptosis (Carrasco-Pozo *et al*., 2019; Chan *et al.*, 2011). Studies have linked these results with its capacity to activate the Wnt/β pathway and GSK-3β (Lee *et al.*, 2013), and to downregulate ERK1/2 and CDK2 pathways (Carrasco-Pozo *et al.*, 2019; Hung *et al.*, 2005).

EGCG also inhibits the insulin-mediated activation of the PI3K/AKT signaling pathway (Kim and Sakamoto, 2012), a potent inducer of adipogenesis, while triggering AMPK, C/EBPA and the PPARG suppressor (Hwang *et al.*, 2005). Consequently, there is a reduction in lipid accumulation, adipocyte expansion, and the expression of other adipogenic markers like SREBP-1c (Furuyashiki *et al.*, 2004; Kim *et al.*, 2010; Wu *et al.*, 2017b). Interestingly, the polyphenols also exert anti-obesogenic roles by stimulating energy expenditure. This was observed in an adipocyte murine model both *in vitro* and *in vivo*, where EGCG increased the expression of UCP-2, a crucial protein in mitochondrial membrane transport and thermogenesis (Klaus *et al.*, 2005; Lee et Kim, 2009).

EGCG affects different mechanisms involved in obesity progression and associated comorbidities. Early studies demonstrated that it modulates lipid metabolism by increasing lipid oxidation and lipolysis (Lee et al., 2009), and reducing lipogenic enzyme activity (Carrasco-Pozo *et al.*, 2019; Yeh *et al.*, 2003). Later, it was described that besides interfering with lipid metabolisms, EGCG could also induce lipid droplet degradation (lipophagy) (Kim *et al.*, 2017a). Mechanistically, EGCG reduces intracellular ATP levels via AMPK activation, which serves as an internal stimulus for autophagy and promotes the recognition of lipid droplets by the RAS oncogene family member 7 (RAB7), a pivotal event to trigger lipophagy (Kim *et al.*, 2017a).

1.4 Extracellular vesicle-mediated regulation of carcinogenesis

Extracellular vesicles (EV) are microparticles delimited by a lipid bilayer and secreted by almost all types of cells, participating in cell-to-cell communication (Thery *et al.*, 2018). They transfer nucleic acids (ADN, mRNA and miRNA), proteins and lipids to distant cells. Therefore, EV are involved in the paracrine regulation of several biological processes (Tkach and Thery, 2016). EV is a global term referring to a heterogeneous population of vesicles with different origins, sizes, and biochemical properties, including oncosomes, ectosomes, microvesicles, exosomes and apoptotic bodies (Zheng *et al.*, 2019).

1.4.1 Classification of extracellular vesicles

The lack of consensus about the markers of each EV' specific subsets make their classification difficult. In this regard, the International Society for Extracellular Vesicles (ISEV) guided the minimal characterization each researcher must perform during their studies. In general, EV must be characterized according to their physical characteristics (size and density), biochemical composition and the description of cell

origin and culture conditions. In terms of size, vesicles < 200nm are considered small (exosomes, exomeres), whereas EV > 200nm are considered medium (microvesicles) to large (apoptotic bodies) (Thery *et al.*, 2018).

The biochemical composition refers to the vesicles' lipid and protein structure, reflecting their origin. Most EV emerge from the plasma membrane, except for the exosomes (Zhang *et al.*, 2019b). They are released from the membrane after the fusion of endosomal multivesicular bodies (MVB). Hence, some proteins are expected to be enriched in each EV subsets. In general, at least three positive markers (transmembrane/lipid-bound and cytosolic) must be detected to confirm the presence of a lipid bi-layer with closed membrane vesicles within the isolation fraction. In cases where a pure vesicle population is required, the absence of at least one negative marker (lipoproteins and serum-derived proteins) must be demonstrated (Thery *et al.*, 2018). Table 1. *2* provided examples of proteins found in different EV populations and considered as positive or negative markers.

Table 1. 2. Proposal of different proteins enriched within the EV.
Adapted from MISEV2018 (Raposo and Stoorvogel, 2013; Thery *et al*., 2018).

Positive Markers		**Negative Markers**	**Present in some EV subtype**	
Transmembrane /Lipid-bound (All EV)	Cytosolic (All EV)	Co-isolated contaminant	Subcellular compartments	Soluble factors
• **Non-tissue specific:** - Tetraspanins: CD63, CD81 and CD82. - Integrins: ITGA/B - Complement binding: CD55 and CD59.	• Protein-binding ability - Alix; FLOT1/2, CAV, Tau, ESCRT I/II/III (TSG101 and TSG102)	- APOA1/2, APOB, ALB	<u>Present in larger EV</u> • Mitochondrial: Cytochrome c • Secretory pathway: BIP and CANX • Cytoskeleton: ACTN1/4	• Growth factors and cytokines: - VEGFA, EGF, ILs
• **Cell/tissue-specific:** - CD9 (not present in B, NK and some MSC). - PECAM (endothelial). - EPCAM (epithelial). - ERBB2 (breast cancer).	• Promiscuous incorporation (Optional) - HSP70 and HSP90 - Tubulin and GAPDH		• Nucleus: - Argonaut/RISC complex (AGO) and histones: HIST1H. <u>Present in Exosomes</u> • Endosome: - Rab GTPase, SNARES, annexins	• Adhesion: - FN and collagen

EV (extracellular vesicles), HSP70/90 (heat shock porteins 70/90), NK (natural killer), MSC (mesenchymal stem cells), PECAM (platelet and endothelial cell adhesion molecule), EPCAM (epithelial cell adhesion molecule), ERBB2/HER2 (epithelial growth factor receptor 2), Alix (programmed cell death 6-interacting protein), FLOT1/2 (Flotillin), CAV (Caveolin), ESCRT (endosomal sorting complex required for transport), GAPDH (glyceraldehyde-3-phosphate dehydrogenase), APOA1/2 and APOB (apolipoproteins), ALB (albumin), BIP (binding immunoglobulin protein), CANX (calnexin), ACTN1/4 (actin 1/4), SNARE (soluble N-ethylmaleimide-sensitive-factor attachment protein receptor), VEGFA (vascular epidermal growth factor alpha), EGF (epidermal growth factor), ILs (interleukins) and FN (fibronectin).

Another critical aspect for vesicle characterization is the description of cell origin, culture conditions such as the number of passages, seeding density/confluence, oxygen level, culture system (static or in bioreactor), and if there was a specific surface coating (Thery *et al.*, 2018).

1.4.2 Biogenesis of the different extracellular vesicles

Exosomes is a term for vesicles with a sucrose gradient density of 1.13-1.19 g/mL and a size ranging from 30-150nm in diameter (Zhang *et al.*, 2019b). They originate from late endosomes, also called the MVB (Raposo et Stoorvogel, 2013), which suffered an inward budding of the membranes forming the intraluminal vesicles (ILV). The MVB can later be fused with lysosomes and degraded, or transported and fused with the extracellular membrane to release ILV as exosomes (Zhang *et al.*, 2019b). Studies have revealed the existence of MVB sub-populations according to the cell type. For instance, in B cells, the MVB with high cholesterol levels are those that fuse with the plasmatic membranes and are released as exosomes (Mobius *et al.*, 2002). In other models, the fusion of the MVB with the plasma membrane is stimulated by the ligand-receptor interaction such as the EGF-mediated activation of the epidermal growth factor receptor (EGF-EGFR) (White *et al.*, 2006), and (Chen *et al.*, 2016; Tauro *et al.*, 2013). Moreover, the TP53 signaling pathway has been linked to regulating exosome biogenesis and secretion (Yu *et al.*, 2006).

In the secretion of exosomes, several proteins are involved, starting with the endosomal sorting complex required for transport (ESCRT), which encompasses four members (0-III) and participates in the MVB formation, protein sorting and vesicle budding (Henne *et al.*, 2013; Hurley, 2015). ESCRT-0 serves as a clathrin adaptor, associated with the clathrin-coated domains within the endosomal membrane, where it encounters ESCRT-I. Then cooperatively, ESCRT-I and II sequester ubiquitinated proteins (ex., tetraspanins) to the endosomal membranes, followed by the interaction

of the other complex members. ESCRT-III is responsible for ILV cleavage, a process that requires the energy provided by the ATPase vacuolar protein sorting 4 homolog A (VPS4) (Henne *et al.*, 2013). Also, the programmed cell death 6-interacting protein (ALIX) binds to ESCRT-III, functioning as an alternative branch to coupling other molecules such as Synthenin, which mediates the recruitment of the Syndecan, often present in exosomes (Hurley, 2015). Hence, ALIX participates in the exosomal sorting cargo and its releasing mechanisms (summarized in Figure 1. *7*). This mechanism is shared among other small vesicles and involves the action of the GTPase ADP-ribosylation factor 6 (ARF6) and phospholipase D2 (Ghossoub *et al.*, 2014). Besides, other GTPases participate in the intracellular trafficking of MVB and small vesicles, such as Rab27a/b, Rab11a, Rab35 and SNAREs (Mathieu *et al.*, 2019).

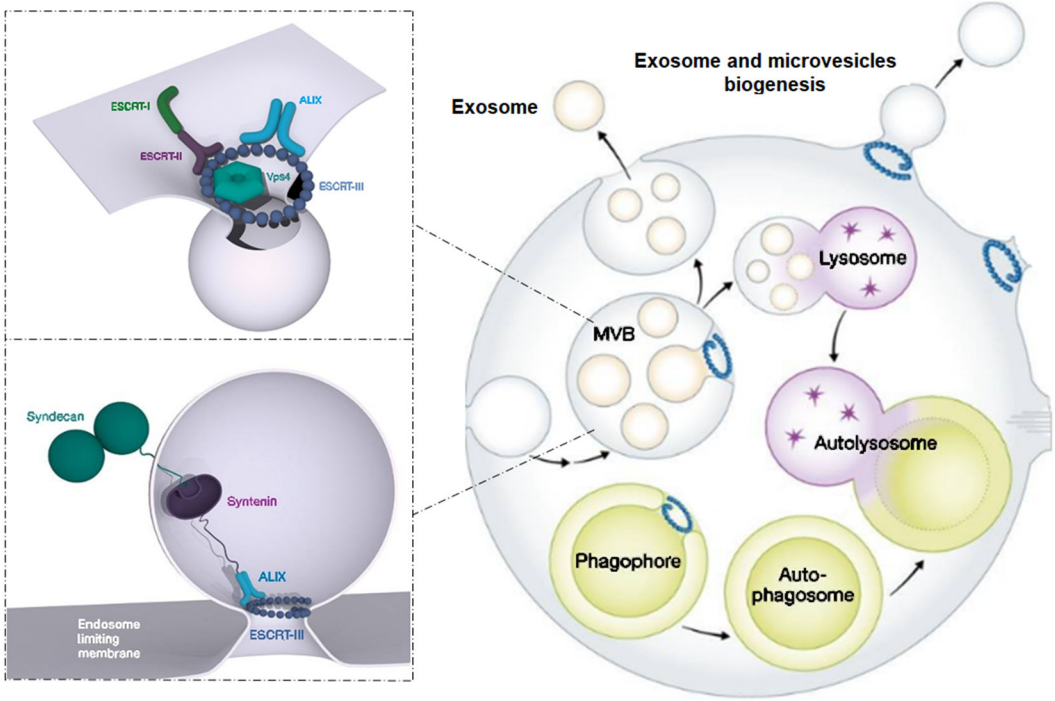

Figure 1. 7. Overview of the ESCRT complexes involved in exosomes budding from the MVB.
Adapted from (Hurley, 2015). ESCRT (endosomal sorting complex required for transport); ALIX (programmed cell death 6-interacting protein); VPS4 (vacuolar protein sorting 4); MVB (multivesicular bodies).

Besides sphingomyelin and ceramides, exosomes are enriched in cholesterol (Raposo and Stoorvogel, 2013). There is also an ESCRT-independent mechanism for the exosome's biogenesis based on raft microdomains causing lateral segregation of sphingomyelinases (SMAse)-enriched microdomains (Castro *et al.*, 2014). This enzyme mediates sphingomyelin hydrolysis generating ceramide, which promotes the budding of the membranes and highlights the role of lipids in this process (Castro et al., 2014). In addition, there is evidence of CD63 participation in the latest mechanism (Edgar *et al.*, 2014).

Since their cargo is intracellular components, exosome biogenesis has been suggested to maintain homeostasis by eliminating intracellular waste (Hessvik and Llorente, 2018). However, only a small portion of the cellular content can be eliminated by exosomes (Hessvik and Llorente, 2018). Meanwhile, they have proven to be key mediators in the paracrine regulation of several biological and cancer-promoting processes (Zhang *et al.*, 2019b; Zheng *et al.*, 2019).

Conversely, microvesicles are a highly heterogeneous population with a size between 100-1000nm and a sucrose gradient density of 1.25-1.30 g/mL (Zhang *et al.*, 2019b). They emerge as a direct outward budding of the plasma membrane in a process that requires the rearrangement of the cytoskeleton and cytosolic Ca^{2+} mobilization (Taylor and Bebawy, 2019). The Ca^{2+} release from the endoplasmatic reticulum to the cytosol involves the participation of channels like transient receptor potential (TRP), inositol triphosphate receptors (IP3R) and ryanodine receptors (RYR). Next, Ca^{2+} mediates the suppression of aminophospholipid translocase (flippase), resulting in a random distribution of phospholipids. Ultimately, this changes the membrane–cytoskeletal anchorage, forming membrane blebs, a structure resolved by the ESCRT machinery (Zheng *et al.*, 2019). Besides, an ADP-ribosylation factor 6 (ARF6)-mediated mechanism for microvesicle release has been reported, where activated phospholipase D caused phospholipids redistribution and ended with the necessary activation of myosin light chain kinase (MLCK). Other shared molecules with exosome biogenesis have been found in this subpopulation, like the ESCRT-I subunit TSG101

and VPS4 (Abels and Breakefield, 2016). They are loaded with proteins, lipids, and all types of nucleic acids, originating from parental cells. There has yet to be a definitive consensus about surface markers to identify this subpopulation, although ARF6 and VCAMP3 have been proposed (Muralidharan-Chari *et al.*, 2009).

Apoptotic bodies originate from apoptotic cells and are characterized by phosphatidylserine and cellular organelles. They have a size of 1–5 μm and a sucrose gradient density from 1.18 to 1.28 g/mL (Thery *et al.*, 2001). Among other characteristics, the oxidation state of surface molecules favours the binding of complement proteins (C3b), mediating recognition and clearance by macrophage (Takizawa *et al.*, 1996). Besides C3b and Annexin V, DNA and histones have been used as specific markers for this population (Zhang *et al.*, 2019b).

1.4.3 Extracellular vesicles in cancer progression

Tumor cells release exosomes and EV, which can trigger phenotypic changes in other cell types present within the tumor microenvironment or at distant places (Hu *et al.*, 2022a). These vesicles are often named oncosomes, or in most studies referred to as exosomes. Studies with EV require a thorough characterization of the vesicle preparation, mainly to discriminate a pure population of exosomes from that of small EV. There is currently a lack of consensus on this point in most papers. Therefore, we will use the term EV in the following sections, to encompass the reports that use both exosomes and EV. In general, EV can fuse with the plasma membrane of the target cells or be internalized through receptor-mediated endocytosis. Then, vesicles can trigger a signalization cascade mediated by receptor activation or the direct release of their molecular content within the cytosol (Raposo and Stoorvogel, 2013). Therefore, EV use several mechanisms to exert their paracrine regulation with a pro-tumoral effect.

For instance, EV originating from tumors can shut down the immune response within the TME, assisting cancer immune evasion. Immune suppressors are among the

proteins detected within tumor-derived EV and are responsible for prompt apoptosis in T and NK cells. Ovarian carcinoma-derived EV, induced FasL–mediated apoptosis of T (CD8+) cells (Taylor *et al.*, 2003). Another inhibitory molecule, PD-1, was found expressed at the surface of BC-released exosomes (Yang *et al.*, 2018). In addition, EV isolated from patients with mesothelioma were TGFB1-loaded and specifically downregulated the expression of killer cell lectin-like receptor K 1 (NKG2D) in the surface of NK cells and T cells (Clayton *et al.*, 2008). The diminishment of this activator receptor provoked the impairment of lymphocyte functionalities (Clayton *et al.*, 2008). More recently, T cell functionality was also abrogated by an immunosuppressive subset of γδT1 cells (CD73+) induced by BC-derived exosomes loaded with the long non-coding RNAs (lncRNAs, SNHG16). Importantly, this regulatory γδT1-subtype within the tumor-infiltrating lymphocytes (TILs) has been associated with poor prognosis in BC patients (Ni *et al.*, 2020).

Tumor-derived EV also mediate the acquisition of pro-tumoral phenotype in different cellular components of the TME. For example, macrophage polarization was induced by BC-derived EV toward a regulatory/immunosuppressive M2 phenotype, characterized by the secretion of the immunoregulatory enzyme Arginase-I and the anti-inflammatory cytokines IL-10 and TGFB (Ahmed et Ismail, 2020). In the murine model, bone marrow-derived macrophages secreted IL-6 due to activating the STAT3 signaling pathway mediated by the BC-EV-derived glycoprotein 130 (gp130) (Ham *et al.*, 2018). The role of the gp130/STAT3 pathway in macrophage polarization was previously documented. This glycoprotein is enriched in exosomes and is stabilized by the tetraspanin CD9 (Shi *et al.*, 2017). During another *in vitro* experiment using human BC-derived EV, macrophage cell lines were activated through toll-like receptor 2 (TLR2)/NF-KB signaling pathway and promoted the secretion of pro-inflammatory molecules such as IL-6, TNFA and CCL2 (Chow *et al.*, 2014).

Tumor-derived EV can also modify adipocytes. It was shown that adipocytes treated with hepatocellular carcinoma-derived EV, were later transferred to tumor-

bearing mice, and stimulated tumor growth, macrophage recruitment and angiogenesis (Wang *et al.*, 2018a). The molecular mechanism by which EV triggered this tumor-promoting capacity in the adipocytes required the activation of the AKT, STAT5A, ERK1/2, NF-KB and GSK-3β pathways, which in turn induced the secretion of the pro-inflammatory cytokines IL-6, IL-8, and CCL2 (Wang *et al.*, 2018a). Furthermore, BC-derived exosomes transferred miRNA-155, mediating metabolic reprogramming of adipocytes and their dedifferentiation into beige/brown. This caused PPARG downregulation, increasing UCP1 levels and augmenting lipolysis (Wu *et al.*, 2018).

Besides activating several pathways within the target cells, EV can also transfer oncoproteins, promoting metastasis and conditioning the pre-metastatic niche. The latter is mediated by tumor-educated bone marrow-derived cells (Kaplan *et al.*, 2005). Patients with advanced Stage IV melanoma were reported to have circulating exosomes with a specific signature, encompassing the tyrosinase-related protein-2 (TYRP2) and the MET oncoprotein. In an *in vitro* study, the researchers showed that bone marrow-derived cells treated with exosomes-enriched MET had high expression of the oncoprotein and enhanced cell mobilization. More importantly, the MET-exosomal transferring seems to mediate the metastatic capacity of bone marrow-derived cells (Peinado *et al.*, 2012).

On the other hand, the EV derived from cells within the TME influence the tumor cells, promoting cancer development. For instance, adipocytes-derived EV induced mitochondrial activity and migration by transferring lipids (lysophosphatidylcholine, sphingomyelin and cholesterol), proteins and substrates involved in fatty acid oxidation to melanoma cancer cells (Clement *et al.*, 2020; Lazar *et al.*, 2016). Additionally, EV can efficiently transfer all types of RNAs to a host cell including lncRNAs and miRNA, regulating the expression of genes involved in diverse biological processes (Statello *et al.*, 2021). It has been documented that TAMs-secreted EV promoted BC progression through several mechanisms, including cancer aerobic glycolysis and tumor invasion (Chen *et al.*, 2019; Yang *et al.*, 2011). TAMs release-EV loaded with HISLA, a HIF-1A-stabilizing lncRNA. This molecule participates in glucose metabolism, increasing

the occurrence of aerobic glycolysis within the tumoral cells and contributing to chemoresistance in patients with BC (Chen *et al.*, 2019). Besides, IL-4 positive TAMs-derived EV promoted the invasiveness of BC cell lines by transferring miR-223 to the cancer cells, which ultimately caused β-catenin nuclear accumulation (Yang *et al.*, 2011).

BC cells acquired a more aggressive phenotype after going through the EMT transition caused by CAF-derived exosomes carrying the Wnt10b protein and activating the canonical Wnt pathway (Chen *et al.*, 2017). Moreover, in samples from human ovarian cancer, CAF-EV were enriched in the TGFB1 cytokine, enhancing migration and metastasis in a BC cell line panel (Li *et al.*, 2017). On the other hand, exosomes isolated from *in vitro* differentiated adipocytes also promoted a BC cell line proliferation and migration capacity. In this case, the exosomes effect was mediated by activating the Hippo signaling pathway within the cancer cell line, inducing proliferation, and conferring resistance to apoptosis (Wang *et al.*, 2019a).

Studies have revealed that transferring oncogenic proteins and RNA by the EV mediates drug resistance. This interchange can happen between resistant and sensitive cells or non-tumorigenic cells (Ozawa *et al.*, 2018). In BC, it has been reported that miR-100, miR-221/222 and miR-30a are among the chemoresistance-mediated RNAs transferred by EV (Pan *et al.*, 2020; Wei *et al.*, 2014). In addition, some exosome-derived miRNAs such as miR-155 (Santos *et al.*, 2018), miRNA-9-5p, miRNA-195-5p, and miRNA-203a-3p (Shen *et al.*, 2019), have been demonstrated to induce resistance by triggering the acquisition of cancer stem cell phenotypes. Recently, studies have documented the involvement of lncRNA in the exosome-mediated transfer of resistance in several cancer models (Wang *et al.*, 2021a). The protein content within the tumor-derived EV has also been documented to mediate drug resistance. For example, a transmembrane glycoprotein (P-gp) responsible for drug substrate efflux was observed to be exosome-transferred from resistant to sensitive BC cell lines, supporting cell survival by keeping drugs at a sublethal concentration (Lv *et al.*, 2014). In another study, the researchers found an increase in the glutathione S-transferase P1

(GSTP1)- containing EV in the serum of BC patients with progressive disease, after an anthracycline/taxane-based neoadjuvant chemotherapy treatment. Concluding that the presence of this detoxifying metabolic enzyme within the EV was associated with chemoresistance (Yang *et al.*, 2017). Remarkably, therapeutic-induced senescent cells are associated with the formation of stem cell niches during metastases. These cells have been shown to secrete more EV than non-senescent cells containing a high expression of P-gp and other critical proteins involved in ATP depletion and proliferation, among others (Kavanagh *et al.*, 2017). Collectively, EV serve as messengers for a tumor cell to transform their surroundings into a suitable environment for their progression, with a broad spectrum of mechanisms of action.

1.4.4 Low oxygen levels impact the extracellular vesicle cargo

Hypoxia is present within extended areas of adipose tissue as well as in the tumor mass. Hence, cells undergo metabolic rearrangement to survive a low oxygen tension environment, affecting the material released in the EV (Kucharzewska *et al.*, 2013). Increased levels of HIF (both intracellular and within the secreted vesicles), is one of the first responses to hypoxic conditions. This family of three isoforms (HIF-1A/2A/4A) regulates tissue remodelling, glucose metabolism, proliferation, and angiogenesis (Finger et Giaccia, 2010). It has been reported that during hypoxia, HIF-1A is stabilized and activates the overexpression of c-Met protein (Pennacchietti *et al.*, 2003), Wnt/beta-catenin signaling (Jiang *et al.*, 2007), and the secretion of VEGF, angiopoietin 2 (Ang-2), and platelet-derived growth factor (PDGF) (Finger et Giaccia, 2010; Ruan *et al.*, 2009). Hypoxic tumors have a more aggressive phenotype since these factors promote cell proliferation, EMT-mediated invasion and angiogenesis.

In BC models, hypoxia-induced HIF-1A-mediated release of EV with high expression of miR-210 (King *et al.*, 2012). The latter is a HIF-1A inducible miRNA linked to neovascularization (Jung *et al.*, 2017) and DNA repair regulation (Fasanaro *et al.*, 2008). Also, lncRNA SNHG1 is enriched in hypoxic BC-derived EV, which

promotes tumor angiogenesis by activating the proliferation and migration of human umbilical vein endothelial cells (HUVECs), and by extending the proliferative phenotype in BC through the miR-216b-5p/JAK2 axis (Dai *et al.*, 2022). Remarkably, BC-derived EV mediates T-cell suppression via delivering TGFB during hypoxic culture conditions (Rong *et al.*, 2016).

EV's capacity to promote aggressiveness has been extensively associated with hypoxic conditions (Jiang *et al.*, 2022), and the research on this topic has been extended to various tumor localizations. EV isolated from hypoxic prostate cancer cells compared with controls, were shown to be loaded with MMP-2 and MMP-9 proteins, as well as cytokines like TGFB2, TNF-1A and IL-6 (Ramteke *et al.*, 2015). Likewise, patients with glioblastoma multiforme showed enrichment of other hypoxia-regulated factors at the protein and mRNA levels, such as IL-8, adrenomedullin (ADM), lysyl oxidase (LOX), caveolin 1, plasminogen activator inhibitor 1 (PAI1), *N*-myelocytomatosis viral related oncogene (myc) downstream regulated 1 (NDRG1) and IGF binding protein 1 and 3(IGFPB1/3), all involved in proliferation, angiogenesis and migration (Kucharzewska *et al.*, 2013). In the *in vitro* setting, most of the hypoxia-upregulated proteins within the EV mirrored the content of their donor cells, and cytokines like IL-1Bwere not detected in the vesicles, suggesting specific sorting mechanisms of the EVs' load (Kucharzewska *et al.*, 2013). Intriguingly, the study did not detect HIF-1A within the EV. Nevertheless, in a nasopharyngeal carcinoma model, the presence of transcriptionally active HIF-1A was detected in the EV, and upon delivery, changed the expression of the EMT-associated markers E and N cadherins in the targeted cells (Aga *et al.*, 2014).

Other cells present within the hypoxic TME can contribute to the progression of the disease. Hypoxic MSC secreted EV packaged with miR-21-5p. This miRNA promotes cancer cell survival by inhibiting the expression of the anti-apoptotic PTEN and programmed cell death 4 (*PDCD4*) protein and increasing tumor chemoresistance by polarizing macrophages toward the M2 phenotype (Ren *et al.*, 2019).This. EV

released by hypoxic human breast CAF were loaded with the autophagy-associated G protein-coupled receptor 64 (GPR64) protein. Upon incubation with BC cell lines, this mediator activated the non-canonical NF-KB pathway, upregulating the expression of MMP-9 and IL-8 and augmenting their invasive capacity (Xi *et al.*, 2021). In contrast, EV released by NK cell culture under low oxygen levels proved to be more cytotoxic due to the high expression of granzyme B, perforin and FasL (Jiang *et al.*, 2021).

1.4.5 Impact of EGCG on the extracellular vesicles' cargo and paracrine regulation

The direct effect of EGCG on cell metabolisms, signaling pathways and gene expression has been extensively studied (Romano and Martel, 2021). However, few studies have documented how the polyphenol might affect what cells secret within their microvesicles and, consequently, their paracrine regulation. In this direction, the focus has been on the modulation of the miRNAs sorting also referred to as exomiR (Table 1. *3*) and regulates gene expression through mRNA binding (Saliminejad *et al.*, 2019). When the 4T1 murine BC cells were treated with EGCG, both cells and secreted vesicles showed an upregulation of miR-16, among others. Nevertheless, the miR-16 transferred by the EV inhibited *in vivo* tumor growth by preventing TAM infiltration and M2 polarization via NF-KB pathway suppression (Jang *et al.*, 2013). This miRNA is often downregulated in human breast cancer cells (Thu *et al.*, 2021), where it acts as a tumor suppressor by targeting genes involved in the cell cycle and apoptosis (Liu *et al.*, 2008). This shows how BC can promote macrophage infiltration and polarization towards the TAM phenotype, which is related to a worse clinical outcome for the patient.

Studies associated with other pathologies have demonstrated the potential of the polyphenol to affect cell-cell communication via EV delivery. For instance, the anti-fibrotic effect of EGCG in a pulmonary fibrosis model was mediated by augmenting the expression levels of miR-6757-3p within the EV secreted from endothelial cells (Murata *et al.*, 2023). This miRNA has been proposed to target TGFB receptor 1 (TGF-

BR1) and to downregulate fibrosis-related genes such as fibronectin α-SMA (Murata, M. 2023). In an ischemia model, vesicles derived from EGCG-treated cardiomyocytes were enriched in miR30a, which reduced the autophagy and apoptotic levels, once transferred to cells during a myocardial infarction (Zhang *et al.*, 2020). Accordingly, the EGCG's potential capacity to ameliorate the damage during coronary artery embolization was mediated by the induction of miR30a (Zhang *et al.*, 2020). Table 1. 3 summarizes the mRNAs modified in the EV upon EGCG treatment of the cells.

Another mechanism, by which EGCG improves myocardial recovery after an infarction, was linked to its action over procoagulant platelets. The EV released by these pro-coagulant platelets are enriched in phosphatidylserine, which upon fusing other platelets, propagate this phenotype and contribute to coagulation and thrombosis. Then, EGCG didn't affect phosphatidylserine serine exposure but rather reduced the number of released EV from pro-coagulant platelets (Millington-Burgess and Harper, 2021). Similar results were obtained during proteomic profiling of EV secreted by intestinal-like cells, in which EGCG reduced both the number and size of the vesicles. Additionally, the EGCG altered the repertoire of enriched proteins within the EV, toward proteins involved in maintaining skin homeostasis, instead of those involved in cell proliferation and immune response, as observed in the control cells (Yano *et al.*, 2022).

Whether the effect of EGCG over EV sorting is specific or is a consequence of the overall modification in cell activation status and gene expression remains an open question. Many factors influence the outcome of what cells are secreted, and it is model-dependent. Some research supports the observation that vesicles reflect the content of their parental cells, while others do not. Interestingly, a study performed in macrophages demonstrated that EGCG could be internalized into cytoplasmic vesicles, triggering an oxidative reaction and causing the selective aggregation and degradation of HMGB1 (Li *et al.*, 2011a), suggesting that some proteins can be targeted intracellularly by the catechin affecting their release as well.

Table 1. 3. Reported miRNAs (miR) modulated by EGCG in the EV.

miRNA	Status	Model	Reference
let-7, miR-16, miR-18b, miR-20a, miR-25, miR-92, miR-93, miR-221, and miR-320	Up (EV and Cells)	BC-Macrophage (Murine)	(Jang *et al.*, 2013)
miR-10a, miR-18a, miR-19a, miR-26b, miR-29b, miR-34b, miR-98, miR-129, miR-181d	Down (EV and Cells)		
miR-6757-3p, miR-1298-5p, miR-3666, miR-4501, miR-6866-3p, miR-562, miR-8055, miR-4690-3p, miR-657, miR-610, miR-4737, miR-509-3-5p, miR-628-3p, miR-550b-2-5p, miR-494-5p, miR-4470, miR-3612, miR-1233-3p, miR-4290, miR-5584-3p, miR-6728-3p, miR-4529-5p 2.02 0.001	Up (EV)	Pulmonary Fibrosis	(Murata *et al.*, 2023)
miR-449b-5p, miR-4710, miR-6801-3p, miR-6827-5p.	Down (EV)		
miR30a	UP (EV and Cells)	Acute myocardial infarction	(Zhang *et al.*, 2020)

miR: micro RNA, EV: extracelular vesicles, BC: breast cancer

RESEARCH PROBLEMATIC, HYPOTHESIS AND OBJECTIVES

Obesity is a condition with a high incidence worldwide. A chronic low inflammation grade is one of the principal characteristics that conditions the development of several comorbidities such as heart disease and cancer (Himbert *et al.*, 2017). The adipose tissue has been acknowledged as an endocrine organ essential in regulating insulin sensitivity and immunological responses (Gregoire, 2001). The presence of hypoxia in extended areas of the adipose tissue promotes and sustains inflammation by recruiting macrophages, which contribute to a pro-angiogenic environment (Nieman *et al.*, 2013). During obesity, the adipocytes' hypertrophy causes a dysfunctional secretory profile toward an inflammatory phenotype. CCL2/MCP-1, TNFA, IL-6, IL-8, PAI-1 and leptin are among the cytokines responsible for triggering the infiltration of lymphocytes, stromal cells and macrophages, altering the tissue microenvironment (Nieman *et al.*, 2013). Hence, the obesogenic condition appears to favor the emergence and development of cancers including breast and endometrial, especially in postmenopausal women (Bjune *et al.*, 2022).

How cancer cells reshape adipocytes is not fully understood. The presence of adipocytes and tumor-reshaped adipocytes (CAA) within the invasive front of breast cancer biopsies has been reported (Duong *et al*., 2017; Nieman *et al*., 2013). Cancer cells can activate lipolysis in the adipocytes by secretion of lipolytic signals like catecholamines, proinflammatory cytokines and adrenomedullin. Then, released FFA can be delivered into the cancer cells by adipose-derived EV, promoting tumor proliferation and migration (Attane and Muller, 2020). Notably, the BC tumor microenvironment is rich in adipose tissue, thereby, it is an excellent model for understanding the molecular intermediates involved in the crosstalk between cancer cells and adipocytes.

Epidemiological studies suggest that consuming a polyphenol-rich diet reduces the incidence of some obesity-related cancers. EGCG, the main catechin in green tea, targets signaling pathways associated with cell survival, proliferation, differentiation,

migration, angiogenesis, hormone activities, detoxification enzymes and immune responses (Bae *et al.*, 2019; Zhou *et al.*, 2016). Besides, EGCG reduces adipocyte markers' expression (PPARG and C/EBPA), proliferation and lipid accumulation (Gonzalez Suarez *et al.*, 2021; Lin *et al.*, 2005). Whether this diet-derived polyphenol can alter the adipocyte secretome profile remains to be addressed.

Considering these facts, we aim to identify the molecular mechanisms involved in the adipocyte paracrine regulation of cancer cells' invasive phenotype and how efficient diet-derived intervention may alter such a phenomenon. To model the interaction between adipose tissue and breast cancer cells, human adipocyte-derived mesenchymal stem cells (h-ADMSC) were used and differentiated into mature adipocytes. As for the tumor cell line, we used MDA-MB-231, a highly aggressive subtype model of TNBC. This is a hard-to-treat subtype because of a lack of recognized targets for molecular-oriented therapy, where little therapeutic progress has been made during the past decades. Thus, new approaches and strategies need to be addressed to prevent the onset of TNBC.

Hypothesis: EGCG alters adipocyte differentiation and signaling pathways involved in the crosstalk between adipocytes and tumor cells.

Objectives:

1) To evaluate the inhibitory capacity of EGCG on adipose-derived mesenchymal stem cell differentiation into adipocytes and the impact on the secretome profile and paracrine regulation of the TNBC invasive phenotype.
2) To characterize the acquisition of a CAA-like phenotype in h-ADMSC and chemotaxis in response to the TNBC-derived secretome.
3) To evaluate the chemopreventive impact of EGCG intervention against acquiring a CAA-like phenotype in the h-ADMSC.
4) To characterize how EGCG alters the TNBC derived-EV cargo and their paracrine regulation over the h-ADMSC.

CHAPTER II

ARTICLE 1

EGCG INHIBITS ADIPOSE-DERIVED MESENCHYMAL STEM CELLS DIFFERENTIATION INTO ADIPOCYTES AND PREVENTS A STAT3-MEDIATED PARACRINE ONCOGENIC CONTROL OF TRIPLE-NEGATIVE BREAST CANCER CELL INVASIVE PHENOTYPE

Narjara Gonzalez Suarez, Sahily Rodriguez Torres, Amira Ouanouki, Layal El Cheikh-Hussein and Borhane Annabi.

Laboratoire d'Oncologie Moléculaire, Département de Chimie, Centre de Recherche CERMO-FC, Université du Québec à Montréal, QC H3C 3P8, Canada.

Manuscript published in Molecules **2021**, 26, 1506.
https://doi.org/10.3390/molecules26061506.

Authors contributions:

Narjara Gonzalez Suarez and *Borhane Annabi*: Designed the experiments of this study and wrote the manuscript.

Narjara Gonzalez Suarez, Sahily Rodriguez Torres, Amira Ouanouki and *Layal El Cheikh-Hussein*: Conducted the experiments, data analysis, and critical discussions of the results.

Borhane Annabi: Provided the financial support.

All authors have read and agreed to the published version of the manuscript.

2.1 Résumé

Les personnes obèses ont un risque accru de développer un cancer du sein triple négatif (TNBC), en partie associé à l'état d'inflammation chronique. De plus, les données épidémiologiques indiquent qu'une consommation accrue de fruits et légumes riches en polyphénols joue un rôle clé dans la réduction de l'incidence de certains types de cancer. Ici, nous avons testé si l'épigallocatéchine-3-gallate (EGCG) dérivée du thé vert pouvait inhiber la différenciation des cellules souches mésenchymateuses adipocytaire en adipocytes, et comment cela impactait le profil du sécrétome et la régulation paracrine du phénotype invasif TNBC. Dans cette étude, les cellules souches mésenchymateuses ont été différenciées en adipocytes, et le milieu conditionné (CM) des préadipocytes et des adipocytes matures a été récolté pour des études de migration et de vasculogenèse. La migration en temps réel des cellules de la lignée MDA-MB-231 dérivée d'un TNBC humain a été réalisée à l'aide du système exCELLigence. Des micropuces d'ADN et la RT-qPCR ont été utilisées pour évaluer les niveaux d'expression géniques. L'immunobuvardage a été utilisé pour évaluer l'expression des protéines et leur statut de phosphorylation. Le mimétisme vasculogénique (VM) *in vitro* a été évalué sur Matrigel. Nos résultats montrent que l'EGCG inhibe l'induction de biomarqueurs adipogéniques clés, notamment la lipoprotéine lipase, l'adiponectine, la leptine, la synthase d'acide gras FABP4. Une augmentation de la chimiotaxie des cellules MDA-MB-231 et du VM ont été observés en réponse au sécrétome des adipocytes matures. Ceci est corrélé à l'augmentation de l'état de phosphorylation de STAT3. Ce phénotype invasif a été inhibé par l'EGCG, les inhibiteurs de JAK/STAT Tofacitinib et AG490, ainsi que par répression génique de STAT3. En conclusion, les catéchines alimentaires pourraient prévenir l'apparition d'un environnement obésogène qui favorise le développement de TNBC en partie à cause de l'inhibition de l'adipogenèse et la modulation du profil du sécrétome des adipocytes.

2.2 Abstract

Obese subjects have an increased risk of developing triple-negative breast cancer (TNBC), in part associated with the chronic low-grade inflammation state. On the other hand, epidemiological data indicates that increased consumption of polyphenol-rich fruits and vegetables plays a key role in reducing incidence of some cancer types. Here, we tested whether green tea-derived epigallocatechin-3-gallate (EGCG) could alter adipose-derived mesenchymal stem cell differentiation into adipocytes, and how this impacts the secretome profile and paracrine regulation of the TNBC invasive phenotype. Here, cell differentiation was performed and conditioned media (CM) from preadipocytes and mature adipocytes harvested. Human TNBC-derived MDA-MB-231 real-time cell migration was performed using the exCELLigence system. Differential gene arrays and RT-qPCR were used to assess gene expression levels. Western blotting was used to assess protein expression and phosphorylation status levels. *In vitro* vasculogenic mimicry (VM) was assessed with Matrigel. EGCG was found to inhibit the induction of key adipogenic biomarkers, including lipoprotein lipase, adiponectin, leptin, fatty acid synthase, and fatty acid binding protein 4. Increased TNBC-derived MDA-MB-231 cell chemotaxis and vasculogenic mimicry were observed in response to mature adipocytes' secretome, and this was correlated with increased STAT3 phosphorylation status. This invasive phenotype was prevented by EGCG, the JAK/STAT inhibitors Tofacitinib and AG490, as well as upon STAT3 gene silencing. In conclusion, dietary catechin-mediated interventions could, in part through the inhibition of adipogenesis and modulation of adipocytes' secretome profile, prevent the onset of an obesogenic environment that favors TNBC development.

2.3 Introduction

Adipogenesis, as defined by the formation of adipocytes from stem cells (Dagpo *et al.*, 2020), and the adipose tissue itself have drawn much attention at the onset of chronic inflammation in metabolic diseases, such as type 2 diabetes mellitus, cardiovascular diseases, and in several types of cancer (Heyn *et al.*, 2020; Himbert *et al.*, 2017). Among the processes involved in the setting of these diseases, the adipose tissue secretome has been inferred to play a crucial paracrine regulatory role in brain cancer (Onzi *et al.*, 2019), prostate cancer (Sacca *et al.*, 2019), bladder cancer (Maj *et al.*, 2018), breast cancer (Chu *et al.*, 2019), and colon cancer (Riondino *et al.*, 2014). Molecular links between central obesity and breast cancer have also been inferred to trigger oncogenic signaling pathways, including NF-KB, JAK, STAT3, and AKT (Zimta *et al.*, 2019).

The adipose tissue functions as an endocrine organ that, in obese people, produces a high level of tumor-promoting hormones such as leptin and estrogen, and a low level of the tumor suppressor hormone, adiponectin (Jasinski-Bergner et Kielstein, 2019). In particular, adipose tissues from tumor-bearing breasts have shown a distinct molecular signature and physiological status from those of tumor-free breasts (Miran *et al.*, 2020). Furthermore, several adipose tissue-derived miRNAs were associated with adipocyte differentiation and identified with essential roles in obesity-associated inflammation, insulin resistance, and tumor microenvironment (Heyn *et al.*, 2020). The efficacy of currently approved drug therapies and understanding of drug mechanisms against obesity remain open for debate (Williams *et al.*, 2020), diet-derived phytochemicals have emerged as potential candidates to combat obesity via adipose non-shivering thermogenesis (Li *et al.*, 2019b), or targeting of the adipose tissue inflammation (Li *et al.*, 2020b; Sudhakaran and Doseff, 2020).

Epidemiological data indicate that increased consumption of fruits and vegetables plays a key role in reducing the incidence of some cancers (Fund., 2007). These foods contain a significant number of polyphenols, which are potential agents that reduce obesity in part through reducing the amount of adipose tissue by stimulating lipolysis

(Andersen *et al.*, 2010). It has been reported that in pre-adipocyte murine models of differentiation, epigallocatechin-3-gallate (EGCG), which is the main compound in green tea, reduced adipocyte proliferation, lipid accumulation and expression of peroxisome proliferator-activated receptor gamma (PPARG) and CCAAT/enhancer-binding protein alpha (C/EBPA) in mature adipocytes (Lin *et al.*, 2005). Whether diet-mediated polyphenols can consequently alter the secretome profile of adipocytes, and how secretome-mediated paracrine regulation of cancer cells' invasive phenotype occurs, remains to be better addressed.

Therefore, the present study aims at exploring the molecular mechanisms involved in the adipocyte paracrine regulation of cancer cells' invasive characteristics, and how efficient diet-derived intervention may prevent such regulation. It was found that the secretome of differentiated adipocytes specifically triggered migration in several TNBC-derived cells, but not the migration of the ovarian or colon cancer cells tested. Chronic exposure of adipose-derived mesenchymal stem cells (ADMSC) to EGCG during their differentiation into mature adipocytes effectively altered adipogenesis and the secretome profile of differentiated adipocytes as TNBC-derived cell chemotaxis and vasculogenic mimicry were inhibited. Finally, adipocyte secretome-mediated paracrine regulation of TNBC-derived cells' invasive phenotype required STAT3 oncogenic signaling, and EGCG was able to acutely inhibit STAT3 phosphorylation.

2.4 Materials and methods

2.4.1 Materials

Sodium dodecylsulfate (SDS), epigallocatechin-3-gallate (EGCG), Tofacitinib, AG490, and bovine serum albumin (BSA) were purchased from Sigma-Aldrich Canada (Oakville, ON). Electrophoresis reagents were purchased from Bio-Rad (Mississauga, ON, Canada). The enhanced chemiluminescence (ECL) reagents were from Amersham Pharmacia Biotech (Baie d'Urfé, QC, Canada). Micro bicinchoninic acid protein assay reagents were purchased from Pierce (Rockford, IL, USA). The polyclonal antibodies against Fibronectin, Tubulin, AKT, phosphorylated AKT, STAT3 and phosphorylated STAT3 were obtained from Cell Signaling Technology Inc. (Danvers, MA, USA). Horseradish peroxidase-conjugated donkey anti-rabbit and anti-mouse IgG secondary antibodies were obtained from Jackson ImmunoResearch Laboratories (West Grove, PA, USA).

2.4.2 Cell Culture

Human serous carcinoma-derived ES-2 ovarian cancer cells, HT-29 colon adenocarcinoma, and triple-negative breast cancer cell lines, including MDA-MB-231, MDA-MB-468, MDA-MB-157, BT-20 and HCC-70, were all purchased from the American Type Culture Collection (ATCC). BT-20, ES-2 and HT-29 cells were grown as monolayers in McCoy's 5a Modified Medium (Wisent, 317-010-CL) containing 10% fetal bovine serum (Life Technologies, 12483-020), 100 U/mL penicillin and 100 mg/mL streptomycin (Wisent, 450-202-EL). MDA-MB-231, MDA-MB-157 and MDA-MB-468 breast cancer cell lines were grown in DMEM Medium (Wisent, 319-005-CL) supplemented with 10% of fetal bovine serum, while HCC-70 cells were cultured in RPMI (Wisent, 350-007-CL). All cells were cultured at 37 °C under a humidified 95%–5% (*v*/*v*) mixture of air and CO_2.

2.4.3 Adipose-Derived Mesenchymal Stem Cell Differentiation

Adipose-derived mesenchymal stem cells (ADMSC; ATCC, PCS-500-011) were grown using the Mesenchymal Stem Cell Basal Medium (ATCC, PCS-500-030), and supplemented with Mesenchymal Stem Cell Growth Kit for adipocyte differentiation-Low Serum (ATCC, PCS-500-040). When cells reached 70–80% confluency, they were seeded at a density of 18,000 cells/cm^2 and differentiated into mature adipocytes with Adipocyte Differentiation Toolkit (ATCC, PCS-500-050) following the manufacturer's instructions. Briefly, cells were incubated at 37 °C with 5% CO_2 for 48 h before initiating adipocyte differentiation. Then, the media was removed, and cell monolayers rinsed with room temperature PBS (ATCC, 302200). Next, 2 mL (for 6-well plates) of pre-warmed (37°C) adipocyte differentiation/initiation medium was added to each well to initiate adipocyte differentiation. After a 48-h incubation, half the volume of media was removed, and the previous steps repeated for another 48 h. Later, the maintenance phase was initiated by carefully removing 2 mL of media from each well (leaving 1 mL) and replacing it with 2 mL of pre-warmed adipocyte differentiation/maintenance medium in each well. The latter step was repeated every 3–4 days for another 11 days until adipocytes reached full maturity (~12–15 days). Conditioned media (CM) was collected at different time points.

2.4.4 Oil Red O Staining

In order to assess adipocyte maturation status and to visualize the lipid droplet formation, medium was removed, and cells were incubated with 10% formalin at room temperature for 5 min, then fresh formalin was added, and cells were stored at 4°C in the dark, for up to 2 days. The wells were next washed with 60% isopropanol and left to dry. Oil Red O (0.5 g/100 isopropanol stock solution; Sigma-Aldrich) was added and left for 10 min. Wells were finally washed with water four times and pictures taken.

2.4.5 Total RNA Isolation, cDNA Synthesis and Real-Time Quantitative PCR

Total RNA was extracted from cell monolayers using TriZol reagent (Life Technologies, Gaithersburg, MD, USA). For cDNA synthesis, two μg of total RNA were reverse-transcribed using a high capacity cDNA reverse transcription kit (Applied Biosystems, Foster City, CA, USA). cDNA was stored at -80°C prior to PCR. Gene expression was quantified by real-time quantitative PCR using iQ SYBR Green Supermix (Bio-Rad, Hercules, CA, USA). DNA amplification was carried out using an Icycler iQ5 (Bio-Rad, Hercules, CA, USA) and product detection was performed by measuring binding of the fluorescent dye SYBR Green I to double-stranded DNA.

2.4.6. Human Adipogenesis and Inflammation PCR Arrays

The Human Adipogenesis RT^2 Profiler PCR Array (PAHS-049Z) and the Human Cancer Inflammation & Immunity Crosstalk RT^2 Profiler™ PCR Array (PAHS-181Z) were used according to the manufacturer's protocol (QIAGEN). The detailed list of the key genes assessed can be found on the manufacturer's website (https://geneglobe.qiagen.com/us/product-groups/rt2-profiler-pcr-arrays) (accessed on 13 February 2021). Using real-time quantitative PCR, we reliably analyzed expression of a focused panel of genes related to adipogenesis and PPARG targets, or to inflammatory cytokines/receptors. Relative gene expressions were calculated using the $2^{-\Delta\Delta C_T}$ method, in which C_T indicates the fractional cycle number where the fluorescent signal reaches detection threshold. The "delta–delta" method uses the normalized ΔC_T value of each sample, calculated using a total of five endogenous control genes (*B2M*, *HPRT1*, *RPL13A*, *GAPDH,* and *ACTB*). Fold change values are then presented as average fold change = 2(average $^{\Delta\Delta C_T}$) for genes in differentiated adipocytes relative to pre-adipocytes. Detectable PCR products were obtained and defined as requiring <35 cycles. The resulting raw data were then analyzed using the PCR Array Data Analysis Template (http://www.sabiosciences.com/pcrarraydataanalysis.php) (accessed on 1

February 2021). This integrated web-based software package automatically performs all $\Delta\Delta C_T$-based fold-change calculations from the uploaded raw threshold cycle data.

2.4.7 Western Blotting

TNBC-derived MDA-MB-231 cells were lysed in a buffer containing 1 mM each of NaF and Na_3VO_4, and proteins (30 μg) were separated by SDS-polyacrylamide gel electrophoresis (PAGE). After electrophoresis, proteins were electro-transferred to polyvinylidene difluoride membranes, which were then blocked for 1 h at room temperature with 5% nonfat dry milk in Tris-buffered saline (150 mM NaCl, 20 mM Tris-HCl, pH 7.5) containing 0.3% Tween-20 (TBST; Bioshop, TWN510-500). Membranes were further washed in TBST and incubated with the appropriate primary antibodies (1/1000 dilution) in TBST containing 3% BSA and 0.1% sodium azide (Sigma-Aldrich), followed by a 1 h incubation with horseradish peroxidase-conjugated donkey anti-rabbit or anti-mouse IgG at 1/2500 dilutions in TBST containing 5% nonfat dry milk. Immunoreactive material was visualized by ECL.

2.4.8 Chemotactic Cell Migration Assay

Cell migration assays were carried out using the Real-Time Cell Analyzer (RTCA) Dual-Plate (DP) Instrument of the xCELLigence system (Roche Diagnostics). Adherent cell monolayers were trypsinized and seeded (30,000 cells/well) onto CIM-Plates 16 (Roche Diagnostics). These migration plates are similar to conventional Transwells (8 μm pore size) but have gold electrode arrays on the bottom side of the membrane to provide real-time measurement of cell migration. Prior to cell seeding, the underside of the wells from the upper chamber were coated with 25 μL of 0.15% gelatin in PBS and incubated for 1 h at 37°C. Chemotaxis was monitored for 8 h using as chemoattractant either media conditioned from serum-starved ADMSC (Preadipo-CM) or from mature adipocytes (Adipo-CM), in the presence or not of EGCG,

Tofacitinib, or AG490. The impedance values were measured by the RTCA DP Instrument software and were expressed in arbitrary units as Normalized Cell Migration Index. Each experiment was performed three times in duplicate.

2.4.9 Wound-Healing Assay

MDA-MB-231 cells were seeded into 6-well tissue culture dishes and grown to nearly confluent cell monolayers. Then, a linear wound was generated in the monolayer with a sterile 200 μL pipette tip creating a cell-free area (Francisco Fernandez *et al.*, 2019). Cultures were gently washed with the growth medium to remove loose cells. The cells were then treated with either Preadipo-CM or Adipo-CM. Immediately after the scratch and at 2, 4, and 8 h, at least four images of the scraped area were captured using phase contrast microscopy and analyzed using NIH ImageJ software (Suarez-Arnedo *et al.*, 2020). Two independent experiments were performed, using three wells for each stimulating condition. The same scratched area was selected for the measurements at each time of the study.

2.4.10 *In Vitro* Vasculogenic Mimicry Assay

In vitro vasculogenic mimicry (VM) of human TNBC-derived MDA-MB-231 cells were assessed by Matrigel tube formation as previously described (Sicard *et al.*, 2021). In brief, each well of a 96-well plate was pre-coated with 50 μL of Matrigel. After gel solidification, MDA-MB-231 cell suspension in culture media (5×10^4 cells/200 μL) was seeded into the wells. Either serum-deprived basal media (unstimulated condition), or stimulation with Preadipo-CM or Adipo-CM (stimulated conditions) were performed. Acute additions of EGCG, Tofacitinib, or AG490 (all at 30 μM) were done in the presence of Adipo-CM to the cell culture and incubated at 37°C in a CO_2 incubator. Pictures were taken overtime using a digital camera attached to a phase-contrast inverted microscope. Images were then placed in bins and subjected

to the “Skeletonize” function of ImageJ software. The corresponding loop area, loop perimeter, branching, and tube elongation parameters were measured using the 2D/3D skeleton PlugIn (Arganda-Carreras *et al.*, 2010) for the NIH ImageJ software (Abramoff, 2004).

2.4.11 Statistical Data Analysis

Unless otherwise stated, data and error bars were expressed as means ± SEM of three or more independent experiments. Statistical analysis of data was performed by Kruskal–Wallis with DunnTukey’s post-test to establish differences among groups or Mann–Whitney for two groups’ comparison. Probability values of less than 0.05 were considered significant and an asterisk identifies such significance in the figures. GraphPad Prism 7 software (San Diego, CA, USA) was used for all analyses.

2.5 Results

2.5.1 Phenotypical and transcriptional assessment of adipose-derived mesenchymal stem cell differentiation and inhibition of adipogenesis by green tea-derived EGCG

The differentiation of human adipose-derived mesenchymal stem cells (ADMSC) into mature adipocytes was first performed according to the manufacturer's instructions. Lipid droplet generation was effectively observed as early as day 6 in mature adipocytes as confirmed by increases in size shape due to lipid vesicles accumulation and by Oil Red O staining (Figure 2. 1A). Interestingly, such differentiation processes were abrogated by the presence of the diet-derived epigallocatechin-3-gallate (EGCG), a flavonoid believed to prevent the obesity-associated mortality (Carrasco-Pozo *et al.*, 2019; Lee *et al.*, 2019; Rufino *et al.*, 2021), as both cell size and Oil Red O staining levels were reduced (Figure 2. 1A). When total RNA was extracted from each condition and RT-qPCR was performed to assess gene expression levels, classical adipogenesis-associated genes were induced, including the transcription factors PPARG and C/EBPA, which promote expression of genes that confer the characteristics of mature adipocytes (Lee *et al.*, 2019). Among those genes are insulin receptors, fatty acid synthase, lipoprotein lipase, adiponectin, leptin, acetyl-CoA carboxylase beta, and fatty acid binding protein 4 (FABP4, Figure 2. 1B) (Rosen *et al.*, 2000), the latter being a new player connecting obesity with breast cancer development (Zeng *et al.*, 2020). Interestingly, EGCG inhibited the induction of these genes by 40–80%, suggesting that the resulting mature adipocytes may additionally exhibit an altered secretome profile (Figure 2. 1C). Finally, differential gene expression of inflammatory biomarkers was assessed comparing genes preferentially expressed in ADMSC (Figure 2. 1D, left) versus genes preferentially expressed in adipocytes (Figure 2. 1D, right). Whereas this does not preclude their overall expression, data confirm that the composition of the respective pro-inflammatory secretome characterizes each of the undifferentiated vs. differentiated adipocyte states.

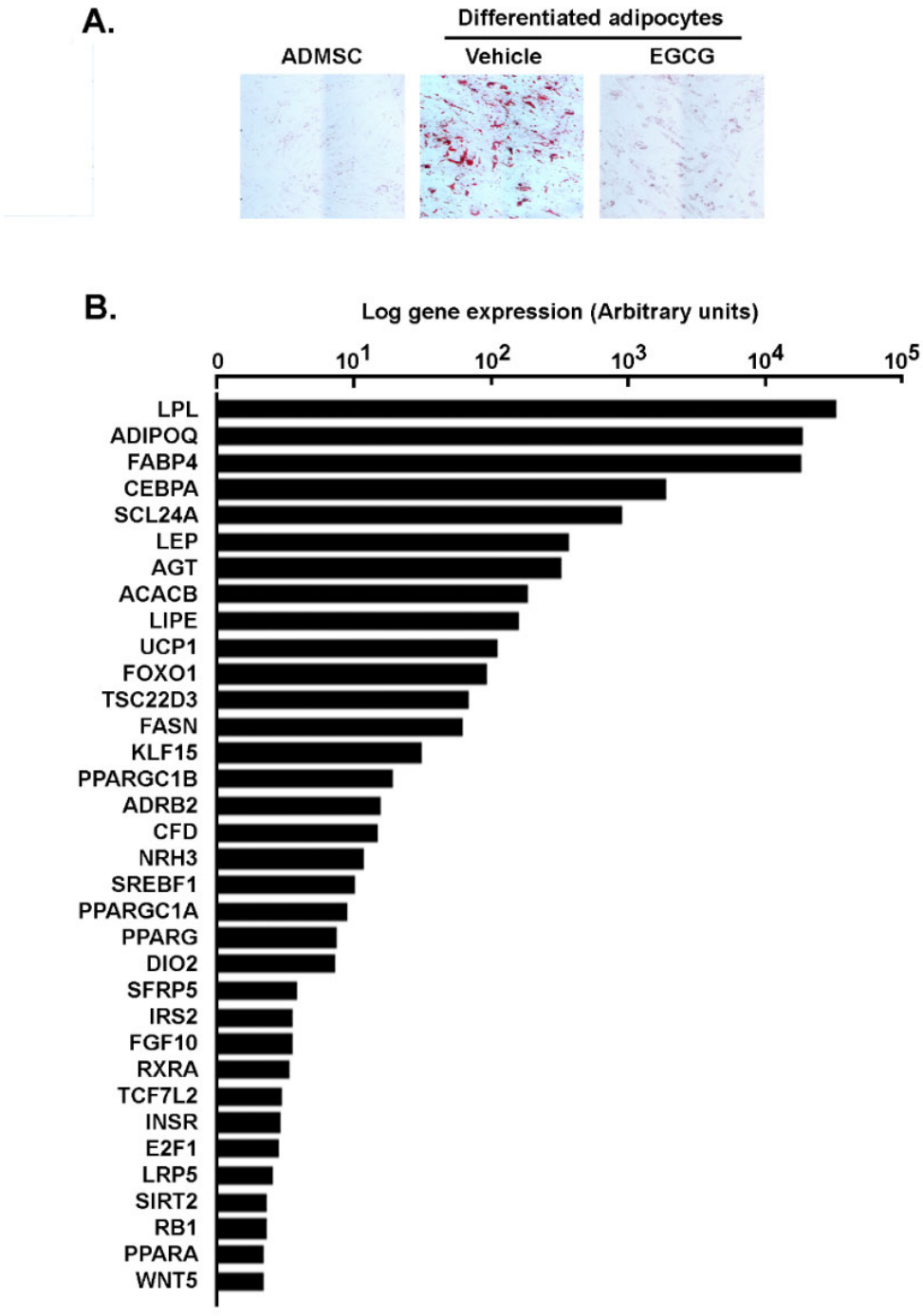
A.
Differentiated adipocytes
ADMSC
Vehicle
EGCG
B.
Log gene expression (Arbitrary units)
0
10^1
10^2
10^3
10^4
10^5
LPL
ADIPOQ
FABP4
CEBPA
SCL24A
LEP
AGT
ACACB
LIPE
UCP1
FOXO1
TSC22D3
FASN
KLF15
PPARGC1B
ADRB2
CFD
NRH3
SREBF1
PPARGC1A
PPARG
DIO2
SFRP5
IRS2
FGF10
RXRA
TCF7L2
INSR
E2F1
LRP5
SIRT2
RB1
PPARA
WNT5

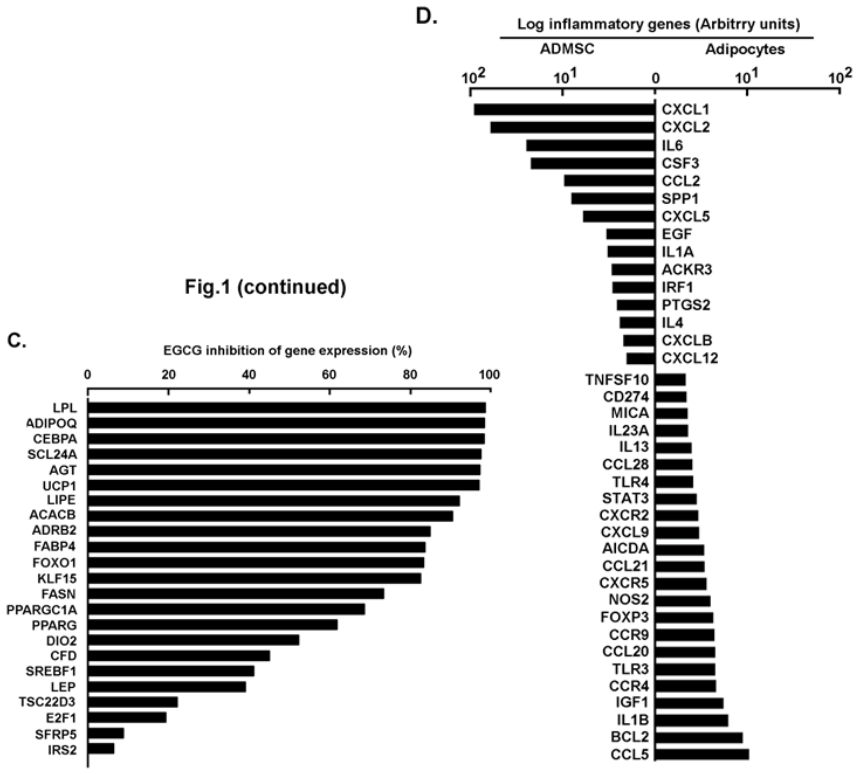

Figure 2. 1. Transcriptional validation of ADMSC differentiation into adipocytes and green tea-derived EGCG inhibition of adipogenesis.

(**A**) ADMSC were differentiated into mature adipocytes in the presence or not of 10 µM EGCG as described in the Methods section. Oil Red O staining was performed at different stages of differentiation to confirm mature adipocyte status through lipid droplets formation, typically observed between day 6 and day 12. (**B**) Total RNA was extracted from ADMSC, adipocytes, as well as ADMSC differentiated in the presence or not of EGCG. RT-qPCR was performed using a RT^2-Profiler gene array to assess adipogenesis gene expression levels. Ratios of adipocytes gene expression on ADMSC gene expression were performed and expressed in a logarithmic scale. (**C**) Ratios of adipocytes differentiated in the presence of EGCG on ADMSC were performed, and EGCG inhibitory potential calculated. (**D**) Total RNA was extracted from ADMSC and from adipocytes. RT-qPCR was performed using a RT^2-Profiler gene array to assess inflammatory-associated gene expression levels. Ratios of adipocytes/ADMSC gene expression (right), and ADMSC/adipocytes (left) gene expression were performed and expressed in a logarithmic scale. Gene arrays data reflect one representative experiment out of two.

2.5.2 Adipocyte Secretome, But Not that of Adipose-Derived Mesenchymal Stem Cells, Triggers Increased TNBC-Derived Cell Migration

Secretome from ADMSC and from adipocyte cell cultures was defined as the conditioned media (CM) collected from each of the respective cell lines, and chemoattractant capacity was assessed on human TNBC-derived MDA-MB-231 cells, ES-2 ovarian cancer cells, and HT-29 colorectal cancer cells. Adipocyte secretome (Adipo-CM; Figure 2. *2* closed circles) was found to trigger a higher chemotactic response in TNBC cells than in any of the two other cancer cell line models tested when compared to ADMSC secretome (Preadipo-CM; Figure 2. *2*, open circles). To further document the evidence of increased chemotaxis observed in MDA-MB-231 cells, a wound-healing assay was performed (Figure 2. 3A) and was found to corroborate the increased invasiveness phenotype as cells recovered the wounded area faster in response to Adipo-CM (Figure 2. 3B). Finally, chemotaxis screening of four other human TNBC-derived cell lines was performed with MDA-MB-468, MDA-MB-157, BT-20, and HCC-70 cells in response to either Preadipo-CM or Adipo-CM. All but HCC-70 cells were found to be more responsive to Adipo-CM than to Preadipo-CM (Figure 2. 3C). This suggests that the mature adipocyte secretome exerts oncogenic paracrine regulation of TNBC cells, increasing their invasiveness.

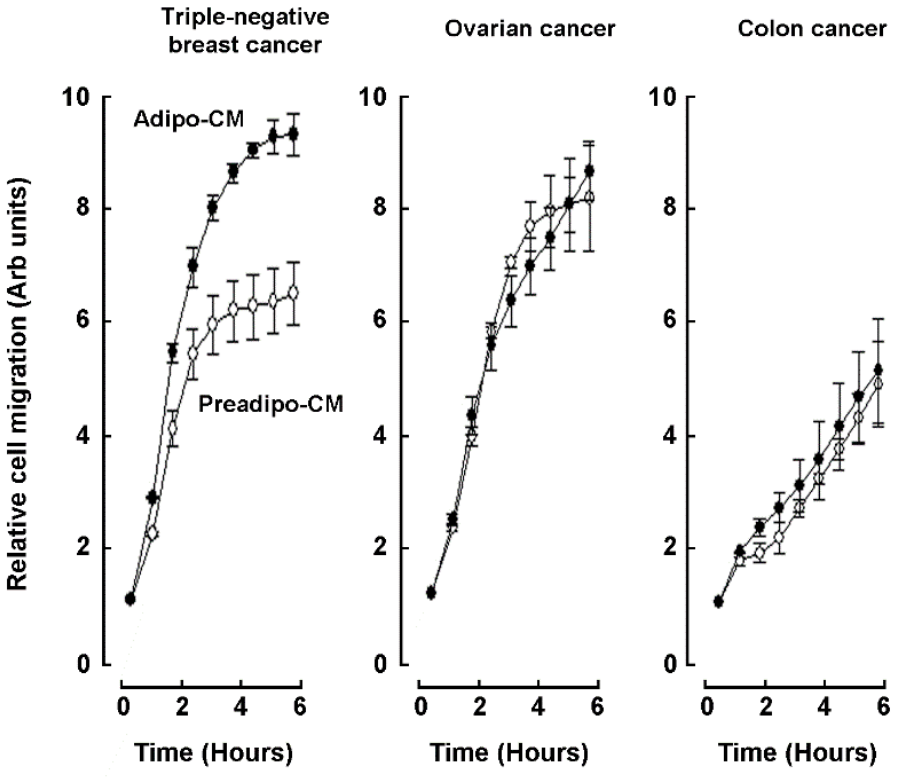

Figure 2. 2. Adipocyte secretome, but not that of ADMSC, triggers increased TNBC-derived cell migration.

Real-time cell migration was performed using the xCELLigence System-RTCA as described in the Methods section in response to ADMSC conditioned media (Preadipo-CM, open circles) or adipocytes' conditioned media (Adipo-CM, closed circles). Cells assessed were human TNBC-derived MDA-MB-231, ES-2 ovarian carcinoma, and HT-29 colorectal adenocarcinoma.

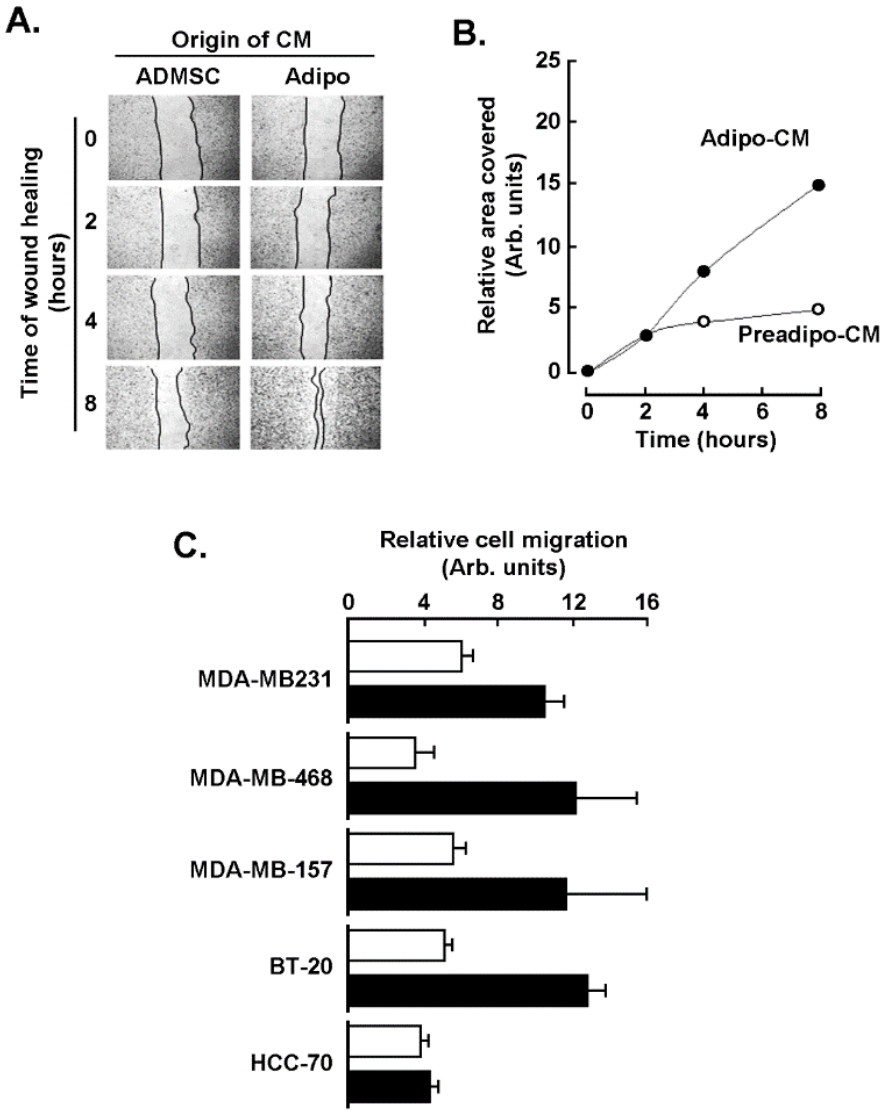

Figure 2. 3. Chemotaxis response of different TNBC-derived cell lines to adipocyte secretome.

(**A**) A wound-healing assay was performed with MDA-MB-231 cells in response to conditioned media isolated from ADMSC (Preadipo-CM) and from adipocyte conditioned media (Adipo-CM), and pictures were taken of the recovered area as described in the Methods section. (**B**) The extent of the recovered area was calculated from a representative experiment. (**C**) Chemotaxis screening of four other human TNBC-derived cell lines was performed with MDA-MB-468, MDA-MB-157, BT-20, and HCC-70 cells in response to either Preadipo-CM (white bars) or Adipo-CM (black bars). Two independent cell migration assays were performed and measured in triplicate.

2.5.3 EGCG Inhibits Both the Acute Response and the Paracrine Regulation of TNBC Cell Chemotaxis Response to Mature Adipocyte Secretome

The capacity of EGCG to regulate the chemotaxis response triggered by the adipocyte secretome was next assessed. Two conditions were tested: first adding the catechin molecule into the Adipo-CM (acute treatment) and second using a CM from ADMSC differentiated in the presence of 10 μM EGCG (paracrine regulation). Whereas little inhibition was found when MDA-MB-231 cells were exposed to Preadipo-CM in the presence of increasing EGCG concentrations (Figure 2. 4A), and a dose-dependent inhibition of chemotaxis was observed in response to Adipo-CM and, when treated at 15 μM EGCG, reached migration levels equivalent to the basal Preadipo-CM response (Figure 2. 4B). When MDA-MB-231 chemotaxis response was assessed with CM isolated from mature adipocytes and from ADMSC differentiated in the presence of EGCG, it was also found to be reduced (Figure 2. 4C). In light of the previously reported involvement of the Fibronectin/STAT3 signaling axis in epithelial-mesenchymal transition (EMT), a process that increases invasion and metastasis of breast cancer cells (Balanis *et al.*, 2013), cell lysates of the above conditions were isolated. Immunoblotting was performed and Adipo-CM was found to trigger Fibronectin expression, a condition which was abrogated by EGCG (Figure 2. 4D). Altogether, these data suggest that specific signaling pathway inhibition may account for the acute EGCG inhibition of chemotaxis. More importantly, EGCG is able to prevent the paracrine regulation of TNBC cell chemotaxis response by altering the adipocyte secretome profile and, ultimately, the acquisition of an EMT-related invasive phenotype.

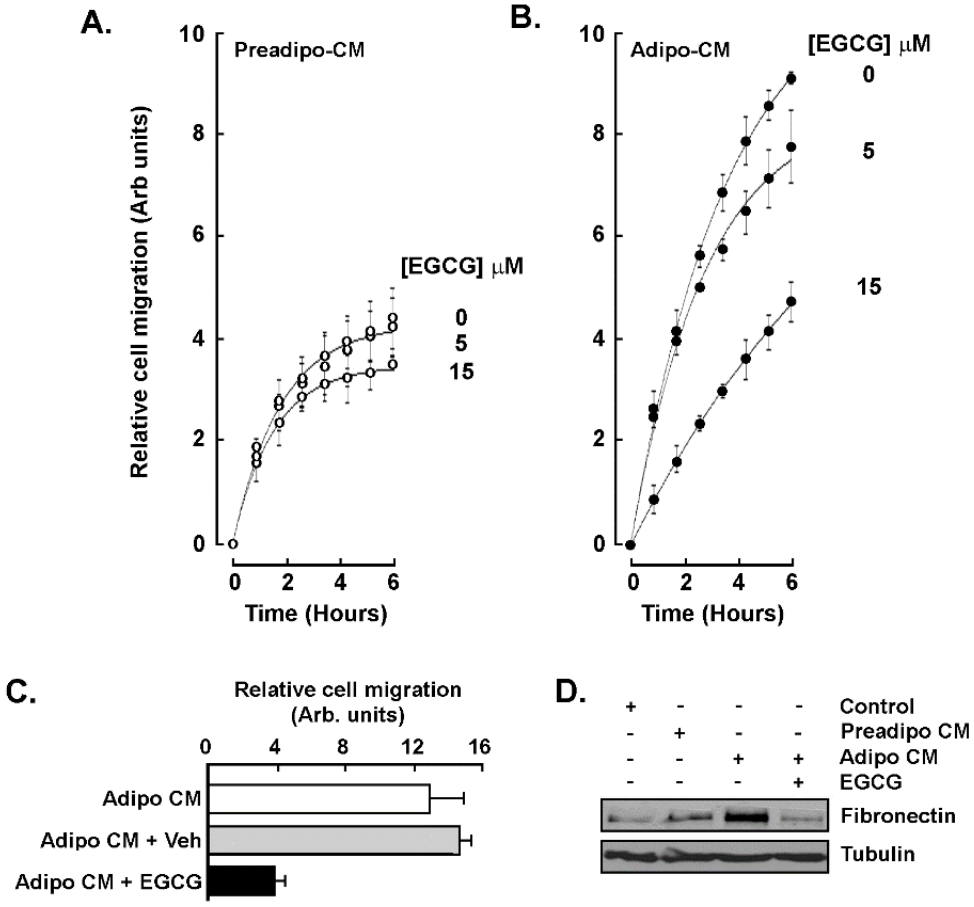

Figure 2. 4. EGCG inhibits the acute response and prevents the paracrine regulation of TNBC cell chemotaxis to adipocyte secretome.

MDA-MB-231 cell migration was assessed as described in the Methods section in the presence of increasing concentrations of EGCG and in response to (**A**) conditioned media isolated from ADMSC (Preadipo-CM), or (**B**) conditioned media isolated from differentiated adipocytes (Adipo-CM). (**C**) Chemotaxis response to conditioned media harvested from adipocytes that were differentiated from ADMSC in untreated (white bar), vehicle-treated (ethanol, grey bars), or differentiated in the presence of 15 μM EGCG (black bars). (**D**) MDA-MB-231 cells were treated for 24 h in basal media (Control), Preadipo-CM, Adipo-CM, or Adipo-CM in the presence of 30 μM EGCG. Fibronectin and Tubulin protein expression were then assessed by immunoblotting using the respective cell lysates. Two independent cell migration assays were performed and measured in triplicate.

2.5.4 STAT3 Is Involved in the Paracrine Chemotaxis Response to Adipocyte Secretome

Stress-induced signaling through signal transducer and activator of transcription 3 (STAT3) is, among other transducing pathways, involved in the initiation, progression, metastasis, and immune evasion of TNBC (Balanis et Carlin, 2017). More recently, STAT3 is further considered as a potential therapeutic target (Bharadwaj *et al.*, 2020; Qin *et al.*, 2019; Wu *et al.*, 2017a). Whether STAT3 is involved in the paracrine response to mature adipocyte secretome was next assessed. MDA-MB-231 cells were exposed to Preadipo-CM or to Adipo-CM for 24 h and STAT3 phosphorylation status assessed by Western blotting. STAT3 phosphorylation was induced in response to Preadipo-CM, whereas phosphorylation was higher in response to Adipo-CM (Figure 2. 5A, upper panels). Interestingly, phosphorylation of the serine/threonine-specific protein kinase AKT, which plays a key role in multiple cellular processes such as cell proliferation, transcription, and cell migration (Jabbarzadeh Kaboli *et al.*, 2020; Lyons, 2019), was only induced in response to Adipo-CM (Figure 2. 5A, lower panels). However, EGCG was able to inhibit STAT3 but not AKT phosphorylation. In addition to EGCG, Tofacitinib and AG490, two pharmacological inhibitors of STAT3 phosphorylation (Hosseini *et al.*, 2020; Jing et Tweardy, 2005), also inhibited Adipo-CM-induced STAT3 phosphorylation (Figure 2. 5B) as well as the MDA-MB-231 chemotactic cell response (Figure 2. 5C). Finally, transient siRNA-mediated gene silencing of STAT3 was performed in MDA-MB-231 cells in order to reduce the STAT3 protein content (Figure 2. 5D, insert). Then, siScrambled or siSTAT3 cells were challenged to migrate in response to Adipo-CM as a chemoattractant. Similarly, to STAT3 pharmacological inhibition, transient silencing of STAT3 was found to reduce the MDA-MB-231 chemotaxis response to the adipocyte secretome (Figure 2. 5D).

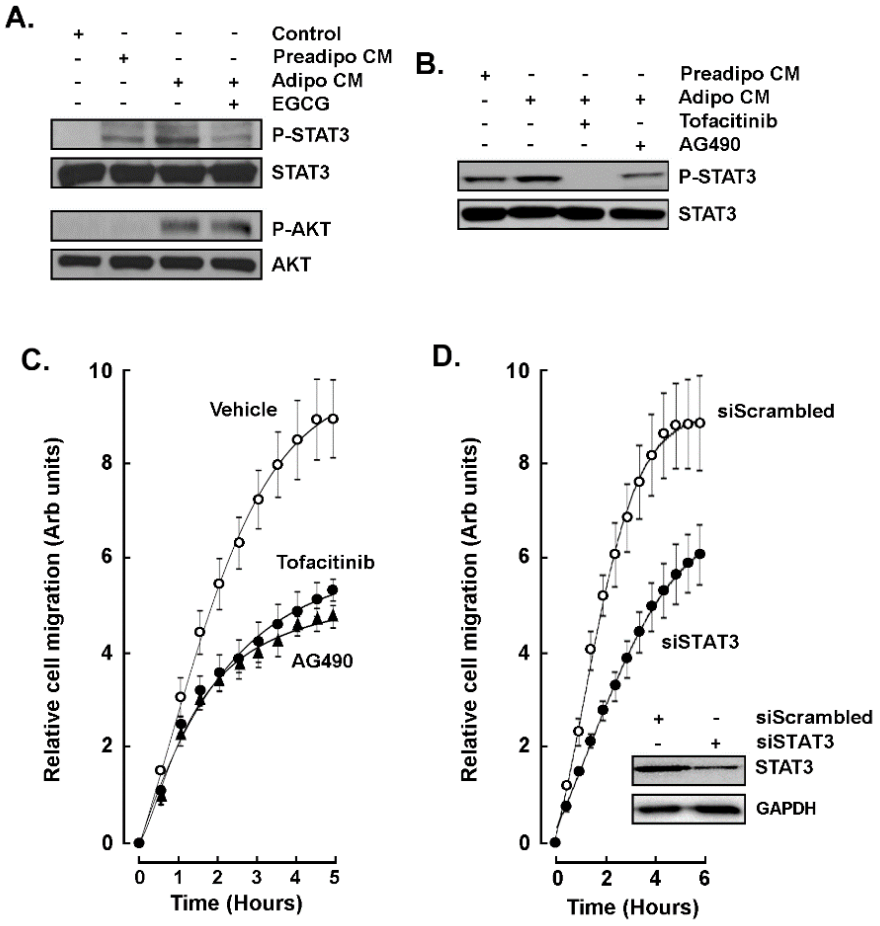

Figure 2. 5. Figure 2.5: STAT3 involvement in the paracrine chemotaxis response to adipocyte secretome.

(**A**) MDA-MB-231 cells were treated for 24 h in the presence of basal media (Control), ADMSC conditioned media (Preadipo-CM), adipocyte conditioned media (Adipo-CM), or Adipo-CM in the presence of 30 μM EGCG. STAT3 and AKT phosphorylation status was then assessed by immunoblotting using the respective cell lysates. (**B**) Cells were similarly treated as in (**A**) with the difference that 30 μM Tofacitinib or AG490 were added to the CM. (**C**) MDA-MB-231 chemotaxis response to conditioned media harvested from adipocytes was performed as described in the Methods section in the absence (vehicle), or presence of Tofacitinib (closed circles), or AG490 (closed triangles). (**D**) MDA-MB-231 chemotaxis response to conditioned media harvested from adipocytes was performed as described in the Methods section in control siScrambled cells (open circles), or in siSTAT3-transfected cells (closed circles). Insert shows a representative Western blot monitoring the extent of STAT3 silencing from siScrambled and siSTAT3-transfected cells. GAPDH was used as a loading control.

2.5.5 Adipocyte Secretome Triggers *In Vitro* 3D-Capillary-Like Structure Maturation, and STAT3 Inhibition Prevents such Maturation.

The paracrine regulation of ADMSC and of mature adipocyte secretome was next assessed on *in vitro* vasculogenic mimicry (VM), a process known to in part be responsible for TNBC chemotherapy resistance (Jitariu *et al.*, 2017). MDA-MB-231 cells were seeded on Matrigel and cultured for 24 h as described in the Methods section in order to generate 3D capillary-like structures. Representative pictures were taken (Figure 2. 6A, upper panels), and digitalized structures were used for the analysis presented (Figure 2. 6A, lower panels). Analysis of the 3D capillary-like structure maturation on Matrigel was performed (Figure 2. 6B) and shows that unstimulated cells cultured on Matrigel and in the presence of serum-deprived basal media (unstimulated condition) led to the formation of 3D structures, which was accelerated by the Preadipo-CM and furthermore by the Adipo-CM (stimulated conditions). The Adipo-CM generated with EGCG added during adipocyte differentiation (Adipo-CM + EGCG (i)), was ineffective in preventing 3D structure maturation. On the contrary, acute additions of EGCG, Tofacitinib, or AG490, were all shown to prevent STAT3 phosphorylation in response to adipocyte secretome, and effectively altered VM processes. Taken together, these results suggest that efficient targeting of the STAT3 signaling pathway may be achieved through diet-derived polyphenols and can prevent the acquisition of an aggressive phenotype in MDA-MB-231 cells, a model of the TNBC.

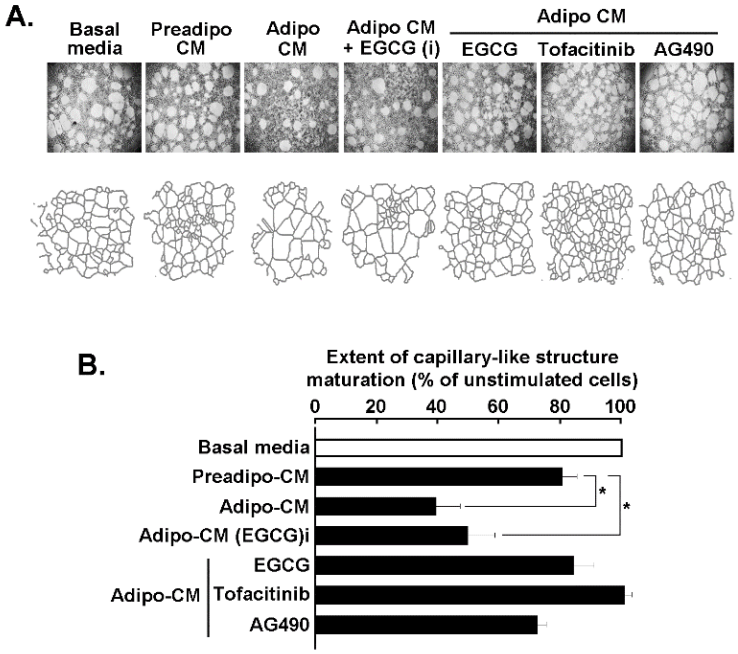

Figure 2. 6: Adipocyte secretome triggers *in vitro* 3D-capillary-like structure maturation, and STAT3 inhibition prevents such maturation.
(**A**) MDA-MB-231 TNBC-derived cells were seeded on Matrigel and cultured for 24 h as described in the Methods section. Representative pictures were taken (upper panels), and digitalized structures used for the analysis presented (lower panels). (**B**) Analysis of the 3D capillary-like structure maturation on Matrigel was performed using ImageJ and was assessed in the presence of either serum-deprived basal media (unstimulated condition), or stimulation with Preadipo-CM, Adipo-CM, or Adipo-CM (i) (CM harvested upon ADMSC differentiation in the presence of 30 µM EGCG). Acute additions of EGCG, Tofacitinib, or AG490 (all at 30 µM) were done in the presence of Adipo-CM to the cell culture. Significance: * $p < 0.05$.

2.6 Discussion

Adipogenesis is a critical step in adipocyte physiology and consists in the terminal differentiation of adipocyte precursor cells (pre-adipocytes) into adipocytes that allows increased storage of fatty acids (Avram *et al.*, 2007). Here, ADMSC differentiation into mature adipocytes has been validated by increased expression of PPARG and C/EBPA, two transcription factors considered among the master regulators of this process (Farmer, 2005). Interestingly, expression of both biomarkers was prevented by

EGCG (Figure 2. *1*), and consequently, it was anticipated that this would alter the state of differentiation as well as the secretome profile of mature adipocytes. Accordingly, distinct pro-inflammatory profiles are shown to characterize the ADMSC and adipocyte respective phenotypes (Figure 2. *1*D). In accordance with previous studies, IL6 was more expressed in ADMSC than in mature adipocytes (Harkins *et al.*, 2004), and the expression of NOS2, IGF-1, and IL-1B were higher in mature adipocytes than in ADMSC (Kloting *et al.*, 2008; Lowenstein and Padalko, 2004; Tang and Lane, 2012). Apart from the regulation of the body's energy balance, factors secreted from adipose tissue in obesity play key roles in the modulation of metabolic processes, insulin sensitivity and immunological responses (Gregoire, 2001), and are believed to provide protumorigenic chemokines to promote breast cancer progression (Raman *et al.*, 2007). Unfortunately, the detailed mechanisms involved in adipose tissue paracrine regulation of breast cancer cells are still not well understood.

Here, we provide evidence for a specific and increased paracrine regulatory impact of the adipocyte secretome on several TNBC-derived cell models. Chemotaxis response was found to be significantly induced by the secretome of differentiated adipocytes when compared to that of undifferentiated adipocytes, and this required the activation of the AKT and STAT3 signaling pathways. EGCG, as well as JAK/STAT inhibitors Tofacitinib and AG490, all prevented the increase in chemotactic response to cytokines and growth factors originating from mature adipocytes. Intriguingly, AKT phosphorylation was also induced but could not be prevented by EGCG. Whereas AKT-targeted therapy is believed to be a promising strategy to overcome drug resistance in breast cancer (Jabbarzadeh Kaboli *et al.*, 2020), such selective targeting of signaling pathways by EGCG prompts for more research.

The adipose microenvironment in obese people bears many similarities with the tumor microenvironment with respect to associated cellular composition, chronic low-grade inflammation, and a high ratio of reactive oxygen species to antioxidants (Zimta *et al.*, 2019). In addition, the secretion of a number of inflammation-related adipokines is upregulated by hypoxia, which is present in some areas of the expanded adipose

tissue (Trayhurn, 2013). Hence, obesity creates a pro-inflammatory environment that is believed to favor the incidence of several cancers (Calle et Thun, 2004) through numerous signal transduction pathways, including the JAK/STAT3 pathway (Loh *et al.*, 2019). Targeting oncogenic transcription factors by polyphenols has recently been inferred (Rajagopal *et al.*, 2018), and inhibition of JAK/STAT3 transducing events by EGCG has been reported in numerous cancers (Farooqi *et al.*, 2020; Wang *et al.*, 2013; Xiao *et al.*, 2019). More recently, emerging evidence of dietary phytochemicals in our fight against cancer has ascribed a role in targeting cancer stem cells (CSC) often associated with chemoresistance and cancer recurrence (Naujokat and McKee, 2021; Singh *et al.*, 2017). Such an avenue towards CSC targeting has prompted preclinical and clinical settings to repurpose pre-existing drugs to treat TNBC on the basis of molecular mechanisms and signaling pathways such as STAT3 (Aggarwal *et al.*, 2021; Avalos-Moreno *et al.*, 2020). In our study, we demonstrate that EGCG prevents the differentiation of ADMSC and modulates the secretome profile of these cells. Furthermore, once the cells are fully mature, EGCG can hinder its paracrine regulation over the TNBC cells within the tumor microenvironment, which highlights the potential benefit of its consumption.

Paracrine-mediated regulation of an increased invasive phenotype can, in part, involve EMT processes (Davis *et al.*, 2014). Here, we show that part of the chemotactic response could be achieved through such processes as the expression of the EMT biomarker Fibronectin and was induced upon incubation with differentiated adipocyte secretome, but not with that from the ADMSC. Interestingly, EGCG prevented both the chemotactic response of TNBC cells as well as the induction of Fibronectin in accordance with its capacity to inhibit EMT (Negri, 2018). EGCG targeting of EMT processes has also recently been documented in ES-2 ovarian cancer cells where cell migration and *in vitro* VM were abrogated (Sicard *et al.*, 2021). In the current study, we demonstrate that the paracrine regulation of MDA-MB-231-mediated *in vitro* VM was abrogated by all three JAK/STAT3 inhibitors (EGCG, Tofacitinib, AG490) tested.

Adipocytes, and their precursors ADMSC, are thought to sustain tumor phenotypes in part through secretion of signaling molecules and vesicles containing proteins, lipids and nucleic acids (D'Esposito *et al.*, 2020). On the other hand, during their interaction with cancer cells, ADMSC can in return be reprogrammed into cancer-associated adipocytes to further secrete adipokines, which stimulate the adhesion, migration, and invasion of cancer cells (Nieman *et al.*, 2013). Such bidirectional communication between adipose and breast cancer cells has laid foundations for the recruitment of macrophages to the mammary tumor inflammatory microenvironment through increased release of cytokines, growth factors and extracellular matrix components (Lengyel *et al.*, 2018; Santander *et al.*, 2015). Our findings are in accordance with the previous statements, as we found that both ADMSC and mature adipocytes secrete factors that could contribute to tumor development like IL-6, EGF, PTGS2 and IL-4 in ADMSC, and CCL5, IL-1Band IGF in adipocytes. Recently, FABP4, a member of a family of circulating adipose fatty acid binding proteins, has emerged as a new link in the obesity-associated breast/mammary tumor development (Hao *et al.*, 2018b; Zeng *et al.*, 2020). Of particular interest, circulating blood concentration FABP4 levels have been proposed as a new independent breast cancer biomarker as it was found increased in breast cancer patients (Guaita-Esteruelas *et al.*, 2017). Here, we report that FABP4 transcript levels were increased upon adipocyte differentiation and, more importantly, that such an induction can efficiently be prevented by EGCG. More studies will be needed to identify, among the secreted factors, which one(s) have a leading role in order to design pharmacological interventions.

In conclusion, this study first validated our preadipocytes differentiation protocol at both the cellular and transcriptional levels. Both the cellular staining and the transcriptomic data demonstrated clear modulation by EGCG. This last evidence strongly suggests that, although beyond the immediate scope of this study, the overall soluble secreted growth factors (secretome) from preadipocytes and mature adipocytes may trigger differential chemotactic response. The exact identification of these

individual growth factors/cytokines would be a logical follow-up although the current approach used, which is the use of the cells' conditioned media to reflect the synergistic action of the complete actors of the secretome, better reflects the pathophysiological tissue microenvironment. One may envision later and address the impact of hypoxia, and EGCG tissue biodistribution/bioavailability using *in vivo* approaches, as these remain major concerns in obesity.

Our study further provides new molecular evidence demonstrating how dietary intervention upon adipogenesis could alter the secretome profile during adipocyte maturation, and the paracrine regulation of TNBC cell acquisition of an invasive phenotype (Figure 2. *7*). Data also highlights the critical role of the JAK/STAT3 signaling pathway in cell chemotaxis and VM, which can be targeted by EGCG as efficiently as by the pharmacological agents Tofacitinib and AG490. Preventing the onset of an obesogenic environment should help reduce the incidence of TNBC development. In Figure 2. 7 we summarized the main findings in our study.

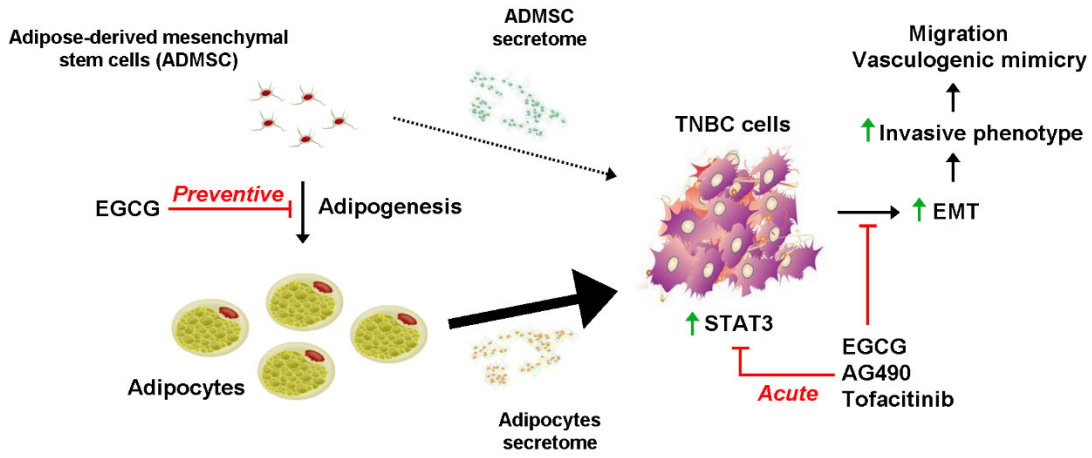

Figure 2. 7. Figure 2.7: Scheme summarizing the preventive and acute effects of EGCG on STAT3-mediated acquisition of an invasive TNBC phenotype.
Adipogenesis is induced during ADMSC differentiation into mature adipocytes. Both of the cell types have characteristic and distinct secretome profiles composed of different levels of pro-inflammatory cytokines, chemokines, and growth factors (Figure

1D). Whereas ADMSC secretome was characterized by some chemotactic properties towards TNBC cells (dotted arrow), this was significantly triggered by the secretome resulting from mature adipocytes (large arrow). EGCG was able to prevent such an effect by inhibiting adipogenesis (Preventive experimental condition). Increased EMT explains, in part, the resulting increases in TNBC cell migration and vasculogenic mimicry in response to the adipocyte secretome, the response of which can be reduced through the inhibition of STAT3-mediated signaling by EGCG, AG490, and Tofacitinib (Acute experimental condition).

CHAPTER III

ARTICLE 2

EGCG PREVENTS THE ONSET OF AN INFLAMMATORY AND CANCER-ASSOCIATED ADIPOCYTE-LIKE PHENOTYPE IN ADIPOSE-DERIVED MESENCHYMAL STEM/STROMAL CELLS IN RESPONSE TO THE TRIPLE-NEGATIVE BREAST CANCER SECRETOME

Narjara Gonzalez Suarez[1], Yuniel Fernandez-Marrero[2], Sima Torabidastgerdooei[1] and Borhane Annabi[1]

[1]Laboratoire d'Oncologie Moléculaire, Département de Chimie, and CERMO-FC, Université du Québec à Montréal, Montreal, QC H3C 3P8, Canada.
[2]Biological Sciences Platform, Sunnybrook Research Institute, Sunnybrook Health Science Centre, Toronto, ON M4N 3M5, Canada.

Manuscript published in Nutrients **2022**, 14, 1099
https://doi.org/10.3390/nu14051099

Authors contributions:

Narjara Gonzalez Suarez: Performed the experiments, analyzed the data, and drafted the manuscript.
Yuniel Fernandez-Marrero: Performed the transcriptomic analysis and reviewed the manuscript.
Sima Torabidastgerdooei: Performed the gene array experiments and analyzed the data.
Borhane Annabi: Designed the study, analyzed the data, drafted the manuscript and provided the financial support.

All authors have read and agreed to the published version of the manuscript.

3.1. Résumé

Contexte: Le sécrétome des cellules du cancer du sein triple négatif (TNBC) induit un microenvironnement pro-inflammatoire au sein du tissu adipeux hébergeant à la fois des adipocytes matures et des cellules souches/stromales mésenchymateuses adipocytaires (ADMSC). Les mécanismes d'acquisition d'un phénotype de type adipocytes associés au cancer (CAA) sont cependant peu connus. Alors que les études épidémiologiques suggèrent que la consommation d'un régime riche en polyphénols réduit l'incidence de certains cancers liés à l'obésité, l'impact chimiopréventif de l'épigallocatéchine-3-gallate (EGCG) dérivée du thé vert envers les signaux qui déclenchent le phénotype CAA reste peu documenté dans les ADMSC. Méthodes : Des cellules ADMSC humaines ont été exposées à du milieux conditionné par les cellules MDA-MB-231 dérivées du TNBC humain (sécrétome des cellules TNBC) en présence ou non d'EGCG. L'expression génique différentielle a été évaluée par analyse RNA-Seq et confirmée par RT-qPCR. Les niveaux d'expression des protéines et l'état d'activation des médiateurs des voies de transduction du signal ont été déterminés par immunobuvardage. La chimiotaxie des ADMSC a été évaluée par un test de migration cellulaire en temps réel. Résultats : Le sécrétome des cellules TNBC induit dans les cellules ADMSC l'expression des cytokines CCL2, CCL5, IL-1Bet IL-6, et des immunomodulateurs COX2, HIF-1A, VEGFA et PD-L1. Nos résultats montrent que le biomarqueur de la transition épithéliale-mésenchymateuse SNAIL1 contrôle le phénotype CAA. L'EGCG inhibe l'induction des gènes liés au phénotype CAA et l'activation de SMAD2 et NF-kB. La réponse chimiotactique induite a également été inhibée par l'EGCG. Conclusion : L'induction d'un phénotype inflammatoire et de type CAA dans les ADMSC peut être déclenchée par le sécrétome des cellules TNBC, tout en étant efficacement empêchée par les polyphénols dérivés de l'alimentation.

3.2. Abstract

Background: Triple-negative breast cancer (TNBC) cells' secretome induces a pro-inflammatory microenvironment within the adipose tissue, which hosts both mature adipocytes and adipose-derived mesenchymal stem/stromal cells (ADMSC). The subsequent acquisition of a cancer-associated adipocyte (CAA)-like phenotype is, however, unknown in ADMSC. Epidemiological studies suggest that consuming a polyphenol-rich diet reduces the incidence of some obesity-related cancers, and the chemopreventive impact of green tea-derived epigallocatechin-3-gallate (EGCG) against the cues that trigger the CAA phenotype remain undocumented in ADMSC. Methods: Human ADMSC were exposed to human TNBC-derived MDA-MB-231 conditioned media (TNBC cell's secretome) supplemented or not with EGCG. Differential gene expression was assessed through RNA-Seq analysis and confirmed by RT-qPCR. Protein expression levels and the activation status of signal transducing pathway mediators were determined by Western blotting. ADMSC chemotaxis was assessed by a real-time cell migration assay. Results: The TNBC cells' secretome induced in ADMSC the expression of the CAA cytokines CCL2, CCL5, IL-1β, and IL-6, and of immunomodulators COX2, HIF-1A, VEGFA, and PD-L1. The epithelial-to-mesenchymal biomarker Snail was found to control the CAA phenotype. EGCG inhibited the induction of CAA genes and the activation status of SMAD2 and NF-KB. The induced chemotactic response was also inhibited by EGCG. Conclusion: The induction of an inflammatory and CAA-like phenotype in ADMSC can be triggered by the TNBC cells' secretome, while still efficiently prevented by diet-derived polyphenols.

3.3 Introduction

The acquisition of a cancer-associated adipocyte (CAA) phenotype can be viewed as an adaptive characteristic of cells residing within the adipose tissue and that respond to cues that originate from the tumor microenvironment (TME) (Lee *et al.*, 2017; Zhao *et al.*, 2020). Accordingly, tumor infiltration of adipocytes has been reported in breast, ovarian, colorectal, and pancreatic cancers, ultimately leading to the instauration of a pro-inflammatory state that promotes carcinogenic events in return (Cai *et al.*, 2019; Pu et Chen, 2021). Such pro-malignancy role of the adipose tissue has been described primarily in breast cancer, where the residing adipocytes represent the most abundant stromal cell type and constitute the main source of pro-inflammatory cytokines and growth factors (Dirat *et al.*, 2011; Rybinska *et al.*, 2021; Wu *et al.*, 2019).

The CAA phenotype characterizes adipose tissue-derived cells with morphologically smaller and irregular sizes, as well as with decreased content and dispersed pattern of lipid droplets (Suarez-Najera *et al.*, 2018). These cells also present an activated state attributable to the overexpression and secretion of the chemokine (C-C motif) ligand 2 (CCL2, also known as MCF-1), the chemokine (C-C motif) ligand 5 (CCL5, also known as RANTES), inflammatory cytokines including interleukin (IL)-1β, IL-6, tumor necrosis factor (TNF)-α, and matrix metalloproteinase (MMP)-11(Dirat *et al.*, 2011). The CAA phenotype further associates with increased releases of metabolites such as lactate, pyruvate, free fatty acids, and ketone bodies (Attane et Muller, 2020). Such adaptive metabolic state is believed to mimic the hypoxic status and to contribute to immunosuppressive events within the TME, in part through the upregulation of hypoxia-inducible factor-1α (HIF-1A) and c-Myc (Brown et Ganapathy, 2020; Masoud et Li, 2015; Wang *et al.*, 2021b). In terms of TME localization, these cells have been ascribed to the invasive front of human breast cancer tumors (Andarawewa, 2005; Bochet *et al.*, 2013; Dirat *et al.*, 2011).

Epidemiological studies have implied the existence of an association between excess adipose tissue and a higher incidence/progression of breast cancer (Protani *et*

al., 2010; Sung *et al.*, 2021). In obesogenic conditions, the excessive expansion in adipose tissue triggers a chronic low-grade inflammation state recognized to create an environment that can sustain tumoral progression (Ramos-Nino, 2013). Therefore, a dynamic crosstalk between resident adipocytes and paracrine response to TME signals appears to play a crucial role in the onset of an aggressive tumor phenotype (Lengyel *et al.*, 2018; Pascut *et al.*, 2020). Epidemiological studies indicate that consumption of a polyphenol-rich diet reduces the incidence of obesity-related cancers (Andersen *et al.*, 2010; Fund, 2018). Nevertheless, the cues triggering the CAA phenotype remain less understood at the early stages of adipocyte maturation as well as in adipocyte-derived mesenchymal stem/stromal cells (ADMSC, also referred to as pre-adipocytes (Gonzalez Suarez *et al.*, 2021; Ullah *et al.*, 2015)). Those cells have been demonstrated to have the ability to differentiate into mesodermal tissue lineages including adipose through the regulation of key transcriptional factors involved in early adipogenesis (Ullah *et al.*, 2015).

Among the phytochemicals targeting adipogenesis, the green-tea-derived epigallocatechin 3-gallate (EGCG) prevented the acquisition of a more invasive phenotype in a triple-negative breast cancer (TNBC)-derived MDA-MB-231 cell model, triggered by the secretome of mature adipocytes but not by the secretome from human ADMSC (Gonzalez Suarez *et al.*, 2021). The adipose tissue microenvironment also promoted TNBC cell invasiveness and dissemination by producing CCL5 (D'Esposito *et al.*, 2016). ADMSC were also suggested to promote progression and metastatic spread in breast cancer by switching to a more malignant phenotype, leading to a worse prognosis (Kamat *et al.*, 2015). The sum of this evidence supports the concept that diet-derived phytochemicals could prevent the onset of an inflammatory obesogenic environment that favors the acquisition of a CAA-like phenotype.

To unveil the key mediators in the crosstalk between cancer cells and resident adipose tissue cells, studies have so far mostly characterized the promoting role of adipocytes in tumor progression (Rybinska *et al.*, 2020). However, fewer have focused on how the TME-mediated reshaping of preadipocytes or ADMSC, or how

dedifferentiated mature adipocytes arise. Therefore, the present study aims at characterizing how soluble factors secreted from the TNBC-derived MDA-MB-231 cell line can mediate the acquisition of an inflammatory and CAA phenotype, and the chemotactic response in ADMSC. Finally, the chemopreventive impact of EGCG was assessed as a model for nutraceutical intervention against the acquisition of a CAA-like phenotype in ADMSC.

3.4 Materials and methods

3.4.1 Materials

Sodium dodecylsulfate (SDS), epigallocatechin-3-gallate (EGCG) and bovine serum albumin (BSA) were purchased from Sigma-Aldrich Canada (Oakville, ON, Canada). Electrophoresis reagents were purchased from Bio-Rad (Mississauga, ON, Canada). The enhanced chemiluminescence (ECL) reagents were from Amersham Pharmacia Biotech (Baie d'Urfé, QC, Canada). Micro bicinchoninic acid protein assay reagents were purchased from Pierce (Rockford, IL, USA). The polyclonal antibodies against Snail, Slug, phosphorylated and total NF-KB (p105), SMAD2, and STAT3 were obtained from Cell Signaling Technology Inc. (Danvers, MA, USA). Monoclonal antibody (mAb) against human IL-6 was purchased from (New England Biolabs Ltd., Whitby, ON, Canada), rabbit IgG isotype control was obtained from Abcam (Toronto, ON, Canada); and a mAb against glyceraldehyde 3-phosphate dehydrogenase (GAPDH) was from Advanced Immunochemical Inc. (Long Beach, CA, USA). Horseradish peroxidase-conjugated donkey anti-rabbit and anti-mouse IgG secondary antibodies were obtained from Jackson ImmunoResearch Laboratories (West Grove, PA, USA). Protein A sepharose beads were obtained from GE Healthcare (Uppsala, Sweden). Gelatin was obtained from Sigma Aldrich (Oakville, ON, Canada).

3.4.2 Cell Culture and TNBC Cells' Secretome Collection

The human adipose-derived mesenchymal stem/stromal cells (ADMSC) and TNBC-derived cell line MDA-MB-231 were purchased from the American Type Culture Collection (ATCC, Manassas, VA, USA). ADMSC were grown in Mesenchymal Stem Cell Basal Medium (ATCC, PCS-500-030) and supplemented with Mesenchymal Stem Cell Growth Kit Low Serum (ATCC, PCS-500-040). They were further reported to have the capacity to undergo adipogenesis (Robert *et al.*, 2020). MDA-MB-231 were grown in EMEM Medium (Wisent, Saint-Jean-Baptiste, QC, Canada) supplemented with 10% of fetal bovine serum. All cells were cultured at 37°C under a humidified 95–5% (v/v) mixture of air and CO2. The TNBC cells' secretome was generated upon a 48h serum deprivation of a ~70% confluent MDA-MB-231 culture. Next, the conditioned media (CM) was harvested and centrifuged at 1500× *g* for 20 min to eliminate cell debris. CM was aliquoted and kept at −20 °C. To evaluate the induction of the CAA phenotype, ADMSC were cultured with the TNBC cells' secretome in the presence or absence of 10 μM EGCG for 24 h. Then, cells were collected for total RNA extraction, protein isolation, or cell migration studies.

3.4.3 Total RNA Isolation, cDNA Synthesis, and Real-Time Quantitative PCR

Total RNA was extracted from cell monolayers using 1 mL of TriZol reagent for a maximum of 3×10^6 cells as recommended by the manufacturer (Life Technologies, Gaithersburg, MD, USA). For cDNA synthesis, 1–2 μg of total RNA was reverse-transcribed using a high-capacity cDNA reverse transcription kit (Applied Biosystems, Foster City, CA) or, in the case of the gene array, R2 First Strand kit (QIAGEN, Valencia, CA, USA). The cDNA was stored at -80°C prior to PCR. Gene expression was quantified by real-time quantitative PCR using iQ SYBR Green Supermix (Bio-Rad, Hercules, CA, USA). DNA amplification was carried out using an Icycler iQ5 (Bio-Rad), and product detection was performed by measuring binding of the fluorescent dye SYBR Green I to double-stranded DNA. The following primer sets

were from QIAGEN: Snail (Hs_SNAI1_1_SG, QT00010010), IL-6 (Hs_IL6_1_SG, QT00083720), RPS18 (Hs_RPS18_2_SG, QT02323251) and PPIA (Hs_PPIA_4_SG, QT01866137). The relative quantities of target gene mRNA were normalized against internal housekeeping genes PPIA and RPS18. The RNA was measured by following a ΔC_T method employing an amplification plot (fluorescence signal vs. cycle number). The difference (ΔC_T) between the mean values in the triplicate samples of target gene and the housekeeping genes was calculated with the CFX manager Software version 2.1 (Bio-Rad), and the relative quantified value (RQV) was expressed as $2^{-\Delta CT}$.

3.4.4 Total RNA Library Preparation and Sequencing

Total RNA (500 ng) was used for library preparation. RNA quality control was assessed with the Bioanalyzer RNA 6000 Nano assay on the 2100 Bioanalyzer system (Agilent technologies, Mississauga, ON, Canada), and all samples had an RNA integrity number (RIN) above eight. Library preparation was carried out with the KAPA mRNA-Seq HyperPrep kit (Roche, Laval, QC, Canada). Ligation was made with Illumina dual-index UMI, and 10 PCR cycles were required to amplify cDNA libraries. Libraries were quantified by QuBit and BioAnalyzer DNA1000. All libraries were diluted to 10 nM and normalized by qPCR using the KAPA library quantification kit (KAPA; Cat no. KK4973). Libraries were pooled to equimolar concentrations. Three biological replicates were generated. Sequencing was performed with the Illumina Nextseq500 using the Nextseq High Output 75 (1 × 75 bp) cycles kit. Around 15–20 M single-end PF reads were generated per sample. Library preparation and sequencing was performed at the Genomic Platform of the Institute for Research in Immunology and Cancer (IRIC, Montreal, QC, Canada).

3.4.5 Reads Alignment and Differential Expression Analysis

Reads were 30 trimmed for quality and adapter sequences using Trimmomatic version 0.35, and only reads with at least 50 bp in length were kept for further analyses. Trimmed reads were aligned to the reference human genome version GRCh38 (gene annotation from Gencode version 37, based on Ensembl 103) using STAR version 2.7.1a (Dobin *et al.*, 2013). Gene expressions were obtained both as read count directly from STAR and computed using RNA-Seq by Expectation Maximization (RSEM) (Li et Dewey, 2011) to obtain normalized gene and transcript-level expression, in TPM values, for these stranded RNA libraries. Differential expression analysis was performed using *DESeq2* version 1.22.2 (Love *et al.*, 2014). The package *limma* (Ritchie *et al.*, 2015) was used to normalize expression data and read counts data were analyzed using DESeq2. Principal component analysis (PCA) for the first two most significant components was conducted with R packages (Team, 2017) found in iDEP (integrated Differential Expression and Pathway) analysis (Ge *et al.*, 2018). iDEP was also used to determine significant differentially expressed genes (DEGs) with DESeq2 false discovery rate (FDR) adjusted *p*-value of 0.05 and fold-change with a cutoff of two.

3.4.6 Gene Ontology Pathway Enrichment Analysis

The genes were filtered by absolute fold change (FC) and FDR ($|FC| > 2$, $FDR < 0.001$) and then used for pathway enrichment analysis on active subnetworks prepared using the library pathfindR (Ulgen *et al.*, 2019). Genes common to samples treated with EGCG or vehicle were z-normalized and clustered using a consensus from ten independent k-means runs. The results were visualized as a heatmap using the package ComplexHeatmap (Gu *et al.*, 2016). All analyses were performed using R version 4.1.1 (10 August 2021). Gene ontology (GO) enrichment analysis for protein class and molecular function of the genes in clusters 5–7 was performed using the GO online resource (geneontology.org). The enrichment of the upregulated genes per cluster was

determined using all genes detected in the control sample as background. An FDR < 0.05 was used as cut off.

3.4.7 Human Cancer Inflammation and Immunity Crosstalk PCR Array

The RT^2 Profiler^{TM} PCR Array for Human Cancer Inflammation and Immunity Crosstalk (PAHS-181Z) was used according to the manufacturer's protocol (QIAGEN). The detailed list of the key genes assessed can be found on the manufacturer's website (https://geneglobe.qiagen.com/us/product-groups/rt2-profiler-pcr-arrays; accessed on 13 January 2022). Using real-time quantitative PCR, we reliably analyzed the expression of a focused panel of genes related to the inflammatory response, including some of the cancer-associated adipocytes markers already published. Relative gene expression was calculated using the $2^{-\Delta\Delta CT}$ method ("delta-delta" method), in which C_T indicates the fractional cycle number where the fluorescent signal crosses the background threshold. This method normalizes the ΔC_T value of each sample, using five housekeeping genes (B2M, HPRT1, RPL13A, GAPDH, and ACTB). The normalized FC values are then presented as average FC = 2 (average $^{\Delta\Delta CT}$). To minimize false positive results, only genes amplified less than 35 cycles were analyzed. The resulting raw data were then analyzed using the PCR Array Data Analysis Template (http://www.sabiosciences.com/pcrarraydataanalysis.php; accessed on 13 January 2022). This integrated web-based software package automatically performs all $\Delta\Delta C_T$-based FC calculations from the uploaded raw threshold cycle data.

3.4.8 RNA Interference

Cells were transiently transfected with siRNA using Lipofectamine-2000 transfection reagent (Thermo Fisher Scientific, Waltham, MA, USA). Gene silencing was performed using 20 nM siRNA against SNAIL1 (Hs_SNAI1_5 HP siRNA, SI02636424), IL-6 (Hs_IL6_1 siRNA, SI00012572) or scrambled sequences (AllStar

Negative Control siRNA, 1027281). The above small interfering RNA and mismatch siRNA were all synthesized by QIAGEN and annealed to form duplexes.

3.4.9 Western Blot

Cells were lysed in a buffer containing 1 mM each of NaF and Na_3VO_4, and proteins (10–20 μg) were separated by SDS-polyacrylamide gel electrophoresis (PAGE). Next, proteins were electro-transferred to polyvinylidene difluoride membranes and blocked for 1 h at room temperature with 5% nonfat dry milk in Tris-buffered saline (150 mM NaCl, 20 mM Tris-HCl, pH 7.5) containing 0.3% Tween-20 (TBST, TWN510-500). Membranes were washed in TBST and incubated over night with the appropriate primary antibodies (1/1000 dilution) in TBST containing 3% BSA and 0.1% sodium azide (Sigma-Aldrich) at 4°C and in a shaker. After three washes with TBST, the membranes were incubated 1 h with horseradish peroxidase-conjugated anti-rabbit or anti-mouse IgG at 1/2500 dilutions in TBST containing 5% nonfat dry milk. Immunoreactive material was visualized by ECL

3.4.10 Multiplex Cytokine ELISA Array

MDA-MB-231 cells were serum-starved for 24 and 48 h. Then, conditioned media was collected, clarified by centrifugation, and stored at −20°C until further evaluations. The relative abundance of the secreted cytokines was determined using a Multiplex Human Cytokine ELISA Kit (MyBioSource, San Diego, CA, USA) and following the manufacturer's instructions. The optical density (OD) values of the samples were obtained at 450 nm.

3.4.11 Immunoprecipitation Procedures

Protein A beads (30 µL slurry) were co-incubated overnight under rotation at 4°C in 4 mL of TNBC conditioned media (CM), with either the anti-IL-6 mAb diluted 1/100 or the IgG isotype control (2 µg). Next, each mixture was centrifuged, the supernatants collected, filtered through a 0.2 µm filter, and frozen until further evaluation. The beads were boiled with Laemmli buffer and applied to a 7.5% SDS-PAGE alongside the supernatants, then transferred to PVDF membranes and immunoblotted to determine the efficiency of the immunoprecipitation.

3.4.12 Chemotactic Cell Migration Assay

Cell migration assays were carried out using the Real-Time Cell Analyzer (RTCA) Dual-Plate (DP) Instrument of the xCELLigence system (Roche Diagnostics, Basel, Switzerland). Adherent ADMSC monolayers were trypsinized and seeded (30,000 cells/well) onto CIM-Plates 16 (Roche Diagnostics). These migration plates are similar to conventional transwells (8 µm pore size) but have gold electrode arrays on their bottom side of the membrane to provide real-time data acquisition of cell migration. Prior to cell seeding, the underside of the wells from the upper chamber were coated with 25 µL of 0.15% gelatin in PBS and incubated for 1 h at 37°C. Cell migration was continuously monitored for 8 h using serum-free, CM obtained from MDA-MB-231 cells (CM or TNBC cells' secretome) grown in the presence or absence of EGCG. Serum-free media was used as a cell migration negative control (NM). Basal migration experiments consisted of pre-treating the cells with NM or CM +/− EGCG 10 µM for 24 h and then allowing cells to migrate without chemoattractant (NM). In all cases, the impedance values were measured by the RTCA DP Instrument software and were expressed as Normalized Cell Migration Index. Each experiment was performed two times in triplicate.

3.4.13. Statistical Data Analysis

Data and error bars were expressed as mean ± standard error of the mean (SEM) of three or more independent experiments unless otherwise stated. Hypothesis testing was conducted using the Kruskal–Wallis test followed by a Dunn Tukey's post-test (data with more than 3 groups) or a Mann–Whitney test (two group comparisons). Probability values of less than 0.05 (*) or 0.01 (**) were considered significant and denoted in the figures. All statistical analyses were performed using the GraphPad Prism 7 software (San Diego, CA, USA).

3.5 Results

3.5.1 Transcriptomic Analysis of Human Adipocyte-Derived Mesenchymal Stem/Stromal Cell Response to Variations of the TNBC Secretome

In order to first identify the genes and molecular pathways involved in the acquisition of a CAA phenotype, human ADMSC were cultured for 24 h in conditioned media (CM) isolated from serum-starved TNBC-derived MDA-MB-231 cells (TNBC cells' secretome). Total RNA was isolated as described in the Methods section and submitted to RNA-Seq. We found 13,284 genes differentially expressed in both conditions (FDR < 0.05), from which roughly two thirds were downregulated in the presence of EGCG (Figure 3. 1A). Next, we selected genes with at least a two-fold change expression variation with respect to the control and a maximum corrected *p*-value of 0.001 to perform gene and pathway enrichment analysis. Using the previous criteria, we found 1331 differentially expressed genes (DEGs), among which 107 were up-regulated and 1224 were down-regulated. The DEGs were cross-referenced with actual protein–protein interactions to build active-subnetworks, onto which pathway enrichment analysis was performed to decipher which biological pathways were enriched in response to the TNBC cells' secretome. Among the pathways involved in the adaptive response of ADMSC to the TNBC cells' secretome, nine reached statistical significance below a *p*-value < 0.01 (Figure 3. 1B, left panel). The following ones were highlighted: nuclear factor-kappa B (NF-KB) signaling, cytokine-cytokine receptor interaction, pathways related to cytokine intracellular signaling such as the tumor necrosis factor (TNF)-α and TGFB, insulin resistance, breast cancer, central carbon metabolism in cancer, HIF-1A, and the interaction between advance glycation end products (AGE)- and their receptors (RAGE). Interestingly, the highlighted pathways have a significant degree of connectivity, with upregulated IL-6, IL-1, and other soluble cytokines acting as network hubs (Figure 3. 1C). In addition, ADMSC exposed to the TNBC cells' secretome acquired a pro-inflammatory phenotype. To

validate the CAA- and immunomodulatory-related genes found in our RNA-Seq experiment, an RT^2 Profiler RT-qPCR gene array was performed. The TNBC cell secretome induced more than 10-fold the expression of CAA genes identified from the RNA-Seq analysis. These included CCL2, CCL5, IL-1β, IL-6, and vascular endothelial growth factor alpha (VEGFα) (Figure 3. 1D). Other upregulated immunomodulatory genes included cytokines with a chemotactic role, such as C-X-C Motif Chemokine Ligand 5 and 8 (CXCL5 and CXCL8), and C-C motif ligand 20 (CCL20). In addition, mediators of the inflammatory response also included cyclooxygenase 2 (COX2), indoleamine 2,3-dioxygenase (IDO), programmed death-ligand 1 (PD-L1), IL-1β, and IL-6. These results confirm the DEG found in our transcriptomic analysis and demonstrate the effective induction of a CAA-like phenotype in ADMSC in response to the TNBC cells' secretome at the gene expression level.

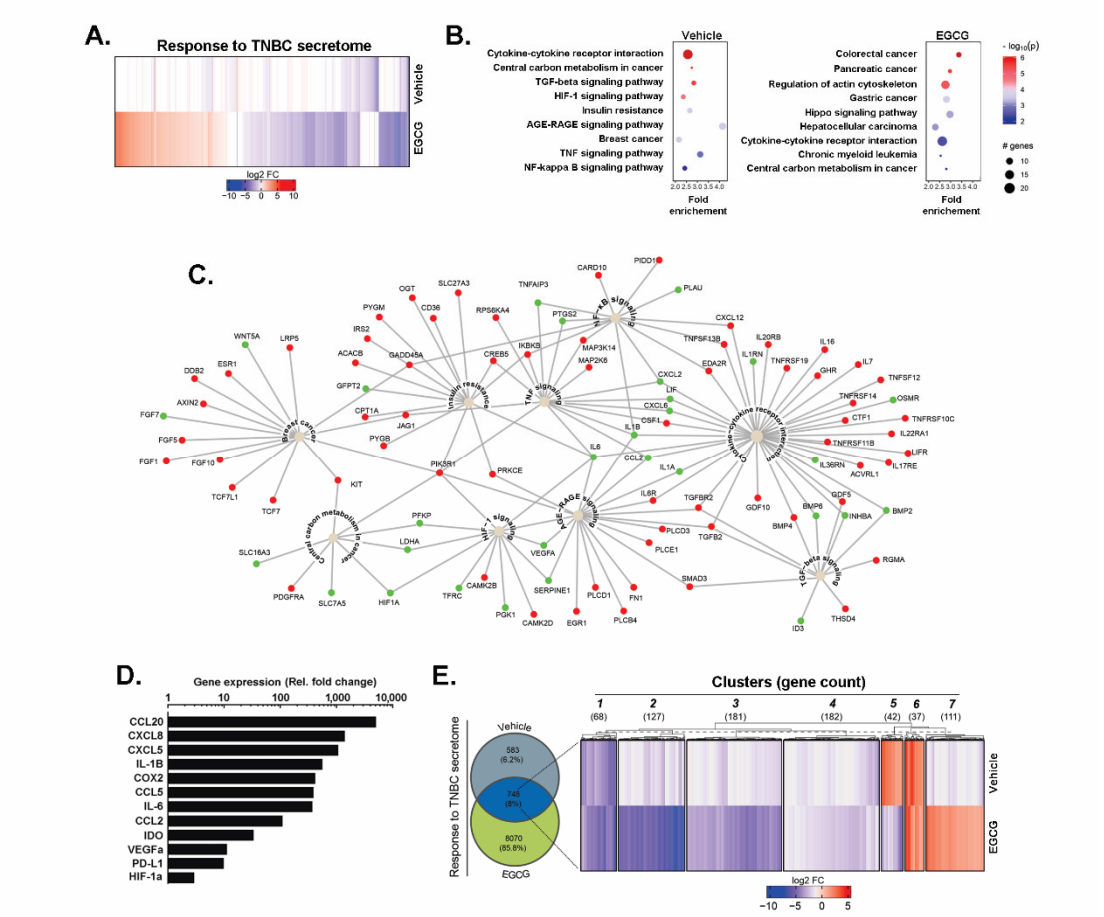

Figure 3. 1. Transcriptomic modulation of ADMSC (adipose-derived mesenchymal stem/stromal cell) response to variations of the TNBC cell secretome.
Human pre-adipocytes mesenchymal stem/stromal cells (ADMSC) were incubated for 24 h with serum-free media conditioned for 48 h by TNBC-derived MDA-MB-231 cells (TNBC cells' secretome) in the presence of 10 µM EGCG (epigallocatechin gallate) or Ethanol (vehicle). Total RNA was extracted from triplicate samples, and gene expression modulation was assessed through RNA-Seq analysis, as described in the Methods section. (**A**) Fold change gene expression compared to control cells considered below the significant threshold (FDR < 0.05) in the presence or absence of EGCG. (**B**) KEGG pathways enrichment analysis of differentially expressed genes (DEGs) with an absolute fold change (FC) > and adjusted p-value < 0.001 in each experimental condition. (**C**) Network graph showing enriched pathways and their respective DEGs in the absence of EGCG. Upregulated and downregulated genes are color-coded in green and red, respectively. (**D**) Expression of selected genes associated with cancer-associated adipocyte (CAA) phenotype and immunomodulation was confirmed by RT-qPCR, as described in the Methods section using a Human Cancer Inflammation and Immunity Crosstalk RT2-Profiler gene array kit. (**E**) Venn diagram

showing the number of DEGs in each experimental condition, followed by a robust k-means clustering visualized as a heatmap. Number of genes per cluster is shown in parenthesis. Representative genes shared in both conditions with a log2FC > 2 and p-value < 0.001. CCL20 (C-C motif ligand 20); CXCL8 and CXCL5 (C-X-C Motif Chemokine Ligand 8 and 5); IL-1_ and IL-6 (interleukin 1 beta and 6); COX2 (cyclooxygenase 2); CCL5 and CCL2 (chemokine C-C motif ligand 5 and 2); VEGFa (vascular endothelial growth factor alpha); IDO (indoleamine 2,3-dioxygenase); HIF1a (hypoxia inducible factor 1 alpha) and PD-L1 (programmed death-ligand 1).

3.5.2 EGCG Inhibits the Expression of Biomarkers Associated with the CAA Phenotype, Epithelial-to-Mesenchymal Transition, and Inflammatory Signaling Pathways induced by the TNBC Cell Secretome

Once the increase in expression of genes linked to a CAA phenotype was demonstrated, we analyzed the effect of EGCG on this adaptive response. ADMSC were incubated 24 h with the TNBC cell secretome in the presence of 10 μM of EGCG, vehicle (ethanol), or negative media (NM). After harvesting the cells and extracting the total RNA, we performed RNASeq and analyzed the output, as described in the Methods section. The cells incubated with NM were used as a control group. Gene and pathway enrichment analysis of the samples challenged with EGCG showed few common pathways compared to the control (Figure 3. 1B, right). Then, we restricted our analysis to those genes with a corrected p-value < 0.001 and an absolute FC greater than two. A Venn diagram depicting the percentage and absolute number of DEGs found in each condition was shown (Figure 3. 1E, left). The cells receiving EGCG had six times more DEGs than the vehicle-treated cells compared to the NM-treated cells. From the 8,818 genes modulated by EGCG, 8070 DEGs were unique to these samples, while 748 were present in both conditions. Our next goal was to identify and characterize the expression pattern of common DEGs. We performed a robust k-means clustering, identifying seven clusters based on the gene expression distribution in the samples (Figure 3. 1E, right). Genes from clusters 1–4 are downregulated in both samples, and their intra-cluster differences result from the magnitude and pattern of

downregulation. On the other hand, cluster 6 contained genes switched-on in both EGCG and vehicle-treated samples compared to NM-treated samples (Supplementary Figure S3. 1. Enrichment analysis of the DEGs in Cluster 6.). The most attractive genes were clustered in groups 5 and 7, with antagonizing expression patterns associated with CM. The EGCG inhibited the genes assigned to cluster 5, which, according to gene ontology (GO) enrichment analysis using an FDR < 0.05 corresponded to growth factors, intracellular signaling molecules and modification enzymes with acyltransferase activity (Supplementary Figure S3. 2). The genes listed in Table 3. 1 evidenced the antagonist effect of EGCG over the CM-mediated induction of genes associated with cholesterol and lipid biogenesis (HMGCS1, HMGCR, IDI1, STARD4, GPAM, and ACSL4), proliferation (PID1, BMP6, and FGF7), invasion and metastasis (PLOD2, MMP1, CEMIP2, PAPPA, COL8A1, and ADAM12), glucose transport (STEAP1, STEAP2), cell survival and oncogenesis (CCN4, WNT5A, and FGF7), and vesicular trafficking (RAB27B, TRFC). Surprisingly, the genes from cluster 7 could not be associated statistically with a particular protein class or molecular functions. More detailed information on all shared genes is provided as a supplementary EXCEL data sheet (Supplementary Table S3. 1).

Following the transcriptomic RNA-Seq analysis, RT-qPCR was performed to validate the inhibition of key CAA markers in ADMSC upon treatment with the TNBC cell secretome in the presence or absence of 10 μM EGCG. The addition of EGCG reduced or completely abrogated the induction of CCL2, CCL5, CXCL8, IL-1β, IL-6, VEGFα, HIF-1α, COX2, and IDO (Figure 3. 2A, black bars), while it did not affect that of PD-L1. In addition to altering ADMSC gene expression plasticity, we assessed the chemotactic response of ADMSC to TNBC cells' secretome by a real-time cell migration assay. An increased ADMSC migration index was observed in response to the direct exposure to TNBC cells' secretome (Figure 3. 2B, black circles), or when ADMSC were cultured for 24 h with it (conditioned ADMSC) and then left to migrate without chemoattractant (Figure 3. 2C, black circles). EGCG prevented the induced chemotactic (Figure 3. 2B) or acquired response (Figure 3. 2C) in both scenarios.

Table 3. 1. The effect of EGCG (epigallocatechin gallate) over Cluster 5 genes upregulated by the TNBC secretome.

ENSEMBL	Gene	FC Vehicle vs. Control	FC EGCG vs. Control	Gene Description	Enriched Terms by KEGG Analysis *
ENSG00000122641	INHBA	5.36	−2.51	Follicle-Stimulating Hormone-Releasing Protein/secreted	- TGF-beta signaling pathway - Signaling pathways regulating pluripotency of stem cells - Cytokine-cytokine receptor interaction - Associated with cancer cachexia in human patients *
ENSG00000152952	PLOD2	4.51	−4.00	2 procollagen-lysine/cisternae of the RER.	- Collagen formation and degradation of the extracellular matrix * - Oxidoreductase activity *
ENSG00000170961	HAS2	4.25	−2.99	Hyaluronan synthase 2 Polysaccharide/extracellular matrix	- Glycosaminoglycan metabolism * - Hyaluronan synthase activity *
ENSG00000105835	NAMPT	3.94	−1.54	Nicotinamide phosphoribosyltransferase; enzime	- NOD-like receptor signaling pathway - Cytokine with immunomodulating properties * - Adipokine with anti-diabetic properties * - Stress response *
ENSG00000104321	TRPA1	3.87	−4.76	Transient receptor potential cation channel, subfamily a/transmembrane proteins	- Regulation of TRP channels - Signal transduction * - Growth control *
ENSG00000112972	HMGCS1	3.73	−2.37	3-α-hydroxy-3-methylglutaryl-coa synthase 1/	- PPAR signaling pathway - Terpenoid backbone biosynthesis - Cholesterol and lipid homeostasis *
ENSG00000196611	MMP1	3.68	−1.80	Matrix metalloproteinase 1/interstitial collagenase	- PPAR and relaxin signaling pathway - Calcium ion binding * - Metallopeptidase activity *
ENSG00000067064	IDI1	3.56	−2.33	Isopentenyl-diphosphate delta isomerase	- Terpenoid backbone biosynthesis - Regulation of cholesterol biosynthesis *

				1/peroxisomally-localized enzyme	- mTOR signalling *
ENSG00000041353	RAB27B	3.40	−6.85	Member RAS oncogene family/membrane-bound proteins involved in vesicular fusion and trafficking	- Vesicular fusion and trafficking * - Autophagy pathway and metabolism of proteins * - GTP binding and protein domain specific binding *
ENSG00000104415	CCN4	3.39	−2.87	Wnt1-inducible signaling pathway protein 1/	- WNT1 signaling pathway - Associated with cell survival *
ENSG00000157214	STEAP2	3.39	−2.92	Six-transmembrane epithelial antigen of prostate/metalloreductase localized in Golgi complex, plasma membrane, and in the cytosol.	- Mineral absorption - Transport of glucose and other sugars, bile salts, and organic acids *
ENSG00000164211	STARD4	3.14	−2.38	Start domain-containing protein 4	- Metabolism of steroid hormones * - Lipid binding *
ENSG00000119927	GPAM	3.13	−4.02	Glycerol-3-phosphate acyltransferase/Mitochondrial	- Regulation of cholesterol biosynthesis * and triacylglycerol biosynthesis. - Acyltransferase activity *
ENSG00000120437	ACAT2	3.11	−2.60	Acetyl-coa acetyltransferase 2/cytosolic	- Terpenoid backbone biosynthesis - Acyltransferase activity *
ENSG00000171208	NETO2	3.09	−1.57	Neuropilin- and tolloid-like 2/transmembrane protein	- Ionotropic glutamate receptor binding in the brain *
ENSG00000153823	PID1	3.00	−1.64	Phosphotyrosine interaction domain-containing 1	- Proliferation of preadipocytes without affecting adipocytic differentiation *
ENSG00000153162	BMP6	2.89	−2.05	Bone morphogenetic protein 6	- Secreted ligand of the TGF-beta superfamily of proteins * - Growth factor activity *
ENSG00000164647	STEAP1	2.80	−2.36	Six-transmembrane epithelial antigen of	- Mineral absorption (copper homeostasis) - Glucose/energy metabolism *

				prostate 1/cell surface antigen significantly expressed at cell-cell junctions.	- Oxidoreductase activity and channel activity *
ENSG00000135048	CEMIP2	2.76	−2.24	Cell migration inducing hyaluronidase 2/transmembrane protein	- Regulator of angiogenesis and VEGF signaling *
ENSG00000113161	HMGCR	2.70	−2.13	3-@hydroxy-3-methylglutaryl-coa reductase/rate-limiting enzyme for cholesterol synthesis	- AMPK signaling pathway - Terpenoid backbone biosynthesis. - Cholesterol and lipid homeostasis * - Protein homodimerization activity and NADP binding *
ENSG00000114251	WNT5A	2.70	−2.10	Wingless-type mmtv integration site family/secreted signaling proteins	- Wnt and Hippo, signaling pathway - Oncogenesis*: Hepatocellular carcinoma, breast cancer and basal cell carcinoma Signaling pathways regulating pluripotency of stem cells - Cushing syndrome - DNA-binding transcription factor activity and protein domain specific binding *
ENSG00000182752	PAPPA	2.67	−1.72	Pregnancy-associated plasma protein/secreted metalloproteinase	- Metabolism of proteins * - Regulation of Insulin-like Growth Factor (IGF) transport * - Metalloendopeptidase activity *
ENSG00000125845	BMP2	2.61	−2.26	Bone morphogenetic protein 2/regulatory element: cis-acting enhancer	- Protein heterodimerization activity * - Cytokine activity *
ENSG00000144810	COL8A1	2.60	−2.67	Collagen, type VIII	- Migration and proliferation of vascular smooth muscle cells *
ENSG00000140416	TPM1	2.40	−3.17	Tropomyosin 1/actin-binding proteins involved in the contractile system of muscles	- Hypertrophic cardiomyopathy - Dilated cardiomyopathy - Cytoskeletal protein binding *

ENSG00000068366	ACSL4	2.34	−5.44	acyl-coa synthetase long chain family	- PPAR signaling pathway. - Lipid biosynthesis and fatty acid degradation *
ENSG00000140285	FGF7	2.30	−5.16	Fibroblast growth factor 7	- Regulation of actin cytoskeleton - Melanoma, gastric and breast cancer - Rap1, Ras and MAPK signaling pathway - Growth factor activity * - Chemoattractant activity *
ENSG00000072274	TFRC	2.07	−2.52	Transferrin receptor/ cell surface receptor	- HIF-1 signaling pathway - Receptor-mediated endocytosis - Clathrin derived vesicle budding *
ENSG00000100644	HIF1A	2.05	−5.07	Hypoxia-inducible factor 1, alpha subunit	- HIF-1 signaling pathway - Central carbon metabolism in cancer - PD-L1 expression and PD-1 checkpoint pathway in cancer - Kaposi sarcoma-associated herpesvirus infectio - Th17 cell differentiation - Thyroid hormone signaling pathway - Proteoglycans in cancer - Choline metabolism in cancer - Autophagy - Renal cell carcinome
ENSG00000148848	ADAM12	2.02	−3.54	A disintegrin and metalloproteinase domain 12	- Cell-cell and cell-matrix interactions * - Metallopeptidase activity *

FC: Fold Change; KEGG: Kyoto Encyclopedia of Genes and Genomes; GO: Gene Ontology; GC GeneCards; RER: rough endoplasmic reticulum; NOD: nucleotide-binding oligomerization domain; PPAR: peroxisome proliferator-activated receptors; mTOR: mechanistic target of rapamycin; GTP: guanine nucleotide-binding proteins; WNT1: wingless-type MMTV integration site family, member 1; TGF-beta: transforming growth factor beta; Rap1: Ras-proximate-1; MAPK: mitogen-activated protein kinase; and JAK-STAT: Janus kinase (JAK)-signal transducer and activator of transcription (STAT).

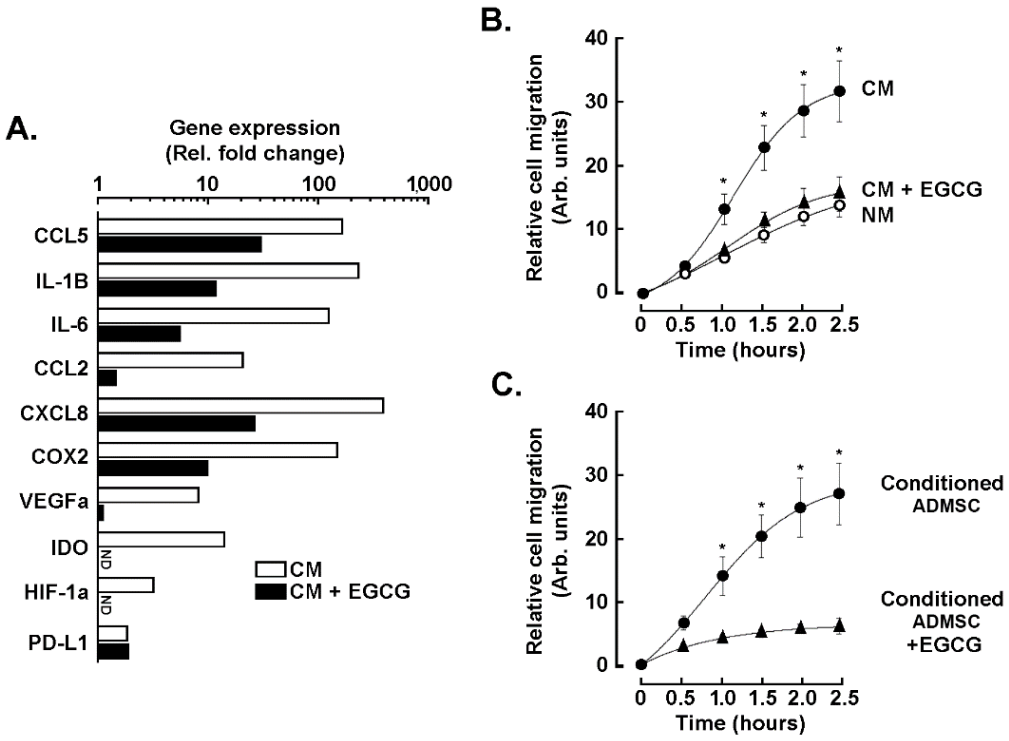

Figure 3. 2. EGCG alters the acquisition of a CAA (cancer-associated adipocyte) phenotype and chemotactic response.
(**A**) ADMSC response to TNBC cells' secretome was monitored after 24 h in vehicle-treated cells (white bars), or in the presence of 10 μM EGCG (black bars). Total RNA was isolated, cDNA was synthetized, and the induction of CAA genes was evaluated using a RT2-Profiler RT-qPCR gene array kit. A representative experiment out of two screens is shown. (**B**) Relative cell migration rate of ADMSC in response to TNBC cells' secretome (CM, closed circles), CM with 30 μM of EGCG (closed triangles), or serum-free negative media (NM, open circles). (**C**) Basal cell migration response: ADMSC were treated for 24 h with CM (closed circles) or in the presence of CM supplemented 10 μM EGCG (closed triangles); then, basal cell migration was assessed. Data are representative from two independent experiments performed in triplicate. (ND, not detectable). Statistical differences were determined with a Mann–Whitney two tail test with a $p < 0.05$ (*). CCL5 and CCL2 (chemokine C-C motif ligand 5 and 2); IL-1_ and IL-6 (interleukin 1 beta and 6); CXCL8 (C-X-C motif chemokine ligand 8); COX2 (cyclooxygenase 2); VEGFa (vascular endothelial growth factor alpha); IDO (indoleamine 2,3-dioxygenase); HIF1a (hypoxia inducible factor 1 alpha) and PD-L1 (programmed death-ligand 1).

3.5.3 The Epithelial-to-Mesenchymal Transition (EMT) Contributes to the CAA-induced Phenotype in ADMSC

We found a robust induction of the transcription factors Slug and Snail and of the pro-inflammatory cytokine IL-6 at the protein level (Figure 3. 3A). As expected, EGCG reduced their expression by at least 50% (Figure 3. 3B). Complementing our transcriptomic results, we also found a CM-dependent activation of signaling cascades involving the phosphorylation of NF-KB and SMAD2 transcription factors (Figure 3. 3A), which was reduced in the presence of EGCG (Figure 3. 3B).

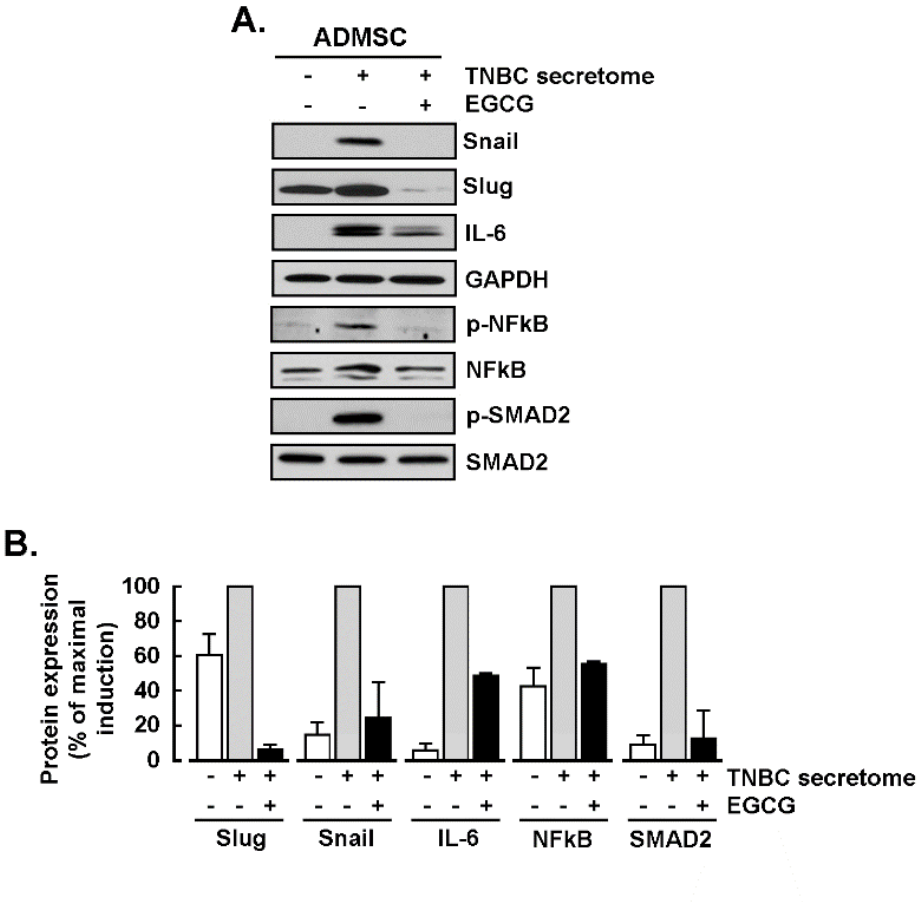

Figure 3. 3. EGCG inhibits the induction of the pro-inflammatory cytokine IL-6, epithelial-to-mesenchymal transition (EMT) markers, and NF-κβ and SMAD2 signal transducing pathways.

ADMSC were incubated for 24 h with the TNBC cells' secretome and protein lysates collected, as described in the Methods section for Western blotting. (**A**) Immunoblotting of Snail, Slug, IL-6, and the phosphorylated and total forms of NF-κβ and SMAD2 (20 µg of protein/well). (**B**) Representative densitometric analysis of Snail, Slug, IL-6, and the ratio of phosphorylated/total forms of NF-κβ and SMAD2. Data are expressed as the percent of maximal effect for each marker in ADMSC treated with the TNBC cell secretome (grey bars). Cells treated with negative media (NM, white bars) and TNBC cell secretome in the presence of 10 µ EGCG (black bars). Data are representative of three independent experiments. Snail (Snail family transcriptional repressor 1); Slug (Snail family transcriptional repressor 2); IL-6 (Interleukin 6); NF-KB (nuclear factor kappa beta); SMAD2 (mothers against decapentaplegic homolog 2); GAPDH (glyceraldehyde 3-phosphate dehydrogenase).

3.5.4 Snail as a Crucial Intermediate in the Upregulation of CAA Genes in Response to TNBC Cell Secretome

Since incubation of the ADMSC with the TNBC cells secretome triggered expression of the EMT biomarker Snail, we investigated its contribution to regulating other CAA genes. We silenced SNAIL in ADMSC using siRNA (siSnail) and then exposed these cells to the TNBC cells' secretome for 24 h. Our siRNA efficiently reduced Snail transcript and protein expression (Figure 3. 4A, B) and impaired the production of CAA genes, except for VEGFα and HIF-1α (Figure 3. 4C). This suggests that selective Snail-mediated transcriptional control is involved in the transcriptional regulation of CAA genes in ADMSC in response to TNBC cells' secretome.

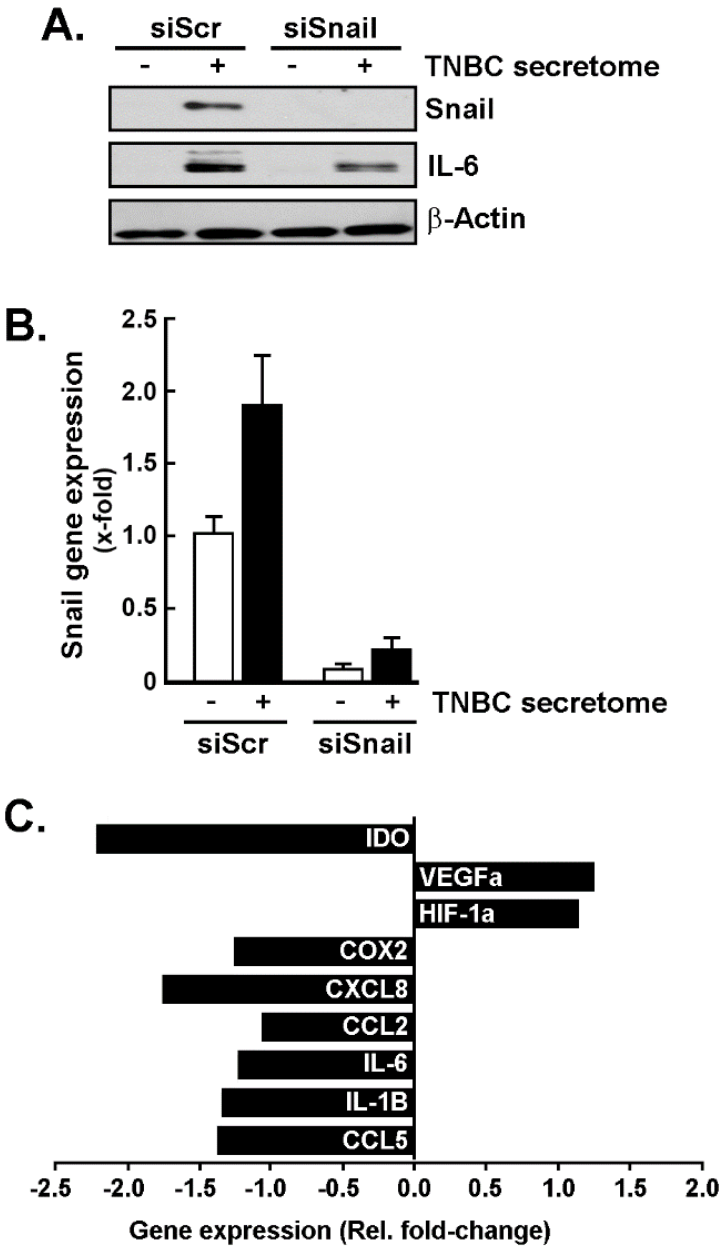

Figure 3. 4. Role of Snail in the upregulation of the CAA phenotype genes.
Transient gene silencing of Snail (siSnail) or of control (siScrambled) was performed in ADMSC, followed by an incubation with the TNBC cells' secretome for 24 h. Cell lysates and total RNA were isolated, and levels of protein and gene expression assessed by Western blotting and RT-qPCR, respectively. (**A**) Protein levels of Snail and IL-6 were assessed by immunoblotting in ADMSC transfected with siScr or siSnail. (**B**) Snail gene expression was evaluated by RT-qPCR in ADMSC transfected with siScr

or siSnail and treated with TNBC cell secretome (black bars) or negative media (white bars). (**C**) CAA gene expression resulting from the comparison of ADMSC transfected with siSnail in response to the TNBC cell secretome vs. siScr cells incubated with the same CM (reference group).

3.5.5 The TNBC-Derived MDA-MB-231 Secrete High Levels of IL-6

Our bio-informatics analysis revealed a strong activation of the cytokine-receptor interaction pathway in the ADMSC response to the TNBC cell secretome (Figure 3. 1). This suggests a contribution of the cytokines secreted by the TNBC cell-derived MDA-MB-231 to the phenotypic modification and chemotaxis of ADMSC. Using a protein cytokine array, we aimed to identify the main cytokines present in the CM upon 24 and 48 h of serum starvation. IL-6 was identified as the preponderant cytokine present in the CM, followed by VEGFα, and to a lesser extent IL-1β, epithermal growth factor (EGF), and transforming growth factor beta (TGFB) (Figure 3. 5A). Interestingly, exogenous addition of IL-6 to ADMSC triggered a biphasic chemotactic dose-response, with the maximal migration rate observed at 10 pg/mL (Figure 3. 5B). This suggests that ADMSC are responsive to both the autocrine and paracrine effects of IL-6.

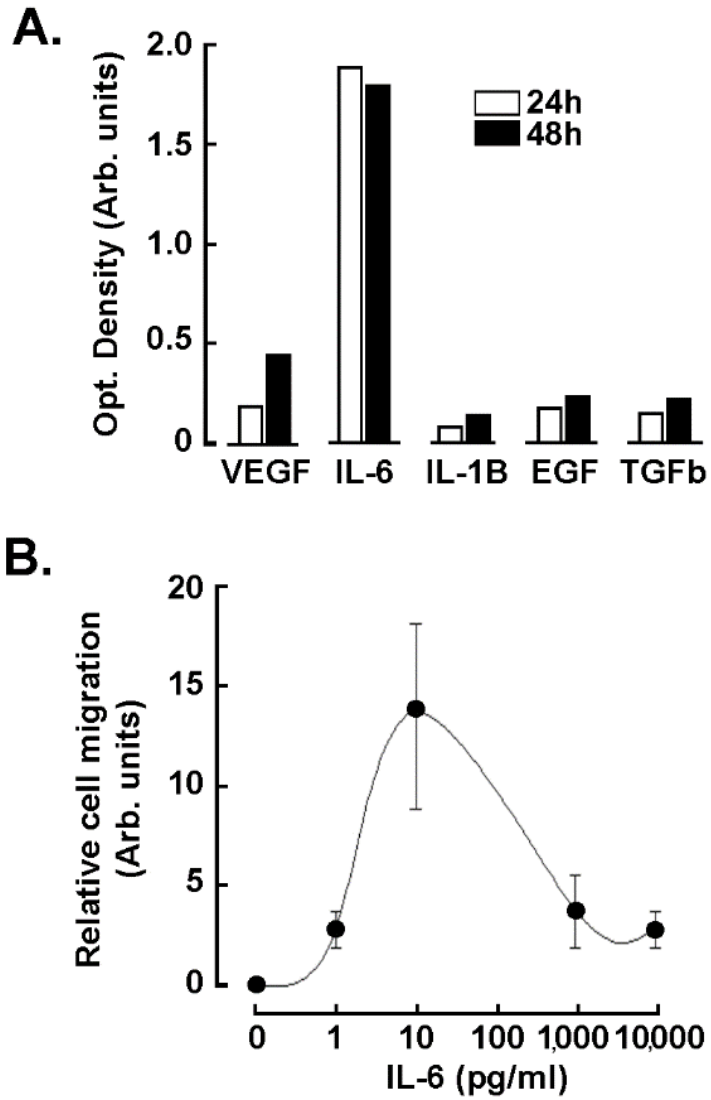

Figure 3. 5. Cytokine levels present in the TNBC cells' secretome.
(**A**) Human TNBC-derived MDA-MB-231 cells were cultured for 24 h (white bars) and 48 h (black bars) in serum free media, and then their respective secretome collected and the cytokine concentrations determined using an ELISA array as described in the Methods section. (**B**) IL-6-mediated chemotaxis of ADMSC was assessed in real time, as described in the Methods section using the exCELLigence system (one out of three independent experiments is shown).

3.5.6 The IL-6 Secreted by the TNBC-Derived MDA-MB-231 Is Required for the Chemotactic Response of the ADMSC but Does not Trigger the CAA Phenotype

To test the role of IL-6 in the chemotactic response of the ADMSC to the TNBC cell secretome, we depleted the CM from IL-6 by immunoprecipitation (CM, Figure 3. 6A). This inhibited ADMSC chemotaxis as we compared the chemotactic capacity of IL-6 immunoprecipitated from the TNBC cell secretome (Figure 3. 6B, black triangles) to that of the CM immunoprecipitated with an IgG isotype control (Figure 3. 6B, black circles). In another approach, IL-6 was silenced in TNBC-derived MDA-MB-231 cells (Figure 3. 6C, left), and then CM harvested upon 24 h of incubation with serum-deprived culture media. Reduced IL-6 concentration was confirmed by ELISA (Figure 3. 6C, right), and the reduced level of IL-6 negatively impacted the ADMSC chemotactic response (Figure 3. 6D). Altogether, these results suggest that IL-6 exerts a significant role in ADMSC mobilization in response to TME cues.

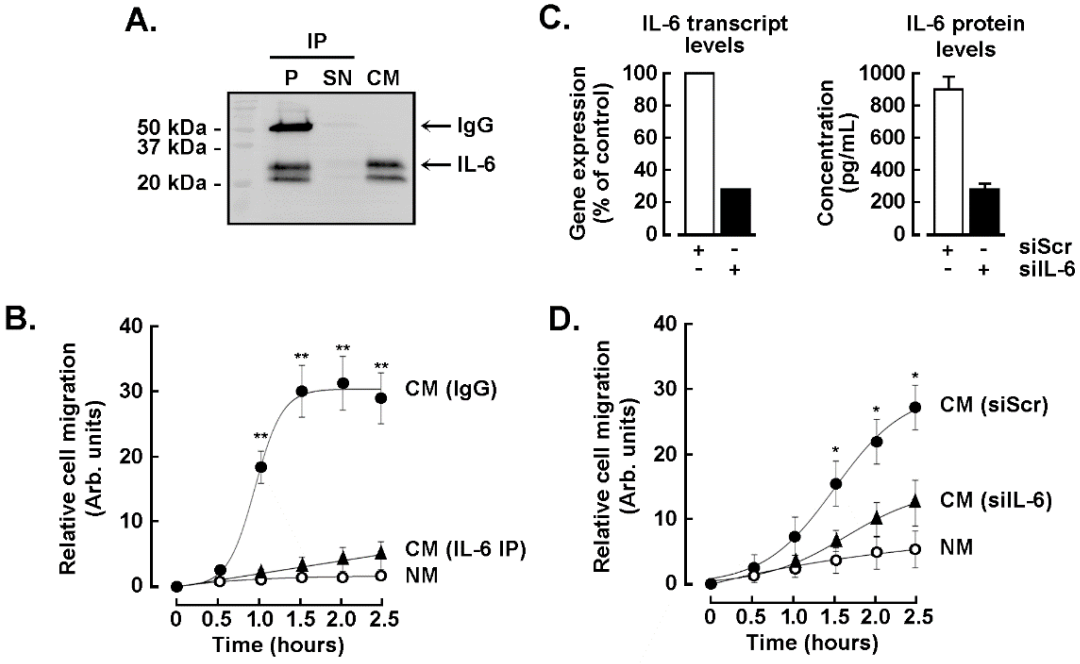

Figure 3. 6. Role of IL-6 in the ADMSC chemotactic response to the TNBC cell secretome.

MDA-MB-231 cells were cultured in serum free media for 48 h and the conditioned media harvested (TNBC cell secretome). (**A**) Immunoprecipitation (IP) of IL-6 from the TNBC cell secretome was performed as described in the Methods section. The efficiency of the IP was evaluated by immunoblotting of the pellet (P), supernatant (SN), or of the conditioned media before the IP (CM). IgG indicates the heavy chain of the anti-IL-6 antibody used for the IP. (**B**) Chemotactic response of the ADMSC in response to negative media (open circles), to CM upon control IgG isotype IP (closed circles), or to CM upon anti-IL-6 IP (closed triangles). (**C**) Transient gene silencing of IL-6 was performed in MDA-MB-231 cells as described in the Methods section. Control cells were transfected with siRNA-Scrambled (siScr). Cells were then serum starved for 24 h. Total RNA was extracted, and RT-qPCR performed to monitor IL-6 silencing efficiency (left). CM was collected to assess secreted IL-6 levels using an ELISA. (**D**) ADMSC chemotactic response to TNBC cell secretome was monitored in CM harvested from siScr-transfected MDA-MB-231 cells (closed circles), CM harvested from siIL-6-transfected cells (closed triangles), or in response to negative media (NM, open circles). One out of two independent experiments performed in triplicate is shown. Statistical differences were determined with a Mann–Whitney two tail test with a $p < 0.05$ (*) or $p < 0.01$(**).

Lastly, we inquired about the extent to which IL-6 contributed to the paracrine upregulation of Snail, autocrine regulation of IL-6, and the signal-transducing pathways activated upon the response to TNBC cells' secretome. ADMSC were thus treated for 24 h with IL-6 at 10 pg/mL, a concentration corresponding to its maximal chemotactic effect, and at 10 ng/mL that corresponded to the naturally occurring concentration of IL-6 in the TNBC cells' secretome (data not shown). Cells were harvested and protein lysates prepared to detect the CAA signature. Unexpectedly, neither Snail nor IL-6 were induced by both of the IL-6 concentrations tested (Figure 3. 7A). However, when ADMSC were incubated with IP-CM (IgG isotype control vs. anti-IL-6 mAb), the IL-6 depleted-CM still induced Snail and IL-6 expression as well as activated the NF-κB and SMAD2 pathways to the same extent as the control IP-CM did (Figure 3. 7B). This suggests that, although Snail controls the acquisition of a CAA phenotype, and that IL-6 is involved in the chemotactic response of ADMSC (Figure 3. 7B), unknown factors within the TNBC cells' secretome, beyond IL-6, are involved in the acquisition of the CAA phenotype in ADMSC.

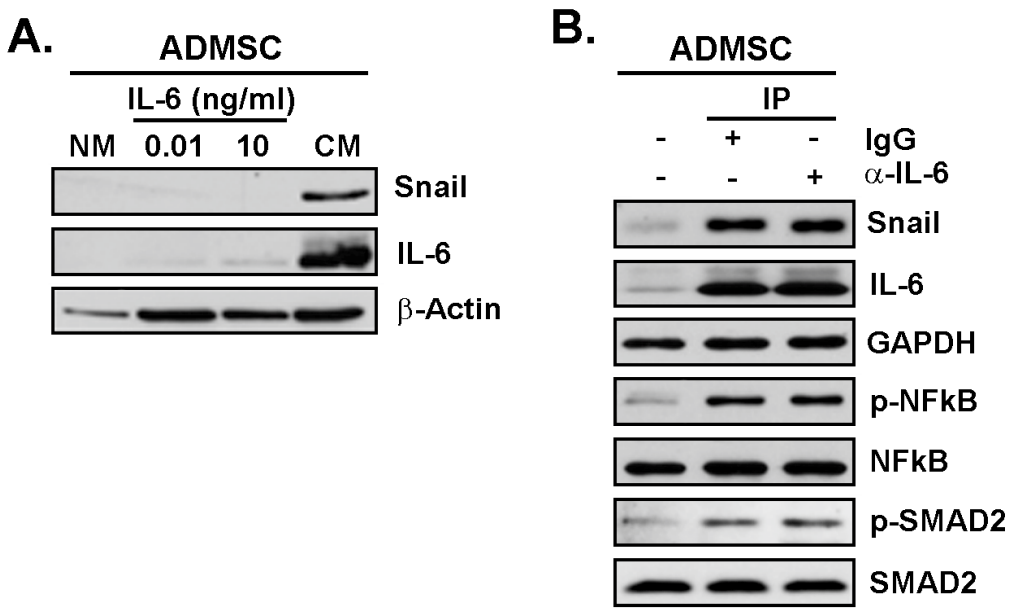

Figure 3. 7. IL-6 is not sufficient to trigger the CAA phenotype in ADMSC.
(**A**) ADMSC were incubated **A**) ADMSC were incubated for 24 h with negative media (NM), TNBC cell-derived secretome (MDA-MB-231 conditioned media, CM), or 10 pg/mL or 10 ng/mL IL-6 in NM. Cell lysates were next isolated and protein expression of Snail, IL-6, and β-Actin assessed by immunoblotting. (**B**) Immunoblots showing the phosphorylation status of SMAD2 and NF-κB, and the expression of Snail and IL-6 in cells treated with NM, IL-6-IP depleted media (αIL-6), or IgG isotype-IP control media (IgG). Data are representative of one experiment out of two.

3.6 Discussion

The TME is a highly dynamic niche composed of multiple cell types constantly interacting with each other. Accordingly, tumor cells can recruit not only immune cells but also those cells residing from adjacent tissues like the adipose tissue (Catalan *et al.*, 2013). The adipose tissue is predominant within the breast anatomy, and its endocrine functions recognized to support tumor cells at their early stages of malignant transformation (Cozzo *et al.*, 2017). To understand the role of adipocytes in tumor progression, previous studies have co-cultured human breast cancer cells with human mature adipocytes (D'Esposito *et al.*, 2016; Dirat *et al.*, 2011; Picon-Ruiz *et al.*, 2016), leading to an increase in the invasiveness of the cancer cells, and the onset of a pro-inflammatory state characterized by the induction of cytokines such as IL-6, IL-1β, and CCL5 (D'Esposito *et al.*, 2016; Picon-Ruiz *et al.*, 2016). Histological analysis of human breast tumors has shown that the adipocytes present at their invasive front also expressed high levels of MMP-11 and IL-6, in contrast to adipocytes from healthy tissues where these proteins are absent (Dirat *et al.*, 2011). This suggests a transducing mechanism that transitions from a healthy adipocyte to a CAA phenotype. Therefore, our findings support that TNBC cells can also mobilize and promote the reprogramming of undifferentiated ADMSC with inflammatory and CAA-like phenotypes. This finding is particularly relevant in the context of obesity, where the abnormal extent of the adipose tissue provides a substantial source of inflammatory cytokines for neoplasms (Picon-Ruiz *et al.*, 2017), and where ADMSC as well as early-stages of adipocyte maturation may also contribute.

Here, the TNBC cells' secretome triggered significant chemotaxis in ADMSC and induced a pro-inflammatory phenotype characterized by the overexpression of IL-1β, COX2, VEGFα, and IL-6 among other immunomodulators, as well as a CAA phenotype including the induction of CCL2 and CCL5. These results were further supported herein by the identification of signaling pathways such as NF-κB, HIF-1α, and AGE-RAGE, all induced as highlighted from the bio-informatics analysis, and

where the upregulation of IL-6 connected pathways was modulated by obesity-like insulin resistance, TNF signaling, AGE-RAGE, and cytokine-receptor interaction (Figure 3. 1). Such evidence at early stages of adipocyte maturation is supported by data showing that ADMSC were primed and permanently altered by tumor presence in breast tissue, resulting in increased tumor cell invasiveness (Plava *et al.*, 2020). Interestingly, our data support these studies as the EMT biomarker Snail is induced in ADMSC in response to the soluble factors present in the MDA-MB-231 CM. More importantly, Snail induction was proved to be essential for sustained upregulation of IL-6, IL-1β, CCL2, and CCL5.

Despite its abundance in the TNBC cells' secretome and its clear contribution to the ADMSC chemotaxis, exogenous addition of IL-6 failed to switch on its autocrine upregulation of Snail. Remarkably, EGCG acted as a potent inhibitor of the pro-inflammatory state triggered by the TNBC cells' secretome, generating a robust inhibition of CAA markers and pro-inflammatory cytokines. This role for EGCG was partially attributed to reduced induction of Snail. Furthermore, EGCG decreased the chemotactic potential of the TNBC cells' secretome and inhibited the activation of the NF-κB and SMAD2 signaling cascades.

The pathway involving HIF-1α, classically activated by low oxygen concentrations (hypoxia), upregulates the expression of pro-angiogenic and mitogenic cytokines such as leptin and VEGFα while reducing the levels of the antimitogenic adipokine adiponectin (Trayhurn, 2013). Harvesting of the TNBC-cells-derived secretome through cell culture serum starvation is typically reflected by enriched lactate levels, which has been proposed to mimic a biochemical "perception" of hypoxia regardless of the level of oxygen, leading to the secretion of angiogenic and inflammatory growth factors/cytokines (Trabold *et al.*, 2003). Besides the increased HIF-1α observed in ADMSC, our transcriptomic screen identified the AGE-RAGE pathway, which may play an important role in acquiring the CAA phenotype; oxidative stress; and activation of the SMAD2 and NF-κB signaling, thus leading to the secretion of inflammatory cytokines and growth factors (Asadipooya and Uy, 2019; Chawla *et*

al., 2014; Tornatore *et al.*, 2012). Interestingly, adipose tissue inflammation occurs in obesogenic conditions due to hypoxia and is thought to originate from enlarged adipocytes distant from the vasculature (Trayhurn *et al.*, 2008). Furthermore, hypoxia has now been directly demonstrated to occur in adipose tissue of several obese mouse models (*ob/ob*, KKAy, diet-induced) and to lead to increased HIF-1α levels (Trayhurn, 2013; Trayhurn *et al.*, 2008).

Our experimental approach exploits the paracrine up-regulation of CCL2, CCL5, IL-1β, and IL-6 in ADMSC in response to TNBC cell secretome, confirming and complementing prior co-culture approaches mixing cancer cells and adipocytes (D'Esposito *et al.*, 2016; Dirat *et al.*, 2011). In addition, relevant cytokines for acquiring a tumor malignancy phenotype, such as CCL5/RANTES, have also been shown to increase cell motility and invasiveness in high-glucose culture conditions (D'Esposito *et al.*, 2016). Interestingly, such conditions mimic the adaptive cellular responses triggered during the onset of insulin resistance associated with obesity. Nevertheless, we still need validation at protein levels for all the genes found in our transcriptomic analysis, those including IL-6, IL-1β, CCL2, CXCL2, and HIF-1α were present in our dataset and bridged several pathways associated with pro-tumoral roles.

On the other hand, we validated the autocrine induction of IL-6 in ADMSC, both at gene and protein levels. Paradoxically, despite ADMSC producing IL-6 after incubation with the TNBC cell secretome, this was not a direct response to paracrine IL-6. One must conclude that irrespective of its massive levels in the CM, the IL-6 paracrine induction certainly requires a combination of stimuli. Noteworthily, the production of IL-6 by ADMSC exposed to the TNBC cell secretome depended on Snail expression. This signaling interplay between Snail and IL-6 has been proposed in myofibroblast trans-differentiation during oral submucosal fibrosis, a premalignant disorder of the oral cavity (Peng *et al.*, 2020).

Once we identified the main upregulated genes and pathways involved in the acquisition of the CAA phenotype in ADMSC in response to the TNBC cell secretome, we investigated the impact of EGCG. This catechin is known to modulate molecular

targets and signaling pathways associated with cell survival, proliferation, differentiation, migration, angiogenesis, hormone activities, detoxification enzymes, and immune response (Chokor *et al.*, 2014; Djediai *et al.*, 2021; Sicard *et al.*, 2021; Zgheib *et al.*, 2013; Zhou *et al.*, 2016). Our differential transcriptomic analysis performed in ADMSC treated in the presence or absence of EGCG revealed six times more modulated genes in samples treated with EGCG (92%, 8070 DEGs). The presence of EGCG drastically reduced the expression of genes encoding growth factors, intracellular signaling intermediates, and cytokines, all of which prevented the acquisition of a CAA-like phenotype.

3.7 Conclusions

The present study revealed EGCG's ability to inhibit the chemotactic properties of the TNBC cells' secretome, primarily through NF-κB and SMAD2 signal-transducing pathways, suggesting that a diet-derived intervention could efficiently alter the signaling crosstalk that links TNBC cells to the CAA phenotype within the adipose tissue environment. Most importantly, our study presents evidence that EGCG can efficiently target the CAA-like phenotype of ADMSC and prevent the onset of a TME that would favor breast cancer development.

3.8 Supporting information

Supplementary Figure S3.1

A.

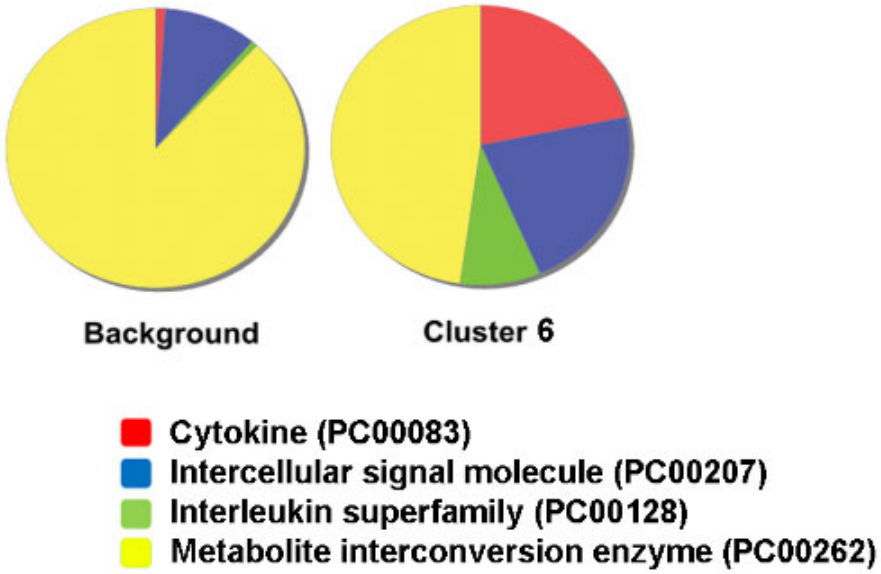

B.

PANTHER Protein Class	Fold Enrichment	FDR
Cytokine	100	1.23E-06
Intercellular signal molecule	11.43	8.10E-03
Interleukin superfamily	67.66	4.03E-02
Metabolite interconversion enzyme	2.88	4.54E-02
GO Molecular Function		
Cytokine activity	23.60	1.04E-03
Cytokine receptor binding	12.53	1.60E-02

Supplementary Figure S3. 1. Enrichment analysis of the DEGs in Cluster 6.
A) Pie charts of protein class variation after a GO enrichment analysis showing the behavior of background genes and genes clustered in 6. **B)** Fold enrichment values for protein class and molecular functions with a FDR ≤0.05 as a cut off, and using as background all genes detected.

Supplementary Figure S3.2

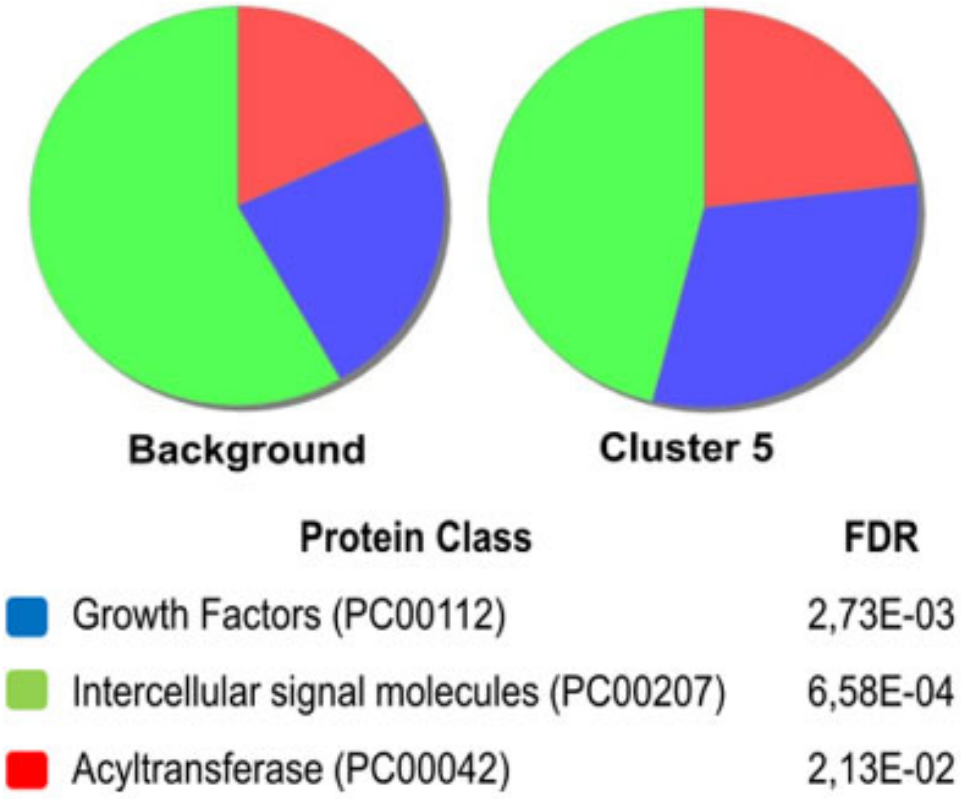

Supplementary Figure S3. 2. Gene ontology (GO) enrichment analysis results of genes from cluster 5.
Pie chart of protein class variation with a false discovery rate (FDR) ≤0.05 as a cutoff, and using all genes detected as background.

Supplementary Table S3.1

Supplementary Table S3. 1. List of the shared DEGs (748 genes) identified within the ADMSC treated with CM or CM+EGCG, with a p-value < 0.001.

ENSEMBL	Gene	CM (FC)	CM + EGCG (FC)	Cluster	Genes minimal description
ENSG00000196616	ADH1B	-1.04	-5.99	Cluster 1	Alcohol dehydrogenase 1b
ENSG00000145242	EPHA5	-2.82	-4.91	Cluster 1	Ephrin receptor 5
ENSG00000101265	RASSF2	-2.88	-4.85	Cluster 1	Ras association domain family protein 2
ENSG00000178573	MAF	-3.16	-4.35	Cluster 1	Zip transcription factor
ENSG00000013297	CLDN11	-3.20	-4.48	Cluster 1	Claudin 11, oligodendrocyte transmembrane protein
ENSG00000116117	PARD3B	-3.21	-4.87	Cluster 1	Par-3 family cell polarity regulator beta
ENSG00000164342	TLR3	-3.22	-4.72	Cluster 1	Toll-like receptor 3
ENSG00000137727	ARHGAP20	-3.29	-4.18	Cluster 1	RHO GTPase-activating protein 20
ENSG00000151322	NPAS3	-3.31	-5.15	Cluster 1	Neuronal pas domain protein 3
ENSG00000136040	PLXNC1	-3.43	-5.07	Cluster 1	Plexin c1, virus-encoded semaphorin protein receptor
ENSG00000239474	KLHL41	-3.44	-4.49	Cluster 1	Kelch-like 41
ENSG00000156486	KCNS2	-3.46	-4.68	Cluster 1	Potassium channel, voltage-gated
ENSG00000126860	EVI2A	-3.46	-5.65	Cluster 1	Ecotropic viral integration site 2a
ENSG00000162981	LRATD1	-3.48	-4.07	Cluster 1	Family with sequence similarity 84
ENSG00000141469	SLC14A1	-3.55	-5.69	Cluster 1	Solute carrier family 14 (urea transporter)
ENSG00000183287	CCBE1	-3.56	-5.75	Cluster 1	Collagen and calcium-binding egf domain-containing protein 1
ENSG00000118898	PPL	-3.58	-3.73	Cluster 1	Periplakin
ENSG00000164440	TXLNB	-3.59	-4.72	Cluster 1	Taxilin beta
ENSG00000121743	GJA3	-3.61	-4.82	Cluster 1	Gap junction protein
ENSG00000144063	MALL	-3.62	-4.49	Cluster 1	T cell differentiation protein like
ENSG00000108381	ASPA	-3.66	-4.60	Cluster 1	Aspartoacylase
ENSG00000138771	SHROOM3	-3.73	-3.01	Cluster 1	Shroom family member 3
ENSG00000204131	NHSL2	-3.77	-4.92	Cluster 1	Nhs-like protein 2

ENSG00000184349	EFNA5	-3.79	-3.26	Cluster 1	Ephrin a5, eph-related receptor tyrosine kinase ligand 7
ENSG00000106819	ASPN	-3.80	-5.52	Cluster 1	Asporin, periodontal ligament-associated protein 1
ENSG00000147481	SNTG1	-3.82	-6.73	Cluster 1	Syntrophin
ENSG00000128594	LRRC4	-3.83	-4.48	Cluster 1	Leucine-rich repeat-containing protein 4
ENSG00000117069	ST6GALNAC5	-3.86	-5.45	Cluster 1	6-sialyltransferase 5
ENSG00000115896	PLCL1	-3.92	-5.34	Cluster 1	Phospholipase c-like 1
ENSG00000172318	B3GALT1	-3.97	-4.48	Cluster 1	Beta-3-galactosyltransferase 1
ENSG00000136999	CCN3	-3.97	-6.42	Cluster 1	Nephroblastoma overexpressed gene
ENSG00000112182	BACH2	-4.00	-3.83	Cluster 1	Basic leucine zipper transcription factor 2
ENSG00000185742	C11orf87	-4.07	-4.40	Cluster 1	Chromosome 11 open reading frame 87
ENSG00000137975	CLCA2	-4.07	-5.42	Cluster 1	Chloride channel accessory 2
ENSG00000204634	TBC1D8	-4.11	-2.67	Cluster 1	Tbc1 domain family member 8
ENSG00000196730	DAPK1	-4.13	-5.21	Cluster 1	Death-associated protein kinase 1
ENSG00000145526	CDH18	-4.15	-5.39	Cluster 1	Cadherin 18
ENSG00000176438	SYNE3	-4.22	-2.91	Cluster 1	Spectrin repeat-containing nuclear envelope protein 3
ENSG00000125378	BMP4	-4.32	-4.44	Cluster 1	Bone morphogenetic protein 4
ENSG00000072952	IRAG1	-4.32	-5.89	Cluster 1	Inositol 1,4,5-trisphosphate-associated CGMP kinase substrate
ENSG00000002587	HS3ST1	-4.33	-5.25	Cluster 1	Heparan sulfate (glucosamine) 3-o-sulfotransferase 1
ENSG00000117425	PTCH2	-4.39	-4.59	Cluster 1	Patched 2
ENSG00000185483	ROR1	-4.53	-4.30	Cluster 1	Receptor tyrosine kinase-like orphan receptor 1
ENSG00000187955	COL14A1	-4.56	-8.12	Cluster 1	Collagen type xiv
ENSG00000171246	NPTX1	-4.59	-3.59	Cluster 1	Pentraxin i
ENSG00000029534	ANK1	-4.59	-3.64	Cluster 1	Ankyrin 1 muscle-specific isoform
ENSG00000164120	HPGD	-4.59	-6.32	Cluster 1	Hydroxyprostaglandin dehydrogenase
ENSG00000133321	PLAAT4	-4.68	-2.60	Cluster 1	Phospholipase a and acyltransferase 4
ENSG00000106809	OGN	-4.75	-6.62	Cluster 1	Osteoglycin, osteoinductive factor
ENSG00000153993	SEMA3D	-4.82	-7.98	Cluster 1	Semaphorin 3d
ENSG00000127083	OMD	-4.87	-4.41	Cluster 1	Osteomodulin
ENSG00000171873	ADRA1D	-4.99	-2.53	Cluster 1	Alpha-1d-adrenergic receptor
ENSG00000164236	ANKRD33B	-5.05	-4.14	Cluster 1	Ankyrin repeat domain 33b
ENSG00000137265	IRF4	-5.06	-4.76	Cluster 1	Interferon regulatory factor 4
ENSG00000122547	EEPD1	-5.14	-4.33	Cluster 1	Endonuclease/exonuclease/phosphatase family domain-containing protein 1

ENSG00000117643	MAN1C1	-5.15	-4.44	Cluster 1	Mannosidase
ENSG00000185924	RTN4RL1	-5.29	-5.21	Cluster 1	Reticulon 4 receptor-like 1
ENSG00000183346	CABCOCO1	-5.44	-4.35	Cluster 1	Ciliary associated calcium binding coiled-coil 1
ENSG00000124749	COL21A1	-5.46	-5.32	Cluster 1	Collagen type xxi
ENSG00000266524	GDF10	-5.55	-5.69	Cluster 1	Growth/differentiation factor 10
ENSG00000250722	SELENOP	-5.69	-5.03	Cluster 1	Selenoprotein p
ENSG00000013293	SLC7A14	-5.91	-7.43	Cluster 1	Solute carrier family 7
ENSG00000168497	CAVIN2	-6.09	-4.47	Cluster 1	Caveolae-associated protein 2, serum deprivation response phosphatidylserine-binding protein
ENSG00000132561	MATN2	-1.00	-5.72	Cluster 2	Matrilin 2
ENSG00000183775	KCTD16	-1.01	-5.38	Cluster 2	Potassium channel tetramerization domain-containing protein 16
ENSG00000163565	IFI16	-1.02	-5.40	Cluster 2	Interferon-gamma-inducible protein 16
ENSG00000173517	PEAK1	-1.03	-5.37	Cluster 2	Pseudopodium-enriched atypical kinase 1
ENSG00000164761	TNFRSF11B	-1.04	-7.94	Cluster 2	Tumor necrosis factor receptor superfamily
ENSG00000138193	PLCE1	-1.05	-5.17	Cluster 2	Phospholipase c epsilon-1
ENSG00000140876	NUDT7	-1.07	-5.72	Cluster 2	Nudix hydrolase 7
ENSG00000162600	OMA1	-1.07	-6.35	Cluster 2	Oma1 zinc metallopeptidase
ENSG00000137831	UACA	-1.10	-7.33	Cluster 2	Uveal autoantigen with coiled-coil domains and ankyrin repeats
ENSG00000188921	HACD4	-1.12	-5.83	Cluster 2	Protein tyrosine phosphatase-like a domain-containing protein 2
ENSG00000152818	UTRN	-1.12	-5.62	Cluster 2	Utrophin
ENSG00000155011	DKK2	-1.12	-6.51	Cluster 2	Dickkopf wnt signaling pathway inhibitor
ENSG00000133026	MYH10	-1.20	-5.49	Cluster 2	Myosin heavy chain 10
ENSG00000189195	BTBD8	-1.20	-5.28	Cluster 2	Kiaa1107 gene
ENSG00000134853	PDGFRA	-1.22	-6.30	Cluster 2	Platelet-derived growth factor receptor alpha
ENSG00000156535	CD109	-1.22	-5.56	Cluster 2	Cd109 platelet-specific antigen system gov
ENSG00000136169	SETDB2	-1.23	-5.27	Cluster 2	Set domain protein bifurcated 2
ENSG00000145390	USP53	-1.24	-6.83	Cluster 2	Ubiquitin-specific peptidase 53
ENSG00000177409	SAMD9L	-1.28	-8.76	Cluster 2	Sterile alpha motif domain-containing protein 9-like
ENSG00000179388	EGR3	-1.28	-5.80	Cluster 2	Early growth response 3
ENSG00000145675	PIK3R1	-1.29	-5.34	Cluster 2	Phosphatidylinositol 3-kinase regulatory subunit 1
ENSG00000145632	PLK2	-1.29	-5.77	Cluster 2	Polo-like kinase 2

ENSG00000128872	TMOD2	-1.32	-7.08	Cluster 2	Tropomodulin 2
ENSG00000138758	SEPTIN11	-1.32	-6.37	Cluster 2	Septin 11
ENSG00000197635	DPP4	-1.33	-7.22	Cluster 2	Dipeptidyl peptidase iv
ENSG00000135205	CCDC146	-1.34	-5.49	Cluster 2	Colied-coil domain containing 146
ENSG00000225830	ERCC6	-1.35	-6.21	Cluster 2	Chromatin remodeling factor
ENSG00000158270	COLEC12	-1.35	-5.48	Cluster 2	Collectin 12, scavenger receptor with c-type lectin domain
ENSG00000144642	RBMS3	-1.37	-5.58	Cluster 2	Rna-binding motif protein single strand-interacting 3
ENSG00000230438	SERPINB9P1	-1.37	-5.73	Cluster 2	Serpin family b member 9 pseudogen 1
ENSG00000170962	PDGFD	-1.37	-6.12	Cluster 2	Platelet-derived growth factor d
ENSG00000153246	PLA2R1	-1.41	-5.56	Cluster 2	Phospholipase a2 receptor 1
ENSG00000136044	APPL2	-1.42	-5.25	Cluster 2	Adaptor protein, phosphotyrosine interaction ph domain and leucine zipper-containing protein 2
ENSG00000154654	NCAM2	-1.46	-5.37	Cluster 2	Cell adhesion molecule
ENSG00000164070	HSPA4L	-1.54	-5.34	Cluster 2	Heat-shock protein family a (hsp70) member 4-like protein
ENSG00000139132	FGD4	-1.55	-8.55	Cluster 2	Rhogef and PH domain containing 4
ENSG00000153291	SLC25A27	-1.66	-5.83	Cluster 2	Solute carrier family 25
ENSG00000187098	MITF	-1.67	-5.99	Cluster 2	Microphthalmia-associated transcription factor
ENSG00000163412	EIF4E3	-1.68	-5.70	Cluster 2	Eukaryotic translation initiation factor 4e family
ENSG00000141447	OSBPL1A	-1.69	-5.39	Cluster 2	Oxysterol-binding protein-like protein 1a
ENSG00000137962	ARHGAP29	-1.70	-5.86	Cluster 2	RHO gtpase-ACTIVATING PROTEIN 29
ENSG00000189184	PCDH18	-1.70	-6.52	Cluster 2	Protocadherin 18
ENSG00000154639	CXADR	-1.73	-5.14	Cluster 2	Coxsackievirus and adenovirus receptor
ENSG00000163617	CCDC191	-1.74	-5.15	Cluster 2	Coiled-coil domain containing 191
ENSG00000196693	ZNF33B	-1.78	-7.32	Cluster 2	Zinc finger protein 33b
ENSG00000163536	SERPINI1	-1.81	-5.93	Cluster 2	Serine protease inhibitor
ENSG00000154822	PLCL2	-1.82	-6.22	Cluster 2	Phospholipase c-like 2
ENSG00000164309	CMYA5	-1.84	-5.96	Cluster 2	Cardiomyopathy-associated protein 5
ENSG00000151491	EPS8	-1.88	-5.48	Cluster 2	Epidermal growth factor receptor pathway substrate 8
ENSG00000187210	GCNT1	-1.92	-5.73	Cluster 2	Glucosaminyl (n-acetyl) transferase 1
ENSG00000206538	VGLL3	-2.03	-5.17	Cluster 2	Vestigial-like 3
ENSG00000188906	LRRK2	-2.05	-6.83	Cluster 2	Leucine-rich repeat kinase 2
ENSG00000131016	AKAP12	-2.06	-6.31	Cluster 2	A-kinase anchor protein 12
ENSG00000169255	B3GALNT1	-2.08	-6.34	Cluster 2	3-N-acetylgalactosaminyltransferase 1 (globoside blood group)

ENSG00000127951	FGL2	-2.08	-7.21	Cluster 2	Fibrinogen-like 2
ENSG00000164330	EBF1	-2.14	-5.61	Cluster 2	Early b-cell factor 1
ENSG00000183049	CAMK1D	-2.15	-5.63	Cluster 2	Calcium/calmodulin-dependent protein kinase i-delta
ENSG00000129682	FGF13	-2.17	-5.12	Cluster 2	Fibroblast growth factor 13
ENSG00000169744	LDB2	-2.25	-5.30	Cluster 2	Lim domain-binding 2
ENSG00000143469	SYT14	-2.33	-7.01	Cluster 2	Synaptotagmin 14
ENSG00000180263	FGD6	-2.33	-7.25	Cluster 2	Rhogef and PH domain containing 6
ENSG00000142149	HUNK	-2.39	-5.35	Cluster 2	Hormonally upregulated neu-associated kinase
ENSG00000134317	GRHL1	-2.39	-5.49	Cluster 2	Grainyhead-like 1
ENSG00000136531	SCN2A	-2.42	-6.11	Cluster 2	Sodium voltage-gated channel alpha subunit 2
ENSG00000197971	MBP	-2.47	-5.40	Cluster 2	Myelin basic protein
ENSG00000168916	ZNF608	-2.55	-5.43	Cluster 2	Zinc FINGER PROTEIN 608
ENSG00000163827	LRRC2	-2.57	-6.76	Cluster 2	Leucine-rich repeat-containing protein 2
ENSG00000154262	ABCA6	-2.58	-8.77	Cluster 2	Atp-binding cassette subfamily a member 6
ENSG00000128536	CDHR3	-2.60	-5.48	Cluster 2	Cadherin-related family member 3
ENSG00000181804	SLC9A9	-2.63	-5.31	Cluster 2	Solute carrier family 9 (sodium/hydrogen exchanger) member 9
ENSG00000145362	ANK2	-2.71	-6.12	Cluster 2	Ankyrin 2
ENSG00000183801	OLFML1	-2.99	-6.68	Cluster 2	Olfactomedin like 1
ENSG00000151150	ANK3	-3.02	-6.89	Cluster 2	Ankyrin 3
ENSG00000154258	ABCA9	-3.06	-6.60	Cluster 2	Atp-binding cassette
ENSG00000138395	CDK15	-3.10	-6.31	Cluster 2	Cyclin-dependent kinase 15
ENSG00000172348	RCAN2	-3.15	-7.42	Cluster 2	Regulator of calcineurin 2
ENSG00000138735	PDE5A	-4.82	-9.95	Cluster 2	Phosphodiesterase 5a
ENSG00000140396	NCOA2	-1.00	-4.60	Cluster 3	Nuclear receptor coactivator 2
ENSG00000156026	MCU	-1.01	-3.25	Cluster 3	Mitochondrial calcium uniporter
ENSG00000150347	ARID5B	-1.02	-4.24	Cluster 3	At-rich interaction domain-containing protein 5b
ENSG00000163879	DNALI1	-1.02	-3.45	Cluster 3	Dynein axonemal light intermediate polypeptide 1
ENSG00000115414	FN1	-1.02	-3.07	Cluster 3	Fibronectin 1
ENSG00000135931	ARMC9	-1.03	-3.42	Cluster 3	Armadillo repeat-containing protein 9
ENSG00000174628	IQCK	-1.04	-3.30	Cluster 3	Iq motif containing k
ENSG00000048740	CELF2	-1.05	-4.69	Cluster 3	Cugbp- and elav-like family member 2
ENSG00000118495	PLAGL1	-1.06	-3.30	Cluster 3	Pleomorphic adenoma gene-like 1
ENSG00000115525	ST3GAL5	-1.06	-3.86	Cluster 3	St3 beta-galactoside alpha-2,3-sialyltransferase 5

ENSG00000144746	ARL6IP5	-1.06	-3.95	Cluster 3	ADP-ribosylation factor-like GTPase 6-interacting protein 5
ENSG00000096093	EFHC1	-1.07	-4.99	Cluster 3	Ef-hand domain (c-terminal)-containing protein 1
ENSG00000155085	AK9	-1.08	-4.47	Cluster 3	Adenylate kinase 9
ENSG00000132849	PATJ	-1.08	-3.73	Cluster 3	Pals1-associated tight junction protein
ENSG00000164099	PRSS12	-1.09	-3.08	Cluster 3	Protease serine 12
ENSG00000077063	CTTNBP2	-1.10	-3.32	Cluster 3	Cortactin-binding protein 2
ENSG00000136960	ENPP2	-1.10	-3.91	Cluster 3	Ectonucleotide pyrophosphatase/phosphodiesterase 2
ENSG00000147162	OGT	-1.12	-3.49	Cluster 3	O-linked n-acetylglucosamine transferase
ENSG00000164463	CREBRF	-1.12	-3.93	Cluster 3	Creb3 recruitment factor
ENSG00000165322	ARHGAP12	-1.12	-4.35	Cluster 3	RHO gtpase-ACTIVATING PROTEIN 12
ENSG00000188312	CENPP	-1.13	-3.53	Cluster 3	Centromeric protein p
ENSG00000164619	BMPER	-1.14	-4.37	Cluster 3	Bone morphogenetic protein-binding endothelial regulator protein
ENSG00000147862	NFIB	-1.14	-4.80	Cluster 3	Nuclear factor i/b
ENSG00000120738	EGR1	-1.14	-4.23	Cluster 3	Early growth response 1
ENSG00000148057	IDNK	-1.15	-4.39	Cluster 3	Chromosome 9 open reading frame 103
ENSG00000147027	TMEM47	-1.15	-4.78	Cluster 3	Transmembrane protein 47
ENSG00000118515	SGK1	-1.16	-3.77	Cluster 3	Serum/glucocorticoid-regulated kinase 1
ENSG00000169432	SCN9A	-1.16	-4.28	Cluster 3	Sodium voltage-gated channel alpha subunit 9
ENSG00000109472	CPE	-1.16	-4.31	Cluster 3	Carboxypeptidase e
ENSG00000126016	AMOT	-1.17	-4.13	Cluster 3	Angiomotin
ENSG00000140199	SLC12A6	-1.17	-3.79	Cluster 3	Solute carrier family 12 (potassium/chloride transporter), member 6
ENSG00000185760	KCNQ5	-1.18	-3.50	Cluster 3	Potassium channel voltage-gated kqt-like subfamily member 5
ENSG00000100490	CDKL1	-1.18	-4.11	Cluster 3	Cyclin-dependent kinase-like 1
ENSG00000122643	NT5C3A	-1.18	-4.41	Cluster 3	CYTOSOLYC IIIA,5-PRIME-αnucleotidase
ENSG00000152217	SETBP1	-1.18	-3.97	Cluster 3	Set-binding protein 1
ENSG00000129675	ARHGEF6	-1.19	-4.90	Cluster 3	Rho guanine nucleotide exchange factor 6
ENSG00000107960	STN1	-1.19	-3.56	Cluster 3	Cst complex subunit
ENSG00000198542	ITGBL1	-1.19	-4.65	Cluster 3	Integrin beta-like 1
ENSG00000110427	KIAA1549L	-1.20	-3.59	Cluster 3	Chromosome 11 open reading frame 41; c11orf41;;g2
ENSG00000168491	CCDC110	-1.20	-4.15	Cluster 3	Cancer/testis antigen km-hn-1
ENSG00000145687	SSBP2	-1.20	-3.33	Cluster 3	Single-stranded dna-binding protein 2

ENSG00000164694	FNDC1	-1.20	-4.09	Cluster 3	Fibronectin type iii domain-containing protein 1
ENSG00000126775	ATG14	-1.21	-3.74	Cluster 3	Autophagy-related 14
ENSG00000173275	ZNF449	-1.23	-4.40	Cluster 3	Zinc finger protein 449
ENSG00000100767	PAPLN	-1.23	-3.29	Cluster 3	Proteoglycan-like sulfated glycoprotein
ENSG00000188993	LRRC66	-1.24	-4.49	Cluster 3	Leucine rich repeat containing 66
ENSG00000144645	OSBPL10	-1.25	-3.64	Cluster 3	Oxysterol-binding protein-like protein 10
ENSG00000163513	TGFBR2	-1.26	-4.29	Cluster 3	Transforming growth factor-beta receptor type ii
ENSG00000149218	ENDOD1	-1.27	-4.56	Cluster 3	Endonucease domain containing 1
ENSG00000170035	UBE2E3	-1.27	-3.40	Cluster 3	Ubiquitin-conjugating enzyme e2e 3
ENSG00000068305	MEF2A	-1.28	-4.42	Cluster 3	Mads box transcription enhancer factor 2
ENSG00000153558	FBXL2	-1.31	-4.79	Cluster 3	F-box and leucine-rich repeat protein 2
ENSG00000214595	EML6	-1.31	-3.48	Cluster 3	Echinoderm microtubule associated protein like 6
ENSG00000066027	PPP2R5A	-1.31	-3.48	Cluster 3	Protein phosphatase 2
ENSG00000172965	MIR4435-2HG	-1.32	-3.66	Cluster 3	Micro rna 4435-2 host gene
ENSG00000127863	TNFRSF19	-1.33	-3.30	Cluster 3	Tumor necrosis factor receptor superfamily member 19
ENSG00000150593	PDCD4	-1.33	-4.09	Cluster 3	Programmed cell death 4, neoplastic transformation inhibitor
ENSG00000143387	CTSK	-1.33	-3.21	Cluster 3	Cathepsin k
ENSG00000137752	CASP1	-1.33	-4.11	Cluster 3	Caspase 1, apoptosis-related cysteine protease
ENSG00000155324	GRAMD2B	-1.36	-3.49	Cluster 3	Gram domain containing 2b
ENSG00000104324	CPQ	-1.37	-3.38	Cluster 3	Carboxypeptidase q
ENSG00000031003	FAM13B	-1.37	-3.93	Cluster 3	Chromosome 5 open reading frame 5
ENSG00000167081	PBX3	-1.38	-3.48	Cluster 3	Pre-b-cell leukemia transcription factor 3
ENSG00000138411	HECW2	-1.40	-3.19	Cluster 3	C2 and ww domains-containing e3 ubiquitin-protein ligase 2
ENSG00000071205	ARHGAP10	-1.41	-3.19	Cluster 3	RHO gtpase-ACTIVATING PROTEIN 10
ENSG00000185745	IFIT1	-1.41	-4.58	Cluster 3	Interferon-induced protein with tetratricopeptide repeats 1
ENSG00000179104	TMTC2	-1.41	-3.54	Cluster 3	Transmembrane and tetratricopeptide repeat domains-containing protein 2
ENSG00000154027	AK5	-1.42	-4.60	Cluster 3	Adenylate kinase 5
ENSG00000134531	EMP1	-1.42	-3.84	Cluster 3	Epithelial membrane protein 1p
ENSG00000205683	DPF3	-1.43	-4.34	Cluster 3	Zinc and double phd fingers family
ENSG00000065534	MYLK	-1.43	-4.26	Cluster 3	Myosin light chain kinase
ENSG00000011523	CEP68	-1.44	-4.56	Cluster 3	Centrosomal protein 68-kd
ENSG00000178695	KCTD12	-1.45	-4.17	Cluster 3	Potassium channel tetramerization domain-containing protein 12

ENSG00000064763	FAR2	-1.46	-4.40	Cluster 3	Fatty acyl CoA reductase 2
ENSG00000158122	PRXL2C	-1.46	-3.55	Cluster 3	Peroxiredoxin like 2c
ENSG00000104435	STMN2	-1.47	-4.73	Cluster 3	Stathmin-like 2
ENSG00000104381	GDAP1	-1.47	-4.87	Cluster 3	Ganglioside-induced differentiation-associated protein 1
ENSG00000156463	SH3RF2	-1.49	-3.99	Cluster 3	Sh3 domain-containing ring finger protein 2
ENSG00000125945	ZNF436	-1.50	-3.41	Cluster 3	Zinc finger protein 436
ENSG00000099204	ABLIM1	-1.53	-5.07	Cluster 3	Actin-binding lim protein family member 1
ENSG00000116667	C1orf21	-1.54	-4.67	Cluster 3	Chromosome 1 open reading frame 21
ENSG00000169239	CA5B	-1.56	-3.41	Cluster 3	Carbonic anhydrase vb mitochondrial
ENSG00000047648	ARHGAP6	-1.56	-3.78	Cluster 3	RHO gtpase-ACTIVATING PROTEIN 6
ENSG00000168016	TRANK1	-1.56	-3.52	Cluster 3	Tetratricopeptide and ankryn repeat containing 1
ENSG00000136235	GPNMB	-1.57	-3.57	Cluster 3	Glycoprotein nmb
ENSG00000163171	CDC42EP3	-1.58	-4.57	Cluster 3	Cdc42 effector protein 3
ENSG00000138119	MYOF	-1.58	-4.81	Cluster 3	Myoferlin
ENSG00000157483	MYO1E	-1.60	-4.62	Cluster 3	Myosin 1E
ENSG00000114670	NEK11	-1.62	-4.52	Cluster 3	Never in mitosis gene a-related kinase 11
ENSG00000139263	LRIG3	-1.63	-4.45	Cluster 3	Leucine-rich repeats- and immunoglobulin-like domains-containing protein 3
ENSG00000155016	CYP2U1	-1.65	-4.52	Cluster 3	Cytochrome p450 family 2 subfamily u
ENSG00000145819	ARHGAP26	-1.68	-4.47	Cluster 3	RHO gtpase-ACTIVATING PROTEIN 26
ENSG00000102387	TAF7L	-1.69	-4.34	Cluster 3	Tata box-binding protein-associated factor 7-like
ENSG00000156299	TIAM1	-1.69	-3.43	Cluster 3	T-cell lymphoma invasion and metastasis 1
ENSG00000112297	CRYBG1	-1.70	-4.60	Cluster 3	Absent in melanoma 1
ENSG00000091656	ZFHX4	-1.70	-3.36	Cluster 3	Zinc finger homeobox 4
ENSG00000166974	MAPRE2	-1.71	-3.33	Cluster 3	Microtubule-associated protein rp/eb family member 2
ENSG00000054654	SYNE2	-1.71	-4.17	Cluster 3	Spectrin repeat-containing nuclear envelope protein 2connecting element
ENSG00000163596	ICA1L	-1.72	-4.21	Cluster 3	Islet cell autoantigen 1 like
ENSG00000166035	LIPC	-1.72	-5.06	Cluster 3	Lipase, hepatic
ENSG00000132274	TRIM22	-1.73	-4.81	Cluster 3	Tripartite motif-containing protein 22
ENSG00000058668	ATP2B4	-1.73	-4.47	Cluster 3	ATPase, Ca (2+)-transporting, plasma membrane, 4
ENSG00000151693	ASAP2	-1.74	-4.54	Cluster 3	Development- and differentiation-enhancing factor 2
ENSG00000185432	METTL7A	-1.74	-4.10	Cluster 3	Methyltransferase-like 7a
ENSG00000120658	ENOX1	-1.76	-4.22	Cluster 3	Ecto-nox disulfide-thiol exchanger 1

ENSG00000124942	AHNAK	-1.76	-4.84	Cluster 3	Ahnak nucleoprotein
ENSG00000138131	LOXL4	-1.77	-3.26	Cluster 3	Lysyl oxidase-like 4
ENSG00000120549	KIAA1217	-1.77	-3.26	Cluster 3	Kiaa1217 gene
ENSG00000081189	MEF2C	-1.78	-3.17	Cluster 3	Mads box transcription enhancer factor 2
ENSG00000138675	FGF5	-1.78	-4.33	Cluster 3	Fibroblast growth factor 5
ENSG00000054392	HHAT	-1.79	-4.50	Cluster 3	Hedgehog acyltransferase, melanoma antigen recognized by t cells 2
ENSG00000091986	CCDC80	-1.80	-4.51	Cluster 3	Coiled-coil domain-containing protein 80
ENSG00000221818	EBF2	-1.80	-4.00	Cluster 3	Early b-cell factor 2
ENSG00000100342	APOL1	-1.80	-3.32	Cluster 3	Apolipoprotein l-i
ENSG00000162407	PLPP3	-1.82	-4.96	Cluster 3	Phospholipid phosphatase 3
ENSG00000035664	DAPK2	-1.82	-3.80	Cluster 3	Death-associated protein kinase 2
ENSG00000197872	CYRIA	-1.83	-4.43	Cluster 3	Cyfip related rac 1 intearctor a
ENSG00000105974	CAV1	-1.84	-3.99	Cluster 3	Caveolin 1
ENSG00000152465	NMT2	-1.85	-4.61	Cluster 3	N-myristoyltransferase 2
ENSG00000138356	AOX1	-1.85	-4.42	Cluster 3	Aldehyde oxidase 1
ENSG00000118777	ABCG2	-1.87	-3.81	Cluster 3	Atp-binding cassette, subfamily g
ENSG00000159784	FAM131B	-1.88	-3.12	Cluster 3	Family with sequence similarity 131 member b
ENSG00000079102	RUNX1T1	-1.88	-4.04	Cluster 3	Runt-related transcription factor 1
ENSG00000160097	FNDC5	-1.91	-4.96	Cluster 3	Fibronectin type iii domain-containing protein 5
ENSG00000196104	SPOCK3	-1.92	-4.50	Cluster 3	Cwcv and kazal like domains proteoglycan 3
ENSG00000110436	SLC1A2	-1.93	-3.82	Cluster 3	Solute carrier family 1 (glial high affinity glutamate transporter), member 2
ENSG00000070882	OSBPL3	-1.93	-4.25	Cluster 3	Oxysterol-binding protein-like protein 3
ENSG00000163947	ARHGEF3	-1.94	-4.15	Cluster 3	Rho guanine nucleotide exchange factor 3
ENSG00000133107	TRPC4	-1.94	-4.31	Cluster 3	Transient receptor potential cation channel subfamily c member 4
ENSG00000071967	CYBRD1	-1.94	-4.85	Cluster 3	CYTOCHROME b REDUCTASE 1
ENSG00000153721	CNKSR3	-1.97	-4.46	Cluster 3	Cnksr family member 3
ENSG00000196639	HRH1	-1.98	-3.25	Cluster 3	Histamine receptor h1
ENSG00000147437	GNRH1	-1.98	-5.05	Cluster 3	Gonadotropin-releasing hormone 1
ENSG00000149256	TENM4	-2.00	-4.05	Cluster 3	Teneurin transmembrane protein 4
ENSG00000196159	FAT4	-2.01	-4.32	Cluster 3	Fat atypical cadherin 4

ENSG00000165124	SVEP1	-2.01	-3.92	Cluster 3	Von Willebrand factor type A, EGF and pentraxin domain containing 1
ENSG00000148798	INA	-2.05	-4.42	Cluster 3	Internexin alpha
ENSG00000081377	CDC14B	-2.11	-3.61	Cluster 3	Cell division cycle 14b; cdc14b;;cell division cycle 14, s. Cerevisiae, homolog b
ENSG00000176771	NCKAP5	-2.13	-4.29	Cluster 3	Nck-associated protein 5
ENSG00000145349	CAMK2D	-2.14	-4.93	Cluster 3	Calcium/calmodulin-dependent protein kinase ii-delta
ENSG00000182836	PLCXD3	-2.16	-4.75	Cluster 3	Phospholipase c phosphatidylinositol-specific x domain-containing protein 3
ENSG00000136826	KLF4	-2.19	-3.44	Cluster 3	Endothelial kruppel-like zinc finger protein
ENSG00000184408	KCND2	-2.21	-4.23	Cluster 3	Potassium voltage-gated channel shal-related subfamily member 2
ENSG00000111261	MANSC1	-2.27	-3.66	Cluster 3	Mansc domain containing 1
ENSG00000183454	GRIN2A	-2.29	-4.72	Cluster 3	Glutamate receptor ionotropic n-methyl-d-aspartate subunit 2a
ENSG00000197321	SVIL	-2.30	-4.93	Cluster 3	Supervillin
ENSG00000061918	GUCY1B1	-2.30	-4.71	Cluster 3	Guanylate cyclase 1, nitric oxide-sensitive guanylyl cyclase, beta-1 subunit
ENSG00000154065	ANKRD29	-2.36	-4.70	Cluster 3	Ankyrin repeat domain 29
ENSG00000170271	FAXDC2	-2.38	-4.10	Cluster 3	Fatty acid hydroxylase domain containing 2
ENSG00000076716	GPC4	-2.42	-3.52	Cluster 3	Glypican 4
ENSG00000135842	NIBAN1	-2.47	-3.22	Cluster 3	Niban apoptosis regulator 1
ENSG00000163071	SPATA18	-2.49	-3.50	Cluster 3	Spermatogenesis-associated protein 18
ENSG00000168079	SCARA5	-2.55	-4.54	Cluster 3	Scavenger receptor class a member 5
ENSG00000149212	SESN3	-2.56	-3.95	Cluster 3	Sestrin 3
ENSG00000126950	TMEM35A	-2.64	-4.10	Cluster 3	Transmembrane protein 35a
ENSG00000107562	CXCL12	-2.64	-3.98	Cluster 3	Chemokine cxc motif ligand 12
ENSG00000172296	SPTLC3	-2.64	-4.16	Cluster 3	Serine palmitoyltransferase long-chain base subunit 3
ENSG00000106823	ECM2	-2.67	-4.76	Cluster 3	Extracellular matrix protein 2
ENSG00000144730	IL17RD	-2.72	-4.37	Cluster 3	Interleukin 17 receptor d
ENSG00000197046	SIGLEC15	-2.80	-3.22	Cluster 3	Sialic acid-binding immunoglobulin-like lectin 15
ENSG00000155792	DEPTOR	-2.81	-4.29	Cluster 3	Dep domain-containing protein 6
ENSG00000053747	LAMA3	-2.87	-3.86	Cluster 3	Laminin alpha-3
ENSG00000166448	TMEM130	-3.10	-3.18	Cluster 3	Transmembrane protein 130

ENSG00000101134	DOK5	-1.01	-1.41	Cluster 4	Docking protein 5
ENSG00000006740	ARHGAP44	-1.01	-3.05	Cluster 4	RHO gtpase-ACTIVATING PROTEIN 44
ENSG00000145358	DDIT4L	-1.01	-1.30	Cluster 4	Dna damage-inducible transcript 4-like
ENSG00000144455	SUMF1	-1.02	-1.03	Cluster 4	Sulfatase-modifying factor 1
ENSG00000173706	HEG1	-1.02	-2.63	Cluster 4	Heart of glass
ENSG00000001461	NIPAL3	-1.03	-2.79	Cluster 4	Nipa like domain containing 3
ENSG00000136003	ISCU	-1.04	-1.49	Cluster 4	Iron-sulfur cluster assembly enzyme
ENSG00000108001	EBF3	-1.04	-2.96	Cluster 4	Early b-cell factor 3, collier/olf1/ebf transcription factor 3
ENSG00000107554	DNMBP	-1.04	-2.45	Cluster 4	Dynamin-binding protein
ENSG00000048471	SNX29	-1.04	-1.03	Cluster 4	Sorting nexin 29
ENSG00000139910	NOVA1	-1.04	-1.80	Cluster 4	Neurooncologic ventral antigen 1
ENSG00000026950	BTN3A1	-1.04	-1.07	Cluster 4	Butyrophilin subfamily 3 member a1
ENSG00000187239	FNBP1	-1.05	-1.98	Cluster 4	Formin-binding protein 1
ENSG00000254122	PCDHGB7	-1.05	-1.37	Cluster 4	Protocadherin-gamma, subfamily b, member 7
ENSG00000119280	C1orf198	-1.05	-1.49	Cluster 4	Chromosome 1 open reading frame 198
ENSG00000110090	CPT1A	-1.05	-2.56	Cluster 4	Carnitine palmitoyltransferase i
ENSG00000186665	C17orf58	-1.07	-2.00	Cluster 4	Chromosome 17 open reading frame 58
ENSG00000239521	CASTOR3	-1.07	-1.97	Cluster 4	Castor family member 3
ENSG00000109787	KLF3	-1.07	-2.32	Cluster 4	Kruppel-like factor 3
ENSG00000162105	SHANK2	-1.08	-2.01	Cluster 4	Sh3 and multiple ankyrin repeat domains 2
ENSG00000133059	DSTYK	-1.08	-2.74	Cluster 4	Dual serine/threonine and tyrosine protein kinase, receptor-interacting serine/threonine kinase 5
ENSG00000167065	DUSP18	-1.09	-1.91	Cluster 4	Dual-specificity phosphatase 18
ENSG00000115935	WIPF1	-1.09	-2.65	Cluster 4	Was/wasl-interacting protein family member 1
ENSG00000108950	FAM20A	-1.09	-2.40	Cluster 4	Family with sequence similarity 20 member a
ENSG00000187391	MAGI2	-1.10	-1.39	Cluster 4	Membrane-associated guanylate kinase, ww and pdz domains-containing, 2
ENSG00000163710	PCOLCE2	-1.10	-2.02	Cluster 4	Procollagen c-endopeptidase enhancer 2
ENSG00000154529	CNTNAP3B	-1.11	-2.14	Cluster 4	Contactin associated protein family member 3b
ENSG00000162599	NFIA	-1.13	-2.13	Cluster 4	Nuclear factor i/a
ENSG00000185189	NRBP2	-1.13	-1.48	Cluster 4	Nuclear receptor-binding protein 2
ENSG00000164938	TP53INP1	-1.14	-1.93	Cluster 4	Tumor protein p53-inducible nuclear protein 1
ENSG00000134698	Aug-04	-1.14	-2.80	Cluster 4	Eukaryotic translation initiation factor 2c, subunit 4
ENSG00000106483	SFRP4	-1.14	-2.60	Cluster 4	Secreted frizzled-related protein 4

ENSG00000101384	JAG1	-1.14	-1.62	Cluster 4	Jagged 1
ENSG00000132793	LPIN3	-1.15	-2.00	Cluster 4	Lipin 3
ENSG00000136002	ARHGEF4	-1.15	-1.89	Cluster 4	Rho guanine nucleotide exchange factor 4
ENSG00000111271	ACAD10	-1.15	-1.06	Cluster 4	Acyl CoA dehydrogenase family member 10; ACAD10
ENSG00000106571	GLI3	-1.15	-2.17	Cluster 4	Gli-kruppel family member 3
ENSG00000104365	IKBKB	-1.17	-1.75	Cluster 4	Inhibitor of nuclear factor kappa-b kinase subunit beta
ENSG00000197256	KANK2	-1.18	-2.63	Cluster 4	Kn motif- and ankyrin repeat domain-containing protein 2
ENSG00000135899	SP110	-1.18	-2.34	Cluster 4	Nuclear body protein sp110, intracellular pathogen resistance 1
ENSG00000266094	RASSF5	-1.18	-1.72	Cluster 4	Ras association domain family protein 5
ENSG00000172667	ZMAT3	-1.20	-2.61	Cluster 4	WILDTYPE p53-INDUCED GENE
ENSG00000138639	ARHGAP24	-1.20	-2.45	Cluster 4	RHO gtpase-ACTIVATING PROTEIN 24
ENSG00000117616	RSRP1	-1.21	-2.25	Cluster 4	Arginine and serine rich protein 1
ENSG00000130956	HABP4	-1.21	-2.90	Cluster 4	Hyaluronan-binding protein 4
ENSG00000183060	LYSMD4	-1.21	-1.84	Cluster 4	Lysm DOMAIN CONTAINING 4
ENSG00000065308	TRAM2	-1.22	-1.39	Cluster 4	Translocation-associated membrane protein 2
ENSG00000132386	SERPINF1	-1.22	-1.48	Cluster 4	Serpin peptidase inhibitor clade f member 1
ENSG00000010278	CD9	-1.22	-1.27	Cluster 4	Leukocyte antigen mic3
ENSG00000116717	GADD45A	-1.23	-1.75	Cluster 4	Growth arrest- and dna damage-inducible gene gadd45
ENSG00000163820	FYCO1	-1.24	-1.88	Cluster 4	Fyve and coiled-coil domain containing 1
ENSG00000164010	ERMAP	-1.24	-1.32	Cluster 4	Erythroblast membrane-associated protein
ENSG00000100100	PIK3IP1	-1.24	-1.16	Cluster 4	Phossphoinositide-3-kinase interacting protein 1
ENSG00000168781	PPIP5K1	-1.24	-2.67	Cluster 4	Diphosphoinositol pentakisphosphate kinase 1
ENSG00000266028	SRGAP2	-1.25	-1.10	Cluster 4	SLIT-ROBO RHO gtpase-ACTIVATING PROTEIN 2
ENSG00000141542	RAB40B	-1.26	-1.66	Cluster 4	Member ras oncogene family
ENSG00000073910	FRY	-1.29	-2.53	Cluster 4	Fry microtubule-binding protein
ENSG00000170734	POLH	-1.29	-2.32	Cluster 4	Polymerase, dna, eta
ENSG00000156113	KCNMA1	-1.30	-2.94	Cluster 4	Potassium channel, calcium-activated, large conductance, subfamily m
ENSG00000109670	FBXW7	-1.30	-3.01	Cluster 4	F-box and wd40 domain protein 7
ENSG00000166780	BMERB1	-1.30	-2.73	Cluster 4	Bmerb domain containiing 1
ENSG00000187720	THSD4	-1.30	-1.27	Cluster 4	Thrombospondin type-1 domain-containing protein 4
ENSG00000026025	VIM	-1.31	-1.77	Cluster 4	Vimentin
ENSG00000168646	AXIN2	-1.31	-2.54	Cluster 4	Axis inhibitor 2

ENSG00000075826	SEC31B	-1.31	-2.55	Cluster 4	COPII coat complex component
ENSG00000146592	CREB5	-1.32	-1.98	Cluster 4	Camp RESPONSE ELEMENT-BINDING PROTEIN 5
ENSG00000167202	TBC1D2B	-1.32	-2.02	Cluster 4	Tbc1 domain family member 2b
ENSG00000088280	ASAP3	-1.33	-1.26	Cluster 4	Ankyrin repeat and PH domain 3, ARF GTPase-activating protein with SH3 domain
ENSG00000213918	DNASE1	-1.34	-2.39	Cluster 4	Deoxyribonuclease ii, lysosomal
ENSG00000119514	GALNT12	-1.35	-2.96	Cluster 4	Udp-n-acetyl-alpha-d-galactosamine:polypeptide n-acetyl galactosaminyl transferase 12
ENSG00000170500	LONRF2	-1.35	-2.46	Cluster 4	Lon peptidase n-terminal domain and ring finger 2
ENSG00000131981	LGALS3	-1.36	-2.18	Cluster 4	Lectin galactoside-binding soluble 3
ENSG00000198873	GRK5	-1.37	-2.51	Cluster 4	G protein-coupled receptor kinase 5
ENSG00000162542	TMCO4	-1.37	-2.04	Cluster 4	Transmembrane and coiled-coil domains 4
ENSG00000197093	GAL3ST4	-1.38	-2.01	Cluster 4	Galactose-3-o-sulfotransferase 4
ENSG00000171533	MAP6	-1.38	-2.78	Cluster 4	Microtubule-associated protein 6
ENSG00000141576	RNF157	-1.40	-1.71	Cluster 4	Ring finger protein 157
ENSG00000121310	ECHDC2	-1.40	-1.80	Cluster 4	ENOYL-coa HYDRATASE DOMAIN CONTAINING 2
ENSG00000130653	PNPLA7	-1.41	-1.34	Cluster 4	Patatin-like phospholipase domain-containing protein 7
ENSG00000150687	PRSS23	-1.41	-1.83	Cluster 4	Protease serine 23
ENSG00000124212	PTGIS	-1.42	-2.17	Cluster 4	Prostaglandin i2 synthase
ENSG00000182606	TRAK1	-1.44	-1.80	Cluster 4	Trafficking protein, kinesin-binding 1
ENSG00000063438	AHRR	-1.44	-1.79	Cluster 4	Arylhydrocarbon receptor repressor
ENSG00000124785	NRN1	-1.45	-2.23	Cluster 4	Neuritin 1
ENSG00000162976	SLC66A3	-1.45	-1.76	Cluster 4	Solute carrier family 66 memeber 3
ENSG00000069535	MAOB	-1.46	-2.90	Cluster 4	Monoamine oxidase (flavin-containing) b
ENSG00000196975	ANXA4	-1.47	-2.92	Cluster 4	Annexin a4
ENSG00000108799	EZH1	-1.47	-1.59	Cluster 4	Enhancer of zeste 1 polycomb repressive complex 2 subunit
ENSG00000109099	PMP22	-1.50	-3.00	Cluster 4	Peripheral myelin protein 22
ENSG00000186073	CDIN1	-1.51	-2.95	Cluster 4	Chromosome 15 open reading frame 41
ENSG00000089225	TBX5	-1.51	-2.49	Cluster 4	T-box transcription factor 5
ENSG00000163661	PTX3	-1.51	-2.86	Cluster 4	Pentraxin 3
ENSG00000134138	MEIS2	-1.55	-2.53	Cluster 4	Meis homeobox 2
ENSG00000167371	PRRT2	-1.55	-2.12	Cluster 4	Proline-rich transmembrane protein 2
ENSG00000153071	DAB2	-1.55	-2.15	Cluster 4	Dab adaptor protein 2

ENSG00000112679	DUSP22	-1.57	-1.76	Cluster 4	Dual-specificity phosphatase 22, jnk pathway-associated phosphatase
ENSG00000196781	TLE1	-1.57	-1.47	Cluster 4	Tle family member 1, transcriptional corepressor
ENSG00000102935	ZNF423	-1.57	-1.65	Cluster 4	Zinc finger protein 423
ENSG00000109794	FAM149A	-1.58	-2.52	Cluster 4	Family with sequence similarity 149 member a
ENSG00000139597	N4BP2L1	-1.60	-3.10	Cluster 4	Nedd4 binding protein 2 like 1
ENSG00000109743	BST1	-1.61	-1.54	Cluster 4	Bone marrow stromal cell antigen 1
ENSG00000154310	TNIK	-1.62	-2.41	Cluster 4	Traf2- and nck-interacting kinase
ENSG00000072195	SPEG	-1.62	-1.43	Cluster 4	Speg aortic preferentially expressed protein 1
ENSG00000135749	PCNX2	-1.62	-2.38	Cluster 4	Pecanex 2
ENSG00000014914	MTMR11	-1.63	-2.21	Cluster 4	Myotubularin related protein 11
ENSG00000123892	RAB38	-1.64	-1.80	Cluster 4	Ras-associated protein rab38
ENSG00000131370	SH3BP5	-1.65	-3.02	Cluster 4	Sh3 domain-binding protein 5
ENSG00000126218	F10	-1.66	-1.45	Cluster 4	Coagulation factor 10
ENSG00000081059	TCF7	-1.69	-1.57	Cluster 4	Transcription factor 7
ENSG00000162804	SNED1	-1.69	-1.40	Cluster 4	Nidogen, and egf-like domains protein 1, stromal nidogen extracellular matrix protein
ENSG00000022267	FHL1	-1.69	-2.63	Cluster 4	Four-and-a-half lim domains 1
ENSG00000123700	KCNJ2	-1.69	-3.01	Cluster 4	Potassium channel
ENSG00000164442	CITED2	-1.70	-1.52	Cluster 4	CBP/p300-interacting transactivator, with GLU/ASP-rich C-terminal domain 2
ENSG00000169184	MN1	-1.70	-2.18	Cluster 4	Mn1 protooncogene, transcriptional regulator;
ENSG00000026297	RNASET2	-1.71	-2.22	Cluster 4	Ribonuclease t2
ENSG00000076356	PLXNA2	-1.72	-2.53	Cluster 4	Plexin a2, transmembrane protein
ENSG00000146776	ATXN7L1	-1.74	-2.17	Cluster 4	Ataxin 7 like protein 1
ENSG00000119943	PYROXD2	-1.77	-1.60	Cluster 4	Pyridine nucleotide-disulphide oxidoreductase domain-containing protein 2
ENSG00000132170	PPARG	-1.80	-1.90	Cluster 4	Peroxisome proliferator-activated receptor-gamma
ENSG00000159023	EPB41	-1.80	-1.47	Cluster 4	Erythrocyte membrane protein band 4.1
ENSG00000008256	CYTH3	-1.81	-3.03	Cluster 4	Cytohesin 3
ENSG00000178031	ADAMTSL1	-1.82	-1.20	Cluster 4	Adamts-like protein 1
ENSG00000166949	SMAD3	-1.82	-1.88	Cluster 4	Smad family member 3
ENSG00000152518	ZFP36L2	-1.82	-2.46	Cluster 4	Zinc finger protein 36-like 2
ENSG00000149294	NCAM1	-1.85	-2.85	Cluster 4	Cell adhesion molecule neural 1

ENSG00000101638	ST8SIA5	-1.85	-1.02	Cluster 4	St8 alpha-n-acetyl-neuraminide alpha-2,8-sialyltransferase 5
ENSG00000196782	MAML3	-1.85	-1.56	Cluster 4	Mastermind-like 3
ENSG00000204219	TCEA3	-1.86	-1.54	Cluster 4	Transcription elongation factor a, 3
ENSG00000064309	CDON	-1.87	-2.19	Cluster 4	Cell adhesion molecule-related/downregulated by oncogenes
ENSG00000110455	ACCS	-1.92	-1.85	Cluster 4	1-αaminocyclopropane-1-CARBOXYLATE SYNTHASE
ENSG00000181350	LRRC75A	-1.95	-1.89	Cluster 4	Leucin riach repeat containing 75a
ENSG00000213366	GSTM2	-1.97	-1.44	Cluster 4	Glutathione s-transferase
ENSG00000152092	ASTN1	-1.97	-2.28	Cluster 4	Astrotactin 1
ENSG00000128284	APOL3	-2.01	-2.60	Cluster 4	Apolipoprotein l-iii
ENSG00000131080	EDA2R	-2.02	-2.85	Cluster 4	Ectodysplasin a2 receptor
ENSG00000225968	ELFN1	-2.02	-1.73	Cluster 4	Extracellular leucine-rich repeat and fibronectin type iii domain-containing protein 1
ENSG00000151623	NR3C2	-2.02	-2.40	Cluster 4	Nuclear receptor subfamily 3, group c, member 2
ENSG00000164237	CMBL	-2.03	-2.92	Cluster 4	Carboxymethylenebutenolidase-like protein
ENSG00000054793	ATP9A	-2.04	-3.00	Cluster 4	Atpase CLASS II TYPE 9A
ENSG00000146674	IGFBP3	-2.06	-2.47	Cluster 4	Insulin-like growth factor-binding protein 3
ENSG00000134508	CABLES1	-2.10	-2.37	Cluster 4	Cdk5 and abl enzyme substrate 1
ENSG00000110002	VWA5A	-2.11	-2.40	Cluster 4	Von willebrand factor a domain-containing protein 5a
ENSG00000214021	TTLL3	-2.12	-2.74	Cluster 4	Tubulin tyrosine ligase like 3
ENSG00000168502	MTCL1	-2.15	-2.83	Cluster 4	Microtubule crosslinking factor 1
ENSG00000108984	MAP2K6	-2.17	-3.00	Cluster 4	Mitogen-activated protein kinase kinase 6
ENSG00000185567	AHNAK2	-2.23	-1.46	Cluster 4	Ahnak nucleoprotein 2
ENSG00000152284	TCF7L1	-2.26	-1.79	Cluster 4	Transcription factor 7-like 1
ENSG00000149451	ADAM33	-2.30	-1.36	Cluster 4	A disintegrin and metalloproteinase domain 33
ENSG00000080854	IGSF9B	-2.37	-2.20	Cluster 4	Immunoglobulin superfamily member 9b
ENSG00000143867	OSR1	-2.48	-1.66	Cluster 4	Odd-skipped-related 1
ENSG00000142611	PRDM16	-2.51	-2.09	Cluster 4	Pr domain-containing protein 16
ENSG00000161381	PLXDC1	-2.60	-2.73	Cluster 4	Plexin domain-containing protein 1
ENSG00000185585	OLFML2A	-2.60	-2.68	Cluster 4	Olfactomedin-like 2a
ENSG00000105339	DENND3	-2.71	-1.60	Cluster 4	Denn domain-containing protein 3
ENSG00000168477	TNXB	-2.76	-1.37	Cluster 4	Tenascin xb
ENSG00000143127	ITGA10	-2.81	-1.95	Cluster 4	Integrin alpha-10
ENSG00000163431	LMOD1	-2.83	-2.50	Cluster 4	Leiomodin 1, thyroid and eye muscle autoantigen, 64-kd
ENSG00000099953	MMP11	-2.85	-2.26	Cluster 4	Matrix metalloproteinase 11

ENSG00000100065	CARD10	-2.93	-1.83	Cluster 4	Caspase recruitment domain-containing protein 10
ENSG00000143772	ITPKB	-2.99	-2.18	Cluster 4	Inositol 1,4,5-trisphosphate 3-kinase b
ENSG00000104368	PLAT	-3.03	-1.73	Cluster 4	Plasminogen activator
ENSG00000174348	PODN	-3.11	-1.30	Cluster 4	Podocan
ENSG00000177363	LRRN4CL	-3.19	-1.54	Cluster 4	Lrrn4 c-terminal like
ENSG00000141574	SECTM1	-3.41	-1.12	Cluster 4	Secreted and transmembrane 1
ENSG00000130592	LSP1	-3.57	-2.72	Cluster 4	Lymphocyte-specific protein
ENSG00000183508	TENT5C	-3.70	-1.37	Cluster 4	Terminal nucleotidyltransferase 5c
ENSG00000169418	NPR1	-3.78	-1.64	Cluster 4	Natriuretic peptide receptor a/guanylate cyclase a
ENSG00000167992	VWCE	-4.01	-1.36	Cluster 4	Von willebrand factor c and egf domain-containing protein
ENSG00000166106	ADAMTS15	-4.73	-1.34	Cluster 4	A disintegrin-like and metalloproteinase with thrombospondin type 1 motif, 15
ENSG00000122641	INHBA	5.36	-2.51	Cluster 5	Inhibin, beta a;follicle-stimulating hormone-releasing protein
ENSG00000152952	PLOD2	4.51	-4.00	Cluster 5	Procollagen-lysine, 2-oxoglutarate 5-dioxygenase 2
ENSG00000170961	HAS2	4.25	-2.99	Cluster 5	Hyaluronan synthase 2
ENSG00000105835	NAMPT	3.94	-1.54	Cluster 5	Nicotinamide phosphoribosyltransferase
ENSG00000104321	TRPA1	3.87	-4.76	Cluster 5	Transient receptor potential cation channel, subfamily a, member 1
ENSG00000112972	HMGCS1	3.73	-2.37	Cluster 5	3-αhydroxy-3-METHYLGLUTARYL-coa SYNTHASE 1
ENSG00000196611	MMP1	3.68	-1.80	Cluster 5	Matrix metalloproteinase 1; mmp1;;collagenase, fibroblast
ENSG00000067064	IDI1	3.56	-2.33	Cluster 5	Isopentenyl-diphosphate delta isomerase 1
ENSG00000041353	RAB27B	3.40	-6.85	Cluster 5	Member ras oncogene family
ENSG00000104415	CCN4	3.39	-2.87	Cluster 5	Wnt1-inducible signaling pathway protein 1
ENSG00000157214	STEAP2	3.39	-2.92	Cluster 5	Steap2 metalloreductase, six-transmembrane epithelial antigen of prostate 2
ENSG00000164211	STARD4	3.14	-2.38	Cluster 5	Start domain-containing protein 4
ENSG00000119927	GPAM	3.13	-4.02	Cluster 5	Mitochondrial glycerol-3-phosphate acyltransferase
ENSG00000120437	ACAT2	3.11	-2.60	Cluster 5	ACETYL-coa ACETYLTRANSFERASE 2
ENSG00000171208	NETO2	3.09	-1.57	Cluster 5	Neuropilin- and tolloid-like 2
ENSG00000153823	PID1	3.00	-1.64	Cluster 5	Phosphotyrosine interaction domain-containing 1
ENSG00000153162	BMP6	2.89	-2.05	Cluster 5	Bone morphogenetic protein 6
ENSG00000164647	STEAP1	2.80	-2.36	Cluster 5	Steap family member 1
ENSG00000135048	CEMIP2	2.76	-2.24	Cluster 5	Transmembrane protein 2
ENSG00000113161	HMGCR	2.70	-2.13	Cluster 5	3-αhydroxy-3-METHYLGLUTARYL-coa REDUCTASE

ENSG00000114251	WNT5A	2.70	-2.10	Cluster 5	Wingless-type mmtv integration site family, member 5a
ENSG00000182752	PAPPA	2.67	-1.72	Cluster 5	Pregnancy-associated plasma protein a
ENSG00000125845	BMP2	2.61	-2.26	Cluster 5	Bone morphogenetic protein 2, regulatory element, cis-acting, enhancer,
ENSG00000144810	COL8A1	2.60	-2.67	Cluster 5	Collagen, type VIII, alpha-1
ENSG00000140416	TPM1	2.40	-3.17	Cluster 5	Tropomyosin 1
ENSG00000068366	ACSL4	2.34	-5.44	Cluster 5	Acyl-CoA synthetase long chain family member 4
ENSG00000140285	FGF7	2.30	-5.16	Cluster 5	Fibroblast growth factor 7
ENSG00000072274	TFRC	2.07	-2.52	Cluster 5	Transferrin receptor
ENSG00000100644	HIF1A	2.05	-5.07	Cluster 5	Hypoxia-inducible factor 1, alpha subunit
ENSG00000148848	ADAM12	2.02	-3.54	Cluster 5	Disintegrin and metalloproteinase domain 12
ENSG00000131459	GFPT2	2.01	-1.74	Cluster 5	Glutamine:fructose-6-phosphate amidotransferase 2
ENSG00000169855	ROBO1	1.95	-3.30	Cluster 5	Roundabout guidance receptor 1
ENSG00000039560	RAI14	1.93	-4.62	Cluster 5	Retinoic acid-induced 14
ENSG00000122884	P4HA1	1.92	-2.81	Cluster 5	Procollagen-proline, 2-oxoglutarate-4-dioxygenase
ENSG00000171617	ENC1	1.85	-4.04	Cluster 5	Ectodermal-neural cortex 1
ENSG00000145555	MYO10	1.62	-2.91	Cluster 5	Myosin x
ENSG00000145623	OSMR	1.55	-2.77	Cluster 5	Oncostatin m receptor
ENSG00000158290	CUL4B	1.51	-5.06	Cluster 5	Cullin 4b
ENSG00000075223	SEMA3C	1.48	-4.85	Cluster 5	Semaphorin 3c
ENSG00000074695	LMAN1	1.47	-3.53	Cluster 5	Lectin, mannose-binding, 1
ENSG00000135919	SERPINE2	1.19	-2.40	Cluster 5	Serpin peptidase inhibitor, clade e (nexin, plasminogen activator inhibitor type 1), member 2
ENSG00000166250	CLMP	1.18	-4.50	Cluster 5	Coxsackievirus- and adenovirus receptor-like membrane protein; adipocyte-specific adhesion molecule
ENSG00000136244	IL6	7.21	3.61	Cluster 6	Interleukin 6
ENSG00000081041	CXCL2	7.09	5.19	Cluster 6	Chemokine, cxc motif, ligand 2
ENSG00000125538	IL1B	6.59	1.76	Cluster 6	Interleukin 1-beta
ENSG00000108691	CCL2	6.30	2.02	Cluster 6	Chemokine, cc motif, ligand 2; monocyte chemotactic protein 1
ENSG00000128342	LIF	5.99	2.48	Cluster 6	Leukemia-inhibitory factor
ENSG00000123610	TNFAIP6	5.27	3.02	Cluster 6	Tumor necrosis factor-alpha-induced protein 6
ENSG00000137331	IER3	5.05	5.01	Cluster 6	Immediate-early response 3

ENSG00000105825	TFPI2	4.97	1.50	Cluster 6	Tissue factor pathway inhibitor 2
ENSG00000099194	SCD	4.82	2.20	Cluster 6	STEAROYL-coa DESATURASE
ENSG00000136689	IL1RN	4.75	4.24	Cluster 6	Interleukin 1 receptor antagonist
ENSG00000172893	DHCR7	4.09	4.14	Cluster 6	7-αdehydrocholesterol REDUCTASE
ENSG00000103257	SLC7A5	4.07	6.54	Cluster 6	Solute carrier family 7 (cationic amino acid transporter)
ENSG00000198959	TGM2	3.81	1.54	Cluster 6	Transglutaminase 2;
ENSG00000186480	INSIG1	3.75	1.18	Cluster 6	Insulin-induced gene 1
ENSG00000173918	C1QTNF1	3.57	4.66	Cluster 6	C1q- and tumor necrosis factor-related protein 1
ENSG00000006118	TMEM132A	3.55	1.95	Cluster 6	Transmembrane protein 132a
ENSG00000148344	PTGES	3.33	3.93	Cluster 6	Prostaglandin e synthase
ENSG00000141526	SLC16A3	3.10	4.56	Cluster 6	Solute carrier family 16 (monocarboxylic acid transporter), member 3
ENSG00000106366	SERPINE1	2.99	2.75	Cluster 6	Serpin peptidase inhibitor, clade e (nexin, plasminogen activator inhibitor type 1), member 1
ENSG00000143878	RHOB	2.96	3.13	Cluster 6	Ras homolog gene family, member b
ENSG00000134107	BHLHE40	2.86	1.24	Cluster 6	Basic helix-loop-helix family, member e40
ENSG00000130164	LDLR	2.85	2.54	Cluster 6	Low density lipoprotein receptorr
ENSG00000088826	SMOX	2.72	4.87	Cluster 6	Spermine oxidase
ENSG00000085662	AKR1B1	2.70	2.43	Cluster 6	Aldo-keto reductase family 1, member b1
ENSG00000168209	DDIT4	2.56	5.07	Cluster 6	Dna damage-inducible transcript 4
ENSG00000085117	CD82	2.52	2.58	Cluster 6	Prostate cancer antimetastasis gene KAI1; leukocyte surface antigen R2
ENSG00000160752	FDPS	2.49	1.18	Cluster 6	Farnesyl diphosphate synthase
ENSG00000104635	SLC39A14	2.46	1.61	Cluster 6	Solute carrier family 39 (zinc transporter), member 14
ENSG00000095303	PTGS1	2.41	2.65	Cluster 6	Prostaglandin-endoperoxide synthase 1; cox1
ENSG00000172061	LRRC15	2.37	1.39	Cluster 6	Leucine rich repeat containing 15
ENSG00000249992	TMEM158	2.25	2.24	Cluster 6	Transmembrane protein 158
ENSG00000086062	B4GALT1	2.14	1.44	Cluster 6	1,beta-1,4-galactosyltransferase 1; b4galt1
ENSG00000067057	PFKP	1.85	1.23	Cluster 6	Hosphofructokinase, platelet type
ENSG00000102144	PGK1	1.82	1.74	Cluster 6	Phosphoglycerate kinase 1
ENSG00000111669	TPI1	1.75	3.94	Cluster 6	Triosephosphate isomerase 1
ENSG00000107957	SH3PXD2A	1.38	1.32	Cluster 6	Sh3 and px domains 2a
ENSG00000175166	PSMD2	1.33	1.52	Cluster 6	Proteasome 26s subunit, non-ATPase, 2; tumor necrosis factor receptor-associated protein 2

ENSG00000163517	HDAC11	-1.01	2.62	Cluster 7	Histone deacetylase 11
ENSG00000075618	FSCN1	-1.02	2.07	Cluster 7	Fascin actin-bundling protein 1
ENSG00000167106	FAM102A	-1.03	3.85	Cluster 7	Family with sequence similarity 102, member a
ENSG00000013364	MVP	-1.03	2.16	Cluster 7	Major vault protein
ENSG00000171045	TSNARE1	-1.04	1.70	Cluster 7	T-snare domain containing 1
ENSG00000110651	CD81	-1.04	1.28	Cluster 7	Cd81 antigen; cd81
ENSG00000117984	CTSD	-1.05	2.46	Cluster 7	Cathepsin d
ENSG00000146054	TRIM7	-1.06	2.98	Cluster 7	Tripartite motif-containing protein 7
ENSG00000168237	GLYCTK	-1.06	2.86	Cluster 7	Glycerate kinase
ENSG00000198715	GLMP	-1.07	2.01	Cluster 7	Glycosylated lysosomal membrane protein
ENSG00000103174	NAGPA	-1.08	1.55	Cluster 7	N-acetylglucosamine-1-phosphodiester alpha-n-acetylglucosaminidase
ENSG00000105516	DBP	-1.09	2.03	Cluster 7	D-BOX-BINDING PAR bzip TRANSCRIPTION FACTOR
ENSG00000162576	MXRA8	-1.09	2.35	Cluster 7	Matrix remodeling-associated protein 8
ENSG00000107731	UNC5B	-1.09	2.22	Cluster 7	Unc5 netrin receptor b
ENSG00000172830	SSH3	-1.09	1.11	Cluster 7	Slingshot protein phosphatase 3
ENSG00000107521	HPS1	-1.09	1.33	Cluster 7	Hps1 biogenesis of lysosomal organelles complex 3, subunit 1
ENSG00000124104	SNX21	-1.10	1.79	Cluster 7	Sorting family member 21
ENSG00000100994	PYGB	-1.10	2.31	Cluster 7	Glycogen phosphorylase, brain type
ENSG00000178980	SELENOW	-1.11	1.28	Cluster 7	Selenoprotein w
ENSG00000175602	CCDC85B	-1.11	1.45	Cluster 7	Coiled-coil domain-containing protein 85b
ENSG00000100307	CBX7	-1.11	1.48	Cluster 7	Chromobox 7
ENSG00000126351	THRA	-1.13	1.14	Cluster 7	Thyroid hormone receptor, alpha-1; thyroid hormone receptor, central nervous system form; thra1; erba-alpha;oncogene erba; erba;;erba-related 7; ear7; v-erb-a avian erythroblastic leukemia viral oncogene homolog 1; erba1 thyroid hormone recep
ENSG00000204851	PNMA8B	-1.14	1.96	Cluster 7	Pnma family member 8b
ENSG00000104936	DMPK	-1.14	1.23	Cluster 7	Dystrophia myotonica protein kinase
ENSG00000142694	EVA1B	-1.15	2.00	Cluster 7	Eva-1 homolog b
ENSG00000108840	HDAC5	-1.16	2.02	Cluster 7	Histone deacetylase 5
ENSG00000211584	SLC48A1	-1.17	1.31	Cluster 7	Heme-responsive gene 1
ENSG00000174791	RIN1	-1.18	3.21	Cluster 7	Ras and rab interactor 1

ENSG00000130244	FAM98C	-1.18	1.61	Cluster 7	Family with sequence similarity 98 member c
ENSG00000006282	SPATA20	-1.19	1.11	Cluster 7	Spermatogenesis-associated protein 20
ENSG00000221995	TIAF1	-1.20	2.56	Cluster 7	Tgfb1-induced antiapoptotic factor 1
ENSG00000142669	SH3BGRL3	-1.21	2.30	Cluster 7	Sh3 domain-binding glutamic acid-rich protein-like protein 3
ENSG00000175573	C11orf68	-1.21	2.06	Cluster 7	Chromosome 11 open reading frame 68
ENSG00000178209	PLEC	-1.21	1.58	Cluster 7	Plectin
ENSG00000090238	YPEL3	-1.22	1.57	Cluster 7	Yippee-like 3
ENSG00000196576	PLXNB2	-1.22	1.49	Cluster 7	Plexin b2
ENSG00000136059	VILL	-1.23	1.35	Cluster 7	Villin like
ENSG00000245532	NEAT1	-1.24	2.35	Cluster 7	Noncoding nuclear-enriched abundant transcript 1
ENSG00000239697	TNFSF12	-1.24	1.17	Cluster 7	Tumor necrosis factor ligand superfamily, member 12
ENSG00000162302	RPS6KA4	-1.25	2.24	Cluster 7	Ribosomal protein s6 kinase, 90-kd, 4
ENSG00000106948	AKNA	-1.26	2.69	Cluster 7	At-hook transcription factor akna
ENSG00000203485	INF2	-1.26	2.58	Cluster 7	Inverted formin 2
ENSG00000160325	CACFD1	-1.27	3.09	Cluster 7	Calcium channel flower-domain containing protein 1
ENSG00000006015	REX1BD	-1.28	1.50	Cluster 7	Required for excision 1-b domain containing
ENSG00000130511	SSBP4	-1.28	1.92	Cluster 7	Single-stranded dna-binding protein 4
ENSG00000177000	MTHFR	-1.29	2.30	Cluster 7	5,10-αmethylenetetrahydrofolate REDUCTASE
ENSG00000175220	ARHGAP1	-1.30	1.76	Cluster 7	RHO gtpase-ACTIVATING PROTEIN 1
ENSG00000102878	HSF4	-1.32	1.79	Cluster 7	Heat-shock transcription factor 4
ENSG00000130787	HIP1R	-1.32	1.50	Cluster 7	Huntingtin-interacting protein 1-related protein
ENSG00000042493	CAPG	-1.36	1.08	Cluster 7	Capping protein (actin filament), gelson-like
ENSG00000187609	EXD3	-1.37	2.13	Cluster 7	Exonuclease 3'-5' domain containing 3
ENSG00000120896	SORBS3	-1.38	1.58	Cluster 7	Sorbin and sh3 domains-containing protein 3; sorbs3; sh3 domain-containing adaptor molecule 1
ENSG00000189129	PLAC9	-1.40	1.41	Cluster 7	Placenta-specific gene 9
ENSG00000114544	SLC41A3	-1.41	1.21	Cluster 7	Solute carrier family 41
ENSG00000175866	BAIAP2	-1.44	2.18	Cluster 7	Bai1-associated protein 2
ENSG00000187091	PLCD1	-1.44	2.41	Cluster 7	Phospholipase c, delta-1
ENSG00000171345	KRT19	-1.44	1.33	Cluster 7	Keratin 19
ENSG00000126107	HECTD3	-1.45	2.24	Cluster 7	Hect domain-containing e3 ubiquitin protein ligase 3
ENSG00000184524	CEND1	-1.46	2.04	Cluster 7	Cell cycle exit and neuronal differentiation 18
ENSG00000213398	LCAT	-1.46	1.02	Cluster 7	Lecithin cholesterol acyltransferase
ENSG00000099377	HSD3B7	-1.47	2.54	Cluster 7	3 beta- and steroid delta-isomerase 7

ENSG00000072163	LIMS2	-1.47	1.57	Cluster 7	Lim and senescent cell antigen-like domains 2
ENSG00000101400	SNTA1	-1.50	2.20	Cluster 7	Syntrophin, alpha-1
ENSG00000242028	HYPK	-1.51	1.63	Cluster 7	Huntingtin-interacting protein k
ENSG00000108828	VAT1	-1.58	2.21	Cluster 7	Vesicle amine transport protein 1
ENSG00000157873	TNFRSF14	-1.58	2.16	Cluster 7	Tumor necrosis factor receptor superfamily, member 14
ENSG00000176428	VPS37D	-1.59	2.94	Cluster 7	Vps37d subunit of escrt-i
ENSG00000140961	OSGIN1	-1.61	5.60	Cluster 7	Oxidative stress-induced growth inhibitor 1
ENSG00000167779	IGFBP6	-1.61	1.47	Cluster 7	Insulin-like growth factor-binding protein 6
ENSG00000128298	BAIAP2L2	-1.61	2.80	Cluster 7	Bai1-associated protein 2-like 2
ENSG00000125966	MMP24	-1.64	1.79	Cluster 7	Matrix metalloproteinase 24
ENSG00000162066	AMDHD2	-1.65	2.20	Cluster 7	Amidohydrolase domain containing 2
ENSG00000124191	TOX2	-1.69	1.77	Cluster 7	Tox high mobility group box family member 2
ENSG00000239857	GET4	-1.72	4.10	Cluster 7	Golgi to er traffic protein 4
ENSG00000160789	LMNA	-1.75	1.22	Cluster 7	Lamin a/c
ENSG00000105327	BBC3	-1.78	2.13	Cluster 7	BCL2-binding component, p53-upregulated modulator of apoptosis; PUMA
ENSG00000148671	ADIRF	-1.82	1.25	Cluster 7	Adipogenesis regulatory factor
ENSG00000132613	MTSS2	-1.87	2.07	Cluster 7	Metastasis suppressor 1-like protein
ENSG00000176909	MAMSTR	-1.89	3.15	Cluster 7	Mef2-activating sap transcriptional regulator
ENSG00000166289	PLEKHF1	-1.90	3.40	Cluster 7	Pleckstrin homology domain-containing protein, family f, member 1
ENSG00000167363	FN3K	-1.92	2.15	Cluster 7	Fructosamine 3-kinase
ENSG00000004776	HSPB6	-1.92	2.10	Cluster 7	Heat-shock 27-kd protein 6
ENSG00000068976	PYGM	-1.93	1.95	Cluster 7	Glycogen phosphorylase, muscle
ENSG00000161513	FDXR	-1.97	1.77	Cluster 7	Ferredoxin reductase
ENSG00000140297	GCNT3	-2.05	1.29	Cluster 7	Glucosaminyl (n-acetyl) transferase 3, mucin-type
ENSG00000177595	PIDD1	-2.19	2.58	Cluster 7	Leucine-rich repeats- and death domain-containing protein
ENSG00000095383	TBC1D2	-2.22	1.52	Cluster 7	Tbc1 domain family, member 2
ENSG00000130518	IQCN	-2.33	2.85	Cluster 7	Iq motif containing n
ENSG00000079337	RAPGEF3	-2.33	1.64	Cluster 7	Rap guanine nucleotide exchange factor 3
ENSG00000167994	RAB3IL1	-2.34	2.27	Cluster 7	Rab3a interacting protein like 1
ENSG00000148426	PROSER2	-2.37	2.79	Cluster 7	Prroline AND SERINE RICH 2
ENSG00000128016	ZFP36	-2.40	1.68	Cluster 7	Zfp36 ring finger protein;
ENSG00000174564	IL20RB	-2.42	1.64	Cluster 7	Interleukin 20 receptor, beta

ENSG00000129194	SOX15	-2.73	1.58	Cluster 7	Transcription factor 15 sry-box 15
ENSG00000165507	DEPP1	-3.59	1.41	Cluster 7	Depp1 autophagy regulator
ENSG00000103316	CRYM	-4.06	2.44	Cluster 7	Crystallin
ENSG00000111728	ST8SIA1	-4.43	5.46	Cluster 7	St8 alpha-n-acetyl-neuraminide alpha-2,8-sialyltransferase 1

Results are shown as fold changes (FC). The *p*-values come from the comparison using NM as baseline. CM (MDA-MB-231 conditioned media), NM (negative media), DEGs (differential expressed genes) and EGCG (epigallocatechin-3-gallate).C

CHAPTER IV

ARTICLE 3

EGCG INHIBITS THE INFLAMMATION AND SENESCENCE-INDUCING PROPERTIES OF MDA-MB-231 TRIPLE-NEGATIVE BREAST CANCER (TNBC) CELLS-DERIVED EXTRACELLULAR VESICLES IN HUMAN ADIPOSE-DERIVED MESENCHYMAL STEM CELLS

Narjara Gonzalez Suarez[1], Yuniel Fernandez-Marrero[2], Mathieu P.A. Hébert[3], Luc H. Boudreau[3], and Borhane Annabi[1].

[1]Laboratoire d'Oncologie Moléculaire, Département de Chimie, Université du Québec à Montréal and CERMO-FC, Montreal, QC, Canada.

[2]Cell Biology Department, NuChem Sciences, Montreal, QC, Canada, H4R 2N6.

[3]Department of Chemistry and Biochemistry, Université de Moncton and New Brunswick Center for Precision Medicine, Moncton, NB, Canada.

Manuscript submitted to Cancer Cell International

Authors contributions:

Narjara Gonzalez Suarez: Data curation, formal analysis, methodology and writing the original draft.

Yuniel Fernandez-Marrero: Formal analysis, methodology, review and editing the original draft.

Mathieu P.A. Hébert: Data curation, formal analysis, review and editing the original draft.

Luc H. Boudreau: Formal analysis, funding acquisition, supervision, review and editing the original draft.

Borhane Annabi: Conceptualization, formal analysis, funding acquisition, supervision, and writing the original draft.

All authors read and approved the final manuscript.

4.1 Résumé

CONTEXTE: Le sécrétome des cellules du cancer du sein triple négatif (TNBC) peut induire un phénotype pro-inflammatoire dans les cellules souches mésenchymateuses adipocytaires humaines (hADMSC). Cela peut être inhibé par l'épigallocatéchine-3-gallate (EGCG), un polyphénol du thé vert. L'impact de l'EGCG sur la régulation paracrine des vésicules extracellulaires (VE) au sein du sécrétome reste très peu compris. MÉTHODES: Les VE ont été obtenues de la lignée cellulaire MDA-MB-231 dérivée de TNBC, dans un milieu dépourvu de sérum et traité ou non avec de l'EGCG dans des conditions de culture normoxiques ou hypoxiques (<1% O_2). L'analyse du contenu génique des VE a été faite par RNASeq. La modulation des marqueurs inflammatoires et de sénescence dans les cellules hADMSC a été évaluée par RT-qPCR à l'aide de puces à ADNc et a été validée par immunobuvardage. Des puces de protéines phospho-kinases ont été utilisées pour évaluer l'induction des voies de signalisation. RÉSULTATS: Alors que les conditions de culture hypoxiques n'ont pas modifié de manière significative le contenu génique des VE sécrétées par les cellules MDA-MB-231, l'ajout d'EGCG a altéré le matériel génique des VE à une faible tension d'oxygène. Les hADMSC traitées avec les VE ont augmenté l'expression des marqueurs adipocytaires associés au cancer *CXCL8*, *CCL2* et *IL-1B*. Les VE isolées des cellules MDA-MB-231 traitées avec l'EGCG (EGCG-EV) régulaient à la baisse l'expression de *CCL2* et *IL-1B*, tout en induisant une expression plus élevée des niveaux de CXCL8 et d'IL-6. Les VE ont activé les voies de signalisation CHK-2, c-Jun, AKT et GSK-3β dans les cellules hADMSC. Les EGCG-VE ont spécifiquement réduit l'expression des marqueurs de sénescence induits par le seriage P21 et β-gal. Enfin, nous avons démontrons que le contenu mitochondrial était réduit dans les VE dérivées de TNBC lors du traitement par EGCG. CONCLUSION: Les polyphénols dérivés de l'alimentation représentent une stratégie de ciblage efficace pour inhiber la régulation pro-tumorale des cellules cancéreuses sur le tissu adipocyte environnant dans le TNBC

4.2 Abstract

BACKGROUND: Triple-negative breast cancer (TNBC) cell secretome can induce a pro-inflammatory phenotype in human adipose-derived mesenchymal stem cells (hADMSC). This can be prevented by the green tea polyphenol epigallocatechin-3-gallate (EGCG). The impact of EGCG on the paracrine regulation that the extracellular vesicles (EV) exert within the TNBC cell secretome remains unknown. METHODS: EV were obtained from a TNBC-derived serum-starved MDA-MB-231 cell model treated or not with EGCG under normoxic or hypoxic (<1% O_2) culture conditions. RNA-Seq analysis was used to assess the EV' genetic content. The modulation of inflammatory and senescence markers in hADMSC was evaluated by RT-qPCR using cDNA arrays and validated by immunoblotting. A protein profiler phospho-kinase array was used to explore signaling pathways. RESULTS: Hypoxic culture conditions did not significantly alter the genetic content of MDA-MB-231-secreted EV, but the addition of EGCG significantly modified EV genetic material at low oxygen tension. Gene expression of cancer-associated adipocyte pro-inflammatory markers *CXCL8*, *CCL2* and *IL-1B* was increased in hADMSC treated with EV. Concomitantly, EV isolated from MDA-MB-231 treated with EGCG (EGCG-EV) downregulated *CCL2* and *IL-1B,* while inducing higher expression of *CXCL8* and *IL-6* levels. EV activated CHK-2, c-Jun, AKT and GSK-3β signaling pathways in hADMSC, whereas EGCG-EV specifically reduced the latter two as well as the serum starvation-induced senescence markers P21 and β-galactosidase. Finally, the mitochondrial content within the TNBC cells-derived EV was found reduced upon EGCG treatment. CONCLUSION: This proof-of-concept study demonstrates that the chemopreventive properties of diet-derived polyphenols may efficiently target the paracrine regulation that TNBC cells could exert upon their surrounding adipose tissue microenvironment.

4.3 Significance statement

The present study reveals that diet-mediated intervention, such as through circulating EGCG, can alter the genetic material found within the TNBC cell-derived extracellular vesicles (EV). EGCG further reduced the capacity of the EV to trigger the pro-inflammatory and senescence processes that often are associated with a chemoresistance phenotype. EGCG caused a reduction in the mitochondrial content of cancer cells-derived EV, reinforcing its overall antitumoral role. Circulating diet-derived polyphenols may therefore represent an efficient chemopreventive strategy to reduce the paracrine regulation that TNBC cells exert within their surrounding adipose tissue environment.

4.4 Introduction

The release of extracellular vesicles (EV) loaded with proteins, lipids, and nucleic acids is an efficient mechanism for cell-to-cell communication (Tkach and Thery, 2016). EV differ in size and origin, but they are all delimited by a phospholipid bilayer. Exosomes are the most accepted term for smaller EV with a diameter between 30-150 nm and from endosomal origin (Stein and Chiang, 2014). On the other hand, microvesicles (also termed microparticles or ectosomes) represent a more heterogeneous population of particles that emerge from the plasmatic membrane budding with a size ranging from 100-1000 nm (Taylor and Bebawy, 2019). Specific RNA, DNA and proteins can be sorted into these secreted vesicles and regulate the gene expression of other cells in distant tissues or within the metastatic niche (Becker *et al.*, 2016; Taylor and Bebawy, 2019). Several studies have reported the role of EV in mediating processes like inflammation (Chimen *et al*., 2020; Duchez *et al.*, 2015; Mause *et al*., 2005; Wadey *et al*., 2019) and tumor progression (Becker *et al*., 2016). For instance, glioma-derived-EV harbouring the mutated variant III of the epidermal growth factor receptor (EGFRvIII) transferred this oncoprotein to other cancer cells and promoted the expansion of a more aggressive tumor phenotype (Al-Nedawi *et al*., 2008).

Nowadays, it is well-accepted that tumors control and pre-condition the metastatic niche in part through the release of EV (Sundararajan *et al*., 2018). However, little is known about the EV-mediated paracrine regulation of cells within the tumor tissue microenvironment and how the neighbouring resident cells, particularly those from the adipose tissue, can be impacted in response to triple-negative breast cancer (TNBC) cells' secretome. In this regard, it has been reported that tumor-derived EV can mediate the differentiation of normal fibroblasts into cancer-associated fibroblasts (CAF) (Wei *et al.*, 2017), induce immune suppression throughout the release of immune checkpoints (Li *et al.*, 2021; Poggio *et al*., 2019), and promote tumor metastasis (Jain, 2014).

Many factors can influence the molecular signature and composition of cell secretome and must be considered during *in vitro* studies using cell cultures. These include low oxygen hypoxic culture conditions, which mimic conditions found within solid tumors and in which cancer cells must survive through high proliferation rates and oxygen consumption (Kucharzewska et al., 2013). The effect of hypoxia on the release mechanisms of EV has been reviewed for different cell types (Bister et al., 2020), and some studies have emphasized its impact on the EV' cargo (Kucharzewska et al., 2013). The main focus has been on the content and identity of the miRNAs (small non-coding RNAs) profile within the hypoxic-EV because of their capacity to regulate gene expression (Bartel, 2004). In addition, EV have been reported to carry and deliver functional mitochondria, free mitochondrial DNA (mtDNA) and their components with a regulatory impact on inflammation (Boudreau et al., 2014; Duchez et al., 2015; Todkar et al., 2021). Consequently, the horizontal transfer of mitochondrial components between cells can modulate the recipient cell's phenotype, including cell respiration (Spees et al., 2006) and cell viability (Kitani et al., 2014; Wang et Gerdes, 2015), and trigger a tumorigenic potential of the recipient cell (Dong et al., 2017; Tan et al., 2015). Studies in this topic have been carried out in platelets (Boudreau et al., 2014) or neutrophils (Yousefi et al., 2009), and only few have investigated the role of tumor-derived EV packed with mitochondrial components. In this regard, Sansone et al. reported that mtDNA transferred from EV leads to the exit from dormancy of therapy-induced cancer stem-like cells, inducing resistance to hormone therapy in metastatic breast cancer patients (Sansone et al., 2017).

Our previous research demonstrated that the secretome of a TNBC-derived cell line triggered the migration and acquisition of a pro-inflammatory phenotype in a human mesenchymal stem cell line derived from the adipose tissue (hADMSC) (Gonzalez Suarez et al., 2022). Furthermore, acquisition of this inflammatory phenotype was prevented by the green tea polyphenol epigallocatechin-3-gallate (EGCG) (Gonzalez Suarez et al., 2022). EGCG has a well-known antitumoral and antioxidant effect (Min et Kwon, 2014). More recently, it has been reported in a murine

model that EGCG inhibited the exosome-mediated infiltration of tumor-associated macrophages (TAM) by transferring miR-16 (Jang et al., 2013). Breast adipose tissue-derived mesenchymal stromal/stem cells are crucial components prone to respond to cues from the tumor microenvironment, and a critical step initially involved in this process, might be their de-differentiation into tumor-supporting phenotypes (Ritter *et al.*, 2023), blocking their response within the tumor microenvironment could therefore serve as a novel chemopreventive strategy effective against breast cancer cell paracrine regulation.

In the present study, we aimed to evaluate the contribution of the tumoral-elicited EV in the induction of a pro-inflammatory phenotype in hADMSC, and whether the genetic content of EV isolated from TNBC-derived MDA-MB-231 cells treated with EGCG was altered. Given the recently discovered link between inflammation and senescence processes (Pribluda et al., 2013; Schmitt et al., 2022), we addressed if EV could trigger senescence in hADMSC and whether this can be prevented by EGCG. Since the mitochondrial content could also contribute to the acquisition of such phenotype in hADMSC, we also analyzed the effect of EGCG on the sorting of mitochondrial components within the EV.

4.5 Materials and methods

4.5.1 Materials

Bovine serum albumin (BSA), sodium dodecyl-sulphate (SDS) and epigallocatechin-3-gallate (EGCG) were obtained from Sigma-Aldrich Canada (Oakville, ON). Phosphate-buffered saline (PBS) buffer solution (pH ~7.4) was purchased from (Wisent, Saint-Jean-Baptiste, QC, Canada). For the SDS-polyacrylamide gel electrophoresis (SDS-PAGE), the reagents were from Bio-Rad (Mississauga, ON), as well as the enhanced chemiluminescence (ECL) reagents. Micro

bicinchoninic acid (BCA) protein assay reagents were purchased from Pierce (Rockford, IL). The antibodies against BIP, P16, IL-6, phospho-AKT, AKT, phospho-GSK-3β, and GSK-3β were obtained from Cell Signaling Technology Inc (Danvers, MA). The anti-Tubulin antibody was purchased from ICN Biomedical (Aurora, OH), anti-P21 was from Abcam (Cambridge, UK), and anti-CD9, CD63 and CD81 from ThermoFisher Scientific (Waltham, MA). Horseradish peroxidase-conjugated anti-rabbit and anti-mouse IgG secondary antibodies were from Jackson ImmunoResearch Laboratories (West Grove, PA).

4.5.2 Cell culture and procedure to generate the conditioned media for EV isolation

The human adipose-derived mesenchymal stem/stromal cells (hADMSC) and TNBC-derived cell line MDA-MB-231 were purchased from the American Type Culture Collection (ATCC, Manassas, VA). hADMSC were grown in Mesenchymal Stem Cell Basal Medium (ATCC, PCS-500-030) and supplemented with Mesenchymal Stem Cell Growth Kit Low Serum (ATCC, PCS-500-040). They were further reported to be able to undergo adipogenesis (Gonzalez Suarez et al., 2022). MDA-MB-231 cells were grown in EMEM Medium (Wisent, 320-036-CL) supplemented with 10% fetal bovine serum (FBS). All cells were cultured at 37°C under a humidified 95-5% (*v*/*v*) mixture of air and CO_2. The TNBC cell secretome was generated upon a 48-hour serum deprivation of a ~70% confluent MDA-MB-231 cell culture. To generate the conditioned media for the vesicle's isolation, approximately 2-5 x 10^6 of MDA-MB-231 cells were seeded in 175 cm^2 cell culture flasks and cultured in EMEM (Wisent, Saint-Jean-Baptiste, QC, Canada) supplemented with 10% FBS. When the cells reached approximately 70-80% confluence, the monolayer was washed twice with negative media (NM) and left in a 20 mL/flask of NM with or without 30 µM of EGCG for 48 hours. Then, the conditioned media was harvested and clarified by centrifugation at 1,500g for 20 minutes to remove cell debris and stored at 4°C for a maximum of one week pending EV's isolation. For the experiments at different oxygen tensions, after

the monolayers reached a 70% of cell confluency, cells were incubated for 48 hours at 37°C under normoxic (21% of O_2 and 5% CO_2) or in hypoxic ($O_2 \leq 1\%$ and 5% CO_2) culture conditions. Next, RNA was extracted for genes expression analysis.

4.5.3 Extracellular vesicle isolation

The clarified conditioned media was concentrated form 40 mL to 10 mL by centrifugation using Amicon Ultra-3K (Millipore, Oakville, ON). EV were then isolated with ExoQuick-TC Exosomes precipitation Solution Kit (SBI) following the manufacturer protocol. The exosomal pellet was resuspended in 500 µL of PBS for dynamic light scattering (DLS) particle size analysis or in Trizol for the RNA-Seq analysis. In the case of *in vitro* experiments, the vesicles' pellet was resuspended in 200 µL of unsupplemented Mesenchymal Stem Cell Basal Medium (BM). Vesicles obtained under normoxia and in the presence of EGCG were labelled as EGCG-EV to distinguish them from those obtained without the catechin (EV).

4.5.4 Extracellular vesicles relative quantification

A portion of the EV's pellet was used for the relative quantification of the particles. Samples were incubated in the presence of membrane-specific dye MemGlowTM 488 (100 nM, Cytoskeleton Inc., Denver, CO) in a total volume of 100 µL containing 20 µL of the EV's pellet suspension and incubating 20 minutes at room temperature in the dark. Samples were then diluted with the addition of 100 µL of PBS and processed for flow cytometry analysis for total number of EV's particles. Briefly, using the high-resolution flow cytometer Cytoflex (Beckman Coulter, Indianapolis, IN), we quantified the number of MemGlow-positive vesicles in an acquisition volume of 30 µL (gating strategy shown in Supplementary Fig.S4.1). EV's count in the original sample was obtained using the following equation: number of particles/µL= (P2*6.7)/20.

4.5.5 Dynamic light scattering

EV's size/diameter was assessed by dynamic light scattering (DLS). The mean hydrodynamic diameter of EV was calculated by fitting a Gaussian function to the measured size distribution. Prior to DLS measurements, each sample was centrifuged at 300g for 10 seconds to pellet large aggregates; 50 µL of the sample was added to a ZEN00400 cuvette, and DLS measurements were conducted at 25°C using a Nano ZSP Zetasizer (Malvern Instruments Ltd., UK) operating at 633 nm and recording the back-scattered light at an angle of 175°. The sample was allowed to equilibrate for 2 minutes before each measurement. DLS was recorded for 200 seconds with three replicate measurements. Signal intensity was transformed to volume distribution, assuming a spherical shape of EV, using the Malvern Instruments Ltd. software.

4.5.6 Western blotting

The hADMSC were lysed in a buffer containing 1 mM NaF, 1 mM Na_3VO_4 and a phosphatase inhibitory cocktail (END Millipore, Germany). Then, the proteins (10 µg) were separated in a polyacrylamide gel at 7.5% or 12% during an SDS-PAGE in denaturing conditions. Next, proteins were electro-transferred to polyvinylidene difluoride (PVDF) membranes and blocked with non-fat dry milk (5%) in Tris-buffered saline (150 mM NaCl, 20 mM Tris-HCl, pH 7.5) at 0.3% Tween-20 (TBS-T, TWN510-500), for 1 hour at room temperature. PVDF membranes were washed three times in TBS-T and incubated with the appropriate primary antibodies (1/1,000 dilution) overnight at 4°C with agitation. All primary antibodies were resuspended in a solution of TBS containing 3% BSA and 0.1% sodium azide (Sigma-Aldrich). Finally, the PVDF membranes were incubated for 1 hour with horseradish peroxidase-conjugated donkey anti-rabbit or anti-mouse IgG at 1/2,500 diluted in TBS-T at 5% of non-fat dry milk. ECL was used to visualize the immunoreactive material (Bio-Rad, Mississauga,

ON, Canada). Tubulin detection within the hADMSC lysates was used as loading control. To confirm the presence of exosomes, the EV were lysed in RIPA buffer 1X (NaCl 150 mM, NP-40 1%, SDS 0.1%, TRIS 50 mM, at pH 7.5), and 4 µg of protein were separated by SDS polyacrylamide, in a 12% gel during electrophoresis (SDS-PAGE), and under non-denaturing conditions. Next, the standard Western blot protocol was used to detect CD63, CD9 and CD81 exosome markers. A human phosphor-kinase array kit (Proteome ProfilerTM, R&D System® Inc, Minneapolis, MN) was used to screen the activated pathways in the hADMSC upon 1 hour treatment with the EV and EGCG-EV. The detection was performed according to the manufacturer's instructions. Densitometry analyses were performed using ImageJ software version 1.53e.

4.5.7 Characterization of MDA-MB-231-derived EV interaction with hADMSC

The EV preparations were evaluated by flow cytometry for their capacity to interact with the targeting hADMSC. Once the vesicles isolated, they were labelled using MemGlowTM 488 as described above, then washed with PBS by ultracentrifugation at 100,000g for 1 hour at 4°C and resuspended in basal media. The hADMSC (10,000 cells/mL) were incubated with the EV at a ratio of 1:1 (cells:EV) in basal media and suspensions kept for 2 hours at 37°C. Next, the population of fluorescent cells was analyzed by flow cytometry using an Accury C6 device (Beckman Coulter, Indianapolis, IN).

4.5.8 Confocal microscopy

To detect the presence of EV within the hADMSC, 10,000 cells were seeded in EBD plates (New Biotechnology Ltd). The next day, growth media was collected, and 500 µL of basal media with and without the MemGlow-labelled EV were added for a 2-hour incubation on cells. Fluorescent vesicles attached to the cells were visualized using a live imaging confocal microscope (Nikon Instruments Inc., Melville, NY). The

experiment was performed two times, and pictures of three different fields were taken. To determine whether the mitochondrial components present within the EV could be efficiently transferred to the hADMSC, MDA-MB-231 cells were seeded in 175 cm flasks and incubated over night with mitoTracker Deep Red (MTR) at a final concentration of 200 nM in negative media (NM). Then, the monolayer of cells was washed with PBS and kept for 24 hours in NM and EV (MTR+EVs) were isolated as described in the Methods section and protected from light. hADMSC were seeded on top of tissue culture glass slides (Falcon, NY, USA) previously coated with Poly-lysine. 200 µl of MTR+EVs were then resuspended in NM and incubated for 4 hours. Cells were then labelled with 100 nM MemGlow, incubated for 20 minutes at RT and in the dark. Finally, cells were fixed in 1% paraformaldehyde solution and DAPI was added to stain the nucleus. Pictures were taken using a fluorescence microscope.

4.5.9 Senescence detection assay

The level of β-galactosidase (β-gal) activity was assessed using the CellEvent™ Senescence Green Detection kit (ThermoFisher Scientific). hADMSC (8,000 cells/well) were seeded onto a poly-L-lysine (Sigma Aldrich, Oakville, ON) pre-coated glass chamber (Nunc, NY, USA). Once the cells adhered, the growth media was removed. EV, EGCG-EV or basal media were added for 24 hours and at a ratio of 1:2 (Cells:EV). Then, cells were washed and stained according to the manufacturer's instructions for the detection of β-gal activity. The nucleus was stained with DAPI. Experiments were performed in duplicate per biological condition, and three pictures/well were taken. The results were presented as the percent (%) of positive cells per field (number of β-gal positive cells/total of cells)*100.

4.5.10 Chemotactic cell migration assay

The experiments performed to evaluate the migration induction caused by the EV were carried out using the Real-Time Cell Analyzer (RTCA) Dual-Plate (DP) Instrument of the xCELLigence system (Roche Diagnostics, Mississauga, ON). The migration plates (CIM-Plates 16) have conventional trans-wells (8 µm pore size) with gold electrode arrays on the upper chamber to record real-time cell migration. Before seeding the cells, the wells of the upper chamber were coated with 25 µL of 0.15% gelatin in PBS and incubated for one hour at 37°C, followed by a wash with PBS. Then, hADMSC (10,000 cells/well) were added and co-cultured with the EV at a ratio of 1:1 (cells:EV) in the upper chamber of the device. The RTCA-DP Instrument software measured the impedance values and expressed them in arbitrary units as Normalized Cell Migration Index. Chemotaxis in response to basal media supplemented with 1% FBS, added to the bottom chamber, was monitored for 8 hours.

4.5.11 Quantification of the mitochondria-containing vesicles

The cell culture media supernatant was filtered using a 1.2 µm syringe filter to remove any remaining cell contaminants. This is a well validated approach to evaluate clinical samples without performing ultracentrifugation (Witwer *et al.*, 2013). For each sample, 5 µL of the supernatant was combined with 1 µL of anti-CD44-FITC (Biolegend), 1 µL of MitoTracker Deep Red (100 nM final concentration, ThermoFisher Scientific) and 93 µL of 0.2 µm filtered PBS (Corning). Labeling was performed by incubating the mixture for 15 minutes at room temperature in the dark. Samples were then processed on the Attune NxT flow cytometer (ThermoFisher Scientific) for quantification of the EV's subpopulation as previously reported (Boudreau *et al.*, 2014; Gharib *et al.*, 2023; Leger *et al.*, 2022). Gating strategies were established using a non-relevant anti-CD41-FITC antibody (Biolegend) for the MDA-MB-231 cell line. EV's subpopulation profile was determined by quantification of the CD44+/MitoTracker Deep Red- events (MPs) and the CD44+/MitoTracker Deep Red+ events (mitoMPs).

4.5.12 Citrate synthase activity assay

The citrate synthase activity was performed as previously described (Thibault, 1997). Briefly, imidazole (Sigma-Aldrich) was resuspended in water at 6.8 mg/mL (pH 8.0). The reaction medium was then prepared by adding 0.1 mM of DTNB (5,5-dithio-bis-(2-nitrobenzoic acid)) sodium salt (Sigma-Aldrich) and 0.1 mM of AcetylCoA (Sigma-Aldrich) to the imidazole solution. The oxaloacetate solution was prepared by dissolving oxaloacetic acid in imidazole buffer at 0.2 mg/mL. The cell culture medium supernatant (100 µL) was centrifuged at 17,800g for 90 minutes with the resulting pellet resuspended in 5 µL of imidazole solution. In a 96-well plate, 200 µL of the reaction medium, 20 µL of the oxaloacetate solution and 5 µL of sample were subsequently added to the wells. The plate was then placed in a Biotek Synergy H1 Hybrid Microplate Reader where the absorbance was measured at 412 nm for 4 minutes at 30-second intervals (9 total reads) with continuous plate shaking between reads. The slopes (ΔA/min) obtained from the reads were used to calculate the activity (AE; U/mL). For consideration, the DTNB has an extinction coefficient (ε) of 13.6 mL/(cm*µmol), the total volume is 225 µL, the sample volume is 5 µL and the light path is 0.643 cm. Each well of the 96-well plate has a diameter (d or 2x radius (r)) of 6.675 mm.

4.5.13 Total RNA isolation, cDNA synthesis, and RT2 Profiler PCR arrays

Total RNA was extracted from cell monolayers using 1 mL of Trizol reagent for a maximum of 3 x 10^6 cells as recommended by the manufacturer (Life Technologies, Gaithersburg, MD). For cDNA synthesis, 1 µg of total RNA was reverse transcribed using the R2 First Strand kit (QIAGEN, Valencia, CA). The cDNA was stored at -80°C prior to PCR. To detect the genes modulated upon treatment with EV and EGCG-EV, the hADMSC (100,000 cells/well) were seeded in a six-well plate (SARSTEDT,

Montreal, QC). The next day the growth media was removed, and the cells were co-incubated with BM or with the EV or EGCG-EV resuspended in BM and at a ratio of 1:0.5 (cells:EV) for twenty-four hours at 37°C and 5% of CO_2. Then, cells were resuspended in Trizol for RNA isolation. The RT2 ProfilerTM PCR Array for Human Inflammatory Cytokines and Receptors (PAHS-181Z) and Human Cellular Senescence (PAHS-050ZD) were used according to the manufacturer's protocol (QIAGEN). The detailed list of the genes assessed can be found at the manufacturer's website (https://geneglobe.qiagen.com/us/product-groups/rt2-profiler-pcr-arrays). Using real-time quantitative PCR, we analyzed the expression of a panel of genes related to the inflammatory response and senescence markers that have already been published. Relative gene expression was calculated using the $2^{\Delta\Delta C_T}$ method ("delta-delta" method), in which C_T indicates the fractional cycle number where the fluorescent signal crosses the background threshold. This method normalizes the $\Delta\Delta C_T$ value of each sample using five housekeeping genes (B2M, HPRT1, RPL13A, GAPDH, and ACTB). The normalized fold change (FC) values are then presented as average FC = 2 (average $\Delta\Delta C_T$). Only genes amplified less than 35 cycles were analyzed. The resulting raw data were then analyzed using the PCR Array Data Analysis Template (http://www.sabiosciences.com/pcrarraydataanalysis.php). This integrated web-based software package automatically performs all $\Delta\Delta C_T$-based FC calculations from the uploaded raw threshold cycle data.

4.5.14 Total RNA library preparation and sequencing

The isolated vesicles preparations were resuspended in 500 µL of Trizol in triplicate per condition for library preparation. Total RNA was isolated using Trizol (ThermoFisher) and RNeasy mini kit (Qiagen) according to the manufacturer's instructions. RNA was quantified using Qubit (ThermoFisher Scientific), and RNA quality control was assessed with the Bioanalyzer RNA 6000 Nano assay on the 2100 Bioanalyzer system (Agilent Technologies, Mississauga, ON). Transcriptome libraries

were generated using the KAPA mRNA-Seq HyperPrep kit (Roche) using a poly-A selection (ThermoFisher Scientific). **S**equencing was performed on the Illumina NextSeq500, obtaining around 20M single-end 75bp reads per sample.

4.5.15 Reads alignment and differential expression analysis

Reads were 30 trimmed for quality and adapter sequences using the Trimmomatic (version 0.35). Only reads with at least 50 bp length were kept for further analyses. Trimmed reads were aligned to the reference human genome version GRCh38 (gene annotation from Gencode version 37, based on Ensembl 103) using STAR version 2.7.1a (Dobin et al., 2013). Gene expressions were obtained as read count directly from STAR and computed using RNA-Seq by Expectation Maximization (RSEM) (Li et Dewey, 2011) to get normalized gene and transcript level expression, in TPM values, for these stranded RNA libraries. Differential expression analysis was performed using DESeq2 version 1.22.2 (Love et al., 2014). The package limma (Ritchie et al., 2015) was used to normalize expression data and read counts data were analyzed using DESeq2. Principal component analysis (PCA) for the first two most significant components was conducted with R packages (Team, 2017). iDEP (integrated Differential Expression and Pathway) analysis (Ge et al., 2018) was also used to determine significant differentially expressed genes (DEG) with a DESeq2 false discovery rate (FDR) adjusted p-value of 0.05 and fold-change with a cut-off of two. Gene expression was scaled and centered across samples using the mean and standard deviation and k-means clustering was performed using the consensus of least 10-independent runs using the R package ComplexHeatmap (Gu et al., 2016). Pathways enrichment analysis were performed with selected genes using the PathfindR package tool (Ulgen et al., 2019). Gene ontology (GO)-SLIM PANTHER 7.0 (protein annotation through evolutionary relationship) analysis of biological process and protein class were performed in the online platform (Gene Ontology Resource), using the Homo sapiens database as reference list.

4.5.16 Statistical data analysis

Unless otherwise stated, data was expressed as mean ± standard error of the mean (SEM) from three or more independent experiments. Hypothesis testing was conducted using the Mann–Whitney test (two-group comparisons) or Wilcoxon signed-rank tests for independent or paired samples respectively. Critical values below 0.05 were deemed statistically significant and accordingly denoted in the figures (*: $p < 0.05$, **: $p < 0.01$). All statistical analyses were performed using the GraphPad Prism 8.0.1 software (San Diego, CA).

4.6 Results

4.6.1 Characterization of the MDA-MB-231-derived EV and validation of the *in vitro* approach.

To characterize the EV's release, serum-starved TNBC-derived MDA-MB-231 cells were cultured in the presence or absence of 30 µM EGCG for 48 hours. This concentration of EGCG has been previously documented to not alter MDA-MB-231 cell viability (Banerjee et Mandal, 2022; Xie *et al.*, 2021). Conditioned media was next collected, and EV were isolated as described in the Methods section. Particle distribution of both EV's preparations were analyzed using DLS. EV samples showed a single peak with a mean diameter of ~100 nm, which corresponds with the expected exosome size, whether isolated from control cells (Figure 4. 1A, upper panel) or EGCG-treated cells (Figure 4. 1B, upper panel). However, when the peaks were analyzed as percent of intensity, we detected the presence of an additional population with sizes bigger than those expected for exosomes (Figure 4. 1A and B, lower panels). This suggests that samples are heterogeneous, and this is also reflected by the polydispersity index which approximated 1. Nevertheless, the expression of the exosome enriched proteins CD9, CD63 and CD81 was confirmed by immunoblotting in the EV lysates (Figure 4. 1C), using BiP as a protein not expected to be enriched within this fraction since it rather associates with secretory pathways (Thery *et al.*, 2018). Hence, one may safely consider our EV samples as a mixture of particles with different origins and will be termed from now on as EV rather than exosomes.

Next, EV capacity to interact with the hADMSC and their impact on the recipient cell's behaviour was investigated. EV were labelled using MemGlow, an amphiphilic probe with high specificity for the plasma membrane and incubated for 2 hours with hADMSC. Flow cytometry analysis confirmed that fluorescent EV highly interacted (≥99%) with hADMSC (Figure 4. 1E). In addition, confocal fluorescent microscopy

further demonstrated the presence of fluorescent EV associated with hADMSC (Fig.4.1F). Finally, hADMSC were treated with the EV at a 1:1 ratio (cell:EV) and cell migration assessed in response to basal media supplemented with 1% FBS. hADMSC treated with EV had a 3-4-fold increase in cell migration rate than untreated cells (Fig.4.1D). These results demonstrate that the MDA-MB-231 derived-EV can trigger a pro-migratory adaptive response in hADMSC, confirming a potential bidirectional movement from adipose tissue cells towards the tumor microenvironment.

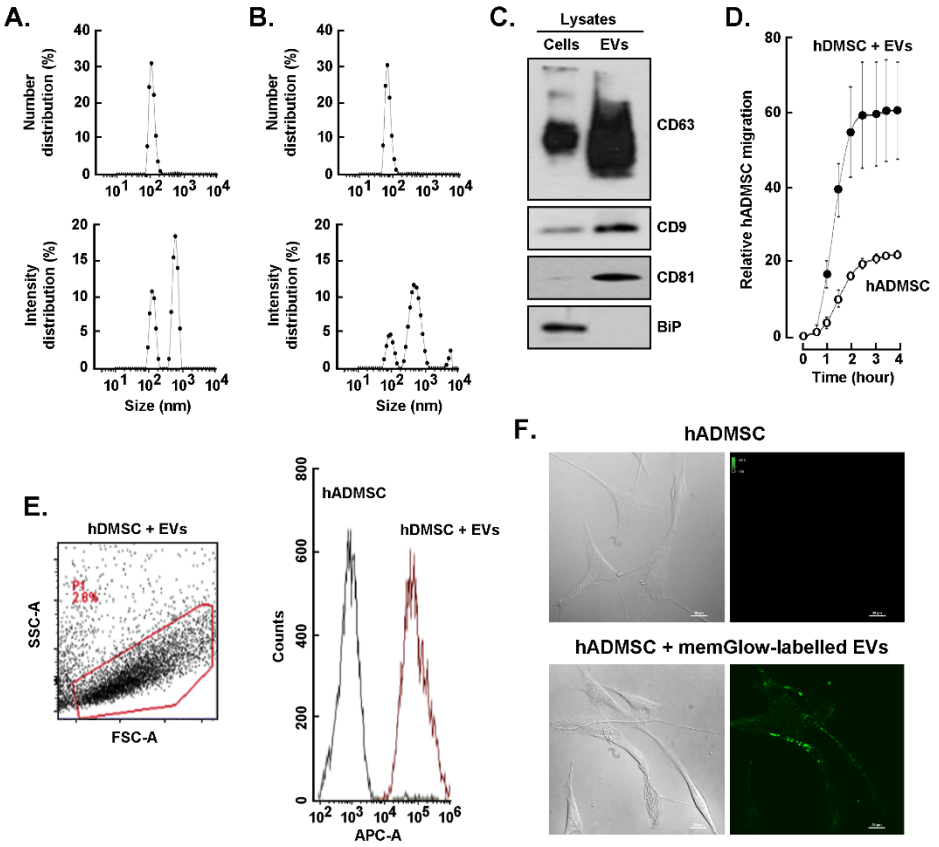

Figure 4. 1. Characterization of the EV isolated from the MDA-MB-231 cells conditioned media.
Serum-starved triple-negative breast cancer-derived MDA-MB-231 cells were cultured for 48 hours in the absence or presence of 30 µM EGCG. Conditioned media was next collected, concentrated, and extracellular vesicles (EV) isolated as described in the Methods section. Dynamic light scattering particle size analysis of the **A)** EV and **B)**

EGCG-EV showing the distribution of the particles by number and by intensity of the refracted light. A representative experiment out of four is presented. **C)** Immunoblotting of the proteins enriched in exosomes CD9, CD63 and CD81, and of the negative marker BIP in MDA-MB-231 cell lysate and EV lysate. **D)** Relative cell migration rate of hADMSC treated with EV (closed circle) or basal media (BM, open circle) in response to basal media supplemented with 1% FBS. Migration experiments were performed three times in quadruplicate. **E)**. Gating strategy of the flow cytometry experiment performed to assess MemGlow-488 labelled EV interaction with hADMSC. Merged histogram was obtained by the measurement by flow cytometry of the untreated cells (black lines) and the cells incubated with stained-EV (red lines). One representative experiment out of two is presented. **F)** Representative microscopy images of hADMSC incubated for two hours with the MDA-MB-231 cells-derived EV labelled with MemGlow-488. One representative experiment out of three is presented (scale bar is 20 µm). *Diameter in nanometers* (d.nm), *polydispersity index* (Pdl), intensity weighted mean hydrodynamic size of the particles (Z-Average). Statistically significant differences were determined by the non-parametric comparison test Mann-Whitney, * $p<0.05$.

4.6.2 Transcriptomic analysis and impact of EGCG on the EV load released by MDA-MB-231 cells.

MDA-MB-231-EV are heterogeneous, and many factors can influence their content. Next, we investigated the specific transcript content packaged into the EV following EGCG treatment. Our RNA-Seq analysis identified a total of 1116 differentially expressed genes (DEG) between EV isolated from control (EV) or EGCG-treated cells (EGCG-EV) (**Error! Reference source not found.**A, and Supplementary Table S4. 1). An asymmetric DEG distribution was observed with a slight tendency to gene downregulation in EGCG-EV (619 downregulated vs 497 upregulated). Next, we searched for pathways enrichment containing the identified DEG using an active subnetwork-based algorithm (Ulgen *et al.*, 2019). Among the pathways enriched, cellular senescence, cell cycle, signaling pathways associated with IL-17, HIF-1 and Notch were observed (**Error! Reference source not found.**B). Interestingly, the highest genes induced in EGCG-EV, were found to associate with mitochondria-related pathways, and further included oxidative phosphorylation,

chemical carcinogenesis-reactive oxygen species, and mitophagy (**Error! Reference source not found.**B). The latter further interconnected with thermogenesis, proteoglycans in cancer and small cell lung cancer biomarkers (**Error! Reference source not found.**C).

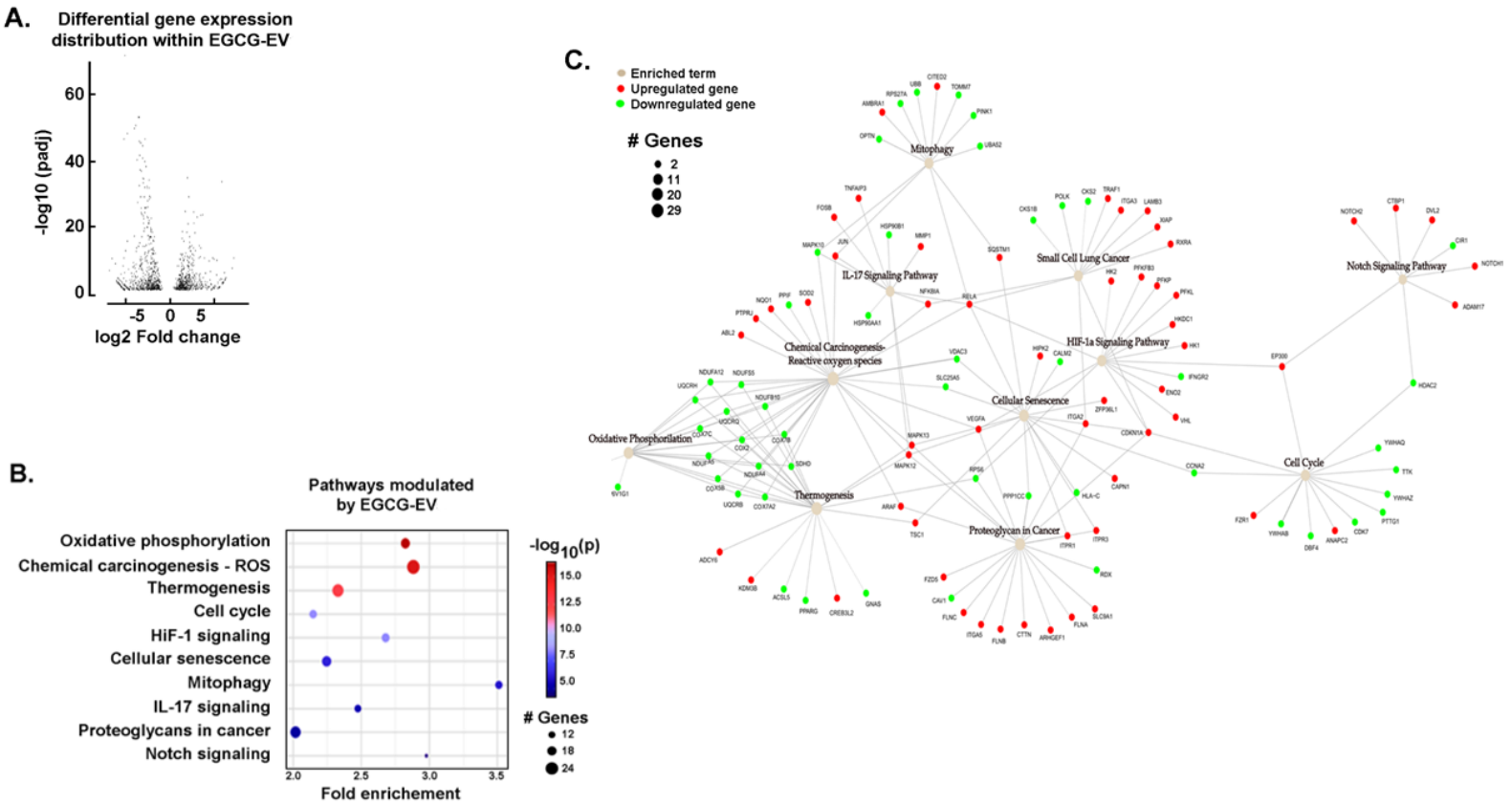

Figure 4. 2. Modulation of the EV's cargo by EGCG.

The extracellular vesicles (EV) were isolated from serum-starved MDA-MB-231 cells treated or not with 30 μM EGCG for 48 hours. **A)** Volcano plot for the expression profile of differentially expressed genes (DEG) with an adjusted *p*-value < 0.05 was selected as the threshold. **B)** KEGG pathway enrichment analysis resulted from the comparison of DEG (EGCG-EV vs EV) with absolute fold change (FC) > 2, and adjusted *p*-value < 0.05. **C)** Network graph showing the enriched pathways and their respective genes. Enriched terms are coloured in beige, while upregulated and downregulated genes are coloured in red and green, respectively.

4.6.3 TNBC cell-derived EV trigger specific signaling pathways in hADMSC.

To address whether both MDA-MB-231-derived EVs' preparations activated different downstream signaling cascades in hADMSC, we first quantified the EV by flow cytometry as described in the Methods section (Supplementary Figure S4. 1A-C). Importantly, no statistical difference in the mean of fluorescence intensity (MFI) between the MemGlow-labelled EV and EGCG-EV was observed (Supplementary Figure S4. 1D), and neither in their interaction capacity with hADMSC (

Supplementary Figure S4. *2*). Interestingly, in terms of number of particles, EGCG-treated MDA-MB-231 were found to release more EV than untreated cells (Supplementary Figure S4. 1E).

Next, downstream phosphorylated intermediates were evaluated with a phospho-kinase immunoblotting array in hADMSC lysates isolated upon incubation with basal media (BM), EV, or EGCG-EV (Figure 4. 3A). Densitometry analysis performed on duplicate lysates from two independent membranes demonstrated that P38A, STAT5A/B and P53 phosphorylation status were induced, but unmodified upon any treatment (Figure 4. 3B). Such screen further revealed that checkpoint kinase 2 (CHK-2) and c-Jun N-terminal kinases JNK (c-Jun) phosphorylation were induced upon EV and EGCG-EV treatments (Figure 4. 3B). Interestingly, EGCG-EV demonstrated an inhibitory effect on the protein kinase B signaling pathway (AKT) and the glycogen synthase kinase-3 beta (GSK-3β) (Figure 4. 3B). The latter two were further validated using individual antibodies against their phosphorylated and total protein states (Figure 4. 3C). Levels of phosphorylation status profiles confirmed the phospho-kinase array results (Figure 4. 3D), suggesting that MDA-MB-231-derived EV and EGCG-EV can exert differential downstream signaling pathways involved in cell survival and proliferation.

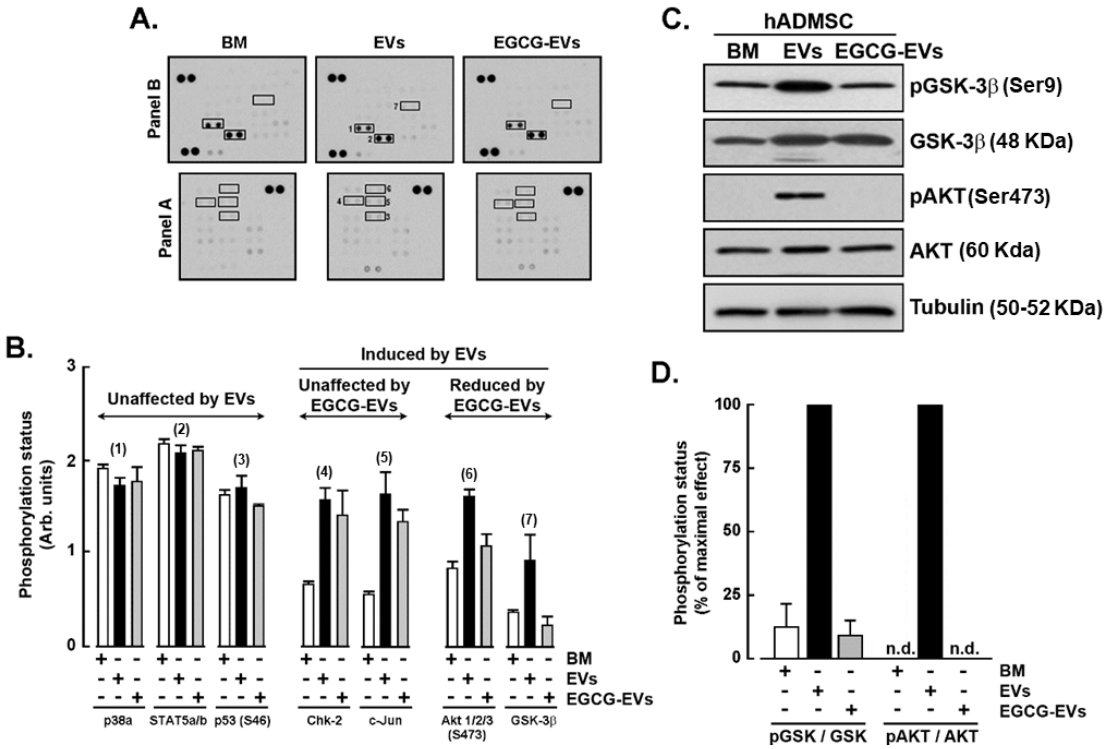

Figure 4. 3. Signaling cascades triggered by the EV.
The hADMSC were incubated for one hour in basal media (BM), EV, or EGCG-EV using a Cell:EV ratio of 1:0,5 (#:#). Cells were next lysed as described in the Methods section for Western blotting analysis. A phospho-kinase array was used to detect the pathways activation state. **A)** Immunoblotting results, and **B)** Densitometric analysis of the highlighted immunoreactive spots was performed using the ImageJ software. **C)** Validation of the phosphorylated and total states of GSK-3β and AKT by immunoblotting. **D)** Ratios of the phosphorylated/total forms of AKT and GSK-3β resulting from the densitometric analysis performed with ImageJ. Mitogen-activated protein kinases (p38); signal transducer and activator of transcription 5A/B (STAT5A/B); Checkpoint kinase-2 (CHK-2); c-Jun N-terminal kinases JNK (c-Jun); protein kinase B signaling pathway (AKT); glycogen synthase kinase-3 (GSK-3); tumor protein 53 (P53).

4.6.4 MDA-MB-231-derived EV trigger the induction of a pro-inflammatory phenotype in hADMSC.

Induction of a pro-inflammatory phenotype by the TNBC secretome was previously reported in hADMSC, and this was prevented by EGCG (Gonzalez Suarez

et al., 2022). Here, we assessed whether the different EV isolated had any biological effect on hADMSC. Then, cells were incubated for 24 hours in serum-free media in the presence of EV or EGCG-EV, and total RNA extracted from hADMSC and transcribed to cDNA. Levels of gene expression associated with inflammation were then assessed by qPCR using the Human Inflammatory Cytokines and Receptors RT^2 Profiler gene array. A cut-off of a fold change (FC) greater or equal to two was defined. Genes related to the cancer-associated adipocytes (CAA) phenotype were induced, and these included the C-C motif chemokine ligand 2 (*CCL2*), interleukin-1 beta (*IL-1B*), and C-X-C motif chemokine ligand 8 (*CXCL8*) (Figure 4. 4A). However, the C-C motif chemokine ligand 5 (*CCL5*) and the tumor necrosis factor (*TNF*) were not induced. Interestingly, the EGCG-EV induced a higher upregulation of *CXCL8* and interleukin-6 (*IL-6*) (Figure 4. 4A), and the latter IL-6 expression was also confirmed at the protein level (Figure 4. 4B).

In addition to the induction of the CAA biomarkers, other pro-inflammatory genes were increased upon incubation with the EV and included the C-C motif chemokine ligands 7, 11, 20 (*CCL7*, *CCL11*, *CCL20*), FAS ligand (*FASLG*), the C-X-C motif chemokine ligands 5 and 10 (*CXCL5*, *CXCL10*), and interleukin-27 (*IL-27*) (Figure 4. 4C). At the same time, EGCG-EV reduced their expression, except for *CXCL5*, while increased the expression of *CXCL1-3*. EGCG-EV also downregulated several interleukins (*IL-16*, *IL-13*, *IL-17C*), and other pro-inflammatory markers such as lymphotoxin-beta also known as tumor necrosis factor C (*LTB/TNF-C*), vascular endothelial growth factor A (*VEGFA*), and the C-X-C motif chemokine ligands 2 (*CXCR2*) (Figure 4. 4C).

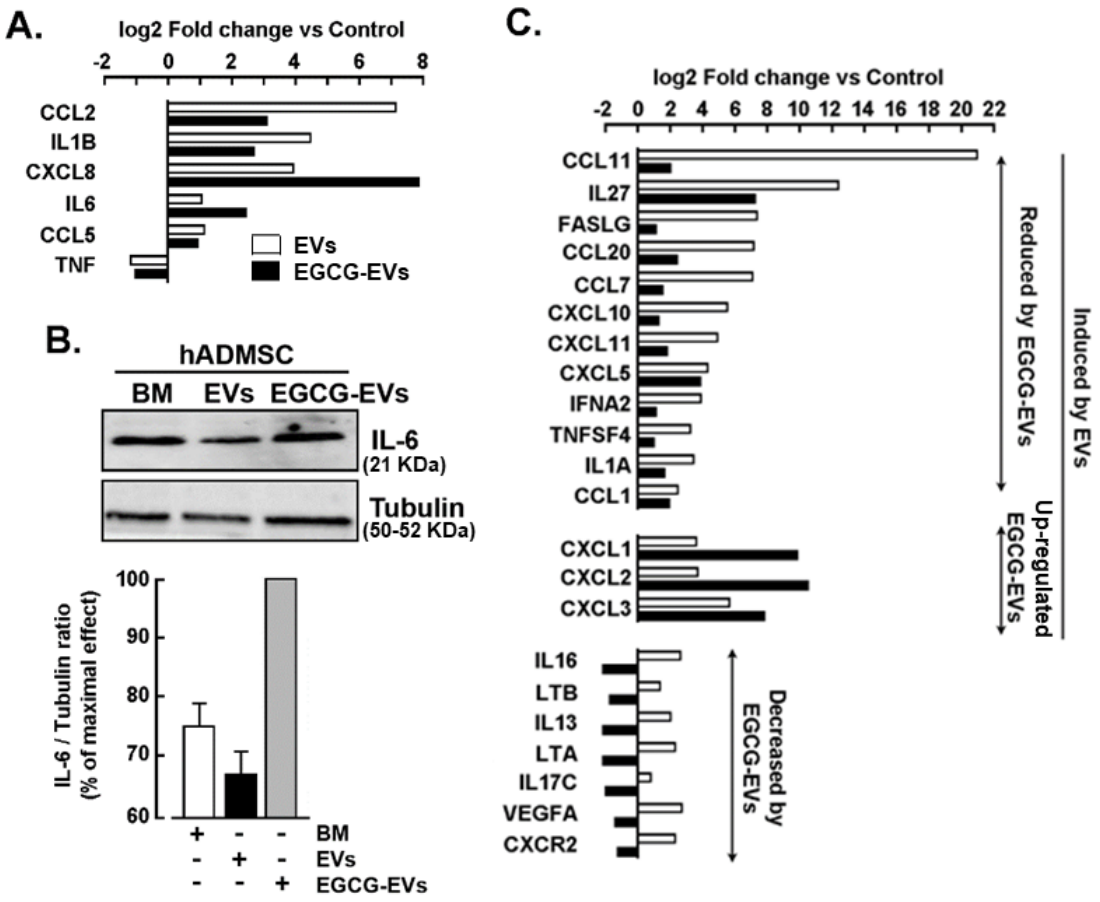

Figure 4. 4. Induction of a pro-inflammatory molecular signature by the MDA-MB-231 cells-derived EV.

The hADMSC were incubated for 24 hours in Basal Media (BM, Control), EV (white bars) or EGCG-EV (black bars) with a Cell:EV ratio of 1:0,5. Next, total RNA was isolated, and cDNA was synthesized. Gene expression levels were determined by qPCR using a Human Inflammatory Cytokine and Receptors RT2-Profiler gene array kit. Densitometric analysis was performed using the ImageJ software. **A)** The fold change (FC) expression of genes related to the cancer-associated adipocyte (CAA) phenotype, using the values obtained with BM as reference. **B)** Immunoblotting of interleukin-6 (IL-6) and tubulin (10 µg protein/well). **C)** FC of selected genes from the array to highlight the modulatory effect of the EGCG-EV.

4.6.5 MDA-MB-231-derived EV trigger hADMSC senescence.

Cancer-associated inflammation is one of the hallmarks of cellular senescence (Pribluda *et al.*, 2013). Since our experiments were performed without growth factors, we wished to assess the impact of serum starvation-induced hADMSC senescence in the presence or not of either EV or EGCG-EV. Senescence was effectively found to be induced upon 24 hours of serum starvation as P21 expression was triggered (BM condition) independently of the presence of EV (Figure 4. 5A). However, EGCG-EV treatment completely prevented serum-starvation induction of senescence. This was further assessed at the cellular level through the expression of primary senescence marker β-galactosidase (β-gal) (Dimri *et al.*, 1995). Hence, hADMSC were incubated with EV or EGCG-EV at 1:2 cells/EV ratio, then washed and stained for the expression of β-gal as described in the Methods section (Figure 4. 5B). In line with the increased expression of P21, the extent of β-gal positive cells increased with either BM or EV-treated cells, and the increase was prevented upon treatment with EGCG-EV (Figure 4. 5C). Total RNA was extracted, and cDNA was synthetized and used to screen for the modulation in the expression of senescence biomarkers with the Human Senescence RT^2-Profiler RT-qPCR gene array. EV treatment triggered NADPH oxidase 4 (*NOX4*), cell division cycle 25C (*CDC25C*), early growth response 1 (*EGR1*), cyclin-dependent kinase inhibitor 2B (*CDKN2B*), plasminogen activator urokinase (*PLAU*), thrombospondin 1 (*THBS1*), insulin-like growth factor 1 (*IGF1*) and the secreted protein acidic and rich in cysteine (*SPARC*) which were all significantly reduced in EGCG-EV-treated hADMSC (Figure 4. 5D). The only gene increased by the EGCG-EV, while not induced by the EV, was the superoxide dismutase 2 (*SOD2,* data not shown). Taking all these results together, it appears that the EGCG-EV can rescue hADMSC from senescence induced by serum starvation.

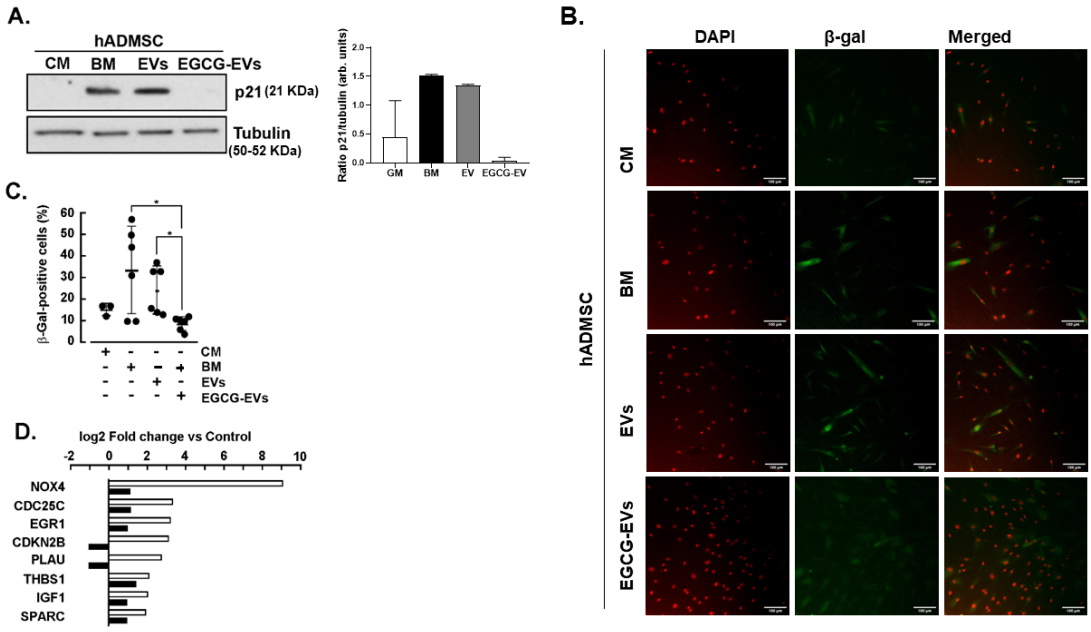

Figure 4. 5. EGCG-EV rescue hADMSC from serum-starvation-induced senescence. hADMSC were incubated for 24 hours in complete media (CM), serum-deprived basal media (BM), EV or EGCG-EV at a ratio Cell:EV of 1:0.5. hADMSC were collected for protein and total RNA as described in the Methods section. **A)** Immunoblotting detection of the senescence biomarker p21 and of the loading control tubulin from control hADMSC lysates, treated with CM, BM, or the respective EV. **B)** Confocal microscopy of hADMSC treated for 48 hours at a Cell:EV ratio of 1:2. The nucleus was stained with DAPI (red), and the expression of the senescence-associated β-galactosidase (β-gal) marker is coloured in green. **C)** Histograms showing the percent of positive β-gal cells obtained upon 48 hours of treatment. **D)** Gene expression of other senescence markers modulated in hADMSC by EGCG-EV compared with the expression level of the genes in cells incubated with EV, using as cut-off a log2 FC ≥ 2 and quantified by qPCR using the Human Senescence RT2-Profiler gene array kit. The percent of positive β-gal cells/field was calculated using the following equation: (number of positive cells /total of cells)*100. The non-parametric two-tailed Mann-Whitney test determined statistically significant differences, showing a ** $p<0.01$.

4.6.6 Presence of mitochondria within MDA-MB-231-derived EV.

Significant expression of genes related to mitochondrial processes were highlighted during the RNA-Seq analysis performed in the genetic material within the EV. Hence, we took a deeper look into those mitochondria-related genes and found that most of them were effectively detected in EV and downregulated in the EGCG-EV samples (Table 4. 1). Consequently, we tracked mitochondrial content within isolated EV and checked whether EGCG treatment altered it. CD44 cell surface expression was used to quantify the total population of MDA-MB-231 derived EV (MPs, Figure 4. 6A) while MitoTracker Deep Red (MTR) was used to identify mitochondrial material in the vesicles (mitoMPs, Figure 4. 6B). EGCG-EV had a tendency to have higher MPs content, but a decrease in the mitoMPs subpopulation. Our flow cytometry results were supported by citrate synthase activity, which correlates with mitochondrial content, and in which the EGCG-EV supernatant had less activity (Figure 4. 6C). Moreover, when hADMSC were incubated with the MTR-stained EV or MTR-stained EGCG-EV, 17% and 13% respectively, of the cells were positive (Figure 4. 6D) whereas the MFI was reduced by more than half for those cells treated with the MTR-stained EGCG-EVs (Figure 4. 6E). The potential inhibitory effect of the EGCG over the mitoTracker dye was ruled out since no variation in the MFI was detected in the stained MDA-MB-231 after being incubated at two different concentrations of the polyphenol (Supplementary Figure S4. 3). Moreover, uptake of mitoMPs within hADMSC and mitochondria delivery were observed confirming that the EVs cargo material can be taken up by the recipient cells (

Supplementary Figure S4. *4*). Altogether, these results suggest that EGCG causes a reduction in the EV mitochondrial content that would eventually be transferred to the recipient cells upon EV fusion (Figure 4. 6F).

Table 4. 1. Fold change regulation of mitochondria-related genes detected in the EGCG-EV vs EV.

Genes	log2 FC	*p*-adjusted value	Protein
MT-ATP8	-6.64	3.99E-33	ATP synthase 8
MCUB	-5.60	0.013846	Mitochondrial Calcium Uniporter Dominant Negative Subunit Beta. An integral component of the mitochondrial inner membrane
MT-ATP6	-4.50	1.75E-11	ATP synthase 6
MT-ND2	-4.33	4.73E-64	NADH dehydrogenase 2
MT-ND4	-3.90	1.67E-44	NADH dehydrogenase 4
MT-CO2	-3.81	8.09E-15	Cytochrome C oxidase II
MT-CYB	-3.38	4.72E-12	Cytochrome b
MT-ND5	-3.35	1.97E-34	NADH dehydrogenase 5
MT-CO3	-3.16	4.84E-11	Cytochrome C oxidase III
MT-ND3	-3.15	4.86E-44	NADH dehydrogenase 3
MT-ND4L	-3.01	3.07E-38	NADH 4L dehydrogenase
MT-ND1	-2.98	3.01E-29	NADH dehydrogenase 1
MT-CO1	-2.41	9.83E-19	Cytochrome C oxidase I
MT-ND6	-2.03	3.01E-10	NADH dehydrogenase 6
FIS1	-2.03	0.0415208	Component of a mitochondrial complex that promotes mitochondrial fission
VDAC1	-1.08	0.0247492	Voltage Dependent Anion Channel 1. A major component of the outer mitochondrial membrane.

FC: fold change

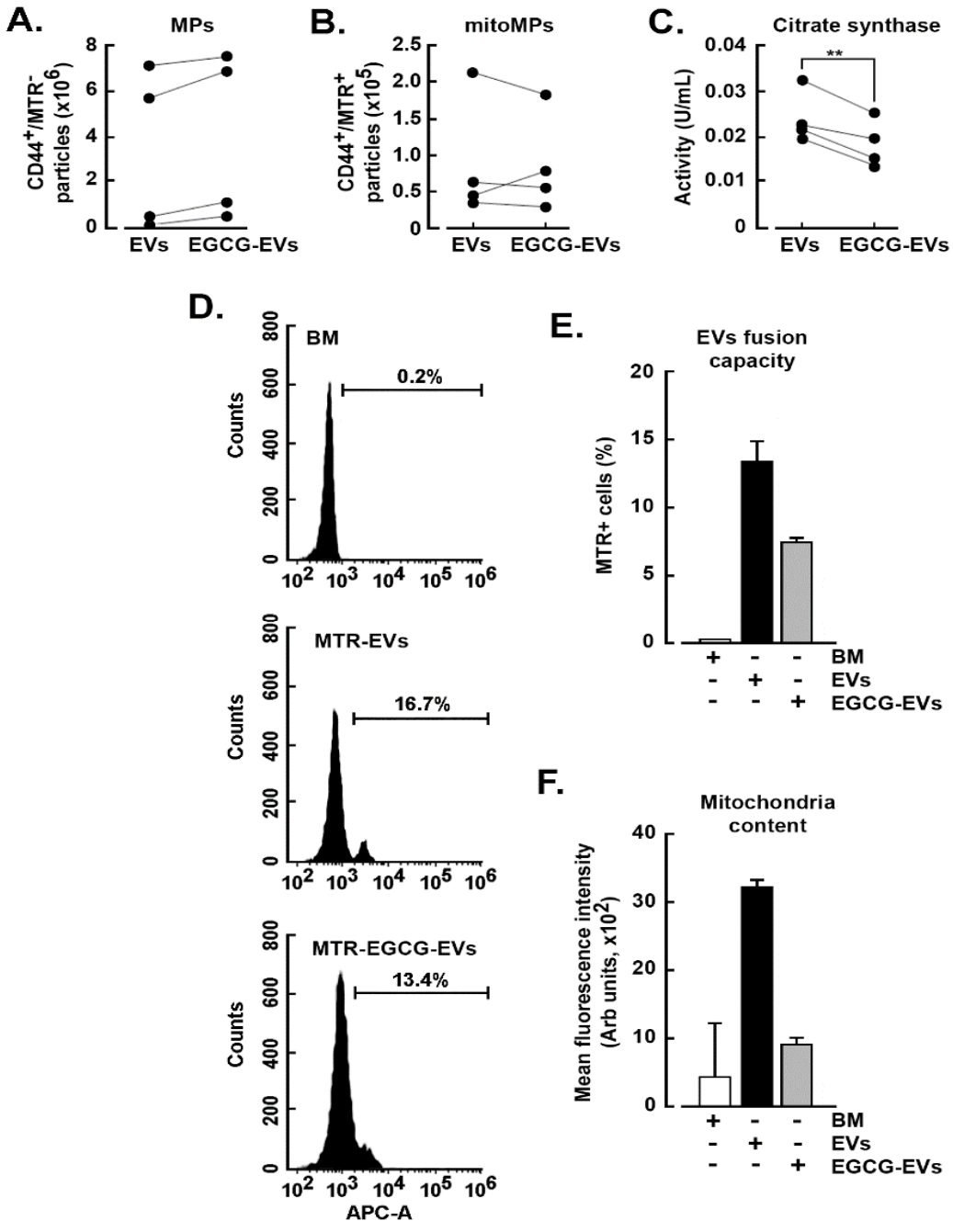

Figure 4. 6. EGCG reduces the mitochondrial content within the EV.
Serum-starved MDA-MB-231 cells were cultured for 48 hours in the presence or absence of 30 μM EGCG. EV were isolated, stained with anti-CD44-FITC and MitoTracker Deep Red (MTR), and analyzed by flow cytometry. Four independent

experiments were spaced in time and with a different cell passage. The dots represent the mean of the counting, and results from the same experimental day, were connected with a line in graphs A-C. Paired *t*-test was performed; $^{**}P < 0.01$. **A)** The total number of $CD44^{+}/MTR^{-}$ microparticles (MPs) detected in EV or EGCG-EV. **B)** Quantification of the mitochondria-containing particles ($CD44^{+}/MTR^{+}$, mitoMPs) in the EV or EGCG-EV. Four independent experiments were performed. **C)** Citrate synthase activity was measured in particles isolated from the conditioned media as described in the Methods section. **D)** Dot plot resulting from the flow cytometry analysis detecting the presence of mitochondria delivered by the EV in hADMSC after incubation with basal media (BM, negative control), mitoTracker-labelled EV (MTR-EV), or mitoTracker-labelled ECGC-EV (MTR-EGCG-EV). **E)** The percent of hADMSC positive for the presence of mitochondria delivered by the EV or EGCG-EV. **F)** Mean of the fluorescence intensity of the EV or EGCG-EV-delivered mitochondria within hADMSC.

4.6.7 Impact of EGCG and low oxygen tension on the sorted genes within the EV.

We next questioned whether EV content is altered in conditions which mimic the patho-physiological conditions of a solid tumor microenvironment, where nutrients are limited, and oxygen tension is low. Given that such starvation and hypoxic conditions have a direct impact on cell metabolism, we assessed the mRNA cargo of the EV derived from MDA-MB-231 cells and whether EGCG additionally altered such content. EV and EGCG-EV were isolated from normoxic (21% O_2) and hypoxic (1% O_2) culture conditions, and total RNA extracted for RNA-Seq analysis. Principal component analysis (PCA) shows that EV samples obtained from cells cultured in normoxia (EV_N) or hypoxia (EV_H) are very similar (cluster 1, C1) (

Figure 4. 7A). Comparing the transcript content of EV_H and EV_N (C1,

Figure 4. 7A), nine DEG were identified (fold change FC > |2| and adjusted *p*-value < 0.05) (Table 4. 2). Among those genes, five were upregulated and were directly involved in the hypoxia-mediated process. These included cell death (*FAM162A*), mitochondrial function (*ISCA1*), metabolism (*PM20D2*, *SLC2A3*), and angiogenesis

(*ADM*). The four downregulated genes were associated with gene expression machinery (*NIP7*, *MRPS7*, *MT-TP*, *ZNF585A*).

Table 4. 2. Genes modulated in hypoxia vs normoxia with a p-adjusted value < 0.05 and a log2 FC > |2|.

Gene Ensemble ID	**log2 FC**	***p*-adjusted value**	**GenCards annotations**
PM20D2 **ENSG00000146281,6**	4.27	0.032	*Peptidase M20 Domain Containing 2*. Hydrolase activity. Function in metabolite repair mechanism.
FAM162A **ENSG00000114023,15**	3.52	0.001	*Family With Sequence Similarity 162 Member A*. Hypoxia-induced cell death, the release of cytochrome C, caspase activation (CASP9) and inducing mitochondrial permeability transition.
ISCA1 **ENSG00000135070,15**	2.60	0.049	*Iron-Sulfur Cluster Assembly 1*. Mitochondrial protein. Function in electron-transfer reactions
ADM **ENSG00000148926,10**	2.23	0.001	*Adrenomedullin*. Functions in vasodilation, hormone secretion regulation, angiogenesis promotion, and antimicrobial activity.
SLC2A3 **ENSG00000059804,16**	2.09	0.001	*GLUT3*. Glucose and other monosaccharides transporter.
NIP7 **ENSG00000132603,15**	-2.20	0.049	*Nucleolar Pre-rRNA Processing Protein NIP7*. RNA binding
MRPS7 **ENSG00000125445,11**	-2.41	0.036	*Mitochondrial Ribosomal Protein S7*. RNA binding and structural constituent of ribosome.
MT-TP **ENSG00000210196,2**	-2.69	0.032	*Mitochondrially Encoded TRNA-Pro (CCN)*. Associated with the tRNA class
ZNF585A **ENSG00000196967,11**	-3.97	0.048	*Zinc Finger Protein 585A*. Function as a transcription factor.

FC: fold change

Interestingly, while oxygen levels have no significant impact on the transcript content of vesicles produced by untreated cells, the addition of EGCG drives the production of vesicles with distinctive transcript signatures linked to oxygen levels (

Figure 4. *7*A, C2 and C3). This suggests that hypoxic conditions may potentiate the action of EGCG. The analysis of the transcripts isolated in EV_HE (C3) vs EV_NE (C2) resulted in the detection of 2,640 gene products, from which 553 were differentially regulated between the experimental conditions (Table 4. 3).

Table 4. 3. DESeq results obtained from the comparison of the EV_HE vs EV_NE

***p*-adjusted value**	**Fold change**	**Numbers of genes**
Significant	Upregulated	107
Significant	Downregulated	446
No significant	-	2087

The Volcano Plot in

Figure 4. *7*B depicts the behaviour of the DEG with an absolute fold change greater than two-fold and colored according to their adjusted *p*-value (red or grey for DEG statistically significant or not respectively). Addition of EGCG in hypoxic cell culture conditions showcases a noticeable gene downregulation (446 downregulated genes vs. 107 upregulated genes). Among the most upregulated genes with the highest statistical differences were the sialic acid acetylesterase enzyme (*SIAE*), the bone morphogenetic protein receptor type 2 (*BMPR2*), the oncogene breast carcinoma amplified sequence 4 (*BCAS4*), genes associated with the vesicular transport like the sorting nexin 32 (*SNX32*), and the GRIP and coiled-coil domain containing 2 (*GCC2*). In contrast, among those genes with the highest downregulation, we found the cytoskeleton constituent tubulin alpha 1c (*TUBA1C*), the high mobility group AT-Hook 1 (*HMGA1*) associated with gene transcription, the scaffolding protein neuroblast differentiation-

associated (*AHNAK*), the coding genes associated with ribosomal functionality, the eukaryotic translation elongation factors 1 alpha 1 and 1 gamma (*EEF1A1* and *EEF1G*), and the transmembrane protein encoded gene solute carrier family 3 member 2 (*SLC3A2*).

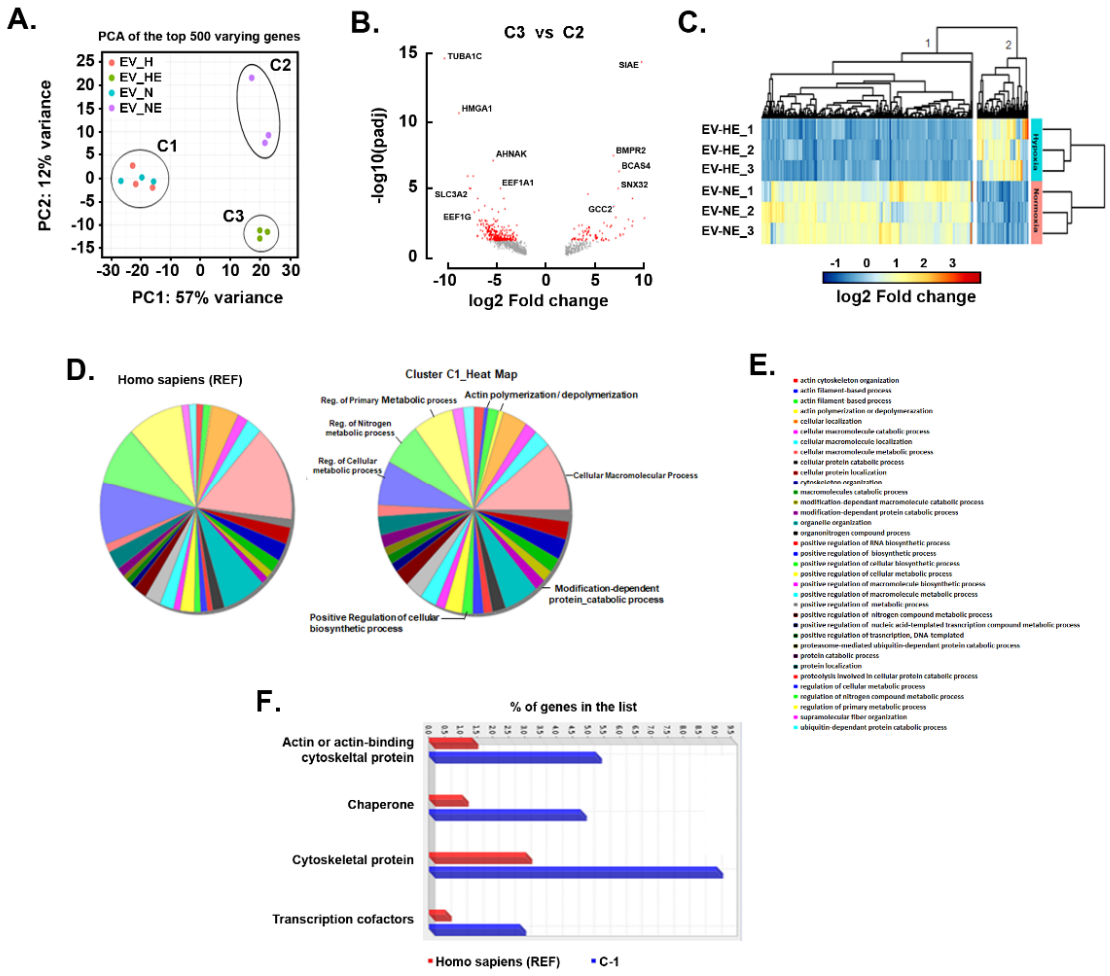

Figure 4. 7. Transcriptomic analysis of the influence of low oxygen tension and EGCG in loading the MDA-MB-231-derived EV.
A) Principal Component Analysis (PCA) of the top 500 differential expressed genes (DEG) identified in the samples. **B)** Volcano Plot showing the number of DEG detected with a log2 FC ≥ |2| in the EV obtained by adding 30 µM EGCG at different oxygen tensions. The analysis was performed by comparing the EGCG-EV obtained in hypoxia (EV_HE, C3) vs EGCG-EV obtained in normoxia (EV_NE, C2). Genes with a

significant or non-significant value were coloured in red and grey respectively. **C)** Robust k-means clustering visualized as a heatmap of the individual samples and their DEG with a log2 FC ≥ |2| and p-adjusted value < 0.05. **D)** Gene ontology (GO)-SLIM PANTHER analysis showing the biological process that involves genes downregulated by HE (cluster 1, heat map). **E)** GO-SLIM PANTHER analysis of the downregulated genes in cluster 1 of the heatmap, showing their protein class. Fisher's exact test and the false discovery rate (FDR) correction were used during the GO-SLIM analysis.

Next, we performed a *k*-means clustering analysis with the 553 DEG and generated the heat map containing each condition replicate (

Figure 4. *7*C). As expected, we detected two major clusters comprising 107 genes, and the other one with the remaining 446 genes. A detailed information of these DEG is provided in a supplementary EXCEL data sheet (Supplementary Table S4. 1). Unfortunately, no association was found upon Gene ontology (GO) enrichment analysis performed (FDR < 0.05) for the upregulated genes (cluster 2,

Figure 4. *7*C). Nevertheless, most of the upregulated genes coded for proteins involved in the regulation of gene expression, mitochondrial components and protein trafficking and recycling. Importantly, there were genes upregulated within the EGCG-EV that associated with the inflammatory response (*HAVCR2*, *LRRFIP2*), cell proliferation (*CCPG1*, *EXOSC2*), apoptosis (*BBC3*) and oncogenesis (*ZMAT3*, *ZNF124*, *ErbB-3*, *SH3D19*, *REL*). When the same analysis was performed with the genes downregulated in EV_HE (cluster 1,

Figure 4. *7*C), we identified genes that were attributed to biological processes associated with regulation of cell metabolism, biosynthesis, and cell mobility like the polymerization/depolymerization of actin (

Figure 4. *7*D). Furthermore, in comparison with the EV_NE, the EV_HE vesicles had less genes coding for cytoskeletal proteins, chaperones, and transcription factors (

Figure 4. *7*E).

4.7 Discussion

The release of small EV loaded with bioactive macromolecules is an efficient communication and paracrine regulation mechanism linking the tumor niche to its neighbouring cells. Cancer cells attract and trigger dedifferentiation of neighbouring cells to acquire a pro-tumoral role like it has been described for the TAM (Wyckoff et al., 2004), cancer-associated fibroblasts (CAF) (Gentric et Mechta-Grigoriou, 2021), and cancer-associated adipocytes (CAA) (Zhao et al., 2020). In our previous study, we demonstrated that the secretome of a TNBC cell line (MDA-MB-231) induced the CAA-like phenotype in hADMSC, a process inhibited by EGCG (Gonzalez Suarez et al., 2022). To decipher the different components within that secretome, the present study focused on the role of the tumor-derived EV and their paracrine regulation over the hADMSC, as well as the effect of EGCG on the vesicle's load and biological effect.

EV have been demonstrated to regulate processes like inflammation and tissue repair, as well as to condition the premetastatic niche (Sundararajan et al., 2018). EV can travel to distant sites and transfer biological information to the recipient cells (Al-Nedawi et al., 2008; Becker et al., 2016; Li et al., 2021). This can be achieved through direct fusion of the vesicles to the plasma membrane via receptor-ligand interactions, membrane fusion or by releasing their load within the cytosol (Nicholson et al., 2020). Our samples were enriched in exosomes according to the isolation method used and the detection of exosomal markers, but the presence of vesicles with different sizes cannot be dismissed. With regards to such size distribution, both EV and EGCG-EV vesicles behaved similarly. In addition to its antioxidant properties, pro-oxidant properties have also been reported for EGCG both *in vitro* and *in vivo* (Kim *et al*., 2014; Li *et al*., 2010). How this could directly affect the membrane composition of the vesicles, as well as the response of the targeted cells, remains to be addressed. However, in our experimental conditions no differences were observed in terms of MFI in the labelled vesicles (**Error! Reference source not found.**D) or in the recipient cells

(**Error! Reference source not found.**C) implying that the staining and interaction capacity of the vesicles remained unaltered.

Here, we demonstrate that TNBC cell-derived EV can interact with hADMSC and induce a pro-migratory and pro-inflammatory phenotype. Accordingly, the inflammation-associated IL-17 pathway was enriched during the transcriptomic analysis of the EV's cargo. Next, we validated the regulation of other inflammatory markers as EV induced several of the genes involved in this signaling cascade including IL-1B, CXCL1 and CXCL2, CCL2, CCL7 and CCL20 (Onishi and Gaffen, 2010), while EGCG-EV reduced most of them. We highlighted the modulation of the CAA markers by the vesicles suggesting that this phenotype can be induced in the hADMSC. Similar observations were found in adipocytes in co-culture with exosomes derived from hepatocellular carcinoma, where the induction of pro-inflammatory cytokines IL-6, IL-8, IL-1Band CCL2 promoted tumor growth and angiogenesis (Wang *et al*., 2018a). Interestingly, EGCG-EV specifically induced IL-6 along with the chemokines CXCL1, CXCL3 and CXCL8. These cytokines are key regulators of the acute response during inflammation and immune response and can contribute to tissue homeostasis by inducing the recruitment of innate immune system cells (Jones et Jenkins, 2018; Vilotic et al., 2022).

By interacting with hADMSC, both preparations of EV (EV and EGCG-EV) specifically triggered the DNA damage response pathway CHK-2 and the stress-activated protein kinase c-Jun/JNK pathway. CHK-2 is activated in response to oxidative stress generated upon nutrient deprivation and maintains the redox homeostasis (Guo et al., 2020). Hence, there appears to be some cellular stress mediated by the EV's preparations, in addition to the nutrient deprivation. In opposition to the EV-mediated effect, the EGCG-EV failed to activate the AKT pathway and reduced the activation state of the GSK-3β pathway. AKT activation has a positive regulation on several processes including metabolism, proliferation, and cell survival (Hemmings et Restuccia, 2012). On the other hand, GSK-3β relays a signal transduction cascade involved in cellular processes like gene transcription, cell

proliferation, and apoptosis (Chargaff et West, 1946). This protein can be phosphorylated on different serine residues by other kinases including AKT (Medina et Wandosell, 2011) and P38 (Thornton et al., 2008), correlating with the inhibition of its kinase activity, or by MEK1/2 leading to its induction (Hartigan et al., 2001). The role of AKT mediating the activation of the c-Jun/caspase-3 axis in response to the endoplasmic reticulum stress, which renders in attenuation of the P21 expression level in a prostate cancer cells' model was recently documented (Rasool et al., 2017). Then, cells exited from a senescence state to enter apoptosis-mediated cell death. Here, the genetic content of EGCG-EV altered pathways associated with ROS, cell cycle, cellular senescence, HIF-1α and Notch. The latter has been also associated with the induction of AKT signaling pathway and P21 expression in T-cell lymphoblastic leukemia (Guo et al., 2009). Besides, we detected a sustained activation of the P38/MAPK pathways that corresponds with the induction of senescence in response to chronic DNA-damage (Ruhland *et al.*, 2016a). These results may suggest that EGCG-EV can rescue cells from senescence since we detected their capacity to reduce the P21 and β-gal expression. In our study, SOD2 was the only senescence marker induced explicitly by the EGCG-EV (data not shown), a fact previously reported for EGCG during an *in vivo* study and linked to its capacity to prevent the oxidative stress caused by free fatty acid-induced insulin resistance (Li et al., 2011b).

The pro-tumoral role of senescent cells has been described as promoting low-grade inflammation (Pribluda et al., 2013) and the CCL2-mediated recruitment of myeloid and NK cells (Lasry et Ben-Neriah, 2015). Also, senescent tumor cells have been reported to have increased migration capacity and to be often present at the tumor invasive front (Kim et al., 2017b). Here, the EV increased the expression of pro-inflammatory and senescence markers in hADMSC, as well as their migration rate. These shreds of evidence highlight the predominant inhibitory effect of EGCG-EV in both biological processes. These vesicles triggered IL-6 and CXCL8 expression, then further studies will be required to clarify how such induction may impact tumor progression.

In addition, we detected the presence of mtDNA and mitochondrial content within a percentage of the isolated vesicles, which could be potentially transferred to the donor cells. It has been reported that mitochondria and their components, when transferred to recipient cells, induce an inflammatory response (Boudreau *et al.*, 2014; Todkar et al., 2021), and increase invasiveness in tumor cells (Rabas *et al*., 2021; Takenaga *et al*., 2021). Previous studies have shown that intercellular transfer of functional mitochondrial content can rescue injured or UV-treated prostate cancer cells (PC12) (Wang et Gerdes, 2015; Yang *et al.*, 2020). Since the integrity of the extracellular mitochondrial content is affected by the EGCG treatment, the bioenergetic state of the recipient cells could be significantly modulated. However, the nature of the factors transmitted varies according to the cell culture conditions (Amari and Germain, 2021) and cell line models used. Our findings support what has been previously reported since mitophagy was detected among the pathways enriched during our transcriptomic analysis of the EGCG-EV, and this was confirmed later by the reduction in the mitochondrial content within these vesicles. Whether this correlates with the anti-inflammatory properties of the EGCG-EV has yet to be established.

The influence of culture conditions in the loading selection of the EV's content has also been extensively studied for the micro-RNA (miRNA) profile (Robert *et al*., 2022). In the present study, we focused on the sorting of the RNA content that can be transcribed and translated into proteins. Considering the impact of hypoxia on cell metabolism and secretory profile, we expanded our analysis on how low oxygen tension influences the transcriptomic profile within the vesicles in combination with EGCG. Contrary to what has been published (Jiang *et al*., 2022), in our experimental condition, hypoxia per se did not affect the transcripts levels sorted into the vesicles. However, when EGCG was added, cells behaved differently, and two different EV clusters were identified (

Figure 4. 7A). Overall, the combined effects of hypoxia and EGCG (EV_HE) caused the downregulation of most genes identified in the EV_NE. The main protein

classes that were downregulated in the EV_HE were associated with cytoskeleton and actin polymerization/depolymerization processes that are involved in exosome biogenesis and secretion mechanisms (Mathieu *et al*., 2019). Transcription factors and chaperones were also identified, suggesting their involvement in the regulation of metabolic and biosynthetic cellular processes. In general, the combination of hypoxia and EGCG appeared to attenuate the paracrine regulatory effect of the vesicles obtained without the stress of low oxygen tension. However, we observed that the EV_HE was enriched in genes associated with inflammation, cell survival and oncogenesis. This further highlights the importance of mimicking *in vitro* as closely as possible the tumor microenvironment through cell culture conditions in studying the paracrine regulation mechanisms of EV.

4.8 Conclusions

The present proof of concept study reveals that EGCG can alter the sorted genetic material found within the TNBC cells-derived EV, and this will require to be further explored in other breast cancer cell models. As evidenced, EGCG reduced the capacity of the EV to trigger the expression of pro-inflammatory and senescence markers that, otherwise, could contribute to the acquisition of a chemoresistance phenotype. How gene expression changes translate into functional consequences upon EGCG treatment, in combination with current chemotherapeutic approaches, should be investigated in further studies to confirm the potential chemoresistance phenotype induced by the horizontal transfer of mitochondrial content. This evidence was further supported by its inhibitory effects over crucial pathways involved in cell proliferation and cell death including, in part, GSK-3β and AKT. Of importance, EGCG caused a reduction in the mitochondrial content of the cancer cells-derived EV, reinforcing its overall antitumoral role. Circulating diet-derived polyphenols may therefore represent an efficient chemopreventive strategy to reduce the paracrine regulation that TNBC cells exert within their surrounding adipose tissue.

4.9 Supporting information

Supplementary Figure S4. 1. Quantification by flow cytometry of the EV samples.

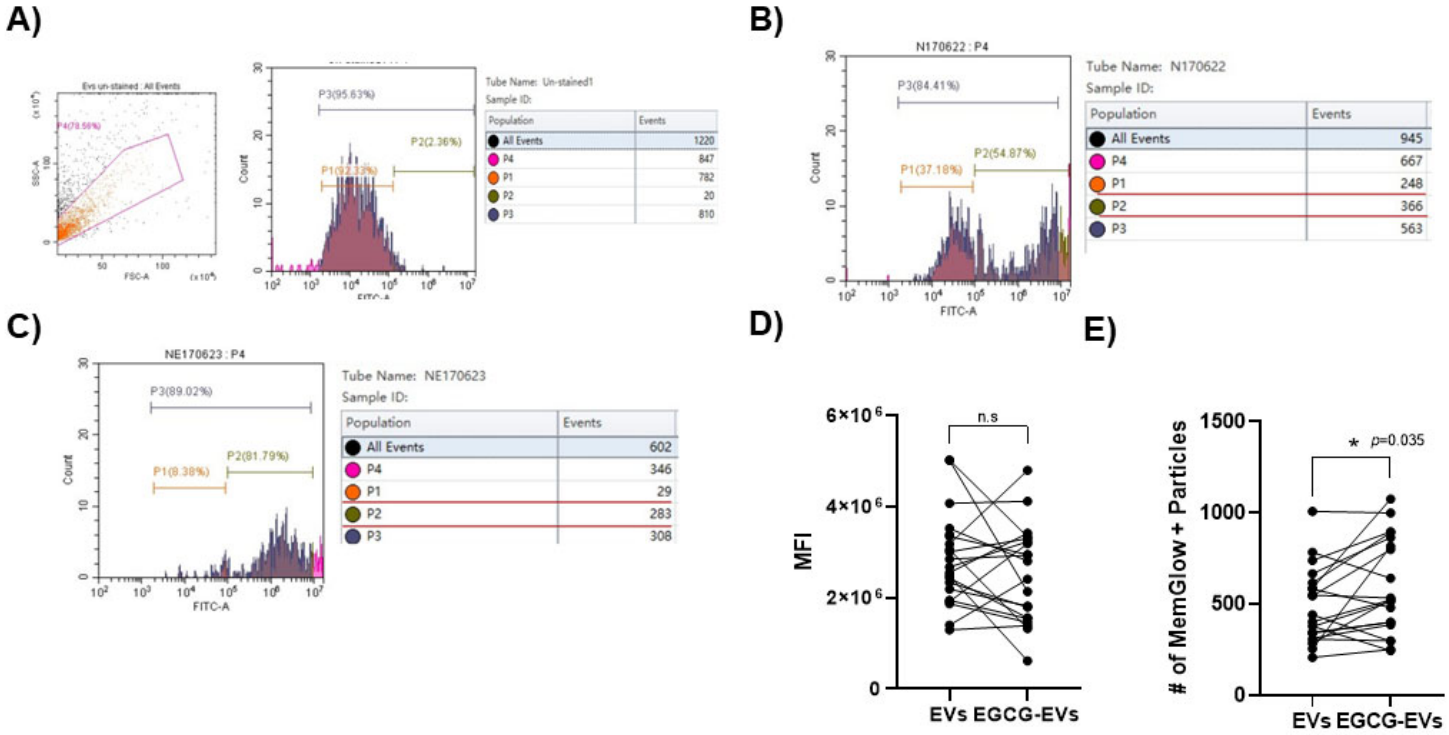

Supplementary Figure S4. 1. Quantification by flow cytometry of the EV samples.
EV and EGCG-EV were isolated, and 20 µL of the samples were stained with 100 nM MemGlow followed by flow cytometry analysis. **A)** Gating strategy and definition of the unstained population. **B)** Representative quantification of a batch of EV (N170622). **C)** Representative quantification of a batch of EGCG-EV (NE170623). Highlighted in red are the P2-positive population with the number of vesicles counted in an acquisition volume of 30 µL. **D)** Paired experimental means of each EV batch's mean fluorescence intensity (MFI). **E)** Paired experimental counting of the number of particles. Wilcoxon-matched pairs signed rank test was used to establish significant statistical differences.

Supplementary Figure S4. *2*

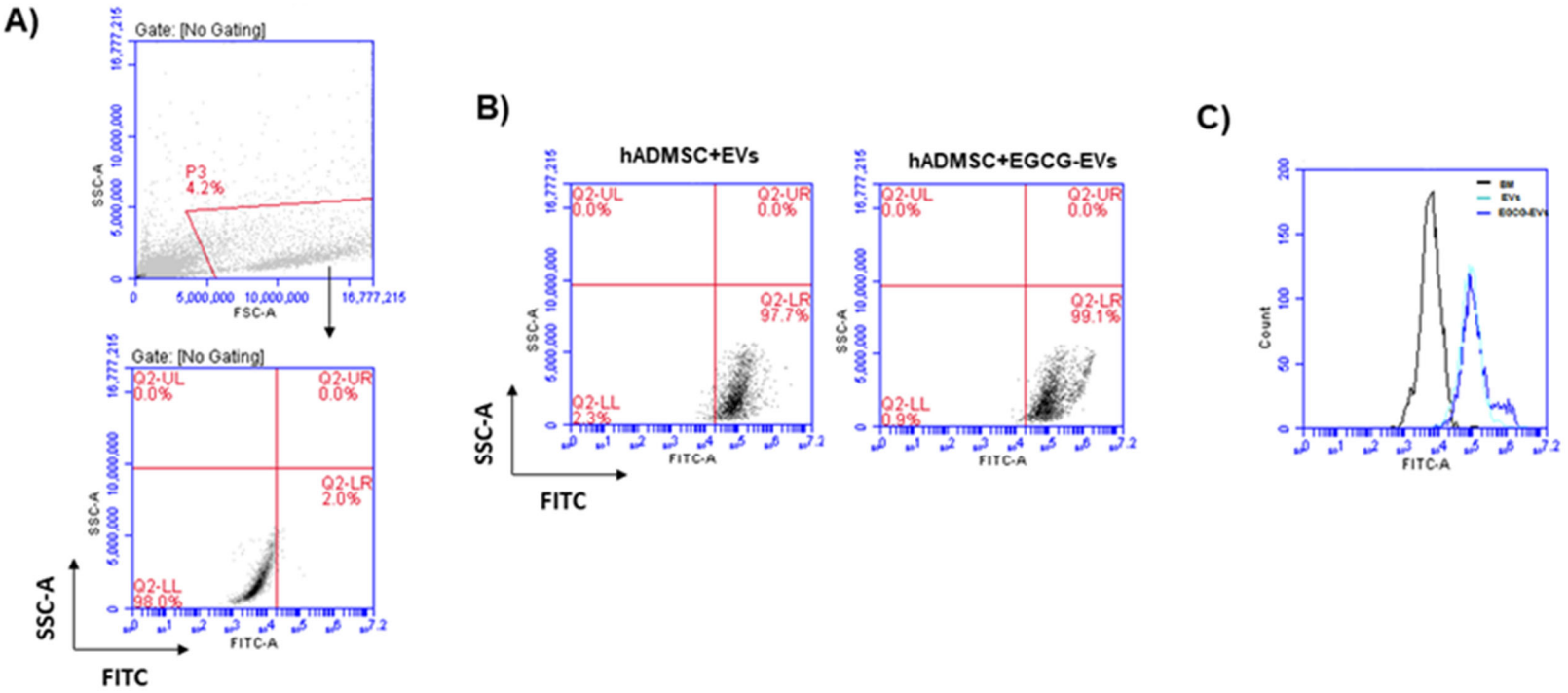

Supplementary Figure S4. 2. Comparing the fusion capacity of MemGlow-stained EV.
EV and EGCG-EV were isolated, labelled with 100 nM MemGlow, washed by ultracentrifugation (1 hour at 100,000g) and resuspended in basal media (BM). Next, hADMSC (10,000 cells/condition) were incubated in suspension with the vesicles at a ratio Cells:EV of 1:1, for 1 hour at 37°C and 5% CO_2 atmosphere. Flow cytometry determination of the number of FL-1-positive cells. **A)** Gating strategy used for samples incubated with BM as a negative control. **B)** Representative plotting of the MemGlow-488-positive cells resulting from the co-incubation with EV or EGCG-EV. **C)** Representative plots of the mean of fluorescence intensity (MFI) of the hADMSC incubated with BM (black line), EV (aqua-coloured line) or with EGCG-EV (dark blue line).

Supplementary Figure S4. 3

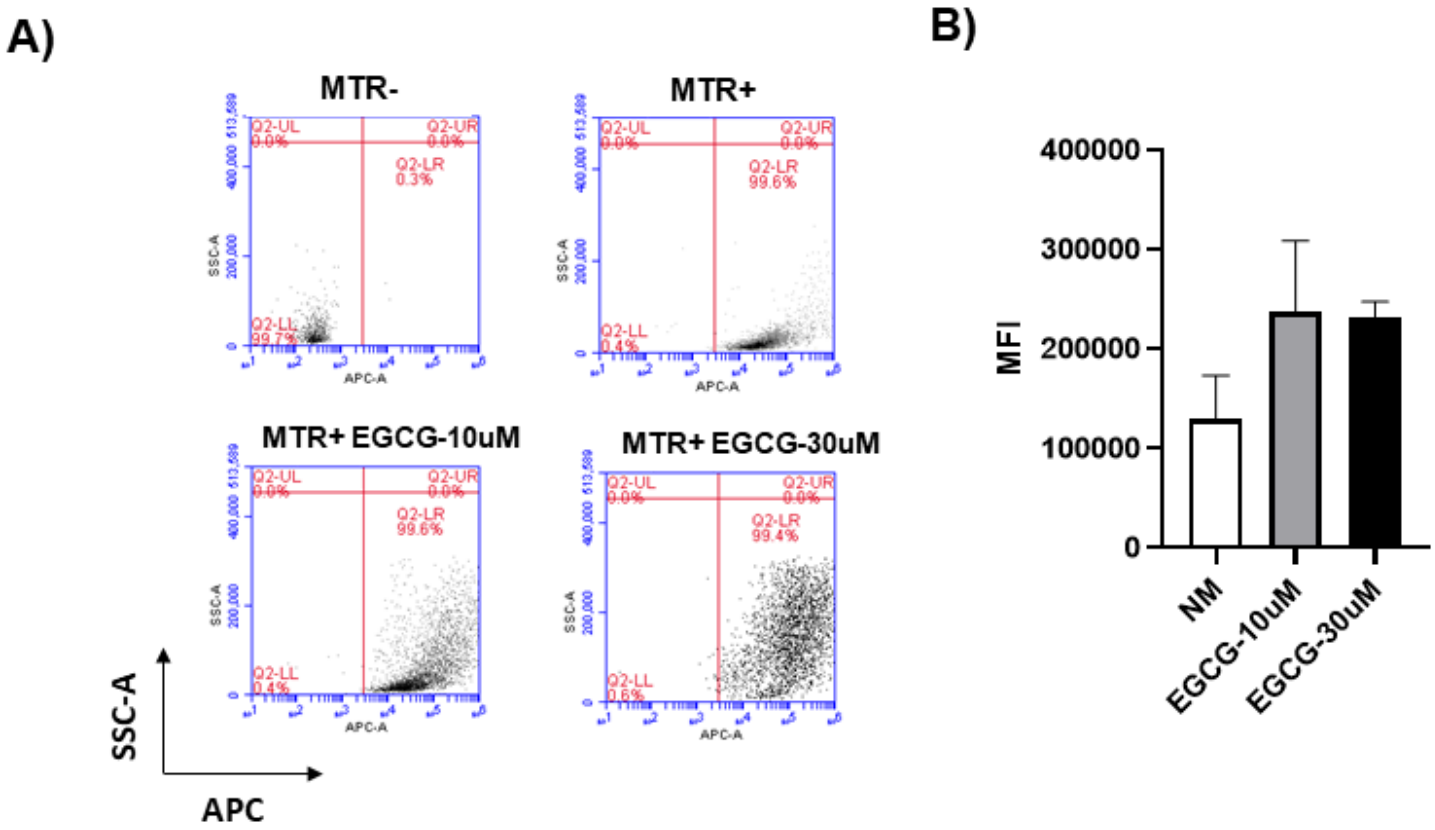

Supplementary Figure S4. 3. Evaluating the effect of EGCG over the mitoTracker dye.
MDA-MB-231 cells were seeded in a 6-well plate, incubated with mitoTracker Deep Red (MT), resuspended in negative media (NM), and added at a final concentration of 200 nM. After washing, the cells were kept for 24 hours in negative media (NM) or NM+EGCG at 10 or 30 µM, respectively. Then, cells were analyzed by flow cytometry. **A)** A representative dot plot of unstained cells (negative control, MT-), cells stained with MT and maintained in NM (positive control, MT+), cells stained and incubated with 10 µM (MT+ EGCG-10) or with 30 µM (MT+ EGCG-30). **B)** Bar graph of the mean of the fluorescence intensity (MFI) of the positive population (n=2).

Supplementary Figure S4. *4*.

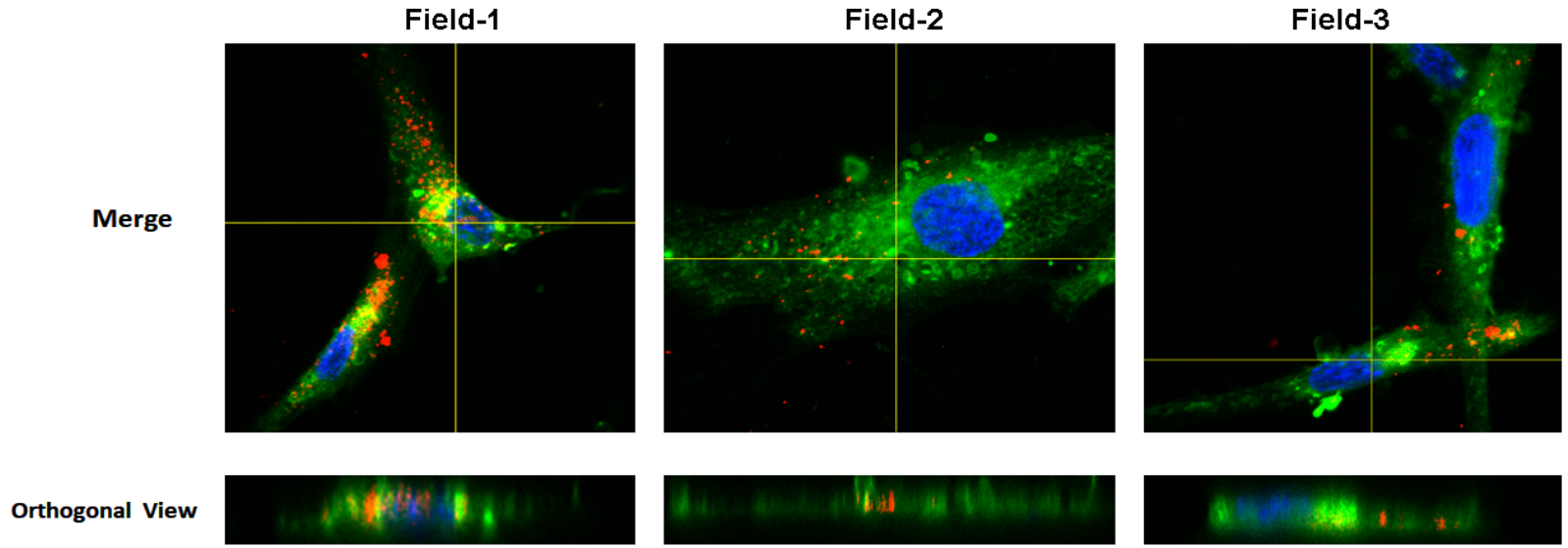

Supplementary Figure S4. 4. Mitochondrial components present within MDA-MB-231-derived EVs can be transferred into hADMSC.

MDA-MB-231 cells were seeded in 175 cm flasks at a 70-80% of confluence. Next, mitoTracker Deep Red (MTR) was added at a final concentration of 200 nM, resuspended in negative media (NM), and cells were incubated overnight. Next day, the monolayer was washed with PBS and kept for 24 hours in NM. Then, cell culture media was collected and EVs were isolated as described in the Methods section and protected from light. hADMSC were then seeded on top of tissue culture glass slides and incubated for 4 hours with 200µL of MTR+EVs resuspended in NM. Afterwards, cells were labelled with 100 nM MemGlow, and fixed. Dapi was added to stain the nucleus and pictures taken using a fluorescence microscope. Pictures from the center section of the cells are represented. Red staining is representative of mitochondrial material delivered within hADMSC (stained in green).

Supplementary Table S4.1

Supplementary Table S4. 1. List of the shared DEGs (1116 genes) identified within the h-ADMSC treated with EGCG-EV vs EV, and with a p-value < 0.05.

Ensemble	Gene	log2FC	padj	Category
ENSG00000212464,1	SNORA12	7.82	7.21E-08	snoRNA
ENSG00000252835,1	SCARNA21	7.73	1.74E-06	scaRNA
ENSG00000212283,1	SNORD89	7.64	3.64E-06	snoRNA
ENSG00000206634,1	SNORA22	7.59	5.47E-06	snoRNA
ENSG00000273768,1	RNVU1-29	7.15	8.03E-05	snRNA
ENSG00000206838,1	SNORA5A	6.88	0.000441461	snoRNA
ENSG00000140320,12	BAHD1	6.74	0.000951438	protein_coding,retained_intron
ENSG00000279133,1	AC018628,1	6.66	8.67E-05	TEC
ENSG00000212607,1	SNORA3B	6.42	0.005676216	snoRNA
ENSG00000272734,1	ADIRF-AS1	6.38	0.000314457	lncRNA,retained_intron
ENSG00000104783,14	KCNN4	6.32	0.007995022	nonsense_mediated_decay, protein_coding, processed transcript, retained_intron
ENSG00000207445,1	SNORD15B	6.30	1.80E-14	snoRNA
ENSG00000235408,6	SNORA71B	6.24	0.000626663	snoRNA
ENSG00000101546,13	RBFA	6.23	0.012249339	protein_coding,processed_transcript,retained_intron
ENSG00000105227,16	PRX	6.21	0.013807783	processed_transcript, protein_coding, nonsense_mediated_decay,retained_intron
ENSG00000135253,15	KCP	6.06	0.00172616	protein_coding, retained_intron,nonsense_mediated_decay,processed_transcript
ENSG00000200434,1	RNA5-8SP2	6.00	1.04E-11	rRNA_pseudogene
ENSG00000251791,1	SCARNA6	5.93	5.20E-05	scaRNA
ENSG00000049249,9	TNFRSF9	5.85	0.004721032	protein_coding,nonsense_mediated_decay
ENSG00000238363,1	SNORA13	5.57	0.012503358	snoRNA
ENSG00000188130,14	MAPK12	5.47	0.016086741	protein_coding,retained_intron,processed_transcript
ENSG00000231721,7	LINC-PINT	5.47	4.90E-07	lncRNA,retained_intron
ENSG00000126214,21	KLC1	5.43	0.00198261	retained_intron,protein_coding,nonsense_mediated_decay
ENSG00000112877,8	CEP72	5.39	0.022693974	protein_coding,retained_intron,processed_transcript
ENSG00000164877,19	MICALL2	5.36	0.023834938	nonsense_mediated_decay, retained_intron,protein_coding,processed_transcript
ENSG00000200959,1	SNORA74A	5.34	0.028745345	snoRNA
ENSG00000212443,1	SNORA53	5.34	1.66E-09	snoRNA
ENSG00000249592,6	AC139887,2	5.32	0.028171239	lncRNA
ENSG00000104936,19	DMPK	5.32	0.028171239	retained_intron, nonsense_mediated_decay,protein_coding,processed_transcript
ENSG00000212232,1	SNORD17	5.31	8.90E-05	snoRNA
ENSG00000148331,12	ASB6	5.29	0.037390971	protein_coding
ENSG00000011132,12	APBA3	5.26	0.006408215	protein_coding,retained_intron
ENSG00000088881,21	EBF4	5.21	0.039432352	protein_coding,processed_transcript,nonsense_mediated_decay

ENSG00000122678,17	POLM	5.21	0.038151278	nonsense_mediated_decay,retained_intron,processed_transcript,protein_coding
ENSG00000130684,14	ZNF337	5.17	0.045836802	processed_transcript,protein_coding
ENSG00000174233,12	ADCY6	5.15	0.006599752	protein_coding,retained_intron,processed_transcript
ENSG00000100034,14	PPM1F	5.04	0.005547963	protein_coding,processed_transcript,retained_intron
ENSG00000189114,8	BLOC1S3	4.87	0.01836295	protein_coding,processed_transcript
ENSG00000134668,12	SPOCD1	4.73	0.029268389	protein_coding,retained_intron
ENSG00000200913,1	SNORD46	4.61	0.046637523	snoRNA
ENSG00000005156,12	LIG3	4.61	2.49E-05	protein_coding,processed_transcript,nonsense_mediated_decay,retained_intron
ENSG00000245532,9	NEAT1	4.55	2.30E-90	lncRNA
ENSG00000105722,10	ERF	4.50	0.048875617	protein_coding,retained_intron,processed_transcript
ENSG00000176248,9	ANAPC2	4.44	0.019027073	protein_coding,retained_intron,processed_transcript
ENSG00000162522,11	KIAA1522	4.43	0.019262146	protein_coding,retained_intron
ENSG00000279602,1	AC109326,1	4.41	0.014604098	TEC
ENSG00000263934,5	SNORD3A	4.40	8.10E-75	snoRNA
ENSG00000150995,20	ITPR1	4.37	0.000182337	protein_coding,processed_transcript,nonsense_mediated_decay,retained_intron,non_stop_decay
ENSG00000208892,1	SNORA49	4.26	2.18E-06	snoRNA
ENSG00000238741,1	SCARNA7	4.23	6.39E-17	scaRNA
ENSG00000136444,10	RSAD1	4.22	0.023958083	nonsense_mediated_decay,protein_coding,retained_intron
ENSG00000239039,1	SNORD13	4.22	0.000467906	snoRNA
ENSG00000101246,20	ARFRP1	4.19	0.005333275	protein_coding,nonsense_mediated_decay,processed_transcript,retained_intron
ENSG00000186350,12	RXRA	4.18	0.015831116	protein_coding,processed_transcript,retained_intron
ENSG00000252947,1	SCARNA1	4.16	0.00089856	scaRNA
ENSG00000054967,13	RELT	4.14	0.020079227	protein_coding,nonsense_mediated_decay,retained_intron
ENSG00000180917,18	CMTR2	4.12	0.026201391	protein_coding,retained_intron
ENSG00000252010,1	SCARNA5	4.05	2.81E-18	scaRNA
ENSG00000197912,16	SPG7	4.04	1.39E-09	protein_coding,nonsense_mediated_decay,retained_intron,processed_transcript
ENSG00000117318,9	ID3	4.02	0.013084692	processed_transcript,protein_coding
ENSG00000226380,9	AC016831,1	4.00	0.032399766	lncRNA
ENSG00000158747,15	NBL1	3.99	0.019292499	protein_coding
ENSG00000214176,9	PLEKHM1P1	3.99	3.17E-05	processed_transcript,transcribed_unprocessed_pseudogene
ENSG00000155744,9	FAM126B	3.96	0.006169037	protein_coding,retained_intron,nonsense_mediated_decay,processed_transcript
ENSG00000202538,1	RNU4-2	3.91	1.63E-20	snRNA
ENSG00000079432,8	CIC	3.90	0.044584156	protein_coding,nonsense_mediated_decay,processed_transcript,retained_intron
ENSG00000038358,15	EDC4	3.82	0.035178065	retained_intron,processed_transcript,protein_coding
ENSG00000073756,13	PTGS2	3.80	0.049165272	nonsense_mediated_decay,retained_intron,protein_coding
ENSG00000223496,3	EXOSC6	3.78	0.003790007	protein_coding
ENSG00000144655,15	CSRNP1	3.66	0.016194629	protein_coding
ENSG00000200795,1	RNU4-1	3.66	7.47E-11	snRNA
ENSG00000144579,8	CTDSP1	3.66	0.019416413	protein_coding,processed_transcript,retained_intron
ENSG00000167395,10	ZNF646	3.64	0.010791257	protein_coding
ENSG00000103249,18	CLCN7	3.62	1.09E-05	protein_coding,retained_intron,processed_transcript

ENSG00000171621,14	SPSB1	3.61	0.014491013	protein_coding
ENSG00000099991,18	CABIN1	3.60	0.016270212	protein_coding,retained_intron,processed_transcript
ENSG00000167378,8	IRGQ	3.53	0.002803776	protein_coding,processed_transcript,retained_intron
ENSG00000131748,16	STARD3	3.53	0.024956292	nonsense_mediated_decay,protein_coding,processed_transcript,retained_intron
ENSG00000188522,15	FAM83G	3.52	1.05E-05	protein_coding,retained_intron
ENSG00000115738,10	ID2	3.50	0.007774496	protein_coding,retained_intron
ENSG00000130158,14	DOCK6	3.50	0.00573122	protein_coding,processed_transcript,retained_intron
ENSG00000125740,14	FOSB	3.48	7.12E-06	retained_intron,protein_coding
ENSG00000059804,16	SLC2A3	3.45	7.96E-13	protein_coding,retained_intron,nonsense_mediated_decay,processed_transcript
ENSG00000069399,15	BCL3	3.45	0.049835677	retained_intron,processed_transcript,protein_coding
ENSG00000153234,15	NR4A2	3.44	0.001037583	nonsense_mediated_decay,protein_coding
ENSG00000251705,1	RNA5-8SP6	3.41	0.014177742	rRNA_pseudogene
ENSG00000216775,3	AL109918,1	3.40	0.014839877	processed_transcript,transcribed_unprocessed_pseudogene
ENSG00000262074,7	SNORD3B-2	3.38	0.04569638	snoRNA
ENSG00000182087,14	TMEM259	3.38	0.023981302	protein_coding,retained_intron,nonsense_mediated_decay
ENSG00000205903,7	ZNF316	3.36	0.009998856	protein_coding,retained_intron
ENSG00000135976,20	ANKRD36	3.35	0.01920445	protein_coding,retained_intron
ENSG00000141298,19	SSH2	3.34	0.005320855	protein_coding,retained_intron,nonsense_mediated_decay
ENSG00000148400,13	NOTCH1	3.32	0.013795109	nonsense_mediated_decay,protein_coding,retained_intron
ENSG00000175471,19	MCTP1	3.31	0.000388337	protein_coding,processed_transcript,retained_intron
ENSG00000151694,14	ADAM17	3.30	2.51E-05	nonsense_mediated_decay,retained_intron,processed_transcript,protein_coding
ENSG00000143878,10	RHOB	3.28	6.21E-11	protein_coding
ENSG00000134070,5	IRAK2	3.28	9.03E-05	protein_coding
ENSG00000148840,11	PPRC1	3.25	4.61E-05	protein_coding,processed_transcript
ENSG00000264229,1	RNU4ATAC	3.21	0.01087643	snRNA
ENSG00000187678,10	SPRY4	3.20	6.36E-15	processed_transcript,protein_coding,retained_intron
ENSG00000177000,13	MTHFR	3.20	0.021722847	processed_transcript,protein_coding,nonsense_mediated_decay,retained_intron
ENSG00000200816,1	SNORA38	3.20	0.017055192	snoRNA
ENSG00000184557,4	SOCS3	3.20	0.03872551	protein_coding
ENSG00000209042,1	SNORD12C	3.17	0.048944693	snoRNA
ENSG00000197355,11	UAP1L1	3.13	0.001367629	protein_coding,nonsense_mediated_decay,retained_intron
ENSG00000101199,13	ARFGAP1	3.13	1.13E-06	protein_coding,nonsense_mediated_decay,processed_transcript,retained_intron
ENSG00000200087,1	SNORA73B	3.13	2.86E-05	snoRNA
ENSG00000033100,16	CHPF2	3.13	0.037714591	protein_coding,nonsense_mediated_decay
ENSG00000074755,15	ZZEF1	3.12	0.012849472	protein_coding,nonsense_mediated_decay,retained_intron,processed_transcript
ENSG00000268205,1	AC005261,1	3.12	0.005501857	lncRNA
ENSG00000149639,15	SOGA1	3.11	1.89E-09	protein_coding,nonsense_mediated_decay,retained_intron
ENSG00000148926,10	ADM	3.11	3.60E-07	protein_coding
ENSG00000160058,19	BSDC1	3.11	0.005790951	protein_coding,nonsense_mediated_decay,processed_transcript,retained_intron
ENSG00000185989,11	RASA3	3.10	9.31E-05	protein_coding,processed_transcript
ENSG00000110046,13	ATG2A	3.09	8.76E-09	protein_coding,retained_intron

ENSG00000142453,12	CARM1	3.03	0.00172616	protein_coding,nonsense_mediated_decay,retained_intron
ENSG00000131899,11	LLGL1	3.02	0.047581409	retained_intron,protein_coding
ENSG00000170525,21	PFKFB3	3.01	5.07E-08	protein_coding,nonsense_mediated_decay,retained_intron
ENSG00000186635,15	ARAP1	3.01	0.002738859	protein_coding,processed_transcript,retained_intron
ENSG00000196968,11	FUT11	3.00	0.018382808	processed_transcript,protein_coding
ENSG00000126003,7	PLAGL2	3.00	0.007046945	protein_coding
ENSG00000143067,5	ZNF697	2.99	0.013015855	protein_coding
ENSG00000104419,17	NDRG1	2.98	3.15E-37	nonsense_mediated_decay,retained_intron,protein_coding,processed_transcript
ENSG00000227036,8	LINC00511	2.98	0.005333275	lncRNA,retained_intron
ENSG00000160285,15	LSS	2.96	3.60E-12	protein_coding,processed_transcript,retained_intron
ENSG00000183826,18	BTBD9	2.95	0.005244564	nonsense_mediated_decay,protein_coding
ENSG00000162413,16	KLHL21	2.94	2.01E-05	protein_coding
ENSG00000144802,11	NFKBIZ	2.93	0.032399766	protein_coding,retained_intron
ENSG00000157637,13	SLC38A10	2.92	0.020318271	protein_coding,processed_transcript,retained_intron
ENSG00000120738,8	EGR1	2.91	1.05E-12	protein_coding
ENSG00000008513,16	ST3GAL1	2.90	7.68E-05	protein_coding,processed_transcript,retained_intron
ENSG00000140750,17	ARHGAP17	2.89	0.010206784	protein_coding,retained_intron,processed_transcript,nonsense_mediated_decay
ENSG00000159399,10	HK2	2.87	1.31E-13	protein_coding,retained_intron
ENSG00000164916,11	FOXK1	2.87	1.48E-10	protein_coding,retained_intron
ENSG00000130560,9	UBAC1	2.86	0.026852652	protein_coding,processed_transcript
ENSG00000139722,7	VPS37B	2.86	0.001379852	protein_coding,retained_intron
ENSG00000090020,11	SLC9A1	2.85	0.017087425	protein_coding,retained_intron,processed_transcript
ENSG00000130787,14	HIP1R	2.84	0.005088212	retained_intron,protein_coding,processed_transcript
ENSG00000115649,16	CNPPD1	2.84	0.020866906	protein_coding
ENSG00000126464,14	PRR12	2.82	0.012948518	protein_coding,retained_intron
ENSG00000183741,12	CBX6	2.79	0.015776726	retained_intron,protein_coding
ENSG00000155363,18	MOV10	2.77	0.008340529	protein_coding,processed_transcript
ENSG00000177225,17	GATD1	2.77	0.017087425	protein_coding,retained_intron,processed_transcript,nonsense_mediated_decay
ENSG00000149115,14	TNKS1BP1	2.76	9.10E-08	nonsense_mediated_decay,protein_coding,retained_intron
ENSG00000107140,16	TESK1	2.76	0.018757718	protein_coding,processed_transcript
ENSG00000123384,14	LRP1	2.74	0.00044759	retained_intron,protein_coding,processed_transcript
ENSG00000104897,10	SF3A2	2.74	0.001392377	protein_coding,retained_intron
ENSG00000070610,14	GBA2	2.74	0.038151278	processed_transcript,protein_coding
ENSG00000101966,13	XIAP	2.73	0.027594721	protein_coding,processed_transcript
ENSG00000185950,9	IRS2	2.73	2.97E-05	protein_coding
ENSG00000154447,15	SH3RF1	2.71	0.003300996	protein_coding,nonsense_mediated_decay,processed_transcript
ENSG00000242125,3	SNHG3	2.69	0.031771535	lncRNA,retained_intron
ENSG00000225190,11	PLEKHM1	2.68	4.64E-05	nonsense_mediated_decay,processed_transcript,protein_coding,retained_intron
ENSG00000118515,11	SGK1	2.68	6.30E-05	protein_coding,retained_intron,processed_transcript
ENSG00000147162,14	OGT	2.68	4.20E-05	protein_coding,processed_transcript,retained_intron
ENSG00000114423,23	CBLB	2.68	0.001152957	nonsense_mediated_decay,protein_coding,processed_transcript,retained_intron

ENSG00000085872,15	CHERP	2.66	0.011978174	protein_coding,processed_transcript,retained_intron
ENSG00000159167,12	STC1	2.66	3.00E-12	protein_coding
ENSG00000173442,13	EHBP1L1	2.65	6.63E-07	protein_coding,processed_transcript,retained_intron
ENSG00000156011,17	PSD3	2.64	0.001588894	protein_coding,nonsense_mediated_decay,processed_transcript,retained_intron
ENSG00000179832,17	MROH1	2.64	0.006952103	protein_coding,retained_intron,processed_transcript
ENSG00000141858,12	SAMD1	2.64	0.039311217	protein_coding,processed_transcript
ENSG00000170581,14	STAT2	2.62	1.64E-05	nonsense_mediated_decay,protein_coding,retained_intron,processed_transcript
ENSG00000154803,13	FLCN	2.61	0.000268586	protein_coding,retained_intron
ENSG00000171295,13	ZNF440	2.61	0.033742751	protein_coding,retained_intron
ENSG00000198018,7	ENTPD7	2.60	0.00231656	protein_coding,nonsense_mediated_decay
ENSG00000128591,16	FLNC	2.60	0.000351179	protein_coding,retained_intron
ENSG00000109046,15	WSB1	2.58	9.43E-08	protein_coding,nonsense_mediated_decay,retained_intron,processed_transcript
ENSG00000233237,8	LINC00472	2.57	0.01527698	lncRNA
ENSG00000108669,16	CYTH1	2.56	0.003323923	retained_intron,protein_coding,processed_transcript,nonsense_mediated_decay
ENSG00000014216,16	CAPN1	2.55	2.32E-06	protein_coding,retained_intron,processed_transcript,nonsense_mediated_decay
ENSG00000137413,16	TAF8	2.52	7.00E-06	protein_coding,processed_transcript,retained_intron
ENSG00000085721,13	RRN3	2.52	0.029834518	protein_coding,retained_intron
ENSG00000009413,16	REV3L	2.51	0.026021735	nonsense_mediated_decay,protein_coding,processed_transcript,retained_intron
ENSG00000008083,14	JARID2	2.51	2.40E-09	protein_coding,processed_transcript
ENSG00000172888,12	ZNF621	2.51	0.029796201	protein_coding,processed_transcript,retained_intron
ENSG00000173120,15	KDM2A	2.50	0.019133929	protein_coding,processed_transcript
ENSG00000143669,14	LYST	2.49	0.01248113	processed_transcript,protein_coding,retained_intron
ENSG00000167548,16	KMT2D	2.48	0.022461179	protein_coding,retained_intron,processed_transcript
ENSG00000198910,14	L1CAM	2.47	0.013709568	protein_coding,retained_intron,processed_transcript
ENSG00000103657,14	HERC1	2.47	0.00707629	protein_coding,nonsense_mediated_decay,retained_intron
ENSG00000105443,15	CYTH2	2.46	0.002292655	protein_coding,processed_transcript,retained_intron,nonsense_mediated_decay
ENSG00000166016,6	ABTB2	2.46	0.028723182	protein_coding,processed_transcript
ENSG00000056558,11	TRAF1	2.45	0.000153483	protein_coding
ENSG00000157933,10	SKI	2.45	0.008129589	processed_transcript,protein_coding,retained_intron
ENSG00000267519,6	MIR23AHG	2.45	1.64E-08	lncRNA
ENSG00000275023,5	MLLT6	2.44	0.000227728	retained_intron,protein_coding,processed_transcript
ENSG00000131165,16	CHMP1A	2.44	0.012948518	retained_intron,protein_coding,nonsense_mediated_decay,processed_transcript
ENSG00000158470,5	B4GALT5	2.44	1.41E-05	protein_coding
ENSG00000127481,15	UBR4	2.43	5.28E-15	protein_coding,retained_intron,processed_transcript
ENSG00000197989,14	SNHG12	2.42	0.002937067	lncRNA,retained_intron
ENSG00000064932,16	SBNO2	2.41	0.001664501	protein_coding,retained_intron
ENSG00000147872,10	PLIN2	2.41	1.09E-16	protein_coding,processed_transcript
ENSG00000126012,12	KDM5C	2.41	0.028317548	processed_transcript,nonsense_mediated_decay,retained_intron,protein_coding
ENSG00000164949,8	GEM	2.40	6.35E-06	protein_coding,retained_intron
ENSG00000197312,12	DDI2	2.40	0.00601616	protein_coding,retained_intron,nonsense_mediated_decay
ENSG00000067798,16	NAV3	2.40	0.028647236	protein_coding,processed_transcript,retained_intron

ENSG00000105953,15	OGDH	2.39	0.000870481	protein_coding,processed_transcript,retained_intron
ENSG00000131389,17	SLC6A6	2.39	0.002409599	nonsense_mediated_decay,protein_coding,processed_transcript,retained_intron
ENSG00000127511,10	SIN3B	2.39	0.002151182	protein_coding,processed_transcript,retained_intron
ENSG00000172534,14	HCFC1	2.38	2.35E-05	protein_coding,processed_transcript
ENSG00000157483,9	MYO1E	2.38	0.016519545	retained_intron,protein_coding,processed_transcript,nonsense_mediated_decay
ENSG00000162402,14	USP24	2.38	7.15E-05	protein_coding,retained_intron,processed_transcript,nonsense_mediated_decay
ENSG00000186918,14	ZNF395	2.38	0.019726551	protein_coding,processed_transcript,retained_intron
ENSG00000065802,12	ASB1	2.37	0.029439739	processed_transcript,protein_coding,nonsense_mediated_decay,retained_intron
ENSG00000112033,14	PPARD	2.37	0.010741509	protein_coding
ENSG00000162231,14	NXF1	2.37	1.13E-06	nonsense_mediated_decay,protein_coding,retained_intron,processed_transcript
ENSG00000164880,16	INTS1	2.37	0.000768589	protein_coding,retained_intron,processed_transcript
ENSG00000137331,12	IER3	2.34	2.33E-23	protein_coding
ENSG00000126883,17	NUP214	2.34	0.001822982	protein_coding,nonsense_mediated_decay,processed_transcript,retained_intron
ENSG00000157227,14	MMP14	2.34	1.24E-12	non_stop_decay,processed_transcript,retained_intron,protein_coding,nonsense_mediated_decay
ENSG00000201998,1	SNORA23	2.34	0.004188497	snoRNA
ENSG00000006432,16	MAP3K9	2.34	0.025227109	protein_coding,retained_intron
ENSG00000197961,12	ZNF121	2.34	0.00323725	protein_coding
ENSG00000164828,18	SUN1	2.34	0.000237965	protein_coding,processed_transcript,retained_intron,nonsense_mediated_decay
ENSG00000089280,19	FUS	2.33	0.007403984	retained_intron,protein_coding,processed_transcript,nonsense_mediated_decay
ENSG00000197714,9	ZNF460	2.32	0.006122352	protein_coding
ENSG00000287080,2	H3C3	2.32	0.0388775	protein_coding
ENSG00000139645,11	ANKRD52	2.32	0.00789788	protein_coding,processed_transcript,retained_intron
ENSG00000141959,17	PFKL	2.30	0.000779841	processed_transcript,retained_intron,protein_coding,nonsense_mediated_decay
ENSG00000197386,13	HTT	2.30	0.001880823	retained_intron,protein_coding,nonsense_mediated_decay,processed_transcript
ENSG00000129003,19	VPS13C	2.30	0.003988115	protein_coding,nonsense_mediated_decay,processed_transcript,retained_intron
ENSG00000189143,10	CLDN4	2.30	0.00017585	protein_coding,processed_transcript
ENSG00000161202,20	DVL3	2.29	0.015887926	processed_transcript,retained_intron,nonsense_mediated_decay,protein_coding
ENSG00000152223,15	EPG5	2.29	5.44E-06	retained_intron,processed_transcript,nonsense_mediated_decay,protein_coding
ENSG00000149716,13	LTO1	2.29	0.032641061	processed_transcript,nonsense_mediated_decay,protein_coding,retained_intron
ENSG00000052795,13	FNIP2	2.28	0.019355817	protein_coding,processed_transcript,retained_intron
ENSG00000270069,1	MIR222HG	2.26	0.007774496	lncRNA
ENSG00000011021,23	CLCN6	2.26	0.019758898	nonsense_mediated_decay,protein_coding,processed_transcript,retained_intron
ENSG00000089902,10	RCOR1	2.26	0.002090189	protein_coding,retained_intron,nonsense_mediated_decay
ENSG00000184634,16	MED12	2.26	0.041017178	protein_coding,processed_transcript
ENSG00000169710,9	FASN	2.26	4.83E-10	protein_coding,retained_intron,nonsense_mediated_decay,processed_transcript
ENSG00000165458,14	INPPL1	2.25	0.008456968	protein_coding,retained_intron,nonsense_mediated_decay
ENSG00000196611,6	MMP1	2.25	1.05E-14	processed_transcript,protein_coding,retained_intron
ENSG00000169155,10	ZBTB43	2.25	0.000259468	protein_coding,processed_transcript
ENSG00000077150,20	NFKB2	2.24	0.000370698	processed_transcript,protein_coding,retained_intron
ENSG00000205189,12	ZBTB10	2.24	0.011564278	protein_coding

ENSG00000175931,13	UBE2O	2.23	0.006640538	protein_coding,retained_intron,processed_transcript
ENSG00000168488,18	ATXN2L	2.23	0.000211844	protein_coding,retained_intron,processed_transcript,nonsense_mediated_decay
ENSG00000143514,17	TP53BP2	2.23	0.000268011	processed_transcript,nonsense_mediated_decay,protein_coding,retained_intron
ENSG00000112511,18	PHF1	2.22	0.000656563	protein_coding,nonsense_mediated_decay,retained_intron
ENSG00000167106,12	FAM102A	2.22	0.002131677	protein_coding,retained_intron,processed_transcript
ENSG00000162775,17	RBM15	2.21	0.004643433	protein_coding
ENSG00000104885,18	DOT1L	2.21	0.015887926	protein_coding,processed_transcript,retained_intron,nonsense_mediated_decay
ENSG00000139354,11	GAS2L3	2.20	0.006195557	protein_coding,retained_intron,processed_transcript,nonsense_mediated_decay
ENSG00000118503,15	TNFAIP3	2.20	0.011496104	protein_coding,processed_transcript
ENSG00000198911,12	SREBF2	2.19	0.001096887	nonsense_mediated_decay,processed_transcript,retained_intron,protein_coding
ENSG00000198517,10	MAFK	2.19	0.008217866	protein_coding,nonsense_mediated_decay
ENSG00000179833,4	SERTAD2	2.18	0.011747591	protein_coding,processed_transcript
ENSG00000013364,19	MVP	2.18	0.000179648	protein_coding,nonsense_mediated_decay,processed_transcript,retained_intron
ENSG00000189241,8	TSPYL1	2.17	0.022437625	protein_coding,nonsense_mediated_decay
ENSG00000132510,11	KDM6B	2.16	0.001084561	processed_transcript,protein_coding
ENSG00000176994,11	SMCR8	2.15	0.002173238	protein_coding
ENSG00000108175,18	ZMIZ1	2.15	0.008057534	protein_coding,processed_transcript
ENSG00000092929,12	UNC13D	2.13	0.002214365	protein_coding,retained_intron,nonsense_mediated_decay,processed_transcript
ENSG00000104880,19	ARHGEF18	2.13	0.005876956	protein_coding,retained_intron
ENSG00000251562,8	MALAT1	2.12	4.65E-23	lncRNA
ENSG00000137628,18	DDX60	2.11	0.013357854	nonsense_mediated_decay,protein_coding,retained_intron,processed_transcript
ENSG00000204569,10	PPP1R10	2.11	5.07E-08	protein_coding,retained_intron,processed_transcript
ENSG00000163814,8	CDCP1	2.10	9.49E-11	protein_coding,processed_transcript
ENSG00000138834,14	MAPK8IP3	2.10	0.010053531	retained_intron,nonsense_mediated_decay,protein_coding,processed_transcript
ENSG00000162298,19	SYVN1	2.07	0.014177742	protein_coding,retained_intron,processed_transcript,nonsense_mediated_decay
ENSG00000105325,15	FZR1	2.07	0.022914346	protein_coding,retained_intron,nonsense_mediated_decay
ENSG00000196182,11	STK40	2.07	0.009212719	processed_transcript,protein_coding
ENSG00000257621,8	PSMA3-AS1	2.07	0.043069818	lncRNA
ENSG00000197217,13	ENTPD4	2.07	0.031188427	protein_coding,processed_transcript,retained_intron
ENSG00000136877,15	FPGS	2.07	0.040950066	processed_transcript,protein_coding
ENSG00000133657,16	ATP13A3	2.07	4.39E-07	protein_coding,retained_intron
ENSG00000148396,18	SEC16A	2.06	0.000873303	protein_coding,processed_transcript
ENSG00000101577,10	LPIN2	2.05	0.002464889	protein_coding,processed_transcript
ENSG00000075426,12	FOSL2	2.05	7.49E-07	protein_coding,processed_transcript
ENSG00000168209,6	DDIT4	2.05	9.34E-08	nonsense_mediated_decay,retained_intron,protein_coding
ENSG00000188157,15	AGRN	2.04	0.038082603	retained_intron,protein_coding
ENSG00000184371,14	CSF1	2.03	0.001995859	protein_coding,processed_transcript
ENSG00000095564,14	BTAF1	2.01	0.002257972	protein_coding,processed_transcript
ENSG00000177733,7	HNRNPA0	2.01	0.032399766	protein_coding
ENSG00000100441,10	KHNYN	2.01	0.049228819	protein_coding,retained_intron
ENSG00000167766,19	ZNF83	2.00	0.002350541	nonsense_mediated_decay,protein_coding,retained_intron,processed_transcript

ENSG00000165861,14	ZFYVE1	2.00	0.045790614	protein_coding,retained_intron,processed_transcript
ENSG00000107185,10	RGP1	1.99	0.01698779	retained_intron,protein_coding
ENSG00000113716,13	HMGXB3	1.98	0.041578324	protein_coding,nonsense_mediated_decay,retained_intron
ENSG00000160209,19	PDXK	1.98	0.001208454	processed_transcript,protein_coding
ENSG00000196367,14	TRRAP	1.98	0.000171674	nonsense_mediated_decay,protein_coding,processed_transcript,retained_intron
ENSG00000137145,21	DENND4C	1.97	0.014483343	protein_coding,retained_intron,nonsense_mediated_decay
ENSG00000198742,10	SMURF1	1.96	0.014867455	protein_coding,processed_transcript
ENSG00000198625,13	MDM4	1.95	0.000358832	protein_coding,processed_transcript
ENSG00000204469,13	PRRC2A	1.95	0.000664601	protein_coding,processed_transcript,retained_intron
ENSG00000124762,14	CDKN1A	1.94	2.50E-05	protein_coding,processed_transcript
ENSG00000141568,21	FOXK2	1.93	0.01279455	processed_transcript,nonsense_mediated_decay,protein_coding,retained_intron,TEC
ENSG00000128016,7	ZFP36	1.93	4.46E-05	protein_coding,processed_transcript
ENSG00000130669,17	PAK4	1.92	0.013015855	protein_coding,retained_intron,processed_transcript
ENSG00000070495,15	JMJD6	1.92	0.027191897	protein_coding,retained_intron,nonsense_mediated_decay
ENSG00000159692,16	CTBP1	1.91	0.008011617	protein_coding,nonsense_mediated_decay,retained_intron,processed_transcript
ENSG00000197226,13	TBC1D9B	1.90	0.016289165	protein_coding,retained_intron,processed_transcript,nonsense_mediated_decay
ENSG00000005884,18	ITGA3	1.90	2.46E-09	protein_coding,retained_intron,nonsense_mediated_decay
ENSG00000004975,12	DVL2	1.89	0.01880383	protein_coding,retained_intron,processed_transcript
ENSG00000174197,16	MGA	1.89	0.007291659	protein_coding,processed_transcript,retained_intron
ENSG00000275110,1	AL928646,1	1.89	0.001996187	miRNA
ENSG00000107263,18	RAPGEF1	1.88	0.006258243	protein_coding,processed_transcript
ENSG00000167615,17	LENG8	1.87	0.004188497	protein_coding,retained_intron
ENSG00000172466,16	ZNF24	1.86	0.026929365	protein_coding
ENSG00000033627,17	ATP6V0A1	1.86	0.024121623	protein_coding,retained_intron,processed_transcript,nonsense_mediated_decay
ENSG00000196924,19	FLNA	1.86	1.76E-10	retained_intron,nonsense_mediated_decay,protein_coding,processed_transcript
ENSG00000101152,11	DNAJC5	1.86	0.015716284	nonsense_mediated_decay,protein_coding
ENSG00000156273,16	BACH1	1.86	0.000673597	protein_coding,processed_transcript
ENSG00000105576,15	TNPO2	1.85	0.002131677	protein_coding,nonsense_mediated_decay,non_stop_decay,retained_intron,processed_transcript
ENSG00000111667,14	USP5	1.85	0.011900088	retained_intron,processed_transcript,protein_coding
ENSG00000161904,12	LEMD2	1.84	0.048831891	retained_intron,protein_coding,nonsense_mediated_decay,processed_transcript
ENSG00000088256,9	GNA11	1.84	0.018233973	protein_coding,processed_transcript,retained_intron
ENSG00000264522,6	OTUD7B	1.84	0.049338772	protein_coding,retained_intron
ENSG00000143442,22	POGZ	1.83	0.034811317	retained_intron,protein_coding,nonsense_mediated_decay
ENSG00000077782,21	FGFR1	1.83	0.021621363	processed_transcript,nonsense_mediated_decay,protein_coding,retained_intron
ENSG00000115977,21	AAK1	1.83	0.006640538	protein_coding,retained_intron,processed_transcript
ENSG00000136830,12	NIBAN2	1.82	3.86E-09	protein_coding,processed_transcript
ENSG00000096433,11	ITPR3	1.82	4.39E-07	protein_coding
ENSG00000071626,17	DAZAP1	1.82	0.001810334	protein_coding,processed_transcript,retained_intron
ENSG00000038382,20	TRIO	1.82	6.19E-06	protein_coding,retained_intron,nonsense_mediated_decay,processed_transcript
ENSG00000240849,11	PEDS1	1.82	0.049686436	protein_coding,nonsense_mediated_decay

ENSG00000164442,10	CITED2	1.82	4.75E-05	protein_coding
ENSG00000111674,9	ENO2	1.82	9.76E-06	retained_intron,protein_coding,nonsense_mediated_decay,processed_transcript
ENSG00000174282,12	ZBTB4	1.81	0.014186397	protein_coding
ENSG00000101654,18	RNMT	1.81	0.007257576	protein_coding,retained_intron,processed_transcript,nonsense_mediated_decay
ENSG00000120129,6	DUSP1	1.80	0.000203824	protein_coding
ENSG00000156711,17	MAPK13	1.80	0.006455577	protein_coding,processed_transcript
ENSG00000095319,14	NUP188	1.80	0.038632198	retained_intron,processed_transcript,protein_coding
ENSG00000116584,20	ARHGEF2	1.79	1.83E-06	protein_coding,nonsense_mediated_decay,processed_transcript,retained_intron
ENSG00000161011,20	SQSTM1	1.78	2.47E-15	protein_coding,retained_intron,nonsense_mediated_decay,processed_transcript
ENSG00000115760,14	BIRC6	1.78	0.000185113	retained_intron,nonsense_mediated_decay,protein_coding
ENSG00000103365,15	GGA2	1.78	0.032224356	nonsense_mediated_decay,protein_coding,processed_transcript,retained_intron
ENSG00000230590,11	FTX	1.78	0.041450404	lncRNA
ENSG00000156030,13	MIDEAS	1.76	0.02005446	nonsense_mediated_decay,protein_coding,retained_intron,processed_transcript
ENSG00000198752,11	CDC42BPB	1.74	0.001674388	protein_coding,processed_transcript,retained_intron
ENSG00000123064,13	DDX54	1.74	0.029268389	processed_transcript,retained_intron,nonsense_mediated_decay,protein_coding
ENSG00000134086,8	VHL	1.74	0.02005446	protein_coding,processed_transcript
ENSG00000198700,10	IPO9	1.73	0.024569875	protein_coding,processed_transcript
ENSG00000088888,18	MAVS	1.73	0.001929135	protein_coding
ENSG00000124181,14	PLCG1	1.73	0.033298422	nonsense_mediated_decay,protein_coding,processed_transcript,retained_intron
ENSG00000130939,20	UBE4B	1.73	0.029439739	protein_coding,retained_intron,nonsense_mediated_decay,processed_transcript
ENSG00000181222,19	POLR2A	1.71	0.002688176	retained_intron,protein_coding,processed_transcript
ENSG00000147133,16	TAF1	1.70	0.011236007	processed_transcript,nonsense_mediated_decay,protein_coding,retained_intron
ENSG00000143322,21	ABL2	1.70	4.86E-06	protein_coding,processed_transcript,retained_intron
ENSG00000147454,14	SLC25A37	1.70	0.001369893	nonsense_mediated_decay,protein_coding,retained_intron,processed_transcript
ENSG00000003756,17	RBM5	1.70	0.020941562	nonsense_mediated_decay,retained_intron,protein_coding,processed_transcript
ENSG00000197102,13	DYNC1H1	1.69	1.36E-10	nonsense_mediated_decay,protein_coding,retained_intron,processed_transcript
ENSG00000066084,13	DIP2B	1.69	0.049704263	nonsense_mediated_decay,retained_intron,protein_coding
ENSG00000067082,15	KLF6	1.69	3.03E-06	protein_coding,processed_transcript
ENSG00000113552,16	GNPDA1	1.68	0.034394689	protein_coding,retained_intron
ENSG00000184014,9	DENND5A	1.67	0.003580397	protein_coding,retained_intron,nonsense_mediated_decay,processed_transcript
ENSG00000107554,17	DNMBP	1.67	0.001822982	protein_coding,retained_intron
ENSG00000149187,18	CELF1	1.66	0.001989513	protein_coding,retained_intron,processed_transcript
ENSG00000124422,12	USP22	1.66	0.001127251	protein_coding,processed_transcript,retained_intron,nonsense_mediated_decay
ENSG00000112096,19	SOD2	1.66	1.94E-08	protein_coding,retained_intron,processed_transcript,nonsense_mediated_decay
ENSG00000137193,14	PIM1	1.65	0.013015855	processed_transcript,protein_coding
ENSG00000197063,11	MAFG	1.65	0.023667535	protein_coding
ENSG00000062716,13	VMP1	1.65	0.000554416	protein_coding,nonsense_mediated_decay,retained_intron,processed_transcript
ENSG00000185567,7	AHNAK2	1.65	1.74E-05	protein_coding,retained_intron
ENSG00000165699,15	TSC1	1.65	0.024871142	protein_coding,nonsense_mediated_decay,retained_intron,processed_transcript
ENSG00000103994,18	ZNF106	1.64	0.028745345	protein_coding,retained_intron,processed_transcript
ENSG00000197077,13	KIAA1671	1.64	0.012975372	protein_coding,retained_intron

ENSG00000142002,18	DPP9	1.64	0.000303549	protein_coding,retained_intron,nonsense_mediated_decay,processed_transcript
ENSG00000177606,8	JUN	1.64	7.92E-05	protein_coding,nonsense_mediated_decay
ENSG00000186174,12	BCL9L	1.63	0.01587033	protein_coding,processed_transcript
ENSG00000182446,14	NPLOC4	1.63	0.01704752	protein_coding,nonsense_mediated_decay,retained_intron,processed_transcript
ENSG00000144136,11	SLC20A1	1.63	0.000529486	protein_coding,nonsense_mediated_decay,retained_intron,processed_transcript
ENSG00000100991,12	TRPC4AP	1.62	0.029439739	protein_coding
ENSG00000178607,17	ERN1	1.62	0.042332002	processed_transcript,retained_intron,protein_coding
ENSG00000160007,19	ARHGAP35	1.62	0.003950207	protein_coding,retained_intron,processed_transcript
ENSG00000136068,15	FLNB	1.62	6.36E-10	protein_coding,nonsense_mediated_decay,retained_intron,processed_transcript
ENSG00000177885,15	GRB2	1.62	0.041578324	protein_coding,processed_transcript,nonsense_mediated_decay,retained_intron
ENSG00000064393,16	HIPK2	1.61	0.000211844	protein_coding
ENSG00000088387,19	DOCK9	1.61	0.001094737	protein_coding,nonsense_mediated_decay,processed_transcript,retained_intron
ENSG00000002834,18	LASP1	1.61	0.000107551	protein_coding,retained_intron,nonsense_mediated_decay
ENSG00000072778,20	ACADVL	1.60	0.001269587	nonsense_mediated_decay,protein_coding,retained_intron,processed_transcript
ENSG00000156515,24	HK1	1.60	0.000194373	protein_coding,processed_transcript,nonsense_mediated_decay,retained_intron
ENSG00000185650,10	ZFP36L1	1.60	8.90E-05	protein_coding
ENSG00000137275,16	RIPK1	1.58	0.032544152	retained_intron,nonsense_mediated_decay,processed_transcript,protein_coding
ENSG00000168092,14	PAFAH1B2	1.58	0.005088212	protein_coding,retained_intron,processed_transcript
ENSG00000159216,19	RUNX1	1.58	0.00226962	protein_coding,retained_intron,processed_transcript,nonsense_mediated_decay
ENSG00000125686,12	MED1	1.58	0.007877973	nonsense_mediated_decay,retained_intron,protein_coding
ENSG00000141522,12	ARHGDIA	1.58	1.59E-05	protein_coding,retained_intron,nonsense_mediated_decay,processed_transcript
ENSG00000182158,15	CREB3L2	1.57	0.012249339	protein_coding,processed_transcript
ENSG00000130513,6	GDF15	1.57	0.049139322	protein_coding,processed_transcript
ENSG00000100650,16	SRSF5	1.56	0.003396482	protein_coding,retained_intron,processed_transcript,nonsense_mediated_decay
ENSG00000120071,15	KANSL1	1.56	0.029268389	protein_coding,processed_transcript,retained_intron
ENSG00000233016,7	SNHG7	1.55	0.021621363	lncRNA
ENSG00000132471,12	WBP2	1.55	0.007046945	nonsense_mediated_decay,protein_coding,retained_intron,processed_transcript
ENSG00000090615,15	GOLGA3	1.55	0.001963565	nonsense_mediated_decay,protein_coding,processed_transcript
ENSG00000013588,9	GPRC5A	1.55	0.010323806	protein_coding,processed_transcript,retained_intron
ENSG00000173064,13	HECTD4	1.55	0.020766726	protein_coding,nonsense_mediated_decay,retained_intron,processed_transcript
ENSG00000137166,17	FOXP4	1.54	0.039070263	protein_coding
ENSG00000137076,21	TLN1	1.54	2.53E-06	protein_coding,processed_transcript,retained_intron
ENSG00000101752,12	MIB1	1.53	0.020766726	processed_transcript,protein_coding,retained_intron
ENSG00000101224,18	CDC25B	1.53	0.019726551	protein_coding,processed_transcript
ENSG00000207340,1	RNVU1-1	1.53	0.030044253	snRNA
ENSG00000161638,11	ITGA5	1.52	0.005044187	retained_intron,nonsense_mediated_decay,processed_transcript,protein_coding
ENSG00000158195,11	WASF2	1.52	0.005764381	protein_coding
ENSG00000167110,18	GOLGA2	1.52	0.002877736	protein_coding,retained_intron
ENSG00000011304,22	PTBP1	1.52	0.003750796	nonsense_mediated_decay,protein_coding,retained_intron
ENSG00000008294,21	SPAG9	1.51	2.46E-05	protein_coding,processed_transcript,retained_intron,nonsense_mediated_decay
ENSG00000134324,12	LPIN1	1.51	0.017150318	protein_coding,nonsense_mediated_decay,processed_transcript,retained_intron

ENSG00000111412,6	SPRING1	1.51	0.016289165	protein_coding,nonsense_mediated_decay
ENSG00000115762,16	PLEKHB2	1.50	0.000276195	protein_coding,processed_transcript,retained_intron
ENSG00000196535,17	MYO18A	1.50	0.00239836	protein_coding,retained_intron,processed_transcript,nonsense_mediated_decay
ENSG00000106070,20	GRB10	1.50	0.003342827	protein_coding,processed_transcript,retained_intron,nonsense_mediated_decay
ENSG00000176619,13	LMNB2	1.50	0.01070394	protein_coding,processed_transcript,retained_intron
ENSG00000157654,19	PALM2AKAP2	1.49	1.48E-05	protein_coding,retained_intron,nonsense_mediated_decay,processed_transcript
ENSG00000130517,14	PGPEP1	1.48	0.045790614	protein_coding,nonsense_mediated_decay
ENSG00000115464,15	USP34	1.48	0.000876323	protein_coding,processed_transcript,retained_intron,nonsense_mediated_decay
ENSG00000108828,16	VAT1	1.46	0.000535491	nonsense_mediated_decay,protein_coding
ENSG00000082641,16	NFE2L1	1.46	0.000870481	protein_coding,processed_transcript
ENSG00000147416,11	ATP6V1B2	1.46	0.046516369	protein_coding,retained_intron,nonsense_mediated_decay
ENSG00000134250,20	NOTCH2	1.46	0.001958541	nonsense_mediated_decay,protein_coding,processed_transcript,retained_intron
ENSG00000167491,17	GATAD2A	1.46	0.026222433	protein_coding,nonsense_mediated_decay,processed_transcript
ENSG00000204463,13	BAG6	1.45	7.56E-06	protein_coding,retained_intron,nonsense_mediated_decay,processed_transcript
ENSG00000253352,10	TUG1	1.45	0.041585096	protein_coding,processed_transcript
ENSG00000278540,5	ACACA	1.44	0.048875617	protein_coding,retained_intron,nonsense_mediated_decay,non_stop_decay,processed_transcript
ENSG00000183696,14	UPP1	1.44	0.004188497	nonsense_mediated_decay,protein_coding,processed_transcript,retained_intron
ENSG00000108510,10	MED13	1.44	0.01098272	protein_coding,retained_intron,processed_transcript
ENSG00000143384,14	MCL1	1.43	0.000350174	protein_coding,processed_transcript,retained_intron
ENSG00000171456,20	ASXL1	1.42	0.022904444	protein_coding,nonsense_mediated_decay,retained_intron,processed_transcript
ENSG00000097007,19	ABL1	1.42	0.041891506	protein_coding
ENSG00000173482,17	PTPRM	1.42	0.010206784	protein_coding,processed_transcript,retained_intron
ENSG00000114867,22	EIF4G1	1.41	1.73E-06	protein_coding,retained_intron,nonsense_mediated_decay
ENSG00000087274,17	ADD1	1.41	0.006122352	protein_coding,nonsense_mediated_decay,retained_intron,processed_transcript
ENSG00000162772,17	ATF3	1.41	0.035875594	protein_coding,processed_transcript,nonsense_mediated_decay,retained_intron
ENSG00000114480,13	GBE1	1.40	0.004245697	protein_coding,retained_intron,processed_transcript
ENSG00000120733,14	KDM3B	1.40	0.040520854	retained_intron,protein_coding,nonsense_mediated_decay,processed_transcript
ENSG00000130726,12	TRIM28	1.39	0.045980896	protein_coding,retained_intron
ENSG00000146112,12	PPP1R18	1.39	0.000326473	protein_coding,processed_transcript
ENSG00000076108,12	BAZ2A	1.38	0.024908987	processed_transcript,protein_coding,retained_intron
ENSG00000215301,11	DDX3X	1.38	2.97E-06	nonsense_mediated_decay,retained_intron,protein_coding,processed_transcript
ENSG00000134107,5	BHLHE40	1.38	0.000298529	protein_coding,retained_intron
ENSG00000135047,16	CTSL	1.37	0.01087643	protein_coding,nonsense_mediated_decay,retained_intron
ENSG00000115963,14	RND3	1.36	0.000108103	protein_coding,retained_intron,processed_transcript
ENSG00000158615,9	PPP1R15B	1.36	0.013526169	protein_coding
ENSG00000175793,12	SFN	1.35	0.038687037	protein_coding
ENSG00000079805,18	DNM2	1.35	0.017450934	retained_intron,protein_coding,processed_transcript
ENSG00000196235,14	SUPT5H	1.35	0.026021735	protein_coding,retained_intron,processed_transcript
ENSG00000238554,1	RNU1-88P	1.35	0.015776726	snRNA
ENSG00000124201,15	ZNFX1	1.35	0.014897272	protein_coding,processed_transcript

ENSG00000145495,16	MARCHF6	1.34	0.032683077	retained_intron,processed_transcript,protein_coding,nonsense_mediated_decay
ENSG00000231925,12	TAPBP	1.32	0.036910788	protein_coding,retained_intron
ENSG00000141458,13	NPC1	1.32	0.018200749	protein_coding,retained_intron,processed_transcript
ENSG00000185658,14	BRWD1	1.32	0.048875617	protein_coding,nonsense_mediated_decay,retained_intron,processed_transcript
ENSG00000112715,25	VEGFA	1.31	9.98E-06	protein_coding,retained_intron
ENSG00000198959,12	TGM2	1.31	0.009168288	protein_coding,retained_intron
ENSG00000164951,16	PDP1	1.31	0.032497118	protein_coding,processed_transcript
ENSG00000182095,14	TNRC18	1.31	0.013015855	protein_coding,retained_intron
ENSG00000121060,18	TRIM25	1.30	0.013845962	retained_intron,nonsense_mediated_decay,protein_coding,processed_transcript
ENSG00000171988,19	JMJD1C	1.30	0.0067383	protein_coding,processed_transcript,retained_intron
ENSG00000165891,16	E2F7	1.29	0.0211254	retained_intron,protein_coding,nonsense_mediated_decay
ENSG00000115295,20	CLIP4	1.29	0.025431263	protein_coding,nonsense_mediated_decay,retained_intron,processed_transcript
ENSG00000123908,12	AGO2	1.27	0.002714871	nonsense_mediated_decay,retained_intron,protein_coding,processed_transcript
ENSG00000173821,19	RNF213	1.27	0.0011651	protein_coding,retained_intron,processed_transcript
ENSG00000164171,11	ITGA2	1.27	0.004221263	protein_coding,nonsense_mediated_decay
ENSG00000035862,12	TIMP2	1.27	0.020817641	protein_coding,nonsense_mediated_decay
ENSG00000110367,13	DDX6	1.26	0.000586727	protein_coding,retained_intron
ENSG00000144028,15	SNRNP200	1.26	0.016298413	retained_intron,protein_coding
ENSG00000276168,1	RN7SL1	1.26	5.76E-05	misc_RNA
ENSG00000185359,14	HGS	1.24	0.029834518	protein_coding,nonsense_mediated_decay,retained_intron,processed_transcript
ENSG00000196365,12	LONP1	1.24	0.028171239	nonsense_mediated_decay,retained_intron,processed_transcript,protein_coding
ENSG00000182944,18	EWSR1	1.23	0.015213542	protein_coding,retained_intron
ENSG00000184640,20	SEPTIN9	1.22	0.006542748	processed_transcript,protein_coding,nonsense_mediated_decay,retained_intron
ENSG00000179820,16	MYADM	1.22	0.020204961	protein_coding,processed_transcript
ENSG00000124942,14	AHNAK	1.20	3.37E-08	protein_coding,processed_transcript
ENSG00000169045,17	HNRNPH1	1.20	0.000107299	protein_coding,retained_intron,nonsense_mediated_decay,processed_transcript
ENSG00000196878,15	LAMB3	1.19	0.019012672	protein_coding
ENSG00000181789,14	COPG1	1.19	0.004438557	retained_intron,protein_coding,nonsense_mediated_decay
ENSG00000186480,13	INSIG1	1.18	0.007439326	protein_coding,retained_intron
ENSG00000168906,13	MAT2A	1.18	0.019726551	protein_coding,retained_intron,processed_transcript
ENSG00000186591,13	UBE2H	1.17	0.020631882	nonsense_mediated_decay,retained_intron,protein_coding
ENSG00000165527,7	ARF6	1.17	0.019570235	protein_coding
ENSG00000143569,19	UBAP2L	1.17	0.028745345	protein_coding,processed_transcript
ENSG00000105568,18	PPP2R1A	1.16	0.01279455	protein_coding,processed_transcript,nonsense_mediated_decay,retained_intron
ENSG00000146674,15	IGFBP3	1.15	0.03815243	protein_coding,processed_transcript,retained_intron
ENSG00000133816,17	MICAL2	1.15	0.014369482	protein_coding,retained_intron,processed_transcript,nonsense_mediated_decay
ENSG00000085733,16	CTTN	1.13	0.032399766	protein_coding,retained_intron,processed_transcript,nonsense_mediated_decay
ENSG00000175592,9	FOSL1	1.13	0.004854265	protein_coding
ENSG00000105701,16	FKBP8	1.13	0.039432352	nonsense_mediated_decay,protein_coding,retained_intron
ENSG00000165029,17	ABCA1	1.10	0.039091715	protein_coding,processed_transcript
ENSG00000067057,18	PFKP	1.08	0.008425831	protein_coding,nonsense_mediated_decay,processed_transcript,retained_intron

ENSG00000166833,22	NAV2	1.07	0.026844542	protein_coding,processed_transcript,retained_intron
ENSG00000172939,9	OXSR1	1.07	0.037589425	retained_intron,protein_coding,processed_transcript,nonsense_mediated_decay
ENSG00000157106,17	SMG1	1.06	0.013301541	protein_coding,processed_transcript,nonsense_mediated_decay,retained_intron
ENSG00000132002,9	DNAJB1	1.06	0.006596274	protein_coding,processed_transcript
ENSG00000130164,14	LDLR	1.06	0.004148745	nonsense_mediated_decay,protein_coding,processed_transcript,retained_intron
ENSG00000116285,13	ERRFI1	1.03	0.000252277	protein_coding,nonsense_mediated_decay
ENSG00000140575,13	IQGAP1	1.02	0.005664796	retained_intron,nonsense_mediated_decay,protein_coding,processed_transcript
ENSG00000265972,6	TXNIP	1.02	0.000194373	protein_coding,retained_intron
ENSG00000198380,13	GFPT1	1.01	0.015887926	protein_coding,nonsense_mediated_decay
ENSG00000086758,16	HUWE1	1.00	0.003300996	protein_coding,processed_transcript,retained_intron,nonsense_mediated_decay
ENSG00000141367,12	CLTC	0.98	0.002391468	protein_coding,processed_transcript,nonsense_mediated_decay,retained_intron
ENSG00000152104,12	PTPN14	0.96	0.016172549	protein_coding,processed_transcript
ENSG00000188229,6	TUBB4B	0.95	0.009494727	retained_intron,protein_coding
ENSG00000139289,14	PHLDA1	0.94	0.001995859	protein_coding
ENSG00000105220,17	GPI	0.93	0.019691269	protein_coding,nonsense_mediated_decay,processed_transcript,retained_intron
ENSG00000198431,16	TXNRD1	0.92	0.000503094	protein_coding,retained_intron,processed_transcript,nonsense_mediated_decay
ENSG00000122218,16	COPA	0.91	0.047538847	nonsense_mediated_decay,protein_coding,retained_intron,processed_transcript
ENSG00000102144,15	PGK1	0.73	0.010640278	protein_coding,processed_transcript
ENSG00000127603,30	MACF1	0.67	0.041765422	protein_coding,nonsense_mediated_decay,retained_intron,processed_transcript
ENSG00000147065,17	MSN	0.66	0.040557283	protein_coding,processed_transcript
ENSG00000087086,15	FTL	-0.59	0.039070263	protein_coding
ENSG00000026025,16	VIM	-0.62	0.016733256	processed_transcript,retained_intron,protein_coding,nonsense_mediated_decay
ENSG00000044574,9	HSPA5	-0.68	0.008202642	retained_intron,protein_coding
ENSG00000156508,19	EEF1A1	-0.68	0.009969445	protein_coding,retained_intron,processed_transcript
ENSG00000136810,13	TXN	-0.73	0.040950066	protein_coding,processed_transcript
ENSG00000140988,16	RPS2	-0.75	0.039432352	retained_intron,protein_coding,nonsense_mediated_decay
ENSG00000147403,18	RPL10	-0.75	0.025429748	protein_coding,processed_transcript,retained_intron
ENSG00000127022,16	CANX	-0.76	0.007001304	nonsense_mediated_decay,protein_coding,retained_intron,processed_transcript
ENSG00000144381,18	HSPD1	-0.78	0.042570137	protein_coding,nonsense_mediated_decay,retained_intron
ENSG00000164924,18	YWHAZ	-0.79	0.019416413	protein_coding,processed_transcript,retained_intron,nonsense_mediated_decay
ENSG00000100097,12	LGALS1	-0.86	0.016194629	protein_coding,retained_intron,nonsense_mediated_decay,processed_transcript
ENSG00000108953,17	YWHAE	-0.88	0.008879793	processed_transcript,protein_coding,nonsense_mediated_decay,retained_intron
ENSG00000084234,18	APLP2	-0.88	0.010750406	nonsense_mediated_decay,protein_coding,processed_transcript,retained_intron
ENSG00000205542,11	TMSB4X	-0.89	0.001101248	protein_coding
ENSG00000100316,16	RPL3	-0.89	0.004463598	protein_coding,retained_intron,nonsense_mediated_decay,processed_transcript
ENSG00000234741,8	GAS5	-0.89	0.03539555	retained_intron,lncRNA
ENSG00000150753,12	CCT5	-0.90	0.035799809	nonsense_mediated_decay,retained_intron,protein_coding
ENSG00000113407,14	TARS1	-0.92	0.012684003	protein_coding,nonsense_mediated_decay,retained_intron,processed_transcript
ENSG00000135404,12	CD63	-0.93	0.026021735	protein_coding,nonsense_mediated_decay,retained_intron
ENSG00000150093,20	ITGB1	-0.96	0.013709568	protein_coding,nonsense_mediated_decay,processed_transcript,retained_intron
ENSG00000131711,15	MAP1B	-0.96	0.000358832	protein_coding,processed_transcript,nonsense_mediated_decay

ENSG00000155660,11	PDIA4	-0.99	0.008670536	protein_coding,retained_intron
ENSG00000173812,11	EIF1	-0.99	0.000810112	protein_coding,retained_intron,processed_transcript
ENSG00000124207,17	CSE1L	-0.99	0.026222433	processed_transcript,protein_coding
ENSG00000118816,11	CCNI	-1.00	0.005671665	protein_coding,retained_intron,nonsense_mediated_decay,processed_transcript
ENSG00000110958,16	PTGES3	-1.00	0.014483343	protein_coding,processed_transcript
ENSG00000169504,15	CLIC4	-1.00	0.015887926	nonsense_mediated_decay,processed_transcript,protein_coding
ENSG00000179218,15	CALR	-1.01	0.000181523	protein_coding,retained_intron,nonsense_mediated_decay
ENSG00000270647,6	TAF15	-1.02	0.039321896	protein_coding,retained_intron,processed_transcript,nonsense_mediated_decay
ENSG00000100664,11	EIF5	-1.02	0.029834518	protein_coding,retained_intron,processed_transcript
ENSG00000107581,13	EIF3A	-1.03	0.005833931	protein_coding,retained_intron
ENSG00000153113,24	CAST	-1.03	0.003947912	nonsense_mediated_decay,protein_coding,retained_intron,processed_transcript
ENSG00000203875,13	SNHG5	-1.04	0.016588614	lncRNA,retained_intron
ENSG00000047410,14	TPR	-1.05	0.040818155	processed_transcript,retained_intron,protein_coding
ENSG00000137818,12	RPLP1	-1.06	0.000771931	protein_coding,retained_intron
ENSG00000170315,14	UBB	-1.06	0.008482433	protein_coding,processed_transcript
ENSG00000141753,7	IGFBP4	-1.06	0.044051163	protein_coding
ENSG00000165732,13	DDX21	-1.06	0.0064376	protein_coding
ENSG00000106052,13	TAX1BP1	-1.07	0.016069035	protein_coding,nonsense_mediated_decay,retained_intron,processed_transcript
ENSG00000102317,18	RBM3	-1.07	0.000631746	processed_transcript,protein_coding
ENSG00000156261,13	CCT8	-1.07	0.034149388	protein_coding,retained_intron,processed_transcript
ENSG00000186298,12	PPP1CC	-1.07	0.039879505	protein_coding,processed_transcript,nonsense_mediated_decay,retained_intron,non_stop_decay
ENSG00000124783,14	SSR1	-1.08	0.005962314	protein_coding,processed_transcript
ENSG00000147010,18	SH3KBP1	-1.08	0.04563222	protein_coding,processed_transcript
ENSG00000149273,15	RPS3	-1.08	1.51E-05	nonsense_mediated_decay,protein_coding,processed_transcript,retained_intron
ENSG00000213585,11	VDAC1	-1.08	0.024749189	protein_coding,retained_intron,processed_transcript
ENSG00000136930,13	PSMB7	-1.09	0.026201391	protein_coding,processed_transcript
ENSG00000165678,21	GHITM	-1.10	0.015041589	protein_coding
ENSG00000184007,22	PTP4A2	-1.12	0.014264892	nonsense_mediated_decay,retained_intron,protein_coding,processed_transcript
ENSG00000134308,14	YWHAQ	-1.12	0.017985914	protein_coding,processed_transcript
ENSG00000161016,18	RPL8	-1.13	4.27E-05	nonsense_mediated_decay,protein_coding,retained_intron,processed_transcript
ENSG00000159377,11	PSMB4	-1.14	0.031736789	protein_coding,retained_intron
ENSG00000147677,11	EIF3H	-1.14	0.012325245	nonsense_mediated_decay,protein_coding,retained_intron
ENSG00000111229,16	ARPC3	-1.15	0.047985138	protein_coding,retained_intron,processed_transcript
ENSG00000146731,11	CCT6A	-1.15	0.020579642	protein_coding,retained_intron,processed_transcript
ENSG00000143621,17	ILF2	-1.15	0.025723937	protein_coding,processed_transcript
ENSG00000164754,15	RAD21	-1.15	0.012447387	protein_coding,processed_transcript,retained_intron
ENSG00000150459,12	SAP18	-1.16	0.029608334	protein_coding,processed_transcript
ENSG00000107223,13	EDF1	-1.16	0.010183581	protein_coding
ENSG00000175061,18	SNHG29	-1.19	1.96E-05	lncRNA,retained_intron
ENSG00000110696,10	C11orf58	-1.20	0.029451904	protein_coding,retained_intron,processed_transcript
ENSG00000142871,18	CCN1	-1.20	0.023842073	protein_coding,retained_intron,processed_transcript,nonsense_mediated_decay

ENSG00000105887,11	MTPN	-1.21	0.013015855	protein_coding
ENSG00000197956,10	S100A6	-1.23	1.69E-07	protein_coding,retained_intron
ENSG00000163466,16	ARPC2	-1.23	0.005421764	protein_coding,retained_intron,processed_transcript,nonsense_mediated_decay
ENSG00000163191,6	S100A11	-1.24	0.000565163	protein_coding,processed_transcript
ENSG00000166913,13	YWHAB	-1.24	0.000351179	nonsense_mediated_decay,protein_coding,retained_intron
ENSG00000122966,17	CIT	-1.25	0.023901883	protein_coding,retained_intron,nonsense_mediated_decay,processed_transcript
ENSG00000118680,14	MYL12B	-1.25	0.000608507	protein_coding
ENSG00000204525,17	HLA-C	-1.25	0.038300918	retained_intron,protein_coding,nonsense_mediated_decay
ENSG00000104408,11	EIF3E	-1.26	0.0004605	protein_coding,retained_intron,nonsense_mediated_decay,processed_transcript
ENSG00000204628,12	RACK1	-1.26	6.52E-07	protein_coding,nonsense_mediated_decay,retained_intron,processed_transcript
ENSG00000070814,22	TCOF1	-1.26	0.040557283	protein_coding,retained_intron,nonsense_mediated_decay,processed_transcript
ENSG00000095787,24	WAC	-1.26	0.015199099	protein_coding,nonsense_mediated_decay,retained_intron,processed_transcript
ENSG00000087460,28	GNAS	-1.27	3.56E-06	protein_coding,nonsense_mediated_decay,processed_transcript,retained_intron
ENSG00000181019,13	NQO1	-1.27	0.022451021	protein_coding,retained_intron
ENSG00000135318,12	NT5E	-1.30	0.013301541	protein_coding
ENSG00000088832,18	FKBP1A	-1.30	0.002806303	protein_coding,nonsense_mediated_decay,processed_transcript,retained_intron
ENSG00000182718,18	ANXA2	-1.31	1.27E-05	protein_coding,nonsense_mediated_decay,retained_intron,processed_transcript
ENSG00000140264,21	SERF2	-1.31	0.01704752	protein_coding,nonsense_mediated_decay,retained_intron,processed_transcript
ENSG00000166441,13	RPL27A	-1.31	1.73E-06	protein_coding,nonsense_mediated_decay,retained_intron,processed_transcript
ENSG00000166794,6	PPIB	-1.32	8.23E-05	protein_coding,nonsense_mediated_decay,retained_intron,processed_transcript
ENSG00000070756,17	PABPC1	-1.32	3.11E-07	protein_coding,nonsense_mediated_decay,retained_intron,processed_transcript
ENSG00000164104,12	HMGB2	-1.32	0.006564414	protein_coding,retained_intron
ENSG00000116288,13	PARK7	-1.32	0.01764519	protein_coding,processed_transcript,retained_intron
ENSG00000181163,14	NPM1	-1.32	2.97E-05	nonsense_mediated_decay,protein_coding,retained_intron
ENSG00000132341,12	RAN	-1.33	0.003396482	protein_coding,retained_intron,nonsense_mediated_decay
ENSG00000079785,16	DDX1	-1.33	0.042996291	nonsense_mediated_decay,protein_coding,retained_intron
ENSG00000237550,5	AC243919,1	-1.34	0.017167021	processed_transcript,transcribed_processed_pseudogene
ENSG00000189060,5	H1-0	-1.34	0.002350541	protein_coding
ENSG00000205581,11	HMGN1	-1.34	0.039321896	nonsense_mediated_decay,protein_coding,processed_transcript,retained_intron
ENSG00000102007,11	PLP2	-1.35	3.22E-05	protein_coding
ENSG00000170759,11	KIF5B	-1.35	0.001219677	protein_coding,processed_transcript
ENSG00000114439,19	BBX	-1.35	0.020866906	protein_coding,retained_intron,processed_transcript
ENSG00000117523,16	PRRC2C	-1.35	4.45E-05	protein_coding,processed_transcript,retained_intron
ENSG00000167526,14	RPL13	-1.36	1.47E-06	protein_coding,retained_intron,nonsense_mediated_decay
ENSG00000167522,16	ANKRD11	-1.37	0.000230304	protein_coding,nonsense_mediated_decay,retained_intron,processed_transcript
ENSG00000115268,10	RPS15	-1.38	4.70E-05	protein_coding,retained_intron
ENSG00000101160,15	CTSZ	-1.38	0.040557283	protein_coding,processed_transcript,retained_intron,nonsense_mediated_decay,non_stop_decay
ENSG00000138069,18	RAB1A	-1.38	0.030981031	nonsense_mediated_decay,protein_coding,processed_transcript
ENSG00000034510,6	TMSB10	-1.39	1.24E-09	protein_coding
ENSG00000124831,19	LRRFIP1	-1.40	0.013015855	protein_coding,retained_intron,processed_transcript

ENSG00000147649,10	MTDH	-1.41	0.000304302	protein_coding,nonsense_mediated_decay,retained_intron
ENSG00000049245,13	VAMP3	-1.41	0.029268389	retained_intron,protein_coding
ENSG00000164611,13	PTTG1	-1.42	0.012697846	protein_coding,retained_intron,processed_transcript
ENSG00000254999,4	BRK1	-1.42	0.041578324	protein_coding
ENSG00000136888,8	ATP6V1G1	-1.42	0.049722952	protein_coding,nonsense_mediated_decay,retained_intron
ENSG00000164134,13	NAA15	-1.42	0.024149002	processed_transcript,retained_intron,protein_coding
ENSG00000144674,16	GOLGA4	-1.42	0.000227183	protein_coding,processed_transcript,retained_intron
ENSG00000067334,14	DNTTIP2	-1.43	0.013015855	protein_coding,nonsense_mediated_decay,processed_transcript,retained_intron
ENSG00000063177,13	RPL18	-1.44	4.38E-07	protein_coding,nonsense_mediated_decay,retained_intron,non_stop_decay
ENSG00000145050,19	MANF	-1.44	0.002517075	retained_intron,nonsense_mediated_decay,protein_coding,processed_transcript
ENSG00000105058,12	FAM32A	-1.44	0.048875617	protein_coding,nonsense_mediated_decay
ENSG00000107957,16	SH3PXD2A	-1.44	0.000954311	protein_coding,processed_transcript
ENSG00000119900,9	OGFRL1	-1.45	0.00295647	protein_coding,processed_transcript
ENSG00000103187,8	COTL1	-1.45	0.015045659	protein_coding,processed_transcript,retained_intron
ENSG00000183255,12	PTTG1IP	-1.45	0.00064039	protein_coding,processed_transcript,retained_intron
ENSG00000115053,17	NCL	-1.46	1.60E-08	protein_coding,retained_intron,nonsense_mediated_decay
ENSG00000103342,13	GSPT1	-1.46	0.037902288	protein_coding,processed_transcript,retained_intron
ENSG00000169908,12	TM4SF1	-1.47	0.007666659	protein_coding,nonsense_mediated_decay
ENSG00000136240,10	KDELR2	-1.47	0.014121631	protein_coding,nonsense_mediated_decay,retained_intron,processed_transcript
ENSG00000106244,13	PDAP1	-1.48	0.024026242	protein_coding,nonsense_mediated_decay,processed_transcript,retained_intron
ENSG00000065000,19	AP3D1	-1.48	7.45E-05	nonsense_mediated_decay,protein_coding,retained_intron,processed_transcript
ENSG00000113810,16	SMC4	-1.48	0.003759463	retained_intron,protein_coding,nonsense_mediated_decay,processed_transcript
ENSG00000119326,15	CTNNAL1	-1.48	0.009962242	processed_transcript,protein_coding
ENSG00000116209,12	TMEM59	-1.49	0.035154432	protein_coding,processed_transcript
ENSG00000133872,14	SARAF	-1.50	0.039961939	protein_coding,retained_intron,nonsense_mediated_decay,processed_transcript
ENSG00000133226,17	SRRM1	-1.50	0.000932328	retained_intron,protein_coding,processed_transcript,nonsense_mediated_decay
ENSG00000090060,18	PAPOLA	-1.51	0.001905129	retained_intron,protein_coding,nonsense_mediated_decay,processed_transcript
ENSG00000164944,12	VIRMA	-1.52	0.019726551	nonsense_mediated_decay,protein_coding,processed_transcript,retained_intron
ENSG00000133131,15	MORC4	-1.52	0.032399766	protein_coding,retained_intron
ENSG00000163938,17	GNL3	-1.53	0.018757718	protein_coding,retained_intron,processed_transcript,nonsense_mediated_decay
ENSG00000178105,11	DDX10	-1.53	0.030981031	protein_coding,processed_transcript,retained_intron,nonsense_mediated_decay
ENSG00000124767,7	GLO1	-1.53	4.42E-05	protein_coding,processed_transcript
ENSG00000171490,13	RSL1D1	-1.53	0.049139322	protein_coding,retained_intron,nonsense_mediated_decay
ENSG00000101439,9	CST3	-1.54	0.025923477	protein_coding
ENSG00000143612,21	C1orf43	-1.55	0.000663607	protein_coding,processed_transcript,nonsense_mediated_decay
ENSG00000138772,13	ANXA3	-1.55	0.009114537	protein_coding,retained_intron
ENSG00000196141,14	SPATS2L	-1.55	0.005407294	protein_coding,processed_transcript,retained_intron
ENSG00000119335,17	SET	-1.55	6.50E-07	protein_coding,processed_transcript,retained_intron
ENSG00000117519,16	CNN3	-1.56	0.000818731	protein_coding,processed_transcript
ENSG00000244038,11	DDOST	-1.56	0.015463035	protein_coding,processed_transcript
ENSG00000166710,21	B2M	-1.57	2.96E-07	nonsense_mediated_decay,processed_transcript,retained_intron,protein_coding

ENSG00000112305,15	SMAP1	-1.57	0.028745345	protein_coding
ENSG00000164587,13	RPS14	-1.57	1.45E-08	protein_coding,nonsense_mediated_decay,retained_intron
ENSG00000198258,11	UBL5	-1.57	0.019416413	protein_coding,processed_transcript,retained_intron
ENSG00000127184,13	COX7C	-1.57	0.000587951	processed_transcript,protein_coding
ENSG00000117724,13	CENPF	-1.58	7.00E-06	protein_coding,processed_transcript
ENSG00000228474,6	OST4	-1.59	0.034970717	protein_coding
ENSG00000089289,16	IGBP1	-1.59	0.02646136	protein_coding
ENSG00000162244,12	RPL29	-1.59	6.09E-05	protein_coding,retained_intron,nonsense_mediated_decay
ENSG00000089009,16	RPL6	-1.59	1.65E-05	retained_intron,protein_coding
ENSG00000174444,15	RPL4	-1.60	1.20E-06	retained_intron,protein_coding,processed_transcript
ENSG00000221983,8	UBA52	-1.60	5.22E-06	protein_coding,retained_intron
ENSG00000230989,7	HSBP1	-1.60	0.031434828	protein_coding,nonsense_mediated_decay,retained_intron
ENSG00000170275,15	CRTAP	-1.60	2.64E-06	protein_coding,processed_transcript
ENSG00000137876,11	RSL24D1	-1.60	0.021542554	protein_coding,retained_intron,nonsense_mediated_decay,processed_transcript
ENSG00000198900,7	TOP1	-1.60	0.000447551	nonsense_mediated_decay,retained_intron,protein_coding
ENSG00000127914,19	AKAP9	-1.61	0.008340529	protein_coding,nonsense_mediated_decay,retained_intron,processed_transcript
ENSG00000167468,18	GPX4	-1.62	0.000276195	protein_coding,non_stop_decay,retained_intron
ENSG00000116754,13	SRSF11	-1.62	0.003479435	protein_coding,nonsense_mediated_decay,processed_transcript
ENSG00000123975,5	CKS2	-1.63	0.004926024	protein_coding
ENSG00000167004,13	PDIA3	-1.64	0.000250045	protein_coding,nonsense_mediated_decay,processed_transcript,retained_intron
ENSG00000142541,18	RPL13A	-1.64	1.16E-08	protein_coding,retained_intron,processed_transcript,nonsense_mediated_decay
ENSG00000143870,13	PDIA6	-1.64	1.89E-05	protein_coding,processed_transcript
ENSG00000145386,11	CCNA2	-1.65	0.023122576	protein_coding
ENSG00000164609,10	SLU7	-1.65	0.040815108	protein_coding,retained_intron
ENSG00000124177,16	CHD6	-1.65	0.001822982	protein_coding,processed_transcript
ENSG00000140319,11	SRP14	-1.65	0.017985914	protein_coding,processed_transcript,retained_intron
ENSG00000130255,13	RPL36	-1.65	1.87E-07	protein_coding,processed_transcript,retained_intron
ENSG00000126698,11	DNAJC8	-1.65	0.014748503	protein_coding,processed_transcript
ENSG00000060339,14	CCAR1	-1.66	0.034468786	protein_coding,nonsense_mediated_decay,retained_intron,processed_transcript
ENSG00000167863,12	ATP5PD	-1.66	0.006592252	protein_coding,nonsense_mediated_decay,retained_intron
ENSG00000166012,17	TAF1D	-1.66	6.45E-05	retained_intron,nonsense_mediated_decay,processed_transcript,protein_coding
ENSG00000184752,13	NDUFA12	-1.67	0.035799809	nonsense_mediated_decay,processed_transcript,protein_coding,retained_intron
ENSG00000126267,11	COX6B1	-1.68	0.033430152	protein_coding
ENSG00000162607,13	USP1	-1.68	0.041520803	protein_coding
ENSG00000115128,7	SF3B6	-1.70	0.014867455	retained_intron,protein_coding
ENSG00000129116,19	PALLD	-1.70	0.000902828	protein_coding,retained_intron
ENSG00000012660,14	ELOVL5	-1.70	0.000249346	protein_coding,processed_transcript
ENSG00000100526,20	CDKN3	-1.70	0.026201391	protein_coding,processed_transcript
ENSG00000136942,15	RPL35	-1.72	1.66E-09	protein_coding,nonsense_mediated_decay,retained_intron
ENSG00000143933,19	CALM2	-1.72	2.95E-08	processed_transcript,protein_coding,retained_intron,nonsense_mediated_decay
ENSG00000101608,13	MYL12A	-1.73	2.92E-05	protein_coding,retained_intron,processed_transcript

ENSG00000116161,18	CACYBP	-1.73	0.007169315	protein_coding,retained_intron
ENSG00000137776,17	SLTM	-1.73	0.013236617	protein_coding,nonsense_mediated_decay,processed_transcript,retained_intron
ENSG00000069275,13	NUCKS1	-1.74	1.18E-08	protein_coding,processed_transcript
ENSG00000117632,23	STMN1	-1.74	6.99E-07	protein_coding,processed_transcript
ENSG00000011426,11	ANLN	-1.75	2.07E-06	protein_coding,nonsense_mediated_decay,retained_intron,processed_transcript
ENSG00000198755,11	RPL10A	-1.75	1.90E-10	protein_coding,processed_transcript
ENSG00000135446,17	CDK4	-1.77	0.019095577	protein_coding,nonsense_mediated_decay,processed_transcript,retained_intron
ENSG00000131981,16	LGALS3	-1.77	0.003252769	protein_coding,processed_transcript,retained_intron
ENSG00000148677,7	ANKRD1	-1.77	0.007382795	protein_coding
ENSG00000134697,13	GNL2	-1.77	0.038601814	protein_coding,processed_transcript
ENSG00000101558,14	VAPA	-1.77	0.000689809	protein_coding,retained_intron,nonsense_mediated_decay,processed_transcript
ENSG00000136108,15	CKAP2	-1.78	0.012849472	retained_intron,protein_coding
ENSG00000198034,11	RPS4X	-1.78	1.02E-09	protein_coding,processed_transcript
ENSG00000143771,12	CNIH4	-1.80	0.032224356	protein_coding,processed_transcript
ENSG00000138160,7	KIF11	-1.81	0.019077638	nonsense_mediated_decay,protein_coding
ENSG00000198898,14	CAPZA2	-1.82	0.013795109	nonsense_mediated_decay,retained_intron,processed_transcript,protein_coding
ENSG00000065548,18	ZC3H15	-1.82	0.021561976	nonsense_mediated_decay,protein_coding,processed_transcript,retained_intron
ENSG00000155368,16	DBI	-1.82	0.00725165	processed_transcript,protein_coding,retained_intron
ENSG00000089220,5	PEBP1	-1.82	0.01279455	processed_transcript,protein_coding
ENSG00000129515,20	SNX6	-1.83	0.02416193	nonsense_mediated_decay,protein_coding,retained_intron
ENSG00000196591,12	HDAC2	-1.84	0.00725165	protein_coding,retained_intron
ENSG00000123240,17	OPTN	-1.85	6.50E-07	protein_coding,nonsense_mediated_decay,processed_transcript
ENSG00000109180,15	OCIAD1	-1.85	0.009998856	protein_coding,retained_intron,processed_transcript,nonsense_mediated_decay
ENSG00000115561,16	CHMP3	-1.86	0.016558364	protein_coding,processed_transcript
ENSG00000113141,18	IK	-1.86	0.013015855	protein_coding,processed_transcript,retained_intron,nonsense_mediated_decay
ENSG00000019582,16	CD74	-1.86	0.01413035	nonsense_mediated_decay,retained_intron,protein_coding
ENSG00000125844,16	RRBP1	-1.87	7.44E-07	protein_coding,retained_intron,nonsense_mediated_decay
ENSG00000164251,5	F2RL1	-1.87	0.024616757	protein_coding
ENSG00000138180,16	CEP55	-1.88	0.013709568	protein_coding,processed_transcript
ENSG00000134186,12	PRPF38B	-1.88	0.035178065	protein_coding,processed_transcript
ENSG00000182220,15	ATP6AP2	-1.89	0.039432352	protein_coding,retained_intron,processed_transcript,nonsense_mediated_decay
ENSG00000174748,22	RPL15	-1.89	2.59E-08	protein_coding,retained_intron
ENSG00000086598,11	TMED2	-1.90	2.53E-06	protein_coding,retained_intron
ENSG00000196154,12	S100A4	-1.90	4.86E-05	protein_coding,processed_transcript
ENSG00000153914,16	SREK1	-1.90	4.04E-05	nonsense_mediated_decay,retained_intron,protein_coding,processed_transcript
ENSG00000122545,20	SEPTIN7	-1.90	0.000136809	retained_intron,protein_coding,processed_transcript,nonsense_mediated_decay
ENSG00000175390,15	EIF3F	-1.90	0.013331259	nonsense_mediated_decay,retained_intron,protein_coding
ENSG00000154723,13	ATP5PF	-1.91	0.021315711	protein_coding,retained_intron
ENSG00000013374,17	NUB1	-1.91	0.015045659	protein_coding,nonsense_mediated_decay,retained_intron,processed_transcript
ENSG00000076043,11	REXO2	-1.91	0.028130386	nonsense_mediated_decay,protein_coding,retained_intron,processed_transcript
ENSG00000105193,9	RPS16	-1.91	4.09E-13	protein_coding,retained_intron

ENSG00000112306,8	RPS12	-1.92	1.01E-10	protein_coding,retained_intron
ENSG00000129250,12	KIF1C	-1.92	2.94E-10	protein_coding,retained_intron,processed_transcript
ENSG00000080824,19	HSP90AA1	-1.92	1.71E-16	protein_coding,nonsense_mediated_decay,retained_intron
ENSG00000091164,13	TXNL1	-1.92	0.049869009	protein_coding,processed_transcript,nonsense_mediated_decay
ENSG00000108298,12	RPL19	-1.92	8.02E-17	protein_coding,retained_intron,nonsense_mediated_decay
ENSG00000139726,11	DENR	-1.93	0.004877896	protein_coding,retained_intron
ENSG00000124356,16	STAMBP	-1.93	0.028745345	protein_coding,processed_transcript
ENSG00000154518,10	ATP5MC3	-1.93	0.021542554	protein_coding,retained_intron
ENSG00000125691,14	RPL23	-1.93	3.01E-14	protein_coding,retained_intron
ENSG00000111011,18	RSRC2	-1.94	0.000503094	retained_intron,protein_coding,nonsense_mediated_decay,processed_transcript
ENSG00000153179,13	RASSF3	-1.95	0.000107299	protein_coding,processed_transcript,nonsense_mediated_decay
ENSG00000145425,10	RPS3A	-1.95	0.013709568	protein_coding,nonsense_mediated_decay,retained_intron
ENSG00000111057,11	KRT18	-1.95	5.85E-07	protein_coding,retained_intron
ENSG00000185222,10	TCEAL9	-1.95	0.0014014	protein_coding
ENSG00000137154,13	RPS6	-1.96	9.07E-12	protein_coding,processed_transcript
ENSG00000164405,11	UQCRQ	-1.96	0.023528157	protein_coding,retained_intron,processed_transcript
ENSG00000143977,14	SNRPG	-1.96	0.049139322	protein_coding,processed_transcript,retained_intron
ENSG00000106028,11	SSBP1	-1.96	0.039070263	protein_coding,retained_intron,processed_transcript
ENSG00000170142,12	UBE2E1	-1.96	0.000537269	protein_coding,retained_intron,processed_transcript
ENSG00000119912,18	IDE	-1.97	0.049473203	nonsense_mediated_decay,retained_intron,protein_coding,processed_transcript
ENSG00000008282,9	SYPL1	-1.98	0.049008652	protein_coding,nonsense_mediated_decay,retained_intron
ENSG00000196704,14	AMZ2	-1.98	0.034192389	protein_coding,processed_transcript,nonsense_mediated_decay,retained_intron
ENSG00000107625,14	DDX50	-1.98	0.029268389	nonsense_mediated_decay,protein_coding,processed_transcript
ENSG00000168653,11	NDUFS5	-1.98	0.000667522	protein_coding
ENSG00000105372,8	RPS19	-1.99	1.19E-11	protein_coding,retained_intron,nonsense_mediated_decay
ENSG00000078804,13	TP53INP2	-1.99	0.005088212	protein_coding
ENSG00000198121,13	LPAR1	-1.99	0.009783146	protein_coding
ENSG00000089157,16	RPLP0	-1.99	1.62E-13	retained_intron,protein_coding,processed_transcript,nonsense_mediated_decay
ENSG00000170017,12	ALCAM	-2.00	0.002213624	protein_coding,processed_transcript,retained_intron
ENSG00000174780,17	SRP72	-2.01	1.84E-05	protein_coding,retained_intron
ENSG00000080200,10	CRYBG3	-2.02	0.031544096	protein_coding,processed_transcript
ENSG00000119185,13	ITGB1BP1	-2.02	0.029746897	retained_intron,protein_coding,processed_transcript,nonsense_mediated_decay
ENSG00000186468,13	RPS23	-2.02	1.51E-05	protein_coding,processed_transcript,retained_intron
ENSG00000148773,14	MKI67	-2.02	1.34E-08	protein_coding,processed_transcript
ENSG00000163636,11	PSMD6	-2.03	0.005624689	protein_coding,retained_intron
ENSG00000214253,9	FIS1	-2.03	0.041520803	nonsense_mediated_decay,protein_coding,processed_transcript
ENSG00000122406,14	RPL5	-2.03	1.01E-10	retained_intron,protein_coding,nonsense_mediated_decay,processed_transcript
ENSG00000198695,2	MT-ND6	-2.03	3.01E-10	protein_coding
ENSG00000198162,12	MAN1A2	-2.04	0.046809901	protein_coding,processed_transcript
ENSG00000175197,12	DDIT3	-2.04	1.73E-06	protein_coding
ENSG00000124596,17	OARD1	-2.04	0.010640278	protein_coding,nonsense_mediated_decay,retained_intron,processed_transcript

ENSG00000142676,14	RPL11	-2.06	9.10E-16	protein_coding,retained_intron,nonsense_mediated_decay
ENSG00000024526,17	DEPDC1	-2.06	0.018617337	protein_coding,nonsense_mediated_decay,retained_intron
ENSG00000111843,14	TMEM14C	-2.06	0.00372046	protein_coding,processed_transcript
ENSG00000197594,13	ENPP1	-2.06	0.017055192	nonsense_mediated_decay,protein_coding,retained_intron,processed_transcript
ENSG00000145741,16	BTF3	-2.07	2.91E-11	protein_coding,retained_intron,nonsense_mediated_decay
ENSG00000140612,14	SEC11A	-2.07	0.047538886	nonsense_mediated_decay,protein_coding,retained_intron
ENSG00000126870,16	DYNC2I1	-2.07	8.81E-05	retained_intron,nonsense_mediated_decay,protein_coding
ENSG00000021355,13	SERPINB1	-2.08	0.000625025	protein_coding,processed_transcript
ENSG00000066455,13	GOLGA5	-2.08	0.028853797	protein_coding,retained_intron
ENSG00000083845,9	RPS5	-2.09	5.54E-11	retained_intron,protein_coding
ENSG00000148516,22	ZEB1	-2.09	2.72E-05	retained_intron,processed_transcript,protein_coding,nonsense_mediated_decay
ENSG00000010278,15	CD9	-2.10	0.005098978	protein_coding,processed_transcript,retained_intron,nonsense_mediated_decay
ENSG00000148303,17	RPL7A	-2.11	2.47E-12	protein_coding,processed_transcript
ENSG00000106443,17	PHF14	-2.11	0.006241057	protein_coding,nonsense_mediated_decay,processed_transcript,retained_intron
ENSG00000145247,12	OCIAD2	-2.12	0.008129589	processed_transcript,protein_coding,nonsense_mediated_decay,retained_intron
ENSG00000168028,14	RPSA	-2.12	6.90E-08	retained_intron,protein_coding,processed_transcript
ENSG00000145555,15	MYO10	-2.13	6.10E-11	protein_coding,processed_transcript,retained_intron
ENSG00000124795,17	DEK	-2.13	6.56E-10	nonsense_mediated_decay,protein_coding,retained_intron
ENSG00000197747,9	S100A10	-2.13	1.43E-12	processed_transcript,protein_coding
ENSG00000101166,16	PRELID3B	-2.13	0.000292978	protein_coding,nonsense_mediated_decay,retained_intron
ENSG00000133112,17	TPT1	-2.13	1.66E-20	protein_coding,retained_intron,processed_transcript
ENSG00000138778,13	CENPE	-2.13	0.000145149	protein_coding,retained_intron
ENSG00000091136,15	LAMB1	-2.14	0.031544096	protein_coding,nonsense_mediated_decay,retained_intron,processed_transcript
ENSG00000144283,22	PKP4	-2.15	0.000919909	nonsense_mediated_decay,processed_transcript,protein_coding,retained_intron
ENSG00000196531,14	NACA	-2.15	1.66E-11	protein_coding,processed_transcript,nonsense_mediated_decay,retained_intron
ENSG00000124562,10	SNRPC	-2.17	0.000545423	protein_coding,processed_transcript
ENSG00000142937,12	RPS8	-2.18	4.19E-16	protein_coding,processed_transcript
ENSG00000162645,13	GBP2	-2.18	0.016489518	protein_coding,nonsense_mediated_decay,retained_intron,processed_transcript
ENSG00000237973,1	MTCO1P12	-2.19	1.82E-06	unprocessed_pseudogene
ENSG00000048544,6	MRPS10	-2.21	0.000145444	protein_coding
ENSG00000122786,20	CALD1	-2.22	3.93E-07	protein_coding,nonsense_mediated_decay,retained_intron,processed_transcript
ENSG00000166598,16	HSP90B1	-2.22	2.57E-23	protein_coding,nonsense_mediated_decay,retained_intron
ENSG00000092010,15	PSME1	-2.23	0.002030256	protein_coding,processed_transcript,retained_intron,nonsense_mediated_decay
ENSG00000152558,15	TMEM123	-2.23	0.01089807	protein_coding,retained_intron,processed_transcript
ENSG00000109321,11	AREG	-2.23	0.007434889	retained_intron,protein_coding
ENSG00000187109,15	NAP1L1	-2.23	2.83E-14	protein_coding,nonsense_mediated_decay,retained_intron
ENSG00000141030,13	COPS3	-2.23	0.018340891	protein_coding,retained_intron,nonsense_mediated_decay
ENSG00000142534,7	RPS11	-2.24	1.75E-15	retained_intron,protein_coding,nonsense_mediated_decay
ENSG00000151725,12	CENPU	-2.25	0.040837852	protein_coding,nonsense_mediated_decay,processed_transcript,retained_intron
ENSG00000198585,12	NUDT16	-2.25	0.009969445	protein_coding
ENSG00000140350,15	ANP32A	-2.25	0.010025153	protein_coding,nonsense_mediated_decay,processed_transcript,retained_intron

ENSG00000005022,6	SLC25A5	-2.26	2.77E-05	protein_coding,processed_transcript
ENSG00000121858,11	TNFSF10	-2.26	0.046708511	protein_coding,nonsense_mediated_decay,retained_intron
ENSG00000143947,15	RPS27A	-2.27	1.24E-12	protein_coding,retained_intron
ENSG00000143401,15	ANP32E	-2.27	9.97E-06	protein_coding
ENSG00000122257,20	RBBP6	-2.29	0.013807783	protein_coding,retained_intron,processed_transcript
ENSG00000108107,15	RPL28	-2.30	8.09E-15	protein_coding,retained_intron
ENSG00000229117,9	RPL41	-2.30	2.78E-07	protein_coding,processed_transcript
ENSG00000131871,15	SELENOS	-2.30	0.013500016	protein_coding,retained_intron
ENSG00000114942,14	EEF1B2	-2.30	6.63E-07	nonsense_mediated_decay,retained_intron,protein_coding
ENSG00000230124,8	ACBD6	-2.31	0.041276712	protein_coding,nonsense_mediated_decay,processed_transcript
ENSG00000233276,8	GPX1	-2.31	0.001907951	protein_coding
ENSG00000104131,13	EIF3J	-2.32	0.010053531	protein_coding,retained_intron,nonsense_mediated_decay
ENSG00000006634,8	DBF4	-2.32	0.029451904	nonsense_mediated_decay,retained_intron,protein_coding
ENSG00000164022,17	AIMP1	-2.33	0.015497396	protein_coding,nonsense_mediated_decay,processed_transcript
ENSG00000137210,14	TMEM14B	-2.33	0.009648673	protein_coding,nonsense_mediated_decay,processed_transcript
ENSG00000115234,11	SNX17	-2.34	0.016643908	retained_intron,nonsense_mediated_decay,protein_coding
ENSG00000137500,9	CCDC90B	-2.34	0.004302359	retained_intron,nonsense_mediated_decay,protein_coding,processed_transcript
ENSG00000125977,7	EIF2S2	-2.34	6.78E-06	protein_coding
ENSG00000180817,12	PPA1	-2.34	0.002953529	protein_coding,retained_intron,nonsense_mediated_decay,processed_transcript
ENSG00000165672,7	PRDX3	-2.36	0.000304302	retained_intron,protein_coding
ENSG00000138182,15	KIF20B	-2.36	0.000564653	protein_coding,processed_transcript
ENSG00000163001,12	CFAP36	-2.37	0.039961939	protein_coding,processed_transcript,retained_intron
ENSG00000165169,11	DYNLT3	-2.37	0.017080755	protein_coding
ENSG00000150687,12	PRSS23	-2.37	0.0004605	nonsense_mediated_decay,protein_coding,processed_transcript,retained_intron
ENSG00000144224,17	UBXN4	-2.38	7.91E-05	protein_coding,nonsense_mediated_decay,processed_transcript,retained_intron
ENSG00000131469,15	RPL27	-2.39	8.40E-13	protein_coding,retained_intron,nonsense_mediated_decay
ENSG00000162368,13	CMPK1	-2.40	0.000203824	protein_coding,nonsense_mediated_decay,retained_intron
ENSG00000126653,18	NSRP1	-2.40	2.47E-05	protein_coding,nonsense_mediated_decay,processed_transcript,retained_intron
ENSG00000171863,15	RPS7	-2.40	2.65E-10	protein_coding,retained_intron,processed_transcript
ENSG00000140990,15	NDUFB10	-2.40	0.01527698	protein_coding,retained_intron
ENSG00000125743,11	SNRPD2	-2.40	1.41E-07	protein_coding,processed_transcript
ENSG00000014824,14	SLC30A9	-2.40	0.029439739	nonsense_mediated_decay,protein_coding,retained_intron
ENSG00000198804,2	MT-CO1	-2.40	9.83E-19	protein_coding
ENSG00000197756,10	RPL37A	-2.41	1.32E-18	protein_coding,retained_intron,nonsense_mediated_decay,processed_transcript
ENSG00000008952,17	SEC62	-2.41	7.82E-05	retained_intron,processed_transcript,nonsense_mediated_decay,protein_coding
ENSG00000123131,13	PRDX4	-2.41	0.001083857	protein_coding,processed_transcript
ENSG00000113387,12	SUB1	-2.41	0.000195645	protein_coding,processed_transcript,retained_intron,nonsense_mediated_decay
ENSG00000182534,13	MXRA7	-2.42	0.032717398	protein_coding
ENSG00000153774,9	CFDP1	-2.43	0.008085672	protein_coding,retained_intron,processed_transcript,nonsense_mediated_decay
ENSG00000173230,15	GOLGB1	-2.44	4.98E-06	protein_coding,nonsense_mediated_decay,processed_transcript
ENSG00000132432,14	SEC61G	-2.44	7.07E-06	protein_coding,retained_intron

ENSG00000231500,7	RPS18	-2.45	4.97E-25	protein_coding,retained_intron,processed_transcript
ENSG00000134419,15	RPS15A	-2.45	0.002064113	nonsense_mediated_decay,protein_coding,processed_transcript
ENSG00000114391,13	RPL24	-2.45	1.87E-12	protein_coding,retained_intron
ENSG00000136156,15	ITM2B	-2.46	0.017167021	nonsense_mediated_decay,protein_coding,processed_transcript
ENSG00000125868,16	DSTN	-2.46	1.43E-12	protein_coding,nonsense_mediated_decay
ENSG00000028310,18	BRD9	-2.47	5.37E-07	processed_transcript,nonsense_mediated_decay,retained_intron,protein_coding
ENSG00000117614,10	SYF2	-2.47	0.001219677	protein_coding,processed_transcript
ENSG00000090054,15	SPTLC1	-2.48	0.038071505	nonsense_mediated_decay,protein_coding,processed_transcript
ENSG00000131174,7	COX7B	-2.48	0.000595448	protein_coding
ENSG00000189043,10	NDUFA4	-2.49	0.006195557	retained_intron,protein_coding,processed_transcript
ENSG00000172809,13	RPL38	-2.51	5.28E-16	protein_coding,retained_intron
ENSG00000129197,15	RPAIN	-2.51	0.04449089	protein_coding,retained_intron,nonsense_mediated_decay
ENSG00000139921,13	TMX1	-2.51	0.019187057	protein_coding,nonsense_mediated_decay,retained_intron
ENSG00000055044,11	NOP58	-2.52	0.000447551	nonsense_mediated_decay,protein_coding,retained_intron,processed_transcript
ENSG00000113328,19	CCNG1	-2.53	0.001733866	protein_coding,processed_transcript,retained_intron
ENSG00000105974,13	CAV1	-2.53	1.49E-11	protein_coding,nonsense_mediated_decay,retained_intron
ENSG00000225921,7	NOL7	-2.53	0.011900088	protein_coding,processed_transcript
ENSG00000122565,19	CBX3	-2.53	7.00E-06	protein_coding,retained_intron,processed_transcript
ENSG00000106541,12	AGR2	-2.54	1.25E-08	protein_coding,retained_intron,processed_transcript
ENSG00000198707,17	CEP290	-2.54	0.049390189	protein_coding,retained_intron,nonsense_mediated_decay,processed_transcript
ENSG00000065978,19	YBX1	-2.54	3.33E-14	protein_coding,processed_transcript
ENSG00000156411,10	ATP5MPL	-2.55	0.011076881	protein_coding,retained_intron,processed_transcript
ENSG00000173674,11	EIF1AX	-2.58	0.017411945	protein_coding
ENSG00000198242,14	RPL23A	-2.62	0.000635668	protein_coding,retained_intron
ENSG00000165629,20	ATP5F1C	-2.62	0.009777018	processed_transcript,protein_coding,retained_intron
ENSG00000128609,16	NDUFA5	-2.65	0.032721092	retained_intron,protein_coding,nonsense_mediated_decay,processed_transcript
ENSG00000133835,17	HSD17B4	-2.65	0.02761815	protein_coding,processed_transcript,nonsense_mediated_decay,retained_intron
ENSG00000008988,11	RPS20	-2.67	1.28E-16	protein_coding,nonsense_mediated_decay,processed_transcript,retained_intron
ENSG00000171530,15	TBCA	-2.68	1.38E-05	protein_coding,retained_intron,processed_transcript
ENSG00000165502,7	RPL36AL	-2.69	1.06E-09	protein_coding
ENSG00000196683,11	TOMM7	-2.69	8.67E-05	protein_coding,retained_intron,processed_transcript
ENSG00000110700,7	RPS13	-2.70	6.46E-17	protein_coding,retained_intron,processed_transcript
ENSG00000171858,18	RPS21	-2.70	4.60E-14	protein_coding,processed_transcript
ENSG00000138430,16	OLA1	-2.70	4.24E-05	processed_transcript,retained_intron,protein_coding
ENSG00000196504,19	PRPF40A	-2.70	7.22E-06	protein_coding,retained_intron,nonsense_mediated_decay,processed_transcript
ENSG00000117751,18	PPP1R8	-2.71	0.046806393	protein_coding,processed_transcript
ENSG00000119707,14	RBM25	-2.71	3.46E-12	retained_intron,protein_coding,nonsense_mediated_decay,processed_transcript
ENSG00000138326,21	RPS24	-2.72	4.10E-18	protein_coding,retained_intron,nonsense_mediated_decay,processed_transcript
ENSG00000163634,12	THOC7	-2.74	0.012886888	protein_coding,nonsense_mediated_decay,processed_transcript,retained_intron
ENSG00000106355,10	LSM5	-2.75	0.008643832	protein_coding,nonsense_mediated_decay,retained_intron
ENSG00000153310,19	CYRIB	-2.75	0.011564278	protein_coding,retained_intron,processed_transcript

ENSG00000147604,14	RPL7	-2.77	0.020249795	protein_coding,retained_intron,processed_transcript
ENSG00000197958,13	RPL12	-2.78	2.75E-25	protein_coding,processed_transcript
ENSG00000156171,15	DRAM2	-2.79	0.03088528	processed_transcript,protein_coding,nonsense_mediated_decay
ENSG00000232112,3	TMA7	-2.79	2.25E-05	protein_coding,retained_intron
ENSG00000109790,17	KLHL5	-2.79	0.000178178	protein_coding,nonsense_mediated_decay
ENSG00000265354,4	TIMM23	-2.80	0.02419363	protein_coding
ENSG00000153132,13	CLGN	-2.81	0.028397389	protein_coding
ENSG00000204370,13	SDHD	-2.81	0.029268389	nonsense_mediated_decay,protein_coding
ENSG00000138433,16	CIR1	-2.81	0.000151322	protein_coding,retained_intron
ENSG00000091986,16	CCDC80	-2.82	0.0064376	protein_coding,processed_transcript
ENSG00000263740,2	RN7SL4P	-2.82	0.008482433	misc_RNA
ENSG00000111142,14	METAP2	-2.83	2.81E-11	protein_coding,nonsense_mediated_decay,retained_intron
ENSG00000153130,18	SCOC	-2.84	0.012684003	protein_coding
ENSG00000188846,14	RPL14	-2.85	3.52E-17	protein_coding,retained_intron,nonsense_mediated_decay,processed_transcript
ENSG00000109929,10	SC5D	-2.86	0.006640538	retained_intron,protein_coding,processed_transcript
ENSG00000213741,11	RPS29	-2.86	1.97E-11	protein_coding,retained_intron,processed_transcript
ENSG00000173905,9	GOLIM4	-2.87	0.040950066	protein_coding,retained_intron
ENSG00000166734,20	GOLM2	-2.87	0.026384199	protein_coding,nonsense_mediated_decay,processed_transcript
ENSG00000169288,18	MRPL1	-2.88	0.043614617	protein_coding,processed_transcript
ENSG00000127920,6	GNG11	-2.89	0.029268389	protein_coding
ENSG00000197579,8	TOPORS	-2.90	0.041578324	protein_coding
ENSG00000173660,12	UQCRH	-2.91	0.000376947	protein_coding,nonsense_mediated_decay,retained_intron
ENSG00000102189,17	EEA1	-2.91	0.005088212	protein_coding,nonsense_mediated_decay,processed_transcript
ENSG00000227234,2	SPANXB1	-2.91	8.82E-05	protein_coding
ENSG00000116191,17	RALGPS2	-2.91	0.043608326	protein_coding,processed_transcript,retained_intron
ENSG00000155115,7	GTF3C6	-2.92	0.03695327	protein_coding,processed_transcript
ENSG00000087502,18	ERGIC2	-2.93	0.031746482	retained_intron,nonsense_mediated_decay,protein_coding
ENSG00000168298,7	H1-4	-2.94	2.66E-17	protein_coding
ENSG00000138398,17	PPIG	-2.94	1.84E-05	retained_intron,protein_coding,nonsense_mediated_decay,processed_transcript
ENSG00000156482,11	RPL30	-2.95	9.10E-19	retained_intron,protein_coding,nonsense_mediated_decay,processed_transcript
ENSG00000151461,20	UPF2	-2.96	2.30E-05	protein_coding,processed_transcript
ENSG00000081154,12	PCNP	-2.96	6.99E-07	protein_coding,nonsense_mediated_decay,processed_transcript,retained_intron
ENSG00000025796,14	SEC63	-2.97	7.15E-05	processed_transcript,protein_coding,retained_intron,nonsense_mediated_decay
ENSG00000198888,2	MT-ND1	-2.98	3.01E-29	protein_coding
ENSG00000089048,15	ESF1	-2.98	5.44E-06	protein_coding
ENSG00000071082,11	RPL31	-2.99	1.75E-21	protein_coding,nonsense_mediated_decay
ENSG00000211459,2	MT-RNR1	-3.00	1.17E-18	Mt_rRNA
ENSG00000163029,16	SMC6	-3.01	0.016318821	protein_coding,nonsense_mediated_decay,processed_transcript,retained_intron
ENSG00000173915,16	ATP5MD	-3.01	7.75E-06	protein_coding
ENSG00000212907,2	MT-ND4L	-3.01	3.07E-38	protein_coding
ENSG00000111639,8	MRPL51	-3.03	0.000124718	protein_coding

ENSG00000112110,10	MRPL18	-3.04	0.021269618	processed_transcript,protein_coding
ENSG00000138385,16	SSB	-3.05	3.46E-05	retained_intron,protein_coding,nonsense_mediated_decay
ENSG00000126777,18	KTN1	-3.06	3.60E-07	retained_intron,protein_coding,nonsense_mediated_decay
ENSG00000183520,12	UTP11	-3.06	0.023380239	processed_transcript,protein_coding
ENSG00000144713,13	RPL32	-3.07	8.28E-27	protein_coding,retained_intron
ENSG00000145592,14	RPL37	-3.08	7.20E-28	protein_coding,processed_transcript
ENSG00000100575,14	TIMM9	-3.09	0.004148745	protein_coding,processed_transcript
ENSG00000113583,8	C5orf15	-3.11	0.015494227	processed_transcript,protein_coding
ENSG00000106399,11	RPA3	-3.11	0.041017178	protein_coding,retained_intron
ENSG00000155959,12	VBP1	-3.13	0.003005974	protein_coding,retained_intron
ENSG00000167283,8	ATP5MG	-3.13	0.047476711	protein_coding,nonsense_mediated_decay,processed_transcript,retained_intron
ENSG00000141429,13	GALNT1	-3.14	0.002409599	protein_coding,nonsense_mediated_decay,processed_transcript
ENSG00000281344,1	HELLPAR	-3.14	0.002486394	lncRNA
ENSG00000198840,2	MT-ND3	-3.15	4.86E-44	protein_coding
ENSG00000169020,10	ATP5ME	-3.15	0.002409599	processed_transcript,protein_coding,retained_intron
ENSG00000198938,2	MT-CO3	-3.16	4.84E-11	protein_coding
ENSG00000122862,5	SRGN	-3.16	0.045526038	protein_coding,processed_transcript
ENSG00000091622,16	PITPNM3	-3.16	8.44E-05	retained_intron,protein_coding,processed_transcript
ENSG00000133142,18	TCEAL4	-3.17	2.99E-05	protein_coding,retained_intron
ENSG00000143228,13	NUF2	-3.17	0.027796711	protein_coding,processed_transcript,nonsense_mediated_decay,retained_intron
ENSG00000166130,15	IKBIP	-3.17	0.004635891	protein_coding
ENSG00000129680,16	MAP7D3	-3.18	0.005044187	protein_coding,processed_transcript
ENSG00000150316,12	CWC15	-3.20	0.000586727	protein_coding,retained_intron
ENSG00000187514,17	PTMA	-3.20	8.40E-21	protein_coding,retained_intron,nonsense_mediated_decay,processed_transcript
ENSG00000123200,17	ZC3H13	-3.21	0.001822982	protein_coding,processed_transcript,retained_intron
ENSG00000100528,12	CNIH1	-3.22	8.67E-05	protein_coding,nonsense_mediated_decay
ENSG00000101132,10	PFDN4	-3.24	0.000689809	protein_coding,nonsense_mediated_decay,processed_transcript
ENSG00000105185,12	PDCD5	-3.24	0.015041589	protein_coding,nonsense_mediated_decay,retained_intron
ENSG00000198826,11	ARHGAP11A	-3.26	0.000203824	protein_coding,processed_transcript,retained_intron
ENSG00000166181,13	API5	-3.27	0.002869989	protein_coding,retained_intron,processed_transcript
ENSG00000198856,13	OSTC	-3.27	2.43E-05	protein_coding,processed_transcript
ENSG00000156467,10	UQCRB	-3.28	5.07E-08	protein_coding,nonsense_mediated_decay,retained_intron
ENSG00000164117,14	FBXO8	-3.30	0.038508508	protein_coding,nonsense_mediated_decay
ENSG00000109475,17	RPL34	-3.30	4.63E-16	protein_coding,retained_intron
ENSG00000113811,11	SELENOK	-3.30	0.008927682	protein_coding,nonsense_mediated_decay,retained_intron,processed_transcript
ENSG00000164172,20	MOCS2	-3.30	0.028102789	protein_coding,retained_intron
ENSG00000124098,10	FAM210B	-3.31	0.028011812	protein_coding
ENSG00000125351,13	UPF3B	-3.32	0.003947912	protein_coding,retained_intron
ENSG00000124172,10	ATP5F1E	-3.33	8.74E-13	protein_coding
ENSG00000118181,11	RPS25	-3.34	2.39E-27	nonsense_mediated_decay,protein_coding,retained_intron,processed_transcript
ENSG00000125870,11	SNRPB2	-3.34	5.20E-05	protein_coding,processed_transcript

ENSG00000198786,2	MT-ND5	-3.35	1.97E-34	protein_coding
ENSG00000174720,16	LARP7	-3.36	3.70E-05	protein_coding,nonsense_mediated_decay,processed_transcript,retained_intron
ENSG00000119655,11	NPC2	-3.37	0.000145514	protein_coding,nonsense_mediated_decay
ENSG00000159335,18	PTMS	-3.37	9.30E-11	protein_coding,processed_transcript
ENSG00000198727,2	MT-CYB	-3.38	4.72E-12	protein_coding
ENSG00000120860,11	WASHC3	-3.39	0.022006606	nonsense_mediated_decay,protein_coding,retained_intron,processed_transcript
ENSG00000163069,13	SGCB	-3.42	0.026021735	protein_coding,nonsense_mediated_decay
ENSG00000169249,13	ZRSR2	-3.42	0.012164054	protein_coding,processed_transcript
ENSG00000143742,14	SRP9	-3.43	0.002400143	protein_coding,nonsense_mediated_decay,retained_intron
ENSG00000182899,17	RPL35A	-3.45	2.16E-24	protein_coding,processed_transcript,nonsense_mediated_decay,retained_intron
ENSG00000152700,14	SAR1B	-3.46	0.014748503	nonsense_mediated_decay,protein_coding,processed_transcript,retained_intron
ENSG00000101052,13	IFT52	-3.48	0.009162113	protein_coding,processed_transcript
ENSG00000170373,9	CST1	-3.49	0.006241057	protein_coding
ENSG00000159128,15	IFNGR2	-3.53	0.009998856	protein_coding,nonsense_mediated_decay
ENSG00000172172,8	MRPL13	-3.53	0.044761906	nonsense_mediated_decay,protein_coding,retained_intron
ENSG00000248527,1	MTATP6P1	-3.54	2.11E-33	unprocessed_pseudogene
ENSG00000137831,15	UACA	-3.55	8.35E-19	protein_coding,retained_intron,processed_transcript
ENSG00000184220,12	CMSS1	-3.55	0.001530455	protein_coding,processed_transcript,nonsense_mediated_decay,retained_intron
ENSG00000100442,11	FKBP3	-3.56	0.000919909	protein_coding,nonsense_mediated_decay,retained_intron
ENSG00000078140,14	UBE2K	-3.57	0.001045119	protein_coding,processed_transcript,nonsense_mediated_decay
ENSG00000164332,8	UBLCP1	-3.60	0.012025803	retained_intron,protein_coding
ENSG00000158417,11	EIF5B	-3.61	1.45E-18	retained_intron,protein_coding
ENSG00000116117,18	PARD3B	-3.66	0.04512733	protein_coding,nonsense_mediated_decay,processed_transcript
ENSG00000167779,9	IGFBP6	-3.67	0.03815243	protein_coding,nonsense_mediated_decay
ENSG00000166557,14	TMED3	-3.69	0.046093348	protein_coding,nonsense_mediated_decay,processed_transcript
ENSG00000134970,14	TMED7	-3.69	0.022905962	protein_coding,processed_transcript
ENSG00000248333,9	CDK11B	-3.72	0.005671665	protein_coding,nonsense_mediated_decay,processed_transcript
ENSG00000210082,2	MT-RNR2	-3.76	4.06E-22	Mt_rRNA
ENSG00000188243,13	COMMD6	-3.80	0.00601616	protein_coding,retained_intron,processed_transcript,nonsense_mediated_decay
ENSG00000225383,8	SFTA1P	-3.81	0.039879505	lncRNA
ENSG00000198712,1	MT-CO2	-3.81	8.09E-15	protein_coding
ENSG00000122034,17	GTF3A	-3.85	4.45E-05	protein_coding,nonsense_mediated_decay,processed_transcript,retained_intron
ENSG00000170860,4	LSM3	-3.86	0.00014177	protein_coding
ENSG00000108848,16	LUC7L3	-3.86	1.29E-14	processed_transcript,protein_coding,nonsense_mediated_decay,retained_intron
ENSG00000126524,10	SBDS	-3.87	2.50E-05	protein_coding,nonsense_mediated_decay,retained_intron
ENSG00000111832,13	RWDD1	-3.88	0.000296445	protein_coding,processed_transcript
ENSG00000198886,2	MT-ND4	-3.90	1.67E-44	protein_coding
ENSG00000161970,15	RPL26	-3.97	6.01E-07	protein_coding,retained_intron,nonsense_mediated_decay,processed_transcript
ENSG00000112144,16	CILK1	-4.06	0.012099596	protein_coding
ENSG00000165632,8	TAF3	-4.09	0.000235896	protein_coding
ENSG00000105821,15	DNAJC2	-4.15	0.000623022	retained_intron,protein_coding,nonsense_mediated_decay

ENSG00000173848,19	NET1	-4.20	3.99E-33	protein_coding,processed_transcript
ENSG00000143162,9	CREG1	-4.22	0.004330704	protein_coding
ENSG00000136104,21	RNASEH2B	-4.27	0.048875617	nonsense_mediated_decay,protein_coding,retained_intron,processed_transcript
ENSG00000145220,14	LYAR	-4.32	0.00044893	protein_coding,retained_intron
ENSG00000133773,12	CCDC59	-4.32	0.000664601	protein_coding,processed_transcript,retained_intron
ENSG00000198763,3	MT-ND2	-4.33	4.73E-64	protein_coding
ENSG00000155657,28	TTN	-4.39	0.04569638	protein_coding,retained_intron
ENSG00000103061,13	SLC7A6OS	-4.42	0.037714591	nonsense_mediated_decay,protein_coding,retained_intron
ENSG00000119328,12	ABITRAM	-4.45	0.03628205	protein_coding,processed_transcript
ENSG00000138175,9	ARL3	-4.46	0.031970718	protein_coding
ENSG00000130032,17	PRRG3	-4.49	8.98E-05	protein_coding
ENSG00000173207,13	CKS1B	-4.50	0.035273285	protein_coding,processed_transcript
ENSG00000198899,2	MT-ATP6	-4.50	1.75E-11	protein_coding
ENSG00000136542,9	GALNT5	-4.54	0.036910788	protein_coding,processed_transcript
ENSG00000163453,11	IGFBP7	-4.54	1.78E-06	protein_coding,processed_transcript
ENSG00000147669,11	POLR2K	-4.55	0.029746897	protein_coding,processed_transcript
ENSG00000109881,17	CCDC34	-4.58	0.029451904	protein_coding,processed_transcript
ENSG00000114446,5	IFT57	-4.63	0.026844542	protein_coding,processed_transcript,nonsense_mediated_decay,retained_intron
ENSG00000198189,11	HSD17B11	-4.63	0.000873303	protein_coding,processed_transcript,retained_intron
ENSG00000091317,8	CMTM6	-4.68	0.001727904	retained_intron,protein_coding
ENSG00000070081,17	NUCB2	-4.72	1.84E-07	protein_coding,nonsense_mediated_decay,retained_intron,processed_transcript
ENSG00000136938,9	ANP32B	-4.72	4.16E-50	processed_transcript,protein_coding
ENSG00000100612,14	DHRS7	-4.74	0.024341232	protein_coding,processed_transcript,retained_intron
ENSG00000167862,10	MRPL58	-4.75	0.017167021	protein_coding,nonsense_mediated_decay,retained_intron
ENSG00000121022,14	COPS5	-4.85	0.013526169	nonsense_mediated_decay,protein_coding,processed_transcript,retained_intron
ENSG00000166562,9	SEC11C	-4.87	0.012849472	protein_coding,nonsense_mediated_decay,retained_intron,processed_transcript
ENSG00000225630,1	MTND2P28	-5.00	3.33E-21	unprocessed_pseudogene
ENSG00000099337,5	KCNK6	-5.06	0.048875617	protein_coding,processed_transcript
ENSG00000119397,18	CNTRL	-5.06	0.008144545	processed_transcript,protein_coding,retained_intron
ENSG00000101441,5	CST4	-5.10	0.045070655	protein_coding
ENSG00000245910,8	SNHG6	-5.13	0.000136809	lncRNA,retained_intron
ENSG00000072571,20	HMMR	-5.13	0.049165272	protein_coding,retained_intron
ENSG00000266472,6	MRPS21	-5.15	0.0388775	protein_coding
ENSG00000172775,17	PSME3IP1	-5.16	0.007129368	processed_transcript,protein_coding,nonsense_mediated_decay
ENSG00000161671,17	EMC10	-5.17	0.045790614	nonsense_mediated_decay,protein_coding,retained_intron
ENSG00000181143,15	MUC16	-5.18	0.041017178	protein_coding,nonsense_mediated_decay,processed_transcript
ENSG00000149218,5	ENDOD1	-5.20	0.045156499	protein_coding
ENSG00000168078,10	PBK	-5.21	0.006357863	protein_coding,nonsense_mediated_decay
ENSG00000145604,17	SKP2	-5.22	0.032717398	nonsense_mediated_decay,protein_coding,retained_intron,processed_transcript
ENSG00000109861,17	CTSC	-5.22	0.040972507	nonsense_mediated_decay,protein_coding,retained_intron,processed_transcript
ENSG00000237190,4	CDKN2AIPNL	-5.24	0.030411064	protein_coding

ENSG00000138036,18	DYNC2LI1	-5.25	0.029268389	protein_coding,nonsense_mediated_decay,retained_intron,processed_transcript
ENSG00000131171,13	SH3BGRL	-5.26	0.041649089	processed_transcript,protein_coding
ENSG00000166503,9	HDGFL3	-5.26	0.03539555	protein_coding,nonsense_mediated_decay,processed_transcript,retained_intron
ENSG00000127125,9	PPCS	-5.27	0.029268389	protein_coding,processed_transcript
ENSG00000210195,2	MT-TT	-5.28	0.028795017	Mt_tRNA
ENSG00000164346,10	NSA2	-5.29	6.82E-07	protein_coding,retained_intron,processed_transcript
ENSG00000172339,10	ALG14	-5.30	0.029439739	processed_transcript,protein_coding
ENSG00000185608,9	MRPL40	-5.31	0.026484003	processed_transcript,protein_coding
ENSG00000176623,12	RMDN1	-5.31	0.028041026	protein_coding,retained_intron,nonsense_mediated_decay,processed_transcript
ENSG00000198157,11	HMGN5	-5.37	0.03083553	protein_coding,processed_transcript
ENSG00000165669,14	FAM204A	-5.41	0.004045619	retained_intron,protein_coding,processed_transcript,nonsense_mediated_decay
ENSG00000152240,13	HAUS1	-5.42	0.022914346	protein_coding,nonsense_mediated_decay,retained_intron,processed_transcript
ENSG00000132664,12	POLR3F	-5.43	0.019915215	processed_transcript,protein_coding
ENSG00000185862,7	EVI2B	-5.44	0.025415459	protein_coding
ENSG00000285219,2	HULC	-5.44	0.018863659	lncRNA
ENSG00000064115,11	TM7SF3	-5.45	0.020318271	processed_transcript,protein_coding,nonsense_mediated_decay,retained_intron
ENSG00000164114,19	MAP9	-5.45	0.017683305	nonsense_mediated_decay,protein_coding,retained_intron
ENSG00000115993,13	TRAK2	-5.46	8.50E-19	protein_coding,retained_intron,processed_transcript
ENSG00000085231,14	AK6	-5.47	0.020105456	protein_coding
ENSG00000111790,14	FGFR1OP2	-5.47	0.023842073	protein_coding,retained_intron
ENSG00000171135,15	JAGN1	-5.49	0.024121623	protein_coding
ENSG00000115514,12	TXNDC9	-5.50	0.016874076	protein_coding,nonsense_mediated_decay,processed_transcript,retained_intron
ENSG00000070785,17	EIF2B3	-5.51	0.017596693	nonsense_mediated_decay,processed_transcript,protein_coding
ENSG00000210107,1	MT-TQ	-5.52	0.015887926	Mt_tRNA
ENSG00000005059,16	MCUB	-5.60	0.013845962	processed_transcript,protein_coding,retained_intron
ENSG00000140307,11	GTF2A2	-5.63	0.013015855	protein_coding,processed_transcript,retained_intron
ENSG00000107890,17	ANKRD26	-5.67	0.01087643	protein_coding,nonsense_mediated_decay,processed_transcript
ENSG00000155868,8	MED7	-5.69	0.011270732	protein_coding
ENSG00000269028,3	MTRNR2L12	-5.71	0.001476164	protein_coding
ENSG00000196151,11	WDSUB1	-5.71	0.013084692	protein_coding
ENSG00000184208,12	C22orf46	-5.74	6.88E-06	processed_transcript,transcribed_unitary_pseudogene
ENSG00000146416,19	AIG1	-5.83	0.00742472	protein_coding,retained_intron
ENSG00000197249,14	SERPINA1	-5.85	0.006679851	protein_coding,processed_transcript,retained_intron,nonsense_mediated_decay
ENSG00000163170,12	BOLA3	-5.85	0.009998856	processed_transcript,protein_coding,retained_intron
ENSG00000026297,16	RNASET2	-5.85	0.007543903	protein_coding,nonsense_mediated_decay,processed_transcript,retained_intron
ENSG00000187118,14	CMC1	-5.90	0.005595636	protein_coding, nonsense_mediated_decay,retained_intron,processed_transcript
ENSG00000101856,10	PGRMC1	-6.48	0.001172357	protein_coding
ENSG00000166164,16	BRD7	-6.51	0.000754869	processed_transcript,retained_intron,protein_coding
ENSG00000134597,16	RBMX2	-6.64	0.000689809	protein_coding,processed_transcript
ENSG00000179630,11	LACC1	-6.64	0.000656563	protein_coding
ENSG00000228253,1	MT-ATP8	-6.64	3.99E-33	protein_coding

ENSG00000210049,1	MT-TF	-7.79	9.09E-06	Mt_tRNA
ENSG00000143545,10	RAB13	-8.17	1.26E-07	protein_coding,processed_transcript

Results are shown as fold changes (FC). The *p*-values come from the comparison using EV as reference. DEGs (differential expressed genes), EV (extracellular vesicles collected from MDA-MB-231 cultured in negative media), EGCG (extracellular vesicles collected from EGCG-treated MDA-MB-231) and EGCG (epigallocatechin-3-gallate).

Supplementary Table S4.2

Supplementary Table S4. 2. List of the shared DEGs (553 genes) identified within the h-ADMSC treated with EV_HE vs EV_NE, with a p-value < 0.05.

Symbol	Gene Name	log2FC	padj	Cluster	Hyp_S1	Hyp_S2	Hyp_S3	Norm_S4	Norm_S5	Norm_S6
AK2	adenylate kinase 2	-3.78	0.0398	Cluster 1	-0.4602	-0.3450	-0.6483	0.2001	0.3776	0.8758
FKBP4	FKBP prolyl isomerase 4	-7.02	0.0170	Cluster 1	-0.5692	-0.5995	-0.5762	-0.4570	2.3467	-0.1448
RBM6	RNA binding motif protein 6	-4.74	0.0248	Cluster 1	-0.6059	-0.4721	-0.4551	0.5736	0.7265	0.2330
AP2B1	adaptor related protein complex 2 subunit beta 1	-5.55	0.0140	Cluster 1	-0.6144	-0.6413	-0.6207	0.4315	0.9934	0.4514
PAFAH1B1	platelet activating factor acetylhydrolase 1b regulatory subunit 1	-4.23	0.0340	Cluster 1	-0.6159	-0.3874	-0.6220	0.7110	0.6072	0.3072
BLTP2	bridge-like lipid transfer protein family member 2	-4.52	0.0462	Cluster 1	-0.4824	-0.5050	-0.4876	0.3142	0.4830	0.6779
SPAG9	sperm associated antigen 9	-5.53	0.0036	Cluster 1	-0.5761	-0.7596	-0.8109	1.2822	0.7191	0.1453
ST3GAL1	ST3 beta-galactoside alpha-2,3-sialyltransferase 1	-5.14	0.0460	Cluster 1	-0.4793	-0.5046	-0.4852	1.3334	0.0446	0.0911
STEEP1	STING1 ER exit protein 1	3.80	0.0439	Cluster 2	-0.5280	1.1706	0.6124	-0.2571	-0.7366	-0.2613
RNF10	ring finger protein 10	-5.14	0.0255	Cluster 1	-0.5532	-0.5786	-0.5591	0.2605	0.4828	0.9476
UBR2	ubiquitin protein ligase E3 component n-recognin 2	-5.99	0.0063	Cluster 1	-0.7439	-0.6561	-0.6343	1.1180	1.0145	-0.0982
VIM	vimentin	-3.39	0.0065	Cluster 1	-0.3642	-0.7573	-0.4824	0.6079	0.4688	0.5272
CD44	CD44 molecule (Indian blood group)	-4.78	0.0211	Cluster 1	-0.3067	-0.7408	-0.7195	0.4763	0.6156	0.6751
BMAL2	basic helix-loop-helix ARNT like 2	-6.30	0.0109	Cluster 1	-0.6733	-0.6058	-0.5834	-0.3360	0.4390	1.7596
RABEP1	rabaptin, RAB GTPase binding effector protein 1	-4.83	0.0282	Cluster 1	-0.5846	-0.4727	-0.4553	0.0889	0.4604	0.9633
SARS1	seryl-tRNA synthetase 1	-4.09	0.0481	Cluster 1	-0.6097	-0.2391	-0.6156	0.3681	0.6024	0.4939

UBA6	ubiquitin like modifier activating enzyme 6	-5.74	0.0058	Cluster 1	-0.5669	-0.5937	-0.7962	0.4905	0.3370	1.1292
VCL	vinculin	-4.81	0.0345	Cluster 1	-0.5824	-0.6089	-0.4174	0.0665	1.0953	0.4470
TIMP2	TIMP metallopeptidase inhibitor 2	-4.50	0.0464	Cluster 1	-0.4802	-0.5027	-0.4854	0.6271	0.5311	0.3101
CAPG	capping actin protein, gelsolin like	-4.33	0.0373	Cluster 1	-0.3030	-0.6394	-0.6197	0.5947	0.3895	0.5779
CTNNA1	catenin alpha 1	-4.71	0.0271	Cluster 1	-0.7153	-0.7433	-0.2223	0.3579	0.4112	0.9117
HSPA5	heat shock protein family A (Hsp70) member 5	-3.17	0.0448	Cluster 1	-1.1694	-0.1635	-0.2632	0.6934	0.6139	0.2888
OFD1	OFD1 centriole and centriolar satellite protein	-5.02	0.0408	Cluster 1	-0.4429	-0.4868	-0.4530	1.0793	1.1896	-0.8861
MAP4	microtubule associated protein 4	-5.98	0.0082	Cluster 1	-0.7591	-0.5761	-0.7661	0.4043	1.3603	0.3367
PLEKHA5	pleckstrin homology domain containing A5	-3.62	0.0359	Cluster 1	-0.4485	-0.7024	-0.2780	1.0970	0.1229	0.2089
MCF2L2	MCF.2 cell line derived transforming sequence-like 2	4.16	0.0420	Cluster 2	-0.5020	0.5522	1.3842	-0.5691	-0.0925	-0.7729
EIF2AK2	eukaryotic translation initiation factor 2 alpha kinase 2	-4.15	0.0463	Cluster 1	-0.4325	-0.5839	-0.3829	0.9471	-0.1453	0.5975
SEC61A1	SEC61 translocon subunit alpha 1	-4.19	0.0372	Cluster 1	-0.3346	-0.6554	-0.6352	0.4485	0.7863	0.3904
WAPL	WAPL cohesin release factor	-4.88	0.0359	Cluster 1	-0.4855	-0.5388	-0.5193	1.0815	0.6954	-0.2334
RPL18	ribosomal protein L18	-5.09	0.0220	Cluster 1	-0.5638	-0.5890	-0.5697	0.7611	0.4673	0.4941
U2AF2	U2 small nuclear RNA auxiliary factor 2	-4.77	0.0373	Cluster 1	-0.5093	-0.5331	-0.5148	0.6335	0.7390	0.1847
EPN1	epsin 1	-5.22	0.0055	Cluster 1	-0.9590	-0.2630	-0.9780	1.5465	0.6542	-0.0007
HIPK2	homeodomain interacting protein kinase 2	-4.97	0.0304	Cluster 1	-0.5331	-0.5578	-0.5389	0.8156	0.6385	0.1757
IPO5	importin 5	-4.43	0.0389	Cluster 1	-0.3193	-0.6591	-0.6382	0.3476	0.1938	1.0752
WDR3	WD repeat domain 3	-5.56	0.0189	Cluster 1	-0.7495	-0.3236	-0.6119	1.5912	-1.0158	1.1095
ERBB3	erb-b2 receptor tyrosine kinase 3	5.07	0.0146	Cluster 2	-0.8912	0.5873	1.8576	-0.1385	-0.6715	-0.7436

CDK13	cyclin dependent kinase 13	-6.03	0.0008	Cluster 1	-0.7696	-0.7289	-0.7714	0.3785	0.5791	1.3122
PFKP	phosphofructokinase, platelet	-4.68	0.0053	Cluster 1	-0.9893	-0.5459	-0.3283	0.5472	0.6176	0.6986
KLF6	KLF transcription factor 6	-5.26	0.0025	Cluster 1	-1.1221	-0.0250	-0.9551	0.8560	0.7486	0.4975
PKM	pyruvate kinase M1/2	-3.33	0.0145	Cluster 1	-0.3604	-0.3004	-0.9516	0.6629	0.6214	0.3281
ACSL4	acyl-CoA synthetase long chain family member 4	-4.86	0.0467	Cluster 1	-0.3475	-0.5444	-0.5242	-0.1666	0.2196	1.3631
PABPC1	poly(A) binding protein cytoplasmic 1	-4.48	0.0201	Cluster 1	-0.2218	-0.8558	-0.8335	0.5612	0.5291	0.8207
TCOF1	treacle ribosome biogenesis factor 1	-4.49	0.0492	Cluster 1	-0.4971	-0.4133	-0.5027	0.2602	0.0683	1.0845
CDC42	cell division cycle 42	-2.92	0.0329	Cluster 1	-0.5719	-0.3964	-0.2656	-0.0001	0.9261	0.3079
ATP2B1	ATPase plasma membrane Ca2+ transporting 1	-4.75	0.0359	Cluster 1	-0.5123	-0.5360	-0.5178	0.3698	0.4329	0.7634
MAP4K4	mitogen-activated protein kinase kinase kinase kinase 4	-5.29	0.0044	Cluster 1	-0.8221	-0.3972	-0.9107	1.0801	-0.1860	1.2360
WDR1	WD repeat domain 1	-4.69	0.0077	Cluster 1	-0.8103	-0.8301	-0.1631	0.8282	0.4819	0.4934
SPP2	secreted phosphoprotein 2	6.54	0.0029	Cluster 2	1.0418	0.3532	0.8474	-0.5402	-0.8850	-0.8174
NFATC3	nuclear factor of activated T cells 3	5.11	0.0255	Cluster 2	-0.5779	-0.2666	2.0096	-0.4908	-0.5880	-0.0862
PICALM	phosphatidylinositol binding clathrin assembly protein	-4.79	0.0348	Cluster 1	-0.5169	-0.5408	-0.5224	0.7694	0.5038	0.3069
ENO1	enolase 1	-3.80	0.0016	Cluster 1	-0.3813	-0.8023	-0.6563	0.6106	0.7107	0.5186
SEMA3C	semaphorin 3C	-5.71	0.0437	Cluster 1	-0.4275	-0.4637	-0.4359	-0.4056	-0.0617	1.7943
RASAL2	RAS protein activator like 2	-4.22	0.0338	Cluster 1	-0.5175	-0.5223	-0.4300	0.8583	0.1860	0.4255
FOSL2	FOS like 2, AP-1 transcription factor subunit	-3.98	0.0326	Cluster 1	-0.7220	-0.2626	-0.7285	0.7358	0.3654	0.6118
ACTB	actin beta	-3.58	0.0032	Cluster 1	-0.2920	-0.7546	-0.6958	0.6624	0.5484	0.5315
RAB7A	RAB7A, member RAS oncogene family	-4.75	0.0337	Cluster 1	-0.5168	-0.5404	-0.5223	0.5006	0.6642	0.4147

PIK3C3	phosphatidylinositol 3-kinase catalytic subunit type 3	-4.70	0.0414	Cluster 1	-0.9056	-0.5942	0.1504	-0.0859	1.3737	0.0616
GNB1	G protein subunit beta 1	-4.26	0.0246	Cluster 1	-0.0352	-0.8115	-0.6863	0.6477	0.3737	0.5115
CIC	capicua transcriptional repressor	-4.94	0.0255	Cluster 1	-0.5437	-0.5682	-0.5494	0.5420	0.4269	0.6925
SRCAP	Snf2 related CREBBP activator protein	-5.00	0.0432	Cluster 1	-0.4928	-0.5176	-0.4985	0.0203	1.1686	0.3200
CPB2	carboxypeptidase B2	7.10	0.0236	Cluster 2	-0.0634	1.6821	-0.0714	-0.5364	-0.4591	-0.5519
PSEN1	presenilin 1	-4.44	0.0236	Cluster 1	-0.5570	-0.5262	-0.5628	0.6809	0.6513	0.3138
HSP90AA1	heat shock protein 90 alpha family class A member 1	-2.56	0.0282	Cluster 1	-0.1336	-0.5943	-0.5400	0.5004	0.4758	0.2916
BZW1	basic leucine zipper and W2 domains 1	-5.07	0.0009	Cluster 1	-0.5160	-0.6719	-1.1380	1.0192	1.0925	0.2141
NFE2L1	NFE2 like bZIP transcription factor 1	-5.80	0.0117	Cluster 1	-0.5458	-0.7410	-0.7183	0.1150	1.3178	0.5722
RPS5	ribosomal protein S5	-3.91	0.0255	Cluster 1	-0.6292	-0.6877	-0.2546	0.5958	0.5178	0.4578
FAT1	FAT atypical cadherin 1	-6.83	0.0001	Cluster 1	-0.9469	-0.7824	-0.8840	1.3254	0.5461	0.7418
EIF3I	eukaryotic translation initiation factor 3 subunit I	-3.19	0.0277	Cluster 1	-0.6231	-0.3463	-0.3405	0.1492	0.2602	0.9005
HUWE1	HECT, UBA and WWE domain containing E3 ubiquitin protein ligase 1	-5.21	0.0154	Cluster 1	0.1153	-0.8732	-1.1878	0.8839	0.5919	0.4700
FTL	ferritin light chain	-5.18	0.0008	Cluster 1	-0.7215	-0.7440	-0.7574	0.8511	0.6561	0.7158
DOCK9	dedicator of cytokinesis 9	-4.04	0.0326	Cluster 1	-0.4549	-0.4457	-0.6352	0.6813	0.4127	0.4419
ANAPC5	anaphase promoting complex subunit 5	-4.48	0.0095	Cluster 1	-0.6705	-0.4918	-0.5919	0.7486	0.6148	0.3908
GCN1	GCN1 activator of EIF2AK4	-6.97	0.0018	Cluster 1	-0.9142	-0.7232	-0.6999	-0.2581	1.3692	1.2262
RPLP0	ribosomal protein lateral stalk subunit P0	-6.02	0.0029	Cluster 1	-0.8355	-0.8653	-0.5983	0.7260	0.6089	0.9642
FUS	FUS RNA binding protein	-5.05	0.0052	Cluster 1	-0.7298	-0.2223	-0.9244	0.5642	0.6556	0.6567
GOLGA3	golgin A3	3.67	0.0011	Cluster 2	0.7560	0.6075	0.4519	-0.3509	-0.6760	-0.7886

HNRNPC	heterogeneous nuclear ribonucleoprotein C	-3.66	0.0211	Cluster 1	-0.3511	-0.4370	-0.8220	0.4582	0.6238	0.5283
TOX4	TOX high mobility group box family member 4	-4.95	0.0169	Cluster 1	-0.4589	-0.6865	-0.4642	0.7414	0.3269	0.5413
DPYSL2	dihydropyrimidinase like 2	-4.66	0.0373	Cluster 1	-0.5044	-0.5277	-0.5098	0.3839	0.5035	0.6544
LRRFIP2	LRR binding FLII interacting protein 2	4.15	0.0236	Cluster 2	0.1892	0.7782	0.6444	-0.3161	-0.4694	-0.8261
OR1I1	olfactory receptor family 1 subfamily I member 1	5.90	0.0011	Cluster 2	0.6389	0.4848	1.1243	-0.6900	-0.9901	-0.5679
ARCN1	archain 1	-6.24	0.0000	Cluster 1	-0.8284	-0.8080	-0.9184	0.8522	0.7640	0.9385
WAC	WW domain containing adaptor with coiled-coil	-2.62	0.0464	Cluster 1	-0.2814	-0.5429	-0.3209	0.2833	0.5834	0.2784
SRPK1	SRSF protein kinase 1	-3.56	0.0314	Cluster 1	-0.2346	-0.7694	-0.5711	0.7758	0.5477	0.2516
SCD	stearoyl-CoA desaturase	-3.92	0.0204	Cluster 1	-0.3108	-0.5492	-0.8363	0.6687	0.6177	0.4099
PCDH11Y	protocadherin 11 Y-linked	5.17	0.0187	Cluster 2	0.8529	0.9249	0.0996	-0.7612	-0.3424	-0.7738
SF3A1	splicing factor 3a subunit 1	-4.72	0.0464	Cluster 1	-0.4860	-0.5097	-0.4915	0.4476	0.0970	0.9425
LGALS1	galectin 1	-4.70	0.0343	Cluster 1	-0.2645	-0.6853	-0.6642	0.0096	0.6503	0.9541
RPL3	ribosomal protein L3	-3.55	0.0246	Cluster 1	-0.5777	-0.4353	-0.4771	0.5479	0.5015	0.4407
EP300	E1A binding protein p300	-5.14	0.0335	Cluster 1	-0.5290	-0.5544	-0.5349	-0.1105	0.7441	0.9848
ZC3H14	zinc finger CCCH-type containing 14	-4.55	0.0052	Cluster 1	-0.5765	-0.6695	-0.5843	0.3537	0.4456	1.0310
YY1	YY1 transcription factor	-4.86	0.0464	Cluster 1	-0.4822	-0.5059	-0.4877	0.0102	1.0821	0.3836
ARHGAP5	Rho GTPase activating protein 5	-4.41	0.0035	Cluster 1	-0.4713	-0.7326	-0.6621	0.5034	0.5180	0.8447
NINL	ninein like	4.48	0.0461	Cluster 2	0.0421	-0.6778	1.8757	-0.2327	0.0076	-1.0149
CSNK2A1	casein kinase 2 alpha 1	-6.20	0.0008	Cluster 1	-0.9646	-0.7176	-0.6516	1.1238	0.7769	0.4330
MAPRE1	microtubule associated protein RP/EB family member 1	-5.25	0.0257	Cluster 1	-0.5539	-0.5798	-0.5599	1.0159	0.6328	0.0448

PGK1	phosphoglycerate kinase 1	-5.58	0.0018	Cluster 1	-0.9268	-0.7090	-0.6687	0.8551	0.7745	0.6748
RBM3	RNA binding motif protein 3	-3.29	0.0431	Cluster 1	-0.7514	-0.2760	-0.2430	0.5503	0.5279	0.1921
TSC22D1	TSC22 domain family member 1	-3.82	0.0418	Cluster 1	-0.5275	-0.1271	-0.7238	0.3082	0.0542	1.0161
COTL1	coactosin like F-actin binding protein 1	-4.72	0.0246	Cluster 1	-0.5121	-0.5770	-0.5178	0.4720	0.1849	0.9500
PIEZO1	piezo type mechanosensitive ion channel component 1	-3.98	0.0216	Cluster 1	-0.6750	-0.6758	-0.3200	0.4570	0.3347	0.8790
EIF3E	eukaryotic translation initiation factor 3 subunit E	-2.76	0.0437	Cluster 1	-0.8157	-0.1292	-0.3474	0.3367	0.3967	0.5588
NDRG1	N-myc downstream regulated 1	-4.87	0.0021	Cluster 1	-0.2810	-1.0173	-1.1251	0.8145	1.0074	0.6016
PLEKHJ1	pleckstrin homology domain containing J1	4.53	0.0117	Cluster 2	0.8570	-0.0263	0.7260	-0.4658	-0.4911	-0.5998
GPI	glucose-6-phosphate isomerase	-2.79	0.0481	Cluster 1	-0.8710	-0.2124	-0.3048	0.6344	0.5867	0.1671
BBC3	BCL2 binding component 3	3.39	0.0417	Cluster 2	-0.0462	0.7993	0.5022	-0.3138	-0.2974	-0.6441
TNPO2	transportin 2	-5.17	0.0359	Cluster 1	-0.5177	-0.5425	-0.5235	0.8349	-0.2414	0.9903
RPL18A	ribosomal protein L18a	-4.28	0.0170	Cluster 1	-0.9707	-1.1771	-0.1092	0.8716	0.7202	0.6651
NAMPT	nicotinamide phosphoribosyltransferase	-7.41	0.0000	Cluster 1	-1.0176	-1.1572	-0.9304	1.3403	1.0508	0.7140
OGDH	oxoglutarate dehydrogenase	-4.46	0.0483	Cluster 1	-0.4750	-0.4972	-0.4801	0.6444	0.3815	0.4265
GRB10	growth factor receptor bound protein 10	-4.35	0.0272	Cluster 1	-0.6490	-0.3994	-0.6552	0.4635	0.7452	0.4949
GARS1	glycyl-tRNA synthetase 1	-5.12	0.0056	Cluster 1	-0.8360	-0.8659	-0.5150	0.9484	0.9810	0.2875
SERPINE1	serpin family E member 1	-4.38	0.0386	Cluster 1	-0.6182	-0.6442	-0.2971	0.4479	0.3428	0.7688
AHR	aryl hydrocarbon receptor	-5.26	0.0281	Cluster 1	-0.5458	-0.5716	-0.5518	0.5360	0.0428	1.0904
GIMAP2	GTPase, IMAP family member 2	3.17	0.0241	Cluster 2	0.1762	0.5742	0.5542	-0.5610	-0.4157	-0.3278
DNMBP	dynamin binding protein	-4.68	0.0430	Cluster 1	-0.4918	-0.5148	-0.4971	0.8505	0.3285	0.3247

GBF1	golgi brefeldin A resistant guanine nucleotide exchange factor 1	-5.37	0.0117	Cluster 1	-0.7969	-0.7188	-0.3242	-0.5855	0.9012	1.5242
ARHGAP21	Rho GTPase activating protein 21	-4.73	0.0467	Cluster 1	-0.5597	-0.3516	-0.5659	-0.4264	0.8347	1.0690
PITRM1	pitrilysin metallopeptidase 1	-5.00	0.0121	Cluster 1	-0.5708	-0.6473	-0.5768	0.3324	0.5731	0.8893
PPIF	peptidylprolyl isomerase F	-4.04	0.0498	Cluster 1	-0.6196	-0.6451	-0.1751	0.5934	0.4144	0.4319
TSPAN14	tetraspanin 14	-3.45	0.0437	Cluster 1	-0.7242	-0.3396	-0.3007	0.6043	-0.2498	1.0100
RGS9	regulator of G protein signaling 9	3.68	0.0291	Cluster 2	0.5127	0.4369	0.8569	-0.2325	-0.4623	-1.1117
KPNB1	karyopherin subunit beta 1	-4.74	0.0086	Cluster 1	-0.4777	-0.7979	-0.7757	0.6205	0.6520	0.7789
CDK5RAP3	CDK5 regulatory subunit associated protein 3	-5.96	0.0014	Cluster 1	-0.5466	-0.9155	-0.5525	0.5585	0.7935	0.6627
PFN1	profilin 1	-6.15	0.0029	Cluster 1	-0.7195	-0.7482	-0.7262	0.6983	0.7589	0.7367
DDX5	DEAD-box helicase 5	-5.45	0.0018	Cluster 1	-0.0334	-1.0905	-1.0379	0.7523	0.7282	0.6813
VAT1	vesicle amine transport 1	-5.95	0.0047	Cluster 1	-0.6901	-0.7183	-0.6967	0.7685	0.6062	0.7305
LRRC59	leucine rich repeat containing 59	-4.56	0.0421	Cluster 1	-0.4902	-0.5130	-0.4955	0.6276	0.4742	0.3969
PRKAR1A	protein kinase cAMP-dependent type I regulatory subunit alpha	-4.71	0.0354	Cluster 1	-0.5116	-0.5351	-0.5171	0.3699	0.6223	0.5717
UBE2D3	ubiquitin conjugating enzyme E2 D3	-3.67	0.0373	Cluster 1	-0.6570	-0.5880	-0.1170	0.7056	0.2579	0.3985
NSD2	nuclear receptor binding SET domain protein 2	-4.44	0.0100	Cluster 1	-0.4142	-0.8264	-0.5927	0.4698	0.5453	0.8181
SH3D19	SH3 domain containing 19	4.41	0.0025	Cluster 2	0.7494	0.2122	0.7756	-0.5088	-0.6272	-0.6012
HSPA8	heat shock protein family A (Hsp70) member 8	-3.04	0.0213	Cluster 1	-0.1978	-0.6542	-0.5758	0.5084	0.6429	0.2764
SIAE	sialic acid acetylesterase	11.03	0.0000	Cluster 2	1.7456	1.3110	1.4196	-1.5853	-1.3277	-1.5632
SNX15	sorting nexin 15	-5.11	0.0187	Cluster 1	-0.4471	-0.7112	-0.4525	0.2444	0.3714	0.9950
ATG2A	autophagy related 2A	-5.01	0.0277	Cluster 1	-0.5416	-0.5665	-0.5474	0.6201	0.8212	0.2142

PDHX	pyruvate dehydrogenase complex component X	4.16	0.0028	Cluster 2	0.7093	0.2448	0.7716	-0.3758	-0.6372	-0.7127
C11orf58	chromosome 11 open reading frame 58	-4.29	0.0117	Cluster 1	-0.5476	-0.4942	-0.6916	0.1802	0.5578	0.9954
ATP5F1B	ATP synthase F1 subunit beta	-4.77	0.0323	Cluster 1	-0.5212	-0.5449	-0.5267	0.5545	0.6189	0.4194
PTGES3	prostaglandin E synthase 3	-5.27	0.0189	Cluster 1	-0.5832	-0.6090	-0.5892	0.5092	0.4035	0.8686
STX2	syntaxin 2	5.00	0.0117	Cluster 2	0.5274	-0.5037	1.5131	-0.6854	-0.4173	-0.4341
RAB5B	RAB5B, member RAS oncogene family	-4.59	0.0282	Cluster 1	-0.5593	-0.4905	-0.5651	0.5826	0.7494	0.2829
GAPDH	glyceraldehyde-3-phosphate dehydrogenase	-2.49	0.0319	Cluster 1	-0.2310	-0.6051	-0.3808	0.5080	0.2775	0.4314
TPI1	triosephosphate isomerase 1	-6.39	0.0013	Cluster 1	-0.7642	-0.8464	-0.8234	0.6071	1.0735	0.7534
ENO2	enolase 2	-4.72	0.0222	Cluster 1	-0.3458	-0.7079	-0.6871	0.5468	0.5509	0.6431
ZNF451	zinc finger protein 451	-4.81	0.0236	Cluster 1	-0.4658	-0.6317	-0.4711	0.1881	0.7925	0.5879
RPS12	ribosomal protein S12	-6.22	0.0167	Cluster 1	-0.6001	-0.6289	-0.6067	0.0158	1.5735	0.2465
CCR6	C-C motif chemokine receptor 6	7.69	0.0005	Cluster 2	0.5025	1.1928	0.5574	-0.6986	-0.8414	-0.7127
HSPA9	heat shock protein family A (Hsp70) member 9	-4.13	0.0220	Cluster 1	-0.8214	-0.8505	-0.2324	0.6805	0.8422	0.3816
ARRDC3	arrestin domain containing 3	-4.28	0.0463	Cluster 1	-0.5277	-0.5518	-0.3936	0.7632	0.2234	0.4865
TARS1	threonyl-tRNA synthetase 1	-5.81	0.0033	Cluster 1	-0.6572	-0.6852	-0.7715	0.9873	0.6136	0.5129
SKP1	S-phase kinase associated protein 1	-5.02	0.0279	Cluster 1	-0.5413	-0.5662	-0.5471	0.3315	0.8965	0.4265
LIFR	LIF receptor subunit alpha	-5.69	0.0431	Cluster 1	-0.4325	-0.4687	-0.4409	1.7516	-0.2433	-0.1663
TBCCD1	TBCC domain containing 1	4.48	0.0117	Cluster 2	1.1781	1.1012	-0.6977	-0.6203	-0.5520	-0.4093
GNAI2	G protein subunit alpha i2	-4.34	0.0389	Cluster 1	-0.3988	-0.5770	-0.5583	0.5716	0.6262	0.3364
RPL24	ribosomal protein L24	-4.81	0.0328	Cluster 1	-0.5222	-0.5462	-0.5278	0.3053	0.5880	0.7030
SSR3	signal sequence receptor subunit 3	-4.97	0.0314	Cluster 1	-0.6187	-0.6459	-0.3920	0.2221	0.2448	1.1896

NRBP1	nuclear receptor binding protein 1	-4.88	0.0296	Cluster 1	-0.5310	-0.5553	-0.5366	0.7680	0.4046	0.4502
RPS15	ribosomal protein S15	-5.27	0.0220	Cluster 1	-0.5712	-0.5971	-0.5773	0.9539	0.5544	0.2374
CLIP4	CAP-Gly domain containing linker protein family member 4	-3.15	0.0482	Cluster 1	-0.7631	-0.7120	-0.0224	0.4196	0.7085	0.3695
CCT4	chaperonin containing TCP1 subunit 4	-4.98	0.0330	Cluster 1	-0.5271	-0.5519	-0.5329	0.9543	0.4567	0.2009
ODC1	ornithine decarboxylase 1	-4.98	0.0241	Cluster 1	-0.5507	-0.5753	-0.5564	0.4599	0.5946	0.6279
BIRC6	baculoviral IAP repeat containing 6	-5.18	0.0255	Cluster 1	-0.5534	-0.5790	-0.5594	0.8623	0.7658	0.0637
MSH6	mutS homolog 6	-4.36	0.0373	Cluster 1	-0.5099	-0.4775	-0.4607	0.6158	0.3563	0.4760
CEP104	centrosomal protein 104	-4.36	0.0384	Cluster 1	-0.5034	-0.4804	-0.4635	0.3812	0.3854	0.6807
QSOX1	quiescin sulfhydryl oxidase 1	-6.10	0.0015	Cluster 1	-0.6812	-0.8676	-0.6880	0.3062	0.8613	1.0693
ERRFI1	ERBB receptor feedback inhibitor 1	-5.29	0.0060	Cluster 1	-0.8371	-0.5048	-0.8440	0.8241	0.8138	0.5479
ASH1L	ASH1 like histone lysine methyltransferase	-3.38	0.0389	Cluster 1	-0.6205	-0.4277	-0.3434	0.6197	0.2581	0.5137
ARHGEF2	Rho/Rac guanine nucleotide exchange factor 2	-4.99	0.0216	Cluster 1	-0.6363	-0.4984	-0.6426	0.9774	0.5244	0.2754
MAP7D1	MAP7 domain containing 1	-4.60	0.0481	Cluster 1	-0.4786	-0.5013	-0.4839	0.7573	0.6153	0.0912
PRDX1	peroxiredoxin 1	-5.45	0.0042	Cluster 1	-0.7390	-0.7679	-0.6441	0.6439	0.5761	0.9310
SLC35A3	solute carrier family 35 member A3	-4.38	0.0449	Cluster 1	-0.7299	-0.2419	-0.1634	1.7244	-0.0216	-0.5676
POLR1G	RNA polymerase I subunit G	3.45	0.0481	Cluster 2	0.8171	-0.5717	0.8764	-0.2806	-0.4854	-0.3559
CTSD	cathepsin D	-3.70	0.0274	Cluster 1	-0.4001	-0.4002	-0.7597	0.4979	0.5827	0.4794
PHF3	PHD finger protein 3	-4.97	0.0348	Cluster 1	-0.5228	-0.5475	-0.5285	0.7017	0.8670	0.0301
SGK1	serum/glucocorticoid regulated kinase 1	-5.46	0.0281	Cluster 1	-0.5484	-0.5750	-0.5546	-0.2927	0.8429	1.1279
GDA	guanine deaminase	7.11	0.0005	Cluster 2	0.8310	0.6689	1.1194	-0.6649	-1.0146	-0.9399

IFIT2	interferon induced protein with tetratricopeptide repeats 2	-4.92	0.0138	Cluster 1	-0.6036	-0.6037	-0.5837	0.7211	0.7729	0.2970
DUSP1	dual specificity phosphatase 1	-4.13	0.0493	Cluster 1	-0.6013	-0.6266	-0.2271	0.3395	0.7121	0.4034
PLEKHG1	pleckstrin homology and RhoGEF domain containing G1	10.02	0.0007	Cluster 2	-0.2621	-0.2997	3.3890	-0.8365	-1.0882	-0.9026
TAF12	TATA-box binding protein associated factor 12	4.17	0.0105	Cluster 2	0.6413	1.0654	0.0209	-0.2924	-0.5109	-0.9243
KDM3B	lysine demethylase 3B	-5.61	0.0333	Cluster 1	-0.5131	-0.5399	-0.5193	0.1750	-0.1039	1.5013
EGR1	early growth response 1	-5.54	0.0127	Cluster 1	-0.6184	-0.6452	-0.6246	0.9090	0.6381	0.3410
GPSM2	G protein signaling modulator 2	-5.12	0.0100	Cluster 1	-0.5990	-0.6316	-0.6430	0.9359	0.0793	0.8583
RPL21	ribosomal protein L21	-3.64	0.0236	Cluster 1	-0.3327	-0.8896	-0.3090	0.4897	0.5872	0.4544
COPA	COPI coat complex subunit alpha	-3.43	0.0421	Cluster 1	-0.6614	-0.0904	-0.7857	0.2830	0.4482	0.8064
HNRNPA2B1	heterogeneous nuclear ribonucleoprotein A2/B1	-2.92	0.0461	Cluster 1	-0.2573	-0.9823	-0.2287	0.4433	0.5980	0.4270
OPTN	optineurin	-5.18	0.0170	Cluster 1	-0.6326	-0.5668	-0.5472	0.6106	0.9999	0.1361
LRP1	LDL receptor related protein 1	-5.80	0.0141	Cluster 1	-0.5936	-0.6560	-0.6001	1.0843	-0.4221	1.1875
TUBA1B	tubulin alpha 1b	-6.70	0.0010	Cluster 1	-0.7949	-0.8247	-0.8019	0.8207	0.7397	0.8611
HJURP	Holliday junction recognition protein	3.86	0.0360	Cluster 2	0.9740	-0.5703	0.9152	-0.1867	-0.4955	-0.6367
AGO2	argonaute RISC catalytic component 2	-5.83	0.0060	Cluster 1	-0.6500	-0.6784	-0.7215	1.0703	0.8829	0.0968
STAU1	staufen double-stranded RNA binding protein 1	-4.73	0.0220	Cluster 1	-0.5800	-0.6054	-0.5171	0.6773	0.5226	0.5026
BCAS4	breast carcinoma amplified sequence 4	7.45	0.0000	Cluster 2	0.9616	0.9832	1.2200	-1.1916	-0.9083	-1.0649
USP22	ubiquitin specific peptidase 22	-5.35	0.0251	Cluster 1	-0.5583	-0.5845	-0.5644	0.0445	1.1076	0.5551
RPS10	ribosomal protein S10	-4.88	0.0373	Cluster 1	-0.5091	-0.5329	-0.5147	0.1013	0.5626	0.8928
CDKN1A	cyclin dependent kinase inhibitor 1A	-4.20	0.0437	Cluster 1	-0.2086	-0.6531	-0.6333	0.5546	0.6327	0.3077

SSR1	signal sequence receptor subunit 1	-3.92	0.0109	Cluster 1	-0.4476	-0.5104	-0.7723	0.3907	0.5909	0.7487
NUP153	nucleoporin 153	-4.46	0.0464	Cluster 1	-0.4785	-0.5008	-0.4837	0.5141	0.5005	0.4484
AHNAK	AHNAK nucleoprotein	-5.38	0.0000	Cluster 1	-0.7937	-0.9798	-0.8056	0.7991	0.8621	0.9179
RPL23	ribosomal protein L23	-3.83	0.0360	Cluster 1	-0.3212	-0.7705	-0.4370	0.5262	0.5742	0.4283
PSMB2	proteasome 20S subunit beta 2	-3.93	0.0481	Cluster 1	-0.3105	-0.6102	-0.5910	0.6276	0.3515	0.5326
AGO3	argonaute RISC catalytic component 3	-3.66	0.0372	Cluster 1	-0.5373	-0.3052	-0.4994	0.1363	0.0917	1.1138
KLC1	kinesin light chain 1	-3.12	0.0170	Cluster 1	-0.5342	-0.4077	-0.4156	0.1598	0.7653	0.4324
CAPNS1	calpain small subunit 1	-4.66	0.0373	Cluster 1	-0.5046	-0.5278	-0.5100	0.5144	0.6181	0.4098
PRDX5	peroxiredoxin 5	-4.44	0.0487	Cluster 1	-0.4738	-0.4960	-0.4790	0.6202	0.3703	0.4583
PCNX4	pecanex 4	-5.72	0.0021	Cluster 1	-0.7705	-0.6420	-0.7201	0.7356	0.3856	1.0114
KTN1	kinectin 1	-3.73	0.0438	Cluster 1	-0.3535	-0.4427	-0.5711	0.6367	-0.0542	0.7849
OR7C1	olfactory receptor family 7 subfamily C member 1	4.78	0.0246	Cluster 2	0.6604	-0.3474	1.0804	-0.5542	-0.4619	-0.3774
SMARCA4	SWI/SNF related, matrix associated, actin dependent regulator of chromatin, subfamily a, member 4	-4.51	0.0099	Cluster 1	-0.4345	-0.6320	-0.7419	0.7394	0.9859	0.0832
KDM4B	lysine demethylase 4B	-4.83	0.0188	Cluster 1	-0.5515	-0.5764	-0.5781	0.6713	0.5884	0.4462
ATF4	activating transcription factor 4	-5.78	0.0060	Cluster 1	-0.6662	-0.6938	-0.6726	0.7208	0.6804	0.6314
CALU	calumenin	-4.76	0.0390	Cluster 1	-0.5020	-0.5253	-0.5074	0.2012	0.8395	0.4939
HERC2	HECT and RLD domain containing E3 ubiquitin protein ligase 2	-4.73	0.0481	Cluster 1	-0.4815	-0.5052	-0.4870	0.9994	0.2283	0.2460
DTD2	D-aminoacyl-tRNA deacylase 2	3.76	0.0194	Cluster 2	0.8696	-0.1866	0.8130	-0.7272	-0.4028	-0.3661
RPL36	ribosomal protein L36	-4.18	0.0461	Cluster 1	-0.2602	-0.6227	-0.6034	0.3620	0.6521	0.4722
TULP4	TUB like protein 4	-6.67	0.0052	Cluster 1	-0.5780	-0.6070	-0.8476	-0.0839	0.4044	1.7122

EXOSC2	exosome component 2	2.62	0.0287	Cluster 2	0.4419	0.6811	0.0439	-0.3749	-0.5149	-0.2771
CHMP2A	charged multivesicular body protein 2A	-4.28	0.0438	Cluster 1	-0.4736	-0.4719	-0.4788	0.2669	0.4042	0.7532
TRIM28	tripartite motif containing 28	-4.43	0.0482	Cluster 1	-0.4739	-0.4960	-0.4791	0.4816	0.4414	0.5260
EIF2S3	eukaryotic translation initiation factor 2 subunit gamma	-4.95	0.0255	Cluster 1	-0.5444	-0.5690	-0.5501	0.6718	0.3662	0.6256
CLIP1	CAP-Gly domain containing linker protein 1	2.48	0.0462	Cluster 2	0.1981	0.5531	0.3455	-0.3164	-0.2690	-0.5113
RPL27	ribosomal protein L27	-4.20	0.0278	Cluster 1	-0.4620	-0.4619	-0.6861	0.3848	0.4191	0.8061
ANKHD1	ankyrin repeat and KH domain containing 1	-3.98	0.0389	Cluster 1	-1.1309	-0.8056	-0.0271	0.1399	0.8422	0.9815
DIAPH1	diaphanous related formin 1	-4.61	0.0155	Cluster 1	-0.4581	-0.6432	-0.6363	0.8637	0.8437	0.0301
MAP1B	microtubule associated protein 1B	-5.33	0.0005	Cluster 1	-0.7715	-0.5938	-0.9211	0.1229	1.1573	1.0063
NUP210	nucleoporin 210	4.03	0.0414	Cluster 2	-0.4817	1.2546	0.6192	-0.3549	-0.2956	-0.7415
RAN	RAN, member RAS oncogene family	-4.93	0.0272	Cluster 1	-0.5396	-0.5641	-0.5453	0.3924	0.5037	0.7529
MYH10	myosin heavy chain 10	-2.19	0.0409	Cluster 1	-0.2874	-0.5788	-0.2116	0.4304	0.5931	0.0542
TPT1	tumor protein, translationally-controlled 1	-3.73	0.0035	Cluster 1	-0.5291	-0.4271	-0.7326	0.5773	0.6503	0.4612
MORC4	MORC family CW-type zinc finger 4	2.70	0.0213	Cluster 2	0.6804	0.2262	0.3700	-0.5244	-0.5233	-0.2290
WDR74	WD repeat domain 74	-2.95	0.0392	Cluster 1	-0.1950	-0.5423	-0.4320	-0.4012	0.9956	0.5748
PDZD2	PDZ domain containing 2	6.25	0.0194	Cluster 2	0.8327	-0.2570	1.1947	-0.6286	-0.5008	-0.6409
BTG1	BTG anti-proliferation factor 1	-4.57	0.0165	Cluster 1	-0.7454	-0.6981	-0.2334	0.7555	0.6635	0.2580
ATP13A3	ATPase 13A3	-5.49	0.0125	Cluster 1	-0.6169	-0.6435	-0.6231	0.5417	0.4650	0.8768
MICAL2	microtubule associated monooxygenase, calponin and LIM domain containing 2	-5.58	0.0071	Cluster 1	-0.5878	-0.7556	-0.7335	0.7045	0.9675	0.4049
ZFC3H1	zinc finger C3H1-type containing	-5.63	0.0052	Cluster 1	-0.5339	-0.8202	-0.5398	0.7294	0.2393	0.9252

CCNB1	cyclin B1	-4.70	0.0389	Cluster 1	-0.5026	-0.5261	-0.5081	0.7102	0.5945	0.2321
BHLHE40	basic helix-loop-helix family member e40	-5.04	0.0249	Cluster 1	-0.5506	-0.5756	-0.5564	0.4423	0.8285	0.4118
EDEM1	ER degradation enhancing alpha-mannosidase like protein 1	-4.56	0.0483	Cluster 1	-0.4785	-0.5014	-0.4838	0.3258	0.3218	0.8160
NOTCH2	notch receptor 2	-5.69	0.0083	Cluster 1	-0.6478	-0.6752	-0.6542	0.5214	0.5901	0.8658
ROCK2	Rho associated coiled-coil containing protein kinase 2	-5.29	0.0164	Cluster 1	-0.6271	-0.5658	-0.5358	0.9726	1.1207	-0.3646
IL6ST	interleukin 6 cytokine family signal transducer	-6.93	0.0166	Cluster 1	-0.5750	-0.6050	-0.5819	-0.1213	2.2016	-0.3184
NAV1	neuron navigator 1	-3.34	0.0492	Cluster 1	-0.6986	-0.4732	-0.2017	0.4401	0.0307	0.9027
ELP2	elongator acetyltransferase complex subunit 2	-5.46	0.0035	Cluster 1	-0.6990	-0.7116	-0.5651	0.9947	0.4984	0.4826
ANXA1	annexin A1	-4.50	0.0082	Cluster 1	-0.1895	-0.8389	-0.9063	0.6230	0.9820	0.3297
CTSL	cathepsin L	-4.62	0.0383	Cluster 1	-0.5007	-0.5238	-0.5061	0.4729	0.5655	0.4922
HAVCR2	hepatitis A virus cellular receptor 2	6.65	0.0021	Cluster 2	1.7462	1.0173	-0.4959	-0.9473	-0.6029	-0.7173
DNAJC14	DnaJ heat shock protein family (Hsp40) member C14	-4.37	0.0236	Cluster 1	-0.5180	-0.5126	-0.5362	0.6506	0.2595	0.6567
HNRNPA1	heterogeneous nuclear ribonucleoprotein A1	-7.99	0.0000	Cluster 1	-1.1690	-1.0043	-0.9807	0.9633	1.0473	1.1435
CCT7	chaperonin containing TCP1 subunit 7	-4.68	0.0358	Cluster 1	-0.5096	-0.5329	-0.5150	0.4531	0.5829	0.5214
GLUL	glutamate-ammonia ligase	-4.65	0.0389	Cluster 1	-0.4019	-0.5879	-0.5680	-0.0909	0.7470	0.9018
GCC2	GRIP and coiled-coil domain containing 2	6.91	0.0001	Cluster 2	0.9629	1.0022	1.2161	-1.3395	-0.6777	-1.1640
FLNB	filamin B	-3.51	0.0324	Cluster 1	-1.0590	0.0889	-0.9274	0.4529	0.7559	0.6886
RNASEH2B	ribonuclease H2 subunit B	4.95	0.0236	Cluster 2	0.9880	-0.3174	0.8352	-0.5046	-0.6726	-0.3286
CALCOCO2	calcium binding and coiled-coil domain 2	-5.00	0.0129	Cluster 1	-0.6296	-0.5791	-0.5599	0.5399	0.6037	0.6251
TEX2	testis expressed 2	3.82	0.0117	Cluster 2	1.1755	0.2767	0.2194	-0.7298	-0.2618	-0.6801

YME1L1	YME1 like 1 ATPase	-4.00	0.0035	Cluster 1	-0.8584	-0.4462	-0.5198	0.8894	0.5387	0.3962
TXN	thioredoxin	-4.94	0.0282	Cluster 1	-0.5364	-0.5609	-0.5421	0.6759	0.7165	0.2471
NIBAN2	niban apoptosis regulator 2	-5.33	0.0108	Cluster 1	-0.7560	-0.7848	-0.4463	0.8535	0.7366	0.3970
RPS6	ribosomal protein S6	-4.02	0.0323	Cluster 1	-0.3797	-0.8244	-0.3897	0.4254	0.3469	0.8214
PIM1	Pim-1 proto-oncogene, serine/threonine kinase	-4.50	0.0467	Cluster 1	-0.4793	-0.5018	-0.4845	0.6852	0.4485	0.3319
HMGA1	high mobility group AT-hook 1	-8.87	0.0000	Cluster 1	-1.0200	-1.4813	-1.5806	1.3023	1.3885	1.3911
MTCH1	mitochondrial carrier 1	-4.62	0.0141	Cluster 1	-0.4633	-0.7647	-0.5945	0.6540	0.7415	0.4270
TAF8	TATA-box binding protein associated factor 8	-4.08	0.0251	Cluster 1	-0.2693	-0.7711	-0.7495	0.6269	0.7034	0.4596
SYTL2	synaptotagmin like 2	8.41	0.0008	Cluster 2	-0.2719	1.6068	1.1045	-0.7406	-0.9411	-0.7576
SDCBP	syndecan binding protein	-5.82	0.0068	Cluster 1	-0.6643	-0.6921	-0.6708	0.6694	0.4707	0.8872
YAP1	Yes1 associated transcriptional regulator	-5.04	0.0358	Cluster 1	-0.5188	-0.5438	-0.5246	0.3117	1.0737	0.2017
SLTM	SAFB like transcription modulator	-4.74	0.0255	Cluster 1	-0.4245	-0.4459	-0.6210	0.2789	0.4191	0.7934
RPLP1	ribosomal protein lateral stalk subunit P1	-4.70	0.0236	Cluster 1	-0.6940	-0.3368	-0.7004	0.6908	0.6284	0.4121
ARHGAP29	Rho GTPase activating protein 29	-4.52	0.0464	Cluster 1	-0.4816	-0.5042	-0.4868	0.2754	0.6675	0.5296
ACTR2	actin related protein 2	-4.59	0.0467	Cluster 1	-0.4811	-0.5037	-0.4864	0.6780	0.1379	0.6553
DUSP5	dual specificity phosphatase 5	-4.67	0.0368	Cluster 1	-0.5062	-0.5295	-0.5116	0.6382	0.4732	0.4359
SMARCAL1	SWI/SNF related, matrix associated, actin dependent regulator of chromatin, subfamily a like 1	5.48	0.0056	Cluster 2	-0.3602	1.3167	1.1453	-1.0365	-0.6020	-0.4633
HNRNPD	heterogeneous nuclear ribonucleoprotein D	-4.53	0.0352	Cluster 1	-0.7467	-0.9229	-0.0045	1.4140	0.0723	0.1878
CENPE	centromere protein E	-5.04	0.0282	Cluster 1	-0.4728	-0.6174	-0.4786	1.0408	0.8804	-0.3524
PHLDA1	pleckstrin homology like domain family A member 1	-5.54	0.0070	Cluster 1	-0.4905	-0.8058	-0.7835	0.8242	0.8256	0.4301

GAS2L3	growth arrest specific 2 like 3	-3.98	0.0236	Cluster 1	-0.7401	-0.6002	-0.2859	0.1645	0.3719	1.0897
SMARCC2	SWI/SNF related, matrix associated, actin dependent regulator of chromatin subfamily c member 2	-5.12	0.0071	Cluster 1	-0.5692	-0.8324	-0.4078	0.2722	0.6724	0.8647
TMBIM6	transmembrane BAX inhibitor motif containing 6	-5.51	0.0115	Cluster 1	-0.6244	-0.6512	-0.6306	0.7949	0.6218	0.4895
MORN3	MORN repeat containing 3	3.39	0.0071	Cluster 2	0.5874	0.6393	0.2642	-0.5135	-0.6056	-0.3718
IQGAP1	IQ motif containing GTPase activating protein 1	-5.76	0.0033	Cluster 1	-0.7444	-0.7738	-0.7007	1.0930	0.3972	0.7287
RPS2	ribosomal protein S2	-3.02	0.0374	Cluster 1	-0.9361	-0.0593	-0.5398	0.5028	0.4334	0.5990
NPC1	NPC intracellular cholesterol transporter 1	-4.92	0.0187	Cluster 1	-0.4709	-0.6857	-0.6649	0.4849	0.6289	0.7078
CSNK1D	casein kinase 1 delta	-3.41	0.0134	Cluster 1	-0.4279	-0.2991	-0.9158	0.3655	0.5783	0.6990
APP	amyloid beta precursor protein	-3.79	0.0246	Cluster 1	-0.6774	-0.5375	-0.3636	0.3750	0.7108	0.4927
RPL13A	ribosomal protein L13a	-3.98	0.0060	Cluster 1	-0.8836	-0.6029	-0.3450	0.6095	0.8010	0.4210
SERBP1	SERPINE1 mRNA binding protein 1	-5.17	0.0213	Cluster 1	-0.5716	-0.5971	-0.5775	0.5881	0.3683	0.7899
RPS8	ribosomal protein S8	-4.14	0.0252	Cluster 1	-0.7641	-0.4601	-0.4283	0.4529	0.4714	0.7282
HDGF	heparin binding growth factor	-5.08	0.0142	Cluster 1	-1.0659	-1.1272	0.2364	0.9192	0.5993	0.4381
SNX27	sorting nexin 27	4.26	0.0060	Cluster 2	0.6700	0.7722	0.8924	-0.1766	-1.0315	-1.1265
DYRK3	dual specificity tyrosine phosphorylation regulated kinase 3	4.04	0.0337	Cluster 2	0.5866	1.2048	-0.5341	-0.5100	-0.4033	-0.3440
TP53BP2	tumor protein p53 binding protein 2	-5.30	0.0464	Cluster 1	-0.4771	-0.5027	-0.4831	0.7351	1.3412	-0.6134
TPM3	tropomyosin 3	-3.98	0.0281	Cluster 1	-0.2883	-0.7419	-0.7206	0.4018	0.6922	0.6568
ARF1	ADP ribosylation factor 1	-4.92	0.0172	Cluster 1	-0.7171	-0.7450	-0.3673	0.5726	0.7077	0.5490
RHOB	ras homolog family member B	-4.82	0.0352	Cluster 1	-0.5166	-0.5406	-0.5222	0.7780	0.5677	0.2338
RPS27A	ribosomal protein S27a	-4.00	0.0437	Cluster 1	-0.2086	-0.7126	-0.6917	0.4801	0.3267	0.8062

SLC20A1	solute carrier family 20 member 1	-5.22	0.0176	Cluster 1	-0.5847	-0.6103	-0.5906	0.5333	0.7299	0.5224
GOLGA4	golgin A4	-4.86	0.0117	Cluster 1	-0.4884	-0.3595	-0.9709	-0.2773	0.9153	1.1807
RPS3A	ribosomal protein S3A	-5.93	0.0052	Cluster 1	-0.6845	-0.7126	-0.6910	0.5368	0.7341	0.8172
MYO10	myosin X	-4.20	0.0398	Cluster 1	-0.5652	-0.4044	-0.5710	0.8323	0.4840	0.2243
PAM	peptidylglycine alpha-amidating monooxygenase	-5.60	0.0052	Cluster 1	-0.5314	-0.5568	-0.8066	0.6998	0.3023	0.8927
IGFBP3	insulin like growth factor binding protein 3	-4.68	0.0389	Cluster 1	-0.5022	-0.5256	-0.5077	0.6625	0.5984	0.2746
SH3KBP1	SH3 domain containing kinase binding protein 1	-4.99	0.0213	Cluster 1	-0.4927	-0.5168	-0.6346	0.8140	0.7521	0.0780
MSN	moesin	-6.95	0.0000	Cluster 1	-0.9192	-0.9689	-0.9415	0.8357	1.0018	0.9922
RPL10	ribosomal protein L10	-3.37	0.0249	Cluster 1	-0.9717	-0.5580	-0.1455	0.5172	0.5274	0.6307
GSN	gelsolin	-4.68	0.0380	Cluster 1	-0.5285	-0.4589	-0.5345	1.1623	0.6463	-0.2867
ASTN2	astrotactin 2	3.34	0.0011	Cluster 2	0.5404	0.4804	0.5631	-0.5166	-0.5799	-0.4874
CIZ1	CDKN1A interacting zinc finger protein 1	-4.19	0.0319	Cluster 1	-0.5359	-0.5601	-0.4758	0.5014	0.4278	0.6426
HERC4	HECT and RLD domain containing E3 ubiquitin protein ligase 4	-3.77	0.0486	Cluster 1	-0.6838	-0.2225	-0.6902	0.8891	0.0668	0.6407
RPS3	ribosomal protein S3	-3.92	0.0141	Cluster 1	-0.2888	-0.9403	-0.5775	0.5743	0.5056	0.7266
HYOU1	hypoxia up-regulated 1	-5.76	0.0255	Cluster 1	-0.5483	-0.5759	-0.5547	1.4809	0.1687	0.0293
ALDOA	aldolase, fructose-bisphosphate A	-3.33	0.0154	Cluster 1	-0.3993	-0.7260	-0.3660	0.6779	0.4743	0.3390
FAM124A	family with sequence similarity 124 member A	7.58	0.0166	Cluster 2	-0.0669	1.8600	-0.0751	-0.4608	-0.6739	-0.5832
DLG2	discs large MAGUK scaffold protein 2	7.87	0.0118	Cluster 2	-0.0887	2.0046	-0.0971	-0.4843	-0.7159	-0.6185
CCT5	chaperonin containing TCP1 subunit 5	-5.07	0.0220	Cluster 1	-0.5623	-0.5873	-0.5681	0.4383	0.6537	0.6257
SLC7A11	solute carrier family 7 member 11	-6.00	0.0226	Cluster 1	-0.5591	-0.5871	-0.5656	-0.1323	1.5768	0.2673

AKAP6	A-kinase anchoring protein 6	6.28	0.0419	Cluster 2	-0.0966	1.5622	-0.1046	-0.5451	-0.2562	-0.5597
NUBPL	NUBP iron-sulfur cluster assembly factor, mitochondrial	6.66	0.0021	Cluster 2	0.6022	1.6404	0.0687	-0.8113	-0.5740	-0.9261
PTPN14	protein tyrosine phosphatase non-receptor type 14	-2.63	0.0364	Cluster 1	-0.3394	-0.3120	-0.5380	0.2723	0.4199	0.4972
NRSN1	neurensin 1	2.87	0.0020	Cluster 2	0.4153	0.4554	0.5745	-0.3535	-0.5145	-0.5772
CWC27	CWC27 spliceosome associated cyclophilin	3.03	0.0398	Cluster 2	0.6371	0.6947	0.2238	-0.1229	-0.4114	-1.0213
AHCTF1	AT-hook containing transcription factor 1	-5.60	0.0220	Cluster 1	-0.4597	-0.6425	-0.6201	-0.3714	0.5032	1.5905
TRIP12	thyroid hormone receptor interactor 12	-4.66	0.0389	Cluster 1	-0.5010	-0.5243	-0.5064	0.6522	0.5822	0.2972
PRKCA	protein kinase C alpha	-5.18	0.0494	Cluster 1	-0.4646	-0.4912	-0.4719	-0.4331	1.3617	0.4991
LARP1	La ribonucleoprotein 1, translational regulator	-4.94	0.0007	Cluster 1	-0.6239	-0.7165	-0.8477	0.8120	0.5890	0.7872
NUP205	nucleoporin 205	-4.39	0.0464	Cluster 1	-0.3760	-0.5658	-0.5468	0.7013	0.0193	0.7681
PDIA4	protein disulfide isomerase family A member 4	-5.07	0.0216	Cluster 1	-0.5646	-0.5897	-0.5705	0.6129	0.5979	0.5140
RPL30	ribosomal protein L30	-4.66	0.0187	Cluster 1	-0.4809	-0.6725	-0.6518	0.4268	0.6131	0.7652
EEF1A1	eukaryotic translation elongation factor 1 alpha 1	-4.65	0.0000	Cluster 1	-0.8409	-0.6066	-0.8258	0.9026	0.7513	0.6194
HKDC1	hexokinase domain containing 1	-4.93	0.0416	Cluster 1	-0.3346	-0.5958	-0.5749	-0.1524	1.3272	0.3306
FRRS1	ferric chelate reductase 1	3.77	0.0120	Cluster 2	0.3300	0.7122	0.6975	-0.7747	-0.7590	-0.2060
EIF4A2	eukaryotic translation initiation factor 4A2	-3.28	0.0052	Cluster 1	-0.4106	-0.6793	-0.4543	0.7609	0.5940	0.1893
SMG1	SMG1 nonsense mediated mRNA decay associated PI3K related kinase	-4.84	0.0001	Cluster 1	-1.0304	-0.7008	-0.5123	0.5263	0.9332	0.7839
CACNA1D	calcium voltage-gated channel subunit alpha1 D	4.54	0.0121	Cluster 2	0.5018	0.5608	1.0195	-1.0285	-0.1928	-0.8607
PALM2AKAP2	PALM2 and AKAP2 fusion	-7.78	0.0000	Cluster 1	-0.8556	-1.1870	-0.8628	1.1890	0.8775	0.8388
B4GALT5	beta-1,4-galactosyltransferase 5	-4.74	0.0465	Cluster 1	-0.4852	-0.5089	-0.4907	0.9391	0.5267	0.0190

ZSCAN12	zinc finger and SCAN domain containing 12	4.33	0.0058	Cluster 2	-0.1499	1.0198	0.7661	-0.4740	-0.6618	-0.5002
TAGLN2	transgelin 2	-4.40	0.0339	Cluster 1	-0.4443	-0.5682	-0.5496	0.5547	0.5011	0.5063
EDA	ectodysplasin A	7.54	0.0117	Cluster 2	-0.2277	-0.2639	2.5284	-0.1865	-0.8846	-0.9657
STC1	stanniocalcin 1	-6.35	0.0022	Cluster 1	-0.7884	-0.7683	-0.7956	1.2619	1.0305	0.0600
RUNX1	RUNX family transcription factor 1	-5.17	0.0255	Cluster 1	-0.5627	-0.5895	-0.5196	1.1280	0.8005	-0.2567
HK2	hexokinase 2	-4.44	0.0339	Cluster 1	-0.2411	-0.7525	-0.7306	1.0762	0.3874	0.2605
ICOSLG	inducible T cell costimulator ligand	2.90	0.0215	Cluster 2	0.5742	0.5452	0.1321	-0.3477	-0.4549	-0.4488
ZNF208	zinc finger protein 208	5.86	0.0358	Cluster 2	-0.1338	-0.1681	1.5894	-0.4511	-0.2344	-0.6019
LMNA	lamin A/C	-3.66	0.0220	Cluster 1	-0.4101	-0.3891	-0.8146	0.5556	0.5444	0.5138
RPL8	ribosomal protein L8	-3.96	0.0255	Cluster 1	-0.8244	-0.1727	-0.8311	0.6258	0.6569	0.5455
ZNF385A	zinc finger protein 385A	4.34	0.0021	Cluster 2	0.6541	0.7673	0.5859	-0.8089	-0.3005	-0.8978
EIF4A1	eukaryotic translation initiation factor 4A1	-4.28	0.0023	Cluster 1	-0.5440	-0.4228	-1.0257	0.6307	0.7788	0.5830
AK4	adenylate kinase 4	-4.69	0.0481	Cluster 1	-0.4831	-0.5066	-0.4886	-0.0208	0.7153	0.7838
JAK1	Janus kinase 1	-4.63	0.0464	Cluster 1	-0.5120	-0.4121	-0.5179	-0.1175	0.4082	1.1513
MYSM1	Myb like, SWIRM and MPN domains 1	6.21	0.0021	Cluster 2	1.4077	-0.5872	1.4707	-0.6748	-0.5081	-1.1083
CAPN2	calpain 2	-5.50	0.0117	Cluster 1	-0.8165	-0.8465	-0.4244	0.2101	0.5498	1.3275
WDR26	WD repeat domain 26	-4.73	0.0364	Cluster 1	-0.5096	-0.5332	-0.5151	0.3225	0.7448	0.4907
REL	REL proto-oncogene, NF-KB subunit	4.14	0.0249	Cluster 2	0.3127	1.2765	-0.1295	-0.5461	-0.2259	-0.6878
MEMO1	mediator of cell motility 1	5.87	0.0373	Cluster 2	-0.1241	-0.1589	1.7625	-0.6172	-0.6954	-0.1668
SSR2	signal sequence receptor subunit 2	-4.72	0.0481	Cluster 1	-0.4828	-0.5064	-0.4883	-0.0723	0.7480	0.8018
CIP2A	cellular inhibitor of PP2A	-4.94	0.0335	Cluster 1	-0.3423	-0.7526	-0.3080	0.2006	1.1933	0.0089

WDFY3	WD repeat and FYVE domain containing 3	-5.07	0.0319	Cluster 1	-0.4560	-0.5910	-0.5704	1.1835	-0.2658	0.6998
RPL9	ribosomal protein L9	-4.90	0.0263	Cluster 1	-0.5396	-0.5640	-0.5453	0.4667	0.5566	0.6256
FANCD2OS	FANCD2 opposite strand	6.40	0.0179	Cluster 2	0.6948	1.3292	-0.2214	-0.6374	-0.5141	-0.6510
SENP2	SUMO specific peptidase 2	-4.57	0.0216	Cluster 1	-0.7119	-0.3012	-0.6652	-0.4193	0.8374	1.2602
TKT	transketolase	-3.92	0.0405	Cluster 1	-0.1213	-0.7819	-0.7604	0.7158	0.5822	0.3657
UBXN7	UBX domain protein 7	-4.48	0.0413	Cluster 1	-0.5229	-0.4404	-0.5285	0.4423	0.9301	0.1195
ANXA5	annexin A5	-6.58	0.0015	Cluster 1	-0.7737	-0.8032	-0.7806	0.9605	0.7905	0.6065
RHOBTB3	Rho related BTB domain containing 3	-3.56	0.0176	Cluster 1	-0.4889	-0.3755	-0.6513	0.5760	0.5907	0.3490
BRI3	brain protein I3	-4.21	0.0044	Cluster 1	-0.6242	-0.3599	-0.8820	0.8399	0.6892	0.3370
DCAF13	DDB1 and CUL4 associated factor 13	-4.19	0.0179	Cluster 1	-0.6985	-0.6768	-0.2894	0.2844	0.5199	0.8604
GEM	GTP binding protein overexpressed in skeletal muscle	-4.93	0.0255	Cluster 1	-0.5430	-0.5675	-0.5487	0.6382	0.6193	0.4015
HNRNPK	heterogeneous nuclear ribonucleoprotein K	-6.52	0.0008	Cluster 1	-0.7525	-0.7822	-0.8935	1.0040	0.9443	0.4798
MID1IP1	MID1 interacting protein 1	-4.92	0.0241	Cluster 1	-0.6519	-0.4369	-0.4183	0.1075	0.8558	0.5437
ATP7A	ATPase copper transporting alpha	3.97	0.0048	Cluster 2	0.9650	0.5342	0.2027	-0.5593	-0.4727	-0.6698
VCP	valosin containing protein	-4.85	0.0187	Cluster 1	-0.2621	-0.7771	-0.7555	0.6100	0.6786	0.5060
SUGT1	SGT1 homolog, MIS12 kinetochore complex assembly cochaperone	-4.30	0.0353	Cluster 1	-0.4528	-0.5340	-0.4578	0.3018	0.6195	0.5233
ARF6	ADP ribosylation factor 6	-5.14	0.0207	Cluster 1	-0.5718	-0.5972	-0.5777	0.7411	0.5219	0.4836
RPL27A	ribosomal protein L27a	-4.49	0.0021	Cluster 1	-0.9518	-0.7971	-0.3550	0.4818	0.8867	0.7354
HDGFL3	HDGF like 3	-5.77	0.0331	Cluster 1	-0.1849	-0.5414	-0.6780	-0.9927	0.2041	2.1930
HSP90B1	heat shock protein 90 beta family member 1	-2.58	0.0373	Cluster 1	-0.8182	-0.2174	-0.2627	0.3646	0.5437	0.3899

PPIB	peptidylprolyl isomerase B	-3.63	0.0287	Cluster 1	-0.6774	-0.4660	-0.3449	0.4724	0.4364	0.5795
SNRPD1	small nuclear ribonucleoprotein D1 polypeptide	-4.49	0.0070	Cluster 1	-0.5631	-0.4717	-0.7283	0.7200	0.3838	0.6593
KATNAL2	katanin catalytic subunit A1 like 2	6.07	0.0266	Cluster 2	1.9082	-0.3042	0.2119	-0.1821	-0.8633	-0.7705
RPL13	ribosomal protein L13	-4.98	0.0063	Cluster 1	-0.6957	-0.8236	-0.4781	0.5618	0.7238	0.7118
TUBA1A	tubulin alpha 1a	-4.79	0.0311	Cluster 1	-0.5246	-0.5484	-0.5301	0.4682	0.5080	0.6269
TUBA1C	tubulin alpha 1c	-10.34	0.0000	Cluster 1	-1.3549	-1.0766	-1.5387	1.0163	1.5106	1.4433
AXL	AXL receptor tyrosine kinase	-3.31	0.0116	Cluster 1	-0.3453	-0.4709	-0.7239	0.5682	0.4326	0.5393
HDGFL2	HDGF like 2	-6.12	0.0117	Cluster 1	-0.6859	-0.3885	-0.5963	-0.2183	-0.0922	1.9812
SRRM2	serine/arginine repetitive matrix 2	-2.63	0.0352	Cluster 1	-0.3794	-0.4713	-0.3466	0.5797	0.4589	0.1587
DDB1	damage specific DNA binding protein 1	-3.92	0.0400	Cluster 1	-0.4952	-0.5679	-0.2689	0.0728	0.0857	1.1735
BEST1	bestrophin 1	4.43	0.0024	Cluster 2	0.5878	1.0547	0.5877	-1.0950	-0.3238	-0.8114
FTH1	ferritin heavy chain 1	-3.56	0.0211	Cluster 1	-0.1490	-0.6315	-1.1408	0.6197	0.7785	0.5232
SLC3A2	solute carrier family 3 member 2	-7.68	0.0000	Cluster 1	-1.1795	-0.8476	-0.8241	0.8879	1.1224	0.8411
CTNNB1	catenin beta 1	-5.59	0.0121	Cluster 1	-0.6233	-0.6503	-0.6296	0.9577	0.3659	0.5797
SETD5	SET domain containing 5	-4.05	0.0395	Cluster 1	-0.5689	-0.2260	-0.6086	0.2379	0.8530	0.3125
MAPK1IP1L	mitogen-activated protein kinase 1 interacting protein 1 like	-4.22	0.0492	Cluster 1	-0.3769	-0.5456	-0.5273	0.5165	0.2018	0.7314
DDIT4	DNA damage inducible transcript 4	-4.98	0.0060	Cluster 1	-0.6752	-0.5429	-0.7693	0.7324	0.7079	0.5471
ATXN2L	ataxin 2 like	-4.57	0.0463	Cluster 1	-0.4817	-0.5042	-0.4870	0.2971	0.7705	0.4053
NSG1	neuronal vesicle trafficking associated 1	8.77	0.0025	Cluster 2	-0.1028	-0.1406	2.2631	-0.7229	-0.6015	-0.6953
LRRC28	leucine rich repeat containing 28	2.66	0.0407	Cluster 2	0.4143	0.1200	0.7014	-0.1270	-0.5586	-0.5502

MAT2A	methionine adenosyltransferase 2A	-5.23	0.0179	Cluster 1	-0.5846	-0.6103	-0.5906	0.7682	0.4592	0.5581
HNRNPH1	heterogeneous nuclear ribonucleoprotein H1	-4.21	0.0250	Cluster 1	-0.8475	-0.4725	-0.2969	1.2348	0.3576	0.0244
CPT1C	carnitine palmitoyltransferase 1C	3.31	0.0215	Cluster 2	0.4470	0.4632	0.6911	-0.1475	-0.6374	-0.8164
CXCL8	C-X-C motif chemokine ligand 8	-4.59	0.0411	Cluster 1	-0.4936	-0.5165	-0.4989	0.5953	0.5688	0.3449
CLIC4	chloride intracellular channel 4	-4.50	0.0442	Cluster 1	-0.4845	-0.5070	-0.4898	0.5366	0.4197	0.5249
FASN	fatty acid synthase	-4.87	0.0217	Cluster 1	-0.7182	-0.3342	-0.7247	0.4310	0.4508	0.8953
CHD3	chromodomain helicase DNA binding protein 3	-5.85	0.0021	Cluster 1	-0.6078	-0.8552	-0.6141	0.6001	0.6187	0.8582
YWHAG	tyrosine 3-monooxygenase/tryptophan 5-monooxygenase activation protein gamma	-4.77	0.0217	Cluster 1	-0.6319	-0.4810	-0.6380	0.5618	0.4730	0.7161
TMED10	transmembrane p24 trafficking protein 10	-5.70	0.0281	Cluster 1	-0.5425	-0.5697	-0.5488	0.7912	-0.4850	1.3549
PFKFB3	6-phosphofructo-2-kinase/fructose-2,6-biphosphatase 3	-5.29	0.0333	Cluster 1	-0.5292	-0.5552	-0.5353	0.6776	1.1465	-0.2044
AKAP13	A-kinase anchoring protein 13	-4.91	0.0274	Cluster 1	-0.5379	-0.5623	-0.5436	0.3556	0.6526	0.6356
PGAM1	phosphoglycerate mutase 1	-4.87	0.0189	Cluster 1	-0.5007	-0.6519	-0.6316	0.5140	0.5622	0.7080
KRT19	keratin 19	-5.21	0.0179	Cluster 1	-0.5828	-0.6084	-0.5888	0.5659	0.7249	0.4892
ZNF562	zinc finger protein 562	-4.13	0.0090	Cluster 1	-0.4904	-0.6465	-0.5401	0.3267	0.4146	0.9357
EXOSC10	exosome component 10	-3.56	0.0434	Cluster 1	-0.6498	-0.1622	-0.6818	0.8894	0.3901	0.2142
GTPBP2	GTP binding protein 2	-5.79	0.0025	Cluster 1	-0.7780	-0.6871	-0.6657	0.7104	0.8061	0.6144
PPP1CA	protein phosphatase 1 catalytic subunit alpha	-4.55	0.0435	Cluster 1	-0.4881	-0.5109	-0.4934	0.5342	0.3265	0.6316
HCFC1	host cell factor C1	-4.76	0.0364	Cluster 1	-0.5113	-0.5351	-0.5169	0.6461	0.2254	0.6918
ZMAT3	zinc finger matrin-type 3	5.73	0.0091	Cluster 2	0.9245	1.5763	-0.4853	-0.5939	-1.0258	-0.3958
SNX32	sorting nexin 32	7.36	0.0000	Cluster 2	1.4243	0.3116	1.1008	-0.8995	-0.9065	-1.0308

OXSR1	oxidative stress responsive kinase 1	-4.79	0.0389	Cluster 1	-0.5045	-0.5280	-0.5099	0.8871	0.2780	0.3773
TRMT112	tRNA methyltransferase activator subunit 11-2	-4.70	0.0389	Cluster 1	-0.5025	-0.5260	-0.5080	0.7394	0.5462	0.2508
KDM2A	lysine demethylase 2A	-3.31	0.0389	Cluster 1	-0.4066	-0.2634	-0.7834	0.8317	0.1683	0.4534
EHBP1L1	EH domain binding protein 1 like 1	-4.65	0.0437	Cluster 1	-0.4888	-0.5117	-0.4941	0.2872	0.8228	0.3846
SMARCC1	SWI/SNF related, matrix associated, actin dependent regulator of chromatin subfamily c member 1	-5.44	0.0398	Cluster 1	-0.4843	-0.5104	-0.4903	-0.0309	0.0130	1.5029
NABP1	nucleic acid binding protein 1	-4.76	0.0220	Cluster 1	-0.4984	-0.5219	-0.5964	0.3751	0.7360	0.5056
CHD2	chromodomain helicase DNA binding protein 2	-3.62	0.0236	Cluster 1	-0.8907	-0.1942	-0.5033	0.3081	0.1907	1.0893
EIF1	eukaryotic translation initiation factor 1	-4.77	0.0121	Cluster 1	-0.8110	-0.3753	-0.8177	0.6914	0.6865	0.6261
RNF213	ring finger protein 213	-3.36	0.0255	Cluster 1	-0.8168	-0.3917	-0.3277	0.2924	0.5769	0.6669
ZDHHC24	zinc finger DHHC-type containing 24	5.72	0.0220	Cluster 2	-0.4412	-0.4783	2.3478	-0.6404	-0.1917	-0.5961
MGA	MAX dimerization protein MGA	-4.66	0.0359	Cluster 1	-0.3936	-0.6176	-0.5968	-0.0619	0.5172	1.1527
PRPF8	pre-mRNA processing factor 8	-5.14	0.0220	Cluster 1	-0.5650	-0.5903	-0.5709	0.2911	0.6858	0.7491
RPL4	ribosomal protein L4	-4.97	0.0155	Cluster 1	-0.3313	-0.7706	-0.7490	0.6620	0.5292	0.6596
ZNF266	zinc finger protein 266	5.68	0.0336	Cluster 2	-0.2276	-0.2635	1.8859	-0.2422	-0.4130	-0.7396
RPL15	ribosomal protein L15	-3.59	0.0266	Cluster 1	-0.9921	-0.4204	-0.1639	0.5537	0.5425	0.4802
CTBP2	C-terminal binding protein 2	-4.51	0.0296	Cluster 1	-0.5452	-0.5094	-0.5511	0.9949	0.4487	0.1621
FOSL1	FOS like 1, AP-1 transcription factor subunit	-5.35	0.0013	Cluster 1	-0.4714	-0.8119	-0.9504	0.7087	0.8346	0.6903
LMNB2	lamin B2	-5.20	0.0282	Cluster 1	-0.5459	-0.5716	-0.5518	0.9157	0.7952	-0.0416
TCEANC	transcription elongation factor A N-terminal and central domain containing	5.29	0.0464	Cluster 2	-0.2613	-0.2962	1.9483	-0.7353	-0.3529	-0.3025
TGIF1	TGFB induced factor homeobox 1	-4.05	0.0448	Cluster 1	-0.5459	-0.5703	-0.3775	0.3926	0.3677	0.7334

CAVIN1	caveolae associated protein 1	-3.43	0.0414	Cluster 1	-0.7263	-0.4032	-0.3109	0.5255	0.5629	0.3520
RPLP2	ribosomal protein lateral stalk subunit P2	-3.50	0.0396	Cluster 1	-0.2147	-0.7785	-0.4909	0.6407	0.5688	0.2745
RIC8A	RIC8 guanine nucleotide exchange factor A	-4.08	0.0246	Cluster 1	-0.6253	-0.3445	-0.6164	0.6682	0.7085	0.2096
PDE4DIP	phosphodiesterase 4D interacting protein	-3.73	0.0109	Cluster 1	-0.7403	-0.5928	-0.2506	0.4250	0.5908	0.5680
ZNF713	zinc finger protein 713	3.33	0.0274	Cluster 2	0.6006	0.6857	0.3202	-0.9288	-0.5304	-0.1473
EXD1	exonuclease 3'-5' domain containing 1	5.92	0.0029	Cluster 2	0.6343	0.9860	0.3418	-0.4831	-0.7288	-0.7501
CALR	calreticulin	-2.56	0.0479	Cluster 1	-0.4262	-0.3750	-0.3340	0.4542	0.3770	0.3038
CIITA	class II major histocompatibility complex transactivator	5.11	0.0121	Cluster 2	0.7286	0.0395	1.4153	-0.9071	-0.2479	-1.0283
SMG1P3	SMG1 pseudogene 3	-5.88	0.0052	Cluster 1	-0.6797	-0.7077	-0.6862	0.7406	0.5868	0.7463
PPA1	inorganic pyrophosphatase 1	5.15	0.0437	Cluster 2	-0.5361	-0.5656	2.1925	-0.3902	0.1535	-0.8541
NPLOC4	NPL4 homolog, ubiquitin recognition factor	-4.71	0.0461	Cluster 1	-0.4878	-0.5114	-0.4933	0.1187	0.9169	0.4568
KPNA2	karyopherin subunit alpha 2	-5.99	0.0066	Cluster 1	-0.7123	-0.6671	-0.7193	1.0681	1.2640	-0.2333
GLRX5	glutaredoxin 5	2.80	0.0164	Cluster 2	0.6656	0.4668	0.2219	-0.2572	-0.4328	-0.6643
TTC3	tetratricopeptide repeat domain 3	-5.96	0.0333	Cluster 1	-0.7255	-0.7586	0.0882	-0.9492	-0.4933	2.8385
ANXA2	annexin A2	-3.11	0.0291	Cluster 1	-0.2854	-0.3055	-0.9574	0.5746	0.4880	0.4856
SRPRA	SRP receptor subunit alpha	-4.84	0.0368	Cluster 1	-0.5129	-0.5371	-0.5185	0.8338	0.6026	0.1322
EWSR1	EWS RNA binding protein 1	-5.21	0.0314	Cluster 1	-0.5335	-0.5591	-0.5394	0.2783	1.1448	0.2089
RUVBL2	RuvB like AAA ATPase 2	-6.46	0.0063	Cluster 1	-0.7865	-0.6103	-0.5879	-0.0111	1.7161	0.2798
TANGO2	transport and golgi organization 2 homolog	3.75	0.0043	Cluster 2	0.7645	0.6529	0.2815	-0.5322	-0.7756	-0.3911
ACTG1	actin gamma 1	-6.14	0.0009	Cluster 1	-0.9826	-0.6143	-0.9897	0.9090	0.9845	0.6931

CMSS1	cms1 ribosomal small subunit homolog	4.19	0.0071	Cluster 2	0.7828	0.8647	0.1192	-0.2799	-0.7864	-0.7004
CSF1	colony stimulating factor 1	-4.59	0.0395	Cluster 1	-0.4964	-0.5193	-0.5017	0.4856	0.5433	0.4885
COPB2	COPI coat complex subunit beta 2	-5.73	0.0164	Cluster 1	-0.5733	-0.6435	-0.6215	-0.1002	0.5100	1.4285
XPOT	exportin for tRNA	-4.80	0.0324	Cluster 1	-0.5225	-0.5465	-0.5281	0.3947	0.4794	0.7230
ATL3	atlastin GTPase 3	-4.87	0.0389	Cluster 1	-0.5048	-0.5285	-0.5103	0.8936	0.6099	0.0401
ADSS1	adenylosuccinate synthase 1	6.39	0.0359	Cluster 2	-0.2418	2.3810	-0.2501	-0.7587	-0.8764	-0.2539
P4HB	prolyl 4-hydroxylase subunit beta	-3.71	0.0217	Cluster 1	-0.0910	-0.7048	-0.9394	0.7330	0.7599	0.2423
SLC36A3	solute carrier family 36 member 3	3.14	0.0463	Cluster 2	0.2433	0.8556	0.3864	-0.7686	-0.6739	-0.0427
INSIG1	insulin induced gene 1	-4.44	0.0352	Cluster 1	-0.6542	-0.6809	-0.2554	0.7789	0.4297	0.3820
UBE2H	ubiquitin conjugating enzyme E2 H	-4.91	0.0308	Cluster 1	-0.5308	-0.5552	-0.5365	0.6726	0.2290	0.7210
PTMA	prothymosin alpha	-3.55	0.0252	Cluster 1	-0.2985	-0.6270	-0.5078	0.8613	0.7071	-0.1351
SPRY4	sprouty RTK signaling antagonist 4	-5.66	0.0115	Cluster 1	-0.6330	-0.6604	-0.6394	0.9884	0.5108	0.4335
FANCM	FA complementation group M	2.93	0.0237	Cluster 2	0.3069	0.8135	0.2228	-0.4732	-0.6455	-0.2245
C17orf99	chromosome 17 open reading frame 99	7.24	0.0069	Cluster 2	1.0575	-0.2481	1.1932	-0.6443	-0.7291	-0.6293
HYKK	hydroxylysine kinase	3.51	0.0226	Cluster 2	-0.1527	0.8014	0.7539	-0.7118	-0.3996	-0.2911
ZNF669	zinc finger protein 669	4.06	0.0048	Cluster 2	0.6953	0.5121	0.6817	-0.3393	-0.5912	-0.9585
PEAK3	PEAK family member 3	5.02	0.0187	Cluster 2	1.3772	1.0894	-0.5988	-1.0360	-0.3497	-0.4820
HMGB1	high mobility group box 1	-6.08	0.0036	Cluster 1	-0.6004	-0.6281	-0.8494	0.0602	0.9749	1.0428
SPATS2L	spermatogenesis associated serine rich 2 like	-5.70	0.0113	Cluster 1	-0.5654	-0.7296	-0.5717	-0.1103	0.7659	1.2110
IARS1	isoleucyl-tRNA synthetase 1	-5.49	0.0001	Cluster 1	-0.8426	-0.5888	-1.0154	0.8695	1.1480	0.4292
CD55	CD55 molecule (Cromer blood group)	-4.17	0.0463	Cluster 1	-0.5537	-0.3678	-0.5593	0.5099	0.5985	0.3724

ZNF124	zinc finger protein 124	5.25	0.0208	Cluster 2	1.0799	-0.3606	0.9844	-0.6452	-0.3128	-0.7458
XRCC6	X-ray repair cross complementing 6	-4.85	0.0282	Cluster 1	-0.5327	-0.5568	-0.5383	0.5593	0.4346	0.6338
NCOR2	nuclear receptor corepressor 2	-4.96	0.0246	Cluster 1	-0.5474	-0.5693	-0.5496	0.6597	0.9729	0.0338
MYO18A	myosin XVIIIA	-4.76	0.0220	Cluster 1	-0.5625	-0.5876	-0.5406	0.6195	0.3839	0.6874
MMP1	matrix metallopeptidase 1	-5.88	0.0040	Cluster 1	-0.4322	-0.9032	-0.8803	0.6571	0.5576	1.0010
SRGAP1	SLIT-ROBO Rho GTPase activating protein 1	-5.02	0.0195	Cluster 1	-0.9870	-1.0089	-0.0148	1.3304	-0.5356	1.2160
ZNF470	zinc finger protein 470	5.12	0.0226	Cluster 2	-0.3464	0.5355	1.3943	-0.7619	-0.4030	-0.4185
DYNC1H1	dynein cytoplasmic 1 heavy chain 1	-4.30	0.0000	Cluster 1	-0.6079	-0.6437	-0.8342	0.6283	0.8133	0.6441
PCBP2	poly(rC) binding protein 2	-5.08	0.0215	Cluster 1	-0.5656	-0.5907	-0.5715	0.5180	0.6580	0.5518
SND1	staphylococcal nuclease and tudor domain containing 1	-5.57	0.0142	Cluster 1	-0.6146	-0.6415	-0.6208	0.5949	0.2832	0.9989
DDI2	DNA damage inducible 1 homolog 2	-4.64	0.0437	Cluster 1	-0.5491	-0.3926	-0.5551	1.1462	0.2311	0.1194
LRP10	LDL receptor related protein 10	-5.34	0.0194	Cluster 1	-0.5447	-0.6352	-0.5509	-0.0453	0.5656	1.2105
SPTAN1	spectrin alpha, non-erythrocytic 1	-5.15	0.0070	Cluster 1	-0.5606	-0.8357	-0.5944	0.9790	-0.0466	1.0583
PARVA	parvin alpha	-4.71	0.0358	Cluster 1	-0.5127	-0.4965	-0.5183	-0.0906	0.9419	0.6762
PSAP	prosaposin	-4.45	0.0373	Cluster 1	-0.1301	-0.8024	-0.7798	0.1934	0.3011	1.2179
CCDC180	coiled-coil domain containing 180	5.63	0.0319	Cluster 2	-0.3303	0.5866	1.5499	-0.7626	-0.8532	-0.1904
MYO1C	myosin IC	-5.30	0.0234	Cluster 1	-0.6581	-0.6867	-0.4369	-0.1467	0.7481	1.1803
PLCG2	phospholipase C gamma 2	-2.97	0.0009	Cluster 1	-0.5172	-0.5152	-0.4469	0.4510	0.5671	0.4612
S100A6	S100 calcium binding protein A6	-3.36	0.0217	Cluster 1	-0.5678	-0.6088	-0.3190	0.5936	0.5964	0.3056
RPL12	ribosomal protein L12	-5.93	0.0052	Cluster 1	-0.6853	-0.7134	-0.6919	0.6590	0.5890	0.8427
RPS4X	ribosomal protein S4 X-linked	-4.18	0.0234	Cluster 1	-0.3838	-0.5020	-0.7984	0.4917	0.7058	0.4867

ZNF273	zinc finger protein 273	3.82	0.0063	Cluster 2	0.2564	0.2985	0.9965	-0.5258	-0.5651	-0.4606
ASPH	aspartate beta-hydroxylase	-4.76	0.0354	Cluster 1	-0.5143	-0.5380	-0.5198	0.5920	0.2870	0.6931
OGA	O-GlcNAcase	-4.59	0.0220	Cluster 1	-0.6588	-0.6859	-0.4402	0.7406	0.7181	0.3262
TXNRD1	thioredoxin reductase 1	-4.15	0.0121	Cluster 1	-0.5920	-0.9520	-0.2951	0.6940	0.6338	0.5113
CALM1	calmodulin 1	-5.11	0.0220	Cluster 1	-0.5612	-0.5875	-0.5603	0.5355	0.0735	1.1000
IPO9	importin 9	-4.71	0.0248	Cluster 1	-0.5057	-0.5073	-0.6075	-0.2118	0.8776	0.9548
COX2	cytochrome c oxidase subunit II	-2.57	0.0386	Cluster 1	-0.2086	-0.4307	-0.5436	0.0327	0.4638	0.6865
CDC42BPB	CDC42 binding protein kinase beta	-5.02	0.0358	Cluster 1	-0.5177	-0.5421	-0.5234	-0.0281	0.9378	0.6735
RPL10A	ribosomal protein L10a	-5.88	0.0055	Cluster 1	-0.6783	-0.7062	-0.6848	0.8247	0.6904	0.5541
ND1	NADH dehydrogenase subunit 1	-3.41	0.0082	Cluster 1	-0.4907	-0.4364	-0.6325	0.2801	0.5335	0.7460
TGM2	transglutaminase 2	-5.25	0.0169	Cluster 1	-0.5886	-0.6143	-0.5946	0.7173	0.5744	0.5058
NA	NA	-3.59	0.0240	Cluster 1	-0.8624	-0.5881	-0.2102	0.6229	0.4672	0.5704
NA	NA	-2.18	0.0364	Cluster 1	-0.4283	-0.4648	-0.1820	0.4008	0.5688	0.1054
NA	NA	2.34	0.0407	Cluster 2	0.5471	0.1219	0.4138	-0.4568	-0.2218	-0.4042
RNA5SP149	RNA, 5S ribosomal pseudogene 149	2.63	0.0220	Cluster 2	0.5101	0.1633	0.6553	-0.3773	-0.2202	-0.7312
BMPR2	bone morphogenetic protein receptor type 2	6.86	0.0000	Cluster 2	0.7576	0.9994	1.2746	-0.9557	-1.2044	-0.8716
MSH5	mutS homolog 5	4.19	0.0494	Cluster 2	0.6284	1.2644	-0.4744	-0.2179	-0.3261	-0.8744
ZNF814	zinc finger protein 814	3.64	0.0282	Cluster 2	0.7343	0.5766	0.6618	-0.3627	-0.3180	-1.2919
RACK1	receptor for activated C kinase 1	-5.12	0.0053	Cluster 1	-0.8630	-0.8021	-0.3338	0.4079	0.9197	0.6713
SNX2	sorting nexin 2	-6.49	0.0246	Cluster 1	-0.3888	-0.6972	-0.3973	0.1372	2.4177	-1.0716
IPO7	importin 7	-6.63	0.0018	Cluster 1	-0.9226	-0.6868	-0.6643	1.4146	0.3426	0.5167

TMSB4X	thymosin beta 4 X-linked	-3.60	0.0116	Cluster 1	-0.2582	-0.7341	-0.7033	0.6891	0.5112	0.4952
MFSD2B	major facilitator superfamily domain containing 2B	4.81	0.0353	Cluster 2	0.1027	1.2933	0.3743	-0.7906	-0.1752	-0.8045
ARL2	ADP ribosylation factor like GTPase 2	-4.85	0.0170	Cluster 1	-0.5397	-0.6137	-0.5455	0.4868	0.5575	0.6546
VDAC1	voltage dependent anion channel 1	-4.79	0.0325	Cluster 1	-0.5216	-0.5455	-0.5272	0.4322	0.4631	0.6989
FOXI3	forkhead box I3	5.94	0.0274	Cluster 2	1.2857	-0.2770	0.6797	-0.6509	-0.3735	-0.6640
HNRNPUL2	heterogeneous nuclear ribonucleoprotein U like 2	-4.43	0.0481	Cluster 1	-0.4744	-0.4966	-0.4796	0.4116	0.5061	0.5330
CSKMT	citrate synthase lysine methyltransferase	-5.19	0.0216	Cluster 1	-0.5707	-0.5963	-0.5767	0.2866	0.6516	0.8054
FNIP1	folliculin interacting protein 1	-5.18	0.0108	Cluster 1	-0.5850	-0.6660	-0.5911	0.3694	0.7787	0.6940
NA	NA	4.27	0.0000	Cluster 2	0.6799	0.6596	0.8133	-0.5100	-0.8026	-0.8403
ARL17A	ADP ribosylation factor like GTPase 17A	2.96	0.0155	Cluster 2	0.6684	0.5319	0.1176	-0.3218	-0.4830	-0.5130
SHISA9	shisa family member 9	2.63	0.0335	Cluster 2	0.4117	0.3526	0.5340	-0.1649	-0.4222	-0.7113
EIF6	eukaryotic translation initiation factor 6	-4.66	0.0397	Cluster 1	-0.4990	-0.5223	-0.5045	0.3776	0.3991	0.7491
APOBEC3D	apolipoprotein B mRNA editing enzyme catalytic subunit 3D	3.93	0.0456	Cluster 2	0.1744	0.7997	0.4384	-0.3135	-0.7815	-0.3175
UBE2V1	ubiquitin conjugating enzyme E2 V1	-4.73	0.0413	Cluster 1	-0.4969	-0.5202	-0.5023	0.7858	0.1158	0.6178
NA	NA	8.83	0.0011	Cluster 2	1.4713	1.4853	-0.3654	-0.8221	-0.9294	-0.8396
RNA5-8SP6	RNA, 5.8S ribosomal pseudogene 6	-4.18	0.0000	Cluster 1	-0.6398	-0.8896	-0.5289	0.8838	0.8132	0.3614
EEF1G	eukaryotic translation elongation factor 1 gamma	-7.30	0.0002	Cluster 1	-0.8763	-0.9067	-0.8834	0.9837	0.9046	0.7780
ZBED6	zinc finger BED-type containing 6	-4.71	0.0400	Cluster 1	-0.4998	-0.5233	-0.5052	0.1895	0.5781	0.7607
CCPG1	cell cycle progression 1	4.37	0.0040	Cluster 2	0.6797	0.3837	0.6662	-0.4763	-0.5517	-0.7016
RPL17	ribosomal protein L17	-4.18	0.0463	Cluster 1	-0.5600	-0.3617	-0.5657	0.5186	0.3502	0.6185

TXNIP	thioredoxin interacting protein	-6.79	0.0008	Cluster 1	-0.8075	-0.8374	-0.8145	0.8059	0.7974	0.8560
NBPF15	NBPF member 15	-5.05	0.0238	Cluster 1	-0.5553	-0.5803	-0.5611	0.5899	0.7478	0.3590
NA	NA	8.81	0.0000	Cluster 2	0.9414	0.7267	1.1913	-0.9166	-1.0104	-0.9323
MAGIX	MAGI family member, X-linked	6.14	0.0271	Cluster 2	-0.2002	-0.2364	2.0097	-0.6796	-0.1656	-0.7279
LOC122539214	Zinc finger protein LOC122539214	-4.96	0.0241	Cluster 1	-0.5500	-0.5746	-0.5557	0.5727	0.6051	0.5026
NUDT3	nudix hydrolase 3	-4.57	0.0411	Cluster 1	-0.4927	-0.5155	-0.4980	0.4790	0.4264	0.6010
NA	NA	4.04	0.0405	Cluster 2	0.9057	0.0560	0.4400	-0.7138	-0.2560	-0.4318
MARCKS	myristoylated alanine rich protein kinase C substrate	-3.66	0.0155	Cluster 1	-0.3526	-0.6057	-0.5910	0.8310	0.4940	0.2243
GRAMD4P3	GRAM domain containing 4 pseudogene 3	8.02	0.0041	Cluster 2	-0.2671	1.1505	1.3400	-0.7055	-0.7972	-0.7206
PRRC2B	proline rich coiled-coil 2B	-5.66	0.0100	Cluster 1	-0.6397	-0.6671	-0.6461	0.9179	0.5990	0.4359
H2AC19	H2A clustered histone 19	-4.66	0.0380	Cluster 1	-0.5033	-0.5266	-0.5087	0.6309	0.5693	0.3386

Results are shown as fold changes (FC). The *p*-values come from the comparison using EV_NE as reference. DEGs (differential expressed genes) and EGCG (epigallocatechin-3-gallate). EV samples obtained from cells cultured with EGCG in normoxia (EV_NE) or hypoxia (EV_HE).

CHAPTER V

GENERAL DISCUSSION

Adipose tissue is more than an energy reservoir; it is a secretory gland that regulates several metabolic pathways and it is one of the main components of the breast (Perez *et al.*, 2016). During the development of obesity, this tissue expands, and adipocytes hypertrophy with an altered pro-inflammatory secretion profile (Pischon and Nimptsch, 2016). It has been reported that it contributes to BC progression through the secretion of FFA (Madak-Erdogan *et al.*, 2019), adipokines and pro-inflammatory cytokines (Avgerinos *et al.*, 2019). Furthermore, adipose tissue serves as a donor of CAF resulting from the differentiation of resident mesenchymal stem cells (Bertolini *et al.*, 2015), and of CAA originating from adipocytes that undergo a dedifferentiation process (Bochet *et al.*, 2013). However, the molecular mechanisms involved in these processes and their impact on tumor development and resistance still need to be fully elucidated. In our study we demonstrated that, besides mature adipocytes, committed preadipocytes (ADMSC) can acquire a CAA-like phenotype, and this can be mediated by soluble factors and EV secreted by the cancer cells. Whether this is a transitional state toward the acquisition of a CAF final phenotype needs to be further addressed. Nevertheless, we are providing insights with our study toward the bidirectional mechanisms of collaboration between the components within the adipose tissue and BC cell development. Therefore, we addressed not only the gap of knowledge in this area but also the contribution of diet-derived polyphenols, like EGCG, in preventing cancer progression by targeting several pathways involved in BC-adipose tissue cooperation. This catechin has anti-inflammatory (Mokra *et al.*, 2022; Nomura *et al.*, 2000), anti-adipogenic (Li *et al.*, 2013), and anti-tumoral (Rady, 2018) effects, which make it a suitable candidate for targeting obesity-associated comorbidities. We confirmed in our experimental conditions that EGCG inhibited adipogenesis by

reducing the expression of adipogenic markers and the proper formation of lipid droplets, in agreement with previously reported data (Kim *et al.*, 2010).

We started by understanding how the secreted factors (secretome) originating from different cellular components of the adipose tissue affected the behavior of tumor cells. Then, we found differences in the composition of the pro-inflammatory genetic profile from ADMSC and adipocytes. The immature phenotype was characterized by a high expression of genes like *IL-6*, *CCL2* and *EGF*; while in adipocytes, *CCL5*, *BCL2*, *IL-1B* and *IGF-1* were among the most upregulated genes. The secretome of both ADMSC and adipocytes, showed chemoattractant capacity in the selected TNBC cell line model, but the secretome of mature adipocytes induced the greatest invasive response. This enhanced chemoattractant effect of the adipocyte secretome was later confirmed using a panel of TNBC, suggesting a global impact on this aggressive subtype. Nevertheless, expanding the study to different BC subtypes will be of interest. Also, it is important to mention that the secretomes were collected from cells cultured without pro-inflammatory or tumor-induced stimulations. Therefore, co-culturing ADMSC and adipocytes with tumor cells or proinflammatory cytokines may impact on their secretory profiles and should be addressed further.

The EGCG-mediated reduction of STAT3 activation appears to be essential to decrease the chemoattractant and proangiogenic potential of the adipocyte secretome. I believe it will be relevant to identify the soluble factors secreted by the mature adipocytes that activate the STAT3-mediated migratory response of the TNBC cell lines. Intriguingly, EGCG showed a selective targeting toward STAT3 in the MDA-MB-231 because it could not prevent the AKT induction. Previous studies have reported contradictory results regarding the capacity of EGCG to regulate the AKT pathway and have been related to the concentration used and the cell line model (Liu *et al.*, 2013). This suggests that even though EGCG has a broad mechanism of action, its molecular targets appear to change according to the cell model investigated.

The IL-6/JAK/STAT3 oncogenic signaling axis has been reported to mediate BC progression by promoting cell proliferation, metastasis, and apoptosis inhibition (Manore *et al.*, 2022; Siersbaek *et al.*, 2020). In BC patients, high circulating IL-6 levels have been associated with poor prognosis (Salgado *et al.*, 2003). Studies have revealed that the STAT3/IL-6 axis has a pro-oncogenic role by upregulating the expression of BCL2 (Real *et al.*, 2002), cyclin D1 (Leslie *et al.*, 2006), c-MYC and metalloproteinases (Hsieh *et al.*, 2005; Zhang *et al.*, 2015). Besides, other EMT markers, such as TWIST and SNAIL, are upregulated in BC cells upon STAT3 activation (Lo *et al.*, 2007; Saitoh *et al.*, 2016). Also, IL-6 impacts the TME by enriching cancer stem cell populations (Sansone *et al.*, 2007) and driving macrophage polarization toward the M2 phenotype (Weng *et al.*, 2019), which increases tumor aggressiveness. Remarkably, this cytokine was upregulated in ADMSC cultured without stimulation and also detected in high levels within the MDA-MB-231 secretome, where it demonstrated a capacity to recruit ADMSC into the TME. More importantly, our study found that IL-6 upregulation is a node that interconnects several intracellular pathways involved in the ADMSC response to the TNBC secretome, such as NF-KB, HIF-1, AGE-RAGE, TNF, and insulin resistance. The AGE-RAGE pathway is essential in diabetes complications and inflammation, increasing oxidative stress and NF-KB activation (Korwar *et al.*, 2012). Besides, it has been proposed to mediate carcinogenesis development in breast cancers by activating pro-tumoral pathways such as VEGF-mediated migration, ERK1/2, STAT3, P38/MAPK and MMP9 (Ishibashi *et al.*, 2012; Sharaf *et al.*, 2015). Taken together, our results emphasize the role of IL-6 as a molecular mediator between BC and adipose tissue crosstalk. In addition, the cellular source of IL-6 also regulates adipose tissue inflammation; when derived from adipocytes it induces macrophage infiltration, while when secreted by myeloid cells it inhibits this process (Han *et al.*, 2020). In the context of obesity, adipocytes become an important source for the pro-inflammatory role of IL-6, contributing to the chemoresistance of anti-VEGF therapies in BC patients (Incio *et*

al., 2018). This highlights the inhibitory effect observed for EGCG over the cytokine expression and associated signalling pathways.

On the other hand, the acquisition of a CAA phenotype by the adipocytes present within the invasive front of the BC has been linked to a process of dedifferentiation defined by the reduction of differentiated terminal markers (PARPG, C/EBPG and FABP4) (Rybinska *et al.*, 2020). In this process, adipocytes acquire an activated phenotype characterized by delipidation and the expression of proinflammatory molecules such as IL-6, IL-8/CXCL8, IL-1B, TNFA, CCL2 and CCL5 (Dirat *et al.*, 2011; Rybinska *et al.*, 2021). The cues that trigger this process have yet to be fully understood. Nevertheless, tumor-secreted soluble factors have been described to mediate this process (Bennett *et al.*, 2002; Bochet *et al.*, 2013; Chirumbolo et Bjorklund, 2016; de Winter et Nusse, 2021; Gustafson et Smith, 2010).We demonstrate that, in addition to adipocytes, ADMSC can also be turned into a CAA-like phenotype in response to the secretome of the TNBC cell line MDA-MB-231. Moreover, the induction of the CAA markers IL-6, CCL5, CCL2, COX2 and IL-1B was partially sustained by SNAIL activation; an EMT marker specifically triggered in the ADMSC in response to the TNBC secretome. Identifying the factors responsible for SNAIL induction will require further assessments. Nevertheless, our findings are relevant, especially in obesity, where the adipose tissues are an abundant source of ADMSC and fully mature adipocytes.

Importantly, recent studies have suggested that the fibroblast-like cells observed at high density in the solid tumor center are derived from dedifferentiated adipocytes (Bochet *et al.*, 2013). In addition, we demonstrated that ADMSC can be reshaped and recruited by tumors in response to soluble factors like IL-6. Besides, most of the studied pathways responsible for the emergence of CAA have been selected based on their role in physiological adipogenesis. However, aberrant signaling can be implied in this phenomenon. We observed the activation of NF-kB and SMAD2 within the ADMSC, in response to the TNBC secretome enriched especially with IL-6 and VEGF. Both

cytokines have been found in high circulating levels in BC patients, associated with advanced tumor stages, and low survival mainly in the HER2- cancer subtypes (Raghunathachar Sahana *et al.*, 2017; Tawara *et al.*, 2019).

EGCG had a potent inhibitory effect on the induction of SNAIL, CAA-associated markers, pro-inflammatory cytokines and pathways, and migration of the ADMSC. This catechin has a broad mechanism of action that goes from impeding receptor signaling by acting as an antagonist (Sicard *et al.*, 2021) or disturbing membrane lipid rafts (Patra *et al.*, 2008) to receptor-mediated signaling activation (Yamada *et al.*, 2016) through passive diffusion into the cytoplasm (Hong *et al.*, 2002). Further studies are needed to clarify the molecular interplays used by EGCG and the concentration range required for its inhibitory effect in our *in vitro* experimental conditions.

Other mechanisms proposed to mediate CAA phenotypes are molecules and mRNAs delivered by BC-secreted EV (Rybinska *et al.*, 2021). The role of EV in cell-to-cell communication has become relevant in the context of cancer and its paracrine regulation of the TME and distant tissues. Exosomes derived from the tumor and associated cellular stroma have been reported to precondition the metastatic niche and determine metastatic organotropism (Becker *et al.*, 2016; Kong *et al.*, 2019; Nogues *et al.*, 2018). For example, it has been reported that EV secreted by BC-associated CAF activate the Wnt pathway in BC cells, promoting their motility (Luga *et al.*, 2012). In the other sense, BC-derived exosomes switched ADMSC into a myofibroblastic phenotype by activating the TGF-B/SMAD2 pathway, inducing the expression of pro-tumoral factors like TGF-B, VEGF and CCL5 (Cho *et al.*, 2012). Also, it has been reported that EV derived from hepatocarcinoma cells induced an inflammatory phenotype in adipocytes by activating the NF-kB signaling pathway (Wang *et al.*, 2018a). Our results agree with these findings since both pathways were induced in the ADMSC in response to the MDA-MB-231 secretome, however when the EV fraction was isolated and used, the pathways induced were AKT and GSK-3B.

Another group documented that adipocytes pre-incubated with tumoral-derived EV promote tumors of a larger size, macrophage infiltration and angiogenesis in a xenograft mice model (Wang *et al.*, 2018a). However, few studies have covered the specific interaction between adipocytes or preadipocytes and BC tumor cells (Wang *et al.*, 2019a). Therefore, we focused on the contribution of TNBC-derived EV in the acquisition of a pro-inflammatory and CAA-like phenotype by the ADMSC. We observed that TNBC-derived EV could bind with the ADMSC, altering their behaviour for a more pro-migratory and pro-inflammatory phenotype. Besides, we found that TNBC-derived EV activate signaling pathways such as CHK-2, c-Jun, AKT and GSK-3β, increasing the expression of some CAA markers (CCL2, CCL5 and IL-1B). Further studies must be conducted to identify whether the EV stimulate the cells by activating receptors and/or releasing their content within the ADMSC. Moreover, an extended protein validation of the inflammatory and CAA markers will be an asset for the study. Nevertheless, we provided evidence that BC cell secreted EV could trigger a CAA phenotype-like within the ADMSC.

To prevent EV-mediated cell-to-cell communication is an attractive strategy to avoid cancer progression, and studies targeting EV biogenesis and release have been conducted in adjuvant therapies (Chalmin *et al.*, 2010; Marleau *et al.*, 2012). Nevertheless, none of these studies have reached clinical trials, mainly due to a lack of knowledge on how to discriminate between EV derived from tumor or normal cells, and concerns about cytotoxicity risks. Therefore, we considered evaluating the chemopreventive effect of a natural, non-toxic polyphenol like EGCG with a broad mechanism of action. However, its impact in altering the cargo of tumor-derived EV and their paracrine regulation of ADMSC has yet to be addressed. In addition to protein interchange, most studies have focused on the EV-mediated regulation of microRNAs expression (Pan *et al.*, 2020; Wei *et al.*, 2014). However, we aimed to start characterizing the mRNA content altered by EGCG within the EV and later complemented the study with proteomic and microRNA characterization.

Our analysis showed that most identified genes in the EV obtained from EGCG-treated TNBC were involved in oxidative stress and mitophagy pathways. Also, ADMSC treated with these vesicles showed a less activated state of the AKT and GSK-3β pathways, which regulate biological processes like adipogenesis (Park *et al.*, 2012) and EMT (Zhang *et al.*, 2021), among others. Despite reducing the induction of most pro-inflammatory and CAA markers, these vesicles triggered the expression of IL-6 and CXCL8/IL-8. A study quantifying the serum levels of both cytokines in patients with BC ductal carcinoma showed their increased level in comparison to healthy controls (Ma *et al.*, 2017). The high levels of IL-6 and CXCL-8/IL-8 correlated with advanced stages of the malignancy (II and III), lymph node metastasis and the expression of ER and HER2 (Ma *et al.*, 2017). Regarding these antigen expressions, they observed a correlation between high levels of IL-6 with ER+ or HER2- tumors and the opposite with higher CXCL-8 levels and no direct correlation between both cytokines was found (Ma *et al.*, 2017). However, whether the cytokines contributed to the tumor progression or resulted from an advanced tumor remains unclear.

Genes related to senescence mechanisms were enriched within the EV and the occurrence of this biological process was subsequently detected in ADMSC cultured under nutrient deprivation and EV. This is a cell program used to switch into a non-proliferative but metabolic active survival state (Hayflick et Moorhead, 1961). A senescent cell can resume proliferation when favourable conditions emerge, hence associated with cancer chemoresistance (Guillon *et al.*, 2019). They are characterized by cell cycle arrest (overexpression of the inhibitors CDKN2A and P21), apoptosis resistance and increased lysosomal activity, expressing high levels of the lysosomal enzyme β-galactosidase (β-gal) (Wang *et al.*, 2022). Senescent cells secrete pro-inflammatory mediators that contribute to tumor growth and progression (Wang *et al.*, 2022), and several studies describe the pro-tumoral role of senescence linked to inflammation and immunosuppression (Pribluda *et al.*, 2013; Ruhland et Alspach, 2021). Obesity increases inflammation mediated by cellular senescence and tissue

dysfunction. (Escande *et al.*, 2015). *In vivo* experiments have revealed that obese mice have an elevated number of senescent cells, that correlates with highly proliferative and poorly immunogenic tumors (Fournier *et al.*, 2023). Activation of senescence has been associated with tumor-derived EV-mediated stimulation of AKT and P38/MAPK pathways, resulting in endoplasmic reticulum stress and chronic DNA damage (Guo *et al.*, 2009; Ruhland *et al.*, 2016a). Remarkably, the EV obtained from EGCG-treated MDA-MB-231 decreased senescence markers. These results suggest the capacity of EGCG-EV to protect the ADMSC from oxidative stress damage. Hence, our findings highlight the indirect effects of EGCG in preventing the acquisition of a senescent phenotype by the ADMSC. Whether this results from more apoptosis induction by the EGCG-EV or restoring an average cell cycle proliferation rate remains to be confirmed.

Mitochondrial dysfunction is another senescence signature hallmark (Wang *et al.*, 2022). Mitochondrial transfer can trigger an inflammatory response in cells (Boudreau *et al.*, 2014), and some mitochondrial components, like DNA, mediate increasing tumor aggressiveness (Takenaga *et al.*, 2021). Cancer cells import these organelles from non-malignant cells through mechanisms including cell-cell fusion, tunneling nanotubes, and gap junctions (Zampieri *et al.*, 2021). Also, it has been reported that EV containing mitochondrial DNA or proteins can trigger an inflammatory response, acting as damage-associated molecular patterns (DAMPs) (Boudreau *et al.*, 2014; Todkar *et al.*, 2021) and enhancing invasiveness in the MDA-MB-231 TNBC cell model via TLR9 activation (Rabas *et al.*, 2021). Remarkably, we detected mitophagy pathway-related genes and reduced mitochondrial content in the EV obtained from EGCG-treated TNBC cells. Besides, we showed that MDA-MB-231-derived EV can transfer mitochondria to the ADMSC. Yet, the functionality of these mitochondria within the EV and their role in the regulation of the ADMSC phenotype must be thoroughly addressed in future studies.

Lastly, we studied the impact of hypoxia on the mRNA load of the EV, considering its *in vivo* relevance during obesity and in the TME. In previous reports, culturing BC

cell lines under hypoxic conditions showed an increase in the release of TGF-β (Rong *et al.*, 2016), miR210 (Jung *et al.*, 2017; King *et al.*, 2012) and lncSNHG1 (Dai *et al.*, 2022) within exosomes; and were associated with T cell suppression, increases in survival, invasion and angiogenesis (Jiang *et al.*, 2022). Our results demonstrate that no significant changes were detected in the sorted mRNA since only nine genes were expressed differentially. From these genes, five were upregulated and related to hypoxia-induced cell death, mitochondrial function, glucose transport and angiogenesis. However, EGCG added to the hypoxic cell cultured caused a significant change in the mRNA content of the TNBC-released EV. Gene downregulation was the tendency in the hypoxic-EGCG-released EV and was associated with processes such as secretion mechanisms and regulation of the metabolic and biosynthetic cellular process, suggesting a reduction of the EV's regulatory capacity. EGCG downregulated an important protooncogene for BC aggressiveness like SLAC3A2 (El Ansari *et al.*, 2018). However, genes associated with inflammation and oncogenesis were detected to be enriched within the TNBC-derived EV cultured under low oxygen tension and EGCG. For instance, we saw the upregulation of BCAS4, an essential gene for the development and progression of breast tumors (Chen *et al.*, 2015). Therefore, the overall impact of EGCG in the axis BC-ADMSC/adipocytes during hypoxic cell culture conditions must be fully addressed in further studies.

CHAPTER VI

CONCLUSIONS AND PERSPECTIVES

In conclusion, we demonstrated that EGCG is a diet-derived compound with the capacity to prevent the onset of an obesogenic environment that favours TNBC development by acting at different nodes:

1) Preventing the expansion of the adipose tissue by targeting the induction of master regulators of adipogenesis, hence reducing the capacity of ADMSC to differentiate into mature adipocytes.
2) Reducing the chemotactic response of TNBC and ADMSC by inhibiting the activation of pathways like JAK/STAT3, NK-κB and SMAD2, and the expression of EMT markers such as SNAIL, SLUG and fibronectin.
3) Abrogating the pro-inflammatory modulation of adipocyte and tumor cells' secretome profile, efficiently altering their signaling crosstalk.
4) Modulating the tumor-derived EV' genetic content and reducing their capacity to trigger pro-inflammatory and senescence markers, potentially impacting chemoresistance.

Importantly, our study proves that ADMSC and adipocytes' secretomes have differential chemoattractant and pro-inflammatory capacities over TNBC cell line models. Besides, we demonstrate that ADMSC can differentiate into a CAA-like phenotype in response to factors secreted by the tumor cells. This represents a molecular insight into the different ways in which adipose tissue contributes to carcinogenesis. In addition, our study discloses the role of tumor-derived EV in acquiring a pro-inflammatory phenotype of the ADMSC. The effect of EGCG on the reduction of mitochondrial content within the EV was a new finding adding a potential anti-tumoral mechanism for the catechin.

Perspectives and open questions of the study:

In our study, we extended the knowledge about possible molecular players that lead to the cooperation between BC tumor cells and the adipose tissue-resident cells within the TME. However, further studies must be performed to fully unveil the missing parts. First, to model the TME, it will be relevant to include hypoxia during the *in vitro* studies since it can affect not only what cells are secreted but also their resulting phenotypes. A crucial missing aspect of our research was the protein validation of the upregulated genes in ADMSC and adipocytes and the inflammatory and CAA markers triggered in the ADMSC by the TNBC secretomes. In this aspect, it raises the question of whether the BC subtypes interact differentially with the preadipocytes or adipocytes. Therefore, it is essential to identify the specific factors present within the TNBC secretome that triggered CAA and the upregulation of SNAIL. In addition, to have a complete picture, it would be relevant to compare the effects of TNBC and other BC subtypes in acquiring a pro-inflammatory phenotype for the ADMSC compared with mature adipocytes. The latter will allow us to determine whether CAA originated from ADMSC, or whether mature adipocytes are phenotypically different, and if there are common mediators in the induction of this phenotype secreted by cancer cells. Likewise, a latter identification of the soluble factors secreted by the adipocytes that mediate the enhanced migration response in the TNBC cell line models would be a logical follow-up for the study.

Our *in vitro* approach agreed with several previously reported studies obtained using co-culture experiments of tumor cells with adipocytes (D'Esposito *et al.*, 2016; Dirat *et al.*, 2011). Nevertheless, it will be pertinent to include aspects of the autocrine regulation to contrast with the paracrine effects. Hence, co-culture experiments can be performed under hypoxic cell culture conditions, followed by detecting the transcribed genes, secreted factors, and protein expression. Additionally, it has been proposed that EGCG added *in vitro* at concentrations higher or equal to 30 μM caused cell production

of H_2O_2, which mediates the induction of apoptosis (Yang *et al.*, 1998; Yang *et al.*, 2000). Therefore, further studies testing the inhibitory effect of EGCG at low physiological concentrations will also be pertinent (Zeng *et al.*, 2014). Indeed, a study in BC patients showed that EGCG detected in human plasma can reach a peak concentration of 7 μM, while maintaining its anti-cancer and pro-apoptotic effects at 1 μM (Zeng *et al.*, 2014). Remarkably, in this study, EGCG inhibited the expression of molecules linked to growth and survival in cancer cells but not in normal cells (Zeng *et al.*, 2014).

Other aspects that need to be addressed in subsequent studies are how the TNBC-derived EV modulate the ADMSC response, whether they bind with the plasma membrane, activate receptor downstream signaling cascades, and/or fuse with the plasma membrane and release their intravesicular content into the ADMSC. Besides, it has been reported that EGCG can bind membranes (Hong *et al.*, 2002). Then, it can be incorporated into the secreted EGCG-EV, transferred into the recipient cells, and mediates some of the described effects for these vesicles. Hence, it is relevant for our study to determine whether EGCG or its oxidative products are present in the EV and if this alters their interaction mechanism with the ADMSC. Additionally, we foresee fully characterizing the EV and EGCG-EV obtained at low oxygen levels, including their protein and microRNA content. Interestingly, we detected the capacity of reduced senescence markers by the EGCG-EV, a result that must be re-evaluated in hypoxic conditions and under lower EGCG concentrations. Then, protein characterization must be extended to other markers besides P21 and β-gal for the senescence phenotype in both the TNBC and ADMSC. The evaluation of the apoptosis levels induced by EGCG-EV will be essential to elucidate their mechanism of action.

One of the most exciting results we obtained was the detection of mitochondria within our vesicles. Competent mitochondria mediate carcinogenic processes involved in proliferation, migration, and metastasis (Nahacka *et al.*, 2021). To our knowledge, its effect on the acquisition of a pro-tumoral phenotype by ADMSC has not been

addressed. Hence, further studies must be conducted to determine 1) whether these tumor-derived EV contain functional mitochondria or components, 2) their direct effect on the ADMSC phenotype, and 3) the mechanisms by which EGCG reduces mitochondrial package within the EV.

Finally, pre-clinical *in vivo* experiments must be performed to evaluate the overall effect of EGCG in obese mice harboring experimentally induced BC tumors. In addition, treatments combining EGCG and clinically approved drugs, are needed in *in vivo* experiments. In this regard, EGCG has been proposed as an adjuvant in cancer therapy for hepatocellular carcinoma during *in vivo* preclinical settings (Bimonte *et al.*, 2019; Li *et al.*, 2016) and with synergic effects during *in vitro* approaches for lung cancer cell models (Zhang *et al.*, 2019a).

BIBLIOGRAPHY

Abels ER et Breakefield XO (2016). Introduction to extracellular vesicles: Biogenesis, RNA cargo selection, content, release, and pptake. *Cell Mol Neurobiol 36*: 301-312.

Abramoff MDM, P.J.; Ram, S.J. (2004). Image processing with ImageJ. *Biophotonics Int 11*: 36-42.

Abramson VG, Lehmann BD, Ballinger TJ et Pietenpol JA (2015). Subtyping of triple-negative breast cancer: implications for therapy. *Cancer 121*: 8-16.

Afaq F, Adhami VM, Ahmad N et Mukhtar H (2003). Inhibition of ultraviolet B-mediated activation of nuclear factor kappaB in normal human epidermal keratinocytes by green tea Constituent (-)-epigallocatechin-3-gallate. *Oncogene 22*: 1035-1044.

Aga M, Bentz GL, Raffa S, Torrisi MR, Kondo S, Wakisaka N, Yoshizaki T, Pagano JS et Shackelford J (2014). Exosomal HIF1alpha supports invasive potential of nasopharyngeal carcinoma-associated LMP1-positive exosomes. *Oncogene 33*: 4613-4622.

Aggarwal S, Verma SS, Aggarwal S et Gupta SC (2021). Drug repurposing for breast cancer therapy: Old weapon for new battle. *Semin Cancer Biol 68*: 8-20.

Aguiar PH, Furtado C, Repoles BM, Ribeiro GA, Mendes IC, Peloso EF, Gadelha FR, Macedo AM, Franco GR, Pena SD, et al. (2013.) Oxidative stress and DNA lesions: the role of 8-oxoguanine lesions in Trypanosoma cruzi cell viability. *PLoS Negl Trop Dis 7*: e2279.

Ahmed I et Ismail N (2020). M1 and M2 Macrophages Polarization via mTORC1 Influences Innate Immunity and Outcome of Ehrlichia Infection. *J Cell Immunol 2*: 108-115.

Al-Nedawi K, Meehan B, Micallef J, Lhotak V, May L, Guha A et Rak J (2008). Intercellular transfer of the oncogenic receptor EGFRvIII by microvesicles derived from tumor cells. *Nat Cell Biol 10*: 619-624.

Alferez DG, Simoes BM, Howell SJ et Clarke RB (2018). The Role of Steroid Hormones in Breast and Effects on Cancer Stem Cells. *Curr Stem Cell Rep 4*: 81-94.

Almatroodi SAA, Alsahli MSMA, A.;, Alhumaydhi FAB, A.Y.; et Khan AAR, A.H. (2022). Potential Therapeutic Targets of Resveratrol, a Plant Polyphenol, and Its Role in the Therapy of Various Types of Cancer. *Molecules 27*:

Amari L et Germain M (2021). Mitochondrial extracellular vesicles - origins and roles. *Front Mol Neurosci 14*: 767219.

Amornsupak K, Insawang T, Thuwajit P, P OC, Eccles SA et Thuwajit C (2014). Cancer-associated fibroblasts induce high mobility group box 1 and contribute to resistance to doxorubicin in breast cancer cells. *BMC Cancer 14*: 955.

Andarawewa KLM, E.R.; Chenard, M.P.; Gansmuller, A.; Stoll, I.; Tomasetto, C.; Rio, M.C. (2005). Stromelysin-3 is a potent negative regulator of adipogenesis

participating to cancer cell-adipocyte interaction/crosstalk at the tumor invasive front. *Cancer Res 65*: 10862–10871.

Anders C et Carey LA (2008). Understanding and treating triple-negative breast cancer. *Oncology (Williston Park) 22*: 1233-1239; discussion 1239-1240, 1243.

Andersen C, Rayalam S, Della-Fera MA et Baile CA (2010). Phytochemicals and adipogenesis. *Biofactors 36*: 415-422.

Andolfi C et Fisichella PM (2018). Epidemiology of obesity and associated comorbidities. *J Laparoendosc Adv Surg Tech A 28*: 919-924.

Arganda-Carreras I, Fernandez-Gonzalez R, Munoz-Barrutia A et Ortiz-De-Solorzano C (2010). 3D reconstruction of histological sections: Application to mammary gland tissue. *Microsc Res Tech 73*: 1019-1029.

Arts IC et Hollman PC (2005). Polyphenols and disease risk in epidemiologic studies. *Am J Clin Nutr 81*: 317S-325S.

Asadipooya K et Uy EM (2019). Advanced Glycation End Products (AGEs), Receptor for AGEs, Diabetes, and Bone: Review of the Literature. *J Endocr Soc 3*: 1799-1818.

Aslan E, Guler C et Adem S (2016). In vitro effects of some flavonoids and phenolic acids on human pyruvate kinase isoenzyme M2. *J Enzyme Inhib Med Chem 31*: 314-317.

Attane C et Muller C (2020). Drilling for oil: tumor-surrounding adipocytes fueling Cancer. *Trends Cancer 6*: 593-604.

Avalos-Moreno M, Lopez-Tejada A, Blaya-Canovas JL, Cara-Lupianez FE, Gonzalez-Gonzalez A, Lorente JA, Sanchez-Rovira P et Granados-Principal S (2020). Drug Repurposing for Triple-Negative Breast Cancer. *J Pers Med 10*:

Avgerinos KI, Spyrou N, Mantzoros CS et Dalamaga M (2019). Obesity and cancer risk: Emerging biological mechanisms and perspectives. *Metabolism 92*: 121-135.

Avram MM, Avram AS et James WD (2007) Subcutaneous fat in normal and diseased states 3. Adipogenesis: from stem cell to fat cell. *J Am Acad Dermatol 56*: 472-492.

Azmanova M et Pitto-Barry A (2022). Oxidative stress in cancer therapy: friend or enemy? *Chembiochem 23*: e202100641.

Bae J, Kumazoe M, Takeuchi C, Hidaka S, Fujimura Y et Tachibana H (2019.) Epigallocatechin-3-O-gallate induces acid sphingomyelinase activation through activation of phospholipase C. *Biochem Biophys Res Commun 520*: 186-191.

Balanis N et Carlin CR (2017). Stress-induced EGF receptor signaling through STAT3 and tumor progression in triple-negative breast cancer. *Mol Cell Endocrinol 451*: 24-30.

Balanis N, Wendt MK, Schiemann BJ, Wang Z, Schiemann WP et Carlin CR (2013). Epithelial to mesenchymal transition promotes breast cancer progression via a fibronectin-dependent STAT3 signaling pathway. *J Biol Chem 288*: 17954-17967.

Banerjee S et Mandal AKA (2022). Role of epigallocatechin-3- gallate in the regulation of known and novel microRNAs in breast carcinoma cells. *Front Genet 13*: 995046.

Bareche Y, Venet D, Ignatiadis M, Aftimos P, Piccart M, Rothe F et Sotiriou C (2018). Unravelling triple-negative breast cancer molecular heterogeneity using an integrative multiomic analysis. *Ann Oncol 29*: 895-902.

Bartel DP (2004). MicroRNAs: genomics, biogenesis, mechanism, and function. *Cell 116*: 281-297.

Barzaman K, Karami J, Zarei Z, Hosseinzadeh A, Kazemi MH, Moradi-Kalbolandi S, Safari E et Farahmand L (2020). Breast cancer: Biology, biomarkers, and treatments. *Int Immunopharmacol 84*: 106535.

Baylin SB et Jones PA (2016). Epigenetic determinants of cancer. *Cold Spring Harb Perspect Biol 8*:

Becker A, Thakur BK, Weiss JM, Kim HS, Peinado H et Lyden D (2016). Extracellular vesicles in cancer: cell-to-cell mediators of metastasis. *Cancer Cell 30*: 836-848.

Bennett CN, Ross SE, Longo KA, Bajnok L, Hemati N, Johnson KW, Harrison SD et MacDougald OA (2002). Regulation of Wnt signaling during adipogenesis. *J Biol Chem 277*: 30998-31004.

Bergenfelz C, Larsson AM, von Stedingk K, Gruvberger-Saal S, Aaltonen K, Jansson S, Jernstrom H, Janols H, Wullt M, Bredberg A, et al. (2015). Systemic monocytic-MDSCs are generated from monocytes and correlate with disease progression in breast cancer patients. *PLoS One 10*: e0127028.

Bergman RN (2012). A better index of body adiposity. *Obesity (Silver Spring) 20*: 1135.

Bertolini F, Petit JY et Kolonin MG (2015). Stem cells from adipose tissue and breast cancer: hype, risks and hope. *Br J Cancer 112*: 419-423.

Bharadwaj U, Kasembeli MM, Robinson P et Tweardy DJ (2020). Targeting Janus kinases and signal transducer and activator of transcription 3 to treat inflammation, fibrosis, and cancer: rationale, progress, and caution. *Pharmacol Rev 72*: 486-526.

Bimonte S, Albino V, Piccirillo M, Nasto A, Molino C, Palaia R et Cascella M (2019.) Epigallocatechin-3-gallate in the prevention and treatment of hepatocellular carcinoma: experimental findings and translational perspectives. *Drug Des Devel Ther 13*: 611-621.

Birsoy K, Chen Z et Friedman J (2008). Transcriptional regulation of adipogenesis by KLF4. *Cell Metab 7*: 339-347.

Bister N, Pistono C, Huremagic B, Jolkkonen J, Giugno R et Malm T (2020). Hypoxia and extracellular vesicles: A review on methods, vesicular cargo and functions. *J Extracell Vesicles 10*: e12002.

Bjune JI, Stromland PP, Jersin RA, Mellgren G et Dankel SN (2022). Metabolic and Epigenetic Regulation by Estrogen in Adipocytes. *Front Endocrinol (Lausanne) 13*: 828780.

Bochet L, Lehuede C, Dauvillier S, Wang YY, Dirat B, Laurent V, Dray C, Guiet R, Maridonneau-Parini I, Le Gonidec S, et al. (2013). Adipocyte-derived fibroblasts promote tumor progression and contribute to the desmoplastic reaction in breast cancer. *Cancer Res 73*: 5657-5668.

Boudreau LH, Duchez AC, Cloutier N, Soulet D, Martin N, Bollinger J, Pare A, Rousseau M, Naika GS, Levesque T, et al. (2014). Platelets release mitochondria serving as substrate for bactericidal group IIA-secreted phospholipase A2 to promote inflammation. *Blood 124*: 2173-2183.

Brown TP et Ganapathy V (2020). Lactate/GPR81 signaling and proton motive force in cancer: Role in angiogenesis, immune escape, nutrition, and Warburg phenomenon. *Pharmacol Ther 206*: 107451.

Bulotta S, Corradino R, Celano M, Maiuolo J, D'Agostino M, Oliverio M, Procopio A, Filetti S et Russo D (2013). Antioxidant and antigrowth action of peracetylated oleuropein in thyroid cancer cells. *J Mol Endocrinol 51*: 181-189.

Burstein MD, Tsimelzon A, Poage GM, Covington KR, Contreras A, Fuqua SA, Savage MI, Osborne CK, Hilsenbeck SG, Chang JC, et al. (2015). Comprehensive genomic analysis identifies novel subtypes and targets of triple-negative breast cancer. *Clin Cancer Res 21*: 1688-1698.

Cabrera MC, Hollingsworth RE et Hurt EM (2015). Cancer stem cell plasticity and tumor hierarchy. *World J Stem Cells 7*: 27-36.

Cai Z, Liang Y, Xing C, Wang H, Hu P, Li J, Huang H, Wang W et Jiang C (2019). Cancer-associated adipocytes exhibit distinct phenotypes and facilitate tumor progression in pancreatic cancer. *Oncol Rep 42*: 2537-2549.

Calle EE et Thun MJ (2004). Obesity and cancer. *Oncogene 23*: 6365-6378.

Cao H (2014). Adipocytokines in obesity and metabolic disease. *J Endocrinol 220*: T47-59.

Cao H, Sekiya M, Ertunc ME, Burak MF, Mayers JR, White A, Inouye K, Rickey LM, Ercal BC, Furuhashi M, et al. (2013). Adipocyte lipid chaperone AP2 is a secreted adipokine regulating hepatic glucose production. *Cell Metab 17*: 768-778.

Carrasco-Pozo C, Cires MJ et Gotteland M (2019). Quercetin and epigallocatechin gallate in the prevention and treatment of obesity: From Molecular to Clinical Studies. *J Med Food 22*: 753-770.

Castaneda S, Remuzgo-Martinez S, Lopez-Mejias R, Genre F, Calvo-Alen J, Llorente I, Aurrecoechea E, Ortiz AM, Triguero A, Blanco R, et al. (2019). Rapid beneficial effect of the IL-6 receptor blockade on insulin resistance and insulin sensitivity in non-diabetic patients with rheumatoid arthritis. *Clin Exp Rheumatol 37*: 465-473.

Castro BM, Prieto M et Silva LC (2014). Ceramide: a simple sphingolipid with unique biophysical properties. *Prog Lipid Res 54*: 53-67.

Catalan V, Gomez-Ambrosi J, Rodriguez A et Fruhbeck G (2013). Adipose tissue immunity and cancer. *Front Physiol 4*: 275.

Catanzaro D, Ragazzi E, Vianello C, Caparrotta L et Montopoli M (2015). Effect of Quercetin on Cell Cycle and Cyclin Expression in Ovarian Carcinoma and Osteosarcoma Cell Lines. *Nat Prod Commun 10*: 1365-1368.

Ceddia RB (2013). The role of AMP-activated protein kinase in regulating white adipose tissue metabolism. *Mol Cell Endocrinol 366*: 194-203.

Chalmin F, Ladoire S, Mignot G, Vincent J, Bruchard M, Remy-Martin JP, Boireau W, Rouleau A, Simon B, Lanneau D, et al. (2010). Membrane-associated Hsp72

from tumor-derived exosomes mediates STAT3-dependent immunosuppressive function of mouse and human myeloid-derived suppressor cells. *J Clin Invest 120*: 457-471.

Chargaff E et West R (1946). The biological significance of the thromboplastic protein of blood. *J Biol Chem 166*: 189-197.

Chawla D, Bansal S, Banerjee BD, Madhu SV, Kalra OP et Tripathi AK (2014). Role of advanced glycation end product (AGE)-induced receptor (RAGE) expression in diabetic vascular complications. *Microvasc Res 95*: 1-6.

Chen F, Chen J, Yang L, Liu J, Zhang X, Zhang Y, Tu Q, Yin D, Lin D, Wong PP, et al. (2019). Extracellular vesicle-packaged HIF-1alpha-stabilizing lncRNA from tumor-associated macrophages regulates aerobic glycolysis of breast cancer cells. *Nat Cell Biol 21*: 498-510.

Chen J, Cao X, Cui Y, Zeng G, Chen J et Zhang G (2018). Resveratrol alleviates lysophosphatidylcholine-induced damage and inflammation in vascular endothelial cells. *Mol Med Rep 17*: 4011-4018.

Chen P, Liu R, Aihara K et Chen L (2015). Identifying critical differentiation state of MCF-7 cells for breast cancer by dynamical network biomarkers. *Frontiers in Genetics 6*:

Chen PN, Chu SC, Kuo WH, Chou MY, Lin JK et Hsieh YS (2011). Epigallocatechin-3 gallate inhibits invasion, epithelial-mesenchymal transition, and tumor growth in oral cancer cells. *J Agric Food Chem 59*: 3836-3844.

Chen Q, Takada R, Noda C, Kobayashi S et Takada S (2016). Different populations of Wnt-containing vesicles are individually released from polarized epithelial cells. *Sci Rep 6*: 35562.

Chen X, Yang M, Yin J, Li P, Zeng S, Zheng G, He Z, Liu H, Wang Q, Zhang F, et al. (2022). Tumor-associated macrophages promote epithelial-mesenchymal transition and the cancer stem cell properties in triple-negative breast cancer through CCL2/AKT/beta-catenin signaling. *Cell Commun Signal 20*: 92.

Chen Y, Zeng C, Zhan Y, Wang H, Jiang X et Li W (2017). Aberrant low expression of p85alpha in stromal fibroblasts promotes breast cancer cell metastasis through exosome-mediated paracrine Wnt10b. *Oncogene 36*: 4692-4705.

Chimen M, Evryviadou A, Box CL, Harrison MJ, Hazeldine J, Dib LH, Kuravi SJ, Payne H, Price JMJ, Kavanagh D, et al. (2020). Appropriation of GPIbalpha from platelet-derived extracellular vesicles supports monocyte recruitment in systemic inflammation. *Haematologica 105*: 1248-1261.

Chirumbolo S et Bjorklund G (2016). Can Wnt5a and Wnt non-canonical pathways really mediate adipocyte de-differentiation in a tumor microenvironment? *Eur J Cancer 64*: 96-100.

Cho JA, Park H, Lim EH et Lee KW (2012). Exosomes from breast cancer cells can convert adipose tissue-derived mesenchymal stem cells into myofibroblast-like cells. *Int J Oncol 40*: 130-138.

Cho SY, Park PJ, Shin HJ, Kim YK, Shin DW, Shin ES, Lee HH, Lee BG, Baik JH et Lee TR (2007). (-)-Catechin suppresses expression of Kruppel-like factor 7 and

increases expression and secretion of adiponectin protein in 3T3-L1 cells. *Am J Physiol Endocrinol Metab 292*: E1166-1172.

Choi EJ, Bae SM et Ahn WS (2008). Antiproliferative effects of quercetin through cell cycle arrest and apoptosis in human breast cancer MDA-MB-453 cells. *Arch Pharm Res 31*: 1281-1285.

Chokor R, Lamy S et Annabi B (2014). Transcriptional targeting of sphingosine-1-phosphate receptor S1P2 by epigallocatechin-3-gallate prevents sphingosine-1-phosphate-mediated signaling in macrophage-differentiated HL-60 promyelomonocytic leukemia cells. *Onco Targets Ther 7*: 667-677.

Chow A, Zhou W, Liu L, Fong MY, Champer J, Van Haute D, Chin AR, Ren X, Gugiu BG, Meng Z, et al. (2014). Macrophage immunomodulation by breast cancer-derived exosomes requires Toll-like receptor 2-mediated activation of NF-kappaB. *Sci Rep 4*: 5750.

Chu DT, Phuong TNT, Tien NLB, Tran DK, Nguyen TT, Thanh VV, Quang TL, Minh LB, Pham VH, Ngoc VTN, et al. (2019). The Effects of Adipocytes on the Regulation of Breast Cancer in the Tumor Microenvironment: An Update. *Cells 8*:

Cinti S (2018) Pink Adipocytes. *Trends Endocrinol Metab 29*: 651-666.

Clayton A, Mitchell JP, Court J, Linnane S, Mason MD et Tabi Z (2008). Human tumor-derived exosomes down-modulate NKG2D expression. *J Immunol 180*: 7249-7258.

Clement E, Lazar I, Attane C, Carrie L, Dauvillier S, Ducoux-Petit M, Esteve D, Menneteau T, Moutahir M, Le Gonidec S, et al. (2020). Adipocyte extracellular vesicles carry enzymes and fatty acids that stimulate mitochondrial metabolism and remodeling in tumor cells. *EMBO J 39*: e102525.

Cochrane CR, Szczepny A, Watkins DN et Cain JE (2015). Hedgehog Signaling in the Maintenance of Cancer Stem Cells. *Cancers (Basel) 7*: 1554-1585.

Cohen P, Miyazaki M, Socci ND, Hagge-Greenberg A, Liedtke W, Soukas AA, Sharma R, Hudgins LC, Ntambi JM et Friedman JM (2002). Role for stearoyl-CoA desaturase-1 in leptin-mediated weight loss. *Science 297*: 240-243.Correa LH, Heyn GS et Magalhaes KG (2019). The Impact of the adipose organ plasticity on inflammation and cancer progression. *Cells 8*:

Cozzo AJ, Fuller AM et Makowski L (2017). Contribution of Adipose Tissue to Development of Cancer. *Compr Physiol 8*: 237-282.

Crosbie EJ, Zwahlen M, Kitchener HC, Egger M et Renehan AG (2010). Body mass index, hormone replacement therapy, and endometrial cancer risk: a meta-analysis. *Cancer Epidemiol Biomarkers Prev 19*: 3119-3130.

Curigliano G et Perez EA (2014). Immunoscoring breast cancer: TILs remember what they target. *Ann Oncol 25*: 1455-1456.

D'Esposito V, Ambrosio MR, Giuliano M, Cabaro S, Miele C, Beguinot F et Formisano P (2020). Mammary adipose tissue control of breast cancer progression: impact of obesity and diabetes. *Front Oncol 10*: 1554.

D'Esposito V, Liguoro D, Ambrosio MR, Collina F, Cantile M, Spinelli R, Raciti GA, Miele C, Valentino R, Campiglia P, et al. (2016). Adipose microenvironment

promotes triple negative breast cancer cell invasiveness and dissemination by producing CCL5. *Oncotarget 7*: 24495-24509.

Dagpo TD, Nolan CJ et Delghingaro-Augusto V (2020). Exploring therapeutic targets to reverse or prevent the transition from metabolically healthy to unhealthy obesity. *Cells 9*:

Dai G, Yang Y, Liu S et Liu H (2022). Hypoxic breast cancer cell-derived exosomal SNHG1 promotes breast cancer growth and angiogenesis via regulating miR-216b-5p/JAK2 Axis. *Cancer Manag Res 14*: 123-133.

Dairkee SH, Puett L et Hackett AJ (1988). Expression of basal and luminal epithelium-specific keratins in normal, benign, and malignant breast tissue. *J Natl Cancer Inst 80*: 691-695.

Daval M, Foufelle F et Ferre P (2006). Functions of AMP-activated protein kinase in adipose tissue. *J Physiol 574*: 55-62.

Davis FM, Stewart TA, Thompson EW et Monteith GR (2014). Targeting EMT in cancer: opportunities for pharmacological intervention. *Trends Pharmacol Sci 35*: 479-488.

De Blander H, Morel AP, Senaratne AP, Ouzounova M et Puisieux A (2021). Cellular P\plasticity: a route to senescence exit and tumorigenesis. *Cancers (Basel) 13*:

de Winter TJJ et Nusse R (2021) Running Against the Wnt: How Wnt/beta-Catenin Suppresses Adipogenesis. *Front Cell Dev Biol 9*: 627429.

Deepak KGK, Vempati R, Nagaraju GP, Dasari VR, S N, Rao DN et Malla RR (2020). Tumor microenvironment: challenges and opportunities in targeting metastasis of triple negative breast cancer. *Pharmacol Res 153*: 104683.

Denduluri SK, Idowu O, Wang Z, Liao Z, Yan Z, Mohammed MK, Ye J, Wei Q, Wang J, Zhao L, et al. (2015). Insulin-like growth factor (IGF) signaling in tumorigenesis and the development of cancer drug resistance. *Genes Dis 2*: 13-25.

Diaz-Montero CM, Salem ML, Nishimura MI, Garrett-Mayer E, Cole DJ et Montero AJ (2009) Increased circulating myeloid-derived suppressor cells correlate with clinical cancer stage, metastatic tumor burden, and doxorubicin-cyclophosphamide chemotherapy. *Cancer Immunol Immunother 58*: 49-59.

Dietze EC, Chavez TA et Seewaldt VL (2018). Obesity and triple-negative breast cancer: disparities, controversies, and biology. *Am J Pathol 188*: 280-290.

Dimri GP, Lee X, Basile G, Acosta M, Scott G, Roskelley C, Medrano EE, Linskens M, Rubelj I, Pereira-Smith O, et al. (1995). A biomarker that identifies senescent human cells in culture and in aging skin in vivo. *Proc Natl Acad Sci U S A 92*: 9363-9367.

Dirat B, Bochet L, Dabek M, Daviaud D, Dauvillier S, Majed B, Wang YY, Meulle A, Salles B, Le Gonidec S, et al. (2011). Cancer-associated adipocytes exhibit an activated phenotype and contribute to breast cancer invasion. *Cancer Res 71*: 2455-2465.

Dixit VD (2010). Thymic fatness and approaches to enhance thymopoietic fitness in aging. *Curr Opin Immunol 22*: 521-528.

Djediai S, Gonzalez Suarez N, El Cheikh-Hussein L, Rodriguez Torres S, Gresseau L, Dhayne S, Joly-Lopez Z et Annabi B (2021). MT1-MMP cooperates with TGF-beta receptor-mediated signaling to trigger SNAIL and induce epithelial-to-mesenchymal-like transition in U87 glioblastoma cells. *Int J Mol Sci 22*:

Dobin A, Davis CA, Schlesinger F, Drenkow J, Zaleski C, Jha S, Batut P, Chaisson M et Gingeras TR (2013). STAR: ultrafast universal RNA-seq aligner. *Bioinformatics 29*: 15-21.

Dommel S et Bluher M (2021). Does C-C motif chemokine ligand 2 (CCL2) link obesity to a pro-Inflammatory state? *Int J Mol Sci 22*:

Dong LF, Kovarova J, Bajzikova M, Bezawork-Geleta A, Svec D, Endaya B, Sachaphibulkij K, Coelho AR, Sebkova N, Ruzickova A, et al. (2017). Horizontal transfer of whole mitochondria restores tumorigenic potential in mitochondrial DNA-deficient cancer cells. *Elife 6*:

Dooley J et Liston A (2012). Molecular control over thymic involution: from cytokines and microRNA to aging and adipose tissue. *Eur J Immunol 42*: 1073-1079.

Duchez AC, Boudreau LH, Naika GS, Bollinger J, Belleannee C, Cloutier N, Laffont B, Mendoza-Villarroel RE, Levesque T, Rollet-Labelle E, et al. (2015). Platelet microparticles are internalized in neutrophils via the concerted activity of 12-lipoxygenase and secreted phospholipase A2-IIA. *Proc Natl Acad Sci U S A 112*: E3564-3573.

Edgar JR, Eden ER et Futter CE (2014). Hrs- and CD63-dependent competing mechanisms make different sized endosomal intraluminal vesicles. *Traffic 15*: 197-211.

Eguchi J, Yan QW, Schones DE, Kamal M, Hsu CH, Zhang MQ, Crawford GE et Rosen ED (2008). Interferon regulatory factors are transcriptional regulators of adipogenesis. *Cell Metab 7*: 86-94.

El Ansari R, Craze ML, Diez-Rodriguez M, Nolan CC, Ellis IO, Rakha EA et Green AR (2018). The multifunctional solute carrier 3A2 (SLC3A2) confers a poor prognosis in the highly proliferative breast cancer subtypes. *Br J Cancer 118*: 1115-1122.

Ellis IO, Galea M, Broughton N, Locker A, Blamey RW et Elston CW (1992). Pathological prognostic factors in breast cancer. II. Histological type. Relationship with survival in a large study with long-term follow-up. *Histopathology 20*: 479-489.

Elston CW et Ellis IO (1991). Pathological prognostic factors in breast cancer. I. The value of histological grade in breast cancer: experience from a large study with long-term follow-up. *Histopathology 19*: 403-410.

Escande C, Nin V, Pirtskhalava T, Chini CC, Tchkonia T, Kirkland JL et Chini EN (2015). Deleted in breast cancer 1 limits adipose tissue fat accumulation and plays a key role in the development of metabolic syndrome phenotype. *Diabetes 64*: 12-22.

Esteve Rafols M (2014). Adipose tissue: cell heterogeneity and functional diversity. *Endocrinol Nutr 61*: 100-112.

Faget DV, Ren Q et Stewart SA (2019). Unmasking senescence: context-dependent effects of SASP in cancer. *Nat Rev Cancer 19*: 439-453.

Fard MK, van der Meer F, Sanchez P, Cantuti-Castelvetri L, Mandad S, Jakel S, Fornasiero EF, Schmitt S, Ehrlich M, Starost L, et al. (2017). BCAS1 expression defines a population of early myelinating oligodendrocytes in multiple sclerosis lesions. *Sci Transl Med 9*:

Farghadani R et Naidu R (2021). Curcumin: Modulator of Key Molecular Signaling Pathways in Hormone-Independent Breast Cancer. *Cancers (Basel) 13*:

Farmer SR (2005). Regulation of PPARgamma activity during adipogenesis. *Int J Obes (Lond) 29 Suppl 1*: S13-16.

Farmer SR (2006). Transcriptional control of adipocyte formation. *Cell Metab 4*: 263-273.

Farooqi AA, Pinheiro M, Granja A, Farabegoli F, Reis S, Attar R, Sabitaliyevich UY, Xu B et Ahmad A (2020). EGCG Mediated Targeting of Deregulated Signaling Pathways and Non-Coding RNAs in Different Cancers: Focus on JAK/STAT, Wnt/beta-Catenin, TGF/SMAD, NOTCH, SHH/GLI, and TRAIL Mediated Signaling Pathways. *Cancers (Basel) 12*:

Fasanaro P, D'Alessandra Y, Di Stefano V, Melchionna R, Romani S, Pompilio G, Capogrossi MC et Martelli F (2008). MicroRNA-210 modulates endothelial cell response to hypoxia and inhibits the receptor tyrosine kinase ligand Ephrin-A3. *J Biol Chem 283*: 15878-15883.

Finger EC et Giaccia AJ (2010). Hypoxia, inflammation, and the tumor microenvironment in metastatic disease. *Cancer Metastasis Rev 29*: 285-293.

Finkel T et Holbrook NJ (2000). Oxidants, oxidative stress and the biology of ageing. *Nature 408*: 239-247.

Fiorillo M, Sotgia F et Lisanti MP (2018). "Energetic" cancer stem cells (e-CSCs): A new hyper-metabolic and proliferative tumor cell phenotype, driven by mitochondrial energy. *Front Oncol 8*: 677.

Fournier F, Diaz-Marin R, Pilon F, Neault M, Juneau R, Girouard G, Wilson AM, Larrivee B, Mallette FA, Crespo-Garcia S, et al. (2023). Obesity triggers tumoral senescence and renders poorly immunogenic malignancies amenable to senolysis. *Proc Natl Acad Sci U S A 120*: e2209973120.

Francisco Fernandez M, Charfi C, Piloto-Ferrer J, Lidia Gonzalez M, Lamy S et Annabi B (2019). Targeting Ovarian Cancer Cell Cytotoxic Drug Resistance Phenotype with Xanthium strumarium L. Extract. *Evid Based Complement Alternat Med 2019*: 6073019.

Fruhbeck G, Catalan V, Rodriguez A et Gomez-Ambrosi J (2018). Adiponectin-leptin ratio: A promising index to estimate adipose tissue dysfunction. Relation with obesity-associated cardiometabolic risk. *Adipocyte 7*: 57-62.

Fruhbeck G, Catalan V, Rodriguez A, Ramirez B, Becerril S, Salvador J, Colina I et Gomez-Ambrosi J (2019). Adiponectin-leptin Ratio is a Functional Biomarker of Adipose Tissue Inflammation. *Nutrients 11*:

Fujisaki K, Fujimoto H, Sangai T, Nagashima T, Sakakibara M, Shiina N, Kuroda M, Aoyagi Y et Miyazaki M (2015) Cancer-mediated adipose reversion promotes cancer cell migration via IL-6 and MCP-1. *Breast Cancer Res Treat 150*: 255-263.

Furuyashiki T, Nagayasu H, Aoki Y, Bessho H, Hashimoto T, Kanazawa K et Ashida H (2004). Tea catechin suppresses adipocyte differentiation accompanied by down-regulation of PPARgamma2 and C/EBPalpha in 3T3-L1 cells. *Biosci Biotechnol Biochem 68*: 2353-2359.

Ge SX, Son EW et Yao R (2018). iDEP: an integrated web application for differential expression and pathway analysis of RNA-Seq data. *BMC Bioinformatics 19*: 534.

Gehler S, Ponik SM, Riching KM et Keely PJ (2013). Bi-directional signaling: extracellular matrix and integrin regulation of breast tumor progression. *Crit Rev Eukaryot Gene Expr 23*: 139-157.

Gentric G et Mechta-Grigoriou F (2021). Tumor Cells and Cancer-Associated Fibroblasts: An Updated Metabolic Perspective. *Cancers (Basel) 13*:

Gharib E, Veilleux V, Boudreau LH, Pichaud N et Robichaud GA (2023) Platelet-derived microparticles provoke chronic lymphocytic leukemia malignancy through metabolic reprogramming. *Front Immunol 14*: 1207631.

Ghossoub R, Lembo F, Rubio A, Gaillard CB, Bouchet J, Vitale N, Slavik J, Machala M et Zimmermann P (2014). Syntenin-ALIX exosome biogenesis and budding into multivesicular bodies are controlled by ARF6 and PLD2. *Nat Commun 5*: 3477.

Gibson GR, Qian D, Ku JK et Lai LL (2005). Metaplastic breast cancer: clinical features and outcomes. *Am Surg 71*: 725-730.

Gilbert CA et Slingerland JM (2013). Cytokines, obesity, and cancer: new insights on mechanisms linking obesity to cancer risk and progression. *Annu Rev Med 64*: 45-57.

Ginestier C, Hur MH, Charafe-Jauffret E, Monville F, Dutcher J, Brown M, Jacquemier J, Viens P, Kleer CG, Liu S, et al. (2007). ALDH1 is a marker of normal and malignant human mammary stem cells and a predictor of poor clinical outcome. *Cell Stem Cell 1*: 555-567.

Giordano A, Smorlesi A, Frontini A, Barbatelli G et Cinti S (2014). White, brown and pink adipocytes: the extraordinary plasticity of the adipose organ. *Eur J Endocrinol 170*: R159-171.

Gonzalez Suarez N, Fernandez-Marrero Y, Torabidastgerdooei S et Annabi B (2022) EGCG Prevents the Onset of an Inflammatory and Cancer-Associated Adipocyte-like Phenotype in Adipose-Derived Mesenchymal Stem/Stromal Cells in Response to the Triple-Negative Breast Cancer Secretome. *Nutrients 14*:

Gonzalez Suarez N, Rodriguez Torres S, Ouanouki A, El Cheikh-Hussein L et Annabi B (2021) EGCG Inhibits Adipose-Derived Mesenchymal Stem Cells Differentiation into Adipocytes and Prevents a STAT3-Mediated Paracrine Oncogenic Control of Triple-Negative Breast Cancer Cell Invasive Phenotype. *Molecules 26*:

Gorgoulis V, Adams PD, Alimonti A, Bennett DC, Bischof O, Bishop C, Campisi J, Collado M, Evangelou K, Ferbeyre G, et al. (2019) Cellular Senescence: Defining a Path Forward. *Cell 179*: 813-827.

Gregoire FM (2001). Adipocyte differentiation: from fibroblast to endocrine cell. *Exp Biol Med (Maywood) 226*: 997-1002.

Gu Z, Eils R et Schlesner M (2016). Complex heatmaps reveal patterns and correlations in multidimensional genomic data. *Bioinformatics 32*: 2847-2849.

Guaita-Esteruelas S, Saavedra-Garcia P, Bosquet A, Borras J, Girona J, Amiliano K, Rodriguez-Balada M, Heras M, Masana L et Guma J (2017). Adipose-Derived Fatty Acid-Binding Proteins Plasma Concentrations Are Increased in Breast Cancer Patients. *Oncologist 22*: 1309-1315.

Guillon J, Petit C, Toutain B, Guette C, Lelievre E et Coqueret O (2019). Chemotherapy-induced senescence, an adaptive mechanism driving resistance and tumor heterogeneity. *Cell Cycle 18*: 2385-2397.

Guo D, Ye J, Dai J, Li L, Chen F, Ma D et Ji C (2009). Notch-1 regulates Akt signaling pathway and the expression of cell cycle regulatory proteins cyclin D1, CDK2 and p21 in T-ALL cell lines. *Leuk Res 33*: 678-685.

Guo QQ, Wang SS, Zhang SS, Xu HD, Li XM, Guan Y, Yi F, Zhou TT, Jiang B, Bai N, et al. (2020). ATM-CHK2-Beclin 1 axis promotes autophagy to maintain ROS homeostasis under oxidative stress. *EMBO J 39*: e103111.

Gupta S, Ahmad N, Nieminen AL et Mukhtar H (2000). Growth inhibition, cell-cycle dysregulation, and induction of apoptosis by green tea constituent (-)-epigallocatechin-3-gallate in androgen-sensitive and androgen-insensitive human prostate carcinoma cells. *Toxicol Appl Pharmacol 164*: 82-90.

Gupta SC, Kunnumakkara AB, Aggarwal S et Aggarwal BB (2018). Inflammation, a double-edge sword for cancer and other age-related diseases. *Front Immunol 9*: 2160.

Gupta SC, Sundaram C, Reuter S et Aggarwal BB (2010). Inhibiting NF-kappaB activation by small molecules as a therapeutic strategy. *Biochim Biophys Acta 1799*: 775-787.

Gustafson B et Smith U (2010). Activation of canonical wingless-type MMTV integration site family (Wnt) signaling in mature adipocytes increases beta-catenin levels and leads to cell dedifferentiation and insulin resistance. *J Biol Chem 285*: 14031-14041.

Haase J, Weyer U, Immig K, Kloting N, Bluher M, Eilers J, Bechmann I et Gericke M (2014). Local proliferation of macrophages in adipose tissue during obesity-induced inflammation. *Diabetologia 57*: 562-571.

Habinowski SA et Witters LA (2001). The effects of AICAR on adipocyte differentiation of 3T3-L1 cells. *Biochem Biophys Res Commun 286*: 852-856.

Haffty BG, Yang Q, Reiss M, Kearney T, Higgins SA, Weidhaas J, Harris L, Hait W et Toppmeyer D (2006). Locoregional relapse and distant metastasis in conservatively managed triple negative early-stage breast cancer. *J Clin Oncol 24*: 5652-5657.

Ham S, Lima LG, Chai EPZ, Muller A, Lobb RJ, Krumeich S, Wen SW, Wiegmans AP et Moller A (2018). Breast Cancer-Derived Exosomes Alter Macrophage Polarization via gp130/STAT3 Signaling. *Front Immunol 9*: 871.

Han MS, White A, Perry RJ, Camporez JP, Hidalgo J, Shulman GI et Davis RJ (2020). Regulation of adipose tissue inflammation by interleukin 6. *Proc Natl Acad Sci U S A 117*: 2751-2760.

Hanahan D (2022). Hallmarks of cancer: new dimensions. *Cancer Discov 12*: 31-46.

Hanahan D et Weinberg RA (2011). Hallmarks of cancer: the next generation. *Cell 144*: 646-674.

Hao J, Yan F, Zhang Y, Triplett A, Zhang Y, Schultz DA, Sun Y, Zeng J, Silverstein KAT, Zheng Q, et al. (2018a). Expression of Adipocyte/Macrophage Fatty Acid-Binding Protein in Tumor-Associated Macrophages Promotes Breast Cancer Progression. *Cancer Res 78*: 2343-2355.

Hao J, Zhang Y, Yan X, Yan F, Sun Y, Zeng J, Waigel S, Yin Y, Fraig MM, Egilmez NK, et al. (2018b). Circulating Adipose Fatty Acid Binding Protein Is a New Link Underlying Obesity-Associated Breast/Mammary Tumor Development. *Cell Metab 28*: 689-705 e685.

Hao Q, Vadgama JV et Wang P (2020). CCL2/CCR2 signaling in cancer pathogenesis. *Cell Commun Signal 18*: 82.

Harkins JM, Moustaid-Moussa N, Chung YJ, Penner KM, Pestka JJ, North CM et Claycombe KJ (2004). Expression of interleukin-6 is greater in preadipocytes than in adipocytes of 3T3-L1 cells and C57BL/6J and ob/ob mice. *J Nutr 134*: 2673-2677.

Hartigan JA, Xiong WC et Johnson GV (2001). Glycogen synthase kinase 3beta is tyrosine phosphorylated by PYK2. *Biochem Biophys Res Commun 284*: 485-489.

Hartung C, Porsch M, Stuckrath K, Kaufhold S, Staege MS, Hanf V, Lantzsch T, Uleer C, Peschel S, John J, et al. (2021). Identifying High-Risk Triple-Negative Breast Cancer Patients by Molecular Subtyping. *Breast Care (Basel) 16*: 637-647.

Harvie MN, Pegington M, Mattson MP, Frystyk J, Dillon B, Evans G, Cuzick J, Jebb SA, Martin B, Cutler RG, et al. (2011). The effects of intermittent or continuous energy restriction on weight loss and metabolic disease risk markers: a randomized trial in young overweight women. *Int J Obes (Lond) 35*: 714-727.

Hayden MS et Ghosh S (2004). Signaling to NF-kappaB. *Genes Dev 18*: 2195-2224.

Hayflick L et Moorhead PS (1961) .The serial cultivation of human diploid cell strains. *Exp Cell Res 25*: 585-621.

He S et Sharpless NE (2017). Senescence in Health and Disease. *Cell 169*: 1000-1011.

He YC, He L, Khoshaba R, Lu FG, Cai C, Zhou FL, Liao DF et Cao D (2019). Curcumin nicotinate selectively induces cancer cell apoptosis and cycle arrest through a P53-mediated mechanism. *Molecules 24*:

Hemmings BA et Restuccia DF (2012). PI3K-PKB/Akt pathway. *Cold Spring Harb Perspect Biol 4*: a011189.

Henne WM, Stenmark H et Emr SD (2013). Molecular mechanisms of the membrane sculpting ESCRT pathway. *Cold Spring Harb Perspect Biol 5*:

Hessvik NP et Llorente A (2018). Current knowledge on exosome biogenesis and release. *Cell Mol Life Sci 75*: 193-208.

Heyn GS, Correa LH et Magalhaes KG (2020). The impact of adipose tissue-derived miRNAs in metabolic syndrome, obesity, and cancer. *Front Endocrinol (Lausanne) 11*: 563816.

Himbert C, Delphan M, Scherer D, Bowers LW, Hursting S et Ulrich CM (2017). Signals from the adipose microenvironment and the obesity-cancer link-a systematic review. *Cancer Prev Res (Phila) 10*: 494-506.

Hong J, Lu H, Meng X, Ryu JH, Hara Y et Yang CS (2002). Stability, cellular uptake, biotransformation, and efflux of tea polyphenol (-)-epigallocatechin-3-gallate in HT-29 human colon adenocarcinoma cells. *Cancer Res 62*: 7241-7246.

Hosseini A, Gharibi T, Marofi F, Javadian M, Babaloo Z et Baradaran B (2020). Janus kinase inhibitors: A therapeutic strategy for cancer and autoimmune diseases. *J Cell Physiol 235*: 5903-5924.

Hotamisligil GS (2006). Inflammation and metabolic disorders. *Nature 444*: 860-867.

Hotamisligil GS, Budavari A, Murray D et Spiegelman BM (1994). Reduced tyrosine kinase activity of the insulin receptor in obesity-diabetes. Central role of tumor necrosis factor-alpha. *J Clin Invest 94*: 1543-1549.

Hotamisligil GS, Shargill NS et Spiegelman BM (1993). Adipose expression of tumor necrosis factor-alpha: direct role in obesity-linked insulin resistance. *Science 259*: 87-91.

Hsieh FC, Cheng G et Lin J (2005). Evaluation of potential Stat3-regulated genes in human breast cancer. *Biochem Biophys Res Commun 335*: 292-299.

Hu C, Jiang W, Lv M, Fan S, Lu Y, Wu Q et Pi J (2022a). Potentiality of Exosomal Proteins as Novel Cancer Biomarkers for Liquid Biopsy. *Front Immunol 13*: 792046.

Hu D, Li Z, Zheng B, Lin X, Pan Y, Gong P, Zhuo W, Hu Y, Chen C, Chen L, et al. (2022b). Cancer-associated fibroblasts in breast cancer: Challenges and opportunities. *Cancer Commun (Lond) 42*: 401-434.

Hu L, Huang X, You C, Li J, Hong K, Li P, Wu Y, Wu Q, Wang Z, Gao R, et al. (2017). Prevalence of overweight, obesity, abdominal obesity and obesity-related risk factors in southern China. *PLoS One 12*: e0183934.

Hu Z, Fan C, Oh DS, Marron JS, He X, Qaqish BF, Livasy C, Carey LA, Reynolds E, Dressler L, et al. (2006). The molecular portraits of breast tumors are conserved across microarray platforms. *BMC Genomics 7*: 96.

Hung PF, Wu BT, Chen HC, Chen YH, Chen CL, Wu MH, Liu HC, Lee MJ et Kao YH (2005). Antimitogenic effect of green tea (-)-epigallocatechin gallate on 3T3-L1 preadipocytes depends on the ERK and Cdk2 pathways. *Am J Physiol Cell Physiol 288*: C1094-1108.

Hurley JH (2015). ESCRTs are everywhere. *EMBO J 34*: 2398-2407.

Hurrle S et Hsu WH (2017). The etiology of oxidative stress in insulin resistance. *Biomed J 40*: 257-262.

Hursting SD et Dunlap SM (2012). Obesity, metabolic dysregulation, and cancer: a growing concern and an inflammatory (and microenvironmental) issue. *Ann N Y Acad Sci 1271*: 82-87.

Hwang HJ, Lee YR, Kang D, Lee HC, Seo HR, Ryu JK, Kim YN, Ko YG, Park HJ et Lee JS (2020). Endothelial cells under therapy-induced senescence secrete CXCL11, which increases aggressiveness of breast cancer cells. *Cancer Lett 490*: 100-110.

Hwang JT, Park IJ, Shin JI, Lee YK, Lee SK, Baik HW, Ha J et Park OJ (2005). Genistein, EGCG, and capsaicin inhibit adipocyte differentiation process via activating AMP-activated protein kinase. *Biochem Biophys Res Commun 338*: 694-699.

Incio J, Ligibel JA, McManus DT, Suboj P, Jung K, Kawaguchi K, Pinter M, Babykutty S, Chin SM, Vardam TD, et al. (2018). Obesity promotes resistance to anti-VEGF therapy in breast cancer by up-regulating IL-6 and potentially FGF-2. *Sci Transl Med 10*:

Ishibashi Y, Matsui T, Takeuchi M et Yamagishi S (2012). Metformin inhibits advanced glycation end products (AGEs)-induced renal tubular cell injury by suppressing reactive oxygen species generation via reducing receptor for AGEs (RAGE) expression. *Horm Metab Res 44*: 891-895.

Iyengar NM, Gucalp A, Dannenberg AJ et Hudis CA (2016). Obesity and Cancer Mechanisms: Tumor Microenvironment and Inflammation. *J Clin Oncol 34*: 4270-4276.

Iyengar P, Espina V, Williams TW, Lin Y, Berry D, Jelicks LA, Lee H, Temple K, Graves R, Pollard J, et al. (2005). Adipocyte-derived collagen VI affects early mammary tumor progression in vivo, demonstrating a critical interaction in the tumor/stroma microenvironment. *J Clin Invest 115*: 1163-1176.

Jabbarzadeh Kaboli P, Salimian F, Aghapour S, Xiang S, Zhao Q, Li M, Wu X, Du F, Zhao Y, Shen J, et al. (2020). Akt-targeted therapy as a promising strategy to overcome drug resistance in breast cancer - A comprehensive review from chemotherapy to immunotherapy. *Pharmacol Res 156*: 104806.

Jain RK (2014). Antiangiogenesis strategies revisited: from starving tumors to alleviating hypoxia. *Cancer Cell 26*: 605-622.

Jang JY, Lee JK, Jeon YK et Kim CW (2013). Exosome derived from epigallocatechin gallate treated breast cancer cells suppresses tumor growth by inhibiting tumor-associated macrophage infiltration and M2 polarization. *BMC Cancer 13*: 421.

Jasinski-Bergner S et Kielstein H (2019). Adipokines regulate the expression of tumor-relevant microRNAs. *Obes Facts 12*: 211-225.

Jia L, Huang S, Yin X, Zan Y, Guo Y et Han L (2018). Quercetin suppresses the mobility of breast cancer by suppressing glycolysis through Akt-mTOR pathway mediated autophagy induction. *Life Sci 208*: 123-130.

Jiang H, Zhao H, Zhang M, He Y, Li X, Xu Y et Liu X (2022). Hypoxia induced changes of exosome cargo and subsequent biological effects. *Front Immunol 13*: 824188.

Jiang Y, Jiang H, Wang K, Liu C, Man X et Fu Q (2021). Hypoxia enhances the production and antitumor effect of exosomes derived from natural killer cells. *Ann Transl Med 9*: 473.

Jiang YG, Luo Y, He DL, Li X, Zhang LL, Peng T, Li MC et Lin YH (2007). Role of Wnt/beta-catenin signaling pathway in epithelial-mesenchymal transition of human prostate cancer induced by hypoxia-inducible factor-1alpha. *Int J Urol 14*: 1034-1039.

Jing N et Tweardy DJ (2005). Targeting Stat3 in cancer therapy. *Anticancer Drugs 16*: 601-607.

Jitariu AA, Cimpean AM, Ribatti D et Raica M (2017). Triple negative breast cancer: the kiss of death. *Oncotarget 8*: 46652-46662.

Jones SA et Jenkins BJ (2018). Recent insights into targeting the IL-6 cytokine family in inflammatory diseases and cancer. *Nat Rev Immunol 18*: 773-789.

Jung KO, Youn H, Lee CH, Kang KW et Chung JK (2017). Visualization of exosome-mediated miR-210 transfer from hypoxic tumor cells. *Oncotarget 8*: 9899-9910.

Kadouh H et Acosta A (2017). Current paradigms in the etiology of obesity. *Techniques in Gastrointestinal Endoscopy 19*: 2-11.

Kamat P, Schweizer R, Kaenel P, Salemi S, Calcagni M, Giovanoli P, Gorantla VS, Eberli D, Andres AC et Plock JA (2015). Human adipose-derived mesenchymal stromal cells may promote breast cancer progression and metastatic Spread. *Plast Reconstr Surg 136*: 76-84.

Kamimura D, Ishihara K et Hirano T (2003). IL-6 signal transduction and its physiological roles: the signal orchestration model. *Rev Physiol Biochem Pharmacol 149*: 1-38.

Kaplan RN, Riba RD, Zacharoulis S, Bramley AH, Vincent L, Costa C, MacDonald DD, Jin DK, Shido K, Kerns SA, et al. (2005). VEGFR1-positive haematopoietic bone marrow progenitors initiate the pre-metastatic niche. *Nature 438*: 820-827.

Katwan OJ, Alghamdi F, Almabrouk TA, Mancini SJ, Kennedy S, Oakhill JS, Scott JW et Salt IP (2019). AMP-activated protein kinase complexes containing the beta2 regulatory subunit are up-regulated during and contribute to adipogenesis. *Biochem J 476*: 1725-1740.

Kavanagh EL, Lindsay S, Halasz M, Gubbins LC, Weiner-Gorzel K, Guang MHZ, McGoldrick A, Collins E, Henry M, Blanco-Fernandez A, et al. (2017). Protein and chemotherapy profiling of extracellular vesicles harvested from therapeutic induced senescent triple negative breast cancer cells. *Oncogenesis 6*: e388.

Keller PJ, Lin AF, Arendt LM, Klebba I, Jones AD, Rudnick JA, DiMeo TA, Gilmore H, Jefferson DM, Graham RA, et al. (2010). Mapping the cellular and molecular heterogeneity of normal and malignant breast tissues and cultured cell lines. *Breast Cancer Res 12*: R87.

Key TJ, Appleby PN, Reeves GK, Roddam A, Dorgan JF, Longcope C, Stanczyk FZ, Stephenson HE, Jr., Falk RT, Miller R, et al. (2003). Body mass index, serum sex hormones, and breast cancer risk in postmenopausal women. *J Natl Cancer Inst 95*: 1218-1226.

Key TJ et Pike MC (1988). The role of oestrogens and progestagens in the epidemiology and prevention of breast cancer. *Eur J Cancer Clin Oncol 24*: 29-43.

Khan J, Deb PK, Priya S, Medina KD, Devi R, Walode SG et Rudrapal M (2021). Dietary Flavonoids: Cardioprotective Potential with Antioxidant Effects and Their Pharmacokinetic, Toxicological and Therapeutic Concerns. *Molecules 26*:

Khansari N, Shakiba Y et Mahmoudi M (2009). Chronic inflammation and oxidative stress as a major cause of age-related diseases and cancer. *Recent Pat Inflamm Allergy Drug Discov 3*: 73-80.

Khorsandi L, Orazizadeh M, Niazvand F, Abbaspour MR, Mansouri E et Khodadadi A (2017). Quercetin induces apoptosis and necroptosis in MCF-7 breast cancer cells. *Bratisl Lek Listy 118*: 123-128.

Kim H, Hiraishi A, Tsuchiya K et Sakamoto K (2010). (-) Epigallocatechin gallate suppresses the differentiation of 3T3-L1 preadipocytes through transcription factors FoxO1 and SREBP1c. *Cytotechnology 62*: 245-255.

Kim H et Sakamoto K (2012). (-)-Epigallocatechin gallate suppresses adipocyte differentiation through the MEK/ERK and PI3K/Akt pathways. *Cell Biol Int 36*: 147-153.

Kim HS, Quon MJ et Kim JA (2014). New insights into the mechanisms of polyphenols beyond antioxidant properties; lessons from the green tea polyphenol, epigallocatechin 3-gallate. *Redox Biol 2*: 187-195.

Kim JB et Spiegelman BM (1996). ADD1/SREBP1 promotes adipocyte differentiation and gene expression linked to fatty acid metabolism. *Genes Dev 10*: 1096-1107.

Kim SH, Yoo ES, Woo JS, Han SH, Lee JH, Jung SH, Kim HJ et Jung JY (2019). Antitumor and apoptotic effects of quercetin on human melanoma cells involving JNK/P38 MAPK signaling activation. *Eur J Pharmacol 860*: 172568.

Kim SN, Kwon HJ, Akindehin S, Jeong HW et Lee YH (2017a). Effects of Epigallocatechin-3-Gallate on Autophagic Lipolysis in Adipocytes. *Nutrients 9*:

Kim SO et Kim MR (2013). (-)-Epigallocatechin 3-gallate inhibits invasion by inducing the expression of Raf kinase inhibitor protein in AsPC-1 human pancreatic adenocarcinoma cells through the modulation of histone deacetylase activity. *Int J Oncol 42*: 349-358.

Kim YH, Choi YW, Lee J, Soh EY, Kim JH et Park TJ (2017b). Senescent tumor cells lead the collective invasion in thyroid cancer. *Nat Commun 8*: 15208.

Kimura Y et Okuda H (2001). Resveratrol isolated from Polygonum cuspidatum root prevents tumor growth and metastasis to lung and tumor-induced neovascularization in Lewis lung carcinoma-bearing mice. *J Nutr 131*: 1844-1849.

King HW, Michael MZ et Gleadle JM (2012). Hypoxic enhancement of exosome release by breast cancer cells. *BMC Cancer 12*: 421.

Kitani T, Kami D, Matoba S et Gojo S (2014). Internalization of isolated functional mitochondria: involvement of macropinocytosis. *J Cell Mol Med 18*: 1694-1703.

Klaus S, Pultz S, Thone-Reineke C et Wolfram S (2005). Epigallocatechin gallate attenuates diet-induced obesity in mice by decreasing energy absorption and increasing fat oxidation. *Int J Obes (Lond) 29*: 615-623.

Klemm DJ, Leitner JW, Watson P, Nesterova A, Reusch JE, Goalstone ML et Draznin B (2001). Insulin-induced adipocyte differentiation. Activation of CREB rescues adipogenesis from the arrest caused by inhibition of prenylation. *J Biol Chem 276*: 28430-28435.

Kloting N, Koch L, Wunderlich T, Kern M, Ruschke K, Krone W, Bruning JC et Bluher M (2008). Autocrine IGF-1 action in adipocytes controls systemic IGF-1 concentrations and growth. *Diabetes 57*: 2074-2082.

Koh YW, Choi EC, Kang SU, Hwang HS, Lee MH, Pyun J, Park R, Lee Y et Kim CH (2011). Green tea (-)-epigallocatechin-3-gallate inhibits HGF-induced progression in oral cavity cancer through suppression of HGF/c-Met. *J Nutr Biochem 22*: 1074-1083.

Kong J, Tian H, Zhang F, Zhang Z, Li J, Liu X, Li X, Liu J, Li X, Jin D, et al. (2019). Extracellular vesicles of carcinoma-associated fibroblasts creates a pre-metastatic niche in the lung through activating fibroblasts. *Mol Cancer 18*: 175.

Korwar AM, Bhonsle HS, Chougale AD, Kote SS, Gawai KR, Ghole VS, Koppikar CB et Kulkarni MJ (2012). Analysis of AGE modified proteins and RAGE expression in HER2/neu negative invasive ductal carcinoma. *Biochem Biophys Res Commun 419*: 490-494.

Krtolica A, Parrinello S, Lockett S, Desprez PY et Campisi J (2001). Senescent fibroblasts promote epithelial cell growth and tumorigenesis: a link between cancer and aging. *Proc Natl Acad Sci U S A 98*: 12072-12077.

Kucharzewska P, Christianson HC, Welch JE, Svensson KJ, Fredlund E, Ringner M, Morgelin M, Bourseau-Guilmain E, Bengzon J et Belting M (2013). Exosomes reflect the hypoxic status of glioma cells and mediate hypoxia-dependent activation of vascular cells during tumor development. *Proc Natl Acad Sci U S A 110*: 7312-7317.

Kwaifa IK, Bahari H, Yong YK et Noor SM (2020). Endothelial dysfunction in obesity-induced inflammation: Molecular mechanisms and clinical implications. *Biomolecules 10*:

Lachapelle J et Foulkes WD (2011). Triple-negative and basal-like breast cancer: implications for oncologists. *Curr Oncol 18*: 161-164.

Lang DR et Racker E (1974). Effects of quercetin and F1 inhibitor on mitochondrial ATPase and energy-linked reactions in submitochondrial particles. *Biochim Biophys Acta 333*: 180-186.

Lasry A et Ben-Neriah Y (2015). Senescence-associated inflammatory responses: aging and cancer perspectives. *Trends Immunol 36*: 217-228.

Lauby-Secretan B, Scoccianti C, Loomis D, Grosse Y, Bianchini F, Straif K et International Agency for Research on Cancer Handbook Working G (2016). Body Fatness and Cancer--Viewpoint of the IARC Working Group. *N Engl J Med 375*: 794-798.

Law BMH, Waye MMY, So WKW et Chair SY (2017). Hypotheses on the Potential of Rice Bran Intake to Prevent Gastrointestinal Cancer through the Modulation of Oxidative Stress. *Int J Mol Sci 18*:

Lazar AD, Dinescu, S., and Costache, M. (2018). Adipose tissue engineering and adipogenesis – a review. *Rev Biol Biomed Sci 1*: 17-26.

Lazar I, Clement E, Dauvillier S, Milhas D, Ducoux-Petit M, LeGonidec S, Moro C, Soldan V, Dalle S, Balor S, et al. (2016). Adipocyte exosomes promote melanoma aggressiveness through fatty acid oxidation: A novel mechanism linking obesity and cancer. *Cancer Res 76*: 4051-4057.

Lee H, Bae S et Yoon Y (2013). The anti-adipogenic effects of (-)epigallocatechin gallate are dependent on the WNT/beta-catenin pathway. *J Nutr Biochem 24*: 1232-1240.

Lee J, Han Y, Wang W, Jo H, Kim H, Kim S, Yang KM, Kim SJ, Dhanasekaran DN et Song YS (2021). Phytochemicals in cancer immune checkpoint inhibitor therapy. *Biomolecules 11*:

Lee J, Hong BS, Ryu HS, Lee HB, Lee M, Park IA, Kim J, Han W, Noh DY et Moon HG (2017). Transition into inflammatory cancer-associated adipocytes in breast cancer microenvironment requires microRNA regulatory mechanism. *PLoS One 12*: e0174126.

Lee JE, Schmidt H, Lai B et Ge K (2019). Transcriptional and epigenomic regulation of adipogenesis. *Mol Cell Biol 39*:

Lee MS et Kim Y (2009). (-)-Epigallocatechin-3-gallate enhances uncoupling protein 2 gene expression in 3T3-L1 adipocytes. *Biosci Biotechnol Biochem 73*: 434-436.

Lee S et Schmitt CA (2019). The dynamic nature of senescence in cancer. *Nat Cell Biol 21*: 94-101.

Lefterova MI et Lazar MA (2009). New developments in adipogenesis. *Trends Endocrinol Metab 20*: 107-114.

Leger JL, Soucy MN, Veilleux V, Foulem RD, Robichaud GA, Surette ME, Allain EP et Boudreau LH (2022). Functional platelet-derived mitochondria induce the release of human neutrophil microvesicles. *EMBO Rep 23*: e54910.

Lehmann BD, Bauer JA, Chen X, Sanders ME, Chakravarthy AB, Shyr Y et Pietenpol JA (2011). Identification of human triple-negative breast cancer subtypes and preclinical models for selection of targeted therapies. *J Clin Invest 121*: 2750-2767.

Lehmann BD et Pietenpol JA (2014). Identification and use of biomarkers in treatment strategies for triple-negative breast cancer subtypes. *J Pathol 232*: 142-150.

Lehrskov LL et Christensen RH (2019). The role of interleukin-6 in glucose homeostasis and lipid metabolism. *Semin Immunopathol 41*: 491-499.

Lengyel E, Makowski L, DiGiovanni J et Kolonin MG (2018). Cancer as a Matter of Fat: The Crosstalk between Adipose Tissue and Tumors. *Trends Cancer 4*: 374-384.

Leslie K, Lang C, Devgan G, Azare J, Berishaj M, Gerald W, Kim YB, Paz K, Darnell JE, Albanese C, et al. (2006). Cyclin D1 is transcriptionally regulated by and required for transformation by activated signal transducer and activator of transcription 3. *Cancer Res 66*: 2544-2552.

Li B et Dewey CN (2011). RSEM: accurate transcript quantification from RNA-Seq data with or without a reference genome. *BMC Bioinformatics 12*: 323.

Li B, Hao J, Yan X, Kong M et Sauter ER (2019a). A-FABP and oestrogens are independently involved in the development of breast cancer. *Adipocyte 8*: 379-385.

Li C, Qiu S, Jin K, Zheng X, Zhou X, Jin D, Xu B et Jin X (2021). Tumor-derived microparticles promote the progression of triple-negative breast cancer via PD-L1-associated immune suppression. *Cancer Lett 523*: 43-56.

Li D, Ji H, Niu X, Yin L, Wang Y, Gu Y, Wang J, Zhou X, Zhang H et Zhang Q (2020a). Tumor-associated macrophages secrete CC-chemokine ligand 2 and induce tamoxifen resistance by activating PI3K/Akt/mTOR in breast cancer. *Cancer Sci 111*: 47-58.

Li D, Zhang T, Lu J, Peng C et Lin L (2020b). Natural constituents from food sources as therapeutic agents for obesity and metabolic diseases targeting adipose tissue inflammation. *Crit Rev Food Sci Nutr* 1-19.

Li FQ, Singh AM, Mofunanya A, Love D, Terada N, Moon RT et Takemaru K (2007). Chibby promotes adipocyte differentiation through inhibition of beta-catenin signaling. *Mol Cell Biol 27*: 4347-4354.

Li GX, Chen YK, Hou Z, Xiao H, Jin H, Lu G, Lee MJ, Liu B, Guan F, Yang Z, et al. (2010). Pro-oxidative activities and dose-response relationship of (-)-epigallocatechin-3-gallate in the inhibition of lung cancer cell growth: a comparative study in vivo and in vitro. *Carcinogenesis 31*: 902-910.

Li H, Qi J et Li L (2019b). Phytochemicals as potential candidates to combat obesity via adipose non-shivering thermogenesis. *Pharmacol Res 147*: 104393.

Li S, Wu L, Feng J, Li J, Liu T, Zhang R, Xu S, Cheng K, Zhou Y, Zhou S, et al. (2016). In vitro and in vivo study of epigallocatechin-3-gallate-induced apoptosis in aerobic glycolytic hepatocellular carcinoma cells involving inhibition of phosphofructokinase activity. *Sci Rep 6*: 28479.

Li W, Zhang X, Wang J, Li M, Cao C, Tan J, Ma D et Gao Q (2017). TGFbeta1 in fibroblasts-derived exosomes promotes epithelial-mesenchymal transition of ovarian cancer cells. *Oncotarget 8*: 96035-96047.

Li W, Zhu S, Li J, Assa A, Jundoria A, Xu J, Fan S, Eissa NT, Tracey KJ, Sama AE, et al. (2011a). EGCG stimulates autophagy and reduces cytoplasmic HMGB1 levels in endotoxin-stimulated macrophages. *Biochem Pharmacol 81*: 1152-1163.

Li X, Feng Y, Liu J, Feng X, Zhou K et Tang X (2013). Epigallocatechin-3-gallate inhibits IGF-I-stimulated lung cancer angiogenesis through downregulation of HIF-1alpha and VEGF expression. *J Nutrigenet Nutrigenomics 6*: 169-178.

Li X, Lewis MT, Huang J, Gutierrez C, Osborne CK, Wu MF, Hilsenbeck SG, Pavlick A, Zhang X, Chamness GC, et al. (2008). Intrinsic resistance of tumorigenic breast cancer cells to chemotherapy. *J Natl Cancer Inst 100*: 672-679.

Li Y, Zhao S, Zhang W, Zhao P, He B, Wu N et Han P (2011b). Epigallocatechin-3-O-gallate (EGCG) attenuates FFAs-induced peripheral insulin resistance through AMPK pathway and insulin signaling pathway in vivo. *Diabetes Res Clin Pract 93*: 205-214.

Lin J, Della-Fera MA et Baile CA (2005). Green tea polyphenol epigallocatechin gallate inhibits adipogenesis and induces apoptosis in 3T3-L1 adipocytes. *Obes Res 13*: 982-990.

Liou GY et Storz P (2010). Reactive oxygen species in cancer. *Free Radic Res 44*: 479-496.

Liu C, Hao K, Liu Z, Liu Z et Guo N (2021). Epigallocatechin gallate (EGCG) attenuates staphylococcal alpha-hemolysin (Hla)-induced NLRP3 inflammasome activation via ROS-MAPK pathways and EGCG-Hla interactions. *Int Immunopharmacol 100*: 108170.

Liu J, Wang H, Zuo Y et Farmer SR (2006). Functional interaction between peroxisome proliferator-activated receptor gamma and beta-catenin. *Mol Cell Biol 26*: 5827-5837.

Liu Q, Fu H, Sun F, Zhang H, Tie Y, Zhu J, Xing R, Sun Z et Zheng X (2008). miR-16 family induces cell cycle arrest by regulating multiple cell cycle genes. *Nucleic Acids Res 36*: 5391-5404.

Liu Q, Liu T, Zheng S, Gao X, Lu M, Sheyhidin I et Lu X (2014). HMGA2 is down-regulated by microRNA let-7 and associated with epithelial-mesenchymal transition in oesophageal squamous cell carcinomas of Kazakhs. *Histopathology 65*: 408-417.

Liu S, Wang XJ, Liu Y et Cui YF (2013). PI3K/AKT/mTOR signaling is involved in (-)-epigallocatechin-3-gallate-induced apoptosis of human pancreatic carcinoma cells. *Am J Chin Med 41*: 629-642.

Liu YR, Jiang YZ, Xu XE, Yu KD, Jin X, Hu X, Zuo WJ, Hao S, Wu J, Liu GY, et al. (2016). Comprehensive transcriptome analysis identifies novel molecular subtypes and subtype-specific RNAs of triple-negative breast cancer. *Breast Cancer Res 18*: 33.

Lo HW, Hsu SC, Xia W, Cao X, Shih JY, Wei Y, Abbruzzese JL, Hortobagyi GN et Hung MC (2007). Epidermal growth factor receptor cooperates with signal transducer and activator of transcription 3 to induce epithelial-mesenchymal transition in cancer cells via up-regulation of TWIST gene expression. *Cancer Res 67*: 9066-9076.

Loh CY, Arya A, Naema AF, Wong WF, Sethi G et Looi CY (2019). Signal Transducer and Activator of Transcription (STATs) Proteins in Cancer and Inflammation: Functions and Therapeutic Implication. *Front Oncol 9*: 48.

Lokuhetty D, White V, Watanabe R et Cree I (2019). WHO Classification of Tumors Editorial Board. Breast Tumors. *WHO Classification of Tumors Series, 5th ed; International Agency for Research on Cancer: Lyon, France 2*: 88-97.

Love MI, Huber W et Anders S (2014). Moderated estimation of fold change and dispersion for RNA-seq data with DESeq2. *Genome Biol 15*: 550.

Lowenstein CJ et Padalko E (2004). iNOS (NOS2) at a glance. *J Cell Sci 117*: 2865-2867.

Lu Z, Zou J, Li S, Topper MJ, Tao Y, Zhang H, Jiao X, Xie W, Kong X, Vaz M, et al. (2020). Epigenetic therapy inhibits metastases by disrupting premetastatic niches. *Nature 579*: 284-290.

Luga V, Zhang L, Viloria-Petit AM, Ogunjimi AA, Inanlou MR, Chiu E, Buchanan M, Hosein AN, Basik M et Wrana JL (2012). Exosomes mediate stromal mobilization of autocrine Wnt-PCP signaling in breast cancer cell migration. *Cell 151*: 1542-1556.

Lv MM, Zhu XY, Chen WX, Zhong SL, Hu Q, Ma TF, Zhang J, Chen L, Tang JH et Zhao JH (2014). Exosomes mediate drug resistance transfer in MCF-7 breast cancer cells and a probable mechanism is delivery of P-glycoprotein. *Tumor Biol 35*: 10773-10779.

Lyons TG (2019). Targeted Therapies for Triple-Negative Breast Cancer. *Curr Treat Options Oncol 20*: 82.

Ma X, Lee P, Chisholm DJ et James DE (2015). Control of adipocyte differentiation in different fat depots; implications for pathophysiology or therapy. *Front Endocrinol (Lausanne) 6*: 1.

Ma Y, Ren Y, Dai ZJ, Wu CJ, Ji YH et Xu J (2017). IL-6, IL-8 and TNF-alpha levels correlate with disease stage in breast cancer patients. *Adv Clin Exp Med 26*: 421-426.

Ma YC, Li C, Gao F, Xu Y, Jiang ZB, Liu JX et Jin LY (2014). Epigallocatechin gallate inhibits the growth of human lung cancer by directly targeting the EGFR signaling pathway. *Oncol Rep 31*: 1343-1349.

Madak-Erdogan Z, Band S, Zhao YC, Smith BP, Kulkoyluoglu-Cotul E, Zuo Q, Santaliz Casiano A, Wrobel K, Rossi G, Smith RL, et al. (2019). Free Fatty Acids Rewire Cancer Metabolism in Obesity-Associated Breast Cancer via Estrogen Receptor and mTOR Signaling. *Cancer Res 79*: 2494-2510.

Magkos F, Wang X et Mittendorfer B (2010) .Metabolic actions of insulin in men and women. *Nutrition 26*: 686-693.

Mahyar-Roemer M, Kohler H et Roemer K (2002). Role of Bax in resveratrol-induced apoptosis of colorectal carcinoma cells. *BMC Cancer 2*: 27.

Maiuolo J, Gliozzi M, Carresi C, Musolino V, Oppedisano F, Scarano F, Nucera S, Scicchitano M, Bosco F, Macri R, et al. (2021). Nutraceuticals and cancer: potential for natural polyphenols. *Nutrients 13*:

Maj M, Kokocha A, Bajek A et Drewa T (2018.) The interplay between adipose-derived stem cells and bladder cancer cells. *Sci Rep 8*: 15118.

Maliniak ML, Miller-Kleinhenz J, Cronin-Fenton DP, Lash TL, Gogineni K, Janssen EAM et McCullough LE (2021). Crown-like structures in breast adipose tissue: early evidence and current issues in breast cancer. *Cancers (Basel) 13*:

Manore SG, Doheny DL, Wong GL et Lo HW (2022). IL-6/JAK/STAT3 signaling in breast cancer metastasis: biology and treatment. *Front Oncol 12*: 866014.

Mao XY, Jin MZ, Chen JF, Zhou HH et Jin WL (2018). Live or let die: Neuroprotective and anti-cancer effects of nutraceutical antioxidants. *Pharmacol Ther 183*: 137-151.

Margoni A, Fotis L et Papavassiliou AG (2012). The transforming growth factor-beta/bone morphogenetic protein signalling pathway in adipogenesis. *Int J Biochem Cell Biol 44*: 475-479.

Marinho HS, Real C, Cyrne L, Soares H et Antunes F (2014). Hydrogen peroxide sensing, signaling and regulation of transcription factors. *Redox Biol 2*: 535-562.

Marleau AM, Chen CS, Joyce JA et Tullis RH (2012). Exosome removal as a therapeutic adjuvant in cancer. *J Transl Med 10*: 134.

Martinez-Outschoorn UE, Goldberg A, Lin Z, Ko YH, Flomenberg N, Wang C, Pavlides S, Pestell RG, Howell A, Sotgia F, et al. (2011). Anti-estrogen resistance in breast cancer is induced by the tumor microenvironment and can be overcome by inhibiting mitochondrial function in epithelial cancer cells. *Cancer Biol Ther 12*: 924-938.

Masoud GN et Li W (2015). HIF-1alpha pathway: role, regulation and intervention for cancer therapy. *Acta Pharm Sin B 5*: 378-389.

Mathieu M, Martin-Jaular L, Lavieu G et Thery C (2019). Specificities of secretion and uptake of exosomes and other extracellular vesicles for cell-to-cell communication. *Nat Cell Biol 21*: 9-17.

Mathieu P, Lemieux I et Despres JP (2010). Obesity, inflammation, and cardiovascular risk. *Clin Pharmacol Ther 87*: 407-416.

Mause SF, von Hundelshausen P, Zernecke A, Koenen RR et Weber C (2005). Platelet microparticles: a transcellular delivery system for RANTES promoting monocyte recruitment on endothelium. *Arterioscler Thromb Vasc Biol 25*: 1512-1518.

McClellan JL, Davis JM, Steiner JL, Enos RT, Jung SH, Carson JA, Pena MM, Carnevale KA, Berger FG et Murphy EA (2012). Linking tumor-associated macrophages, inflammation, and intestinal tumorigenesis: role of MCP-1. *Am J Physiol Gastrointest Liver Physiol 303*: G1087-1095.

Medina M et Wandosell F (2011). Deconstructing GSK-3: The Fine Regulation of Its Activity. *Int J Alzheimers Dis 2011*: 479249.

Millington-Burgess SL et Harper MT (2021). Epigallocatechin gallate inhibits release of extracellular vesicles from platelets without inhibiting phosphatidylserine exposure. *Sci Rep 11*: 17678.

Min KJ et Kwon TK (2014). Anticancer effects and molecular mechanisms of epigallocatechin-3-gallate. *Integr Med Res 3*: 16-24.

Mineva ND, Paulson KE, Naber SP, Yee AS et Sonenshein GE (2013). Epigallocatechin-3-gallate inhibits stem-like inflammatory breast cancer cells. *PLoS One 8*: e73464.

Miran I, Scherer D, Ostyn P, Mazouni C, Drusch F, Bernard M, Louvet E, Adam J, Mathieu MC, Haffa M, et al. (2020). Adipose tissue properties in tumor-bearing breasts. *Front Oncol 10*: 1506.

Mittal S, Brown NJ et Holen I (2018). The breast tumor microenvironment: role in cancer development, progression and response to therapy. *Expert Rev Mol Diagn 18*: 227-243.

Mobius W, Ohno-Iwashita Y, van Donselaar EG, Oorschot VM, Shimada Y, Fujimoto T, Heijnen HF, Geuze HJ et Slot JW (2002). Immunoelectron microscopic localization of cholesterol using biotinylated and non-cytolytic perfringolysin O. *J Histochem Cytochem 50*: 43-55.

Mokra D, Joskova M et Mokry J (2022). Therapeutic effects of green tea polyphenol (–)-epigallocatechin-3-gallate (EGCG) in relation to molecular pathways controlling inflammation, oxidative stress, and apoptosis. *Int J Mol Sci 24*:

Moschos SJ et Mantzoros CS (2002). The role of the IGF system in cancer: from basic to clinical studies and clinical applications. *Oncology 63*: 317-332.

Moseti D, Regassa A et Kim WK (2016). Molecular regulation of adipogenesis and potential anti-adipogenic bioactive molecules. *Int J Mol Sci 17*:

Moulana M, Lima R et Reckelhoff JF (2011). Metabolic syndrome, androgens, and hypertension. *Curr Hypertens Rep 13*: 158-162.

Muralidharan-Chari V, Clancy J, Plou C, Romao M, Chavrier P, Raposo G et D'Souza-Schorey C (2009). ARF6-regulated shedding of tumor cell-derived plasma membrane microvesicles. *Curr Biol 19*: 1875-1885.

Murata M, Marugame Y, Morozumi M, Murata K, Kumazoe M, Fujimura Y et Tachibana H (2023). (-)-Epigallocatechin-3-O-gallate upregulates the expression levels of miR-6757-3p, a suppressor of fibrosis-related gene expression, in extracellular vesicles derived from human umbilical vein endothelial cells. *Biomed Rep 18*: 19.

Nahacka Z, Zobalova R, Dubisova M, Rohlena J et Neuzil J (2021). Miro proteins connect mitochondrial function and intercellular transport. *Crit Rev Biochem Mol Biol 56*: 401-425.

Naik A, Monjazeb AM et Decock J (2019). The Obesity Paradox in Cancer, Tumor Immunology, and Immunotherapy: Potential Therapeutic Implications in Triple Negative Breast Cancer. *Front Immunol 10*: 1940.

Naujokat C et McKee DL (2021). The "big five" phytochemicals targeting cancer stem cells: Curcumin, EGCG, sulforaphane, resveratrol and genistein. *Curr Med Chem 28*: 4321-4342.

Negri AN, V.; Rizzi, F.; Bettuzzi, S. (2018). Molecular targets of epigallocatechin-gallate (EGCG): A special focus on signal transduction and cancer. *Nutrients 10*: 1936.

Neveu V, Perez-Jimenez J, Vos F, Crespy V, du Chaffaut L, Mennen L, Knox C, Eisner R, Cruz J, Wishart D, et al. (2010). Phenol-Explorer: an online comprehensive database on polyphenol contents in foods. *Database (Oxford) 2010*: bap024.

Nguyen MT, Satoh H, Favelyukis S, Babendure JL, Imamura T, Sbodio JI, Zalevsky J, Dahiyat BI, Chi NW et Olefsky JM (2005). JNK and tumor necrosis factor-alpha mediate free fatty acid-induced insulin resistance in 3T3-L1 adipocytes. *J Biol Chem 280*: 35361-35371.

Nguyen TNQ, Jung S, Nguyen HA, Lee B, Vu SH, Myagmarjav D, Eum HH, Lee HO, Jo T, Choi Y, et al. (2022). The regulation of insulin receptor/insulin-like growth factor 1 receptor ratio, an important factor for breast cancer prognosis, by TRIP-Br1. *J Hematol Oncol 15*: 82.

Ni C, Fang QQ, Chen WZ, Jiang JX, Jiang Z, Ye J, Zhang T, Yang L, Meng FB, Xia WJ, et al. (2020). Breast cancer-derived exosomes transmit lncRNA SNHG16 to induce CD73+gammadelta1 Treg cells. *Signal Transduct Target Ther 5*: 41.

Nicholson C, Shah N, Ishii M, Annamalai B, Brandon C, Rodgers J, Nowling T et Rohrer B (2020). Mechanisms of extracellular vesicle uptake in stressed retinal pigment epithelial cell monolayers. *Biochim Biophys Acta Mol Basis Dis 1866*: 165608.

Nieman KM, Romero IL, Van Houten B et Lengyel E (2013). Adipose tissue and adipocytes support tumorigenesis and metastasis. *Biochim Biophys Acta 1831*: 1533-1541.

Nishimura N, Hartomo TB, Pham TV, Lee MJ, Yamamoto T, Morikawa S, Hasegawa D, Takeda H, Kawasaki K, Kosaka Y, et al. (2012). Epigallocatechin gallate inhibits sphere formation of neuroblastoma BE(2)-C cells. *Environ Health Prev Med 17*: 246-251.

Nogues L, Benito-Martin A, Hergueta-Redondo M et Peinado H (2018). The influence of tumor-derived extracellular vesicles on local and distal metastatic dissemination. *Mol Aspects Med 60*: 15-26.

Nomura M, Ma W, Chen N, Bode AM et Dong Z (2000). Inhibition of 12-O-tetradecanoylphorbol-13-acetate-induced NF-kappaB activation by tea polyphenols, (-)-epigallocatechin gallate and theaflavins. *Carcinogenesis 21*: 1885-1890.

O'Meara T, Marczyk M, Qing T, Yaghoobi V, Blenman K, Cole K, Pelekanou V, Rimm DL et Pusztai L (2020). Immunological differences between immune-rich estrogen receptor-positive and immune-rich triple-negative breast cancers. *JCO Precis Oncol 4*:

Oishi Y, Manabe I, Tobe K, Tsushima K, Shindo T, Fujiu K, Nishimura G, Maemura K, Yamauchi T, Kubota N, et al. (2005). Kruppel-like transcription factor KLF5 is a key regulator of adipocyte differentiation. *Cell Metab 1*: 27-39.

Onishi RM et Gaffen SL (2010). Interleukin-17 and its target genes: mechanisms of interleukin-17 function in disease. *Immunology 129*: 311-321.

Onzi GR, Faccioni JL, Pereira LC, Thome MP, Bertoni APS, Buss JH, Fazolo T, Filippi-Chiela E, Wink MR et Lenz G (2019). Adipose-derived stromal cell secretome disrupts autophagy in glioblastoma. *J Mol Med (Berl) 97*: 1491-1506.

Orimo A, Gupta PB, Sgroi DC, Arenzana-Seisdedos F, Delaunay T, Naeem R, Carey VJ, Richardson AL et Weinberg RA (2005). Stromal fibroblasts present in invasive human breast carcinomas promote tumor growth and angiogenesis through elevated SDF-1/CXCL12 secretion. *Cell 121*: 335-348.

Orrantia-Borunda E, Anchondo-Nunez P, Acuna-Aguilar LE, Gomez-Valles FO et Ramirez-Valdespino CA (2022). Subtypes of breast cancer. Dans *Breast Cancer*. Mayrovitz HN, ed. Brisbane (AU).

Ozawa PMM, Alkhilaiwi F, Cavalli IJ, Malheiros D, de Souza Fonseca Ribeiro EM et Cavalli LR (2018). Extracellular vesicles from triple-negative breast cancer cells promote proliferation and drug resistance in non-tumorigenic breast cells. *Breast Cancer Res Treat 172*: 713-723.

Pan X, Hong X, Lai J, Cheng L, Cheng Y, Yao M, Wang R et Hu N (2020). Exosomal microRNA-221-3p confers adriamycin resistance in breast cancer cells by targeting PIK3R1. *Front Oncol 10*: 441.

Pare M, Darini CY, Yao X, Chignon-Sicard B, Rekima S, Lachambre S, Virolle V, Aguilar-Mahecha A, Basik M, Dani C, et al. (2020). Breast cancer mammospheres secrete Adrenomedullin to induce lipolysis and browning of adjacent adipocytes. *BMC Cancer 20*: 784.

Park EJ, Lee JH, Yu GY, He G, Ali SR, Holzer RG, Osterreicher CH, Takahashi H et Karin M (2010a). Dietary and genetic obesity promote liver inflammation and tumorigenesis by enhancing IL-6 and TNF expression. *Cell 140*: 197-208.

Park HJ, Chung BY, Lee MK, Song Y, Lee SS, Chu GM, Kang SN, Song YM, Kim GS et Cho JH (2012). Centipede grass exerts anti-adipogenic activity through inhibition of C/EBPbeta, C/EBPalpha, and PPARgamma expression and the AKT signaling pathway in 3T3-L1 adipocytes. *BMC Complement Altern Med 12*: 230.

Park J, Wysocki RW, Amoozgar Z, Maiorino L, Fein MR, Jorns J, Schott AF, Kinugasa-Katayama Y, Lee Y, Won NH, et al. (2016). Cancer cells induce metastasis-supporting neutrophil extracellular DNA traps. *Sci Transl Med 8*: 361ra138.

Park SY, Lee HE, Li H, Shipitsin M, Gelman R et Polyak K (2010b). Heterogeneity for stem cell-related markers according to tumor subtype and histologic stage in breast cancer. *Clin Cancer Res 16*: 876-887.

Pascut D, Pratama MY, Vo NVT, Masadah R et Tiribelli C (2020). The crosstalk between tumor cells and the microenvironment in hepatocellular carcinoma: The role of exosomal microRNAs and their clinical implications. *Cancers (Basel) 12*:

Patra SK, Rizzi F, Silva A, Rugina DO et Bettuzzi S (2008) Molecular targets of (-)-epigallocatechin-3-gallate (EGCG): specificity and interaction with membrane lipid rafts. *J Physiol Pharmacol 59 Suppl 9*: 217-235.

Peinado H, Aleckovic M, Lavotshkin S, Matei I, Costa-Silva B, Moreno-Bueno G, Hergueta-Redondo M, Williams C, Garcia-Santos G, Ghajar C, et al. (2012). Melanoma exosomes educate bone marrow progenitor cells toward a pro-metastatic phenotype through MET. *Nat Med 18*: 883-891.

Peng CY, Liao YW, Lu MY, Yang CM, Hsieh PL et Yu CC (2020). Positive feedback loop of SNAIL-IL-6 mediates myofibroblastic differentiation activity in precancerous oral submucous fibrosis. *Cancers (Basel) 12*:

Pennacchietti S, Michieli P, Galluzzo M, Mazzone M, Giordano S et Comoglio PM (2003). Hypoxia promotes invasive growth by transcriptional activation of the met protooncogene. *Cancer Cell 3*: 347-361.

Perez LM, Pareja-Galeano H, Sanchis-Gomar F, Emanuele E, Lucia A et Galvez BG (2016). 'Adipaging': ageing and obesity share biological hallmarks related to a dysfunctional adipose tissue. *J Physiol 594*: 3187-3207.

Perou CM, Sorlie T, Eisen MB, van de Rijn M, Jeffrey SS, Rees CA, Pollack JR, Ross DT, Johnsen H, Akslen LA, et al. (2000). Molecular portraits of human breast tumors. *Nature 406*: 747-752.

Picon-Ruiz M, Morata-Tarifa C, Valle-Goffin JJ, Friedman ER et Slingerland JM (2017) Obesity and adverse breast cancer risk and outcome: Mechanistic insights and strategies for intervention. *CA Cancer J Clin 67*: 378-397.

Picon-Ruiz M, Pan C, Drews-Elger K, Jang K, Besser AH, Zhao D, Morata-Tarifa C, Kim M, Ince TA, Azzam DJ, et al. (2016). Interactions between adipocytes and breast cancer cells stimulate cytokine production and drive Src/Sox2/miR-302b-mediated malignant progression. *Cancer Res 76*: 491-504.

Pires BR, IS DEA, Souza LD, Rodrigues JA et Mencalha AL (2016). Targeting Cellular signaling pathways in breast cancer stem cells and its implication for cancer treatment. *Anticancer Res 36*: 5681-5691.

Pischon T et Nimptsch K (2016). Obesity and risk of cancer: an introductory overview. *Recent Results Cancer Res 208*: 1-15.

Plava J, Cihova M, Burikova M, Bohac M, Adamkov M, Drahosova S, Rusnakova D, Pindak D, Karaba M, Simo J, et al. (2020) Permanent pro-tumorigenic shift in adipose tissue-derived mesenchymal stromal cells induced by breast malignancy. *Cells 9*:

Poggio M, Hu T, Pai CC, Chu B, Belair CD, Chang A, Montabana E, Lang UE, Fu Q, Fong L, et al. (2019). Suppression of exosomal PD-L1 induces systemic anti-tumor immunity and memory. *Cell 177*: 414-427 e413.

Pribluda A, Elyada E, Wiener Z, Hamza H, Goldstein RE, Biton M, Burstain I, Morgenstern Y, Brachya G, Billauer H, et al. (2013). A senescence-inflammatory switch from cancer-inhibitory to cancer-promoting mechanism. *Cancer Cell 24*: 242-256.

Protani M, Coory M et Martin JH (2010). Effect of obesity on survival of women with breast cancer: systematic review and meta-analysis. *Breast Cancer Res Treat 123*: 627-635.

Pu X et Chen D (2021). Targeting Adipokines in Obesity-Related Tumors. *Front Oncol 11*: 685923.

Qian Y, Ding P, Xu J, Nie X et Lu B (2022). CCL2 activates AKT signaling to promote glycolysis and chemoresistance in glioma cells. *Cell Biol Int 46*: 819-828.

Qin JJ, Yan L, Zhang J et Zhang WD (2019). STAT3 as a potential therapeutic target in triple negative breast cancer: a systematic review. *J Exp Clin Cancer Res 38*: 195.

Qin W, Zhang K, Clarke K, Weiland T et Sauter ER (2014). Methylation and miRNA effects of resveratrol on mammary tumors vs. normal tissue. *Nutr Cancer 66*: 270-277.

Quail DF et Dannenberg AJ (2019). The obese adipose tissue microenvironment in cancer development and progression. *Nat Rev Endocrinol 15*: 139-154.

Rabas N, Palmer S, Mitchell L, Ismail S, Gohlke A, Riley JS, Tait SWG, Gammage P, Soares LL, Macpherson IR, et al. (2021). PINK1 drives production of mtDNA-containing extracellular vesicles to promote invasiveness. *J Cell Biol 220*:

Rady IM, H.; Siddiqui, I.A.; Mukhtar, H. (2018). Cancer preventive and therapeutic effects of EGCG, the major polyphenol in green tea. *Egypt j basic appl sci 5*: 1-23.

Raghunathachar Sahana K, Akila P, Prashant V, Sharath Chandra B et Nataraj Suma M (2017). Quantitation of Vascular Endothelial Growth Factor and Interleukin-6 in Different Stages of Breast Cancer. *Rep Biochem Mol Biol 6*: 33-39.

Rajagopal C, Lankadasari MB, Aranjani JM et Harikumar KB (2018). Targeting oncogenic transcription factors by polyphenols: A novel approach for cancer therapy. *Pharmacol Res 130*: 273-291.

Rakha EA, El-Sayed ME, Green AR, Lee AH, Robertson JF et Ellis IO (2007). Prognostic markers in triple-negative breast cancer. *Cancer 109*: 25-32.

Raman D, Baugher PJ, Thu YM et Richmond A (2007). Role of chemokines in tumor growth. *Cancer Lett 256*: 137-165.

Ramos-Nino ME (2013). The role of chronic inflammation in obesity-associated cancers. *ISRN Oncol 2013*: 697521.

Ramteke A, Ting H, Agarwal C, Mateen S, Somasagara R, Hussain A, Graner M, Frederick B, Agarwal R et Deep G (2015). Exosomes secreted under hypoxia enhance invasiveness and stemness of prostate cancer cells by targeting adherens junction molecules. *Mol Carcinog 54*: 554-565.

Raouf A, Zhao Y, To K, Stingl J, Delaney A, Barbara M, Iscove N, Jones S, McKinney S, Emerman J, et al. (2008). Transcriptome analysis of the normal human mammary cell commitment and differentiation process. *Cell Stem Cell 3*: 109-118.

Raposo G et Stoorvogel W (2013). Extracellular vesicles: exosomes, microvesicles, and friends. *J Cell Biol 200*: 373-383.

Rasool RU, Nayak D, Chakraborty S, Faheem MM, Rah B, Mahajan P, Gopinath V, Katoch A, Iqra Z, Yousuf SK, et al. (2017). AKT is indispensable for coordinating Par-4/JNK cross talk in p21 downmodulation during ER stress. *Oncogenesis 6*: e341.

Real PJ, Sierra A, De Juan A, Segovia JC, Lopez-Vega JM et Fernandez-Luna JL (2002). Resistance to chemotherapy via Stat3-dependent overexpression of Bcl-2 in metastatic breast cancer cells. *Oncogene 21*: 7611-7618.

Ren W, Hou J, Yang C, Wang H, Wu S, Wu Y, Zhao X et Lu C (2019). Extracellular vesicles secreted by hypoxia pre-challenged mesenchymal stem cells promote non-small cell lung cancer cell growth and mobility as well as macrophage M2 polarization via miR-21-5p delivery. *J Exp Clin Cancer Res 38*: 62.

Renehan AG, Tyson M, Egger M, Heller RF et Zwahlen M (2008). Body-mass index and incidence of cancer: a systematic review and meta-analysis of prospective observational studies. *Lancet 371*: 569-578.

Reusch JE, Colton LA et Klemm DJ (2000). CREB activation induces adipogenesis in 3T3-L1 cells. *Mol Cell Biol 20*: 1008-1020.

Reyes-Farias M et Carrasco-Pozo C (2019). The Anti-Cancer Effect of Quercetin: Molecular Implications in Cancer Metabolism. *Int J Mol Sci 20*:

Riondino S, Roselli M, Palmirotta R, Della-Morte D, Ferroni P et Guadagni F (2014). Obesity and colorectal cancer: role of adipokines in tumor initiation and progression. *World J Gastroenterol 20*: 5177-5190.

Ritchie ME, Phipson B, Wu D, Hu Y, Law CW, Shi W et Smyth GK (2015). limma powers differential expression analyses for RNA-sequencing and microarray studies. *Nucleic Acids Res 43*: e47.

Ritter A, Kreis NN, Roth S, Friemel A, Safdar BK, Hoock SC, Wildner JM, Allert R, Louwen F, Solbach C, et al. (2023). Cancer-educated mammary adipose tissue-derived stromal/stem cells in obesity and breast cancer: spatial regulation and function. *J Exp Clin Cancer Res 42*: 35.

Robert AW, Marcon BH, Angulski ABB, Martins ST, Leitolis A, Stimamiglio MA, Senegaglia AC, Correa A et Alves LR (2022). Selective Loading and Variations in the miRNA Profile of Extracellular Vesicles from Endothelial-like Cells Cultivated under Normoxia and Hypoxia. *Int J Mol Sci 23*:

Robert AW, Marcon BH, Dallagiovanna B et Shigunov P (2020). Adipogenesis, osteogenesis, and chondrogenesis of human mesenchymal stem/stromal cells: a comparative transcriptome approach. *Front Cell Dev Biol 8*: 561.

Romano A et Martel F (2021). The role of EGCG in breast cancer prevention and therapy. *Mini Rev Med Chem 21*: 883-898.

Rong L, Li R, Li S et Luo R (2016). Immunosuppression of breast cancer cells mediated by transforming growth factor-beta in exosomes from cancer cells. *Oncol Lett 11*: 500-504.

Rosen E, Eguchi J et Xu Z (2009). Transcriptional targets in adipocyte biology. *Expert Opin Ther Targets 13*: 975-986.

Rosen ED, Sarraf P, Troy AE, Bradwin G, Moore K, Milstone DS, Spiegelman BM et Mortensen RM (1999). PPAR gamma is required for the differentiation of adipose tissue in vivo and in vitro. *Mol Cell 4*: 611-617.

Rosen ED, Walkey CJ, Puigserver P et Spiegelman BM (2000). Transcriptional regulation of adipogenesis. *Genes Dev 14*: 1293-1307.

Ruan K, Song G et Ouyang G (2009). Role of hypoxia in the hallmarks of human cancer. *J Cell Biochem 107*: 1053-1062.

Rudrapal M, Khairnar SJ, Khan J, Dukhyil AB, Ansari MA, Alomary MN, Alshabrmi FM, Palai S, Deb PK et Devi R (2022). Dietary polyphenols and their role in oxidative stress-induced human diseases: insights into protective effects, antioxidant potentials and mechanism(s) of action. *Front Pharmacol 13*: 806470.

Rufino AT, Costa VM, Carvalho F et Fernandes E (2021). Flavonoids as antiobesity agents: A review. *Med Res Rev 41*: 556-585.

Ruhland MK et Alspach E (2021). Senescence and Immunoregulation in the Tumor Microenvironment. *Front Cell Dev Biol 9*: 754069.

Ruhland MK, Coussens LM et Stewart SA (2016a). Senescence and cancer: An evolving inflammatory paradox. *Biochim Biophys Acta 1865*: 14-22.

Ruhland MK, Loza AJ, Capietto AH, Luo X, Knolhoff BL, Flanagan KC, Belt BA, Alspach E, Leahy K, Luo J, et al. (2016b). Stromal senescence establishes an immunosuppressive microenvironment that drives tumorigenesis. *Nat Commun 7*: 11762.

Rybinska I, Agresti R, Trapani A, Tagliabue E et Triulzi T (2020). Adipocytes in Breast Cancer, the Thick and the Thin. *Cells 9*:

Rybinska I, Mangano N, Tagliabue E et Triulzi T (2021). Cancer-Associated Adipocytes in Breast Cancer: Causes and Consequences. *Int J Mol Sci 22*:

Sabharwal SS et Schumacker PT (2014). Mitochondrial ROS in cancer: initiators, amplifiers or an Achilles' heel? *Nat Rev Cancer 14*: 709-721.

Sacca PA, Mazza ON, Scorticati C, Vitagliano G, Casas G et Calvo JC (2019). Human Periprostatic adipose tissue: secretome from patients with prostate cancer or benign prostate hyperplasia. *Cancer Genomics Proteomics 16*: 29-58.

Safaei M, Sundararajan EA, Driss M, Boulila W et Shapi'i A (2021). A systematic literature review on obesity: Understanding the causes & consequences of obesity and reviewing various machine learning approaches used to predict obesity. *Comput Biol Med 136*: 104754.

Saitoh M, Endo K, Furuya S, Minami M, Fukasawa A, Imamura T et Miyazawa K (2016). STAT3 integrates cooperative Ras and TGF-beta signals that induce SNAIL expression. *Oncogene 35*: 1049-1057.

Salgado R, Junius S, Benoy I, Van Dam P, Vermeulen P, Van Marck E, Huget P et Dirix LY (2003). Circulating interleukin-6 predicts survival in patients with metastatic breast cancer. *Int J Cancer 103*: 642-646.

Saliminejad K, Khorram Khorshid HR, Soleymani Fard S et Ghaffari SH (2019). An overview of microRNAs: Biology, functions, therapeutics, and analysis methods. *J Cell Physiol 234*: 5451-5465.

Sansone P, Savini C, Kurelac I, Chang Q, Amato LB, Strillacci A, Stepanova A, Iommarini L, Mastroleo C, Daly L, et al. (2017). Packaging and transfer of mitochondrial DNA via exosomes regulate escape from dormancy in hormonal therapy-resistant breast cancer. *Proc Natl Acad Sci U S A 114*: E9066-E9075.

Sansone P, Storci G, Tavolari S, Guarnieri T, Giovannini C, Taffurelli M, Ceccarelli C, Santini D, Paterini P, Marcu KB, et al. (2007). IL-6 triggers malignant features in mammospheres from human ductal breast carcinoma and normal mammary gland. *J Clin Invest 117*: 3988-4002.

Santander AM, Lopez-Ocejo O, Casas O, Agostini T, Sanchez L, Lamas-Basulto E, Carrio R, Cleary MP, Gonzalez-Perez RR et Torroella-Kouri M (2015). Paracrine Interactions between Adipocytes and Tumor Cells Recruit and Modify Macrophages to the Mammary Tumor Microenvironment: The Role of Obesity and Inflammation in Breast Adipose Tissue. *Cancers (Basel) 7*: 143-178.

Santos JC, Lima NDS, Sarian LO, Matheu A, Ribeiro ML et Derchain SFM (2018). Exosome-mediated breast cancer chemoresistance via miR-155 transfer. *Sci Rep 8*: 829.

Sarjeant K et Stephens JM (2012). Adipogenesis. *Cold Spring Harb Perspect Biol 4*: a008417.

Satpathi S, Gaukar S, Potdukhe A et Wanjari M (2023). Unveiling the role of hormonal imbalance in breast cancer development: a comprehensive review. *Cureus 15*: e41737.

Schmid P, Adams S, Rugo HS, Schneeweiss A, Barrios CH, Iwata H, Dieras V, Hegg R, Im SA, Shaw Wright G, et al. (2018). Atezolizumab and Nab-Paclitaxel in Advanced Triple-Negative Breast Cancer. *N Engl J Med 379*: 2108-2121.

Schmitt CA, Wang B et Demaria M (2022). Senescence and cancer - role and therapeutic opportunities. *Nat Rev Clin Oncol 19*: 619-636.

Sen T et Chatterjee A (2011). Epigallocatechin-3-gallate (EGCG) downregulates EGF-induced MMP-9 in breast cancer cells: involvement of integrin receptor alpha5beta1 in the process. *Eur J Nutr 50*: 465-478.

Shankar S, Ganapathy S, Hingorani SR et Srivastava RK (2008). EGCG inhibits growth, invasion, angiogenesis and metastasis of pancreatic cancer. *Front Biosci 13*: 440-452.

Shankar S, Suthakar G et Srivastava RK (2007). Epigallocatechin-3-gallate inhibits cell cycle and induces apoptosis in pancreatic cancer. *Front Biosci 12*: 5039-5051.

Sharaf H, Matou-Nasri S, Wang Q, Rabhan Z, Al-Eidi H, Al Abdulrahman A et Ahmed N (2015). Advanced glycation endproducts increase proliferation, migration and invasion of the breast cancer cell line MDA-MB-231. *Biochim Biophys Acta 1852*: 429-441.

Sharma C, Nusri Qel A, Begum S, Javed E, Rizvi TA et Hussain A (2012). (-)-Epigallocatechin-3-gallate induces apoptosis and inhibits invasion and migration of human cervical cancer cells. *Asian Pac J Cancer Prev 13*: 4815-4822.

Shaw E, Farris M, McNeil J et Friedenreich C (2016). Obesity and endometrial cancer. *Recent Results Cancer Res 208*: 107-136.

She QB, Bode AM, Ma WY, Chen NY et Dong Z (2001). Resveratrol-induced activation of p53 and apoptosis is mediated by extracellular-signal-regulated protein kinases and p38 kinase. *Cancer Res 61*: 1604-1610.

Shekhar MP, Santner S, Carolin KA et Tait L (2007). Direct involvement of breast tumor fibroblasts in the modulation of tamoxifen sensitivity. *Am J Pathol 170*: 1546-1560.

Shen M, Dong C, Ruan X, Yan W, Cao M, Pizzo D, Wu X, Yang L, Liu L, Ren X, et al. (2019). Chemotherapy-induced extracellular vesicle miRNAs Promote breast cancer stemness by targeting ONECUT2. *Cancer Res 79*: 3608-3621.

Shi J, Liu F, Zhang W, Liu X, Lin B et Tang X (2015). Epigallocatechin-3-gallate inhibits nicotine-induced migration and invasion by the suppression of angiogenesis and epithelial-mesenchymal transition in non-small cell lung cancer cells. *Oncol Rep 33*: 2972-2980.

Shi Y, Zhou W, Cheng L, Chen C, Huang Z, Fang X, Wu Q, He Z, Xu S, Lathia JD, et al. (2017). Tetraspanin CD9 stabilizes gp130 by preventing its ubiquitin-dependent lysosomal degradation to promote STAT3 activation in glioma stem cells. *Cell Death Differ 24*: 167-180.

Shin MJ, Hyun YJ, Kim OY, Kim JY, Jang Y et Lee JH (2006). Weight loss effect on inflammation and LDL oxidation in metabolically healthy but obese (MHO) individuals: low inflammation and LDL oxidation in MHO women. *Int J Obes (Lond) 30*: 1529-1534.

Shipitsin M, Campbell LL, Argani P, Weremowicz S, Bloushtain-Qimron N, Yao J, Nikolskaya T, Serebryiskaya T, Beroukhim R, Hu M, et al. (2007). Molecular definition of breast tumor heterogeneity. *Cancer Cell 11*: 259-273.

Sicard AA, Dao T, Suarez NG et Annabi B (2021). Diet-derived gallated catechins prevent TGF-beta-mediated epithelial-mesenchymal transition, cell migration and vasculogenic mimicry in chemosensitive ES-2 ovarian cancer cells. *Nutr Cancer 73*: 169-180.

Siersbaek R, Scabia V, Nagarajan S, Chernukhin I, Papachristou EK, Broome R, Johnston SJ, Joosten SEP, Green AR, Kumar S, et al. (2020). IL6/STAT3 Signaling Hijacks Estrogen Receptor alpha Enhancers to Drive Breast Cancer Metastasis. *Cancer Cell 38*: 412-423 e419.

Siiteri P (1987). Adipose tissue as a source of hormones. *The American Journal of Clinical Nutrition 45*: 277–282.

Singh AK, Sharma N, Ghosh M, Park YH et Jeong DK (2017). Emerging importance of dietary phytochemicals in fight against cancer: Role in targeting cancer stem cells. *Crit Rev Food Sci Nutr 57*: 3449-3463.

Soda Y, Marumoto T, Friedmann-Morvinski D, Soda M, Liu F, Michiue H, Pastorino S, Yang M, Hoffman RM, Kesari S, et al. (2011). Transdifferentiation of glioblastoma cells into vascular endothelial cells. *Proc Natl Acad Sci U S A 108*: 4274-4280.

Soria G, Yaal-Hahoshen N, Azenshtein E, Shina S, Leider-Trejo L, Ryvo L, Cohen-Hillel E, Shtabsky A, Ehrlich M, Meshel T, et al. (2008). Concomitant expression of the chemokines RANTES and MCP-1 in human breast cancer: a basis for tumor-promoting interactions. *Cytokine 44*: 191-200.

Sorlie T, Perou CM, Tibshirani R, Aas T, Geisler S, Johnsen H, Hastie T, Eisen MB, van de Rijn M, Jeffrey SS, et al. (2001). Gene expression patterns of breast carcinomas distinguish tumor subclasses with clinical implications. *Proc Natl Acad Sci U S A 98*: 10869-10874.

Sotgia F, Fiorillo M et Lisanti MP (2019). Hallmarks of the cancer cell of origin: Comparisons with "energetic" cancer stem cells (e-CSCs). *Aging (Albany NY) 11*: 1065-1068.

Spees JL, Olson SD, Whitney MJ et Prockop DJ (2006). Mitochondrial transfer between cells can rescue aerobic respiration. *Proc Natl Acad Sci U S A 103*: 1283-1288.

Spiegel A, Brooks MW, Houshyar S, Reinhardt F, Ardolino M, Fessler E, Chen MB, Krall JA, DeCock J, Zervantonakis IK, et al. (2016). Neutrophils suppress intraluminal nk cell-mediated tumor cell clearance and enhance extravasation of disseminated carcinoma cells. *Cancer Discov 6*: 630-649.

Stanford KI, Middelbeek RJ et Goodyear LJ (2015). Exercise effects on white adipose tissue: beiging and metabolic adaptations. *Diabetes 64*: 2361-2368.

Statello L, Guo CJ, Chen LL et Huarte M (2021). Gene regulation by long non-coding RNAs and its biological functions. *Nat Rev Mol Cell Biol 22*: 96-118.

Stein K et Chiang HL (2014). Exocytosis and endocytosis of small vesicles across the plasma membrane in Saccharomyces cerevisiae. *Membranes (Basel) 4*: 608-629.

Suarez-Arnedo A, Torres Figueroa F, Clavijo C, Arbelaez P, Cruz JC et Munoz-Camargo C (2020). An image J plugin for the high throughput image analysis of in vitro scratch wound healing assays. *PLoS One 15*: e0232565.

Suarez-Najera LE, Chanona-Perez JJ, Valdivia-Flores A, Marrero-Rodriguez D, Salcedo-Vargas M, Garcia-Ruiz DI et Castro-Reyes MA (2018). Morphometric study of adipocytes on breast cancer by means of photonic microscopy and image analysis. *Microsc Res Tech 81*: 240-249.

Sudhakaran M et Doseff AI (2020). The Targeted Impact of Flavones on Obesity-Induced Inflammation and the Potential Synergistic Role in Cancer and the Gut Microbiota. *Molecules 25*:

Sue N, Jack BH, Eaton SA, Pearson RC, Funnell AP, Turner J, Czolij R, Denyer G, Bao S, Molero-Navajas JC, et al. (2008). Targeted disruption of the basic Kruppel-like factor gene (Klf3) reveals a role in adipogenesis. *Mol Cell Biol 28*: 3967-3978.

Sun H, Zou J, Chen L, Zu X, Wen G et Zhong J (2017). Triple-negative breast cancer and its association with obesity. *Mol Clin Oncol 7*: 935-942.

Sundararajan V, Sarkar FH et Ramasamy TS (2018). Correction to: The versatile role of exosomes in cancer progression: diagnostic and therapeutic implications. *Cell Oncol (Dordr) 41*: 463.

Sung H, Ferlay J, Siegel RL, Laversanne M, Soerjomataram I, Jemal A et Bray F (2021). Global Cancer Statistics 2020: GLOBOCAN Estimates of incidence and mortality worldwide for 36 cancers in 185 countries. *CA Cancer J Clin 71*: 209-249.

Takenaga K, Koshikawa N et Nagase H (2021) .Intercellular transfer of mitochondrial DNA carrying metastasis-enhancing pathogenic mutations from high- to low-metastatic tumor cells and stromal cells via extracellular vesicles. *BMC Mol Cell Biol 22*: 52.

Takizawa F, Tsuji S et Nagasawa S (1996). Enhancement of macrophage phagocytosis upon iC3b deposition on apoptotic cells. *FEBS Lett 397*: 269-272.

Tan AS, Baty JW, Dong LF, Bezawork-Geleta A, Endaya B, Goodwin J, Bajzikova M, Kovarova J, Peterka M, Yan B, et al. (2015). Mitochondrial genome acquisition restores respiratory function and tumorigenic potential of cancer cells without mitochondrial DNA. *Cell Metab 21*: 81-94.

Tanaka T, Narazaki M et Kishimoto T (2014). IL-6 in inflammation, immunity, and disease. *Cold Spring Harb Perspect Biol 6*: a016295.

Tang QQ et Lane MD (2012). Adipogenesis: from stem cell to adipocyte. *Annu Rev Biochem 81*: 715-736.

Tang SN, Singh C, Nall D, Meeker D, Shankar S et Srivastava RK (2010). The dietary bioflavonoid quercetin synergizes with epigallocathechin gallate (EGCG) to inhibit

prostate cancer stem cell characteristics, invasion, migration and epithelial-mesenchymal transition. *J Mol Signal 5*: 14.

Tauro BJ, Greening DW, Mathias RA, Mathivanan S, Ji H et Simpson RJ (2013). Two distinct populations of exosomes are released from LIM1863 colon carcinoma cell-derived organoids. *Mol Cell Proteomics 12*: 587-598.

Tawara K, Scott H, Emathinger J, Ide A, Fox R, Greiner D, LaJoie D, Hedeen D, Nandakumar M, Oler AJ, et al. (2019). Co-Expression of VEGF and IL-6 Family cytokines is associated with decreased survival in HER2 negative breast cancer patients: subtype-specific IL-6 family cytokine-mediated VEGF secretion. *Transl Oncol 12*: 245-255.

Taylor DD, Gercel-Taylor C, Lyons KS, Stanson J et Whiteside TL (2003). T-cell apoptosis and suppression of T-cell receptor/CD3-zeta by Fas ligand-containing membrane vesicles shed from ovarian tumors. *Clin Cancer Res 9*: 5113-5119.

Taylor J et Bebawy M (2019). Proteins Regulating Microvesicle Biogenesis and Multidrug Resistance in Cancer. *Proteomics 19*: e1800165.

Taylor NA, Vick SC, Iglesia MD, Brickey WJ, Midkiff BR, McKinnon KP, Reisdorf S, Anders CK, Carey LA, Parker JS, et al. (2017). Treg depletion potentiates checkpoint inhibition in claudin-low breast cancer. *J Clin Invest 127*: 3472-3483.

Thery C, Boussac M, Veron P, Ricciardi-Castagnoli P, Raposo G, Garin J et Amigorena S (2001). Proteomic analysis of dendritic cell-derived exosomes: a secreted subcellular compartment distinct from apoptotic vesicles. *J Immunol 166*: 7309-7318.

Thery C, Witwer KW, Aikawa E, Alcaraz MJ, Anderson JD, Andriantsitohaina R, Antoniou A, Arab T, Archer F, Atkin-Smith GK, et al. (2018). Minimal information for studies of extracellular vesicles 2018 (MISEV2018): a position statement of the International Society for Extracellular Vesicles and update of the MISEV2014 guidelines. *J Extracell Vesicles 7*: 1535750.

Thibault M, Blier, P.U. & Guderley, H (1997). Seasonal variation of muscle metabolic organization in rainbow trout (Oncorhynchus mykiss). *Fish Physiol Biochem 16*: 139-155.

Thornton TM, Pedraza-Alva G, Deng B, Wood CD, Aronshtam A, Clements JL, Sabio G, Davis RJ, Matthews DE, Doble B, et al. (2008). Phosphorylation by p38 MAPK as an alternative pathway for GSK3beta inactivation. *Science 320*: 667-670.

Thu HNN, Vy HTN, Thanh TNN, Giang DTN, Nhan TN, Hoang NP et Hue TN (2021). [miRNA-16 AS an Internal Control in Breast Cancer Studies: A Systematic Review and Meta-analysis]. *Mol Biol (Mosk) 55*: 1045-1056.

Tkach M et Thery C (2016). Communication by extracellular vesicles: where we are and where we need to go. *Cell 164*: 1226-1232.

Toden S, Tran HM, Tovar-Camargo OA, Okugawa Y et Goel A (2016). Epigallocatechin-3-gallate targets cancer stem-like cells and enhances 5-fluorouracil chemosensitivity in colorectal cancer. *Oncotarget 7*: 16158-16171.

Todkar K, Chikhi L, Desjardins V, El-Mortada F, Pepin G et Germain M (2021). Selective packaging of mitochondrial proteins into extracellular vesicles prevents the release of mitochondrial DAMPs. *Nat Commun 12*: 1971.

Tong Q, Tsai J, Tan G, Dalgin G et Hotamisligil GS (2005). Interaction between GATA and the C/EBP family of transcription factors is critical in GATA-mediated suppression of adipocyte differentiation. *Mol Cell Biol 25*: 706-715.

Tornatore L, Thotakura AK, Bennett J, Moretti M et Franzoso G (2012). The nuclear factor kappa B signaling pathway: integrating metabolism with inflammation. *Trends Cell Biol 22*: 557-566.

Trabold O, Wagner S, Wicke C, Scheuenstuhl H, Hussain MZ, Rosen N, Seremetiev A, Becker HD et Hunt TK (2003). Lactate and oxygen constitute a fundamental regulatory mechanism in wound healing. *Wound Repair Regen 11*: 504-509.

Trayhurn P (2013). Hypoxia and adipose tissue function and dysfunction in obesity. *Physiol Rev 93*: 1-21.

Trayhurn P, Wang B et Wood IS (2008). Hypoxia in adipose tissue: a basis for the dysregulation of tissue function in obesity? *Br J Nutr 100*: 227-235.

Tsao R (2010). Chemistry and biochemistry of dietary polyphenols. *Nutrients 2*: 1231-1246.

Ulgen E, Ozisik O et Sezerman OU (2019). pathfindR: An R Package for Comprehensive Identification of Enriched Pathways in Omics Data Through Active Subnetworks. *Front Genet 10*: 858.

Ullah I, Subbarao RB et Rho GJ (2015). Human mesenchymal stem cells - current trends and future prospective. *Biosci Rep 35*:

Vaitkus JA et Celi FS (2017). The role of adipose tissue in cancer-associated cachexia. *Exp Biol Med (Maywood) 242*: 473-481.

Van Baelen K, Geukens T, Maetens M, Tjan-Heijnen V, Lord CJ, Linn S, Bidard FC, Richard F, Yang WW, Steele RE, et al. (2023). Corrigendum to "Current and future diagnostic and treatment strategies for patients with invasive lobular breast cancer": [Annals of Oncology 33 (2022) 769-785]. *Ann Oncol 34*: 326.

van Tienen FH, Laeremans H, van der Kallen CJ et Smeets HJ (2009). Wnt5b stimulates adipogenesis by activating PPARgamma, and inhibiting the beta-catenin dependent Wnt signaling pathway together with Wnt5a. *Biochem Biophys Res Commun 387*: 207-211.

Vigneri R, Goldfine ID et Frittitta L (2016). Insulin, insulin receptors, and cancer. *J Endocrinol Invest 39*: 1365-1376.

Vilotic A, Nacka-Aleksic M, Pirkovic A, Bojic-Trbojevic Z, Dekanski D et Jovanovic Krivokuca M (2022) IL-6 and IL-8: An Overview of their roles in healthy and pathological pregnancies. *Int J Mol Sci 23*:

Vinayak M et Maurya AK (2019). Quercetin Loaded nanoparticles in targeting cancer: recent development. *Anticancer Agents Med Chem 19*: 1560-1576.

Vonderheide RH, Domchek SM et Clark AS (2017). Immunotherapy for Breast Cancer: What Are We Missing? *Clin Cancer Res 23*: 2640-2646.

Vozarova B, Weyer C, Hanson K, Tataranni PA, Bogardus C et Pratley RE (2001). Circulating interleukin-6 in relation to adiposity, insulin action, and insulin secretion. *Obes Res 9*: 414-417.

Wadey RM, Connolly KD, Mathew D, Walters G, Rees DA et James PE (2019.) Inflammatory adipocyte-derived extracellular vesicles promote leukocyte attachment to vascular endothelial cells. *Atherosclerosis 283*: 19-27.

Wahli W (2002). Peroxisome proliferator-activated receptors (PPARs): from metabolic control to epidermal wound healing. *Swiss Med Wkly 132*: 83-91.

Wang B, Kohli J et Demaria M (2020a). Senescent cells in cancer therapy: friends or foes? *Trends Cancer 6*: 838-857.

Wang D, Xiao F, Feng Z, Li M, Kong L, Huang L, Wei Y, Li H, Liu F, Zhang H, et al. (2020b). Sunitinib facilitates metastatic breast cancer spreading by inducing endothelial cell senescence. *Breast Cancer Res 22*: 103.

Wang F, Gao S, Chen F, Fu Z, Yin H, Lu X, Yu J et Lu C (2014). Mammary fat of breast cancer: gene expression profiling and functional characterization. *PLoS One 9*: e109742.

Wang L, Lankhorst L et Bernards R (2022). Exploiting senescence for the treatment of cancer. *Nat Rev Cancer 22*: 340-355.

Wang S, Su X, Xu M, Xiao X, Li X, Li H, Keating A et Zhao RC (2019a). Exosomes secreted by mesenchymal stromal/stem cell-derived adipocytes promote breast cancer cell growth via activation of Hippo signaling pathway. *Stem Cell Res Ther 10*: 117.

Wang S, Xu M, Li X, Su X, Xiao X, Keating A et Zhao RC (2018a). Exosomes released by hepatocarcinoma cells endow adipocytes with tumor-promoting properties. *J Hematol Oncol 11*: 82.

Wang T, Fahrmann JF, Lee H, Li YJ, Tripathi SC, Yue C, Zhang C, Lifshitz V, Song J, Yuan Y, et al. (2018b). JAK/STAT3-Regulated Fatty Acid beta-Oxidation Is Critical for Breast Cancer Stem Cell Self-Renewal and Chemoresistance. *Cell Metab 27*: 136-150 e135.

Wang X et Gerdes HH (2015). Transfer of mitochondria via tunneling nanotubes rescues apoptotic PC12 cells. *Cell Death Differ 22*: 1181-1191.

Wang X, Qi Y, Kong X, Zhai J, Li Y, Song Y, Wang J, Feng X et Fang Y (2019b). Immunological therapy: A novel thriving area for triple-negative breast cancer treatment. *Cancer Lett 442*: 409-428.

Wang X, Sun C, Huang X, Li J, Fu Z, Li W et Yin Y (2021a). The Advancing Roles of Exosomes in Breast Cancer. *Front Cell Dev Biol 9*: 731062.

Wang Y, Ren X, Deng C, Yang L, Yan E, Guo T, Li Y et Xu MX (2013). Mechanism of the inhibition of the STAT3 signaling pathway by EGCG. *Oncol Rep 30*: 2691-2696.

Wang Z, Aguilar EG, Luna JI, Dunai C, Khuat LT, Le CT, Mirsoian A, Minnar CM, Stoffel KM, Sturgill IR, et al. (2019c). Paradoxical effects of obesity on T cell

function during tumor progression and PD-1 checkpoint blockade. *Nat Med 25*: 141-151.

Wang Z, Monjazeb AM et Murphy WJ (2019d). The complicated effects of obesity on cancer and immunotherapy. *Immunotherapy 11*: 11-14.

Wang ZH, Peng WB, Zhang P, Yang XP et Zhou Q (2021b). Lactate in the tumor microenvironment: From immune modulation to therapy. *EBioMedicine 73*: 103627.

Wankhade UD, Shen M, Yadav H et Thakali KM (2016). Novel Browning Agents, Mechanisms, and Therapeutic Potentials of Brown Adipose Tissue. *Biomed Res Int 2016*: 2365609.

Ward AB, Mir H, Kapur N, Gales DN, Carriere PP et Singh S (2018). Quercetin inhibits prostate cancer by attenuating cell survival and inhibiting anti-apoptotic pathways. *World J Surg Oncol 16*: 108.

Wei M, Yang T, Chen X, Wu Y, Deng X, He W, Yang J et Wang Z (2017). Malignant ascites-derived exosomes promote proliferation and induce carcinoma-associated fibroblasts transition in peritoneal mesothelial cells. *Oncotarget 8*: 42262-42271.

Wei X, Li S, He J, Du H, Liu Y, Yu W, Hu H, Han L, Wang C, Li H, et al. (2019). Tumor-secreted PAI-1 promotes breast cancer metastasis via the induction of adipocyte-derived collagen remodeling. *Cell Commun Signal 17*: 58.

Wei Y, Lai X, Yu S, Chen S, Ma Y, Zhang Y, Li H, Zhu X, Yao L et Zhang J (2014.) Exosomal miR-221/222 enhances tamoxifen resistance in recipient ER-positive breast cancer cells. *Breast Cancer Res Treat 147*: 423-431.

Weigelt B, Geyer FC et Reis-Filho JS (2010). Histological types of breast cancer: how special are they? *Mol Oncol 4*: 192-208.

Weigelt B, Horlings HM, Kreike B, Hayes MM, Hauptmann M, Wessels LF, de Jong D, Van de Vijver MJ, Van't Veer LJ et Peterse JL (2008). Refinement of breast cancer classification by molecular characterization of histological special types. *J Pathol 216*: 141-150.

Weigelt B et Reis-Filho JS (2009). Histological and molecular types of breast cancer: is there a unifying taxonomy? *Nat Rev Clin Oncol 6*: 718-730.

Weisberg SP, McCann D, Desai M, Rosenbaum M, Leibel RL et Ferrante AW, Jr. (2003). Obesity is associated with macrophage accumulation in adipose tissue. *J Clin Invest 112*: 1796-1808.

Weng YS, Tseng HY, Chen YA, Shen PC, Al Haq AT, Chen LM, Tung YC et Hsu HL (2019). MCT-1/miR-34a/IL-6/IL-6R signaling axis promotes EMT progression, cancer stemness and M2 macrophage polarization in triple-negative breast cancer. *Mol Cancer 18*: 42.

White IJ, Bailey LM, Aghakhani MR, Moss SE et Futter CE (2006). EGF stimulates annexin 1-dependent inward vesiculation in a multivesicular endosome subpopulation. *EMBO J 25*: 1-12.

World Health Organization (WHO). (2021). Dans breast cancer. Récupéré le 2023, 07-03-2023 de

Williams DM, Nawaz A et Evans M (2020). Drug therapy in obesity: a review of current and emerging treatments. *Diabetes Ther 11*: 1199-1216.

Witwer KW, Buzas EI, Bemis LT, Bora A, Lasser C, Lotvall J, Nolte-'t Hoen EN, Piper MG, Sivaraman S, Skog J, et al. (2013). Standardization of sample collection, isolation and analysis methods in extracellular vesicle research. *J Extracell Vesicles 2*:

Wu HT, Liu J, Li GW, Shen JX et Huang YT (2017a). The transcriptional STAT3 is a potential target, whereas transcriptional STAT5A/5B/6 are new biomarkers for prognosis in human breast carcinoma. *Oncotarget 8*: 36279-36288.

Wu M, Liu D, Zeng R, Xian T, Lu Y, Zeng G, Sun Z, Huang B et Huang Q (2017b). Epigallocatechin-3-gallate inhibits adipogenesis through down-regulation of PPARgamma and FAS expression mediated by PI3K-AKT signaling in 3T3-L1 cells. *Eur J Pharmacol 795*: 134-142.

Wu PP, Kuo SC, Huang WW, Yang JS, Lai KC, Chen HJ, Lin KL, Chiu YJ, Huang LJ et Chung JG (2009). (-)-Epigallocatechin gallate induced apoptosis in human adrenal cancer NCI-H295 cells through caspase-dependent and caspase-independent pathway. *Anticancer Res 29*: 1435-1442.

Wu Q, Li B, Li Z, Li J, Sun S et Sun S (2019). Cancer-associated adipocytes: key players in breast cancer progression. *J Hematol Oncol 12*: 95.

Wu Q, Siddharth S et Sharma D (2021). Triple negative breast cancer: a mountain yet to be scaled despite the triumphs. *Cancers (Basel) 13*:

Wu Q, Sun S, Li Z, Yang Q, Li B, Zhu S, Wang L, Wu J, Yuan J, Yang C, et al. (2018). Tumor-originated exosomal miR-155 triggers cancer-associated cachexia to promote tumor progression. *Mol Cancer 17*: 155.

Wyckoff J, Wang W, Lin EY, Wang Y, Pixley F, Stanley ER, Graf T, Pollard JW, Segall J et Condeelis J (2004). A paracrine loop between tumor cells and macrophages is required for tumor cell migration in mammary tumors. *Cancer Res 64*: 7022-7029.

Xi L, Peng M, Liu S, Liu Y, Wan X, Hou Y, Qin Y, Yang L, Chen S, Zeng H, et al. (2021)/ Hypoxia-stimulated ATM activation regulates autophagy-associated exosome release from cancer-associated fibroblasts to promote cancer cell invasion. *J Extracell Vesicles 10*: e12146.

Xiao X, Jiang K, Xu Y, Peng H, Wang Z, Liu S et Zhang G (2019). (-)-Epigallocatechin-3-gallate induces cell apoptosis in chronic myeloid leukaemia by regulating Bcr/Abl-mediated p38-MAPK/JNK and JAK2/STAT3/AKT signalling pathways. *Clin Exp Pharmacol Physiol 46*: 126-136.

Xie L, Yi J, Song Y, Zhao M, Fan L et Zhao L (2021). Suppression of GOLM1 by EGCG through HGF/HGFR/AKT/GSK-3beta/beta-catenin/c-Myc signaling pathway inhibits cell migration of MDA-MB-231. *Food Chem Toxicol 157*: 112574.

Xu MJ, Liu BJ, Wang CL, Wang GH, Tian Y, Wang SH, Li J, Li PY, Zhang RH, Wei D, et al. (2017). Epigallocatechin-3-gallate inhibits TLR4 signaling through the 67-kDa laminin receptor and effectively alleviates acute lung injury induced by H9N2 swine influenza virus. *Int Immunopharmacol 52*: 24-33.

Xu XJ, Gauthier MS, Hess DT, Apovian CM, Cacicedo JM, Gokce N, Farb M, Valentine RJ et Ruderman NB (2012). Insulin sensitive and resistant obesity in humans: AMPK activity, oxidative stress, and depot-specific changes in gene expression in adipose tissue. *J Lipid Res 53*: 792-801.

Yamada S, Tsukamoto S, Huang Y, Makio A, Kumazoe M, Yamashita S et Tachibana H (2016). Epigallocatechin-3-O-gallate up-regulates microRNA-let-7b expression by activating 67-kDa laminin receptor signaling in melanoma cells. *Sci Rep 6*: 19225.

Yamauchi T, Kamon J, Minokoshi Y, Ito Y, Waki H, Uchida S, Yamashita S, Noda M, Kita S, Ueki K, et al. (2002). Adiponectin stimulates glucose utilization and fatty-acid oxidation by activating AMP-activated protein kinase. *Nat Med 8*: 1288-1295.

Yamauchi T, Kamon J, Waki H, Terauchi Y, Kubota N, Hara K, Mori Y, Ide T, Murakami K, Tsuboyama-Kasaoka N, et al. (2001). The fat-derived hormone adiponectin reverses insulin resistance associated with both lipoatrophy and obesity. *Nat Med 7*: 941-946.

Yang GY, Liao J, Kim K, Yurkow EJ et Yang CS (1998). Inhibition of growth and induction of apoptosis in human cancer cell lines by tea polyphenols. *Carcinogenesis 19*: 611-616.

Yang GY, Liao J, Li C, Chung J, Yurkow EJ, Ho CT et Yang CS (2000). Effect of black and green tea polyphenols on c-jun phosphorylation and H(2)O(2) production in transformed and non-transformed human bronchial cell lines: possible mechanisms of cell growth inhibition and apoptosis induction. *Carcinogenesis 21*: 2035-2039.

Yang L, Wang L, Lin HK, Kan PY, Xie S, Tsai MY, Wang PH, Chen YT et Chang C (2003). Interleukin-6 differentially regulates androgen receptor transactivation via PI3K-Akt, STAT3, and MAPK, three distinct signal pathways in prostate cancer cells. *Biochem Biophys Res Commun 305*: 462-469.

Yang M, Chen J, Su F, Yu B, Su F, Lin L, Liu Y, Huang JD et Song E (2011). Microvesicles secreted by macrophages shuttle invasion-potentiating microRNAs into breast cancer cells. *Mol Cancer 10*: 117.

Yang M, Ma B, Shao H, Clark AM et Wells A (2016). Macrophage phenotypic subtypes diametrically regulate epithelial-mesenchymal plasticity in breast cancer cells. *BMC Cancer 16*: 419.

Yang SJ, Wang DD, Li J, Xu HZ, Shen HY, Chen X, Zhou SY, Zhong SL, Zhao JH et Tang JH (2017). Predictive role of GSTP1-containing exosomes in chemotherapy-resistant breast cancer. *Gene 623*: 5-14.

Yang XR, Sherman ME, Rimm DL, Lissowska J, Brinton LA, Peplonska B, Hewitt SM, Anderson WF, Szeszenia-Dabrowska N, Bardin-Mikolajczak A, et al. (2007). Differences in risk factors for breast cancer molecular subtypes in a population-based study. *Cancer Epidemiol Biomarkers Prev 16*: 439-443.

Yang Y, Li CW, Chan LC, Wei Y, Hsu JM, Xia W, Cha JH, Hou J, Hsu JL, Sun L, et al. (2018). Exosomal PD-L1 harbors active defense function to suppress T cell killing of breast cancer cells and promote tumor growth. *Cell Res 28*: 862-864.

Yang Y, Ye G, Zhang YL, He HW, Yu BQ, Hong YM, You W et Li X (2020). Transfer of mitochondria from mesenchymal stem cells derived from induced pluripotent stem cells attenuates hypoxia-ischemia-induced mitochondrial dysfunction in PC12 cells. *Neural Regen Res 15*: 464-472.

Yano S, Suzuki K et Hara T (2022). Proteomic profiling of intestinal epithelial-like cell-derived exosomes regulated by epigallocatechin gallate. *Biofactors*

Yeh CW, Chen WJ, Chiang CT, Lin-Shiau SY et Lin JK (2003). Suppression of fatty acid synthase in MCF-7 breast cancer cells by tea and tea polyphenols: a possible mechanism for their hypolipidemic effects. *Pharmacogenomics J 3*: 267-276.

Yeong J, Thike AA, Lim JC, Lee B, Li H, Wong SC, Hue SS, Tan PH et Iqbal J (2017). Higher densities of Foxp3(+) regulatory T cells are associated with better prognosis in triple-negative breast cancer. *Breast Cancer Res Treat 163*: 21-35.

Yin L, Duan JJ, Bian XW et Yu SC (2020). Triple-negative breast cancer molecular subtyping and treatment progress. *Breast Cancer Res 22*: 61.

Yoshida K et Miki Y (2004). Role of BRCA1 and BRCA2 as regulators of DNA repair, transcription, and cell cycle in response to DNA damage. *Cancer Sci 95*: 866-871.

Yousefi S, Mihalache C, Kozlowski E, Schmid I et Simon HU (2009). Viable neutrophils release mitochondrial DNA to form neutrophil extracellular traps. *Cell Death Differ 16*: 1438-1444.

Yu J, Wang Y, Yan F, Zhang P, Li H, Zhao H, Yan C, Yan F et Ren X (2014). Noncanonical NF-kappaB activation mediates STAT3-stimulated IDO upregulation in myeloid-derived suppressor cells in breast cancer. *J Immunol 193*: 2574-2586.

Yu X, Harris SL et Levine AJ (2006). The regulation of exosome secretion: a novel function of the p53 protein. *Cancer Res 66*: 4795-4801.

Yuan S, Norgard RJ et Stanger BZ (2019). Cellular Plasticity in Cancer. *Cancer Discov 9*: 837-851.

Zampieri LX, Silva-Almeida C, Rondeau JD et Sonveaux P (2021). Mitochondrial Transfer in Cancer: A Comprehensive Review. *Int J Mol Sci 22*:

Zatterale F, Longo M, Naderi J, Raciti GA, Desiderio A, Miele C et Beguinot F (2019). Chronic Adipose Tissue Inflammation Linking Obesity to Insulin Resistance and Type 2 Diabetes. *Front Physiol 10*: 1607.

Zeleniuch-Jacquotte A, Afanasyeva Y, Kaaks R, Rinaldi S, Scarmo S, Liu M, Arslan AA, Toniolo P, Shore RE et Koenig KL (2012). Premenopausal serum androgens and breast cancer risk: a nested case-control study. *Breast Cancer Res 14*: R32.

Zeng J, Sauter ER et Li B (2020). FABP4: A New Player in Obesity-Associated Breast Cancer. *Trends Mol Med 26*: 437-440.

Zeng L, Holly JM et Perks CM (2014). Effects of physiological levels of the green tea extract epigallocatechin-3-gallate on breast cancer cells. *Front Endocrinol (Lausanne) 5*: 61.

Zgheib A, Lamy S et Annabi B (2013). Epigallocatechin gallate targeting of membrane type 1 matrix metalloproteinase-mediated Src and Janus kinase/signal transducers and activators of transcription 3 signaling inhibits transcription of colony-

stimulating factors 2 and 3 in mesenchymal stromal cells. *J Biol Chem 288*: 13378-13386.

Zha J et Lackner MR (2010). Targeting the insulin-like growth factor receptor-1R pathway for cancer therapy. *Clin Cancer Res 16*: 2512-2517.

Zhang C, Gan X, Liang R et Jian J (2020). Exosomes derived from epigallocatechin gallate-treated cardiomyocytes attenuated acute myocardial infarction by modulating microRNA-30a. *Front Pharmacol 11*: 126.

Zhang F, Wang Z, Fan Y, Xu Q, Ji W, Tian R et Niu R (2015). Elevated STAT3 signaling-mediated upregulation of MMP-2/9 confers enhanced invasion ability in multidrug-resistant breast cancer cells. *Int J Mol Sci 16*: 24772-24790.

Zhang H, and Tsao, R (2016). Dietary polyphenols, oxidative stress and antioxidant and anti-inflammatory *Curr Opin Food Sci 8*: 33-42.

Zhang L, Xie J, Gan R, Wu Z, Luo H, Chen X, Lu Y, Wu L et Zheng D (2019a). Synergistic inhibition of lung cancer cells by EGCG and NF-kappaB inhibitor BAY11-7082. *J Cancer 10*: 6543-6556.

Zhang S, Wang J, Chen T, Wang J, Wang Y, Yu Z, Zhao K, Zheng K, Chen Y, Wang Z, et al. (2021). Alpha-Actinin1 promotes tumorigenesis and epithelial-mesenchymal transition of gastric cancer via the AKT/GSK3beta/beta-Catenin pathway. *Bioengineered 12*: 5688-5704.

Zhang X, Min KW, Wimalasena J et Baek SJ (2012). Cyclin D1 degradation and p21 induction contribute to growth inhibition of colorectal cancer cells induced by epigallocatechin-3-gallate. *J Cancer Res Clin Oncol 138*: 2051-2060.

Zhang Y, Bellows CF et Kolonin MG (2010). Adipose tissue-derived progenitor cells and cancer. *World J Stem Cells 2*: 103-113.

Zhang Y, Liu Y, Liu H et Tang WH (2019b). Exosomes: biogenesis, biologic function and clinical potential. *Cell Biosci 9*: 19.

Zhao C, Wu M, Zeng N, Xiong M, Hu W, Lv W, Yi Y, Zhang Q et Wu Y (2020). Cancer-associated adipocytes: emerging supporters in breast cancer. *J Exp Clin Cancer Res 39*: 156.

Zheng X, Bahr M et Doeppner TR (2019). From tumor metastasis towards cerebral ischemia-extracellular vesicles as a general concept of intercellular communication processes. *Int J Mol Sci 20*:

Zhou B, Chen WL, Wang YY, Lin ZY, Zhang DM, Fan S et Li JS (2014). A role for cancer-associated fibroblasts in inducing the epithelial-to-mesenchymal transition in human tongue squamous cell carcinoma. *J Oral Pathol Med 43*: 585-592.

Zhou F, Zhou H, Wang T, Mu Y, Wu B, Guo DL, Zhang XM et Wu Y (2012). Epigallocatechin-3-gallate inhibits proliferation and migration of human colon cancer SW620 cells in vitro. *Acta Pharmacol Sin 33*: 120-126.

Zhou Y, Zheng J, Li Y, Xu DP, Li S, Chen YM et Li HB (2016). Natural polyphenols for prevention and treatment of cancer. *Nutrients 8*:

Zhu BH, Chen HY, Zhan WH, Wang CY, Cai SR, Wang Z, Zhang CH et He YL (2011). (-)-Epigallocatechin-3-gallate inhibits VEGF expression induced by IL-6 via Stat3 in gastric cancer. *World J Gastroenterol 17*: 2315-2325.

Zhu BH, Zhan WH, Li ZR, Wang Z, He YL, Peng JS, Cai SR, Ma JP et Zhang CH (2007). (-)-Epigallocatechin-3-gallate inhibits growth of gastric cancer by reducing VEGF production and angiogenesis. *World J Gastroenterol 13*: 1162-1169.

Zimta AA, Tigu AB, Muntean M, Cenariu D, Slaby O et Berindan-Neagoe I (2019). Molecular links between central obesity and breast cancer. *Int J Mol Sci 20*: